UNIVERSIDAD DE CÓRDOBA

DOCTORAL THESIS

Quantitative proteomics in the bioremediation of cyanide, arsenic and metals by *Pseudomonas pseudoalcaligenes* CECT 5344

Proteómica cuantitativa en la biorremediación de cianuro, arsénico y metales por *Pseudomonas pseudoalcaligenes* CECT 5344

MEMORIA PARA OPTAR AL GRADO DE DOCTOR

Karolina Angelika Biełło

Directores

Conrado Moreno Vivián

Alfonso Olaya Abril

Departamento de Bioquímica y Biología Molecular

Programa de Doctorado de Biociencias y Ciencias Agroalimentarias

Córdoba, 23 de octubre 2023

TITULO: *Quantitative proteomics in the bioremediation of cyanide, arsenic and metals by Pseudomonas pseudoalcaligenes CECT 5344*

AUTOR: *Karolina Biello*

Campus de Rabanales
Ctra. Nacional IV, Km. 396 A
14071 Córdoba

https://www.uco.es/ucopress/index.php/es/
ucopress@uco.es

INFORME RAZONADO DE LAS/LOS DIRECTORAS/ES DE LA TESIS

Este documento se presentará junto con el depósito de la tesis en https://moodle.uco.es/ctp3/

DOCTORANDA/O

Karolina Angelika Biełło

TÍTULO DE LA TESIS:

Quantitative proteomics in the bioremediation of cyanide, arsenic and metals by Pseudomonas pseudoalcaligenes CECT 5344.

INFORME RAZONADO DE LAS/LOS DIRECTORAS/ES DE LA TESIS
(se hará mención a la evolución y desarrollo de la tesis, así como a trabajos y publicaciones derivados de la misma)

Conrado Moreno Vivián, Catedrático de Bioquímica y Biología Molecular de la Universidad de Córdoba y Alfonso Olaya Abril, Profesor Titular de Bioquímica y Biología Molecular de la Universidad de Córdoba,

Informan que,

La presente Tesis Doctoral, titulada "Quantitative proteomcis in the bioremediation of cyanide, arsenic and metals by Pseudomonas pseudoalcaligenes CECT 5344", realizada por Dª Karolina Angelika Biełło, se ha desarrollado en los laboratorios del Departamento de Bioquímica y Biología Molecular de la Universidad de Córdoba bajo nuestra dirección.

Esta Tesis Doctoral reúne todas las condiciones exigidas, según la legalidad vigente. Su evolución y desarrollo ha seguido el plan de trabajo inicialmente previsto, alcanzándose los objetivos previamente marcados. Durante el desarrollo de la Tesis la doctoranda ha realizado una labor altamente satisfactoria en el grupo de investigación, se ha implicado en el desarrollo y aprendizaje de nuevas metodologías y se ha mostrado altamente motivada, habiendo probado con solvencia sus capacidades investigadoras.

Actualmente, cuenta con tres publicaciones en revistas de prestigio internacional como primera autora de trabajos originales de su Tesis. Asimismo, ha defendido su trabajo de investigación en seis Congresos Nacionales y en uno Internacional, siendo galardonada con el premio a la mejor presentación oral de su sesión en el 44º Congreso de la Sociedad Española de Bioquímica y Biología Molecular. Su formación predoctoral ha incluido también actividades docentes, divulgativas y de perfeccionamiento. Ha impartido 6,6 ETCS en diversas asignaturas de varios Grados, como Bioquímica del Grado de Fisioterapia o Biotecnología Ambiental en el Grado de Ciencias Ambientales. En cuanto a la divulgación, ha participado en actividades como el "Paseo por la Ciencia" o "Cuéntame tu tesis", donde ganó el tercer premio. Finalmente, se ha seguido formando mediante la superación de diferentes cursos que le han permitido un mayor perfeccionamiento, como "Introducción a R para análisis de datos" o "Formación Doctoral en Investigación: Herramientas para la Investigación".

Por todo ello, se autoriza la presentación de la tesis doctoral.

Córdoba, a 11 de septiembre de 2023

Las/los directoras/es

MORENO VIVIAN CONRADO - 29750929S
Firmado digitalmente por MORENO VIVIAN CONRADO - 29750929S
Fecha: 2023.09.11 12:35:49 +02'00'

Fdo.: Conrado Moreno Vivián

OLAYA ABRIL ALFONSO - 30975964R
Firmado digitalmente por OLAYA ABRIL ALFONSO - 30975964R
Fecha: 2023.09.07 12:51:05 +02'00'

Fdo.: Alfonso Olaya Abril

Financiación

Este trabajo ha sido financiado con el proyecto P18-RT-3048 de la Junta de Andalucía en titulado: “Cianuro, arsénico y metales. Biodegradación de residuos de la minería y la industria joyera mediante bacterias (CAMBIO)”.

A mi abuelo Eugenio

A mis padres

Mojemu Dziadkowi Eugeniuszowi

Moim Rodzicom

Agradecimientos

Puede parecer que escribir un agradecimiento debería ser una tarea fácil, pero es una de las partes más difíciles de este trabajo a las que me he enfrentado. A pesar de que solo hay un autor en la portada de la obra, esta ha contado con muchos escritores fantasmas a lo largo del proceso, sin los cuales la realización de este trabajo hubiera sido imposible y a quienes debo muchos reconocimientos.

Me gustaría comenzar dando mi más sincero agradecimiento a mis tutores, los profesores Conrado y Alfonso, sin los cuales la realización de este viaje científico no sería posible.

Conrado, me gustaría agradecerte profundamente no solo la oportunidad de realizar mi investigación doctoral sino, más importante aún, el hacerme parte de la increíble familia del grupo BIO-117. Gracias por tu confianza y guía invaluable que me has brindado durante todo este tiempo. Por las innumerables conversaciones esclarecedoras y anécdotas interesantes sobre la ciencia. Por compartir conmigo tu gran conocimiento y experiencia. Por las críticas constructivas cuando fueran necesarias. Por tu apoyo y palabras de aliento recordando que un buen científico obtiene un experimento positivo entre noventa y nueve fracasos. Por tu total atención y tiempo siempre que lo necesité.

Alfonso, es muy difícil decir en pocas palabras “gracias” por los cinco años de guía, ayuda y apoyo que me has brindado durante los primeros pasos de mi aventura científica. Me gustaría agradecerte por ser el MEJOR profesor con el que todos podrían soñar. Por enseñarme desde el principio, ya que era estudiante de grado y mis conocimientos y habilidades eran muy escasos. Por las incontables horas de tu tiempo y tu paciencia conmigo cuando estaba confundida con mi trabajo o llegaba a un callejón sin salida. Por tu gran entusiasmo por la investigación y voluntad de compartirla conmigo. Por tu energía y chistes cotidianos. Por entender mi español, a veces extraño. Gracias por tu apoyo y por tu ayuda cada vez que la necesité. Gracias por cada experimento difícil y tarea desafiante que me formó y me fortaleció en la ética de trabajo.

María Dolores, te agradezco profundamente que me hayas abierto la puerta del laboratorio cuando por primera vez vine como estudiante Erasmus y una tesis doctoral con el grupo estaba más allá de mi imaginación. Gracias por la oportunidad y la cálida bienvenida cuando volví para realizar mis estudios de máster y doctorado. Por ser una supervisora increíble y por tus innumerables palabras de aliento.

Lara, me gustaría agradecerte tu amabilidad, disposición para ayudar y mucha paciencia al responder a mis infinitas preguntas. Gracias por tu energía optimista y tu sonrisa que nunca desaparece.

Víctor, gracias por tus consejos, ayuda y nuestras conversaciones diarias en el laboratorio.

K.A. Biełło 2023

Lolita, me gustaría darte las gracias por enseñarme todo en el laboratorio y compartir conmigo tus "trucos" para que el experimento saliera mejor. Por tu gran ayuda incluso cuando mi español era terrible y apenas podíamos comunicarnos. Por tus palabras de consuelo después de cada experimento fallido. Por tu gran paciencia y tu gran corazón. Por cada risa y lágrima que compartimos.

Gema, mi compi! Me gustaría agradecerte por todo este tiempo que pasamos juntas charlando, riéndonos y discutiendo. Por cada una de tus palabras de valentía. Por permitirme aprender mucho de ti, por brindarme tu tiempo y atención cada vez que lo necesité incluso cuando estabas extremadamente ocupada. Gracias por tu gran ayuda con el cuidado de mis *Pseudomonas*. Gracias por las amables notas (y el chocolate) que dejaste en mi escritorio cuando tuve que quedarme hasta tarde en el laboratorio. Gracias por tus sugerencias y los consejos que me han ayudado a superar las situaciones difíciles.

Noelia, gracias por tu sonrisa y la energía que trajiste al laboratorio. Por tu gran ayuda siempre que la necesitaba.

Me gustaría también dar gracias al grupo BIO-128 por recibirme siempre con una cálida sonrisa durante mis innumerables visitas.

Muchas gracias al grupo BIO-115 por hacerme sentir siempre bienvenida en vuestro laboratorio y por vuestra energía positiva.

Niemożliwym jest opisanie jak duże i serdeczne podziękowania kieruje w stronę moich kochanych rodziców Iwony i Przemysława. Wam zawdzięczam wszystko co udało mi się osiągnąć do tej pory w życiu. Dziękuję za wasze wsparcie, miłość i wiarę we mnie. Za stworzenie rodziny, w której czułam się bezpiecznie i mogłam rozwijać swoje pasje i umiejętności.

Tato, za wszystkie nasze rejsy, długie konwersacje, twoją pasję do sportu i żeglarstwa, którą mnie zaraziłeś. Za wszystkie rady i złote myśli.

Mamo, za wychowanie mnie na silna i niezależna kobietę. Za twoja troskę i słowa otuchy w trudnych momentach.

Dziękuję za waszą pomoc i czas w każdej chwili kiedy tylko potrzebowałam. Za słowa krytyki kiedy te były jak najbardziej potrzebne. Za pomoc w zdobywaniu moich własnych biegunów.

Jestem dumna, że jesteście moimi rodzicami!

K.A. Biełło 2023

Moim drogim dziadkom Basi i Edkowi, za najwspanialsze dzieciństwo jakie miałam. Za wsparcie, miłości i ciepło jakie od was otrzymałam.

Mojej drogiej babci Ali, za każdą cenną poradę i słowa otuchy. Za Twoje zainteresowanie moimi studiami i nauką. Za długie konwersacje i niepodzielną uwagę kiedy opowiadałam Ci o moich pierwszych doświadczeniach w świecie naukowym.

It is impossible to describe how big and heartfelt words of gratitude I direct towards my beloved parents Iwona and Przemysław. I owe you everything that I have achieved so far in my life. Thank you for your support, love and faith in me. For creating a family where I felt safe and could develop my passions and skills.

Dad, for all our cruises, long conversations, your passion for sports and sailing, which you passed on to me. For all your advices and golden thoughts.

Mom, for raising me to be a strong and independent woman. For your concern and words of encouragement in difficult times.

Thank you for your help and time whenever I needed it. For words of criticism when they were most needed. For helping me conquer my own poles.

I am proud of having you as my parents!

To my dear grandparents Basia and Edek, for the most wonderful childhood I ever had. For the support, love and warmth I received from you.

To my dear grandmother Alicja, for every valuable advice and words of encouragement. For your interest in my studies and learning. For long conversations and undivided attention when I was telling you about my first experiences in the scientific world.

También me gustaría expresar mis agradecimientos a mi familia española, Beatriz y Luis.

Beatriz, por tus palabras de aliento, increíble energía positiva, sonrisa constante y tu enorme corazón.

Luis, por las interesantes conversaciones y anécdotas sobre ciencia, tu apoyo, tus chistes y espíritu crítico.

Estoy muy agradecida de que me hagáis parte de vuestra familia.

K.A. Biełło 2023

Me gustaría dar las gracias a todos mis amigos tanto en Polonia como en España que me han apoyado durante este período.

Por último, me gustaría darle las gracias a mi novio Luis. Por tu angélica paciencia conmigo, tu constante apoyo y tu amor. Por llevarme al laboratorio a altas horas de la noche siempre cuando lo necesitaba. Por calmarme en momentos de pánico. Por siempre creer en mí. A ti te debo esta tesis.

He aprendido mucho durante este período de mi aventura científica y sigo aprendiendo, porque a medida que he entrado en el mundo científico me he dado cuenta de lo poco que sé y de lo mucho que me queda por descubrir.

Abstract/Resumen

Abstract

Proteomics is a high-throughput and relatively new technology that has gained a lot of interest during last decades. Proteomics belongs to the family of “omics” techniques together with genomics, transcriptomics and metabolomics, among others, and it aims to investigate the functional relevance of all expressed proteins in cells, tissues or organisms, providing a holistic view. Despite its broad applications in clinical field, the proteomics studies focused on microbial bioremediation of wastewaters and soils contaminated with toxic pollutants remain scarce.

Pseudomonas pseudoalcaligenes CECT 5344 is a cyanotrophic Gram-negative bacterium isolated form sludges of Guadalquivir River that is able to use free cyanide, metal-cyanide complexes and cyano-derivatives as sole nitrogen source under alkaline conditions, thus preventing the formation of highly toxic cyanhydric acid. *P. pseudoalcaligenes* CECT 5344 is a versatile organism with great biotechnological potential in bioremediation treatments. Intense industrial and mining activities generate large amounts of wastes that usually are rich in arsenic, mercury, and cyanide. In this work the quantitative proteomic liquid chromatography-mass spectrometry/mass spectrometry (LC-MS/MS) technique complemented with transcriptional quantitative reverse transcription polymerase chain reaction (*q*RT-PCR) analysis has been used to unravel the molecular mechanisms triggered by the simultaneous presence of toxic compounds in the cyanide-assimilating bacterium *P. pseudoalcaligenes* CECT 5433. Firstly, the combined effect of arsenic and cyanide on the metabolism of the strain CECT 5344 was investigated. Several proteins encoded by two *ars* gene clusters of this bacterium, as well as other As-related proteins, were induced by the presence of arsenic. The nitrilase NitC, required for cyanide assimilation was found unaffected in the analysis, thereby allowing bacterial growth with both cyanide and arsenic. The expression of ArsH2 protein increased in the presence of arsenite or cyanide, suggesting its role in the protection from oxidative stress caused by both toxics. Tetrahydrofolate metabolism was also stimulated by arsenite. Finally, two As-resistance mechanisms were characterized in the strain CECT 5344, the extrusion of As(III) and its extracellular sequestration in biofilm, whose synthesis increased in the presence of arsenite, and the formation of organoarsenicals such as arseno-phosphoglycerate and methyl-As.

Subsequently, the proteomic approach has been applied to disclose the molecular basis of the detoxification of cyanide and mercury by *P. pseudoalcaligenes* CECT 5344. This bacterium harbors two *mer* gene clusters, whose expression was stimulated by the presence of mercury chloride. The cyanide-insensitive alternative oxidase CioAB and the nitrilase NitC were not significantly affected by Hg, thus highlighting their importance in the tolerance and assimilation of cyanide in the presence of this heavy

metal. The CECT 5344 strain demonstrated significantly higher mercury resistance when the bacterium was grown with cyanide than with ammonium, probably due to the formation of cyanide-mercury complexes. Furthermore, the integration of proteomic, bioinformatic and transcriptional data suggested a potential role of the MerR2 protein as a master regulator in media with cyanide and mercury. In general, the Hg-resistance mechanism in the CECT 5344 strain was based on the activity of mercuric reductase MerA and the extrusion from the cells of the volatile form Hg^0, with a residual accumulation inside the cells, probably through chelation to biomolecules.

Finally, a quantitative proteomic LC-MS/MS analysis was also applied to characterize the metabolic changes in *P. pseudoalcaligenes* CECT 5344 during an anaerobic lifestyle in a presence of iron and ammonium. The proteomic analysis revealed induction under anoxic conditions of proteins associated with the tricarboxylic acid cycle, fatty acid metabolism, polyhydroxyalkanoates metabolism, as well as iron-related proteins, among others. It is suggested that ammonium, in addition to acting as a N-source, participates in the Fe(III) reduction via the Fe-dependent ammonium oxidation (Feammox) process, and the respiratory electron transport chain of this bacterium would be involved in the regeneration of Fe(III) from Fe(II) for the Feammox reaction coupled to fumarate respiration. Additionally, the excess of carbon source was directed into synthesis of polyhydroxyalkanoates. These results are a preliminary view on the anaerobic metabolism of the strain CECT 5344, which requires further studies to corroborate this hypothesis.

In general, all the results presented in this work highlight the great and versatile biotechnological potential of the cyanotrophic bacterium *P. pseudoalcaligenes* CECT 5344, and could be useful not only for the design of strategies for bioremediation of complex industrial wastes co-contaminated with cyanide, arsenic, and mercury, but also for the development of alternative anaerobic technologies.

Resumen

La proteómica es una tecnología de alto rendimiento y relativamente nueva que ha adquirido mucho interés durante las últimas décadas. La proteómica pertenece a la familia de las técnicas "ómicas" junto con la genómica, la transcriptómica y la metabolómica, y tiene como objetivo investigar la relevancia funcional de todas las proteínas expresadas en células, tejidos u organismos, aportando una visión holística. A pesar de sus amplias aplicaciones en el campo clínico, los estudios de proteómica centrados en la biorremediación microbiana de aguas residuales y suelos contaminados con sustancias tóxicas siguen siendo escasos.

*Pseudomonas pseudoalcaligene*s CECT 5344 es una bacteria Gram-negativa aislada de los lodos del río Guadalquivir que es capaz de utilizar cianuro libre, complejos metal-cianuro y cianoderivados como única fuente de nitrógeno en condiciones alcalinas, lo que evita la formación de ácido cianhídrico volátil. *P. pseudoalcaligenes* CECT 5344 es un organismo versátil con gran potencial biotecnológico para su aplicación en tratamientos de biorremediación. Las intensas actividades industriales y mineras generan grandes cantidades de residuos que suelen ser ricos en cianuro, arsénico, mercurio y otros metales. En este trabajo se ha utilizado la proteómica cuantitativa (LC-MS/MS) complementada con análisis transcripcional mediante *q*RT-PCR para dilucidar los mecanismos moleculares desencadenados por la presencia simultánea de compuestos tóxicos en la bacteria asimiladora de cianuro *P. pseudoalcaligenes* CECT 5433. En primer lugar, se investigó el efecto combinado del arsénico y el cianuro sobre el metabolismo de la cepa CECT 5344. Varias proteínas codificadas por dos agrupaciones de genes *ars*, así como otras proteínas relacionadas con la tolerancia al As, resultaron inducidas por la presencia de arsénico. La nitrilasa NitC, necesaria para la asimilación del cianuro, no se vio afectada en el análisis, lo que permitió el crecimiento bacteriano tanto con cianuro como con arsénico. La expresión de la proteína ArsH2 aumentó en presencia de arsenito o cianuro, lo que sugiere su papel en la protección del estrés oxidativo causado por ambos tóxicos. El arsenito también estimuló el metabolismo del tetrahidrofolato. Finalmente, se caracterizaron dos mecanismos de resistencia al As en la cepa CECT 5344, la extrusión de As(III) y su secuestro extracelular en la matriz extracelular (biofilm), cuya síntesis aumentó en presencia de arsenito, y la formación de compuestos organoarsenicales como el arseno-fosfoglicerato y el metil-As.

Posteriormente, se aplicó el enfoque proteómico para revelar las bases moleculares de la destoxificación de cianuro y mercurio por *P. pseudoalcaligenes* CECT 5344. Esta bacteria alberga dos agrupaciones de genes *mer*, cuya expresión se estimuló en presencia de cloruro de mercurio. La oxidasa alternativa insensible al cianuro CioAB y la nitrilasa NitC no se afectaron significativamente por

el Hg, destacando así su importancia en la tolerancia y asimilación del cianuro en presencia de este metal pesado. La cepa CECT 5344 demostró una resistencia al mercurio significativamente mayor cuando la bacteria se cultivó con cianuro que con amonio, probablemente debido a la formación de complejos cianuro-mercurio. Además, la integración de datos proteómicos, bioinformáticos y transcripcionales sugirió un papel potencial de la proteína MerR2 como un regulador maestro en presencia de cianuro y mercurio. En general, el mecanismo de resistencia al Hg en la cepa CECT 5344 se basó en la actividad de la mercurio reductasa MerA y la extrusión de la forma volátil Hg^0, con una acumulación residual dentro de las células, probablemente a través de la quelación a biomoléculas.

Finalmente, también se aplicó un análisis proteómico cuantitativo por LC-MS/MS para caracterizar los cambios metabólicos en *P. pseudoalcaligenes* CECT 5344 durante un estilo de vida anaeróbica en presencia de hierro y amonio. El análisis proteómico reveló la inducción en condiciones anóxicas de proteínas asociadas al ciclo de los ácidos tricarboxílicos, metabolismo de ácidos grasos, metabolismo de polihidroxialcanoatos, así como proteínas relacionadas con el hierro, entre otras. Se sugiera que el amonio, además de ser una fuente de N, participa en la reducción de Fe(III) a través del proceso de oxidación de amonio dependiente de Fe (Feammox), y la cadena respiratoria de transporte de electrones de esta bacteria estaría involucrada en la regeneración de Fe(III) a partir de Fe(II) para la reacción de Feammox acoplada a respiración de fumarato. Además, el exceso de fuente de carbono se derivó a la síntesis de polihidroxialcanoatos. Estos resultados son una visión preliminar sobre el metabolismo anaeróbico de la cepa CECT 5344, pero se requieren más estudios para corroborar esta hipótesis.

En general, todos los resultados presentados en este trabajo destacan el gran y versátil potencial biotecnológico de la bacteria cianotrófica *P. pseudoalcaligenes* CECT 5344, y podrían ser útiles no solo para el diseño de estrategias de biorremediación de residuos industriales complejos co-contaminados con cianuro, arsénico y mercurio, sino también para el desarrollo de tecnologías anaeróbicas alternativas.

Abbreviations

A	Absorbance
AMD	Acid mine drainage
Anammox	Anaerobic ammonium oxidation
ATSDR	Agency for Toxic Substances and Disease Registry
BLAST	Basic Local Alignment Search Tool
CFU	Colony forming unit
CHAPS	3-[(3-Cholamidopropyl)dimethylammonio]-1-propanesulfonate
DDA	Data-dependent analysis
DIA	Data-independent analysis
EDTA	Ethylenediaminetetraacetic acid
Feammox	Anaerobic ammonium oxidation coupled to Fe(III)
HCl	Hydrochloric acid
IARC	International Agency for Research on Cancer
ICP-MS	Inductively Coupled Plasma Mass Spectrometry
LB	Medio Luria Bertani
LC-MS/MS	Liquid Chromatography with tandem mass spectrometry
M9	Minimal mineral media
MBC	Minimum bactericidal concentration
MIC	Minimum inhibitory concentration
min	Minutes
N-source	Nitrogen source
PHA	Polyhydroxyalkanoates
*q*RT-PCR	Real-Time Quantitative Reverse Transcription PCR
RNA	Ribonucleic acid
ROS	Oxygen reactive species
Rpm	Revolutions per minute
TEG	Triethylene glycol
Tris	Tris(hydroxymethyl)aminomethane

Index

Figure index

General introduction

Chapter I

Chapter II

Chapter III

Table index

General introduction

Chapter I

Chapter II

Chapter III

General introduction

1. General introduction

1.1. Environmental contamination

Over last few decades, the environmental pollution has become one of the greatest concern that the world needed to face. Rapid economic, agricultural and industrial development, deforestation, expansion of urbanization, and intense population growth have contributed to the excessive rise of the concentration of pollutants in nature. Pollution is the introduction of contaminants in the environment that, due to chemical composition or quantity, may cause harm to living organisms and/or damage the environment (Castillo et al., 2005; Özkara and Akyil, 2018; Woundefiraw, 2021). Since 1930, and until 2000, the worldwide production of anthropogenic chemicals has increased dramatically from 1 to 400 million tons/year (Özkara and Akyil, 2018). Industrial development, constantly increasing living standards and consumers demand, have magnified the air, water and soils contamination with a wide range of toxic compounds like sulphur dioxide ($S0_2$), carbon dioxide ($C0_2$), ozone (0_3) and nitrogen oxides ($N0_x$), as well as many different hazardous organic compounds wide spread among atmosphere, waters, sludges and soils (Gavrilescu, 2010; Gavrilescu et al., 2015). Pollutants may also be substances that are already present in nature, but they are accumulated in excess due to human activity, such as heavy metals, metalloids or cyanide. On the other hand, the technological revolution has increased the synthesis of xenobiotics, which are substances that do not occur naturally in the environment. These anthropogenic compounds are very difficult to remove, due to their molecular structures, water solubility, ionizability, polarity, lipophilicity and/or volatility. Xenobiotics encompass a broad range of substances like aliphatic and (poly)aromatic hydrocarbons, chlorinated solvents, alkylphenols, and other organic compounds used as herbicides, pharmaceuticals, antibiotics, antioxidants and sunscreen agents, among other applications (Castillo et al., 2005; De Oliveira et al., 2020; Štefanac et al., 2021). Furthermore, contaminants might by categorized either in biodegradable, which can be broken down and transformed by living organisms (inorganic salts, phosphates and organic wastes like paper), or in non-biodegradable, which cannot be degraded, and hence are persistent in the environment for an extended period of time, such as plastics, glass, radioactive isotopes and recalcitrant xenobiotics (Santos, 1990; Özkara and Akyil, 2016).

The expansion of polluted sites and migration of toxic substances into drinking water and food expose human health at great risk (Hu et al., 2006; Jiang et al., 2018; Liu et al., 2018). Heavy metals and organic contaminants are most often found in soils and groundwaters (Liu et al., 2017; Song et al., 2017). Only in Europe, more than 342,000 highly contaminated areas have been identified and 2.5

million are estimated to exist. Also, only in Europe, the mortality rate caused by air pollution is estimated at 790,000 annually (Lelieveld et al., 2019). The cost of remediation of already identified sites is estimated at 6 billion euros per year (Panagos et al., 2013). Therefore, the development of remediation strategies and their application in order to treat polluted sites is of a great importance to solve the contamination-derived problems (Song et al., 2017).

1.1.1. Remediation methods and approaches

The remediation strategies could be classified in two main types: *in-situ* and *ex-situ*. The *in-situ* strategies imply the treatment of pollutants at the place of origin. On the other hand, *ex-situ* methods are based on soils and sediments treatment outside the contaminated sites. The *in-situ* strategies are low-cost approaches, and they are the only solution to remediate contaminated sites with extended surfaces (Castillo et al., 2005; Song et al., 2017). Recently, both *in-situ* and *ex-situ* techniques have been extensively developed to be applied to decontaminate or remediate polluted areas. These include processes like immobilization, degradation, transformation and extraction. Furthermore, they could be split into four main categories: chemical, physical, thermal and biological, which can be also combined (Khalid et al., 2017; Liu et al., 2018). To choose the correct remediation technique, several factors need to be considered like volume and type of contaminated soils, or its risk and toxicity.

The main methods used in the removal of contaminants are chemical processes like adsorption, oxidation, reduction, retaliation and load exchange, which can be applied in combination. Some important chemical methods are:

a) Solidification and stabilization: an *in-situ* or *ex-situ* capture or immobilization of contaminants, based on the introduction of chemical agents (carbonates, phosphates, alkaline agents or chelators) that strongly absorb pollutants. This approach does not remove the contaminants from the soils, but prevent them from spreading (Xie et al., 2014; Reddy et al., 2015; Tajudin et al., 2016; Seshadri et al., 2017; Liu et al., 2018).
b) Soil washing: a technology that uses aqueous solutions to extract pollutants from the soils (Morillo and Villaverde, 2017).
c) Nanotechnology: application of green nanomaterials (1-100 nm) like zero-valent metals (iron or carbon-based nanoparticles, among others) and nanofiltration membranes used for the removal of inorganic and organic contaminants from industrial wastewaters (Mandeep and

Shukla, 2020). This technology could be applied for *in-* or *ex-situ* remediation of contaminated sites, due to its small size and high surface area (Crane and Scott 2012; Thomé et al., 2015).

Physical processes aim to immobilize and withdraw contaminants from the soils and sediments, and they include techniques like:

a) Surface capping: a process of containment of the pollutant based on covering the contaminated site with a low permeability material, to prevent further risk of exposure and spreading of toxic substance (Tomaszewski et al., 2006).
b) Vapor extraction: applied *in-situ* to remove volatile and subvolatile organic contaminants from the soils with the subsequent treatment of toxic vapors (Albergaria et al., 2012; Lim et al., 2016).
c) Electrokinetic remediation: usually applied *in-situ* to remove organic and inorganic pollutants, by using electrical current of low-density (Lim et al., 2016; Liu et al., 2018).

Thermal processes are special physical methods based on heating the contaminated surface, which leads to the mobilization, volatilization or destruction of the pollutants in soils or sediments through conductive, electric resistance, steam and radio-frequency heating. The most frequent thermal technologies are:

a) Vitrification: used for very toxic and radioactive compounds, in which heat is applied to transform soils into a glassy matrix that traps the contaminants. It may be applied both *in-situ* and *ex-situ* (Meuser, 2013; Liu et al., 2018).
b) Thermal desorption: based on application of increased temperature with the aim to provoke volatilization of organic compounds, and subsequently their desorption from soils. The generated gases must be treated before their disposal into the atmosphere (Lim et al., 2016).

Finally, the biological processes involved in the transformation and degradation of toxic substances (bioremediation) are carried out by living organisms, mainly bacteria and plants, or their enzymes or products. There are a variety of bioremediation techniques, with names that depend on the organisms used like vermiremediation (applications of worms to remove organic contaminants from the soils) and phytoremediation (decontamination of the soils by using plants and their associated microbial communities) (Germida et al., 2002; Rodriguez-Campos et al., 2014; Lim et al., 2016). In any case, the main bioremediation techniques that use microorganisms to treat the polluted sites are:

a) Bioaugmentation: based on introduction of new microorganisms (isolated or forming consortia) (Abdulsalam et al., 2011).

b) Biostimulation: based on the increment of already existing microbes by the adjustment of several parameters like temperature, humidity and pH, as well as addition of nitrogen, phosphorus and potassium as nutrients, in order to provide optimal growth of the microorganisms. It also includes addition of biosurfactants and biopolymers, or electron acceptors (like oxygen). In this sense, bioventing or bioventilation provides the oxygen necessary for biodegradation while minimizes volatilization and the release of pollutants into the atmosphere, and it is usually used when contamination is located in deep soils (Karamalidis et al., 2010; Abed et al., 2015; Lim et al., 2016).

1.1.2. Environmental contamination by heavy metals and cyanide

Environmental contamination with heavy metals, metalloids and other pollutants like cyanide has become a great concern and a threat over the past decades. Hazardous wastes containing inorganic and organic toxic elements or xenobiotic compounds like fertilizers and pesticides are being discharged into the atmosphere, soils and water due to intense agriculture and industrial activities. Some of the most abundant inorganic contaminants that could be found in soils and wastewaters are heavy metals. They are defined as metallic elements with a density higher than 5 g/cm^3 or with an atomic number greater than 20, including cadmium, chrome, copper, iron, lead and mercury (Wu et al., 2016a; Ali and Khan, 2017). These elements are usually toxic to humans and living organisms. In addition, metalloids like arsenic and selenium are also referred as “heavy metals” due to their great toxicity (Duffus, 2002; Wang, 2009; Tchounwou et al., 2012). Furthermore, heavy metals could be classified as essential and nonessential, depending on their role in biological systems. Thereby, elements like molybdenum, zinc, copper, cobalt and iron are required by all living organisms for biochemical and physiological processes. On the other hand, mercury, cadmium and lead are considered as nonessential metals that have unknown beneficial function to organisms. Nonetheless, any given metal is toxic at a high concentration, regardless its role or importance in biological systems (Chronopoulos et al., 1997). Heavy metals have always been present in nature due to natural origin like volcanic activity and weathering of metal-bearing rocks (Ali et al., 2019). However, the main sources of these inorganic elements are anthropic activities like agriculture, mining and industrial processing, nuclear power plants or plastic and paper processing (Nagajyoti et al., 2010; Khalid et al., 2017). It is estimated that more than 5 million sites worldwide are contaminated by heavy metals (Khalid et al., 2017). One of the main characteristics of heavy metals is their non-biodegradability, and once they are released to the environment, they remain present in the biogeochemical cycles for decades.

Cyanide is a highly toxic compound that is usually found as both free (CN^-) and metal-complexed forms, in many areas that are also polluted with heavy metals. Thus, the majority of toxic wastes generated by tailing in mining, jewelry and gold industries are rich in cyanide and heavy metals, in which they occur as co-contaminants in mixtures characterized by a complex chemistry (Luque-Almagro et al., 2016, Alvillo-Rivera et al., 2021). These pollutants leach out usually in uncontrolled manner into the surrounding environment and they are scattered by the wind (Singh et al., 2011). Treatment of cyanide residues are based on alkaline chlorination, biological and/or chemical oxidation processes or cyanide recovery by acidification (Dash et al., 2009, Malmir et al., 2022). However, these methods are very expensive and only effective for free cyanide and cyanide weakly bound to metals. Besides, they require special equipment, maintenance and licenses for the discharge of the new generated residues, which could also contain toxic pollutants as chlorine (Nyamunda, 2017). On the other hand, in the treatment of these complex wastes, the presence of heavy metals must be considered and specific treatments for a given heavy metal may not be compatible with treatments for cyanide removal (Coudert et al., 2020; Róldan et al., 2021).

Microorganisms are able to endure high concentrations of heavy metals and other contaminants that may be present in some environments. The resistance and detoxification mechanisms that bacteria display might benefit, as essential tools, the bioremediation of polluted areas (Fashola et al., 2016). The use of microorganisms in bioremediation is a low-cost and environmentally friendly approach to remove toxic residues.

To adapt to hazardous environmental conditions, microorganisms have developed resistance strategies like biotransformation, bioaccumulation and biosorption that might be applied to *ex-situ* or *in-situ* bioremediation of polluted sites (Gadd, 2010). Their advantageous properties like small genome size, relative simplicity of the cell, short replication times and rapid evolution and adaptation, make bacteria good candidates for bioremediation technologies. Also, they are already able to tolerate and transform/detoxify cyanide, metals, and metalloids (Newsome and Falagán, 2021). In this sense, the microbe-metal, microbe-cyanide and metal-cyanide interactions should be defined in cyanurated wastewaters, because bioremediation mechanisms and strategies will be also conditioned by both the forms of cyanide originally present in the samples and the possible enzymatic and non-enzymatic reactions that occur, considering the great reactivity of cyanide. In addition, tolerance to different heavy metals is different for each organism (González-Henao and Ghneim-Herrera, 2021; Kabiraj et al., 2022).

1.2. Cyanide

1.2.1. Forms of cyanide

Cyanides and cyano-derivatives are compounds that contain the cyano group (-C≡N), which reactivity and toxicity depend on their chemical structure (Raybuck, 1992; Razanamahandry et al., 2017). The simplest and most toxic form of cyanide is hydrogen cyanide (HCN) gas, which in solution dissociates to free cyanide (CN^-), in an equilibrium with a pKa of 9.2. Thereby, an alkaline pH is required to avoid HCN volatilization from solutions. Other forms of cyanide are inorganic salts (NaCN and KCN), metal-cyanide complexes, and nitriles (organic cyanides) (Ghosh et al., 2006). Depending on the stability and dissociation capacity, there are two classes of metal-cyanide complexes: the so-called weak acid dissociable (WAD) metal-cyanide complexes (with nickel, copper, mercury, or zinc), which may dissociate with a weak acid, usually at pH 4.5, releasing significant concentrations of free cyanide under acidic conditions, and the strong acid dissociable (SAD) metal-cyanide complexes (with iron, calcium or cobalt), which only dissociate in the presence of a strong acid, at pH 2 or lower (Ibáñez et al., 2017). On the other hand, organic compounds that incorporate the cyano group (-C≡N), also known as nitriles, are widely distributed in nature and include, among others, cyanohydrins (2-hydroxynitriles), aliphatic, aryl-aliphatic and aromatic nitriles, and also carbohydrates and lipids cyano-derivatives (Roldán et al., 2021).

In addition, two main oxidized cyanide-derivatives are found in nature: thiocyanate (SCN^-) and cyanate (OCN^-). The first one is a result of the interaction between free cyanide, oxygen and reduced forms of sulfur, which are usually present in minerals like pyrite or pyrrhotite. Cyanate is also generated during mineral processing, via the reaction between cyanide and a metal ion, such as cupric ion, or during treatment of effluents containing cyanide with an oxidizing agent like hydrogen peroxide or hypochlorite. In solution, cyanate is in equilibrium with isocyanic acid (HNCO), which can react with various organic and inorganic compounds (Cabello et al., 2018; Luque-Almagro et al., 2018). Cyanate could be also considered as a putative intermediate in the cyanide biodegradation process (Estepa, 2012). The toxicity of cyanides depends on their capacity to release free cyanide, and therefore it could be presented as follows:

free cyanide (HCN/CN^-) > WAD/SAD metal-cyanide complexes > SCN^-/OCN^- > nitriles

1.2.2. Sources of cyanide

Cyanide is a natural compound that has been omnipresent in nature before the beginning of life. Recent studies have highlighted the essential role of cyanide in the origin of life, allowing the prebiotic synthesis of amino acids, nucleotides and lipid precursors (Toner and Catling, 2019). It is considered that numerous prebiotic organic compounds could have been generated from cyanide in mechanisms involving copper, phosphorus, sulfur and UV radiation (Patel et al., 2015; Ritson et al., 2018). It was postulated that high concentrations of ferrocyanide salts were present on the early Earth. Due to ferrocyanide salts thermal decomposition to NaCN in aqueous solution, they could eventually form free cyanide (Toner and Catling, 2019).

Cyanide is synthesized by many taxa of plants, fungi, algae, bacteria and even animals like some insects, myriapods and other arthropods (Table 1.1) (Cabello et al., 2018). Due to cyanide high toxicity, its synthesis is associated commonly with defensive or offensive functions against predators and pathogens (Dwivedi et al., 2018). The biosynthesis of cyanide is called cyanogenesis and it was described for the first time in 1802 by a German pharmacist (Rosenthaler, 1919). Hydrogen cyanide may be released from cyanogenic glycosides, cyanohydrins or cyano-lipids as a result of damage by hydrolysis or decomposition. So far, more than 60 cyanogenic glycosides have been described (Lechtenberg, 2011). Plants are considered the main cyanogenic organisms, with more than 2,000 cyanogenic species, many of them being foods like almonds (297 mg/kg of plant tissue), cassava (104 mg/kg), wild cherries (up to 370 mg/kg), lima beans (1-3 g/kg) and sorghum (2.5 g/kg). Cyanide is also found in bamboo shoots, apple, apricot, peach and even strawberries (Kuyucak and Akcil 2013), and many other plant species (Table 1.1). The main route of cyanide production in plants is the synthesis of ethylene, a plant hormone of great importance, by the so-called methionine or Yang cycle (Peiser et al., 1984; Manning, 1986; Seo et al., 2011). In bacteria, the cyanogenesis has been intensively studied in *Pseudomonas, Chromobacterium* and *Rhizobium* species (Freeman et al., 1975; Blumer and Haas, 2000; Fairbrother et al., 2009; Lenney and Gilchrist, 2011; Rijavec and Lapanje, 2017). HCN is mainly produced during the transition from the exponential growth phase to the stationary phase, and the enzyme HCN synthase is responsible for the synthesis of cyanide from glycine, generating CO_2 and HCN. This process can be influenced by several factors, such as the concentration and availability of oxygen, iron and phosphate. Additionally, this process was also reported in several cyanobacteria, such as *Anacystis nidulans*, *Plectonema boryanum* and *Nostoc muscorum* (Rudrappa et al., 2008). Cyanogenic glucosides where also found in different Arthropoda, mainly myriapods (*Oxidus gracilis* and *Harpaphe haydeniana*), and insects, including Coleoptera (*Paropsis atomaria*, *Chrysophtharta variicollis* and *C. amoena*) and Lepidoptera like butterflies belonging to the subfamilies Heliconiinae,

Nymphalinae and Polyommatinae (Zagrobelny et al., 2004). Recently, cyanide synthesis in several mammalian cells and tissues have also been reported, were its presence could lead to calcium mobilization, N-methyl-D-aspartate receptor (NMDA) activation, and DNA fragmentation, among others processes. It was proposed that a low concentration of cyanide may have beneficial and cytoprotective effects on mammalian cells and tissues (Zuhra and Szabo, 2022).

Table 1.1. Biological cyanide production.

Natural sources	
Plants	*Acacia* spp., *Bahia oppositifolia*, *Bambusa* spp., *Cercocarpus* spp., *Mountain mahogany*, *Eucalyptus cladocalyx*, *Glyceria striata*, *Heteromeles arbutifolia*, *Manihot esculenta*, *Prunus* spp., *Pyrus malus*, *Mandragora* spp., *Atropa belladonna*
Algae and cyanobacteria	*Chlorella vulgaris, Anacystis nidulans, Nostroc muscorum, Plectonema boryanum*
Bacteria	*Rhizobium* spp., *Chromobacterium violaceum*, *Pseudomonas* (*P. chlorophis, P. aureofaciens, P. aeruginosa, P. fluorescens*)
Fungi	*Actinomycetes, Basidiomycetes, Clitocybe, Marasmius, Pholiota, Polyporus, Tricholoma*
Animals	Arthropoda: Myriapoda, Insecta (Coleoptera, Lepidoptera)

(Ghosh et al., 2006; Rudrappa et al., 2008; Zagrobelny et al., 2004).

The amount of cyanide generated via natural pathways is relatively low and harmless for the environment, allowing its elimination by natural biodegradation. Nonetheless, the intense and progressive human activities have contributed to the significant increase and accumulation of cyanide in the nature, mainly in industrial processes like electroplating, metal finishing, steel tempering, coal processing, jewelry and mining, especially for gold and silver extraction from the ores (Dash et al., 2009; Luque-Almagro et al., 2016). Due to its high reactivity, cyanide is used for the synthesis of numerous chemical compounds, such as paints, nylon, pesticides, synthetic rubber, photographic chemicals, drugs and pharmaceutical products (Homan, 1987; Pesce, 1993; Dwivedi et al, 2018). The requirement for sodium cyanide is almost one million tons per year (Mudder and Botz, 2004), most of which is being used in the cyanidation process, for the extraction of gold through the reaction:

$$4\ Au + 8\ NaCN + O_2 + 2\ H_2O \rightarrow 4\ Na[Au(CN)_2] + 4\ NaOH$$

The immense volume of cyanide-containing residues are produced in the range from 10,000 to 30,000 mg/L, but even reaching up to 100,000 mg/L. These levels are remarkably high when compared to cyanide found in uncontaminated streams and lakes waters, usually lower than 10-50

µg/L (Wild et al., 1994). Only in Córdoba (Spain), the jewelry industry produce about 10 tons/year of an alkaline waste (pH > 13) containing approximately 40 g/L of cyanide (1.5 M), including both free cyanide and metal-cyanide complexes (Ibáñez et al., 2017). Additionally, high amounts of heavy metals and metalloids like mercury, lead, zinc, copper, cadmium, chromium and arsenic are also found in those wastes, forming mixtures of complex chemistry and toxicity that may vary from extreme alkaline to acidic pH (Luque-Almagro et al., 2016; Alvillo-Rivera et al., 2021). Taking under consideration the fact that heavy metals contribute to the formation of reactive oxygen species (ROS), the oxidative damage caused by cyanide is probably magnified in these wastes (Valko et al., 2005). The industrial toxic residues are usually stored in artificial ponds that are prone to leaching, discharges or dam breaks, causing environmental disasters at national or global scale (Table 1.2). Due to cyanide great toxicity and environmental impacts, entities such as the European Parliament have requested to stop using cyanide in mining activities. Nonetheless, to date, legislation has not been developed, and in some countries, including USA, it is still allowed to apply cyanide for other purposes like pest control in agriculture (Roldán et al., 2021).

Table 1.2. Relevant mine tailings dam failures.

Mine (location, year)	Principal material released	Volume of tailings released (m^3)	Direct human effects
Kearl oil and sands mine (Canada, 2023)	bitumen	5,300	unknown
Williamson Mine (Tanzania, 2022)	mixture	12,800,000	Household and agricultural damage. Numerous people affected and hurt
Jagersfontein (South Africa, 2022)	mixture	5,040,000	Agricultural damage. Human fatalities: 2, 76 people severely injured
Brumadinho dam (Brazil, 2019)	Fe	12,000,000	Human fatalities: 134
Kokoya Gold Mine (Liberia, 2017)	CN	11,500	
Bento Rodrigues dam (Brazil, 2015)	Fe	60,000,000	Human fatalities: 19
Proyecto Magistral Mine (Mexico, 2014)	CN	1,900	
Kingston plant (Tennessee, USA, 2008)	As, Hg	4,100,000	Cleanup workers suffered severe health problems
Baia Mare/Baia Borsa (Romania, 2000)	Ag, Au, CN	100,000	Interruption of water supply
Aznalcóllar (Spain, 1998)	S^{2-}, As	1,300,000	Agricultural and natural reserve damage
Omai gold mine (Guyana, 1995)	CN	4,200,000	
Harmony, Merriespruit (South Africa, 1994)	Au	600,000	Human fatalities: 17
Cerro Negro No. 4 (Chile, 1985)	Cu	2,000,000	
El Cobre Old Dam (Chile, 1965)	Cu	1,900,000	Human fatalities: ~300

1.2.3. Cyanide toxicity

Cyanide is a highly hazardous molecule that poses a great threat for all living organisms and it is included in the Comprehensive Environmental Response, Compensation and Liability Act (CERCLA) priority list of most hazardous substance (ATSDR, 2015). It was used during II World War as a genocidal agent and it is also applied nowadays in some parts of the world for judicial executions (Dwivedi et al, 2018). Cyanide exposure has negative impact on metabolic functions, in both aerobic and anaerobic conditions (Luque-Almagro et al., 2018), through three main mechanisms: reaction with keto-compounds like pyruvate, 2-oxoglutarate and oxaloacetate, forming cyanohydrins; reaction with Schiff-base intermediates, giving nitriles; and chelation of metals in metalloenzymes like cytochrome *c* oxidase (Chena and Liu, 1999; Luque-Almagro et al., 2011b, Ibáñez et al., 2017; Malmir et al., 2022). This causes important changes in the general metabolism, the respiratory electron chain and the generation of oxidative stress (Hariharakrishnan et al., 2009). Cyanide is easily and rapidly absorbed through the skin, and via digestive and respiratory systems, causing acute or chronic poisoning. Cyanide exposure causes dizziness, headache, loss of conscious, low blood pressure, and respiratory failure that leads to heart pain, coma and death (Dwivedi et al, 2018). Furthermore, the lowest oral lethal dose reported in humans is 0.54 mg/kg of body weight, whereas the permissible amount in drinking water oscillate around 0.2 mg/L (USEPA, 1985; Zagury et al., 2004).

Several treatments have been developed to palliate cyanide poisoning, including the use of methemoglobin, nitric oxide, sodium nitrite and dimethylaminophenol, due to the high affinity of cyanide to these compounds. Moreover, sodium thiosulfate and glutathione are also applied as sulfur donors for the rhodonese activity to form thiocyante, which is less toxic than cyanide, and direct binding agents like hydroxocobalamin and dicobalt-EDTA are also used as antidotes (Petrikovics et al., 2015).

1.2.4. Physico-chemical treatments to remove cyanide

To protect nature and human health, cyanide-polluted wastes must be treated before their deposition in the environment (Patil and Paknikar, 2000; Kao et al., 2003). There are several well-known physico-chemical treatments used for cyanide and metal recovery or transformation into less toxic forms (Table 1.3). To select the appropriate treatment for cyanide removal it is necessary to take into account several factors like the form of cyanide, the volume to be treated, or the environment where the treatment is applied. Most of these methods are based on cyanide recovery by acidification and/or destruction by chemical oxidation (Young and Jordan, 1995; Akcil, 2003). The most frequently

applied technique is the alkaline-chlorination-oxidation process that takes place in two stages. Firstly, cyanogen chloride is produced by adding chlorine or hypochlorite, which is subsequently transformed into cyanate. Secondly, cyanate is oxidized to ammonium and carbon dioxide (Wild et al*.,* 1994; Dash at al., 2009). Methods based on ozonation, electrolytic decomposition and copper-catalyzed hydrogen peroxide oxidation are very expensive and demand special equipment for their application and maintenance (Dash at al., 2009; Nyamunda, 2017). In addition, active carbon can be also used as both absorbent and catalyst for the oxidation of cyanide. This treatment requires the sparging of the solution with air or oxygen, and cyanide is oxidized to cyanate (Adams, 1994; Dash et al., 2008).

Table 1.3. Physico-chemical treatments for cyanide removal.

Cyanide removal treatments	Reactions
Alkaline chlorination	$Cl_2 + CN^- \rightarrow CNCl + Cl^-$
	$CNCl + H_2O \rightarrow CNO^- + Cl^- + 2H^+$
	$CNO^- + 2\ H_2O \rightarrow CO_2 + NH_4^+ + OH^-$
Hydrogen peroxide	$H_2O_2 + CN^- \rightarrow CNO^- + H_2O$
Ozonation	$CN^- + O_3 \rightarrow CNO^- + O_2$
	$2\ CN^- + O_2 \rightarrow 2\ CNO^-$
	Global: $3\ CN^- + O_3 \rightarrow 3\ CNO^-$
SO_2/air (INCO) process	$CN^- + SO_2 + O_2 + H_2O \rightarrow CNO^- + SO_4^{2-} + 2H^+$
Active carbon (cyanide oxidation)	$CN^- + 1/2O_2 \rightarrow CNO^-$

The previously described methods to remove cyanide are usually expensive and only effective for the removal of free cyanide or WAD metal-cyanide complexes. Additionally, they require equipment, maintenance and permissions in order to discharge the new generated wastes that might contain toxic pollutants (Nyamunda, 2017). Hence, there is an increased demand for the treatments that are able to degrade cyanide from residues in a most effective and economical way. Furthermore, in regard to co-contaminated wastes, some specific treatments for a given pollutant may not be compatible with treatments for cyanide removal (Coudert et al., 2020). Therefore, biodegradation carried out by microorganisms has been suggested as a suitable and environmental-friendly alternative (Roldán et al., 2021).

1.2.5. Cyanide biodegradation

During evolution some organisms have acquired different mechanisms to cope with cyanide toxicity, either by increasing the tolerance to cyanide or by transforming this compound into less- or non-toxic products, such as ammonia and carbon dioxide. The essential machinery against cyanide toxicity is based on cyanide-insensitive respiration. It encompasses the ubiquinol alternative oxidase described in plants (Berthold et al., 2000) or the cytochrome *bd* cyanide-insensitive oxidase found in bacteria (Jünemann, 1997; Richardson, 2000). On the other hand, some microorganisms may degrade cyanide by metabolic pathways that include oxidation, reduction, hydrolysis or substitution/transfer reactions (Fig. 1.1) (Cabello et al., 2018; Luque-Almagro et al., 2018). In the oxidative pathways, ammonia and CO_2 are formed as the final products, either directly through the enzyme cyanide dioxygenase, which is present in *Pseudomonas fluorescens*, *P. cereus* and *Bacillus pumillus*, or in two-steps catalyzed by the enzymes cyanide monooxygenase and cyanase. The existence of a putative cyanide moooxyganse has not been demonstrated, but it was suggested in *Pseudomonas* sp. to transform cyanide into cyanate, which could be subsequently converted into ammonia and carbon dioxide by the cyanase, a well-known enzyme involved in cyanate assimilation in many bacteria (Acheampong et al., 2010; Park et al., 2017; Parmar et al., 2013). The reductive reaction takes place in anaerobiosis, through the nitrogenase, which converts HCN into methane and ammonia, but it was described in only a few microorganisms like *Klebsiella oxytoca, Herbaspirillum seropedicae* or *Azotobacter* sp. The hydrolytic pathways encompass the enzymes cyanide hydratase and cyanidase, which act on HCN, or nitrile hydratase and nitrilase, which act on nitriles. Cyanide hydratase is a lyase responsible for carbon-nitrogen bond cleavage in the cyano-amino acid metabolism of *Fusarium* sp. and *Pseudomonas fluorescens* (Gupta et al., 2010; Dwivedi et al, 2018; Alvillo-Rivera et al., 2021). Cyanidase or cyanide dehydratase (CynD) converts directly cyanide into formate and ammonia. This enzyme was described in *Bacillus pumilus*, *Alcaligenes xylosoxidans* and *Pseudomonas strutzeri* (Ingvorsen et al., 1991; Meyers et al., 1993). On the other hand, nitrile hydratase converts nitriles to amides, and it is present in *Corynebacterium, Brevibacterium, Rhodococcus rhodochrous* and *Pseudomonas putida*, among others (Alvillo-Riviera et al., 2021), whereas nitrilases are responsible for the hydrolysis of nitriles to ammonia and carboxylic acid avoiding the formation of amide intermediates. Nitrilases have been described in a broad range of microorganisms including *Arthrobacter*, *Alcaligenes*, *Acinetobacter*, *Nocardia*, *Klebsiella*, *Pseudomonas* and *Rhodococcus* species (Dwivedi et al., 2018; Alvillo-Riviera et al., 2021). Substitution/transfer reactions are involved in the assimilation of 3-cyanoalanine in some bacteria, also allowing the growth with cyanide as nitrogen source and preventing cyanide toxicity. In *Chromobacterium violoaceum, Bacillus megaterium* or *Pseudomonas* sp. this pathway includes the 3-

cyanoalanine synthase (CAS), which catalyzes the transformation of cyanide and cysteine into sulfide and 3-cyanoalanine. This nitrile may be converted into asparagine, through the 3-cyanoalanine hydratase, or directly into aspartate and ammonium, by the 3-cyanoalanine nitrilase. In addition, the rhodanese (thiosulfate sulfurtransferase) catalyzes the conversion of cyanide and thiosulfate into thiocyanate and sulfite. This enzyme is found in *Azotobacter vinelandii, E. coli, Pseudomonas aeruginosa, Ferrobacillus ferroxidans, Thermobacillus denitrificans* and *Desulfotomaculum nigrificans* (Dash et al., 2009; Park et al., 2017; Dwivedi et al, 2018; Alvillo-Riveria et al., 2021). Thiocyanate may be further converted into H_2S and CO_2 by hydrolytic/oxidative reactions (Cabello et al., 2018; Luque-Almagro et al., 2018).

Microorganisms are obligated to adapt to the presence of different contaminants in nature. To obtain positive results and good efficiency in the bioremediation of industrial wastes containing both cyanide and cyanide-metal complexes is crucial to consider that metals biodegradation is very reduced, and instead majority of defense mechanisms against heavy metals are based on detoxification and immobilization reactions (Das et al., 2016). Thus, the following five essential mechanisms have been described: i) extracellular barriers (cell wall, plasma membrane, capsule), ii) extrusion via efflux pumps or diffusion, iii) intracellular sequestration, iv) extracellular sequestration, and v) biotransformation/detoxification of metal ions (Choudhury and Srivastava, 2001; Bazzi et al., 2020; Kabiraj et al., 2022). These mechanisms could be targets for biotechnological approaches. For example, the efflux systems that are the most prevalent bacterial mechanisms for conferring heavy metals resistance may be modified or over-expressed in order to increase the resistance or to confer metal tolerance (Delmar et al., 2015; Abbas et al., 2017; Bazzi et al., 2020). This will allow to carry out with a cyanide biodegradation process, even in the presence of high concentrations of heavy metals. Thus, *Serratia marcescens* may degrade up to 200 mg/L cyanide complexed with metals (Ag, Au, Zn, Cu, Pb and Hg), and removal of cyanide reached to 25% in the presence of Hg and up to 88% with other metals (Karamba et al., 2014, 2017). Additionally, *Pseudomonas pseudoalcaligenes* CECT 5344 was shown to be able to degrade at pH 9, up to 12 M (0.3 g/L) of total cyanide present in an industrial residue that includes both free cyanide and metal-cyanide complexes (Ibáñez et al., 2017).

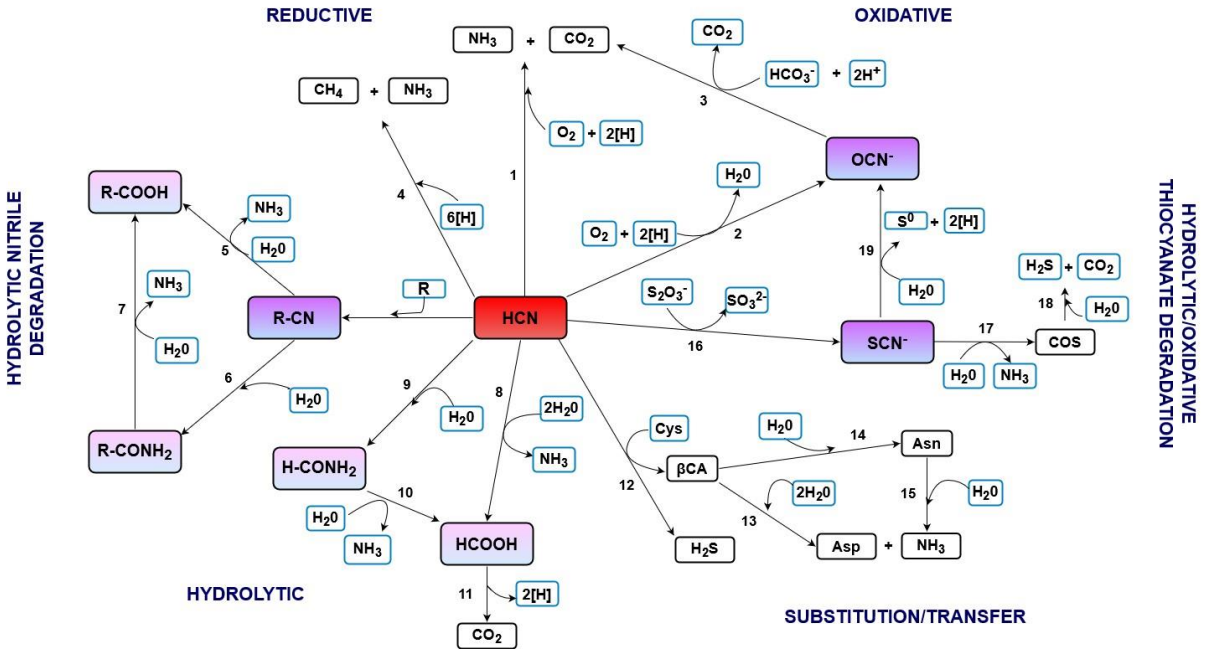

Figure 1.1. Biochemical pathways for the biodegradation of cyanide and its derivatives. The cyano-compounds are boxed and highlighted in colors. Symbols: R-CN, nitrile (organic cyanide); R, organic compound; [H], hydrogen atom; βCA, 3-cyanoalanine. Enzymes: 1, cyanide dioxygenase; 2, cyanide monooxygenase; 3, cyanase; 4, nitrogenase; 5, nitrilase; 6, nitrile hydratase; 7, amidase; 8, cyanidase (cyanide dihydratase); 9, cyanide hydratase; 10, formamidase; 11, formate dehydrogenase; 12, 3-cyanoalanine synthase; 13, 3-cyanoalanine nitrilase; 14, 3-cyanoalanine hydratase; 15, asparaginase; 16, rhodanese; 17, thiocyanate hydrolase; 18, carbonyl sulfide (COS) hydrolase; 19, thiocyanate dehydrogenase (modified from Luque-Almagro et al., 2018).

1.3. Arsenic

1.3.1. Chemical forms of arsenic

Arsenic (As) is a metalloid widely distributed in both terrestrial and aquatic environment (Tsai et al., 2009). It appears in various forms like elemental, carbonate and sulfide (Genchi et al., 2022), and it is a component in more than 200 minerals, including realgar (As_4S_4), orpiment (As_2S_3) and arsenopyrite (FeAsS), the main arsenic ore (Mandal and Suzuki, 2002). Arsenic might be present in different oxidation states: -3 (arsine); 0 (arsenic); +3 (arsenite) and +5 (arsenate). The ability of arsenic species to undergo various chemical reactions by changing their oxidation state affects their toxicity and mobility (Smedley and Kinniburgh, 2002; Raju, 2022). However, arsenic is mostly present in nature as arsenate, As(V), in aerobic environments or as arsenite, As(III), in anoxic conditions (Roberts et al., 2010). Organic methylarsenicals, such as trimethylarsine (TMA), dimethylarsenate (DMAV) and monomethylarsenate (MMAV), are also found in the environment. These organoarsenicals are less

toxic than their inorganic analogues, except for the highly toxic trivalent derivatives monomethylarsenite (MMAIII) and dimethylarsenite (DMAIII) (Oremland et al., 2017).

1.3.2. Sources of arsenic

Arsenic can be easily found in oceans, rivers, soils and air. Its natural concentration in the environment is caused by volcanic eruptions (production of ashes), volatilization from the soils, geothermal activity and wind erosion (Fig. 1.2). However, arsenic biochemical cycle is mostly affected by anthropogenic sources. Recent human activities have significantly contributed to arise arsenic concentration in nature (Fig. 1.2). Gold mining, smelter slag, coal combustion, glass manufacturing, pesticide and herbicide production, processing of pressure-treated wood or fertilization practices are the main anthropic contributions to arsenic pollution (Oremland and Stolz, 2003; Hery et al., 2015; Sher and Rehman, 2019). Therefore, arsenic concentration in soils and waters reaches approximately 100 mg/kg and 10 µg/L, respectively (WHO, 1993; Rimondi et al., 2022). Besides, crops, particularly rice *(Oryza sativa)*, accumulate in seeds great amounts of arsenic (Meharg and Zhao, 2012; Gu et al., 2020). In addition, mining residues consist of other toxic elements like cyanide and heavy metals, which may react with arsenic (Coudert et al., 2020). Drinking water polluted with arsenic has caused a global environmental problem (Nordstrom, 2002; McCarty et al*.,* 2011), and in fact, As-contaminated groundwaters provoked the largest poisoning in human history in Bangladesh (Smith et al., 2000). There are almost 100 countries, including China, India, Bangladesh and USA, with more than 200 million people highly exposed to arsenic (Nordstorm, 2002). Although, the permissible limit for arsenic in drinking water is 10 µg/L (WHO, 2014), seafood may contain great amounts of this metalloid, up to 10-100 mg/kg dry weight. Further, terrestrial animals may contain arsenic in form of arsenobetaine, which is a relatively less toxic arsenical compound (Newcome et al., 2010; Hackethal et al., 2021).

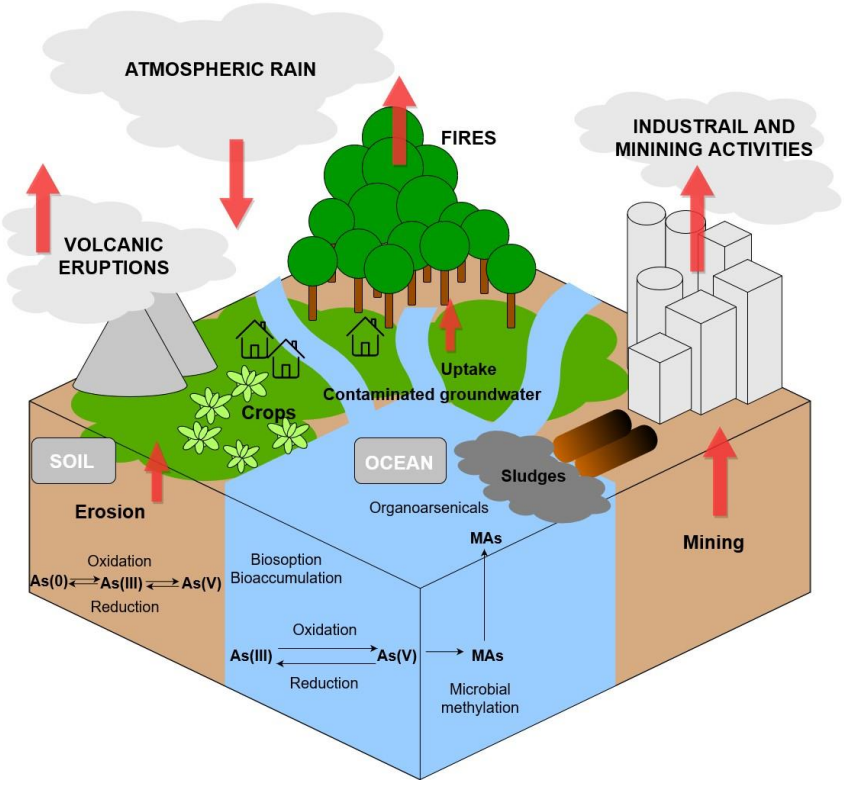

Figure 1.2. Biochemical cycle of arsenic (adapted from Sohn, 2014; De Francisco et al., 2021).

1.3.3. Arsenic toxicity

Arsenic is considered a redox sensible and hazardous element for all living organisms (Mandal and Suzuki, 2002; Oremland and Stolz, 2005). It is considered an human carcinogen by the International Agency for Research on Cancer (IARC), and is the major inorganic pollutant according to the Toxic Substances and Disease Registration Agency (ATSDR) (Martínez et al., 2011). Both pentavalent and trivalent forms of arsenic enter to the cell via two different uptake systems (Garbinski et al., 2019). Arsenate is a phosphate analog that uses phosphate permeases like Pit or Pst (Rosen and Liu, 2009), meanwhile arsenite penetrates the cells through aquaglyceroporins, such as GlpF in *E. coli* and AqpS in *Sinorhizobium meliloti* (Mukhopadhyay et al., 2014). The toxicity of As(V) is based on its ability to compete with phosphate, thus impairing the electron transport chain and energy generation systems (Yang et al., 2005). On the other hand, As(III) inactivates over 200 enzymes through binding to glutathione, lipoic acid and other compounds containing thiol or sulfhydryl groups (Hughes, 2002; Oremland and Stolz, 2003). Also, it has the ability to interact with glucocorticoid receptors (Oremland and Stolz, 2003). As(III) primarily exists as uncharged As_2O_3 or as AsO_3^{3-} anion with a pKa of 9.2 (Rosen, 2002). As(III) adsorbs or binds to minerals, which makes it a more mobile and soluble oxyanion than

arsenate in the majority of environments (Smedley and Kinniburgh, 2002). The toxicity of various arsenicals occurs in the following order: As(V) < MMA(V) < DMA(V) < As(III) < MMA(III) ≈ DMA(III) (Petrick et al., 2000).

Arsenic may be absorbed through skin, ingested or inhaled. The fatal dose of the arsine gas (AsH_3), which is the most toxic form, is 250 mg/m^3 during exposure for 30 minutes, whereas the lethal dose (*LD*50) for arsenic trioxide (As_2O_3) is 34.5 mg/kg, for sodium arsenite ($NaAsO_2$) is 4.5 mg/kg, and for sodium arsenate (Na_3AsO_4) varies from 14 to 18 mg/kg (Marquardt and Schäfer, 1994; Yamauchi and Fowler, 1994). Arsenic easily accumulates in tissues, skin, nails and bones, and causes acute and chronic poisoning, with symptoms like weight and hair loss, anorexia, gastritis or chronic weakness. Long-term exposure is much more severe. The main accompanying symptoms are cardiovascular diseases, eczema, liver and kidney disorders, hyperkeratosis and hyperpigmentation. Vomits, muscles cramps or impairment of circulatory system may also occur (Bissen and Frimmel, 2003). Additionally, arsenic is associated with skin, lungs and liver cancer development, by impairing the reparation of DNA damage. Nonetheless, it is not considered as a mutagen because gene alternations provoked by arsenic are not yet clear and its effect may rely on epigenetic levels. Arsenic also generates reactive oxygen species (ROS) and leads to lipid peroxidation and other oxidative damages (Kligerman and Tennant, 2007).

For many years arsenic has been used in medicine and military conflicts, and it is also used as a pigment (Paris and Scheele green). During the Vietnam War, the United States used a mix of cacodylic (dimethylarsenic) acid and sodium cacodylate to poison food sources for Vietnamese soldiers and depraving them from rice (Olson and Cihacek, 2020). Despite its toxicity, arsenic has been applied to the treatment of several diseases. Thus, human trypanosomiasis (sleeping sickness) would be fatal without the arsenical-based medicament called melarsoprol. Furthermore, patients with acute promyelocytic leukemia may be treated with arsenic trioxide (Pott et al*.,* 2001).

1.3.4. Arsenic resistance in microorganisms

High concentration of heavy metals and other pollutants constitutes a selective pressure that forces microbes to develop different mechanisms of resistance to survive in adverse environmental conditions. Intracellular chelation, bioaccumulation, immobilization, extrusion from the cytosol and transformation to less toxic forms are metabolic reactions performed by bacteria to deal with arsenic

toxicity (Tsai et al., 2009; Yang and Rosen, 2016; Barral-Fraga et al., 2018; Garbinski et al., 2019; Diba et al., 2021).

Prokaryotes present the vastest metabolic diversity regarding arsenic detoxification (Fig. 1.3). Some bacteria are able to conduct oxidation of arsenite to arsenate, thus reducing arsenic toxicity. This reaction may occur under both aerobic and anaerobic condition with simultaneous generation of energy, due to electron transfer to oxygen or nitrate (Mazumder et al., 2020). Arsenic aerobic oxidizers, such as *Alcaligenes feacelis* use the Mo/Fe-containing arsenite oxidase AioAB that allows the production of ATP coupled to oxygen reduction to water (Anderson et al., 1992; Kabiraj et al., 2022), while in anaerobiosis the arsenite oxidase ArxA allows As(III) oxidation in some nitrate-respiring or anoxygenic photosynthetic bacteria (Oremland et al., 2017). Conversely, the arsenate reduction to arsenite increases arsenic toxicity and mobility. This process is conducted intracellularly by aerobic arsenate-resistant microorganisms or extracellularly by anaerobic dissimilatory arsenate-reducing (arsenate-respiring) bacteria (Kulp et al., 2004; Song et al., 2009). The periplasmic arsenate reductase ArrAB, which is encoded by the *arr* operon and presents high similarity to molybdoenzymes of the DMSO reductase family, is associated with the respiratory reduction of As(V) to As(III) (Kabiraj et al., 2022). In this pathway, As(V) is used as terminal electron acceptor, whereas acetate, formate or hydrogen may act as electron donors (Saleem et al., 2019). The arsenite generated is released to the extracellular environment (Dowdle et al., 1996; Blum et al., 2018). However, the most common and well-known arsenic detoxification system is encoded by the *ars* genes, which are widely distributed in arsenic-resistant bacteria and archaea, although with different gene composition and organization (Fekih et al., 2018; Yan et al., 2019). The *arsRBC* genes are proposed as the core *ars* cluster, in which ArsR acts as a negative regulatory protein that senses As(III) and ArsB is an arsenic energy-dependent efflux pump with 12 transmembrane helices. When As(III) is present, it binds to ArsR and causes its dissociation from the promoter region, allowing transcription of *ars* genes (Yang et al., 2012a). Arsenic tolerance in aerobic prokaryotes is usually associated with the arsenate reductase ArsC that converts arsenate to arsenite, which is subsequently extruded by the ArsB pump. Considering the electron donor used, two unrelated types of arsenate reductase are described, which are dependent on thioredoxin or glutaredoxin (Slyemi and Bonnefoy, 2012; Yan et al., 2019). The *arsRDABC* gene cluster that was previously described in the plasmid R773 of *E.coli*, encompasses two additional genes, *arsA* and *arsD*, which code for the ATPase ArsA that forms a complex with ArsB, yielding a high-efficiency, ATP-driven arsenite efflux pump, and the putative As(III)-metallochaperone ArsD that binds arsenite for its transfer to the ArsA component of the efflux pump complex, also exhibiting a weak repressor activity (Lin et al., 2006; Slyemi and Bonnefoy, 2012). Additionally, other *ars* genes have been described to be involved in arsenic detoxification. Thus, some microorganisms possess the Acr3 transmembrane

As-efflux protein in addition or in replacement of the ArsB protein (Ghosh et al., 1999), and additional genes of unknown function like *arsT* or *arsN* are included in other bacterial *ars* gene clusters (Wang et al., 2006; Chauhan et al., 2009).

The arsenic biogeochemical cycle also involves microbial synthesis and transformation of organoarsenicals, mainly through methylation and demethylation (Slyemi and Bonnefoy, 2012; Andres and Bertin, 2016; Yan et al., 2019). These processes generate several arsenical forms including MMA(III), MMA(V), DMA(III), DMA(V), TMA(V), and TMA(III), of which MMA(III) and DMA(III) are highly toxic (Di et al., 2019). Methylation pathway is directly associated with the *S*-adenosylmethionine (SAM)-dependent methyltransferase ArsM, which presents both methylating and demethylating activities. Furthermore, the methylarsenite oxidase ArsH confers resistance to methyl-As(III) derivatives and protects against oxidative stress caused by arsenic (Páez-Espino et al., 2020). The permease ArsP, which also protects from MMA(III) and DMA(III), and the non-heme iron-dependent deoxygenase ArsI, which shows C-As lyase activity, are also involved in methylarsenic metabolism (Huang et al., 2018). In *Pseudomonas aeruginosa* DK2, a different pathway has been described for organoarsenical detoxification operating through the glyceraldehyde-3-phosphate dehydrogenase (GADPH) and the *arsJ* gene product. GADPH uses arsenate, an inorganic phosphate analog, to form 1-arseno-3-phosphoglycerate. This unstable organoarsenical compound is extruded by the permease ArsJ, which belongs to the major facilitator superfamily (MFS), before its extracellular dissociation into As(V) and 3-phosphoglycerate (Chen et al., 2016). In addition, it has been recently described another arsenic efflux transporter (ArsK), which remains under the control of the *arsR*2 gene and it confers resistance to inorganic arsenite, trivalent roxarosone and methylarsenite (Shi et al., 2018).

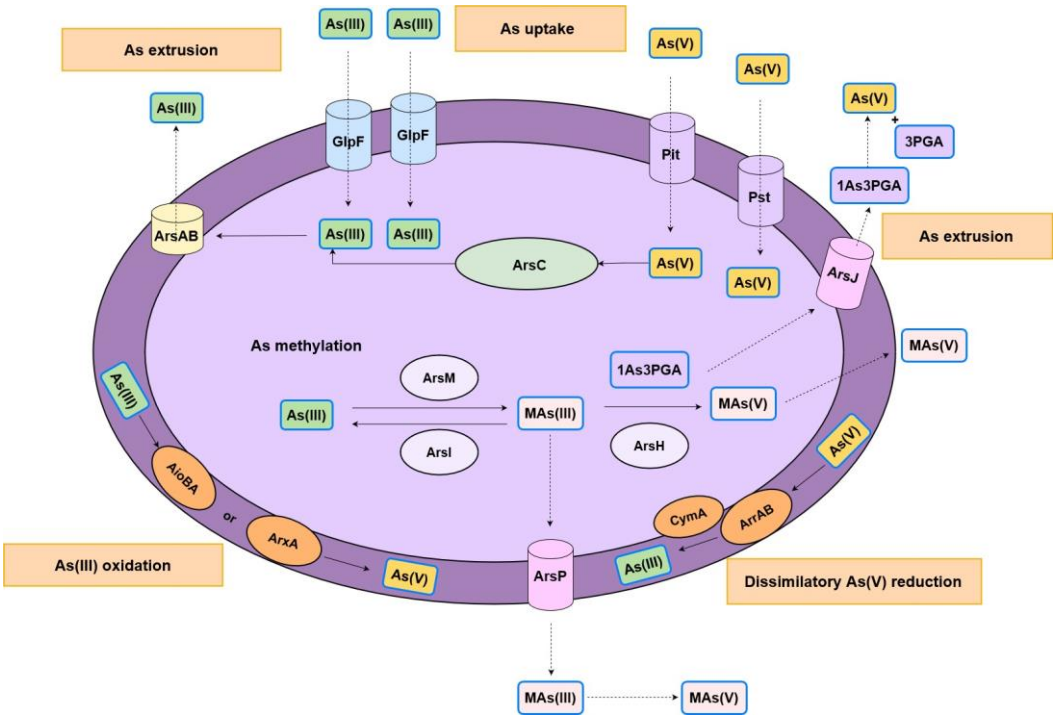

Figure 1.3. Arsenic detoxification and metabolism in bacteria (adapted from Slyemi and Bonnefoy, 2012; Yan et al., 2019).

1.3.5. Physico-chemical treatments for arsenic removal

There are several arsenic removal technologies, which could be divided into chemical, physical and biological (bioremediation by microorganisms). The chemical approaches encompass adsorption by using specific media, immobilization, coagulation combined with filtration, precipitation, complex reactions and formation of stable phases ($FeAsO_4$) or stabilization using nanosized oxides and Fe(0) (Mahimairaja et al., 2005; Duarte et al., 2009; Mueller and Nowack, 2010; Kim et al., 2012; Komarek et al., 2013). The chemical technologies were quite popular and successful, although for remediation of large areas, a significant increase in costs is expected (Mahimairaja et al., 2005; Duarte et al., 2009). The physical methods to reduce arsenic concentration in soils are based on minimalization of the pollutant level by mixing together both contaminated and non-contaminated soils, soil washing with the use of chemicals like nitric acid, sulfuric acid or hydrogen bromide, and immobilization of soluble arsenites by using cement in terms of stabilization/solidification (Mahimairaja et al., 2005; Sullivan et al., 2010).

1.3.6. Arsenic bioremediation by microorganisms

In the past few decades, the demand for efficient and affordable bioremediation strategies has increased significantly. The physico-chemical technologies applied to remove arsenic from drinking water are usually expensive and relatively inefficient, being not completely effective. Microbial bioremediation has become a suitable approach, and for a better adaptation, various microorganisms have been genetically modified with the introduction in their genome of the *arsM* gene, responsible for arsenic methylation. In *Sphingomonas desiccabilis* and *Bacillus idriensis*, the presence of ArsM increased volatilization up to 10 times, and in *Bacillus subtilis* it also enables volatilization of dimethylarsine and trimethylarsine (Kostal et al., 2004; Liu et al., 2011). Likewise, a genetically modified *Pseudomonas putida* strain was able to produce organoarsenicals (Chen et al., 2013). On the other hand, many bacteria are able to tolerate a high concentration of arsenic, such as facultative anaerobic *Bacillus* sp. that resists up to 50 mM arsenate, which is used as an ultimate electron acceptor (Kabiraj et al., 2022). Furthermore, *Staptohylococcus xylosus*, *Acidithiobacillus ferrooxidans* and *Brevibacillus brevis* were reported to accumulate arsenic species in their biomass, hence being promising candidates for bioabsorption of this metalloid (Aryal et al., 2010; Yan et al., 2010; Banerjee et al., 2013). Additionally, *Arthrobacter* species were able to absorb efficiently up to 74.91 mg/g of arsenite and 81.63 mg/g of arsenate, at pH 7 (Kabiraj et al., 2022). Several microorganisms, such as *Pseudomonas*, *Bacillus*, *Variovorax* or *Pseudoxanthomonas* are part of consortia that enhance and promote uptake of this metalloid by plants (Antenozio et al., 2021). In this regard, *Ptaris vittata* treated with bacteria increased arsenic removal by 20% and its biomass by 45% (Lampis et al., 2015), whereas *Brassica juncea* achieved up to 140% arsenic accumulation (Franchi et al., 2019).

1.4. Mercury

1.4.1. Chemical forms of mercury

Mercury (Hg) is a very potent and pervasive heavy metal. This non-essential chemical element has unique characteristics of being liquid at room pressure and temperature. However, it may be found under gaseous colorless form, because it shows a high vapor pressure (Priyadarshanee, 2022). Mercury is placed on the third position in the list of the most toxic elements for human health by US Government Registration Agency for Toxic Substance and Diseases (Antoszczyszyn and Michalska,

2016). Mercury appears in the environment as inorganic and organic forms, including elemental (Hg^0) or divalent (Hg^{2+}) mercury and methylated compounds like methylmercury (MeHg) (Burger et al., 2019; Priyadarshanee et al., 2022). It possesses seven stable isotopes from Hg^{196} to Hg^{204} and it is constituent of more than 90 minerals, mainly livingstonite ($HgSb_4S_8$), corderoite ($Hg_3S_2Cl_2$) and cinnabar (HgS), the most abundant (Beckers and Rinklebe, 2017). Mercury has great affinity to form complexes with organic and inorganic compounds, which depend on nature, amount and characteristics of the ligands (Coulibaly et al., 2016). In terms of organic substrates, mercury reacts strongly with cysteine and mercaptoacetate, whereas sulfide and oxygen-containing functional groups are consider weak ligands. On the other hand, mercury forms strong complexes with inorganic particles like chloride, hydroxide and sulfide, which play an important role in heavy metal speciation in aquatic system. Interestingly, mercury has a strong association to dissolved organic matter (DOM). DOM stands for a heterogenous complex of low and high molecular weight organic compounds that present different solubilities and reactivities. The different fractions, such as carboxylic (COOH), phenolic and alcoholic (OH), carbonyl (C=O) and amine (NH_2) groups may interact with mercury and influence the metal-DOM interactions. Furthermore, mercury interacts with several metals like gold and silver (Matlock et al., 2002; Vázquez et al., 2014), and it is able to react with one or more carbon-containing molecules (Priyadarshanee et al., 2022; Sun et al., 2022). Mercury may also bind to cyanide forming toxic and water soluble complexes like $HgCN^+$, $Hg(CN)_2$, $Hg(CN)_3^-$ and $Hg(CN)_4^{2-}$ (Drace et al., 2016; Marshall et al., 2018). Additionally, cyanide might facilitate mercury methylation and solubility in the environment (Tulasi et al., 2021).

1.4.2. Sources of mercury

Mercury is commonly present in the ecosystems due to natural sources, such as geothermal activity, volcanic eruptions, wildfires, volatilization from the ocean surface and weathering of mercury-containing minerals (Fig. 1.4) (Gaffney and Marley, 2014; Burger et al., 2019; Priyadarshanee et al., 2022). However, the amount of this heavy metal emitted to the atmosphere by natural processes is relatively low when compared to human activities (Fig. 1.4), which produce globally an estimated total amount of 643 tons Hg per year (Pacyna et al., 2010; Pirrone and Keating, 2010). Furthermore, intense industrial enterprise and economic development have increased up to 1.5 to 3 times the concentration of mercury in the environment compared to the ancient times (Ruelas-Inzunza et al., 2013). Frequently, mercury has been used in barometers, thermometers, batteries or dental amalgams, and it is also found in paints, pharmaceuticals and paper (Lin et al., 2016; Priyadarshanee et al., 2022). Additionally,

coal burning, oil and gas combustion, and chlor-alkali industry have large contributions to mercury emissions, and electrical power plants generate large amounts of mercury. Nonetheless, the largest concentration of mercury are related to mining and gold digging, being artisanal small-scales gold mining the main producer of toxic mercury-containing wastes (Bridges and Zalups, 2017). Almost 95% of the mercury used in this type of gold mining is released to the environment, with total mercury emissions of over 1,000 tons per year. Furthermore, despite the prohibition of this activity, almost 16 million of artisanal mines remain active, located mainly in South America and Africa (Seccatore et al., 2014; Tulasi et al., 2021).

Mercury is a hazardous substance, and hence, its pollution provokes a critical and disturbing problem that is not restricted to one specific area (Bridges and Zalups, 2017; Priyadarshanee et al., 2022). Once mercury is released as a volatile elemental form to the atmosphere, it is scattered by wind even during 2 years, before its deposition in aquatic and terrestrial ecosystems as oxidized bivalent mercury (Holzamn, 2010). Further, mercury may undergo different reactions, such as reduction followed by reemission to the atmosphere and methylation, or may be placed into sediments (Grégoire and Poulain, 2018). Additionally, during methylation process, inorganic mercury is converted to its methylated form that bioaccumulates mainly in sea living organisms, especially big-size fishes like tuna, shark, swordfish and salmon, and also in plants like rice (Bridges and Zalups, 2017).

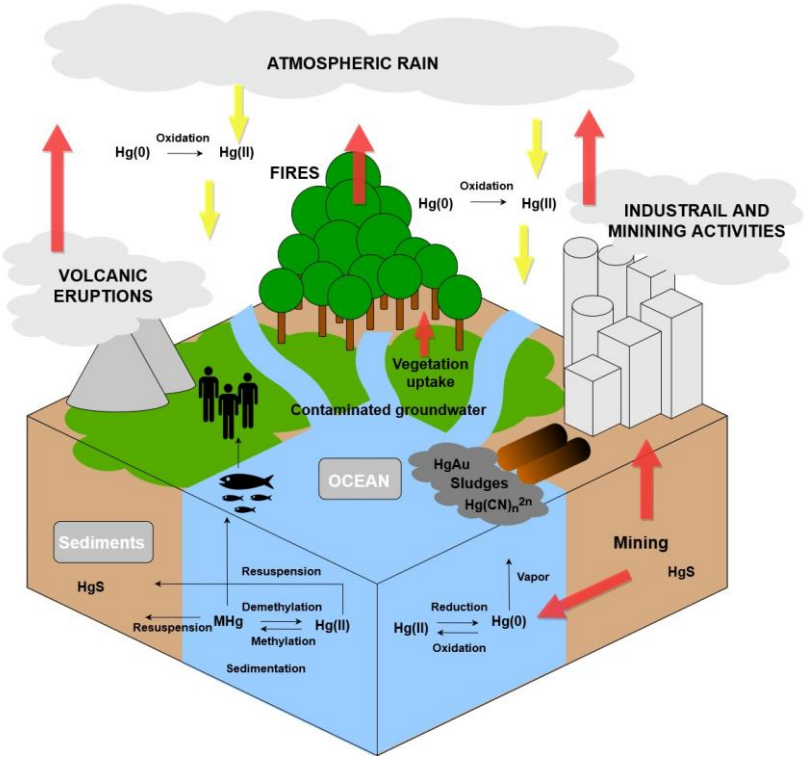

Figure 1.4. Mercury biochemical cycle in the environment (adapted from Busairi and Syahir, 2018).

1.4.3. Toxicity of mercury

The limit of mercury concentration in drinking water established by WHO is 6 µg/mL. In human body, the half-live of methylmercury is estimated around 44 days and 1-4 g of mercury constitute a fatal dose in adults (Von Burg, 1995; Rand and Caito, 2019). Its toxicity and chemical traits are based primarily on the oxidation state of particular mercury forms. Thus, the less toxic form of this pollutant is Hg^0 (Broussard et al., 2002; González-Raymant et al., 2017). However, its volatile proprieties facilitates its entrance into the human body through the respiratory system (Priyadarshanee et al., 2022). On the other hand, methylmercury is described as a remarkably potent neurotoxin with the ability to cross the blood-brain barrier, although with lower efficiency than Hg^0 (Hong et al., 2012; Park and Zheng, 2012). Hence, it accumulates in the brain, liver or kidney, and it is able to easily pass-through placenta and affects fetus (Park and Zheng, 2012; Priyadarshanee et al., 2022). Furthermore, methylmercury is responsible for mitochondrial dysfunction, provokes changes in membrane permeability, and increases the level of ROS. In addition, it triggers lipid peroxidation and disruption of microtubule composition, synapse transmission and transport of amino acids (Sager and Matheson, 1988; Zhao et al., 2021). Mercury presents high affinity to sulfhydryl groups, thus binding to cysteine, glutathione, homocysteine and proteins (Hughes, 1957). Methylmercury is also associated with a wide range of severe diseases like attention-deficit hyperactivity, acrodynia, attention deficient disorder, and the most famous and well-known Minamata disease, which was caused by a mercury waste disposal from a chemical plant in Japan in 1956, affecting 2252 people, of which 1043 died (Harada, 1995; Kerrie and Austin, 2011; Kim et al., 2013).

1.4.4. Mercury removal treatments

Mercury removal from wastewaters emphases various physical and chemical approaches like reverse osmosis, ion exchange, nanomembrane filtration, coagulation or coprecipitation and adsorption with application of various absorbent (Adams, 1991; Richard et al., 2016; Wu et al., 2016b; Yu et al., 2016; Bashir et al., 2019; Zunita, 2021). Nonetheless, majority of these technologies require great amount of chemicals and a lot of energy. In addition, the application of activated carbon has been considered as a suitable absorbent for mercury removal due to its availability, low generation of secondary wastes and high absorbability (Hadi et al., 2015; Heidarinejad et al., 2020).

1.4.5. Mercury resistance in microorganisms

The presence of mercury in nature pressed diverse range of organisms as fungi, bacteria and plants to develop different detoxification mechanisms to cope with the great toxicity of mercurial species. Nonetheless, microorganisms play a main role in the mercury biological cycle, by oxidizing, reducing or sequestering different forms of mercury (Cardona et al., 2022). In this regard, the main resistance mechanism triggered as a response to the toxicity of mercury is based on the presence of the *mer* genes, which are ubiquitous in a variety of Gram-positive and Gram-negative bacteria, presumably by spreading via vertical and horizontal gene transfer (Fig. 1.5) (Bhakta et al., 2011). The *mer* genes may be located as a part of genomic DNA, plasmids and integrons, or as a component of Tn21 and Tn501 transposons (Summers and Silver, 1972; Hamlett et al., 1992; Wireman et al., 1997; Liebert et al., 1999; Nascimento and Chartone-Souza, 2003; Schelert et al., 2004; Zeng et al., 2010). The mechanism of mercury detoxification is based on enzymatic degradation of organomercury compounds, which are further reduced to less toxic and volatile forms (Sone et al., 2013a). To date, two type of *mer* gene clusters have been described: the narrow-spectrum operons (*merRTPAD*), which confer resistance only to inorganic mercury salts (Mergeay et al., 2003), and the broad-spectrum systems that promote resistance to both inorganic mercury and organomercurials like methylmercury (Osborn et al., 1997). Expression of *mer* operons is strictly associated with the MerR regulatory protein that acts as a transcriptional repressor in the absence of mercury. However, when Hg^{2+} is present, MerR undergoes an allosteric change that activates the transcription of the *mer* genes (Mathema et al., 2011; Rojas et al., 2011). It has been suggested that MerD may have a co-regulatory role in the expression of the *mer* genes, possibly through formation of a complex with MerR (Champier et al., 2004). MerP and MerT are essential for the transport of mercury forms in bacteria. Mercury binds to two cysteine residues of the periplasmic protein MerP, and then is translocated into the cells by the membrane protein MerT, which contains four cysteine residues, and is also involved in the uptake of organomercurials (Zheng et al., 2018). Thus, Hg^{2+} is transported from the periplasmic side to the cytosolic compartment, through the cysteine residues of MerP and MerT (Sone et al., 2013b). It is remarkable that the lack of *merT* gene is more lethal for bacterial cells than the lack of *merP* (Wilson et al., 2000). Furthermore, upon binding to MerT in the cytosol, Hg^{2+} migrates straight to the active side of MerA, a homodimeric mercury reductase that uses NADPH as electron donor and acts as an integral part of the mercury detoxifications system (Schue et al., 2007; Barkay et al., 2010). In addition, certain bacteria also possess the organomercury lyase MerB that facilitates the C-Hg bond cleavage (Mathema et al., 2011; Naguib et al., 2018), and additional genes coding for transport proteins may be found in other *mer* gene clusters. Thus, the *merE* gene codes for a Hg^{2+} or methylmercury transporter

(Amin et al., 2019), the *merF* gene codes for a protein with similar function to MerT that may be involved in the transport of ionic mercury from the periplasmic protein MerP to the mercuric reductase MerA (Barkay et al., 2003), the *merH* gene also supports the transport of mercuric species (Schue et al., 2009), and the *merG* gene facilitates phenylmercury permeability (Priyadarshanee et al., 2022).

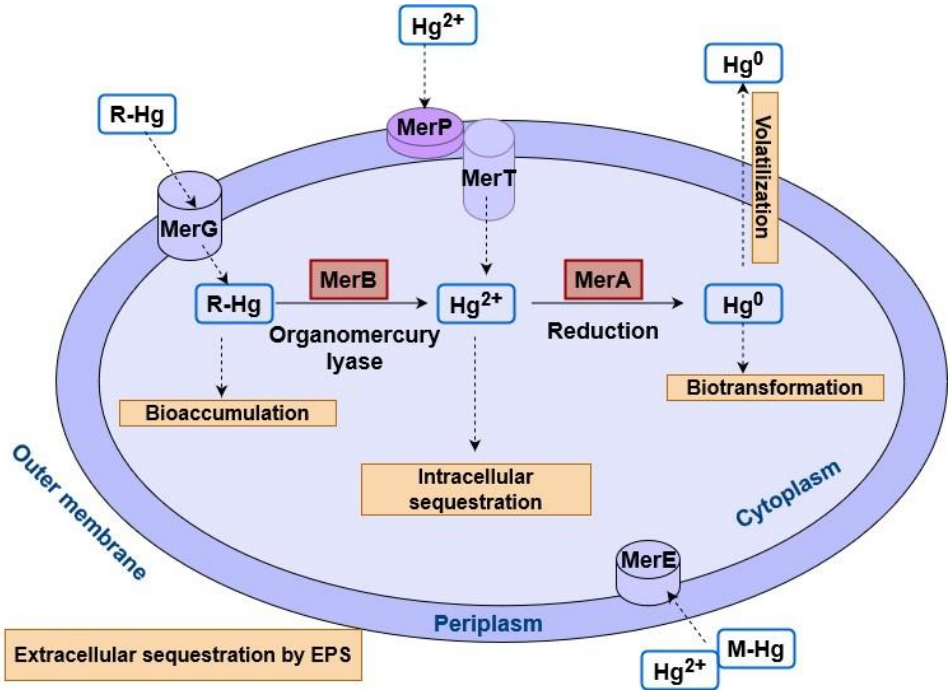

Figure 1.5. Mercury resistance mechanism in bacteria (adapted from Boyd and Barkay, 2012; Priyadarshanee et al., 2021).

Volatile forms of mercury may escape from the cell by simply diffusing through the membrane (Barkay et al., 2003; Priyadarshanee et al., 2022). Furthermore, proteins of the heavy metal efflux resistance-nodulation-cell division (HME-RND) protein superfamily facilitate the efflux of mercury forms (Das et al., 2016). However, some anaerobic bacteria may also oxidize Hg(0) to Hg(II) (Smith et al., 1998; Colombo et al., 2014). Various bacterial strains like *Bacillus cereus*, *Ochrobactrum* sp. HG16, *Klebsiella rosea* EP1, *Lysinibacillus* sp. HG17 or *Bacillus* sp. CM11 are able to bind inorganic forms of mercury (III) in extracellular polymeric substance (EPS) (François et al., 2012). Recently, it has been described that biofilm formation is highly correlated with pH, and low pH stimulates chelation of mercury in EPS (Gupta and Diwan, 2017).

1.4.6. Mercury biodegradation

Several bacterial strains have been reported to be able to growth in the presence of $HgCl_2$. *Pseudomonas mohni* was able to tolerate up to 59 mg/L $HgCl_2$, whereas *Burkholderia contaminans* tolerated up to 86 mg/L $HgCl_2$ (Cardona et al., 2022). Additionally, *Pseudomonas putida* SP-1, a biofilm-forming bacterium, was able to volatilize 89% of mercury (Zhang et al., 2012). *Vibrio fluvialis* may resist up to 100 mg/L of mercury and other bacteria like *Pseudomonas aeruginosa, Brevibacterium casei, Bacillus* sp. and *Bacillus thuringiensis*, have been also described with the capacity to tolerate mercury, and being able to bioremediate between 42 and 80% of mercury (Saranya et al., 2017).

1.5. Iron

1.5.1. Role and properties of iron

Iron (Fe) is a first row transition metal and the fourth most abundant element after Si, O and Al in the Earth crust (approximately 5%), meanwhile soils are estimated to have an average of 3.8%. Iron is a highly reactive metal with a particular electron structure that allows reversible changes in its different oxidation states. Due to its redox versatility, iron participates as a cofactor in many enzymes and regulatory proteins in the form of heme group (i.e. cytochromes), or different Fe-S centers that display a wide range of redox potentials from + 0.3 V in cytochrome *a* to - 0.49 V in sulfoferric proteins (Castillo et al., 2005). Iron is usually found in nature in two oxidation states: ferrous (Fe^{2+}) or ferric (Fe^{3+}). In anoxic conditions iron appears as soluble ferrous form, while ferric iron is the most abundant under aerobic conditions (Melton et al., 2014). Iron usually forms insoluble hydroxides that limit the availability of this metal. The solubilization of iron in these minerals may be achieved by various organic chelating molecules, called siderophores (Castillo et al., 2005). Elemental iron (Fe^0) is generally a product of human activity to obtain molten iron and it does not appear naturally (Battle et al., 2014). Therefore, the biological cycle of iron is reduced to the chemical or biological conversion between ferrous and ferric forms, which depends on the environmental conditions, and it may be coupled to energy conservation processes. Iron is an essential oligonutrient/micronutrient for all living organisms to grow and survive, being crucial in many biological processes like photosynthesis, N_2 fixation, respiration, central metabolic reactions, oxygen transport, gene regulation, and biosynthesis of DNA (Andrews et al., 2003). Its biological functionality is almost entirely dependent upon its incorporation

into proteins, either as mono or binuclear species, or in a more complex form as part of iron-sulfur clusters or heme groups (Beinert et al., 1997; Andreini et al., 2008). Nonetheless, its reactivity and low solubility lead to problems of toxicity and poor availability. Through the Fenton and Haber-Weiss reactions, iron generates ROS like the hydroxyl radical (HO•), the superoxide anion radical ($O_2^{\cdot-}$) and peroxides (O_2^{2-}) that contribute to the generation of oxidative stress (Touati, 2000). ROS can damage lipids, proteins and DNA by oxidation, and therefore cells must remove them before they cause significant damages (Hansberg, 2002).

1.5.2. Iron toxicity and pollution

Despite the fact that iron is an essential element required by almost all living organisms to survive, at high concentration it might be harmful. Ingestion of less than 20 mg/kg of elemental iron is nontoxic, between 20-60 mg/kg results in moderate symptoms, and ingestion of more than 60 mg/kg can result in severe toxicity, even leading to elevated morbidity and mortality (Yuen and Becker, 2022). Intense urbanization and agriculture are main contributors to air and water pollution with iron. Disturbingly high levels of iron, above the acceptable limit (1 mg/L) (BIS, 1991) were detected in waters from almost all parts of India, being a threat to millions of people that depend on natural water sources (Sarkar and Shekhar, 2018). The appearance of a high concentration of iron in water leads to various problems like clogging of water treatment setups, acidification of water leading to corrosion of pipes, decline in soil cultivation productivity, and undesired taste in drinking water (Mehta and Shrivastava, 2012). Furthermore, it might have a negative impact on human health by causing hemochromatosis, a disorder leading to frequent transfusions of blood (WHO, 2003). Another great concern is the abundant presence of iron as air pollution nanoparticles emitted from a range of industries and traffic-related sources. They constitute a major environmental risk factor regarding cardiovascular mortality and morbidity on a global scale (Pope et al., 2006; Newby et al., 2015; Rajagopalan et al., 2018; Miller and Newby, 2020). These nanoparticles reache a size of approximately 15-40 nm diameter, and are found within abnormal myocardial mitochondria like ruptured membranes or deformed cristae. In addition, iron might generate ROS that leads to oxidative stress and cell damage. Regardless, high toxicity of iron-rich nanoparticles and their ability to gain access to any organ in the body through inhalation or ingestion, they are neither monitored nor regulated at the current time (De Jesus et al., 2019).

1.5.3. Iron acquisition and storage

Considering iron properties like low solubility and availability, microorganisms have developed several strategies to maintain intracellular iron homeostasis. Many bacteria and fungi, and also some plants generate siderophores, which act as extracellular ferric chelators. Usually, they are compounds with low molecular weight and high-affinity to iron that convert Fe^{3+} to Fe^{2+} facilitating iron uptake via active transport (Byers and Arceneux, 1998). Approximately 500 siderophores have been characterized so far, which are classified according to the functional group used as iron ligand (Drechsel and Winkelmann, 1997; Boukhalfa and Crumbliss, 2002). The most common siderophores are enterobactin and aquachelin, among others. The siderophore-Fe^{3+} complexes are too large to pass through the porins, thus they require receptors or permeases that bind siderophores with high specificity. In Gram-negative bacteria, the siderophores are taken up by specific outer membrane (OM) receptor proteins in a process mediated by the energy transducing TonB-ExbB-ExbD system (Larsen et al., 1994; Higgs et al., 1998; Koster, 2001). All known OM receptors are related, although there are many different types like FhuA, FecA, or FepA (Ferguson et al., 1998; Buchanan et al., 1999; Koster, 2001; Ferguson et al., 2002). Once internalized, the ferric-siderophore complex must be dissociated to liberate iron for cellular metabolism. This process involves the reduction of the siderophore-associated ferric iron, which results in the dissociation of the complex due to the relatively low affinity of siderophores to ferrous iron. On the other hand, since Gram-positive bacteria are lacking both OM receptors and the complex TonB-ExbB-ExbD system, they use ABC-type permeases, with high affinity to iron, which are homologous to the SfuABC, SitABCD, YfeABCD, FbpABC and FutABC transporters found in Gram-negative bacteria like *Serratia marcescens*, *Salmonella typhimurium*, *Yersinia pestis*, *Neisseria gonorrhoeae* and *Synechocystis* PCC (Angerer et al., 1990; Adhikari et al., 1996; Bearden and Perry, 1999; Zhou et al., 1999; Janakiraman and Slauch, 2000; Katoh et al., 2001). Many bacteria are able to accumulate iron in the intracellular space within iron storage proteins (Andrews, 1998). There are three main type of iron-storing molecules: ferritins that are also found in eukaryotes; heme-containing bacterioferritin found only in eubacteria; and small Dps proteins found only in prokaryotes. They consist of similar subunits (24 in ferritins and bacterioferritins or 12 in Dps proteins) that assemble to form a spherical protein shell surrounding a central cavity that acts as iron storage reservoir. Regarding ferritins and bacterioferritins, in the first step of the iron storage process, the ferrous ions are taken up and bound through highly conserved ligands in the ferroxidase center. Then, Fe^{2+} ions are oxidized by oxygen and an oxo-bridged di-ferric intermediate is formed as a result. Subsequently, the ferric ions are directed to the central cavity where, depending on the presence of phosphate, either a ferrihydrite core or an amorphous ferric phosphate core is formed. In the Dps proteins, the ferroxidase residues

are not conserved, and biding and oxidation of ferric ions occur in the site located at the two-fold interface between subunits (Ilari et al., 2000; Andrews et al., 2003).

1.5.4. Iron homeostasis: the ferric uptake regulator (Fur)

In response to iron availability, bacteria regulate their iron metabolism via the ferric uptake regulator (Fur protein), which was firstly described in *E. coli* (Stojiljkovic et al., 1994). It is a metalloprotein that binds Fe^{2+} and acts as global homeostatic regulator, controlling the expression of more than 90 genes (Hantke, 2002; Braun, 2003; Lee and Helmann, 2007). Recently, it has been established that Fur also acts in various important processes, such as nitrogen metabolism, synthesis of nucleic acids, signal transduction, intermediary metabolism, photosynthesis, respiration, motility, glycolysis, virulence and protection against oxidative stress (Touati, 2000; Delany et al., 2004; Zhou et al., 2006; Gao et al., 2008; Cornelis et al., 2011; González et al., 2014; Chareyre and Mandin, 2018).

To maintain homeostasis, the Fur protein acts as a repressor of the iron uptake genes. Thus, when the intracellular concentration of Fe^{2+} exceeds the threshold level, Fur protein binds to the opposite sites of DNA at the so called “Fur boxes” or “iron boxes”, and in this way represses the expression of over 100 target genes, which are involved mostly in iron uptake (Fillat, 2014; Seo et al., 2014; Beauchene et al., 2015). On the other hand, when concentration of ferrous iron drops, the Fur protein dissociates from DNA to increase iron capturing to recover normal levels of iron. Additionally, other members of the Fur family are involved in the maintenance of homeostasis of other metal ions, such as Mur (manganese), Nur (nickel) or Zur (zinc) (Lee and Helmann, 2007).

In early 2000s, it was proposed that RhyB, a small RNA (sRNA), plays a key role in iron homeostasis. RhyB has been shown to be responsible for controlling over 50 genes involved in iron usage and import. Nonetheless, the expression of *rhyB* gene remains under strict negative control of the Fur protein (Massé and Gottesman, 2002). Under iron starvation, inactivation of Fur causes rapid induction of *rhyB* and the Fe acquisition genes. Furthermore, RhyB rapidly blocks the synthesis of non-essential iron proteins, allowing essential proteins to use the iron that remains available. On the other hand, when the free concentrations of iron are high, Fur is activated and expression of the *rhyB* gene is repressed (Chareyre and Mandin, 2018).

1.5.5. Iron reduction/oxidation for energy metabolism

The iron biochemical cycle encompasses numerous redox reactions driven by microbial activity or by chemical agents. The majority of these reactions occurs at circumneutral pH (Fig. 1.6). However, a few prokaryotes are able to perform iron oxidation or reduction under extreme pH conditions (Johnson et al., 2012). The Fe^{3+} bioavailability might be affected by redox potential, activation energies, aqueous speciation and sorption. The form in which ferric iron occurs is also critical. Microorganisms reduce iron to further incorporate the Fe^{2+} ion as a cofactor of many regulatory proteins and metabolic enzymes. In the suitable environments like flooded soils, anoxic lakes sediments, and peat bogs, several species of *Pseudomonas*, *Proteus*, *Alcaligenes* or *Bacillus* are able to use ferric iron as an electron acceptor for anaerobic respiratory processes (Castillo et al., 2005). The process of iron reduction, where Fe^{3+} acts as electron acceptor, is one of the most important geochemical reaction in anoxic aquatic sediments. Iron reduction is associated with oxidation of organic compounds, such as methane, ethanol, acetate, pyruvate, propanol, fatty acids, carbohydrates, amino acids, aromatic compounds, or inorganic substances like H_2S, S^0, H_2 or NH_4^+ (Castillo et al., 2005; Kappler et al., 2021). Electrons are transferred from these donors via electron transport chain to the ferric iron reductase system, giving rise to a proton motive force that can be used for ATP synthesis. Thus, an anaerobic respiration process through ferric iron reduction coupled with H_2 oxidation was described in the chemolithoautotrophic bacterium *Acidithiobacillus ferrooxidan.* Fe^{3+} reduction requires a *c*-type cytochrome, which is responsible for the reduction of ferric iron. This mechanism serves as a primary energy source and plays an important role in the primary mechanism of energy production under anaerobic conditions (Ohmura et al., 2002). In some bacteria like *Shewanella, Geobacter* or *Magnetospirillum*, the ferric iron reductase consists of a monomeric protein that is associated with the membrane and the electron transport chain. The enzyme activity is regulated, in addition to the iron concentration, by the presence of nitrate because iron and nitrate compete for the common reductants.

Recently a novel anaerobic pathway for Fe(III) reduction coupled to ammonium oxidation (Feammox) was described, in which ammonium is oxidized to dinitrogen gas, nitrite or nitrate (Fig. 1.6) (Clément et al., 2005; Ding et al., 2014). Feammox mostly occurs in lake sediments, marine environment, forests soils, and wetlands (Yang et al., 2012b; Ding et al., 2014; Huang and Jaffé, 2018; Ríos-Del Toro et al., 2018). It plays a significant role in natural nitrogen cycle and has been proposed as a promising treatment for biological removal of nitrogen excess (Yang et al., 2018). Microbial anaerobic Fe(III) reduction may also be linked to methane oxidation, being performed by anaerobic methane oxidizing archaea (Scheller et al., 2016).

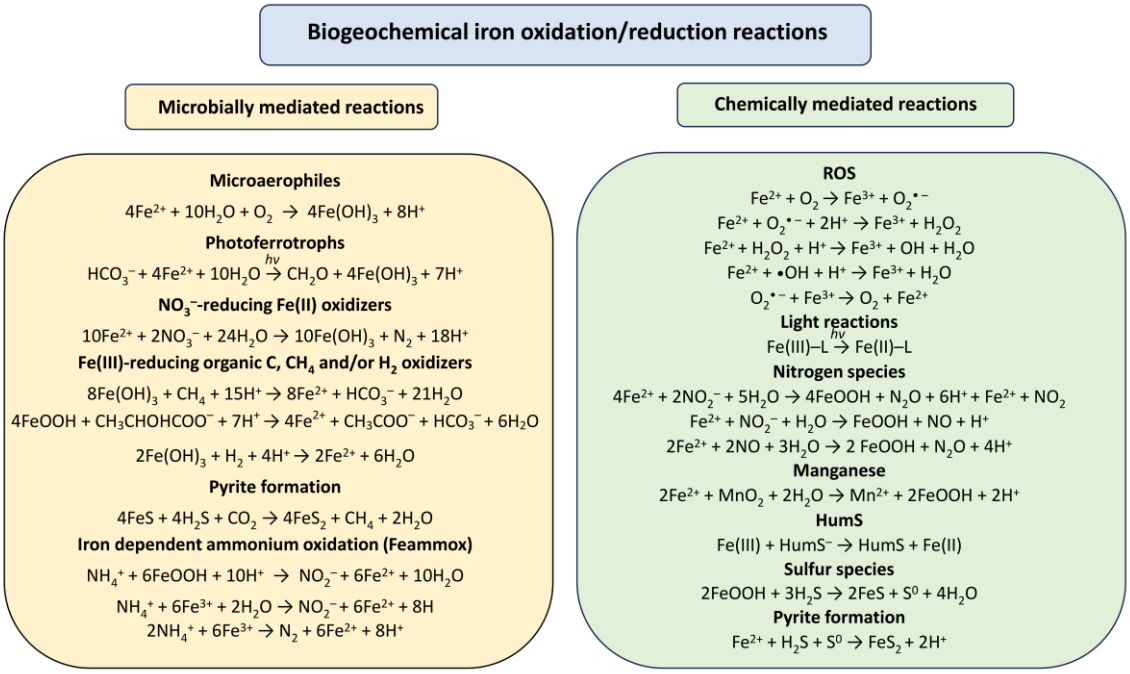

Figure 1.6. Iron redox reactions that occur at circumneutral pH (based on Melton et al., 2014; Kuypers et al., 2018; Kappler et al., 2021). ROS, reactive oxygen species; L, organic ligands; HumS, humic substances.

On the other hand, many microorganisms benefit on the reaction of iron oxidation as a mechanism for obtaining energy. In 1837, *Gallionella ferruginea* was described as the first iron oxidizing bacteria (Ehrenberg, 1837). Iron oxidizers are known to control the fate of many metals and nutrients like manganese, copper, chromium, phosphate, nitrate, bicarbonate or sulfate (Singh et al., 2018). Ferric iron, generated after bacterial iron oxidation, interacts with metals and nutrients to form metal-nutrient-complexes, which settle down in the aquatic system for a very long period of time. Depending on the pH and redox potential, iron forms a variety of oxidized and reduced compounds. Alkaline to neutral pH, and presence of oxygen, favor the oxidation of ferrous iron, which spontaneously oxidizes to ferric iron (Druschel et al., 2008). On the other hand, acidic pH provides stability to the ferrous form, allowing iron oxidation by some acidophilic bacteria like *Thiobacillus ferrooxidans, Sulfolobus acidocaldarius* or *Leptospirillum* (Jones, 1986). As a reduced amount of energy may be generated during iron oxidation, these bacteria need to oxidize large amounts of this metal to sustain growth, leading to an abundant formation of insoluble Fe^{3+}, which further precipitates as $Fe(OH)_3$ (Castillo et al., 2005).

Fe^{2+} oxidation takes place in the periplasm mediated by rusticyanin, a copper-containing protein encoded by *rus* operon that presents high redox potential (+ 0.68 V at pH 2) and great stability in acidic environments (Castillo et al., 2005). Rusticyanin acts as an intermediate electron acceptor, and together with two additional small cytochromes (Cyc-A1 and Cyc-1), it transfers electrons from ferrous

iron to oxygen. Protons required to form H_2O are obtained from the cytoplasm (Singh et al., 2018). The naturally occurring high proton gradient between outside and inside the cell (pH 6 in the cytoplasm and pH 2 in the periplasm), leads to proton inflow and consequently to the production of ATP by the ATP synthase (Quatrini et al., 2009). In addition, a reverse flow of electrons allows NADH production, which is essential for CO_2 fixation (Castillo et al., 2005).

1.6. *Pseudomonas pseudoalcaligenes* CECT 5344

1.6.1. Isolation and genome sequencing

Pseudomonas pseudoalcaligenes CECT 5344 is a nonpathogenic, alkaliphilic Gram-negative bacterium that belongs to the class of γ-proteobacteria. It was isolated from sludges of Guadalquivir River in Spain, Córdoba, by application of enrichment techniques with minimal medium containing 2 mM sodium cyanide as the sole nitrogen source, at pH 9.5 (Luque-Almagro et al., 2005). The *P. pseudoalcaligenes* CECT 5344 genome was completely sequenced and consists of 4,696,984 bp chromosome featuring a GC-content of 62.34% and including a total of 4514 genes, of which 4435 are protein coding genes. Furthermore, this strain is closely related to *Pseudomonas mendocina* ymp by sharing 75% of the genes (Luque-Almagro et al., 2013; Wibberg et al., 2014, 2016). The remarkable feature of *P. pseudoalcaligenes* CECT 5344 lies upon its ability to tolerate and assimilate cyanide, cyanate, metal-cyanide complexes and nitriles, under alkaline conditions, avoiding formation of toxic and highly volatile HCN. Several bacteria have been described so far that are able to tolerate cyanide, however only the *P. pseudoalcaligenes* CECT 5344 strain is able to use cyanide as the sole nitrogen source under alkaline conditions. In addition, this bacterium is able to detoxify up to 12 mM cyanide from a jewelry waste, and it tolerates up to 30 mM cyanide or 100 mM cyanate (Luque-Almagro et al., 2005, 2008; Ibáñez et al., 2017).

1.6.2. Cyanide-assimilation capacity and biotechnological potential of *P. pseudoalcaligenes* CECT 5344

In general, microorganisms may have different metabolic tools for both cyanide resistance and degradation. In *P. pseudoalcaligenes* CECT 5344 these two processes are connected through the

malate:quinone oxidoreductase (MQO) (Fig. 1.7). This enzyme is responsible for the formation of oxaloacetate, crucial for cyanide assimilation, coupled to the electron transfer to the alternative cyanide-insensitive terminal oxidase (CioAB), a membrane integral cytochrome *bd*-type complex (Luque-Almagro et al., 2011b). Previous work demonstrated that a mutant defective in the *cioA* gene was unable to grow on cyanide, and did not use this compound as the sole nitrogen source, demonstrating that the alternative quinol oxidase CioAB was essential for cyanide tolerance (Quesada et al., 2007). In *P. pseudoalcaligenes* CECT 5344, cyanide provokes the induction of the MQO, which transfers electrons directly from malate to the quinone pool, yielding oxaloacetate, which may spontaneously react with cyanide to generate a cyanohydrin (2-hydroxynitrile). This nitrile is hydrolyzed further by the nitrilase NitC, forming ammonium, which is subsequently incorporated into carbon skeletons by the glutamine synthetase/glutamate synthase (GS/GOGAT) cycle (Luque-Almagro et al., 2011b; Estepa et al., 2012).

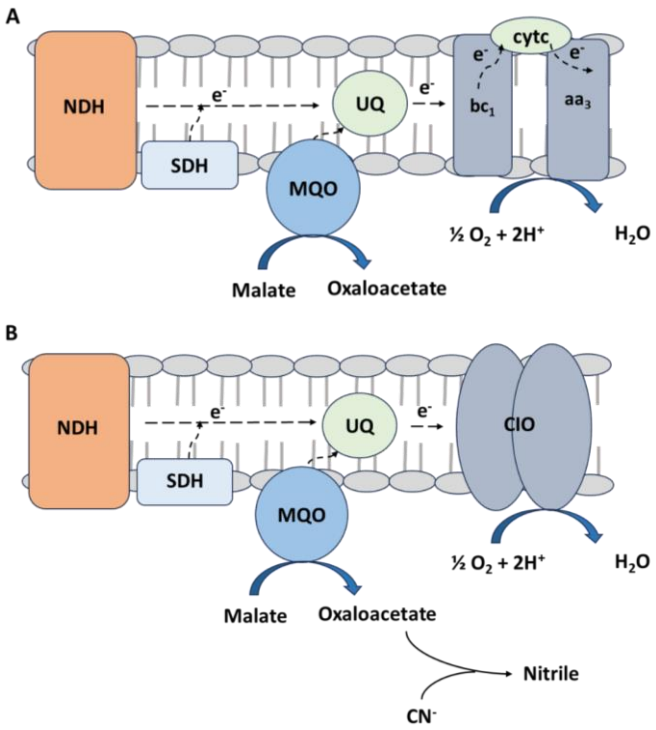

Figure 1.7. Components of the electron transfer chain in *P. pseudoalcaligenes* CECT5344 cells grown without (A) or with (B) cyanide. The cyanide degradation process includes an early response by which oxaloacetate is produced as a consequence of the stimulation of the glyoxylate cycle and the cyanide-insensitive respiratory system. Abbreviations: CIO, cyanide-insensitive oxidase; MQO, malate:quinione oxidoreductase; NDH, NADH:ubiquinone oxidoreductase (complex I); SDH, succinate dehydrogenase; UQ, ubiquinol/ubiquinone pool. For simplicity, proton translocation coupled to the electron transport chain has been omitted (Luque-Almagro et al., 2011b).

In *P. pseudoalcaligenes* CECT 5344, the nitrilase NitC that is essential for the assimilation of free cyanide and nitriles is encoded by the *nit1C* (*nitABCDEFGH*) gene cluster. This cluster encodes the following proteins: NitA, a Fis-family σ^{54}-dependent transcriptional activator; NitC, a nitrilase enzyme; NitD, an *S*-adenosylmethionine superfamily member; NitE, an *N*-acyltransferase superfamily member; NitF, a trifunctional polypeptide of the AIRS/GARS family; NitH, an NADH-dependent oxidoreductase, and NitB and NitG, two hypothetical proteins of unknown function (Estepa et al., 2012). *P. pseudoalcaligenes* CECT 5344 is also able to growth with 3-cyanoalanine as the sole nitrogen source. However, this strain does not use this particular nitrile as an intermediate in the cyanide assimilation pathway. Both proteomic and phenotypic analyses of several nitrilase defective mutants of this bacterium have demonstrated that the nitrilase NitC participates in a novel alternative 3-cyanoalanine assimilation pathway in absence of cyanide, while the nitrilase Nit4 is involved in 3-cyanoalanine assimilation only when cyanide is also present (Pérez et al., 2021).

Furthermore, the strain CECT 5344 is also able to assimilate cyanate, which is used as the sole nitrogen source via a cyanide-independent pathway, which requires cyanate degradation to ammonia and carbon dioxide by the cyanase CynS, which is encoded by the *cynFABDS* gene cluster (Luque-Almagro et al., 2008; Cabello et al., 2018; Sáez et al., 2019).

In the presence of cyanide, the CECT 5344 strain is able to resist and adapt to some additional factors, such as cell damage caused by oxidative stress or the decreased bioavailability of essential metals like iron and copper due to the formation of metal-cyanide complexes. Previous studies based on DNA microarray analysis and quantitative proteomics by Liquid-Chromatography-Mass Spectrometry/Mass Spectrometry (LC-MS/MS) that were performed to analyze the global response of this bacterium to cyanide and metals present in a jewelry residue, have confirmed that oxidative stress defense and iron homeostasis are important during cyanide assimilation. Thus, the alkyl hydroperoxide reductase AhpC1 and the dihydrodipicolinate synthase DapA1, among other proteins, are crucial not only for cyanide resistance but also for oxidative stress and iron homeostasis responses mediated by the ferric uptake regulator Fur (Luque-Almagro et al., 2007, 2015; Ibáñez et al., 2017). The dihydrodipicolinate synthase is essential for production of dipcolinates that act as iron chelators, conferring protection against oxidative stress and allowing the regeneration of Fe-S centers to reactivate cyanide-damaged metalloproteins (Olaya-Abril et al., 2020). Cyanide toxicity is derived from its ability to bind to metal cofactors present in essential metalloproteins (Gupta et al., 2010; Luque-Almagro et al., 2011a), especially heme-containing proteins like cytochromes and iron-sulfur enzymes like fumarase and aconitase. In this regard, the presence in *P*. *pseudoalcaligenes* CECT5344 of different isoforms of key iron-containing enzymes, such as the tricarboxylic acid cycle enzymes fumarase and

aconitase, may also contribute to cyanide resistance (Igeño et al., 2011). In the Figure 1.8 is shown an overview of the metabolic responses triggered by cyanide in the strain CECT 5344.

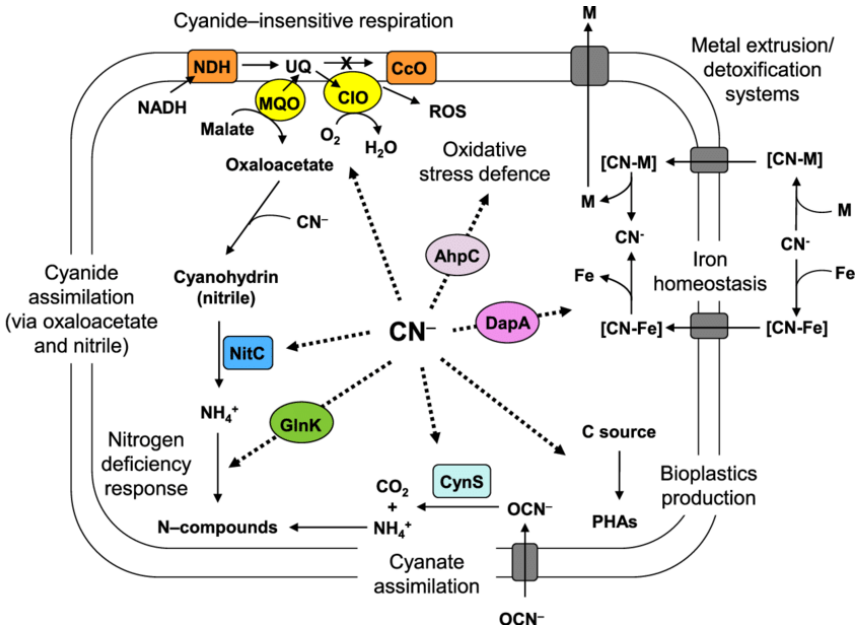

Figure 1.8. Metabolic responses to cyanide and cyano-compounds in *P. pseudoalcaligenes* CECT5344. Dotted arrows indicate the different cyanide-induced responses. Some relevant cyanide-induced proteins like the nitrilase NitC, the cyanase CynS, the PII-type nitrogen regulator GlnK, the alkyl-hydroperoxide reductase AhpC and the dihydropicolinate synthase DapA are also shown. NDH, NADH dehydrogenase complex; UQ, ubiquinone; CcO, cytochrome c oxidase; MQO, malate:quinone oxidoreductase; CIO, cyanide-insensitive quinol oxidase; ROS, reactive oxygen species, PHAs, polyhydroxyalkanoates; M, metals; [CN-M], metal-cyanide complexes; [CN-Fe], iron-cyanide complexes (Cabello et al., 2018).

1.6.3. Polyhydroxyalkanoates production in *P. pseudoalcaligenes* CECT 5344

Polyhydroxyalkanoates (PHA) are polymers with water insoluble thermoplastics properties (bioplastics), which accumulate inside the bacterial cells as intracellular, circular-shaped, nano-sized granules (0.2-0.5 µm diameter). They are covered with a layer of phospholipids, and are covalently bound to proteins called phasins (Steinbüchel et al., 1995; Jurasek and Marchessault, 2002; York et al., 2002; Verlinden et al., 2007; Obulisamy and Mehariya, 2021). Under nutrition limitation or oxidative stress conditions, PHA are produced by several bacteria, archaea or algae to serve as a carbon storage (García et al., 1999; Madison and Huisman, 1999; Rehm and Steinbuchel, 1999; Prieto et al., 2007; Anjum et al., 2016). Generally, the synthesis of PHA occurs under carbon excess and strong macro- and/or microelement limitation like nitrogen, magnesium, sulfur or oxygen (Shang et al., 2003). It was proposed that the most effective limitation factor is oxygen, although for many bacteria the same

effect on PHA synthesis has the lack of nitrogen (Dawes, 1990). Interestingly, the production of bioplastics does not affect bacterial metabolism, hence it is a process that does not require any additional energy (Verlinden et al., 2007). The genome of *P. pseudoalcaligenes* CECT 5344 contains three gene clusters involved in the metabolism of PHA and it has been demonstrated that this strain may accumulate PHA under cyanotrophic conditions (Luque-Almagro et al., 2013; Manso et al., 2015).

1.7. Omic techniques as a tool for development of bioremediation strategies

The development of new high-throughput resolution technologies and bioinformatics has made possible the appearance of the so-called "omics", which allow the study of the genome (genomics), as well as the set of mRNA (transcriptomics), proteins (proteomics) and metabolites (metabolomics) that an organism contains under certain conditions (Fig. 1.9). These techniques allow for extraction of large amount of information, providing a holistic view of multiple cellular processes with possible biotechnological applications, implementing key information to understand the different mechanisms involved in the bioremediation of toxic compounds (Chakraborty et al., 2012). New generation of omic techniques are currently revolutionizing our knowledge of biological processes, because they allow collection of substantial data for a general and global analysis of these processes. Cyanomics, a recently coined term, encompasses the global application of these omic techniques to the study of cyanide biodegradation to provide a holistic view of this process (Luque-Almagro et al., 2016; Roldán et al., 2021).

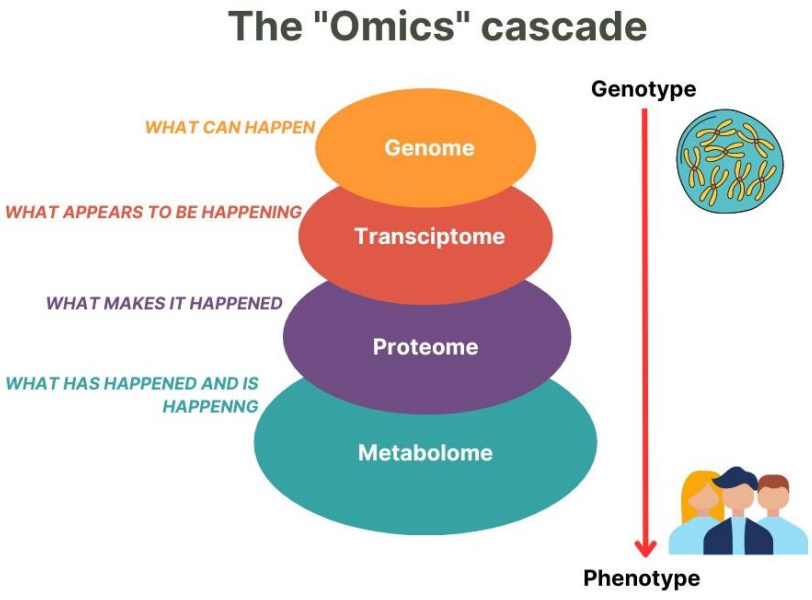

Figure 1.9. Scheme of omic techniques cascade (based on Cortes et al., 2016).

1.7.1. Genomics

Genomics encompasses all the techniques that are dedicated to the comprehensive study of the origin, evolution, content and functioning of genomes, based on the knowledge of different disciplines, such as Molecular Biology, Biochemistry, Genetics and Computer Sciences. Genomics could be subdivided into different areas, such as functional, structural and comparative genomics. The development of genomics has allowed great advances in the fields of medicine and agriculture, but also in environmental biotechnology.

Although there are many microorganisms that use cyanide as a nitrogen source, to date the genomes of only few cyanotrophic bacteria have been sequenced, such as *Pseudomonas pseudoalcaligenes* CECT 5344, *Pseudomonas fluorescens* NCIMB 11764 and *Azotobacter chroococcum* NCIMB 8003 (Vilo et al., 2012; Luque-Almagro et al., 2013; Wibberg et al., 2014; Robson et al., 2015). The first completely sequenced genome of a bacterium capable of assimilating cyanide was from *P. pseudoalcaligenes* CECT 5344 (Luque-Almagro et al., 2013; Wibberg et al., 2014; 2016). Contrary to cyanide-assimilating bacteria, a large number of cyanogenic bacteria have been sequenced, to date, including *Chromobacterium violaceum, Burkholderia cepacia* and different strains of the genus *Pseudomonas* (Ryall et al., 2008; Smits et al., 2015). Recently, genome sequencing was also achieved in arsenic resistant bacteria from arsenic nearing gold ores and As-contaminated soils, such as *Brevibacterium* sp. CS2, *Micrococcus luteus* AS2, *Microbacterium* sp. SZ1, *Brevindumonas* sp., and *Alicylobacillus mali* FL18 (Mohd et al., 2017; Sher et al., 2019; Aulitto et al., 2021; Soto et al., 2021). Genome comparison between two *Exiguonactreium* strains, S17 and N139, was also applied for 3D modeling application to Acr3 efflux pump (Ordoñez et al., 2015). Additionally, whole genome characterization was conducted for mercury resistance in *Arthrobacter* sp. H-02-3 and *Enterobacteriaceae* to identify the plasmids encoding mercury resistance (Pathak et al., 2020; Heiden et al., 2021).

1.7.2. Transcriptomics

Transcriptomics analyzes the expression profile of all the genes within a genome in response to certain conditions. The first transcriptomic studies began in the 1990s and one of the most significant techniques in the initial transcriptomic studies were the DNA chips or “microarrays”, which allow the analysis of simultaneous expression of thousands of genes under different experimental conditions.

Microarrays arise from the need to analyze the large amount of information regarding sequencing projects. They allow the generation of transcriptional maps and provide indirect information on gene expression. Today, more massive sequencing techniques using RNA-seq are used. Transcriptomic analysis using DNA chips to study the global bacterial response to cyanide has only been carried out in *P. pseudoalcaligenes* CECT 5344. In this line, a transcriptomic analysis was performed with cells cultured in the absence of nitrogen or with different sources of nitrogen, such as ammonium, sodium cyanide and a cyanide-rich residue from the jewelry industry (Luque-Almagro et al., 2015).

Another cyanide-related transcriptomic study was carried out in *Nitrosomonas europaea* with the aim of identifying genes that respond to stress caused by cyanide (Park and Ely, 2009). This nitrifying bacterium is used to remove nitrogen from wastewaters, but the nitrification process is sensitive to very low cyanide concentrations.

Transcriptomic techniques were also applied to study arsenite/antimonite oxidation in *Bosea* AS-1 (Wu et al., 2022) and *Thioalkalivibrio jannaschii* ALM2 (Ahn et al., 2019). In *Rhodococcus aetherivorans* BCP1 they were used to analyze the response to inorganic arsenic oxyanions (Firrincieli et al., 2022). Additionally, RNA-sequencing of a *fur*$^{-}$ mutant defective in the ferric uptake regulator was performed in *P. pseudoalcaligenes* CECT 5344 (Becerra et al., 2020).

1.7.3. Proteomics

The term “proteomics” was coined for the first time by Wilkins et al. (1995) to describe the protein complement to genome. Nowadays this term refers to the set of proteins that are present in an organism under determined experimental conditions. This high-throughput analysis for identification of proteins was developed successfully over past 40 years, and combined with other “omic” approaches like transcriptomic and metabolomic, allows to obtain satisfactory results about the global view of biological responses. The first generation of proteomic techniques was based on the sodium dodecyl sulfate denaturing polyacrylamide gel electrophoresis (SDS-PAGE). It was reported for the first time in 1970 by Laemmli, and it has been commonly used until today. It is a very simple and relatively low-cost technique, based on protein separation according to size. Nonetheless, it is not adequate for accurate quantitative analysis. The SDS-PAGE, two-dimensional (2D) gel electrophoresis is used for protein separation based on the isoelectric points (first dimension) and molecular weight (second dimension) by applying SDS-polyacrylamide gel electrophoresis (O’Farrell, 1975; Magdeldin et al., 2014). Additionally, the covalent labeling with fluorescent Cy-dyes may be used to increase the

sensitivity (May et al., 2012; Drabik et al., 2016). However, 2D gel electrophoresis has several disadvantages, mainly because it is not suitable to detect small quantities of proteins and it is not adequate for detection of post-translational modifications of proteins (Novotny et al., 2013; Venne et al., 2014). Different proteomic studies on various bacteria have been carried out by applying this method, including *Mycobacterium tuberculosis*, *Scheffersomyces stipites*, *Staphylococcus aureus* and *Klebsiella pneumoniae* (Huang et al., 2012; Liu et al., 2014; Kamaladevi et al., 2017; Bespyatykh et al., 2019).

Protein sequencing had become an essential nexus between the activity of purified proteins and their amino acid sequences. Therefore, the rapid development of proteomic techniques was particularly focused on the increase in sensitivity of the methods for identification of proteins that are separated within a gel. Hence, the Edman degradation method (1973) was a prevailing approach to identify gel-separated proteins. It was based on sequencing of the amino acids in peptides of intact proteins or in enzymatically digested fragments (Vandekerckhove et al., 1985; Aebersold et al., 1987). Despite reliability and maturity, this technique was characterized by poor sensitivity and slowness (Patterson and Aebersold, 2003). Furthermore, the intense development of gene sequence libraries has provoked the emergence of more advanced proteomic analytical methods, defined as second generation, such as tandem mass spectrometry (MS/MS) that provides structural information of molecular ions (peptides). This approach allows the measurement of the mass-to-charge ratio (m/z) of a molecule. It is performed on previously ionized samples in a high vacuum system. Shortly after, the mass spectrometry gave rise to two very successful methods, the electrospray ionization (ESI) combined with ion-trap or triple-quadrupole MS/MS spectrometers, and matrix-assisted laser desorption ionization (MALDI) associated with time-of-flight (TOF) mass analyzer (Patterson and Aebersold, 2003). Further development of MS-based quantitative proteomics introduced methods like chemical or enzymatic labeling, including isotope-coded affinity tag (ICAT) (Inal et al., 2013), isobaric tag for absolute quantitation (iTRAQ) (Wiese et al., 2007), dimethyl labeling (Boersema et al., 2009; Hsu et al., 2016), the standard tandem mass tag labeling (TMT) (Thompson et al., 2003), and metabolic labeling techniques (Ong et al., 2002; Krijgsveld et al., 2003).

The introduction of label-free methods like the label-free quantification based on MS/MS liquid chromatography (LC) is considered as a third generation of proteomics. This technique allows the separation of previously digested peptides and their transfer to MS1 - first mass spectrometer, in which abundance of each peptide is measured (Schlichtemeieret et al., 2019). Then, the deeper fragmentation and parent ion determination occurs in MS2 (Anand et al., 2017). Therefore, this method provide a wide protein quantification (Bereman, 2015). Additionally, it does not require large sample amounts and guarantee a high proteome coverage. However, it might not be suitable for low

abundant proteins, and the probability of errors by incomplete digestion is high (Zhang et al., 2015a). LC-MS/MS is also referred as shot-gun proteomics, since beforehand the analysis, proteins are enzymatically hydrolyzed into peptides. This technique is usually conducted by using the data-depended acquisition (DDA) mode, in which peptides with the highest intensity are selected by mass spectrometer to be further fragmented by collision with an inert gas, and analyzed during a second step (Meyer, 2021). The latest advances in the field of proteome analyses is the application of data-independent acquisition (DIA or SWATCH) mass spectrometry, which grants higher sensitivity and larger protein coverage than the DDA mode (Liu et al., 2013; Li et al., 2020). In general, the third generation is a multiapproach technique based on multidimensional data analysis and modelling. It encompasses the MS-based proteomics used for analysis of multi-proteins structure and dynamic responses of proteomes, as well as analyzing patterns of reversible post-translation modifications (Lamond et al., 2012).

With regards to cyanide biodegradation, only few proteomic studies have been performed to described the effect of cyanide on the proteome of cyanotrophic microorganisms. The two-dimensional electrophoresis (2D-PAGE) coupled with mass spectrometry was applied to identify the molecular responses of *P. pseudoalcaligenes* CECT5344 and *Klebsiella oxytoca* to cyanide (Huertas et al., 2006; Luque-Almagro et al., 2007; Tang et al., 2010; Chen et al., 2011). Later, different proteomic techniques were applied to investigate the response of *P. pseudoalcaligenes* CECT 5344 to cyanide and cyanide-metal complexes. The two-dimensional gel revealed that cyanide induces responses to iron depletion, oxidative stress and nitrogen starvation (Luque-Almagro et al., 2007). Further, application of second-generation gel-free quantitative proteomic technique allowed identification of over 150 proteins that were overexpressed in cells degrading a cyanide-containing jewelry residue, including proteins associated with metal resistance and detoxification, oxidative stress response, cyanide assimilation, and cyanide-insensitive respiration (Ibáñez et al., 2017). Recently, the proteomic label-free liquid chromatography-tandem mass (LC-MS/MS) analysis was performed to study the assimilation of 3-cyanoalanine in the CECT 5344 strain (Pérez et al., 2021).

Concerning arsenic and mercury, several proteomic analyses have been reported. Two dimension gel electrophoresis proteomics, together with transcriptomic analysis, were applied in *Micrococcus luteus* AS2 under arsenic stress (Sher and Rehman, 2021). In *Exiguobacterium* sp. S17*,* MALDI-TOF/MS was apply to identify proteins involved in arsenic-stress response (Belfiore et al., 2013). Furthermore, label-free LC-MS/MS-based proteomics was reported in *Dunaliella salina* to analyze the proteomic response to arsenate (Ge et al., 2016). Quantitative proteomic analysis was also performed to identify changes in potential functional processes related to *hgcAB* gene deletion in the case of mercury methylating bacterium *Desulfovibrio desulfuricans* ND132 (Qian et al., 2018).

1.7.4. Metabolomics

Metabolomics, together with genomics, proteomics and transcriptomics, is a rapidly developing branch of “omic” techniques. The concept of metabolomics was introduced for the first time in 1999 by Jeremy Nicholson (Nicholson et al., 1999), and since then it has been applied as a useful tool for discovery and development of new drugs, biomarkers and enzymes (Goodcare, 2005; Harrigan, 2006; Saito et al., 2006; Schlotterbeck et al., 2006; Villas-Bôas et al., 2006; Aderem et al., 2021), but also to investigate the mechanisms of various diseases like cancer (Hartmann et al., 2006; Malhi and Gores, 2006) or Alzheimer (Yilmaz et al., 2017; Wilkins et al., 2018). It is often used in discovery of new bacterial species (Palama et al., 2016) and functional genes (Mapelli et al., 2008), and to investigate antibiotic resistance (Belenky et al., 2015; Stokes et al., 2019), and is also applied in agriculture (Bender, 2005; Dixon et al., 2006) and bioremediation (Singh, 2006), among other purposes (Ye et al., 2022).

Microbial metabolomics is based on qualitative and quantitative global analysis of low-molecular weight (< 1500 Da) intracellular and extracellular metabolites, hormones, signaling molecules and secondary metabolites (Muthubharathi et al., 2021). It is applied to investigate and explain metabolite changes, interactions and the information flow in order to understand the physiological state of microorganisms or their effects on host metabolism (Lobritz et al., 2015; Covington et al., 2017). The most commonly applied tool in metabolomics, which provides high sensitivity and separation efficiency and robustness of the data, is mass spectrometry (MS) often coupled with gas or liquid chromatography, as gas chromatography-mass spectrometry (GC-MS) and liquid chromatography-mass spectrometry (LC-MS), respectively. The magnetic resonance spectroscopy (NMR) with the use of hydrogen (^{1}H-NMR), carbon (^{13}C-NMR) or phosphorus (^{31}P-NMR) spectrum is also used in metabolomic analysis (Dong et al., 2012; Zhang et al., 2013; Larive et al., 2015; Zhang et al., 2019). With regards to the large size of obtained data and complexity of metabolic maps, the processing of the data requires a special analysis, including a first step of data extraction by visualization of the metabolic maps, further data processing by filtering the noise, overlapping the peak resolution, performing peak alignment, matching or data normalization, and finally a pattern recognition by using either a supervised or an unsupervised mode.

Only few metabolomics studies have been performed regarding cyanide, arsenic or mercury effect on microorganisms. The high-resolution HPLC-MS was applied in *Aspergillus fumigatus* to analyze the biosynthesis of isocyanide under copper starvation (Won et al., 2022). The LC-MS comparative metabolomic analysis with electrospray ionization tandem mass spectrometry was used

to investigate secondary metabolites from the fungal genus *Podaxis*, which led to identification of podaxisterols that carries a nitrosyl cyanide moiety (Guo et al., 2022). Further, the LC-MS analysis coupled to ^{1}H-NMR was reported in *Agrobacterium tumefaciens* to investigate metabolic changes after exposure to 100 µM As(III) (Tokmina-Lukaszewska et al., 2017). However, in general, the majority of metabolomic approaches are angled to investigate alteration of microbiota gut composition and metabolite disruption (Lu et al., 2014; Lin et al., 2021a,b; Wang et al., 2021; Tu et al., 2023), or aim to analyze paddy soils rich in arsenic (Qian et al., 2022).

1.7.5. Metaomics

In addition to the omic techniques, metaomics aims to identify the diversity of the microbial population, genes, pathways and metabolic functions. It also investigates their interaction, activity, cooperation and growth by analyzing uncultured organisms (Handelsman et al., 1998; Lloyd et al., 2018). This technique has emerged in recent decades as a powerful tool for the genetics, biochemistry, and physiology of populations of non-culturable microorganisms (Handelsman, 2004). It has been applied to samples of natural coking processes and artificial residual waters with thiocyanate and cyanide, making it possible to reconstruct the genomes of the microorganisms and identifying the metabolic potential of the complex bacterial community present in the wastewater studied (Kantor et al., 2015; Wang et al., 2015). To date, there are only few metaomic studies focused on sites contaminated by cyanide and metals like mining areas and rivers. Metaomics targeted directly on bacterial communities could surely enrich the current knowledge about the mechanisms used by living organisms against environmental pollutants (Dvořák et al., 2017, Roldán et al., 2021). Sadly, studies concerning heavy metals are focused particularly on the characterization of biological speciation and diversity of already-well known resistance mechanisms against a specific metal, such as *arsC*, *arsM*, *arrA* or *aioA* genes in the case of arsenic (Halter et al., 2011; Costa et al., 2014; Reis et al., 2016; Sonthiphand et al., 2019; Hemmat-Jou et al., 2021; Li et al., 2021; López-Pérez et al., 2021). Furthermore, considering the limitations of techniques such as proteomics and metaproteomics (Kunath et al., 2019), the use of cutting-edge methodologies as data-independent acquisition (DIA) mode, the construction of *in-silico* libraries (Rosenberg et al., 2017), and the application of deep learning for proteomics (Distler et al., 2014; Wen et al., 2020) and proteogenomic strategies could provide essential information for the development of bioremediation strategies.

Metaomics and direct analysis on microbial communities have been applied to investigate contaminant biotransformation (Kantor et al., 2017; Birrer et al., 2019). However, omic analysis

directly applied on environments contaminated by cyanide and metals, such as mining areas, are remarkably scarce. Most of these studies are focused on acid mine drainage (AMD) ecosystems, which are generated in mining gold, copper, and nickel ores. AMD environments are characterized by low pH and high concentrations of metals and sulfate. In addition, cyanidation in gold mining can also contribute to the presence of cyanide in these acid drainages. In the last decades, culture-independent approaches have revealed the diversity and metabolic potentials and activities of AMD communities, although these studies have not analyzed specifically genes for cyanide assimilation (Munyai et al., 2021). In the case of metals, some studies at the proteomic level have been focused on sentinel organisms (Abril et al., 2015; Kwan et al., 2019; Michán et al., 2019).

In any case, it is necessary to develop metaomic analysis on sites contaminated by cyanide and metals in order to have a global and holistic view of the processes triggered by the presence of both types of pollutants. Metaomics could enrich current knowledge about the mechanisms used by living organisms against environmental contaminants (Dvořák et al., 2017, Roldán et al., 2021).

Objectives

Within this work, the following objectives have been specified and investigated:

1. Proteomic analysis of the alkalophilic cyanotrophic bacterium *Pseudomonas pseudoalcaligenes* CECT 5344 cultured in the simultaneous presence of cyanide and arsenic, or cyanide and mercury, to define the metabolism and strategies associated to the resistance and detoxification mechanisms for bioremediation purposes.

2. Proteomic analysis of *P. pseudoalcaligenes* CECT 5344 grown under anaerobic lifestyle in the presence of iron and ammonium to decipher the metabolic adaptations in order to develop anaerobic bioremediation strategies.

2. Chapter I

Proteomic analysis of arsenic resistance during cyanide assimilation by *Pseudomonas pseudoalcaligenes* CECT 5344

Results described in this chapter have been published in the article

Biełło, K.A.; Cabello, P.; Rodríguez-Caballero, G.; Sáez, L.P.; Luque-Almagro, V.M.; Roldán, M.D.; Olaya-Abril, A.; Moreno-Vivián, C. Proteomic Analysis of Arsenic Resistance during Cyanide Assimilation by *Pseudomonas pseudoalcaligenes* CECT 5344. *International Journal of Molecular Sciences* (2023), *24*:7232. doi:10.3390/ijms24087232.

2.1. Introduction

Mining activities are generating wastes on a great scale, of which near 80% are disposed to the environment without any treatment (Rorat et al., 2019). These residues might contain high levels of various toxic pollutants, such as cyanide, arsenic and heavy metals. Particularly, gold leaching by cyanidation generates high amounts of wastewaters containing free cyanide and different cyanide-arsenic and cyanide-metal complexes (Feng et al., 2018). Considering that chemical and psychical treatments of these wastes are proven to be expensive and insufficient, attention has been paid to the development of bioremediation approaches based on the use of microorganisms. Recently, many microbes have been investigated in terms of resistance to arsenic, and/or cyanide, several of which belong to the *Pseudomonas* genus. Thus, *Pseudomonas alcaligenes* NBRC14159 was reported to be able to methylate arsenic due to the arsenite *S*-adenosylmethionine methyltransferase (ArsM) activity (Zhang et al., 2015b) and *Pseudomonas* sp. HN-2 is able to perform both oxidation of As(III) and reduction of As(V) (Zhang et al., 2016). Furthermore, the cyanotrophic bacterium *Pseudomonas mendocina* P6115 was described as an arsenic oxidizer (Miranda-Carrazco et al., 2018), and in *Pseudomonas putida* KT 2440 the presence of the *arsH* gene enhances the resistance to both arsenic forms, As(V) and As(III) (Páez-Espino et al., 2020).

In this Chapter I, the global response of *Pseudomonas pseudoalcaligenes* CECT 5344 to arsenic was studied in the presence or absence of cyanide. The CECT 5344 strain is able to grow with cyanate, nitriles, cyanide and industrial residues containing both cyanide and metals (Luque-Almagro et al., 2005; Cabello et al., 2018; Sáez et al., 2019). The genome of this bacterium has been completely sequenced (Luque-Almagro et al., 2013; Wibberg et al., 2014, 2016) and the cyanide degradation process has been properly characterized by biochemical and omic approaches (Luque-Almagro et al., 2015, 2016; Ibáñez et al., 2017; Olaya-Abril et al., 2019, 2020; Pérez et al., 2021), which make *Pseudomonas pseudoalcaligenes* CECT 5344 an excellent model to develop synthetic biology strategies for bioremediation of cyanide-containing industrial wastes (Roldán et al., 2021).

2.2. Materials and methods

2.2.1. Culture media and growth conditions

Pseudomonas pseudoalcaligenes CECT 5344 was cultured in M9 minimal medium (Sambrook and Russel, 2001) with pH adjusted to 9.5, at 30 °C and under aerobic conditions in an orbital shaker MAXQ

4000 (Thermo-Scientific) (Luque-Almagro et al., 2005). The M9 medium consists of the following reagents (per liter): 6 g Na_2HPO_4, 3 g KH_2PO_4, 0.5 g NaCl, 4.1 g sodium acetate and 1.25 mL of a trace metal solution that contains (per liter): 10.75 g $MgCl_2$, 2 g $CaCO_3$, 6.16 g $MgS0_4$ x $7H_2O$, 4.75 g $FeSO_4$ x $7H_2O$, 1.12 g $MnSO_4$ x $7H_2O$, 0.25 g $CuSO_4$ x $5H_2O$, 0.28 g $CoSO_4$ x $7H_2O$, 0.06 g H_3BO_3 and 51.13 mL HCl 12 N. Furthermore, 2 mM ammonium chloride or 2 mM sodium cyanide (prepared from 200 mM stock solutions) were used as the sole nitrogen source, whereas 50 mM sodium acetate was added to the medium as a carbon source. In addition, media was supplemented with 10 µg/mL of nalidixic acid (from a stock solution of 10 mg/mL in 0.1 M NaOH). When applicable, different concentrations of arsenite as sodium dioxoarsenate ($NaAsO_2$, Sigma-Aldrich) from a 500 mM stock solution, or arsenate, as arsenate dibasic heptahydrate (Na_2HAsO_4 x $7H_2O$, Sigma Aldrich), were also added. When agar-plates were required, 15 g/L bacteriological agar was added to liquid LB medium (10 g bactotryptone, 5 g yeast extract, 5 g NaCl and 15 g agar) prior sterilization in autoclave (Green and Sambrook, 2012).

2.2.2. Determination of ammonium concentration

The determination of extracellular ammonium was performed by using the previously described colorimetrical method based on the Nessler reagent (Morrison, 1971), which was prepared by mixing 0.09 M K_2HgI_4 - solution A (Merck) with 1 N NaOH - solution B (Merck) (stoichiometry 1:1), and afterwards, it was diluted in distilled water in 1:3 ratio. Subsequently, 0.5 mL of previously diluted sample was incubated with 0.5 mL of Nessler reagent for 5 min at room temperature, and absorbance was measured at 420 nm. Finally, the ammonium concentration was estimated by using a calibration plot previously elaborated with known concentrations of ammonium chloride.

2.2.3. Determination of free cyanide concentration

Free cyanide concentration in the media was measured as described by Asmus and Garschagen (1953). Briefly, 10 µL supernatant was added to 2.5 mL of distilled water. Further, 100 µL of 1% ice cold chloramine T were added and samples were incubated for 1 min at room temperature. Subsequently, 300 µL of reagent B, containing 3 g barbituric acid (Sigma Aldrich), 15 mL pyridine (PanReacAppliChem), 3 mL HCl 12 N and water up to 50 mL were added. After 8 min incubation at room temperature, the absorbance at 578 nm was measured. The concentration of cyanide was estimated by using a calibration plot previously elaborated with known concentrations of sodium cyanide.

2.2.4. Determination of bacterial growth

Bacterial growth was monitored in liquid medium, per triplicate, by measuring the absorbance at 600 nm (A_{600}) in a spectrophotometer (Herigstad et al., 2001), or in agar-plates, by counting colony forming units (CFU) with the drop plate technique, per quintuplicate (Naghili et al., 2013).

2.2.5. Determination of arsenic tolerance

Bacterial tolerance to arsenite and arsenate was established by calculating the minimum inhibitory concentration (MIC) and the minimum bactericidal concentration (MBC) (Andrews, 2001). For this purpose, *P. pseudoalcaligenes* CECT 5344 was precultured in M9 liquid medium with 5 mM ammonium chloride. After 24 hours, when the nitrogen source was completely depleted, the cells were used to inoculate (at $A_{600} \approx 0.1$) fresh M9 medium with 2 mM ammonium or 2 mM cyanide as the nitrogen source. Increasing concentrations of arsenite (up to 75 mM) or arsenate (up to 2.5 M) were added. Furthermore, 200 µL of the inoculated media were placed in sterile U-shaped 96-well microtiter plates, in quintuplicate (one column on each side of the plate was filled with sterile water to prevent evaporation and to maintain humidity) (Naghili et al., 2013). After 48 h incubation at 30 °C in an orbital shaker at 220 rpm, MIC was calculated as the lowest arsenic concentration that inhibits the visible bacterial growth (as a dot at the bottom of the well), meanwhile MBC was estimated as the lowest arsenic concentration that kills the bacteria, checked by CFU counting. The influence of As(III) in the cyanide tolerance was established by calculating the MIC and MBC values for cyanide (with increasing concentrations of cyanide from 0 to 100 mM), in the absence or presence of 0.25 mM arsenite by following the protocol previously described.

2.2.6. Determination of arsenic intracellular concentration

The intracellular arsenic concentration was determined as previously described (Olaya-Abril et al., 2022). Briefly, *P. pseudoalcaligenes* CECT 5344 was inoculated in minimal medium M9 using 2 mM ammonium chloride (“N” condition) or 2 mM of sodium cyanide (“CN” condition) as the sole nitrogen source in the presence of 250 µM arsenite (“NAs” and “CNAs” conditions, depending on the nitrogen source). Before nitrogen source was completely consumed (at the same point as for quantitative proteomic and real-time PCR analyses), cells were harvested and centrifuged at 10,000 rpm at 4 °C during 10 min. Afterwards, samples were washed with 1 mL buffer, containing 20 mM Tris-HCl (pH 8),

4 mM EDTA, and they were dried at 80 °C for 96 h to determine cell dry weight. Then, pellets were resuspended in HNO_3 (69%, trace-metal grade, Fisher) for acid digestion. Finally, samples were provided to the Mass Spectrometry Facility of the Central Service for Research Support of the University of Córdoba (SCAI, UCO) and analyzed by Inductively Coupled Plasma Mass Spectrometry (ICP-MS) equipment (PerkinElmer model Nexion 350X). Three biological samples were analyzed for each previously mentioned condition. Statistical significance was analyzed by applying a two-tailed *t*-test analysis corrected with the Benjamini-Hochberg method.

2.2.7. Biofilm quantification

The effect of arsenic in the formation of biofilm, when ammonium or cyanide was used as nitrogen source, was tested as previously described (Lundholt et al., 2003; Shukla and Rao, 2017). For this purpose, *P. pseudoalcaligenes* CECT 5344 was cultured in the four conditions previously mentioned: 2 mM ammonium chloride or 2 mM sodium cyanide, without or with the addition of 250 µM arsenite (N, CN, NAs and CNAs, respectively). The A_{600} was adjusted to 0.1, and cells were subsequently placed on microtiter plates, using six wells per replicate, and considering the "edge effect" (Naghili et al., 2013). After 48 h incubation on orbital shaker at 220 rpm at 30 °C, the plates were washed twice with sterile 0.85% NaCl and air dried. Then, wells were incubated during 10 min with 200 µL 0.02% crystal violet solution. Afterwards, plates were washed again twice with sterile 0.85% NaCl and air dried. Finally, the crystal violet bound to the biofilm was dissolved in 200 µL 33% acetic acid. Biofilm was measured at 570 nm by using a micro plate reader (VarioskanLux, Thermo Fisher Scientific). In parallel, the same number of wells for each condition were used for protein quantification (Bradford, 1976) to avoid possible differences as a consequence of different growth rates derived from the nitrogen source used. Statistical significance was analyzed by applying a two-tailed *t*-test analysis with the Benjamini-Hochberg correction on the crystal violet measurements normalized by protein amount.

2.2.8. Determination of protein concentration

Determination of protein concentration was carried out as previously described (Bradford, 1976), along with proteomic analysis as well as biofilm quantification. Therefore, cell samples from biofilm or liquid cultures from formerly indicated conditions (N, NAs, CN and CNAs) were collected by using 100 µL of lysis buffer containing 8 M urea, 50 mM Tris-HCl (pH 7.5), and 4% CHAPS. Then, samples were disrupted by sonication in a Bandelin Sonoplus H20070 equipment (5 pulses for 20 sec at 25 W).

Afterwards, 100 µL of previously diluted samples were mixed on the U-shaped 96-well microtiter plates with 100 µL of Bradford solution (Biorad) (diluted 1:5 with distilled water). After 5 min incubation time in darkness, protein concentration was determined by measuring absorbance at 595 nm by using a microplate reader (VarioskanLux, Thermo Fisher Scientific). Each sample was measured by maintaining three technical replicates. The concentration of protein was estimated by using a calibration plot previously elaborated with known concentrations of bovine serum albumin.

2.2.9. Determination of arsenic concentration in biofilm

The samples for arsenic determination in biofilm were collected in parallel to biofilm quantification. Thus, after 48 hours incubation on orbital shaker at 220 rpm at 30 °C, biofilm from formerly indicated conditions (N, NAs, CN and CNAs) were collected by using 100 µL of HNO_3. Subsequently, samples were heated up to 95 °C and digested at 25 °C for 1 h with shaking. After diluting the samples in 2% HNO_3, arsenic content was analyzed on an ICP/MS equipment (PerkinElmer, model Nexion 350X) at the SCAI, UCO. Three biological samples, with three technical replicates, were analyzed for each condition (N, CN, NAs, CNAs). Statistical significance was measured by applying a two-tailed *t*-test analysis with the Benjamini-Hochberg correction.

2.2.10. Quantitative proteomic analysis

P. pseudoalcaligenes CECT 5344 cells were grown in M9 minimal medium under the four aerobic conditions mentioned above: 2 mM ammonium chloride as the sole nitrogen source, without arsenite (N) or with 250 µM arsenite (NAs); and 2 mM cyanide as the sole nitrogen source, without arsenite (CN) or with 250 µM arsenite (CNAs). Before the nitrogen source was entirely consumed, three independent cultures of each condition were harvested by centrifugation at 12,000 rpm for 10 min at 4 °C and stored at -80 °C until used. Samples for LC-MS/MS proteomic (data-dependent acquisition) analysis were prepared by resuspension of frozen cells in 300 µL lysis buffer. Subsequently, cells were disrupted by cavitation with ultrasounds with 8 pulses for 20 second each at 25 W (Bandelin Sonoplus H2070). To eliminate cell debris, extracts were centrifuged at 12,000 rpm for 10 min at 4 °C and supernatants were precipitated by using the commercial 2D-Clean Up Kit (Amershamm GE Healthcare). Protein concentration was estimated as previously described (Bradford, 1976). Afterwards, samples were digested with trypsin overnight at 37 °C without agitation. Finally, samples were provided to the SCAI, UCO. All the analysis were performed by using a Dionex Ultimate 3000 nano UHPLC system

connected to a mass spectrometer Orbitrap Fusion (Thermo Fisher Scientific, San Jose, CA, USA) equipped with nanoelectrospray ionization interface. The separation column was Acclaim Pepmap C18, 500 mm x 0.075 mm, 2 mm pore size, and the 5 mm x 0.3 mm precolumn Acclaim Pepmap C18 (Thermo Fisher Scientific, San Jose, CA, USA) was used for trapping the digest. The samples, containing 0.2 mg/mL, were trapped at 10 mL/min flow rate, for 5 min, with 2% acetonitrile/0.05% trifluoroacetic acid. Subsequently, the trapping column was switched on-line with the separation column and the gradient was started. Peptides were eluted with a 60-min gradient 5-40% acetonitrile/0.1% formic acid solution at a flow rate of 300 nL/min. Survey scans of peptide precursors from 400 to 1500 m/z were performed at 120 K resolution (at 200 m/z) with a 5 x 10^5 ion count target. Tandem MS was performed by isolation at 1.6 Da with the quadrupole, fragmentation by collision-induced dissociation (CID) with normalized collision energy of 35, and rapid scan MS analysis in the ion trap. The automatic gain control (AGC) ion count target was set to 2 x 10^3 and the max injection time was 75 ms. Only those precursors with charge state 2-5 were sampled for MS2. The dynamic exclusion duration was set to 15 s with 10 ppm tolerance around the selected precursor and its isotopes. Monoisotopic precursor selection was turned on. The instrument was run in top speed mode with 3 s cycles, meaning the instrument would continuously perform MS2 events until the list of non-excluded precursors diminishes to zero or 3 s, whichever is shorter. Charge state deconvolution and deisotoping were not performed. MS2 spectra were analyzed by using MaxQuant software version 1.5.7.4 (Cox and Mann, 2008). MS2 spectra were searched with Andromeda search engine against a database of *P. pseudoalcaligenes* CECT 5344 (deposited in the Uniprot database under the accession number UP000032841). Peptides generated from a tryptic digestion were searched by using the following parameters: up to one missed cleavage, carbamidomethylation of cysteines as fixed modifications, and oxidation of methionine as variable modifications. Precursor mass tolerance was 10 ppm and product ions were searched at 0.6 Da tolerances. Peptides were validated by filtering according with 1% FDR *q*-value. A target-decoy search strategy was applied, which integrates multiple peptide parameters such as length, charge, number of modifications and the identification score into a single quality that acts as the statistical evidence on the quality of each single peptide spectrum match. Relative protein quantification after LC-MS/MS procedure was performed by using MaxQuant (Cox and Mann, 2008), which uses the free available software Perseus (version 1.6.12.1) (https://maxquant.org/perseus/). The exploratory qualitative analysis was achieved by running principal component analysis (PCA) and representing relationships between expressed proteins in four experimental conditions by Venn diagram. Subsequently, the quantitative analysis was performed to define proteins differentially expressed. Proteins identified from only one peptide and/or in only one replicate were discarded. Proteins identified in at least two replicates out of three, per each condition, were used for differential pairwise comparison analysis if they were positive after considering a two-way Student-test *t*-test with the Benjamini-Hochberg

correction (Olaya-Abril et al., 2018). Proteins were considered differentially expressed when the fold change (FC) was ≥ 2, which is equal to $\log_2$ FC ≥ 1 (over-expressed), or FC ≤ 0.5, which is equal to $\log_2$ FC ≥ -1 (down-regulated), with a corrected *p* value < 0.05. Furthermore, proteins which were identified in at least two of three replicates out of one condition and undetectable in the other condition were considered as exclusive. The mass spectrometry data were deposited to the ProteomeXchange Consortium (http://proteomecentral.proteomexchange.org) with the dataset identifier PXD033539. GO analysis was performed using the web application ComparativeGO (Fruzangohar et al., 2013). For that, only those changes with a *p* value < 0.05 after a hyper-geometric distribution [E(GO)] test of the third level of GO biological function were shown. The whole genome of *P. pseudoalcaligenes* CECT 5344 was used as reference and the parameter [E(GOi)], which is used to determine the GO enrichment, was calculated by using the formula: [E(GOi)] = sample size/genome size x GOi. Integration of final proteomic data were performed by using the tool KEGG Mapper.

2.2.11. Quantitative real-time PCR analysis

P. pseudoalcaligenes CECT 5344 cells were cultured under four previously mentioned conditions (N, NAS, CN, CNAs). Then, samples were collected (along with samples for proteomic analysis) by centrifugation at 12,000 for 10 min at 4°C, before complete consumption of the nitrogen source. Further, cells were washed in 1 mL TEG buffer containing (per liter): 25 mL 1 M Tris-HCl (pH 8), 20 mL 0.5 M EDTA, 50 mL 20% glucose, and distillated water up to 1 L; and they were stored at -80 °C until further use. RNA isolation was carried out by using commercial Direct-zol RNA MiniPrep Kit (Zymo Research, Irvine, CA, USA). Subsequently, additional post-column treatment was required with DNase I (Ambion-Thermo Fisher Scientific, Waltham, MA, USA). The purity and concentration of the RNA samples were measured by using a ND1000 spectrophotometer (Nanodrop Technologies, Waltham, MA, USA). The synthesis of total cDNA was performed by using the commercial RevertAid RT Reverse Transcription Kit (Thermo Fisher Scientific, Waltham, MA, USA). Further, for transcriptional analysis, gene-specific primers were designed by using the Oligo 7.0 software (Supplementary Materials, Table S1). PCR reaction was carried out by using the SYBR Green PCR Master Mix (BioRad), with following setting: an initial activation step (95 °C, 3 min), followed by 40 cycles containing a denaturation step (95 °C, 20 s), a primer annealing step (62 °C, 20 s) and a primer extension (72 °C, 15 s). A final extension step was added, consisting of 65 °C for 10 s. Each reaction was carried out with three biological replicates, and with three technical replicates. Calibration curve was performed for relative quantitation of the fluorescence values, by using serial dilutions of gDNA, from *P. pseudoalcaligenes* CECT5344 isolated by using the PROMEGA commercial kit, following the instructions of the

manufacturer, with final concentrations from 50 ng/µL to 0.0005 ng/µL. The obtained data were normalized to the *rpoB* and 23S rRNA housekeeping genes. Finally, relative fold gene expression was calculated by the ΔΔCt method (Olaya-Abril et al., 2022) and data were analyzed by a *t*-test analysis with the Benjamini-Hochberg correction by using Perseus software (1.6.12.1).

2.3. Results

2.3.1. Bioinformatic analysis of arsenic detoxifying potential in *Pseudomonas pseudoalcaligenes* CECT 5344

To determine the putative potential of *P. pseudoalcaligenes* CECT 5344 to resist and detoxify arsenic, the genome of this bacterium was analyzed. Thus, two separate *ars* gene clusters were identified (Fig. 2.1), which code for three arsenate reductases (ArsC), two arsenite efflux pumps (ArsB), two regulatory proteins (ArsR), and several putative proteins associated with arsenic detoxification. In addition, other putative *ars*-related genes were distributed throughout the genome. Nonetheless, homologs to the *aio*, *arx* or *arr* genes, which are involved in As(III) oxidation or dissimilatory As(V) reduction, were not found in the genome of *P. pseudoalcaligenes* CECT 5344. The first characterized *ars* gene cluster presented the *arsRICBCH* gene arrangement (BN5_1989-BN5_1994) and codes for the thioredoxin-dependent and the glutaredoxin-dependent arsenate reductases ArsC1 (BN5_1991) and ArsC2 (BN5_1993), among other proteins. The second *ars* gene cluster (BN5_2705-BN5_2712) showed the *arsABRCH* gene organization and codes for the thioredoxin-dependent arsenate reductase ArsC3 (BN5_2708), among other proteins. In addition, genes coding for the glyceraldehyde-3-phosphate dehydrogenase GAPDH (BN5_2711) and the organoarsenical MSF-type transporter ArsJ (BN5_2712) were also included in this cluster 2. Also, as previously mentioned, various genes involved in arsenic detoxification were found outside these *ars* clusters, such as those encoding two additional glutaredoxin-dependent arsenate reductases, ArsC4 and ArsC5 (BN5_2838 and BN5_2786, respectively), and an ArsR-family transcriptional regulator (BN5_0252). Furthermore, other proteins that could be potentially related to arsenic metabolism in the strain CECT 5344 were searched by using protein-BLAST database and available information from sequences deposited in Uniport database. Thus, the Acr3-type permease/multidrug resistance protein MdtC (BN5_2698) and an uncharacterized multi-transmembrane protein W6QSH3 (BN5_1279), that contains an ArsP domain according to Pfam protein family database, were also identified. Additionally, some proteins with moderate similarity (40-50%) to putative ArsM methyltransferases of γ-proteobacteria, which chiefly aligned in the central methylase domain, were found. These ArsM-like proteins (genes) are annotated in the genome of *P.*

pseudoalcaligenes CECT 5344 as 3-demethylubiquinone-9/3-methyltransferase W6QUY3 (BN5_1671), bifunctional demethylmenaquinone methyltransferase/2-methoxy-6-polyprenyl-1,4-benzoquinol methylase UbiE W6QXX4 (BN5_0407), quinone oxidoreductase W6QQQ6 (BN5_0233), ubiquinone/menaquinone biosynthesis methylase W6R1I2 (BN5_3586), biotin synthesis protein BioC W6R7T1 (BN5_3914), and uncharacterized protein W6R0V8 (BN5_4176).

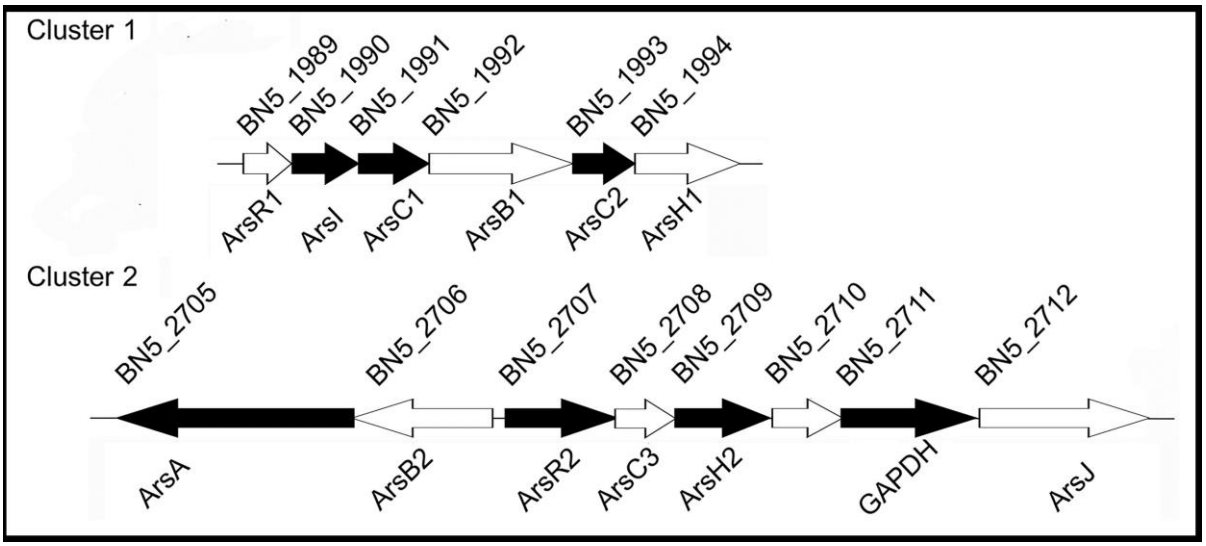

Figure 2.1. *P. pseudoalcaligenes* CECT 5344 *ars* gene clusters encoding putative proteins related to arsenic detoxification. Reference numbers correspond with UniProt annotation (UP000032841). Black genes code for proteins identified by LC-MS/MS proteomic analysis in cells grown in the presence of arsenite (see Section 2.3.3).

2.3.2. Arsenic resistance of *Pseudomonas pseudoalcaligenes* CECT 5344

To determine the minimum inhibitory concentration (MIC) and the minimum bactericidal concentration (MBC) for As(III) and As(V), *P. pseudoalcaligenes* CECT 5344 was cultured with ammonium chloride or sodium cyanide as the sole nitrogen source in the presence of different concentrations of arsenite or arsenate. For As(III), the MIC and MBC values obtained were 35 and 40 mM, respectively, regardless the nitrogen source used. Regarding arsenate, the minimal inhibitory concentration was established at 1.25 M in the presence of cyanide as N-source and 1.75 M with ammonium, whereas the minimal bactericidal concentration was 2 M (with cyanide) or 2.5 M (with ammonium).

Interestingly, the MIC and MBC values calculated for cyanide in absence of As(III) were 25 and 50 mM respectively, whereas in the presence of 0.25 mM arsenite, these values dropped to 20 and 25

mM respectively, thus suggesting a negative effect of arsenite on the cyanide tolerance in the bacterium *P. pseudoalcaligenes* CECT 5344.

Subsequently, a physiological characterization was performed to determine an adequate arsenite concentration that could affect cell growth and metabolism, without a complete inhibition of bacterial growth. Therefore, *P. pseudoalcaligenes* CECT 5344 was cultured with different arsenite concentration (up to 1 M), using either ammonium or cyanide as the sole nitrogen source. A significant effect, but without being highly detrimental for bacterial growth, was detected with both nitrogen sources at a concentration 0.25 mM of arsenite (Fig. 2.2). Alongside, a similar analysis was performed for arsenate. *P. pseudoalcaligenes* CECT 5344 was highly resistance to the presence of As(V), growing even with 200 mM arsenate (Fig. 2.3). Therefore, 0.25 mM arsenite, and 200 mM arsenate, were used in the subsequent proteomic and *q*RT-PCR analyses.

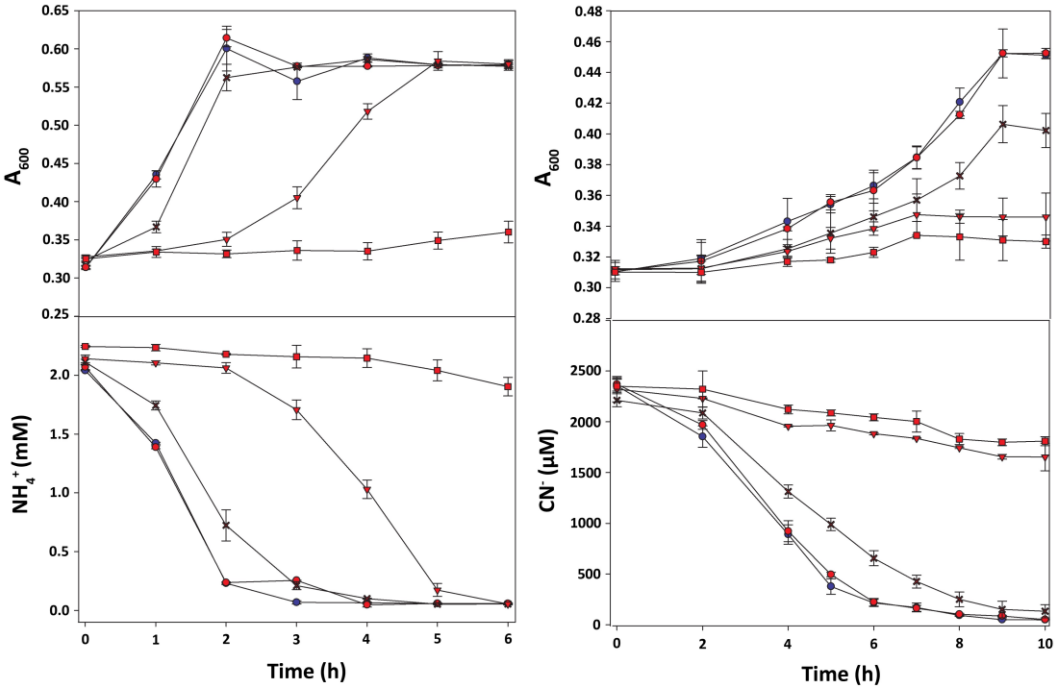

Figure 2.2. Physiological characterization of arsenite tolerance in *P. pseudoalcaligenes* CECT 5344. Cells were grown in M9 minimal medium with 50 mM sodium acetate as carbon source and 2 mM ammonium chloride (panels left) or 2 mM sodium cyanide (panels right) as sole nitrogen source, without (blue circles) or with arsenite (red symbols): 0.1 mM (filled circles), 0.25 mM (asterisks), 0.5 mM (triangles), and 1 mM (squares). Bacterial growth, upper panels; N-source consumption, lower panels.

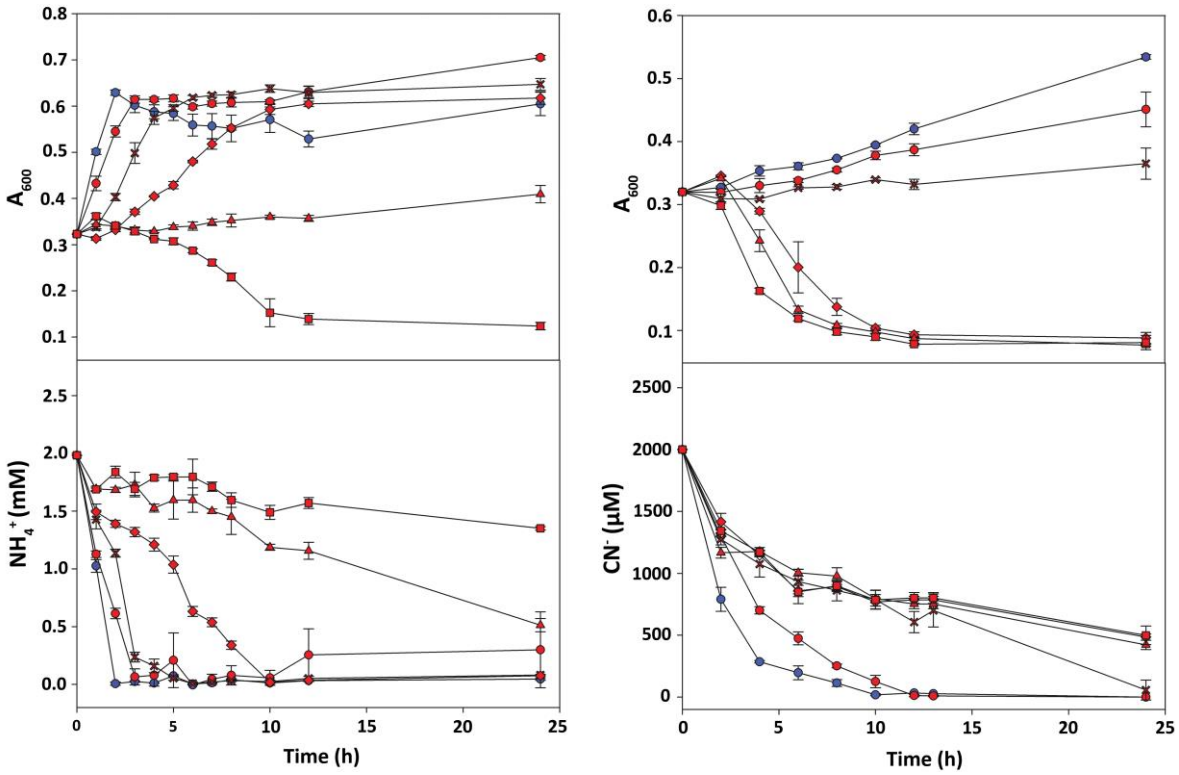

Figure 2.3. Physiological characterization of arsenate tolerance in *P. pseudoalcaligenes* CECT 5344. Cells were grown in M9 minimal medium with 50 mM sodium acetate as carbon source and 2 mM ammonium chloride (panels left) or 2 mM sodium cyanide (panels right) as nitrogen source, without (blue circles) or with arsenate (red symbols): 100 mM (circles), 200 mM (asterisks), 300 mM (diamonds), 400 mM (triangles) and 500 mM (squares). Bacterial growth, upper panels; N-source consumption, lower panels.

2.3.3. Global changes in the proteome of *P. pseudoalcaligenes* CECT 5344 in response to arsenite

Quantitative proteomic analysis by LC-MS/MS was performed to study the general response of this bacterium against arsenite. The bacterial cells were cultured under four conditions, ammonium without (N) or with 0.25 mM arsenite (NAs), and cyanide without (CN) or with 0.25 mM arsenite (CNAs), as previously described (Section 2.2.10). Subsequently, samples were harvested before nitrogen source was completely depleted to prevent a response to nitrogen starvation. After the exploratory principal component analysis (PCA) (Fig. 2.4), the three biological replicates were selected and grouped according to the nitrogen source and the presence or absence of 0.25 mM As(III). A total of 1659 unique proteins were identified from more than one peptide: 1177 in N, 1312 in NAs, 1591 in CN, and 1581 in CNAs (Table 2.1), although most of them (1105 proteins; 66.6% of identified proteins) were shared among all conditions (Fig. 2.5).

Table 2.1. Number of proteins identified per biological replicate and condition in the proteomic analysis.

Sample	Replicate	# Proteins	# Uniques Proteins
N	1	924	1177
	2	1105	
	3	1031	
NAs	1	1145	1312
	2	1205	
	3	1204	
CN	1	1446	1591
	2	1480	
	3	1525	
CNAs	1	1506	1581
	2	1511	
	3	1484	

In the quantitative differential expression analysis, the comparisons CNAs *vs* CN and NAs *vs* N revealed changes of protein expression as consequence of the presence of arsenite, when ammonium or cyanide were used as nitrogen source. The comparison CNAs *vs* CN revealed 24 up-regulated proteins in the CNAs proteome, of which 17 were "exclusive" (proteins found in, at least, two replicates of the condition CNAs and not detected in CN), and 7 were over-represented in the presence of As(III), with fold change (FC) ≥ 2 (the FC parameter was calculated as the ratio of normalized peptide intensities NAs/N and CNAs/CN). Oppositely, 41 proteins were found up-regulated in the CN condition, with 18 exclusive proteins and 23 proteins over-represented in absence of arsenite. The comparison NAs *vs* N showed that 87 proteins were up-regulated by arsenite in the NAs proteome, of which 86 were exclusive (not found in N) and only one protein was over-represented in NAs respect to N, whereas 18 proteins were exclusive of the N cultures (not detected in NAs).

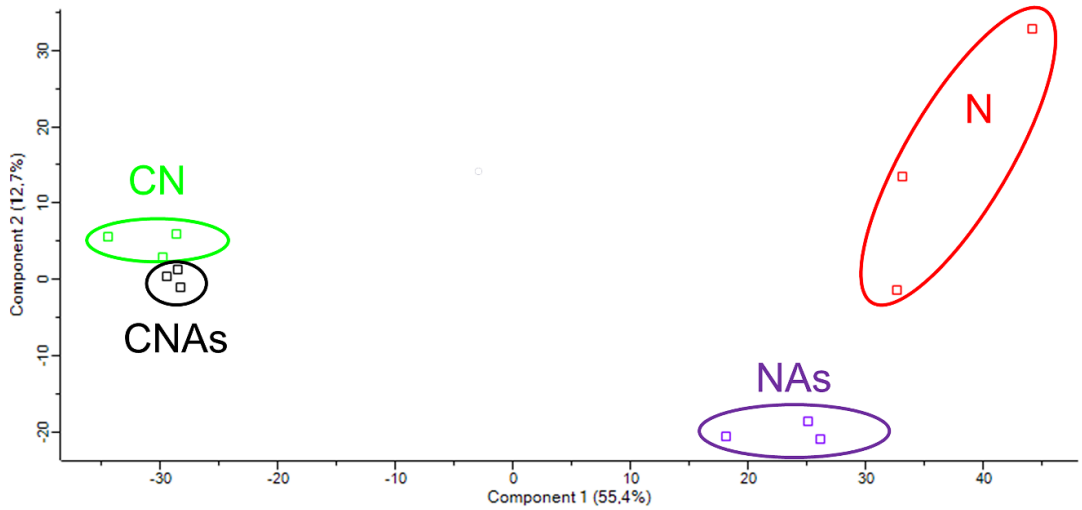

Figure 2.4. Principal component analysis (PCA) of *P. pseudoalcaligenes* CECT 5344. Cells were grown with 2 mM cyanide without (green color) or with 0.25 mM arsenite (black color), or with 2 mM ammonium in the absence (red color) or presence of 0.25 mM arsenite (purple color).

The differential proteomic analyses CN *vs* N and CNAs *vs* NAs showed the molecular mechanism by which the CECT 5344 strain responds to cyanide in absence or presence of arsenite, respectively. The analysis CN *vs* N showed 353 proteins exclusive plus 188 proteins over-represented in CN, and 18 proteins exclusive plus 164 proteins over-represented in N. Comparing CNAs *vs* NAs, 241 proteins were found exclusively in CNAs, and 168 proteins were over-represented, whereas 23 proteins were exclusive, and 137 proteins were over-represented in NAs. The detailed information of the proteins detected differentially expressed in the different comparisons is shown as supplementary material in the publication Biełło et al. (2023a), and the link is given in the Annex I.

Comparative gene ontology (GO enrichment) was carried out to analyze the arsenite effect on the global metabolism (Fig. 2.6). In general, the response of the bacterium to the presence of arsenite was influenced by the nitrogen source. Thus, in ammonium-grown cells, proteins up-regulated by As gave an enrichment in the GO categories SOS response proteins, nucleoside metabolic process related proteins, and aromatic amino acid family biosynthetic process/chorismate biosynthetic process proteins. On the other hand, the response to arsenite in presence of cyanide triggered non-specific responses related to nitrate assimilation and redox processes through down-regulation of the assimilatory nitrate and nitrite reductases and the cytochrome *c* oxidase *cbb3*-type CcoG, among other proteins.

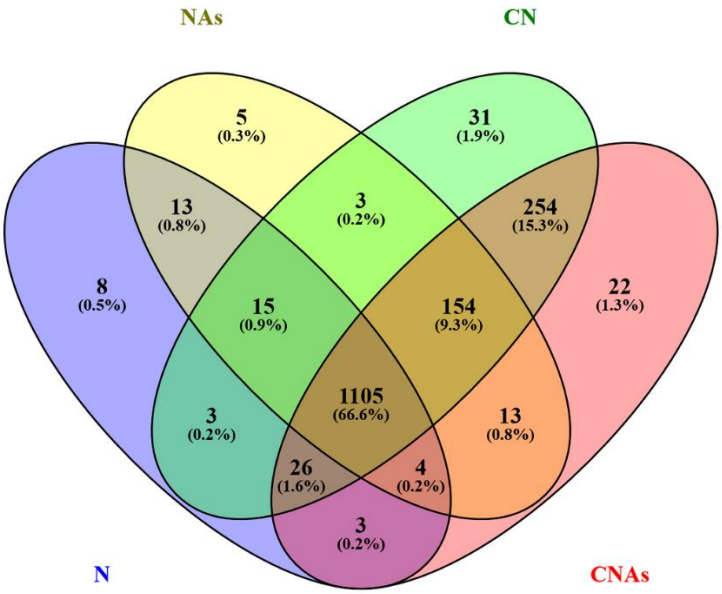

Figure 2.5. Venn diagram of identified proteins in proteomic analysis of *P. pseudoalcaligenes* CECT 5344. The blue color shows protein identified in N proteome, the yellow color represents proteins from NAs condition, the green color demonstrates proteins in CN proteome and the red color indicates protein identified in CNAs condition.

The four nitrilases (NitC, Nit4, Nit1 and Nit2) previously described in *P. pseudoalcaligenes* CECT 5344, were identified in the differential proteomic analyses CN *vs* N (Fig. 2.7). The nitrilase NitC was not significantly affected by arsenite (FC 0.91 in CNAs/CN), but other two proteins encoded by the *nit1C* gene cluster, NitD and NitG, were decreased in the CNAs condition. Similarly, Nit4 and most proteins encoded by the *cio* gene cluster were up-regulated by cyanide, but decreased significantly in presence of arsenite, showing FC values lower than 0.5 in the CNAs/CN comparison. Induction by arsenite, regardless of the nitrogen source used, was observed for the phosphate permease PstA, the protein PilJ involved in type IV pili formation, mobility and biofilm synthesis (Kuchma and O'Toole, 2022), the multidrug resistance/Acr3-type permease MdtC, the glycerol-3-phosphate dehydrogenase GlpD1, the translocase component SecY, and a LuxR family regulator, whereas the DNA repair protein RecN, the diguanylate cyclase YddV, and the membrane transport ATPase component ZntA, among others, were exclusive of CNAs (Fig. 2.7). When comparing proteins up-regulated by cyanide in the absence of arsenite (CN *vs* N) with those induced by arsenite in the absence of cyanide (NAs *vs* N), it was found that 77 exclusive proteins were shared between the CN and NAs proteomes. Some of these proteins are related to oxidative stress, such as the glutathione *S*-transferase and the hydrogen peroxide-inducible activator encoded by the BN5_4225 gene; mobility, cell communication, and biofilm formation, such as FlgN and PilJ proteins; cyanide metabolism, such as the aliphatic nitrilase Nit1; and arsenic metabolism like the ArsA and ArsH2 proteins, among others (Fig. 2.7). Concerning

other metabolic processes, the induction of enzymes involved in tetrahydrofolate (THF) metabolism was also observed in both arsenic cultures, NAs and CNAs (Figs. 2.7 and 2.8).

Regarding to the metabolism of arsenite, the differential proteomic analyses NAs *vs* N and CNAs *vs* CN revealed the metabolic strategy followed by *P. pseudoalcaligenes* to resist and detoxify arsenic. According to proteomic data, the *ars* gene clusters 1 and 2 responded significantly to the presence of As(III) (Fig. 2.7). Thus, several proteins encoded by these gene clusters, such as the arsenate reductases ArsC1 and ArsC2, the pump-driving ATPase ArsA, the regulatory protein ArsR2, and the glyceraldehyde-3-phosphate dehydrogenase GAPDH, among other proteins, were up-regulated by arsenite. Additionally, the glycerol-3-phosphate dehydrogenase GlpD1 was induced in both NAs and CNAs conditions. Furthermore, the ArsH2 protein, encoded by the BN5_2709 gene of the *ars* gene cluster 2, was up-regulated by arsenite, and also by cyanide in absence of arsenite, being exclusive of the CN condition in the CN *vs* N comparison. In contrast, the ArsB proteins were not identified by proteomics, probably because technical limitations due to their transmembrane location (Bogdanow et al., 2016). Nonetheless, the ArsA component of the ArsBA efflux pump, which is encoded by the *ars* cluster 2, was up-regulated by arsenite. The presence of arsenite also induced the expression of an arsenate transporter, the phosphate permease PstA, and the multidrug resistance Acr3-type permease (Fig. 2.7). However, the putative arsenate reductases encoded by the non-clustered *arsC* genes BN5_2786 (ArsC5) and BN5_2838 (ArsC4) were not detected in the proteomic analysis.

On the other hand, induction of proteins related to intracellular bioaccumulation of arsenic was not observed in the CECT 5344 strain. Furthermore, the proteomic analyses demonstrated that some ArsM like proteins were constitutively expressed, or induced by cyanide, suggesting that As(III) methylation may occur in *P. pseudoalcaligenes* CECT 5344, although these putative methyltransferases were not directly regulated by arsenite. Proteins related to THF metabolism, and also proteins involved in the synthesis of chorismate, a precursor of *p*-aminobenzoate, were induced in the presence of As(III) as well (Fig. 2.8).

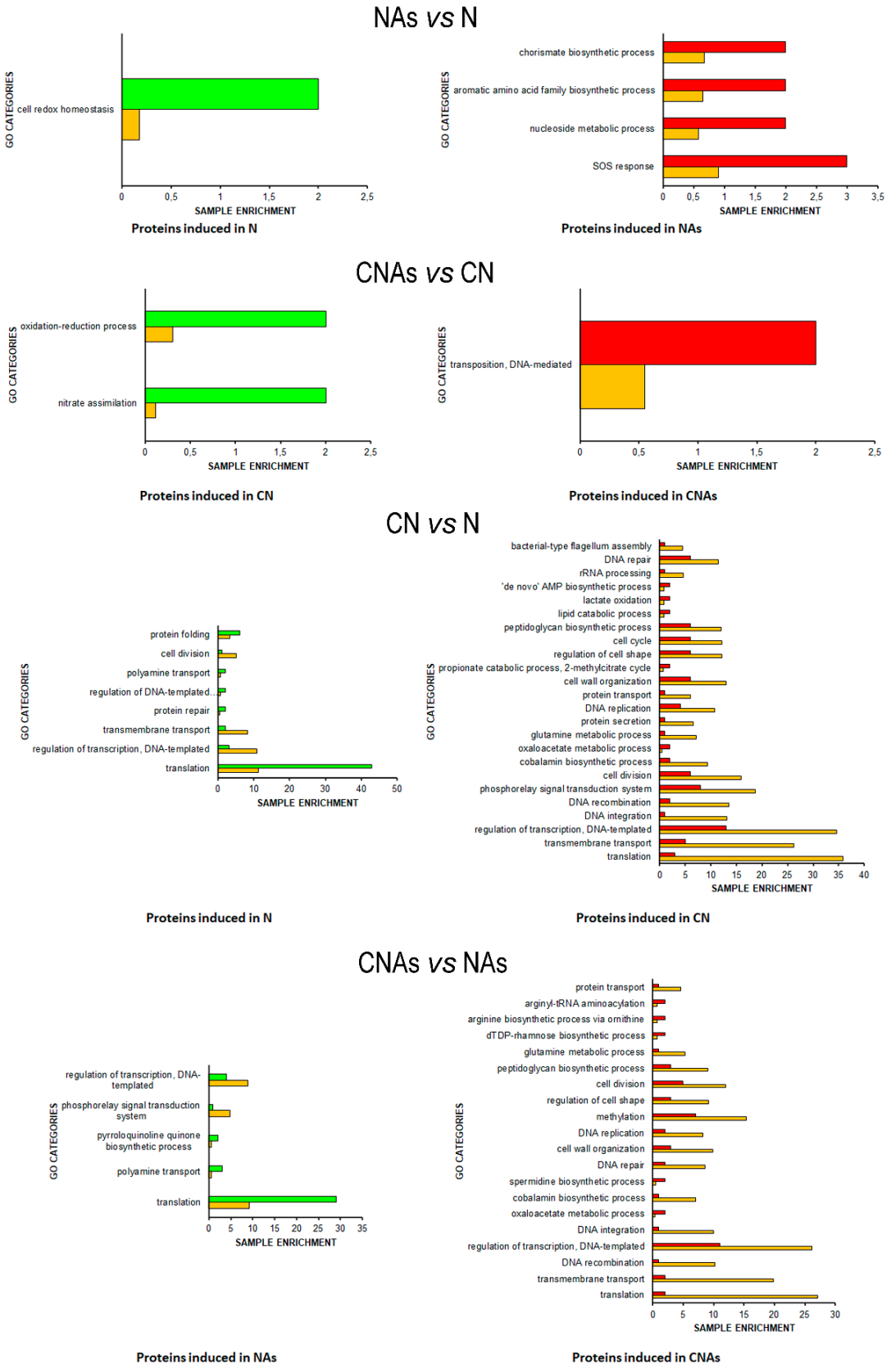

Figure 2.6. GO enrichment analysis of the different proteomic comparisons. Significative changes in GO groups with proteins over-represented in each condition (green or red) for each comparation analysis are shown. The genome of the wild-type strain was considered as reference (yellow).

Protein ID	Locus	Protein names	Short name	Log$_2$ FC NAs/N	CNAs/CN	CN/N	CNAs/NAs
		***ars* gene cluster 1**					
W6QX55	BN5_1989	Putative transcriptional regulator ArsR	ArsR1				
W6RF96	BN5_1990	Lactoylglutathione lyase, C-As lyase	ArsI				
W6QUH3	BN5_1991	Arsenate reductase (thioredoxin-dependent)	ArsC1				
W6R2E3	BN5_1992	Arsenical-resistance protein (arsenite ArsB efflux pump)	ArsB1				
W6QVQ7	BN5_1993	Arsenate reductase (glutaredoxin-dependent)	ArsC2				
W6QX59	BN5_1994	Arsenical resistance protein	ArsH1				
		***ars* gene cluster 2**					
W6RHD6	BN5_2705	Arsenical pump-driving ATPase, ArsA	ArsA				
W6QWP7	BN5_2706	Arsenite transporter ArsB efflux pump	ArsB2				
W6R4K3	BN5_2707	Regulatory protein ArsR	ArsR2				
W6QXT2	BN5_2708	Arsenate reductase (thioredoxin-dependent)	ArsC3				
W6QZ50	BN5_2709	Arsenical resistance protein, ArsH	ArsH2				
W6RHD9	BN5_2710	Protein tyrosine phosphatase domain-containing protein 1	-				
W6QWQ1	BN5_2711	Glyceraldehyde-3-phosphate dehydrogenase	GADPH				
W6R4K6	BN5_2712	MFS transporter 1-arseno-3-phosphoglycerate exporter	ArsJ				
		***nit1C* gene cluster**					
H9N5E0	BN5_1630	Sigma-54-dependent transcriptional regulator	NitA				
H9N5E2	BN5_1631	Uncharacterized protein	NitB				
H9N5E1	BN5_1632	Nitrilase NitC	NitC				
H9N5E3	BN5_1633	Radical SAM domain-containing protein	NitD				
H9N5E4	BN5_1634	GCN5-related N-acetyltransferase	NitE				
H9N5E5	BN5_1635	AIR synthase-like protein	NitF				
H9N5D9	BN5_1636	Uncharacterized protein	NitG				
H9N5D8	BN5_1637	FAD dependent oxidoreductase	NitH				
		***cio* gene cluster**					
W6QWX1	BN5_1899	GntR family transcriptional regulator	MocR				
W6RF17	BN5_1900	Sulfite reductase (NADPH) hemoprotein beta-component	CysL3				
W6QU90	BN5_1901	Uncharacterized protein	CioC3				
W6R254	BN5_1902	Terminal oxidase subunit I	CioA3				
W6QVH5	BN5_1903	Cytochrome *d* ubiquinol oxidase, subunit II	CioB3				
W6QWX6	BN5_1904	Phosphoserine aminotransferase	SerC3				
W6RF21	BN5_1905	Histidinol-phosphate aminotransferase	HisC3				
W6QU95	BN5_1906	Acetylornithine aminotransferase	ArgD3				
W6R260	BN5_1907	4-hydroxy-tetrahydrodipicolinate synthase	DapA1				
W6QVI0	BN5_1908	High-affinity glucose transporter	-				
W6QWY1	BN5_1909	Methylenetetrahydrofolate reductase	MetF3				
W6RF25	BN5_1910	Cysteine synthase	CysM3				
W6QUA1	BN5_1911	NADP-dependent malic enzyme	MaeB3				
W6R265	BN5_1912	Nitrilase Nit4	Nit4				

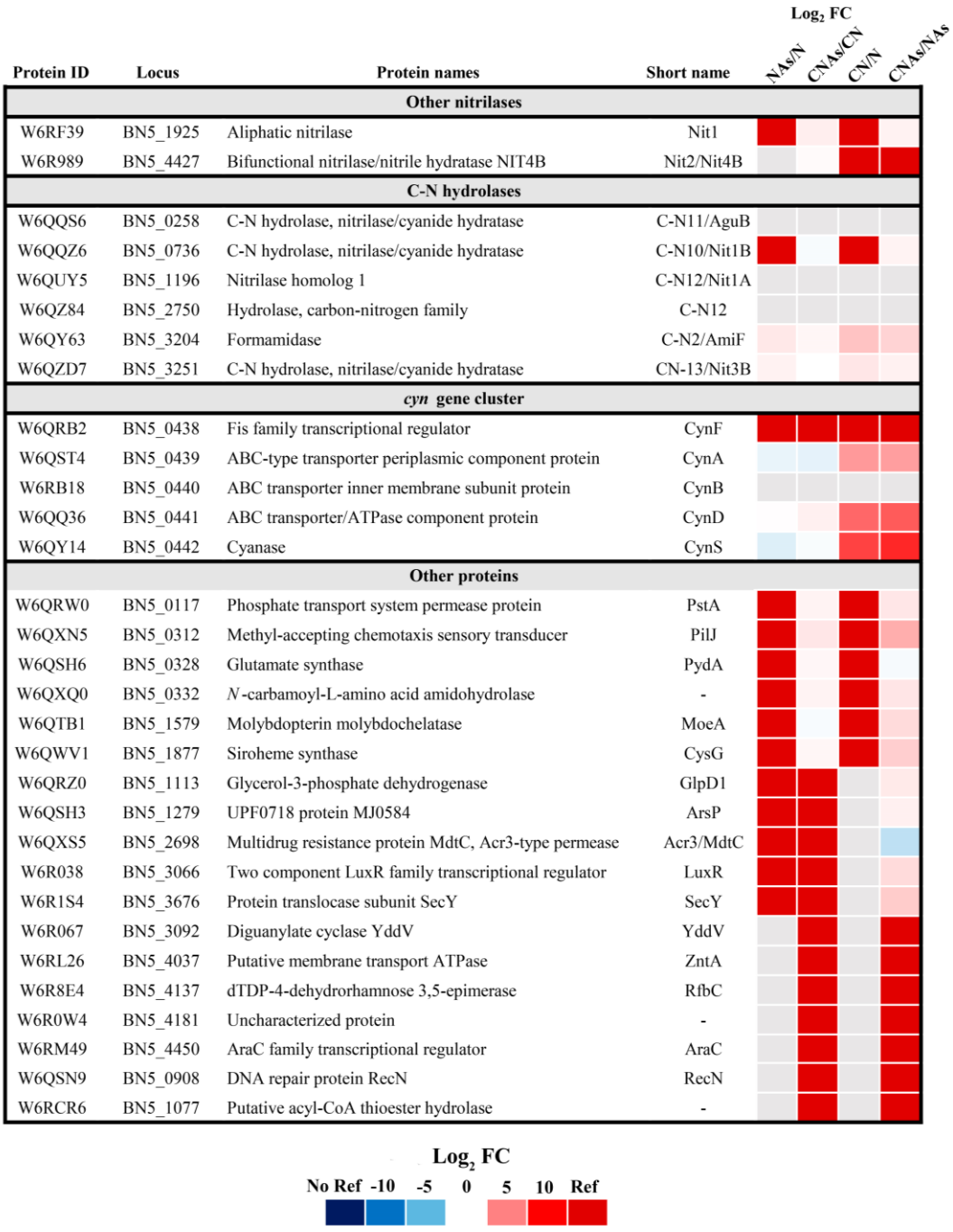

Protein ID	Locus	Protein names	Short name
		Other nitrilases	
W6RF39	BN5_1925	Aliphatic nitrilase	Nit1
W6R989	BN5_4427	Bifunctional nitrilase/nitrile hydratase NIT4B	Nit2/Nit4B
		C-N hydrolases	
W6QQS6	BN5_0258	C-N hydrolase, nitrilase/cyanide hydratase	C-N11/AguB
W6QQZ6	BN5_0736	C-N hydrolase, nitrilase/cyanide hydratase	C-N10/Nit1B
W6QUY5	BN5_1196	Nitrilase homolog 1	C-N12/Nit1A
W6QZ84	BN5_2750	Hydrolase, carbon-nitrogen family	C-N12
W6QY63	BN5_3204	Formamidase	C-N2/AmiF
W6QZD7	BN5_3251	C-N hydrolase, nitrilase/cyanide hydratase	CN-13/Nit3B
		***cyn* gene cluster**	
W6QRB2	BN5_0438	Fis family transcriptional regulator	CynF
W6QST4	BN5_0439	ABC-type transporter periplasmic component protein	CynA
W6RB18	BN5_0440	ABC transporter inner membrane subunit protein	CynB
W6QQ36	BN5_0441	ABC transporter/ATPase component protein	CynD
W6QY14	BN5_0442	Cyanase	CynS
		Other proteins	
W6QRW0	BN5_0117	Phosphate transport system permease protein	PstA
W6QXN5	BN5_0312	Methyl-accepting chemotaxis sensory transducer	PilJ
W6QSH6	BN5_0328	Glutamate synthase	PydA
W6QXQ0	BN5_0332	*N*-carbamoyl-L-amino acid amidohydrolase	-
W6QTB1	BN5_1579	Molybdopterin molybdochelatase	MoeA
W6QWV1	BN5_1877	Siroheme synthase	CysG
W6QRZ0	BN5_1113	Glycerol-3-phosphate dehydrogenase	GlpD1
W6QSH3	BN5_1279	UPF0718 protein MJ0584	ArsP
W6QXS5	BN5_2698	Multidrug resistance protein MdtC, Acr3-type permease	Acr3/MdtC
W6R038	BN5_3066	Two component LuxR family transcriptional regulator	LuxR
W6R1S4	BN5_3676	Protein translocase subunit SecY	SecY
W6R067	BN5_3092	Diguanylate cyclase YddV	YddV
W6RL26	BN5_4037	Putative membrane transport ATPase	ZntA
W6R8E4	BN5_4137	dTDP-4-dehydrorhamnose 3,5-epimerase	RfbC
W6R0W4	BN5_4181	Uncharacterized protein	-
W6RM49	BN5_4450	AraC family transcriptional regulator	AraC
W6QSN9	BN5_0908	DNA repair protein RecN	RecN
W6RCR6	BN5_1077	Putative acyl-CoA thioester hydrolase	-

Figure 2.7. Heatmap of *P. pseudoalcaligenes* CECT5344 proteins identified in proteomic analysis with a possible role in arsenic and/or cyanide detoxification. The differential expression of proteins is represented as Log_2 fold change (FC). The fold change has been calculated as the ratio normalized peptide intensity in the four comparisons NAs/N, CNAs/CN, CN/N, and CNAs/NAs. NAs, ammonium as N-source, with 0.25 mM arsenite; N, ammonium as N-source, without arsenite; CNAs, cyanide as N-source, with 0.25 mM arsenite; and CN, cyanide as N-source, without arsenite. Proteins not detected (gris color). Protein code according to Uniprot database under the accession number UP000032841. Genes annotation from GeneBank (Accession HG916826.1).

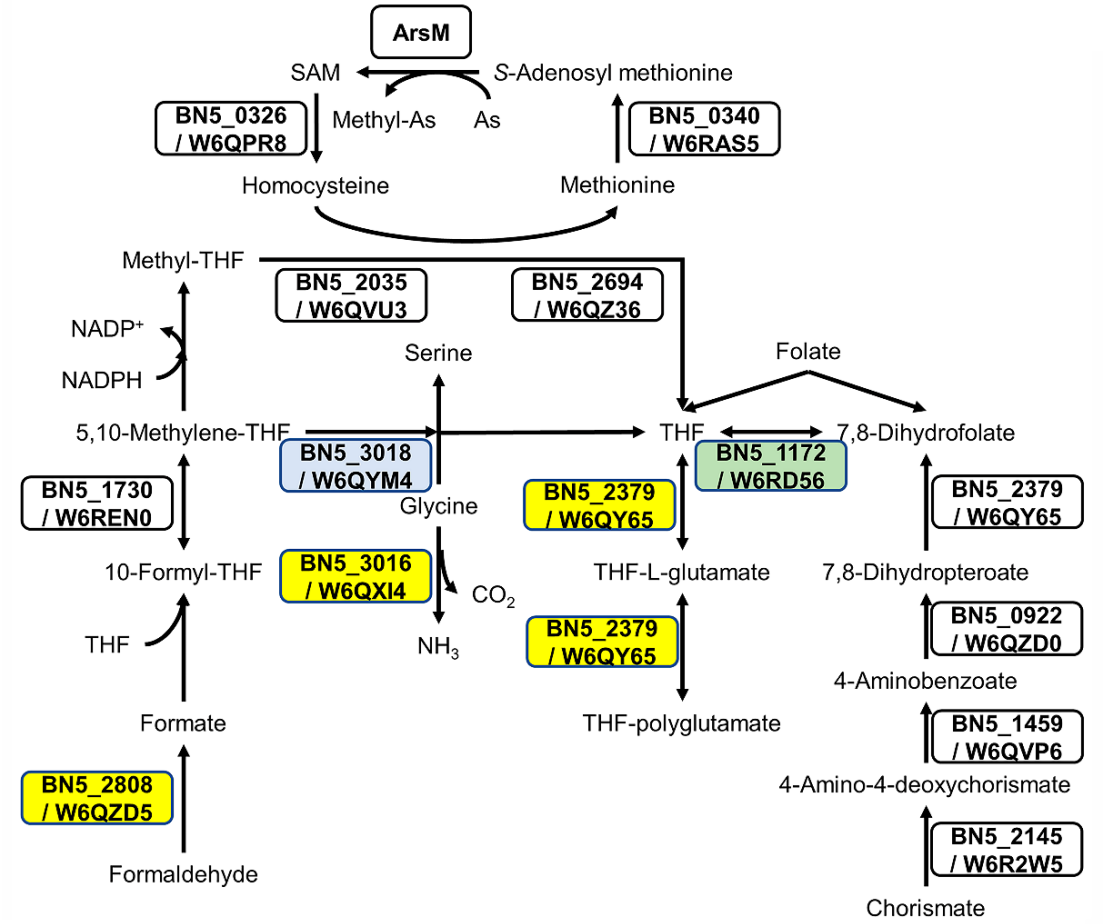

Figure 2.8. Effect of arsenite on proteins involved in tetrahydrofolate (THF) metabolism. Folate biosynthesis (ppse00790), biosynthesis of cofactors (ppse01240), and carbon metabolism (ppse01200) from KEGG were analyzed to build the metabolic pathways. Proteins W6QZD5 (*S*-formylglutathione hydrolase encoded by BN5_2808), W6QXI4 (glycine cleavage system H protein encoded by BN5_3016), and W6QY65 (dihydrofolate/folylpolyglutamate synthase encoded by BN5_2379), marked in yellow boxes, were induced by As(III) when ammonium was used as N-source. The protein W6QYM4 (serine methylase encoded by BN5_3018), shown in a blue box, was induced by As(III) with cyanide as N-source. The protein W6RD56 (dihydrofolate reductase encoded by BN5_1172), boxed in green, was identified only in cyanide, with or without arsenite.

2.3.4. Accumulation of arsenic in biofilm

Biofilm formation by *P. pseudoalcaligenes* CECT 5344 was significantly increased in cells grown with 0.25 mM arsenite (Fig. 2.9). Bacterial cells incubated with CNAs showed the highest amount of biofilm production, when compared to NAs condition. Furthermore, significative arsenic retention was detected by ICP-MS analysis in the biofilm, whereas the intercellular concentration of As was residual. The accumulation of arsenic in biofilm was also significantly higher with cyanide (CNAs) than in the NAs condition.

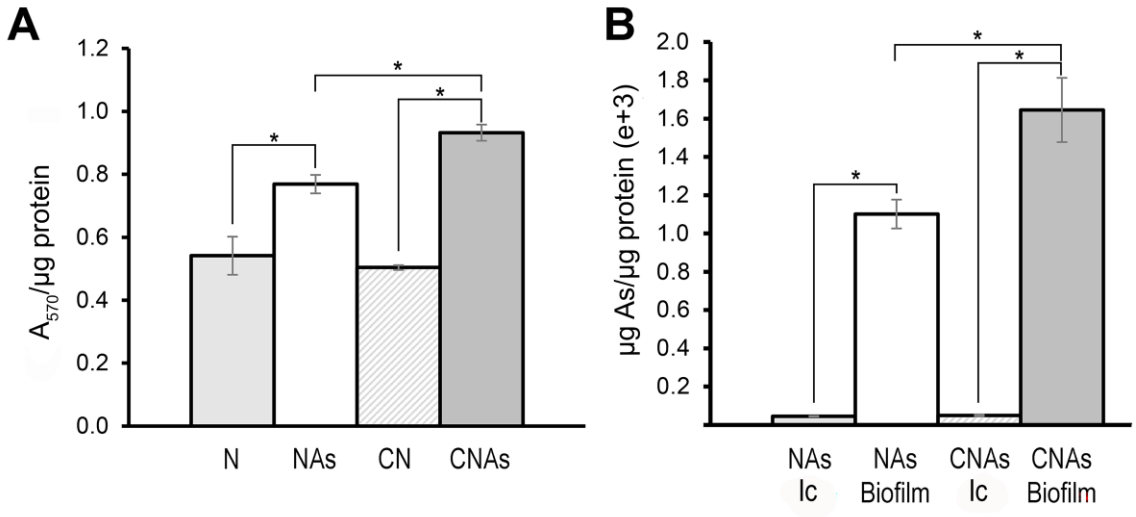

Figure 2.9. Biofilm production in *P. pseudoalcaligenes* CECT 5344 and arsenic accumulation in the biofilm. (A) Biofilm formation (measured with crystal violet as A_{570}) normalized by protein amount (µg) in cells grown with 2 mM ammonium as nitrogen source in the absence (N) or the presence of 0.25 mM arsenite (NAs), or with 2 mM cyanide as nitrogen source, without (CN) or with 0.25 arsenite (CNAs). (B) Intracellular (Ic) and biofilm arsenic accumulation in cells grown with 0.25 mM arsenite using ammonium (NAs) or cyanide (CNAs) as the sole nitrogen source. Asterisks indicate that the differences are significant ($p < 0.05$) according to a *t*-test

2.3.5. Transcriptional *q*RT-PCR analysis

Taking into account the limitations of the proteomic LC-MS/MS technique, for example the poor detection of peptides and proteins with low abundance, membrane location and/or with post-translational modifications, which may lead to misidentification of proteins (Bogdanow et al., 2016; Pappireddi et al., 2019; Dupree et al., 2020; Bugyi et al., 2021), a *q*RT-PCR transcriptional analysis of some genes coding for some relevant proteins identified by proteomics, or not detected but putatively related to arsenic resistance, was performed. In the first place, the arsenate reductase genes of the *P. pseudoalcaligenes* CECT 5344 were analyzed in cells grown in the presence of 0.25 mM arsenite or 200 mM arsenate, with ammonium or cyanide (2 mM) as the sole nitrogen source (Fig. 2.10). The

expression of the arsenate reductases *arsC1* and *arsC2* genes (BN5_1991 and BN5_1993, respectively), located in the *ars* cluster 1, as well as *arsC3* (BN5_2708), located in the *ars* cluster 2, was induced by As(III) and As(V) regardless the nitrogen source, cyanide or ammonium (Fig. 2.10). However, expression of the putative non-clustered *arsC5* (BN5_2786) and *arsC4* (BN5_2838) genes was residual and resulted unaffected by arsenite or arsenate (not shown).

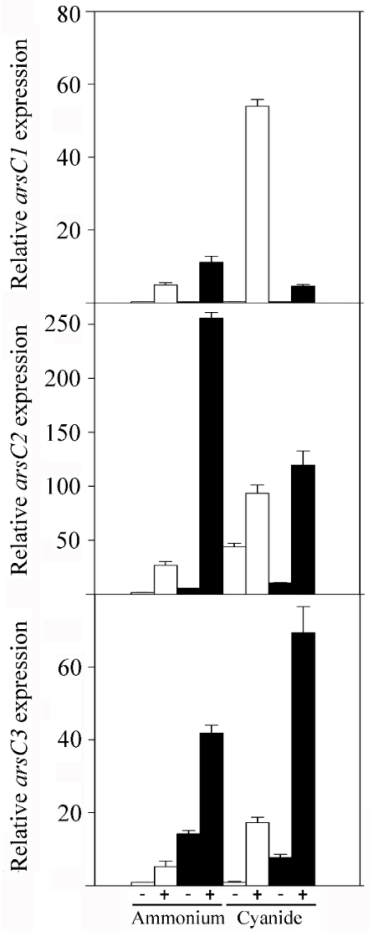

Figure 2.10. Relative expression of arsenate reductase *arsC1*, *arsC2*, and *arsC3* genes of the CECT 5344 strain in response to arsenic. Gene expression was analyzed by *q*RT-PCR in cells grown with 2 mM ammonium chloride or 2 mM sodium cyanide, without (-) or with (+) arsenite 0.25 mM (white bars) or arsenate 200 mM (black bars).

In general, the *q*RT-PCR analysis carried out to determine the expression of selected genes confirmed the proteomic results previously obtained (Fig. 2.11). The *q*RT-PCR analysis demonstrated that expression of the *arsP* gene (BN5_1279) encoding a putative permease, and the *gcvH3* (BN5_3016) and *glyA5* (BN5_3018) genes, which are related to THF biosynthesis, were induced by arsenite. The increase of both protein and mRNA levels in presence of arsenite was also observed for the phosphate permease PstA. However, the induction by arsenite of the *arsB1* (BN5_1992) and *arsR1* (BN5_1989) genes of the *ars* cluster 1 was observed only at transcriptional level (Fig. 2.11). This may be due to the

difficulty to detect by proteomics membrane proteins or regulators that may be present in the cells at very low concentrations (Bogdanow et al., 2016).

On the other hand, the negative effect of arsenite on the *cio* gene cluster (*cioA3* and *maeB3* genes) was also confirmed by *q*RT-PCR (Fig. 2.11). For the *maeB3* gene, this inhibition was observed both by transcriptional and proteomic analyses, but for the *cioA3* gene it was observed only at the protein level. Proteomic and *q*RT-PCR data revealed that the nitrilase NitC, which is essential for cyanide assimilation, was not affected by arsenite. However, the proteins NitD and NitG, which are also encoded by the *nit1C* gene cluster, were found decreased in the presence of arsenite. Significant differences were not observed at the transcript level for *nitD* and *nitG* in the CN and CNAs conditions, suggesting that As(III) affects NitD and NitG only post-translationally.

2.4. Discussion

The main aim of the research presented in this Chapter I was to study the comprehensive response of *Pseudomonas pseudoalcaligenes* CECT 5344 to arsenite in the presence of cyanide under aerobic conditions. The holistic approach was applied by combining LC-MS/MS proteomics and *q*RT-PCR transcriptional analyses. Previous works demonstrated that the strain CECT 5344 is able to assimilate cyanide, cyanate, metal-cyanide complexes and different nitriles as nitrogen source under alkaline pH (Luque-Almagro et al., 2005). Nonetheless, the potential of *P. pseudoalcaligenes* CECT 5344 to resist and degrade metalloids like arsenic, especially in the presence of cyanide, has not been described yet.

There is a wide range of microbial *ars* gene clusters that have been described so far, such as the *arsRBC* cluster reported in *E.coli* (Carlin et al., 1995), *Staphyloccocus xylosus* pSx267 (Rosenstein et al., 1992), *Staphylococcus aureus* pI258 (Ji and Silver, 1992) and *Pseudomonas aeruginosa* pKW301 (Cai et al., 1998); the *arsRDABC* cluster described in *E. coli* R773 (Chen et al., 1986) and *Acidiphilium multivorum* pKW301 (Suzuki et al., 1998); or even more complex *ars* operons that contain two or more *arsC* (arsenate reductase) and other *ars* genes like *arsH*, *arsD* and *arsA,* as reported in *Acidithiobacillus caldus* (Tuffin et al., 2005), *Corynebacterium glutamicum* (Ordóñez et al., 2005), *Pseudomonas putida* (Páez-Espino et al., 2015) and *Caenibacter arsenoxydans* (Muller et al., 2007). The bioinformatic analysis by using protein-Blast platform and Uniprot database revealed that the CECT 5344 strain harbors two *ars* gene clusters, *arsRICBCH* and *arsABRCH*, respectively, which encode several genes involved in arsenic detoxification (Fig. 2.1). Moreover, several proteins were detected that presented 40-50% similarity with microbial methyltransferases ArsM, mainly aligned in the central methylase domain.

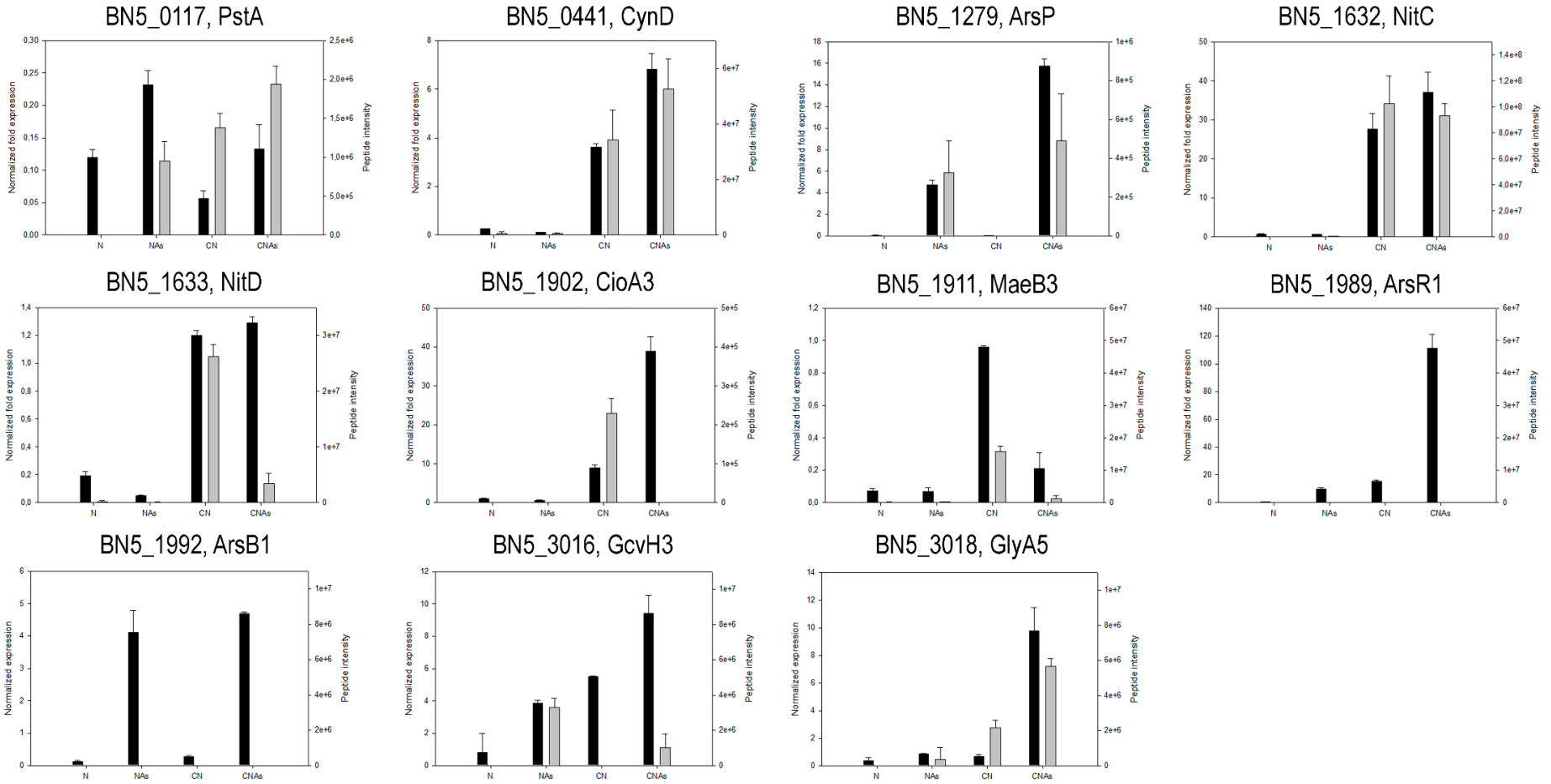

Figure 2.11. Comparison of the transcriptional and proteomic analyses for some genes of *P. pseudoalcaligenes* CECT 5344 and their products. The relative gene expression determined by *q*RT-PCR (black bars), and the normalized peptide intensities of its encoded proteins (grey bars), are shown for the different culture conditions: N, ammonium chloride as nitrogen source, without arsenite; NAs, ammonium chloride as nitrogen source, plus 0.25 mM As(III); CN, sodium cyanide as nitrogen source, without arsenite; and CNAs, sodium cyanide as nitrogen source, plus 0.25 mM As(III).

However, *aio*, *arx* or *arr* homologues, which are genes associated with arsenite oxidation or dissimilatory arsenate reduction, respectively, in *Rhizobium* sp., *Alkalilimnicola ehrlichii*, *Chrysiogenes arsenatis*, and other bacteria (Badilla et al., 2018) were not found in the genome of *P. pseudoalcaligenes* CECT 5344. This suggests that the CECT 5344 strain may tolerate and detoxify arsenite and arsenate, but it cannot use these compounds to gain metabolic energy.

To establish the tolerance range of *P. pseudoalcaligenes* CECT 5344 to arsenic, the minimum inhibitory concentration (MIC) and the minimum bactericidal concentration (MBC) were calculated. Many tolerance determination assays are performed by growing the bacterial strains in LB rich medium, which might be helpful to overcome toxicity of hazardous metalloids and heavy metals (Páez-Espino et al., 2020; Bermanec et al., 2021). Nonetheless, to develop the bioremediation treatments, the composition of the culture medium, among many other factors, is essential to control growth conditions. Therefore, the CECT 5344 strain was cultured in M9 minimal medium with 2 mM ammonium chloride or 2 mM sodium cyanide as the sole nitrogen source in the presence of different As(III) or As(V) concentrations. The assays revealed that *P. pseudoalcaligenes* CECT 5344 was able to resist arsenite in the range of 35 mM (MIC) and 40 mM (MBC), regardless the nitrogen source used. These values are similar to those found in *Bacillus licheniformis* DAS1 (Tripti et al., 2014), *Bacillus* sp. DT10 (Bachate et al., 2009), *Bacillus* sp. WK3 (Anderson and Cook, 2004)*, Achromobacter* sp. Kas3-1 (Sarkar et al., 2013)*, Acinetobacter brisoui* RCd3 (Bhakta et al., 2014), *Enterobacter* sp. (Chitpirom et al., 2009), *Microbacterium hydrocaboxydans* Rice F (Bachate et al., 2009), *Pseudomonas* sp. (Anderson and Cook, 2004; Chitpirom et al., 2009) and several bacterial isolates from tannery wastes (Chitpriom et al., 2009). With regards to the MIC and MBC for cyanide, which were 25 and 50 mM in absence of arsenite, it was found that these values dropped to 20 and 25 mM, respectively, in the presence of 0.25 mM arsenite, thus indicating that As(III) decreases cyanide tolerance of *P. pseudoalcaligenes* CECT 5344. Nonetheless, the obtained MIC value was significantly higher than those reported for *Pseudomonas mendocina* (10 mM) (Miranda-Carrazco et al., 2018), *P. stutzeri* (4.6 mM) (Singh et al., 2018) or *Rhodococcus* sp. (15 mM) (Maniyam et al., 2011). This fact should be considered for the bioremediation of wastes co-contaminated with both toxic compounds. In the case of As(V), this bacterium showed MIC values of 1.25 M (with cyanide as N-source) or 1.75 M (with ammonium), and MBC values of 2 M (with cyanide) or 2.5 M (with ammonium), in accordance with the lower toxicity of arsenate compared to arsenite described by other authors (Cai et al., 2009; Byeon et al., 2021; Kabiraj et al., 2022).

Subsequently, the physiological characterization aimed to determine the arsenic concentration that might alter cell metabolism and growth without completely inhibiting the bacterial growth. The CECT 5344 strain was cultured with different concentrations of arsenite, up to 1 mM, using

either ammonium or cyanide as the sole nitrogen source (Fig. 2.2). It was found that 0.25 mM arsenite, which is almost 10 times higher than the average concentration of arsenic in the lithosphere (Newsome and Falagán, 2021), allowed cell growth without being highly detrimental for the bacterium. Additionally, *P. pseudoalcaligenes* CECT 5344 was highly resistant to As(V), and a significant negative effect on bacterial growth was only observed for 400 mM arsenate with ammonium, or 200 mM arsenate with cyanide (Fig. 2.3). In terms of As(III), the obtained values are significantly lower than those reported for *Pseudomonas putida* KT2440, which is able to resist up to 10-20 mM. Regarding the As(V) concentration, the values obtained for *P. pseudoalcaligenes* CECT 5344 are similar to those for *P. putida* KT2440 (300 mM) (Fernández et al., 2014; Páez-Espino et al., 2015). Nonetheless, in both cases the strain KT2440 was cultured in LB rich medium, which may significantly increase tolerance to both forms of arsenic. Furthermore, the cyanotrophic bacterium *Pseudomonas mendocina* was reported to resist 8 mM As(III) and 140 mM As(V), and also could oxidize 0.5 mM As(III) (Miranda-Carrazco et al., 2018). Although, *P. mendocina* shows high genome similarity (94.8%) to the CECT 5344 strain (Luque-Almagro et al., 2013), its ability to resist arsenic or cyanide is significantly lower than in *P. pseudoalcaligenes* CECT 5344. In general, a more accurate comparison of the tolerance to toxic elements of these microorganisms is difficult, due to the differences in the composition of the media and growth conditions (Miranda-Carrazco et al., 2018).

LC-MS/MS proteomic analysis provided a holistic view on the *P. pseudoalcaligenes* CECT 5344 response to the presence of 0.25 mM arsenite in the media (Fig. 2.7). Foremost, the data obtained from differential proteomic analysis comparing CN *vs* N samples confirmed on a high degree the results previously described in this cyanide-degrading strain (Luque-Almagro et al., 2015; Ibáñez et al., 2017; Olaya-Abril et al., 2020; Pérez et al., 2021), thus supporting the robustness and reliability of the analysis performed in this Chapter I. The four nitrilases (NitC, Nit4, Nit1 and Nit2) that are present in *P. pseudoalcaligenes* CECT 5344 (Luque-Almagro et al., 2013) were identified in the proteomic analysis (Fig. 2.7). As previously described, cyanide up-regulated the nitrilases NitC and Nit4, which are required for cyanide assimilation and for 3-cyanoalanine assimilation, respectively (Estepa et al., 2012; Pérez et al., 2021). NitC is encoded by the *nitC* gene (BN5_1632) located on the *nit1C* cluster required for cyanide assimilation, whereas *nit4* (BN5_1912) belongs to the *cio* gene cluster involved in the cyanide-insensitive respiration (Estepa et al., 2012; Luque-Almagro et al., 2013). Additionally, the majority of proteins encoded by *cio* gene cluster that were up-regulated by cyanide, declined significantly in the presence of arsenite. This may explain the decrease of the MIC and MBC values for cyanide observed when the *P. pseudoalcaligenes* CECT 5344 was cultured in presence of 0.25 mM arsenite. The proteomic differential analysis performed by comparing proteins up-regulated by cyanide in the absence of arsenite (CN *vs* N) with those induced by arsenite in the absence of cyanide (NAs *vs* N)

revealed that several proteins associated with oxidative stress, mobility, cell communication, biofilm formation and cyanide and arsenic metabolism were up-regulated by both toxics (Fig. 2.7). This might indicate that cyanide and arsenic detoxification processes present a certain degree of interrelation, being affected by each other, probably because both toxic compounds trigger general stress response mechanisms in bacteria. Proteomic analysis also revealed the induction by arsenite of the glutamate synthase, the *N*-carbamoyl-L-amino acid amidohydrolase, and the molybdopterin molybdochelatase MoeA and the siroheme synthase CysG proteins involved in the biosynthesis of the molybdopterin and siroheme cofactors of the nitrate and nitrite reductases, respectively (Figs. 2.6 and 2.7). This suggests that arsenite may provoke changes in the metabolism of nitrogenous compounds.

Interestingly, proteins related to THF metabolism, and also proteins involved in the synthesis of chorismate, a precursor of *p*-aminobenzoate, were induced in the presence of As(III), suggesting a relationship between THF metabolism and arsenic resistance (Fig. 2.8). It has been shown that administration of folic acid reduces arsenic toxicity in humans (Bae et al., 2021), and this effect could be due to the requirement of THF for arsenic methylation, either directly or allowing synthesis and recycling of SAM, which is required for ArsM-type methyltransferases (Bustaffa et al., 2020; Abuawad et al., 2021). Also, the GAPDH enzymes may catalyze the formation of arseno-phosphoglycerate, which is exported by the permease ArsJ (Chen et al., 2016; Huang et al., 2018). In *P. pseudoalcaligenes* CECT 5344, both *gapdh* (BN5_2711) and *arsJ* (BN5_2712) genes are present in the arsenite-induced *ars* cluster 2. On the other hand, nitriles and cyanoderivatives may react with arsenic forming Lewis adducts (Saal et al., 2018). Dissociation of these possible adducts could be mediated by the putative C-As lyase ArsI, encoded by the BN5_1990 gene of the *ars* cluster 1, which was found induced by arsenite. Proteomic and *q*RT-PCR data are coincident (Figs. 2.7 and 2.10) and suggest that the *arsC1-C3* genes are involved in As-resistance, but the *arsC4* and *arsC5* genes could be the result of gene duplications or horizontal gene transfer events, being either non-functional or controlled by different environmental conditions, like in *P. putida* (Páez-Espino et al., 2015) and *Rhodopseudomonas palustris* (Zhao et al., 2015).

According to the proteomic differential analysis, the *ars* clusters 1 and 2 of the strain CECT 5344 responded significantly to the presence of arsenite. In addition, As(III) also induced the phosphate permease PstA, an arsenate transporter. Hence, once inside the cells, As(V) could be reduced to As(III) by the arsenate reductases ArsC1-C3, being arsenite directly expelled to the extracellular media by the ATP-driven efflux pump ArsBA or the multidrug resistance Acr3-type permease, which is also induced by As (Fig. 2.7). Intracellular arsenic bioaccumulation is not common in prokaryotes (Bazzi et al., 2020). However, it has been recently reported that As may be retained by the bacterial biofilm (Barral-Fraga et al., 2018; Mathivanan et al., 2021; Maity et al., 2022). In addition, some proteins like PilJ (BN5_0312),

RfbA (BN5_4136) and RfbC (BN5_4137), which are involved in biofilm formation (Kim and Wei, 2009; Li and Wang, 2011; Kuchma and O'Toole, 2022), were found up-regulated by arsenite in the proteomic analysis. Furthermore, it was observed that arsenic is being accumulated in biofilm with significantly higher amounts in the presence of cyanide, while intracellular concentration of this metalloid remains residual (Fig. 2.9).

In light of all the results presented in this Chapter I, the arsenic metabolism in *P. pseudoalcaligenes* CECT 5344 could be summarize as shown in the Figure 2.12. Arsenite induces the expression of the *ars* gene clusters 1 and 2, through ArsR. Arsenite may enter the cells through the aquaglyceroporins meanwhile arsenate uses the PstA phosphate permease, and then it is reduced to As(III) by the arsenate reductases ArsC1-C3. The main mechanism of arsenite tolerance is its extrusion through the ArsBA-type efflux pump. Formation of organoarsenical compounds also contributes to As detoxification. Methylated derivatives could be formed by methyltransferases that show partial similarity to bacterial ArsM proteins, and proteomic data suggest that THF metabolism may play a role in the methylation processes. Moreover, an arsenic-phosphoglycerate derivative may be formed by the arsenite-inducible glyceraldehyde-3-phosphate dehydrogenase GAPDH. Organoarsenicals could be extruded by ArsJ, Acr3 and ArsP permeases. Once outside, arsenic is retained and accumulated on the bacterial biofilm. Moreover, when cyanide is used as the nitrogen source, arsenite and cyanide could form Lewis adducts, which could be processed by ArsI. Additionally, the ArsH2 protein, which is induced by both arsenite and cyanide, could increase the tolerance to these compounds by protecting from oxidative stress caused by these toxics (Páez-Espino et al., 2020). Results derived from this work may contribute to the development of strategies for bioremediation of wastes, in which cyanide and arsenic are co-pollutants, by using the *P. pseudoalcaligenes* CECT 5344 strain.

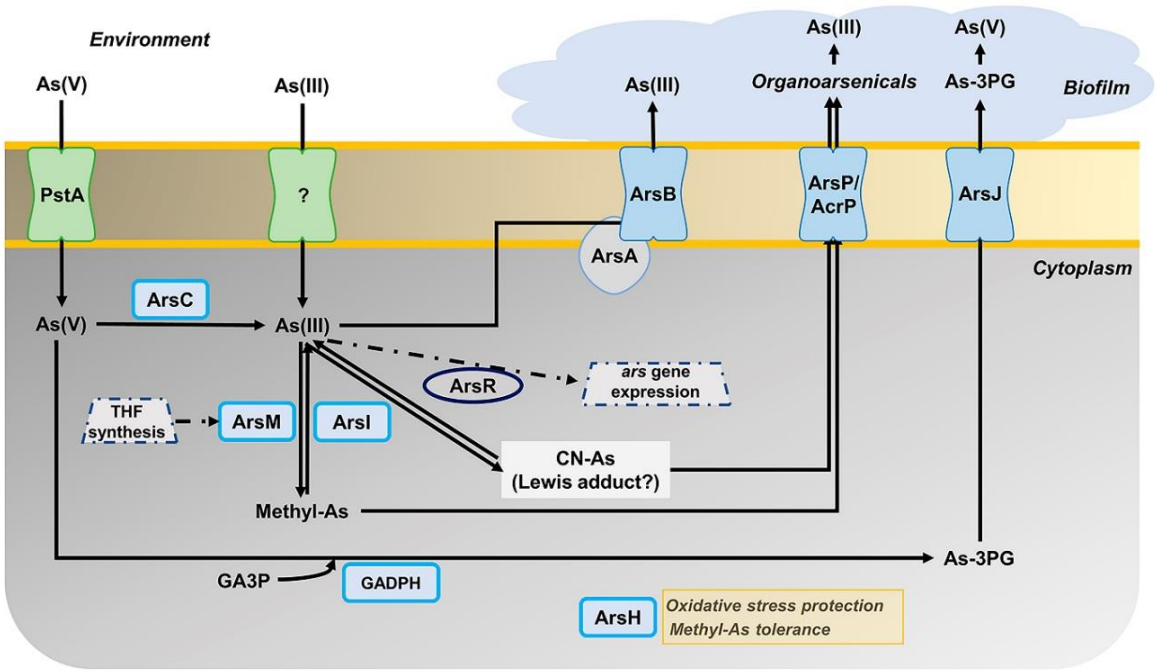

Figure 2.12. Overview of the arsenic metabolism in *P. pseudoalcaligenes* CECT 5344. The different proteins (encoded by the genes indicated in brackets) that are involved in the As tolerance of the strain CECT 5344 are: ArsC (BN5_1991; BN5_1993; BN5_2708); ArsR (BN5_1989; BN5_2707); ArsB (BN5_1992; BN5_2706); ArsA (BN5_2705); ArsI (BN5_1990); ArsH (BN5_1994; BN5_2709); glyceraldehyde-3-phosphate dehydrogenase GAPDH (BN5_2711); ArsJ (BN5_2712); ArsP (BN5_1279); Acr3 (BN5_2698); ArsM (BN5_1671; BN5_0407; BN5_4176); PstA (BN5_0117).

2.5. Conclusions

The main conclusions of this Chapter I are:

1. *Pseudomonas pseudoalcaligenes* CECT 5344 contains two main *ars* gene clusters that respond to arsenite, regardless of the nitrogen source used, although As-resistance response shows some differences between ammonium and cyanide. Therefore, *P. pseudoalcaligenes* CECT 5344 could be used for bioremediation of wastes from mining and other industries co-contaminated with cyanide and arsenic.

2. The main basis of As-resistance in this bacterium is the extrusion of As(III) through the ArsBA efflux pumps, or as organic derivatives exported through ArsP, Acr3 and ArsJ permeases. After extrusion of As(III) or organoarsenicals, As is accumulated in the bacterial biofilm, whose synthesis is enhanced in the presence of arsenite.

3. Production of arseno-phosphoglycerate by the As-inducible GAPDH enzyme, As methylation, THF metabolism, and perhaps formation of Lewis adducts in the presence of cyanide, seem to be also

relevant processes involved in As detoxification. The ArsH2 protein, which is induced regardless the nitrogen source, may protect from the oxidative stress caused by both arsenic and cyanide

3. Chapter II

Quantitative proteomic analysis of cyanide and mercury detoxification by *Pseudomonas pseudoalcaligenes* CECT 5344

Part of the results described in this Chapter have been published in the article:

Biełło, K.A.; Olaya-Abril, A.; Cabello, P., Rodríguez-Caballero, G.; Sáez, L.P.; Moreno-Vivián, C.; Luque-Almagro, V.M.; Roldán, M.D. Quantitative proteomic analysis of cyanide and mercury detoxification by *Pseudomonas pseudoalcaligenes* CECT 5344. *Microbiology Spectrum* (2023), *11*:e0055323. doi:10.1128/spectrum.00553-23.

3.1. Introduction

Currently, there are 95 countries involved in gold-mining activities, generating great amounts of industrial wastes that contribute to release a total mercury amount of over 1,000 tons per year (Suhadi et al., 2019). Almost 16 million of artisanal mines remain active, mainly in South America and Africa, despite general prohibition of their activity (Seccatore et al., 2014; Tulasi et al., 2021). In addition, cyanide is commonly used for gold extraction from mercury-rich tailings, which leads to the generation of residues where cyanide and mercury, among other metals, co-exist at high concentrations (Esdaile and Charker, 2018).

At laboratory scale, the treatment methods most extensively applied for mercury removal from polluted wastewaters are based on ion-exchange resin adsorption. However, they are not suitable for environmental conditions. Thus, the development of bacterial-based mercury detoxification is an advantageous technology due to its low cost, practicability and possibility to sequester Hg in diverse environments (Priyadarshanee et al., 2022). Bacterial strains from the *Pseudomonas* genus demonstrate great resistance to heavy metals, including mercury (Nascimento and Chartone-Souza, 2003). Up to date, several *Pseudomonas* species have been isolated and investigated to be applied to mercury removal from wastes (Giovanella et al., 2016; Yin et al., 2016; Neneng and Gunawan, 2018; Xue et al., 2022). However, a microorganism that is able to resist and detoxify two or more highly toxic pollutants in co-occurrence, such as cyanide and mercury, has not been described yet. Therefore, in this Chapter II, the molecular response to simultaneous toxicity of cyanide and mercury was characterized in *Pseudomonas pseudoalcaligenes* CECT 5344 thorough proteomic, *q*RT-PCR and bioinformatic approaches. Considering the already demonstrated great biotechnological potential of this strain CECT 5344 in bioremediation of cyanide-rich residues, the results obtained could be profitable to develop further treatment techniques for detoxification of industrial wastes co-contaminated with cyanide, mercury and arsenic.

3.2. Materials and methods

3.2.1. Culture media, bacterial growth conditions and mercury tolerance

P. pseudoalcaligenes CECT 5344 was cultured under aerobic conditions in M9 minimal media (pH adjusted to 9.5) at 30 °C as previously described (see Chapter I, Section 2.2.1). Sodium acetate was used as carbon source and 2 mM sodium cyanide or 2 mM ammonium chloride were used as sole nitrogen source. When applicable, mercury chloride was added to the M9 media, to achieve the indicated

concentration for each experiment. When required, agar-plates were also prepared as indicated previously (Chapter I, Section 2.2.1).

Bacterial growth was determined in liquid minimal media, per triplicate, by measuring the absorbance at 600 nm (A_{600}) in a spectrophotometer, or in agar-plates, by counting colony forming units (CFU) with the drop plate technique, per quintuplicate (Naghili et al., 2013). The tolerance of *P. pseudoalcaligenes* CECT 5344 to mercury was characterized by calculation of the minimum inhibitory concentration (MIC) and the minimum bactericidal concentration (MBC) (Andrews, 2001) with 2 mM ammonium or 2 mM cyanide as the nitrogen source in sterile U-shaped 96-well microtiter plates, in quintuplicate, as described in Chapter I, Section 2.2.5, but using increasing mercury concentrations (up to 500 µM). One column on each side of the plate was filled with sterile water to prevent evaporation and maintain humidity (Naghili et al., 2013). The effect of $HgCl_2$ on the cyanide tolerance was established by calculating the MIC and MBC values for cyanide (or ammonium as a control) with increasing concentrations of cyanide (from 0 to 100 mM) or ammonium (from 0 to 500 mM), with or without mercury (75 µM mercury for cyanide or 7.5 µM mercury for ammonium), and following the protocol previously described. Finally, the combined toxicity of mercury and arsenic was determined by simultaneously applying 5 µM mercury chloride and 200 µM arsenite with cyanide concentrations increasing up to 100 mM, and by following the protocol described above.

3.2.2. Analytical determinations

The precise methodology for each analytical determination method was described in details in the Chapter I, Section 2.2. Free cyanide in the media was measured colorimetrically in the presence of chloramine T, barbituric acid and pyridine reagents (Asmus and Garschagen, 1953). Extracellular ammonium concentration was determined colorimetrically using the Nessler reagent (Morrison, 1971). Protein concentration was quantified by the protein-Coomassie dye binding method (Bradford, 1976).

3.2.3. Determination of extra- and intra-cellular mercury concentration and biofilm quantification

The concentration of mercury in the culture media, or accumulated extracellularly (biosorption) or intracellularly (chelated to biomolecules), was determined by Inductively Coupled Plasma-Mass-Spectrometry ICP-MS (PerkinElmer, model Nexion 350X) at the Central Service for Research Support of the University of Córdoba (SCAI-UCO). Liquid cultures (100 mL) carried out in M9 minimal media with

75 µM $HgCl_2$ and 2 mM cyanide as the sole nitrogen source (CN+Hg) were centrifuged at 10,000 rpm for 10 min at 4 °C after 7.5 h of growth. Supernatants were used to determine extracellular mercury concentration. Cell pellets were washed with 1 mL of a solution containing 1 mL 20 mM Tris-HCl (pH 8) and 4 mM EDTA. To determine intracellular concentration of mercury, pellets were heated at 80 °C for 96 h and cell dry weight was determined, and then cells were digested in 69% HNO_3 (trace-metal grade, Fisher). Four biological samples were analyzed**.** Statistical significance was analyzed by applying a two-tailed *t*-test analysis corrected with the Benjamini-Hochberg method.

The effect of mercury on biofilm formation was determined as previously described (Chapter 1, Section 2.7.7), but growing *P. pseudoalcaligenes* CECT 5344 cells with 2 mM cyanide, in the absence (CN) or the presence of 75 µM $HgCl_2$ (CN+Hg).

3.2.4. Quantitative proteomic analysis

P. pseudoalcaligenes CECT 5344 cells were grown in M9 minimal medium under aerobic condition with 2 mM sodium cyanide as sole nitrogen source, without mercury chloride (condition CN) or with 75 µM mercury chloride (condition CN+Hg). Cells were harvested after 7.5 h growth, when they were actively growing and most of the cyanide was consumed. Samples for LC-MS/MS proteomic (data-independent acquisition) analysis were prepared as described previously (Chapter I, Section 2.2.10), and four independent replicates of each condition were performed. Protein concentration was estimated as previously (Bradford, 1976). In this case, the samples for proteomic analysis were provided to the Maimonides Institute for Biomedical Research of Córdoba (IMIBIC). Peptides were diluted using LC-MS grade water and 0.1% (v/v) formic acid to achieve a concentration of 10 ng/µL. A pool of samples was created by mixing the same volume of each sample. Peptides (200 ng) were loaded onto Evotips (Evosep, Odense, Demark), and Pierce™ Hela Tryptic Digest Standard (Thermo Fisher Scientific, Washington, DC, USA) was also prepared and loaded onto Evotips for quality control and system equilibration. Purified tryptic digests were separated by using the predefined 60 SPD method (21-min gradient time, 200 ng peptides) on an Evosep One LC system (Evosep, Odense, Demark) (Bache et al., 2018). A fused silica 10 µm ID emitter (Bruker Daltonics, Billerica, MA, USA) was placed inside a nanoelectrospray source (CaptiveSpray source, Bruker Daltonics, MA, USA). The emitter was connected to an 8 cm x 150 µm reverse phase column, packed with 1.5 µm C18 beads. The column was heated to 40 °C in an oven compartment. Mobile phases were water and acetonitrile, buffered with 0.1% formic acid (LC-MS grade, Fisher Scientific). Liquid chromatography was coupled online to a TIMS Q-TOFinstrument (timsTOF Pro, Bruker Daltonics, MA, USA) with data dependent acquisition-parallel

accumulation serial fragmentation (ddaPASEF) for HeLa Digest and pooled quality control (QC) analysis and data-independent acquisition-parallel accumulation serial fragmentation (dia-PASEF) for sample analysis through a CaptiveSpray nano-electrospray ion source (Meier et al., 2018, 2020). For both acquisition modes, the ion mobility dimension was calibrated with three Agilent ESI-L tuning mix ions (m/z, 1/K0: 622.0289 Th, 0.9848 Vs cm^{-2}; 922.0097 Th, 1.1895 Vs cm^{-2}; 1221.9906 Th, 1.3820 Vs cm^{-2}). The collision energy decreased linearly from 59 eV at 1/K0 = 1.6 Vs cm^{-2} to 20 eV at 1/K0 = 0.6 Vs cm^{-2}. To carry out the DDA-PASEF method, each top N acquisition cycle consisted of four PASEF MS/MS. The accumulation and ramp times were set to 100 ms. Singly charged precursors were excluded from fragmentation using a polygon filter in the (m/z, 1/K0) plane. All precursors that reached a target value of 20,000 were excluded for 0.4 min. Precursors were isolated using a Q window of 2 Th for m/z < 700 and 3 Th for m/z > 800. For DIA-PASEF, the 'long gradient' method (m/z range: 400-1200 Th, 1/K0 range: 0.6-1.6 Vs cm^{-2}, DIA-PASEF windows: 16 x 25 Th) was applied. The experiment was analyzed running first 10 QCs to condition the system and following the sequence HeLa-QC-10 samples analysis-HeLa-QC. The order of the samples was randomly defined. Data from the FASTA *P. pseudoalcaligenes* CECT 5344 strain (Uniprot, UP000032841) were used to build an in-silico library with DIA-NN 1.8 (https://github.com/vdemichev/DiaNN/releases/tag/1.8, accessed on 8 October 2021). The options 'FASTA digest for library-free search/library generation', 'Deep learning-based spectra', and 'RTs and IMs prediction' were enabled. Missed cleavages were set to 1, precursor change range 2-4, and precursor m/z range 100-1700, neural network classifier set to double-pass mode, quantification strategy was set to 'Any LC (high accuracy)', and match between runs (MBR) option was also enabled. MS1 and MS2 accuracy and retention time window scans were set to 0 to let DIA-NN to perform its automatic inference for the first run in the experiment. Following previously published recommendations (Rosenberger et al., 2017), DIA-NN output was filtered at precursor *q* value < 1% and global protein *q* value < 1%. FDR validation benchmark was filtered to include only unmodified peptides or peptides with carbamidomethylated cysteines, oxidated methionine, or excised N-terminal from methionine. The numbers of precursors/proteins were obtained based on filtering the library for precursors within charge range from 2 to 4 and mass range 100.0-1700.0 m/z. All other DIA-NN settings were left default, using RT-dependent cross-run normalization and filtering the output at 1% FDR. The number of threads used by DIA-NN was 52, as automatically suggested by the software. Finally, for DIA-PASEF analysis, spectral library generated in the previous step was added. MS1 and MS2 accuracy and retention time window scans were set to 0 to let DIA-NN to perform their automatic inference for the first run in the experiment. Protein inference in DIA-NN was configured to use the protein names from FASTA file (the same used for the generation of the spectral library) with enabled MBR. When reporting protein numbers and quantities, Protein.Group column in the DIA-NN report was used to identify the protein group, and PG-MaxLFQ was used to obtain the normalized quantity. Quantification

mode was set to 'Any LC (high accuracy)'. All other settings were set as described above for the generation of the spectral library. The analysis of the obtained data was performed by using available software Perseus (version 1.6.12.1) (https://maxquant.org/perseus/). The exploratory analysis was carried out including PCA analysis, and generation of heat-map and volcano plot, by using defaults parameters. Furthermore, the quantitative differential analysis was performed in order to identified proteins differentially expressed. Proteins identified from only one peptide and/or in only one replicate were discarded. Proteins identified in at least three replicates out of four, per each condition, were used for differential pairwise comparison analysis if they were positive after considering a two-way Student-test *t*-test with the Benjamini-Hochberg correction (Olaya-Abril et al., 2021). Proteins were considered differentially expressed when the fold change (FC) was ≥ 2, which is equal to $\log_2$ FC ≥ 1 (up-regulated by Hg), or FC ≤ 0.5, which is equal to $\log_2$ FC ≤ -1 (down-regulated by Hg), with a *p* value < 0.05. Furthermore, proteins which were identified in at least three out of four replicates out of one condition and undetectable in the other condition were considered as exclusive. The mass spectrometry data were deposited to the ProteomeXchange Consortium (http://proteomecentral.proteomexchange.org) with the dataset identifier PXD038659. GO analysis was performed using the ClueGo software on the Cytoscape platform (version 3.10.1) (https://cytoscape.org/). Integration of final proteomic data were performed by using the tool KEGG Mapper.

3.2.5. Quantitative real-time PCR analysis

P. pseudoalcaligenes CECT 5344 was cultured in M9 minimal media containing 50 mM sodium acetate as carbon source and 2 mM sodium cyanide as the sole nitrogen source, in the presence of 75 µM mercury chloride (CN+Hg) or without mercury (CN). As control, cells grown with 2 mM of ammonium chloride as the sole nitrogen source, with 7.5 µM mercury chloride (NH_4^++Hg) or without mercury (NH_4^+) were also collected. Cells were harvested by centrifugation (12,000 rpm, 10 min, 4 °C) before consumption of the N-source was completed to avoid a nitrogen starvation response. Thus, cells were collected after 7.5 h, when cyanide was used as nitrogen source (CN and CN+Hg) and after 30 min or 6 h, when ammonium was used as the sole nitrogen source NH_4^+ and NH_4^++Hg. Cells treatments, determination of the purity and concentration of RNA samples, synthesis of cDNA and PCR reactions were carried out as described in Chapter I, Section 2.2.11. The gene-specific primers were designed by using the Oligo 7.0 software (Supplementary Materials, Table S2). The obtained data were normalized to *dnaQ1* (BN5_2215) and the *dnaE* (BN5_2819) housekeeping genes. The relative fold gene expression

was calculated by the ΔΔCt method (Olaya-Abril et al., 2022) and data were analyzed by a *t*-test analysis with the Benjamini-Hochberg correction by using Perseus software (1.6.12.1).

3.2.6. Bioinformatic analysis of MerR binding sequences in the genome of *P. pseudoalcaligenes* CECT 5344

The identification of putative MerR binding boxes in the genome of *P. pseudoalcaligenes* CECT 5344 was performed by using the previously described pattern locator software, PatLoc (https://www.cmbl.uga.edu/software/patloc.html). The search was restricted to "intergenic" regions of the genome. The sequence 5'-(T/C)GTA(G/C)-N4-GTAC-3' previously described in *E. coli* (Brown et al., 2003) was used as the predicted MerR-binding box in the CECT 5344 strain.

3.3. Results

3.3.1. Mercury detoxification by *Pseudomonas pseudoalcaligenes* CECT 5433

P. pseudoalcaligenes CECT 5344 resistance towards mercury was firstly addressed by analyzing the sequenced genome of this strain. The presence of two *mer* gene clusters located in the *loci* BN5_3800-BN5_3802 (*merP1T1R5*) and BN5_4473-BN5_4479 (*merR6T3P3T5ADE*) was revealed (Fig. 3.1). These mercury resistance genes code for putative transcriptional regulators (two MerR proteins), a co-regulatory protein (MerD), mercuric transport proteins (three MerT proteins, two MerP proteins and MerE), and mercuric reductase (MerA). In both clusters the regulatory genes (*merR5* and *merR6*) are oriented divergently to the structural genes (Fig. 3.1). Additionally, other four *merR* genes (BN5_0701, BN5_2264, BN5_2322 and BN5_3351) encoding putative MerR transcriptional regulators were scattered throughout the genome of *P. pseudoalcaligenes*. The *merB* gene that codes for the organomercury lyase MerB was not detected in the genome of this bacterium.

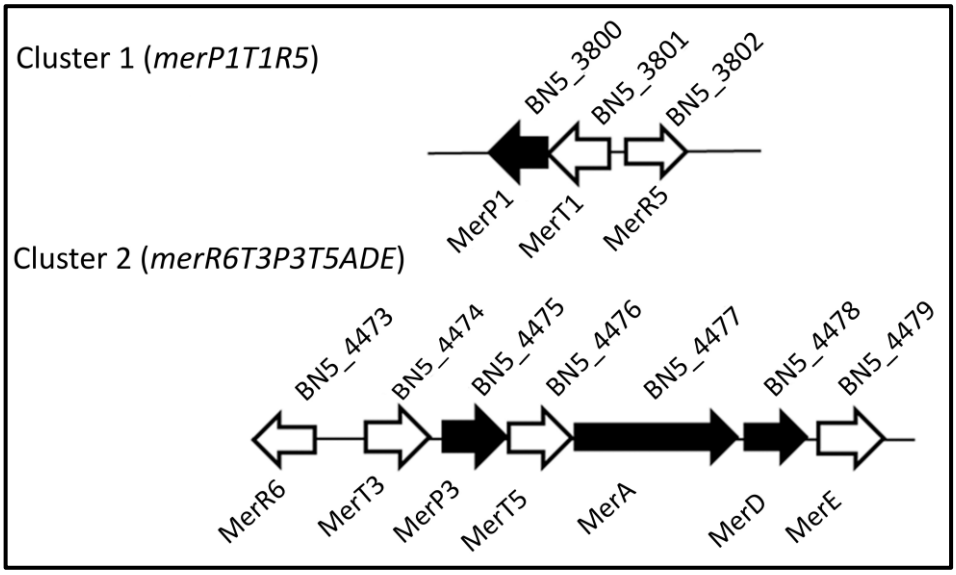

Figure 3.1. *P. pseudoalcaligenes* CECT 5344 gene clusters encoding putative Mer proteins related to mercury detoxification. Reference numbers correspond to UniProt annotation (UP000032841). Black genes code for proteins identified by LC-MS/MS proteomic analysis from cells grown in the presence of mercury chloride (see Section 3.3.3).

To evaluate the ability of the cyanide-degrading strain CECT 5344 to detoxify cyanide in the presence of mercury chloride, the minimum inhibitory concentration (MIC) and the minimum bactericidal concentration (MBC) were calculated in this bacterium. Cells were grown aerobically in M9 minimal media with 50 mM acetate as carbon source and 2 mM sodium cyanide or 2 mM ammonium chloride as the sole nitrogen source in the presence of increasing concentrations of mercury chloride, up to 500 µM. MIC and MBC values for Hg in the presence of cyanide were 200 µM and 300 µM respectively, while MIC and MBC values for Hg were considerably lower, 10 µM and 17.5 µM respectively, when ammonium was used as N-source. To characterize further the tolerance to mercury, growth curves of the CECT 5344 strain were carried out in M9 minimal media with different concentrations of mercury; 75, 100 and 150 µM with cyanide as N-source, or 7.5 and 10 µM in media with ammonium (Fig. 3.2). *P. pseudoalcaligenes* CECT 5344 was able to grow in the presence of 100 µM mercury, consuming cyanide from the extracellular medium, although this growth was slower than with 75 µM mercury. Accordingly, cyanide was totally removed from the medium after 12 h, in the presence of 75 µM mercury, but about 18 h were required for the complete consumption of cyanide in the presence of 100 mM mercury. Higher mercury concentrations, such as 150 mM, were required to severely impair bacterial growth and cyanide uptake (Fig. 3.2A). Therefore, to perform a proteomic analysis under cyanotrophic conditions, a concentration 75 µM mercury was used and cells were harvested after 7.5 h of growth. On the other hand, in the presence of ammonium, this bacterium was able to resist only 7.5 µM mercury, with a significant delay in growth and a slower ammonium

consumption in comparison with the control without mercury. In the presence of 10 µM mercury, the bacterial growth was significantly delayed and the nitrogen source was completely depleted later than in the control and in the presence of 7.5 µM mercury (Fig. 3.2B).

Additionally, the effect of mercury toxicity on the cyanide and ammonium assimilation in the CECT 5344 strain was also evaluated by determining the MIC and MBC values for these compounds. As indicated before, the MIC and MBC values for cyanide were 25 mM and 50 mM (see Chapter I, Section 2.3.2). However, the MIC and MBC values for cyanide in the presence of 7.5 µM mercury were 25 mM and 35 mM, respectively. Additionally, MIC and MBC determination assays for cyanide were performed in the presence of 5 µM mercury and 200 µM As(III). The MIC and MBC values for cyanide in the presence of both mercury and arsenite were 20 mM and 40 mM, respectively, thus suggesting that cyanide assimilation is not greatly affected by the simultaneous presence of both Hg(II) and As(III). On the other hand, both MIC and MBC values for ammonium were higher than 400 mM, meanwhile these values for ammonium strongly decreased to 10 mM and 20 mM, respectively, in the presence of 7.5 µM mercury. In addition, the MIC and MBC values for ammonium in the presence of 5 µM mercury and 200 µM As(III), were 20 mM and 30 mM, respectively.

Finally, the combined effect of both mercury and arsenite on bacterial growth was also characterized using different concentrations of both toxics, which were selected taking under consideration the results mentioned above and those previously presented in the Chapter I (Fig. 3.3). *P. pseudoalcaligenes* CECT 5344 was able to grow with 2 mM cyanide in the presence of 50 µM $HgCl_2$ and 200 µM As(III), and also with 75 µM $HgCl_2$ and 250 µM As(III). Although, cyanide consumption was delayed with respect to the control, in both cases cyanide was consumed at 15 hours of growth (Fig. 3.3A). On the other hand, the CECT 5344 strain cultured with 2 mM ammonium as the nitrogen source was able to resist up to 7.5 µM $HgCl_2$ and 250 µM As(III), nonetheless presenting significantly lower growth and ammonium consumption rates (Fig. 3.3B).

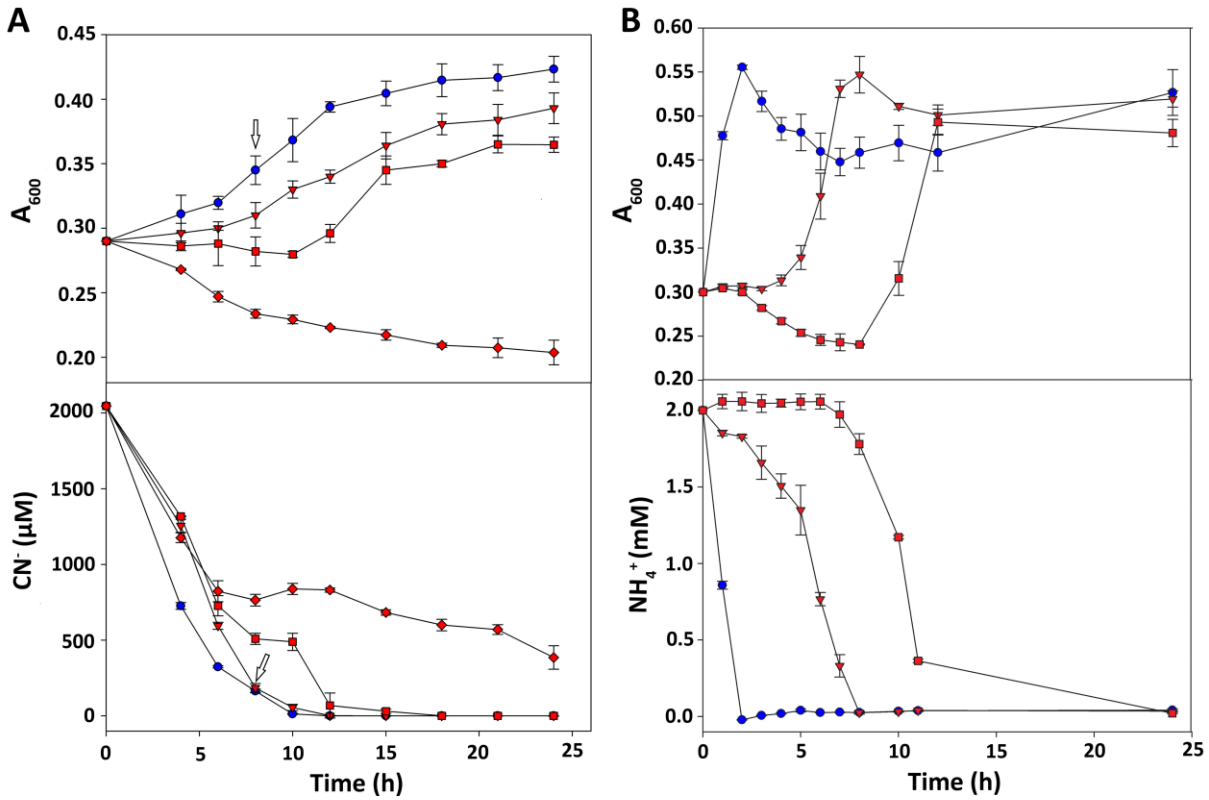

Figure 3.2. Physiological characterization of *P. pseudoalcaligenes* CECT 5344 cells grown with cyanide (A) and ammonium (B) as the sole nitrogen source in the presence or absence of mercury chloride. Cells were grown in M9 minimal medium with 50 mM sodium acetate and 2 mM sodium cyanide or 2 mM ammonium chloride as the carbon and nitrogen source, respectively. For proteomic analysis, the cells grown with cyanide were harvested after 7.5 h of growth (time indicated by arrows). Panel A represents growth (upper panel) and cyanide consumption (lower panel) of the CECT 5344 cells cultured in media without mercury (blue circles) or with mercury (red symbols): 75 µM (triangles), 100 µM (squares) and 150 µM (diamonds). Panel B represents growth (upper panel) and ammonium consumption (lower panel) in media without mercury (blue circles) or with mercury (red symbols): 7.5 µM (triangles) and 10 µM (squares).

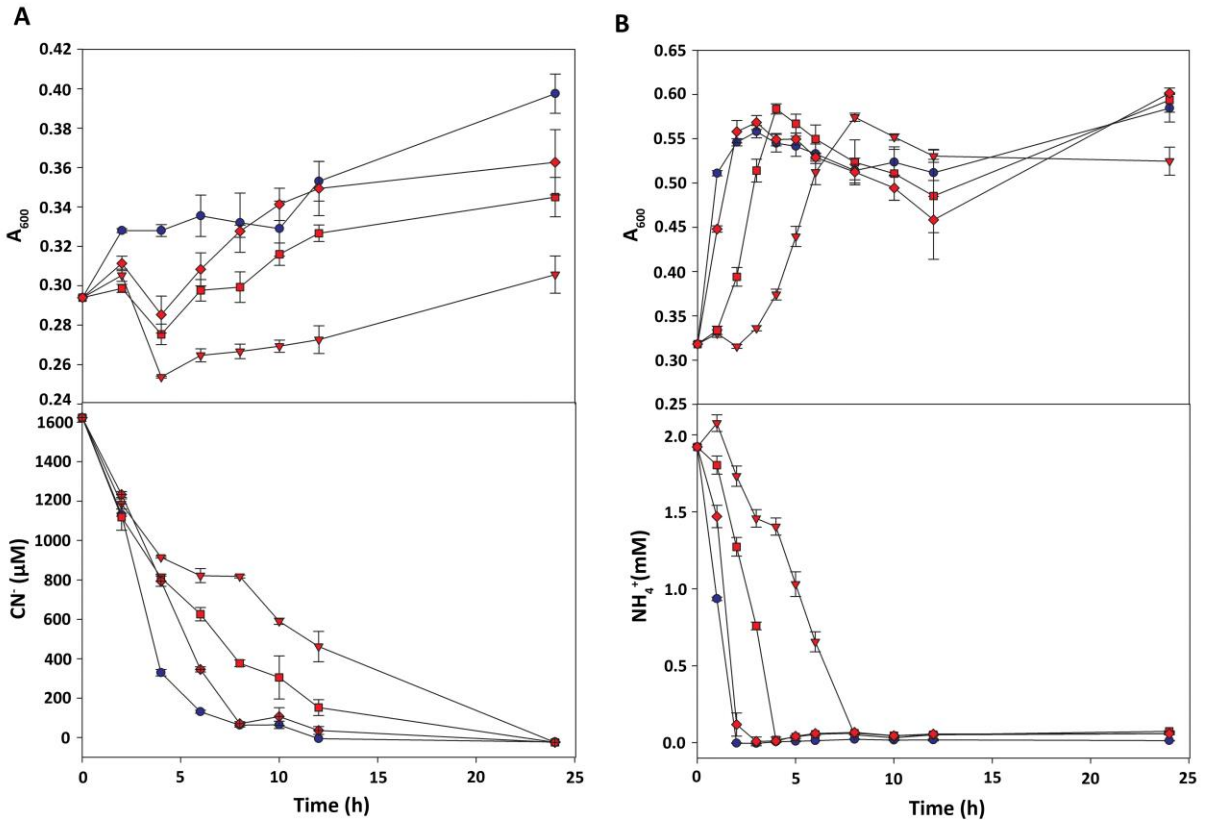

Figure 3.3. Physiological characterization of *P. pseudoalcaligenes* CECT 5344 cells grown with ammonium (A) and cyanide (B) as the sole nitrogen source in the presence or absence of mercury chloride and arsenite. Cells were grown in M9 minimal medium with 50 mM sodium acetate and 2 mM sodium cyanide or 2 mM ammonium chloride as the carbon and nitrogen sources, respectively. Panel A represents growth (upper panel) and cyanide consumption (lower panel) of the CECT 5344 cells cultured in media without mercury and arsenite (blue circles) or with the following concentrations of mercury and arsenite (red symbols): 25 μM $HgCl_2$ and 150 μM As(III) (diamonds), 50 μM $HgCl_2$ and 200 μM As(III) (squares) and 75 μM $HgCl_2$ and 250 μM As(III) (triangles). Panel B represents growth (upper panel) and ammonium consumption (lower panel) in media without mercury and arsenite (blue circles) or with the following concentration of mercury and arsenite (red symbols): 2.5 μM $HgCl_2$ and 150 μM As(III) (diamonds), 5 μM $HgCl_2$ and 200 μM As(III) (squares) and 7.5 μM $HgCl_2$ and 250 μM As(III) (triangles).

3.3.2. Evaluation of the accumulation of mercury in biofilm

The concentration of mercury remaining in the extracellular media, or bioaccumulated extracellularly (biosorption) and intracellularly (chelated to biomolecules), was determined by ICP-MS from *P. pseudoalcaligenes* CECT 5344 cultures after 7.5 h of growth in media with 2 mM NaCN and 75 μM $HgCl_2$, as described in the Section 3.2.3 of this Chapter II. Mercury was neither detected in the extracellular media nor bioaccumulated extracellularly, while the intracellular concentration of mercury was 0.010 ± 0.003 μg/mg protein.

3.3.3. Proteomic analysis of *P. pseudoalcaligenes* CECT 5344 grown with mercury under cyanotrophic conditions

The global changes in the proteome of the strain CECT 5344 in response to mercury, when the cells were grown with cyanide as the sole nitrogen source, were investigated by performing a proteomic analysis by Liquid Chromatography-Mass Spectrometry/Mass Spectrometry (LC-MS/MS). Cells grown under aerobic cyanotrophic conditions (2 mM sodium cyanide as the sole nitrogen source) in absence (CN) or presence of 75 µM $HgCl_2$ (CN+Hg) were harvested after 7.5 h, when they were actively growing and low concentrations of cyanide remained in the media (Fig. 3.2A). Four independent biological replicates were used in this study, and the principal component analysis (PCA), clustering of the replicates, and volcano plot were performed (Fig. 3.4). The preliminary qualitative analysis revealed that the overall number of identified proteins (2689) represented about 60% of the total predicted proteins (4435) encoded by the genome of the CECT 5344 strain (Wibberg et al., 2016).

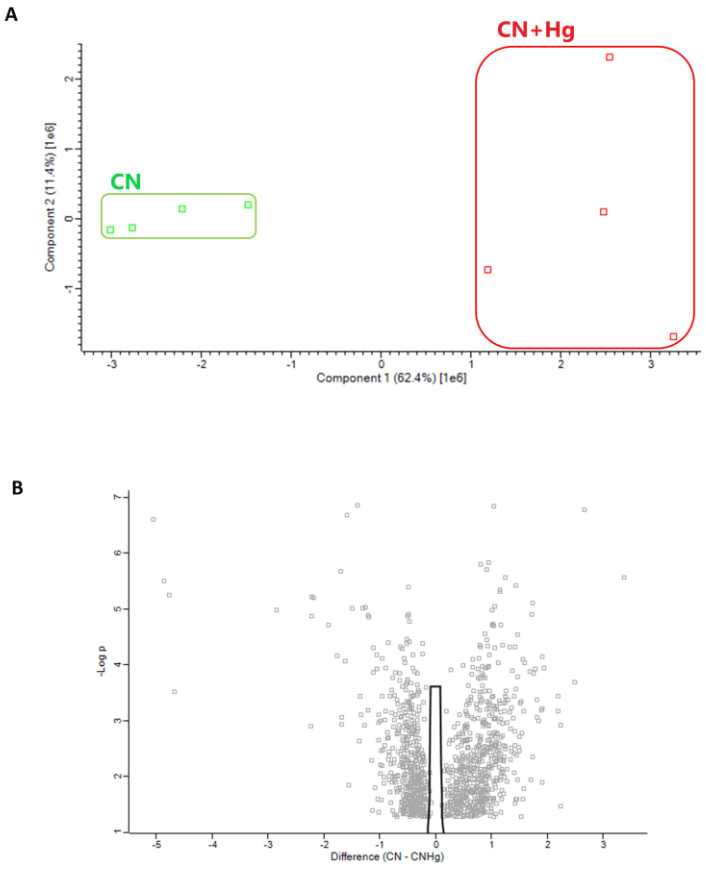

Figure 3.4. Principal component analysis (A) and volcano plot (B) of the *P. pseudoalcaligenes* CECT5344 proteomic analysis. Green color corresponds to samples with cyanide as N-source without mercury (CN), while red color represents samples with cyanide and mercury (CN+Hg).

The differential quantitative analysis was performed by comparison of the CN+Hg *vs* CN proteomes (see the Supplementary Materials available online in the reference Biełło et al., 2023b). In this analysis, the fold change (FC) parameter was applied to measure differences in protein expression, being calculated as the ratio of normalized peptide intensities CN+Hg/CN. Therefore, proteins shared by both CN+Hg and CN proteomes, but nevertheless differentially expressed, were considered 'over-represented' (up-regulated) in the CN+Hg proteome when the $\log_2$ FC was ≥ 1 (FC ≥ 2) or 'down-represented' (down-regulated) in the CN+Hg proteome when the $\log_2$ FC was ≤ -1 (FC ≤ 0.5). Proteins that were found only in one proteome (CN+Hg or CN) were considered 'exclusive' of that condition. In this quantitative analysis, 21 proteins were exclusive of the CN+Hg proteome and 209 proteins were found differentially expressed, of which 45 proteins were up-regulated and 164 proteins were down-regulated in the presence of mercury (Fig. 3.5).

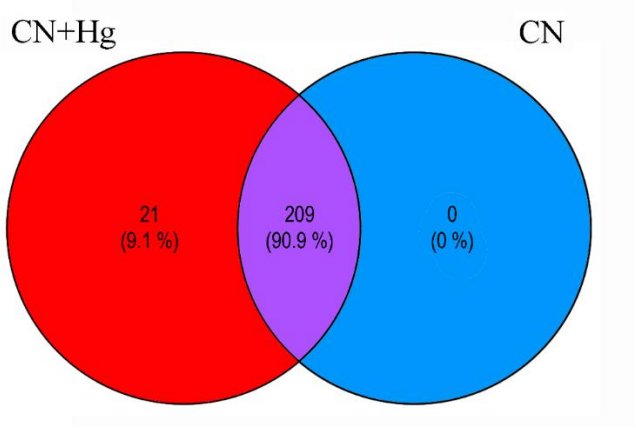

Figure 3.5. Venn diagram of identified proteins in the differential proteomic analysis of *P. pseudoalcaligenes* CECT 5344 cells grown with cyanide as N-source with or without 75 µM mercury. Red color, proteins exclusively found in the CN+Hg proteome; blue color, proteins exclusively found in the CN conditions; purple color, proteins shared between these two conditions, but differentially expressed.

The gene ontology (GO) analysis using the comparative study between the proteomes CN and CN+Hg revealed insight into functional protein categories that were affected by the presence of mercury under cyanotrophic conditions (Fig. 3.6). Proteins over-represented in the control without mercury (or down-represented in the presence of mercury) belonged mainly to the GO category 'urea metabolism' (not shown), while proteins over-represented in the presence of mercury (or down-represented without mercury) belonged to the GO groups 'response to metal ion', 'response to toxic substance', 'response to mercury ion', 'detoxification of mercury ion', 'detoxification of inorganic compound', and 'oxidoreductase activity, acting on the CH-NH_2 group of donors', among others (Fig. 3.6).

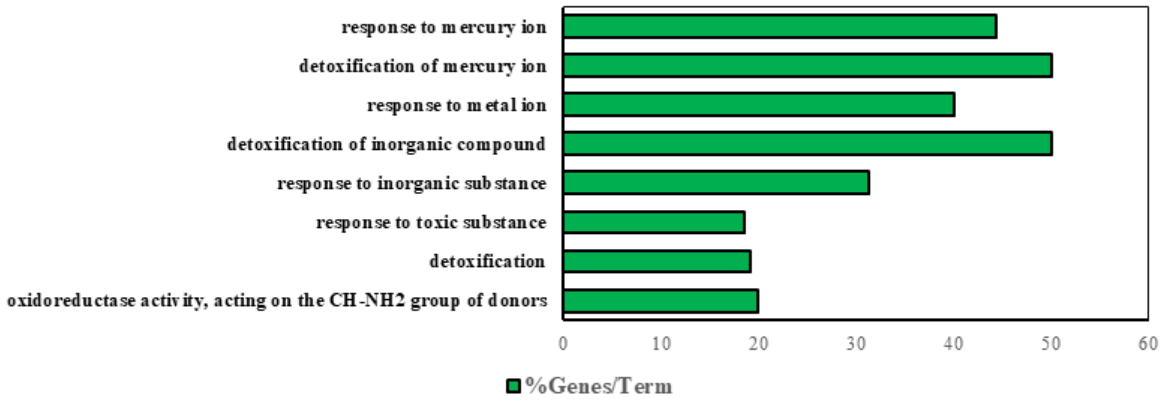

Figure 3.6. GO enrichment analysis among proteins induced in the presence mercury. Enrichment is shown as % genes/GO term.

Interestingly, the proteins encoded by the *nit1C* and *cio* gene clusters, which are essential for cyanide assimilation and cyanide-insensitive respiration, respectively, were detected in both CN and CN+Hg conditions, and were not affected significantly by the presence of mercury (Fig. 3.7). However, cyanase and other proteins involved in cyanate assimilation, which are encoded by the *cynABDS* gene cluster, were down-regulated by mercury (Fig. 3.8.). Other proteins identified in the quantitative analysis were classified functionally and grouped into carbohydrate and energy metabolism, nucleotide metabolism, amino acid metabolism, metabolism of cofactors and vitamins, transporters, regulators, mercury and arsenic resistance, and other proteins (Fig. 3.8). Proteins exclusively found in the proteome from *P. pseudoalcaligenes* cells grown in CN+Hg included the hemin import ATP-binding HmuV protein (W6QZG3 protein/BN5_0959 gene), a thioesterase (W6QVD5/BN5_2259), the cobalamin-independent methionine synthase MetE (W6QZ36/BN5_2694), and the aliphatic sulfonate transport components SsuC (W6R0T9/BN5_4161) and SsuB (W6RLD8/BN5_4160), among others (Fig. 3.8). Additionally, some proteins over-represented in the CN+Hg proteome were mercuric (II) reductase MerA (W6R9E5/BN5_4477), periplasmic mercury ion-binding proteins MerP1 (W6R0W8/BN5_3800) and MerP3 (W6RM71/BN5_4475), arsenical resistance protein ArsH2 (W6QZ50/BN5_2709), arsenate reductase ArsC3 (W6QXT2/BN5_2708), phosphorus metabolism related protein PhoH (W6RJF8/BN5_3397), alkanesulfonate monooxygenase SsuD (W6R8H1/BN5_4162), sulfate-binding protein (W6R1W0/BN5_4183), cysteine desulfurase IscS (W6RJ61/BN5_3268), thioredoxin reductase (W6QYN2/BN5_3403), glutathione *S*-transferase (W6R3L0/BN5_2412), dihydropyrimidine dehydrogenase (W6QQZ8/BN5_0328), dihydropyrimidinase (W6RAR6/BN5_0330), uracil-xanthine permease (W6RJI7/BN5_3437), ribonucleoside-diphosphate reductase subunits (W6QTT2/BN5_1291 and W6R0E8/BN5_1290), alanine racemase (W6QPB8/BN5_0166), β-alanine-pyruvate transaminase (W6QZ51/BN5_0842), precorrin-2 C20-methyltransferase (W6R2H6/BN5_4378), D-amino acid dehydrogenase (W6QS35/BN5_0164), and antioxidant alkyl hydroperoxide reductase AhpC

(W6RLE3/BN5_4165). Additionally, transcriptional regulators that were exclusive or over-represented in the CN+Hg proteome were the MerR-family transcriptional regulator MerD (W6R2U3/BN5_4478), the ArsR2 protein (W6R4K3/BN5_2707), the AraC protein (W6QY08/BN5_2307), the RegB protein (W6QQY1/BN5_0721), and transcriptional regulators of the GntR (W6QWV0/BN5_2413) and MarR families (W6QY91/BN5_2414) (Fig. 3.8).

Protein ID[1]	Gene ID[2]	Protein description/name	CN	CN+Hg
		nit gene cluster		
H9N5E0	BN5_1630	Sigma-54-dependent transcriptional regulator (NitA)		
H9N5E2	BN5_1631	Uncharacterized protein (NitB)		
H9N5E1	BN5_1632	Nitrilase (NitC)		
H9N5E3	BN5_1633	Radical SAM domain-containing protein (NitD)		
H9N5E4	BN5_1634	GCN5-related *N*-acetyltransferase (NitE)		
H9N5E5	BN5_1635	AIR synthase-like protein (NitF)		
H9N5D9	BN5_1636	Uncharacterized protein (NitG)		
H9N5D8	BN5_1637	FAD-dependent oxidoreductase (NitH)		
		cio gene cluster		
W6QWX1	BN5_1899	GntR family transcriptional regulator (MocR)		
W6RF17	BN5_1900	Sulfite reductase (NADPH) hemoprotein beta-component (CysL3)		
W6QU90	BN5_1901	Uncharacterized protein (CioC3)		
W6R254	BN5_1902	Terminal oxidase subunit I (CioA3)		
W6QVH5	BN5_1903	Cytochrome *d* ubiquinol oxidase, subunit II (CioB3)		
W6QWX6	BN5_1904	Phosphoserine aminotransferase (SerC3)		
W6RF21	BN5_1905	Histidinol-phosphate aminotransferase (HisC3)		
W6QU95	BN5_1906	Acetylornithine aminotransferase (ArgD3)		
W6R260	BN5_1907	4-hydroxy-tetrahydrodipicolinate synthase (DapA1)		
W6QVI0	BN5_1908	High-affinity glucose transporter		
W6QWY1	BN5_1909	Methylenetetrahydrofolate reductase (MetF3)		
W6RF25	BN5_1910	Cysteine synthase (CysM3)		
W6QUA1	BN5_1911	NADP-dependent malic enzyme (MaeB3)		
W6R265	BN5_1912	Nitrilase (Nit4)		
		Other nitrilases genes		
W6RF39	BN5_1925	Aliphatic nitrilase (Nit1)		
W6R989	BN5_4427	Bifunctional nitrilase/nitrile hydratase NIT4B (Nit2)		
		C-N hydrolases genes		
W6QQS6	BN5_0258	C-N hydrolase, nitrilase/cyanide hydratase (AguB)		
W6QQZ6	BN5_0736	C-N hydrolase, nitrilase/cyanide hydratase (Nit1B)		
W6QUY5	BN5_1196	Nitrilase homolog 1 (Nit1A)		
W6QZ84	BN5_2750	Hydrolase, carbon-nitrogen family		
W6QY63	BN5_3204	Formamidase (AmiF)		
W6QZD7	BN5_3251	C-N hydrolase, nitrilase/cyanide hydratase (Nit3B)		

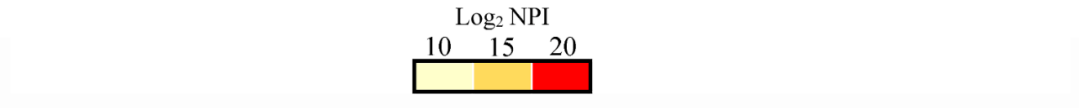

Figure 3.7. Effect of mercury on proteins involved in cyanide detoxification/assimilation by *P. pseudoalcaligenes* CECT 5344. Data are shown as heatmap of Log_2 of normalized peptide intensity (Log_2 NPI). CN, cyanide-containing media without added mercury; CN+Hg, cyanide-containing media with 75 µM $HgCl_2$. (1) Protein code according to Uniprot database under the accession number UP000032841. (2) Genes annotation from GeneBank (accession HG916826).

On the other hand, proteins that were down-represented in the CN+Hg proteome were thioredoxin (W6QS83/BN5_0229), thiol-disulfide isomerase/thioredoxin (W6R248/BN5_1897), glutaredoxin (W6RM46/BN5_4445), glutathione peroxidase (W6R1A5/BN5_1595), ring-cleaving dioxygenase (W6RFG7/BN5_2062), quercetin 2,3-dioxygenase (W6QXS7/BN5_3119), cytochrome c_{550} (W6R3F4/BN5_2347), cytochrome *c* (W6RAS2/ BN5_0335), bacterioferritin (W6RCV7/BN5_1112), cytochrome *c* oxidase-subunit 2 (W6QRT0/BN5_0092), superoxide dismutase SodC (W6RIH7/BN5_3015), DNA-binding protein HU (W6QWH2/BN5_1752), TusC protein (W6QWV6/BN5_1882), translation initiation factor IF-1 (W6REZ4/BN5_1868), ribosome-binding factor A (W6QU93/BN5_0931), and ribosome-recycling factor RRF (W6R4U4/BN5_2831) (Fig. 3.8).

Protein ID[1]	Gene ID[2]	Protein description/name	FC[3]
Carbohydrate and energy metabolism			
W6QRT0	BN5_0092	Cytochrome *c* oxidase subunit 2 (CoxB)	
W6QST4	BN5_0439	ABC-type transporter periplasmic component protein (CynA)	
W6RB18	BN5_0440	ABC transporter inner membrane subunit protein (CynB)	
W6QQ36	BN5_0441	ABC transporter/ATPase component protein (CynD)	
W6QY14	BN5_0442	Cyanase (CynS)	
W6QZN2	BN5_1039	2-isopropylmalate synthase (LeuA)	
W6QTU1	BN5_1301	6-phosphogluconolactonase (Pgl)	
W6QV86	BN5_1302	2-dehydro-3-deoxyphosphogluconate aldolase (Eda)	
W6R1N1	BN5_1685	UDP-*N*-acetylglucosamine 2-epimerase (WecB)	
W6QWV3	BN5_2780	Periplasmic nitrate reductase (NapB)	
W6QY63	BN5_3204	Formamidase (AmiF)	
W6QYN2	BN5_3403	Thioredoxin reductase	
W6RLD8	BN5_4160	Aliphatic sulfonates import ATP-binding protein (SsuB)	
W6R0T9	BN5_4161	Putative aliphatic sulfonates transport permease protein (SsuC3)	
W6R8H1	BN5_4162	Alkanesulfonate monooxygenase (SsuD)	
W6R1W0	BN5_4183	Sulfate-binding protein (CysP3)	
Amino acid metabolism			
W6QS35	BN5_0164	D-amino acid dehydrogenase (DadA3)	
W6QPB8	BN5_0166	Alanine racemase (DadX)	
W6QYG3	BN5_0579	Urease subunit beta (UreB)	
W6QT84	BN5_0581	Urease subunit gamma (UreA)	
W6QZ51	BN5_0842	Beta-alanine-pyruvate transaminase	
W6R1A5	BN5_1595	Glutathione peroxidase	
W6RE84	BN5_1603	Glutamate dehydrogenase	
W6QVQ2	BN5_2381	*N*-(5'-phosphoribosyl)anthranilate isomerase (TrpF)	
W6R3L0	BN5_2412	Glutathione S-transferase family protein	
W6QWV0	BN5_2413	GntR family transcriptional regulator	
W6QZ36	BN5_2694	Cobalamin-independent methionine synthase (MetE)	
Nucleotide metabolism			
W6QQZ8	BN5_0328	Dihydropyrimidine dehydrogenase (PydA)	
W6RAR6	BN5_0330	Dihydropyrimidinase (HydA)	
W6R0E8	BN5_1290	Ribonucleoside-diphosphate reductase subunit beta (NrdB)	
W6QTT2	BN5_1291	Ribonucleoside-diphosphate reductase (NrdA)	
W6QYA3	BN5_2424	Orotidine 5'-phosphate decarboxylase (PyrF)	
Metabolism of cofactors and vitamins			
W6RCV7	BN5_1112	Bacterioferritin (Bfr2)	
W6RI94	BN5_2964	Isochorismatase hydrolase	
W6RJ61	BN5_3268	Cysteine desulfurase (IscS)	
W6R2H6	BN5_4378	Precorrin-2 C20-methyltransferase (CobI)	

Protein ID[(1)]	Gene ID[(2)]	Protein description/name	FC[(3)]
Transporters			
W6QQ87	BN5_0036	Substrate-binding region of ABC-type glycine betaine transport system (ProX1)	
W6QQ99	BN5_0056	TRAP dicarboxylate transporter-DctP subunit	
W6QSM0	BN5_0374	Substrate-binding region of ABC-type glycine betaine transport system (ProX3)	
W6QQH3	BN5_0593	ABC-type branched-chain amino acid transport systems (UrtA)	
W6QZG3	BN5_0959	Hemin import ATP-binding protein (HmuV)	
W6QUE9	BN5_1006	Putative amino-acid ABC transporter-binding protein (AapJ)	
W6QYJ4	BN5_2987	Branched-chain amino acid transport system substrate-binding protein (LivK)	
W6RJI7	BN5_3437	Uracil-xanthine permease	
Regulators			
W6RAQ0	BN5_0310	Response regulator receiver protein (PilH)	
W6QQY1	BN5_0721	Sensor histidine kinase (RegB)	
W6QY08	BN5_2307	AraC-family regulatory protein	
W6QY91	BN5_2414	MarR family transcriptional reglator	
Mercury and arsenic resitance			
W6R4K3	BN5_2707	ArsR family transcriptional regulator (ArsR2)	
W6QXT2	BN5_2708	Arsenate reductase (ArsC3)	
W6QZ50	BN5_2709	Arsenical resistance protein (ArsH2)	
W6R0W8	BN5_3800	Periplasmic mercury ion-binding protein (MerP1)	
W6RM71	BN5_4475	Periplasmic mercury ion-binding protein (MerP3)	
W6R9E5	BN5_4477	Mercuric reductase (MerA)	
W6R2U3	BN5_4478	Mer family transcriptional regulator (MerD)	
Other proteins			
W6QPA6	BN5_0150	Cytochrome C6 (CccA)	
W6QS83	BN5_0229	Thioredoxin (TrxA)	
W6QSQ4	BN5_0409	Poly(Hydroxyalkanoate) granule-associated protein (Phasin)	
W6QZS8	BN5_1079	Thiol:disulfide interchange protein (DsbC)	
W6R248	BN5_1897	Thiol-disulfide isomerase and thioredoxins protein	
W6QXU7	BN5_2242	Rhodanese domain-containing protein	
W6QVD5	BN5_2259	Thioesterase superfamily protein	
W6RIH7	BN5_3015	Superoxide dismutase (SodC)	
W6RLE3	BN5_4165	Antioxidant, AhpC/Tsa family (AhpC3)	
W6RM46	BN5_4445	Glutaredoxin 3	

Figure 3.8. Heatmap of *P. pseudoalcaligenes* CECT 5344 proteins affected by mercury under cyanotrophic conditions. The differential expression of proteins is represented as Log_2 fold change (FC). The fold change has been calculated as the ratio normalized peptide intensity in CN+Hg/normalized peptide intensity in CN. (1) Protein code according to Uniprot database under the accession number UP000032841. (2) Genes annotation from GeneBank (accession HG916826.1).

3.3.4. Bioinformatic analyses of MerR regulators

The analysis of *P. pseudoalcaligenes* CECT 5344 genome revealed the presence of six genes that could encode putative MerR-type transcriptional regulators: MerR1 (BN5_0701 gene/W6QQW2 protein), MerR2 (BN5_2264/W6QVE0), MerR3 (BN5_2322/W6QWL9), MerR4 (BN5_3351/W6R6A1), MerR5 (BN5_3802/W6RKL7) and MerR6 (BN5_4473/W6R2T8). BLASTP sequence comparisons of these six regulators revealed that MerR5 and MerR6 were homologs, displaying 50% identity. MerR2 showed

only 33% and 34% identity with MerR1 and MerR6, respectively, and MerR5 presented 36% identity when compared to MerR1. Other comparisons yielded less than 30% identity (Table 3.1).

Table 3.1. Sequence comparisons (% identity) of the *P. pseudoalcaligenes* CECT 5344 MerR transcriptional regulators.

% Identity	MerR1	MerR2	MerR3	MerR4	MerR5	MerR6
MerR1	100.0	33.3	-	-	36.5	28.9
MerR2		100.0	-	-	29.9	34.3
MerR3			100.0	24.4	28.0	-
MerR4				100.0	29.5	26.5
MerR5					100.0	50.0
MerR6						100.0

In order to identify MerR orthologs in bacteria and archaea, a bioinformatic analysis by using KEGG database was performed. It was demonstrated that MerR-type transcriptional regulators are widely distributed among proteobacteria and other bacteria, without relevant differences in their distribution within the different phyla. Among previously described six MerR-type regulators of *P. pseudoalcaligenes* CECT 5344, MerR1 was the closest relative to MerR2 in the phylogenetic tree. Curiously, the transcriptional regulator MerR2 was also very close, in evolutive distance, to those found in archaea and thermophilic bacteria (Fig. 3.9). In addition, the regulator pairs MerR5 and MerR6, and MerR3 and MerR4, were more similar to each other (Fig. 3.9).

To identify putative MerR binding boxes in the promoter gene regions of *P. pseudoalcaligenes* CECT 5344, an additional bioinformatic analysis was carried out, using the MerR2 binding sequence previously described in *Escherichia coli* (Brown et al., 2003). Hence, the predicted MerR2 binding sequence 5'-(T/C)GTA(G/C)-N4-GTAC-3' was identified in the CECT 5433 strain. This sequence was found in the promoters of several regulatory genes, including those involved in mercuric resistance, *merR5* (BN5_3802) and *merR6* (BN5_4473), in arsenic resistance, *arsR* (BN5_0252), and in phosphate metabolism, *phoR* (BN5_4234). This putative MerR2 binding site was also present in the promoters of structural genes for metal resistance *cpxP* (BN5_2475), ribonucleoside-diphosphate reductase/β-subunit *nrdB* (BN5_1290), dithiol oxidoreductase/disulfide-forming *dsbA* (BN5_0108), glutathione *S*-transferases *yghU* (BN5_2864) and *fosA* (BN5_3450), 3-octaprenyl-4-hydroxybenzoate carboxy-lyase *ubiD* (BN5_0231), and amino acid/peptide exporter *virD* (BN5_3536).

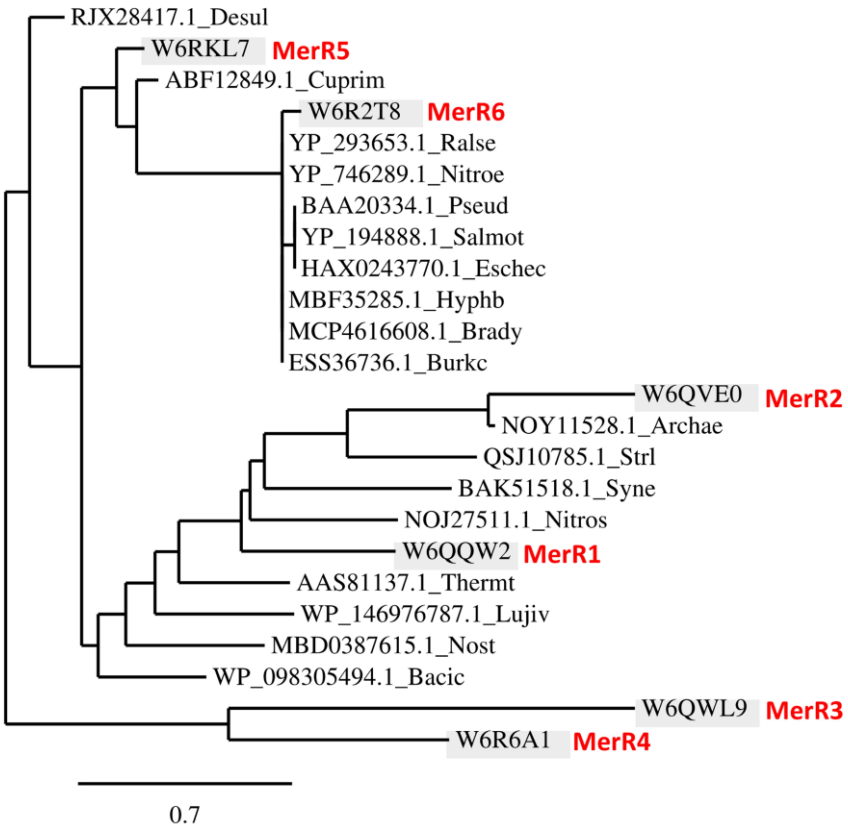

Figure 3.9. Phylogenetic distribution of MerR proteins in bacteria and archaea. Tree was constructed using the Phylogeny.fr platform (Dereeper et al., 2008). Sequences were aligned with MUSCLE v3.8.31 with default settings. Ambiguous regions were removed with Gblocks v0.91b. The phylogenetic tree was reconstructed using the maximum likelihood method implemented in the PhyML program 3.1/3.0 aLRT. Graphical representation and edition of the phylogenetic tree were performed with TreeDyn v198.3. The *P. pseudoalcaligenes* CECT 5344 MerR sequences are highlighted in red color. Protein name (protein/gene IDs): MerR1 (W6QQW2/BN5_0701), MerR2 (W6QVE0/BN5_2264), MerR3 (W6QWL9/BN5_2322), MerR4 (W6R6A1/BN5_3351), MerR5 (W6RKL7/BN5_3802) and MerR6 (W6R2T8/BN5_4473). Protein sequences correspond to the following phyla and organisms: α-proteobacteria (Hyphb, *Hyphomonadaceae bacterium*; Brady, *Bradyrhizobium* sp.), β-proteobacteria (Burkc, *Burkholderia cenocepacia* KC-01; Nitroe, *Nitrosomonas eutropha* C91; Ralse, *Ralstonia eutropha* JMP134; Cuprim, *Cupriavidus metallidurans* CH34), δ-proteobacteria (Desul, *Desulfarculus* sp.; Lujiv, *Lujinxingia vulgaris*), γ-proteobacteria (Pseud, *Pseudomonas* sp. K-62), enterobacteria (Salmot, *Salmonella enteria* subsp. enterica serovar *Thyphimurium*; Eschec, *Escherichia coli* JJ1897), firmicutes (Bacic, *Bacillus cereus*), actinobacteria (Strl, *Streptomyces lividans*), cyanobacteria (Syne, *Synechocystis* sp. PCC 6803; Nost, *Nostoc* sp. C3-bin3), *Deinococcus-Thermus* (Thermt, *Thermus thermophilus* HB27), and archaea (Nitros, *Nitrososphaera* sp.; Archae, *Archaeoglobi archaeon*).

3.3.5. Quantitative transcriptional analysis by *q*RT-PCR

In order to study the transcriptional expression of several genes that were found over- or down-represented in the previously described proteomic analysis, a quantitative transcriptional analysis by *q*RT-PCR was performed using cells grown with 2 mM sodium cyanide as sole nitrogen source in the presence or absence of 75 µM mercury chloride. The structural genes belonging to the two *mer* clusters of the CECT 5344 strain were highly induced in the presence of mercury, although transcriptional

expression of the *merP1* and *merT1* genes, which are located in the *merP1T1R5* gene cluster, was higher than that displayed by the structural genes of the *merR6T3P3T5ADE* gene cluster (Fig. 3.10A).

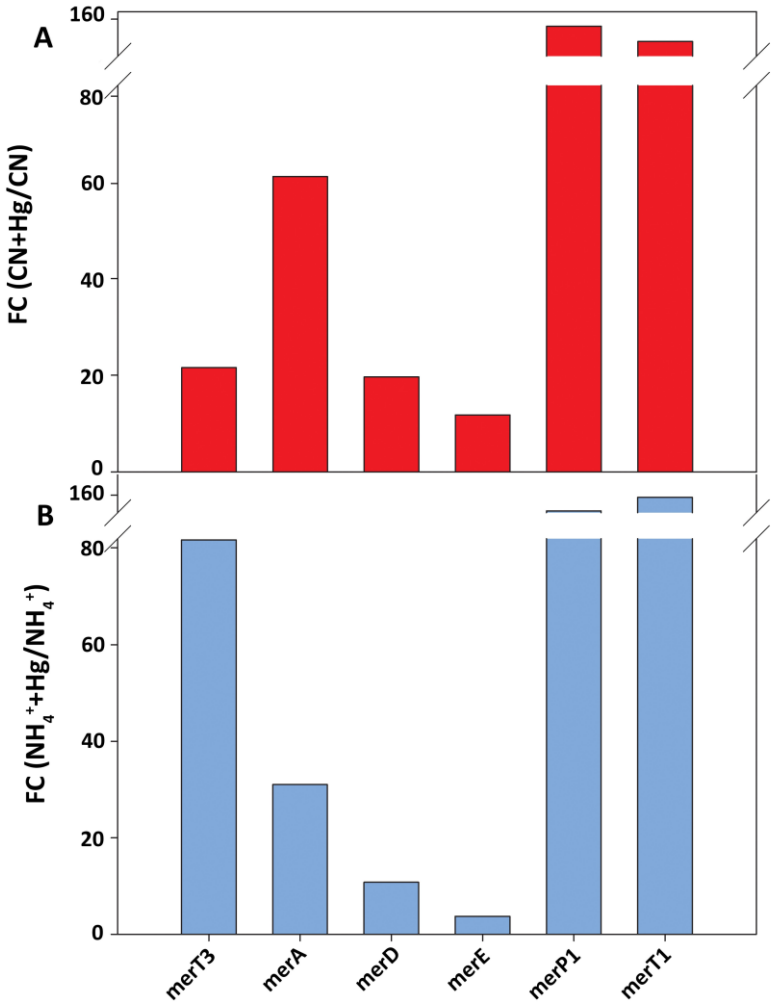

Figure 3.10. Transcriptional expression analysis by *q*RT-PCR of the *P. pseudoalcaligenes* CECT 5344 *mer* structural genes. Cells were grown with 2 mM sodium cyanide without or with 75 µM $HgCl_2$ (A) or 2 mM ammonium chloride, without or with 7.5 µM $HgCl_2$ (B). The differential gene expression is represented as fold change (FC) of the relative gene expression ratio (CN+Hg/CN or NH_4^++Hg/NH_4^+). Gene IDs: *merT3* (BN5_4474), *merA* (BN5_4477), *merD* (BN5_4478), *merE* (BN5_4479), *merP1* (BN5_3800), and *merT1* (BN5_3801).

In addition, the transcriptional expression of the mercuric (II) reductase *merA* gene (BN5_4477) was higher than expression of the *merT3*, *merD* and *merE* genes that are located in the same gene cluster (Fig. 3.10A). Concerning to the six previously mentioned *merR* genes (*merR1-merR6*), only *merR2* (BN5_2264) showed a significative induction by mercury (FC > 2), although expression of the *merR3* and *merR6* genes was also slightly increased in the presence of mercury (FC > 1). By contrast, expression of *merR4* was down-regulated in the presence of mercury (Fig 3.11A).

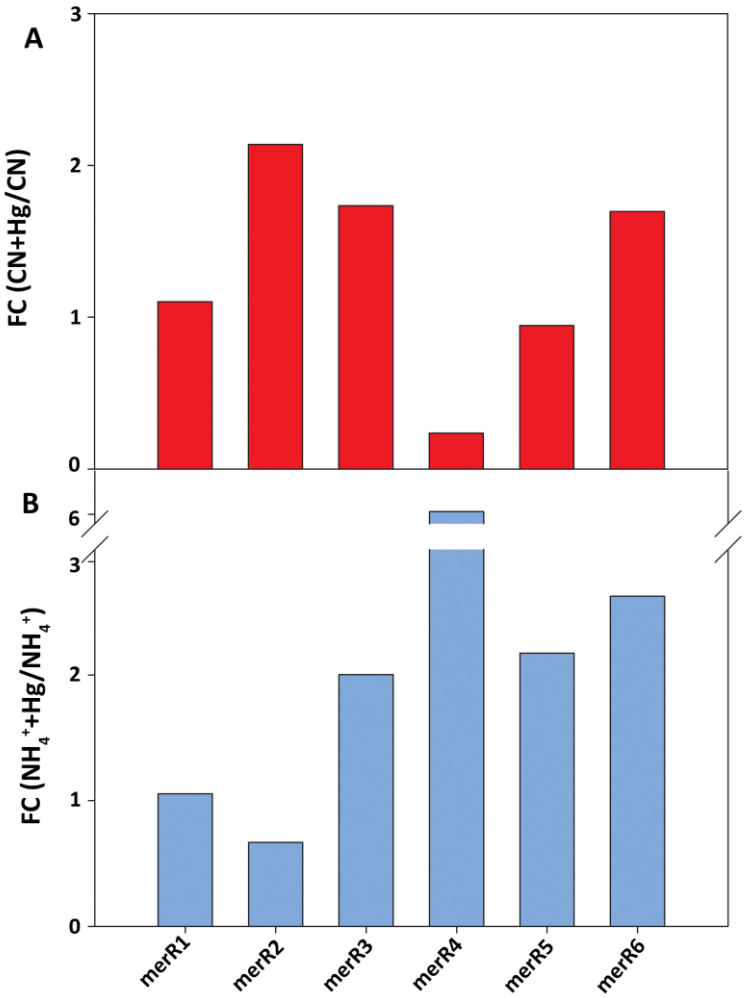

Figure 3.11. Transcriptional expression analysis by *q*RT-PCR of the *P. pseudoalcaligenes* CECT 5344 *merR* regulatory genes. Cells were grown with 2 mM sodium cyanide without or with 75 µM $HgCl_2$ (A) or 2 mM ammonium chloride, without or with 7.5 µM $HgCl_2$ (B). The differential gene expression is represented as fold change (FC) of the relative gene expression ratio (CN+Hg/CN or NH_4^++Hg/NH_4^+). Gene IDs: *merR1* (BN5_0701), *merR2* (BN5_2264), *merR3* (BN5_2322), *merR4* (BN5_3351), *merR5* (BN5_3802), and *merR6* (BN5_4473).

Additionally, many of the predicted MerR2-target genes identified by informatic analysis were significantly induced (FC > 2) in the presence of mercury, including *arsR*, *cpxP*, *nrdB*, *dsbA*, *yghU* and *fosA* genes. However, the expression of the genes *merR5*, *merR6, ubiD, virD* and *phoR* was not significantly affected by mercury (FC < 2) (Fig. 3.12).

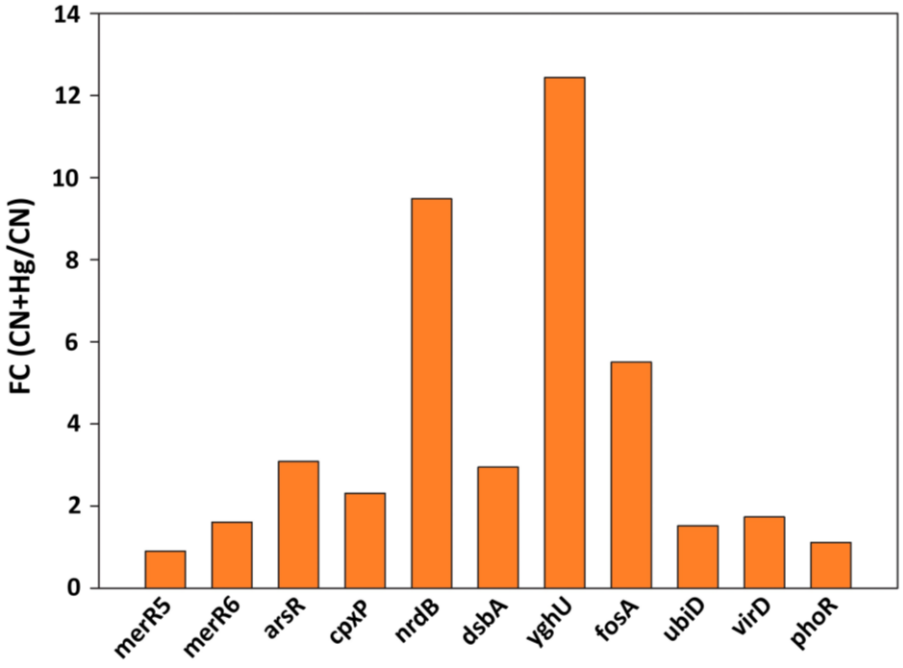

Figure 3.12. Transcriptional *q*RT-PCR analysis of some MerR2-regulated genes. The CECT 5344 cells were harvested after 10 h of growth, when these genes showed their maxima expression. Gene IDs: *merR5* (BN5_3802), *merR6* (BN5_4473), *arsR* (BN5_0252), *cpxP* (BN5_2475), *nrdB* (BN5_1290), *dsbA* (BN5_0108), *yghU* (BN5_2864), *fosA* (BN5_3450), *ubiD* (BN5_0231), *virD* (BN5_3536), *phoR* (BN5_4234).

Furthermore, in accordance with proteomic data, other genes that were found induced by mercury in the *q*RT-PCR, analysis were those coding for phosphate starvation-induced protein PhoH, precorrin-2 C20-methyltransferase CobI, alkanesulfonate monooxygenase SsuD, alkyl hydroperoxide reductase AhpC, thioredoxin reductase, transcriptional regulator ArsR2, arsenate reductase ArsC3, glutathione *S*-transferase, and ribonucleoside-diphosphate reductase NrdB (Table 3.2). Conversely, genes with decreased expression in the presence of mercury included those coding for glutathione peroxidase and formamidase. Expression of the *nitC* gene coding for the nitrilase NitC that is essential for cyanide assimilation was also slightly decreased in the presence of mercury, although mercury had no effect on the expression of the *nitD* gene that is clustered together with the *nitC* gene (Table 3.2).

Table 3.2. Transcriptional expression analysis by *q*RT-PCR of some *P. pseudoalcaligenes* CECT 5344 genes encoding proteins that were found affected by mercury in the proteomic analysis.

Gene[1]/protein ID[2]	Gene/protein name	2 mM cyanide as N-source			2 mM ammonium as N-source		
		CN + Hg	CN	FC (CN+Hg/CN)	NH_4^++Hg	NH_4^+	FC (NH_4^++Hg/NH_4^+)
BN5_3397/W6RJF8	PhoH family protein	0.156	0.086	1.82	0.78	0.823	0.95
BN5_4378/W6R2H6	Precorrin-2 C20-methyltransferase (CobI)	0.026	0.011	2.38	0.118	0.054	2.19
BN5_4162/W6R8H1	Alkanesulfonate monooxygenase (SsuD)	0.041	0.009	4.18	0.136	0.316	0.43
BN5_4165/W6RLE3	Antioxidant AhpC/Tsa family (AhpC)	0.293	0.066	4.43	3.982	6.531	0.61
BN5_3403/W6QYN2	Thioredoxin reductase	0.418	0.083	5.00	0.822	0.182	4.52
BN5_2707/W6R4K3	ArsR family transcriptional regulator (ArsR2)	4.655	1.380	3.37	5.85	11.13	1.9
BN5_2708/W6QXT2	Arsenate reductase (ArsC3)	0.785	0.077	10.25	ND	ND	ND
BN5_2709/W6QZ50	Arsenical resistance protein ArsH	1.833	1.748	1.05	2.3	1.4	1.64
BN5_2412/W6R3L0	Glutathione *S*-transferase family protein	0.701	0.189	3.69	ND	ND	ND
BN5_2413/W6QWV0	GntR family transcritpional regulator	0.076	0.042	1.83	0.454	0.037	12.33
BN5_1290/W6R0E8	Ribonucleoside-diphosphate reductase (NrdB)	5.802	2.154	2.69	ND	ND	ND
BN5_1595/W6R1A5	Glutathione peroxidase	0.528	0.65	0.81	ND	ND	ND
BN5_3204/W6QY63	Formamidase (AmiF)	0.27	0.512	0.53	0.935	0.362	2.58
BN5_1632/H9N5E1	Nitrilase (NitC)	7.40	9.40	0.79	0.035	0.021	1.68
BN5_1633/H9N5E3	Radical SAM domain-containing protein (NitD)	5.524	5.536	1.00	0.02	0.007	2.71

Cells were grown with 2 mM cyanide as the sole N-source in the absence (CN) or the presence of 75 µM $HgCl_2$ (CN+Hg). Also, 2 mM ammonium was used as the sole N-source, without (NH_4^+) or with 7.5 µM $HgCl_2$ (NH_4^++Hg). Fold change (FC) represents the ratio between the relative gene expression with and without mercury. (1) Protein code according to Uniprot database under the accession number UP000032841. (2) Genes annotation from GeneBank (Accession HG916826.1).

Additionally, a complementary *q*RT-PCR analysis was carried out with the cells of *P. pseudoalcaligenes* CECT 5344 grown with 2 mM ammonium chloride as the sole nitrogen source in the absence or presence of 7.5 µM mercury. Cells were harvested after 30 min (NH_4^+) or 6 h (NH_4^++Hg), when they were actively growing and ammonium was not completely consumed (Fig. 3.2B). Both *mer* gene clusters, *merP1T1R5* (BN5_3800-BN5_3802) and *merR6T3P3T5ADE* (BN5_4473-BN5_4479), were also found significantly induced by Hg in media with ammonium (Figs. 3.10B and 3.11B). Interestingly, the *merR2* gene (BN5_2264) was slightly down-regulated by Hg (FC < 1) in the NH_4^++Hg condition, while it was over-expressed (FC > 2) in CN+Hg condition (Fig. 3.11). Conversely, the expression of *merR4* was significantly induced by Hg with ammonium (FC > 2), but it was down-regulated by Hg with cyanide (FC < 0.5) (Fig. 3.11). Furthermore, genes encoding the GntR-family transcriptional regulator (BN5_2413), the precorrin-2 C20-methyltransferase CobI (BN5_4378), the thioredoxin reductase (BN5_3403), and the formamidase AmiF (BN5_3204) were found significantly induced by mercury in media with ammonium (Table 3.2). Also, the genes coding for the nitrilase NitC (BN5_1632), the radical SAM-domain containing protein NitD (BN5_1633), the transcriptional regulator ArsR2 (BN5_2707) and the arsenical resistance protein ArsH (BN5_2709), were found slightly induced in the NH_4^++Hg condition (Table 3.2). Contrarywise, the genes found down-regulated by mercury in media with ammonium were those coding for the alkanesulfonate monooxygenase SsuD (BN5_4162), the alkyl hydroperoxide reductase AhpC (BN5_4165), and the phosphate starvation-induced protein PhoH (BN5_3397) (Table 3.2).

3.4. Discussion

Several bacteria that resist mercury toxicity have been recently characterized, including *Pseudomonas*, *Bacillus*, *Brevundimonas*, *Nitrococcus*, and *Fusobacterium* species, among others (Chasanah et al., 2018; Kotwal et al., 2018; Cardona et al., 2022). However, microorganisms able to cope with toxicity of both cyanide and mercury have not been described yet. Therefore, in this Chapter II, the mercury tolerance and detoxification capacity of the cyanotrophic bacterium *Pseudomonas pseudoalcaligenes* CECT 5344, with particular attention to simultaneous cyanide assimilation, was characterized by applying a proteomic approach. This bacterium was cultured in M9 minimal media with acetate as the sole carbon source and cyanide or ammonium as the sole nitrogen source, in the absence or presence of increasing concentrations of mercury chloride. The MIC and MBC values obtained for mercury in the CECT 5344 strain were significantly higher when cyanide was the N-source (200 µM and 300 µM, respectively) than with ammonium (10 µM and 17.5 µM, respectively), probably due to a lower toxicity of this metal when it forms complexes with cyanide. These MIC values for Hg are in the same range

that those reported for *Pseudomonas mohnii* (217 µM), *Burkholderia contaminans* (316 µM) and *Seratia marcescens* (7 µM), respectively (Cardona et al., 2022), although, these bacterial strains were grown in LB-rich medium without cyanide, which makes difficult to compare the abilities of those microorganisms with the CECT 5344 strain, since the composition of the media varies (Miranda-Carrazco et al., 2018). Interestingly, the MIC value for cyanide was the same (25 mM) in the absence or in the presence of 7.5 µM $HgCl_2$, and the MBC value for cyanide dropped only from 50 mM to 35 mM in the presence of 7.5 µM $HgCl_2$. The MIC values obtained for cyanide were significantly higher than those described for *Pseudomonas putida* (5.2 mM) (Singh et al., 2018) or *Rhodococcus* sp. (15 mM) (Maniyam et al., 2011). Therefore, 7.5 µM mercury does not significantly affect the cyanide assimilation in the strain CECT 5344. Even more, under cyanotrophic conditions, this bacterium tolerated higher concentrations of mercury, displaying a significant growth even in the presence of 100 µM mercuric chloride, although better growth and cyanide consumption rates were achieved in the presence of 75 µM mercuric chloride (Fig. 3.2A). On the other hand, the MIC and MBC values for ammonium in the presence of 7.5 µM mercury were only 10 mM and 20 mM, respectively, when ammonium is fairly well tolerated at very high concentrations in absence of Hg (the MBC value for ammonium was higher than 400 mM). Accordingly, with ammonium as nitrogen source, the bacterial growth of *P. pseudoalcaligenes* CECT 5344 was significantly impaired in the presence of 10 µM mercuric chloride (Fig. 3.2B). These outcomes demonstrate that the negative effect of mercury on bacterial growth and metabolism is significantly higher in the presence of ammonium than when cyanide is used as N-source. Therefore, these results show the advantage of applying the strain CECT 5344 in detoxification of industrial wastewaters containing both cyanide and mercury.

Resistance to heavy metals has been characterized in numerous bacterial species, and strains able to tolerate mercury were, among others, *Pseudomonas* sp. (up to 1.6 mM), *Brevundimonas* sp. (2.8 mM), *Staphylococcus aureus* (3.2 mM), *Corynebacterium xerosis* (0.8 mM), and some transgenic clones of *E. coli* (5-120 µM) (Pan-Hou et al., 2002; Keramati et al., 2011; Pepi et al., 2011; Ruiz et al., 2011). A broad range of microorganisms were also recognized for their tolerance towards arsenite, as described in Chapter I. Nonetheless, the majority of these studies were focused on the physiological and/or metabolic responses towards toxicity of a single metal, rather than simultaneous effect of two or more contaminants. The effect of heavy metals on cyanide biodegradation was only reported in *Serratia marcescens* by Karamba et al. (2014). In this bacterium, cyanide biodegradation was strongly inhibited (more than 75%) in the presence of 1 ppm mercury, whereas other metals like Cu, Cd, Ni, Pb and As inhibited less than 20%. Therefore, *P. pseudoalcaligenes* CECT 5344 seems to be much more resistance to mercury than *S. marcescens*, although, unfortunately, an accurate comparison of

resistance and tolerance of these strains to cyanide and mercury is difficult, due to differences in growth conditions and the composition of the media.

Intracellular mercury accumulation is not a common resistance mechanism in microorganisms; nonetheless, in some bacterial strains like *Pseudomonas pseudoalcaligenes* S1, *Bacillus* sp., or *Ficitibacillus* sp., among others, this type of bioaccumulation was reported (De et al., 2014; Dash and Das, 2016; Nurfitirani et al., 2020; Zhang et al., 2020). The extracellular and intracellular determination of mercury by ICP-MS in the cells grown with cyanide and mercury revealed that *P. pseudoalcaligenes* CECT 5344 accumulated intracellularly a very low amount of mercury, probably chelated to biomolecules. Likewise, most of the mercury added to the media was rapidly removed because mercury was not detected in the extracellular media after 7.5 h of growth. This may be due to the rapid reduction of Hg^{2+} to the volatile Hg^0 by the mercuric reductase MerA. In addition, the potential formation of organomercurials could not be ruled out, although the organomercurial lyase MerB was not detected in the genome of *P. pseudoalcaligenes* CECT 5344. All this results indicate that this strain may detoxify mercury very efficiently through a mercuric reductase (MerA) that converts Hg^{2+} into the volatile form Hg^0, without discarding other resistance mechanisms like formation of organomercurials. Additionally, it has been suggested that biofilm formation is highly correlated with the pH of the media, since a low pH facilitates the chelation of Hg in the exopolysaccharide matrix (Gupta and Diwan, 2017). Thus, it may be proposed that the lack of extracellular mercury sequestration by the biofilm of the CECT 5344 strain, could be due to the alkaline conditions (pH 9.5) used for the bacteria.

The growth of *P. pseudoalcaligenes* CECT 5344 was also characterized in the presence of cyanide, mercury and arsenite. The strain CECT 5344 cultured with 2 mM sodium cyanide was able to grow with 50 µM $HgCl_2$ and 200 µM As(III), whereas 75 µM $HgCl_2$ and 250 µM As(III) significantly impaired the bacterial growth, mainly at the beginning of the experiment (Fig. 3.3A). On the other hand, with 2 mM ammonium as N-source, this bacterium could resist only 7.5 µM $HgCl_2$ and 250 µM As(III), although with delayed growth compared to lower concentrations of these metals (Fig. 3.3B). In addition, the MIC and MBC values for cyanide only decreased from 25 mM and 50 mM in absence of Hg and As(III) to 20 mM and 40 mM, respectively, in the presence of 5 µM mercury and 200 µM As(III). However, the MIC and MBC values for ammonium drastically decreased from values higher than 400 mM in absence of metals to 20 and 30 mM, respectively, in the presence of both Hg and As(III). The higher metal resistance under cyanotrophic conditions might indicate the possible formation of complexes between cyanide and metals, thus reducing the toxicity of these contaminants on bacterial metabolism. Therefore, these results indicate that *P. pseudoalcaligenes* CECT 5344 is a suitable candidate for bioremediation of industrial wastewaters, containing high concentrations of different co-pollutants, including cyanide, mercury and arsenic.

Taking under consideration that *P. pseudoalcaligenes* CECT 5344 demonstrated significantly higher resistance to mercury in the presence of cyanide than with ammonium (Fig. 3.2), the quantitative proteomic analysis to study mercury tolerance and detoxification was performed using cells grown with 2 mM sodium cyanide as the sole nitrogen source, with 75 µM mercury chloride (CN+Hg) or without mercury (CN). In both proteomes a total of 2689 unique proteins were identified, with 209 proteins differentially expressed and 21 proteins found exclusively in the CN+Hg condition (Fig. 3.5). Several proteins that were found over-represented or exclusive in the CN+Hg proteome were encoded by the two *mer* gene clusters, *merP1T1R5* and *merR6T3P3T5ADE*, previously identified in the *P. pseudoalcaligenes* CECT 5344 genome. These proteins included the periplasmic mercury ion-binding proteins MerP1 and MerP3, the MerR-family transcriptional regulator MerD, and the mercuric reductase MerA (Figs. 3.1 and 3.8.). Nonetheless, products of some *mer* genes like the mercuric resistance regulatory proteins MerR6 and MerR5, the mercuric transport proteins MerT3, MerT5 and MerT1, and the mercuric resistance protein MerE, which functions as an inorganic/organic mercury transporter (Naguib et al., 2018; Amin et al., 2019), were not identified in the proteomic analysis. The detection of such hydrophobic integral membrane proteins, and some regulatory proteins that are usually present at low concentration in the cells, are well-known limitations of proteomic techniques (Bogdanow et al., 2016).

Among proteins identified in both proteomes, CN and CN+Hg, were some products of the *nit1C* gene cluster, which codes for the nitrilase NitC and other proteins essential for cyanide assimilation in the strain CECT 5344 (Estepa et al., 2012). In addition, proteins encoded by the *cio* gene cluster were also identified in both proteomes (Fig. 3.7). These proteins include the cytochrome *bd*-type alternative oxidase CioAB that replaces the cytochrome *c* oxidase for a cyanide-independent respiration, and the 4-hydroxy-tetrahydropicolinate synthase DapA1 and the nitrilase Nit4, which play a key role in intracellular iron homeostasis and 3-cyanoalanine assimilation, respectively (Olaya-Abril et al., 2020; Pérez et al., 2021). Other members of the C-N hydrolase superfamily, including the nitrilases Nit1 and Nit2, were also detected in the proteomes from cells grown in both CN and CN+Hg media (Fig. 3.7). Recently, a mutational analysis has demonstrated that these nitrilases Nit1 and Nit2 are not essential for cyanide degradation in *P. pseudoalcaligenes* CECT 5344, but they could contribute to soothe cyanide toxicity, thus contributing to bacterial cyanide resistance (Pérez et al., 2021). Therefore, all these results indicate that mercury does not affect significantly proteins involved in cyanide resistance and assimilation, which constitutes an advantage to apply *P. pseudoalcaligenes* CECT 5344 for cyanide and mercury bioremediation processes.

The comparative gene ontology analysis (GO enrichment) of CN *vs* CN+Hg proteomes revealed that proteins over-represented in the presence of mercury chloride belonged to GO categories related

to response to toxic substance, mercury ion, and detoxification of inorganic compounds (Fig. 3.6). Mercury affects numerous metabolic pathways and provokes many changes in cell functions. It alters the permeability of the cell membrane and induces changes in the DNA structure. Mercury also triggers modifications in the structure and functions of proteins, by showing high affinity to sulfhydryl groups (Bjørklund et al., 2019). In the proteomic analysis carried out in this Chapter II, a glutathione *S*-transferase (encoded by the BN5_2412 gene) was found over-represented in the presence of mercury (Fig. 3.8). The primary role of this enzyme is the conjugation of toxic substances to glutathione (GSH), an essential antioxidant that prevents damage of crucial cellular molecules in the presence of some metals and peroxides. Furthermore, mercury preferably binds to glutathione, cysteine, or homocysteine, as a part of mercury resistance mechanism. GSH is also able to conjugate organomercurial compounds like methylmercury. Thus, the glutathione *S*-transferase probably plays a crucial role in the cellular detoxification of Hg (Bjørklund et al., 2019). Additionally, two GSH-dependent enzymes, glutaredoxin and glutathione peroxidase, which are involved in redox reactions and protection from oxidative damage, were found down-represented in the presence of mercury (Fig. 3.8). This could be due to the decreased pool of biologically active glutathione in the presence of Hg. In this regard, thioesterases, which catalyze the cleavage of thioester groups present in a wide variety of molecules like coenzyme-A, acyl carrier protein, and GSH, among others (Cantu et al., 2020), were found exclusively in the CN+Hg proteome.

The comparative proteomic analysis also demonstrated the induction in the CN+Hg proteome of the thiol-based redox sensor RegB and the alkyl hydroperoxide reductase AhpC, which is an antioxidant thiol-dependent enzyme (Fig. 3.8). This might be due to the fact that mercury acts as a catalyst in Fenton-type reactions (Zhao et al., 2021), hence increasing the level of oxygen reactive species (ROS) and oxidative stress. Furthermore, a component of an ABC-type sulfonate transporter, and an alkanesulfonate monooxygenase that catalyzes the conversion of sulfonates into sulfite and the corresponding aldehyde, were found over-represented in the CN+Hg proteome (Fig. 3.8). The majority of redox signals are recognized by cysteine residues, which can be oxidized to different redox states like sulfenic, sulfinic and sulfonic groups that can sense a range of oxidative signals. Therefore, sulfenic acids can form complexes with GSH, and also two adjacent cysteines can form intra- or inter-molecular disulfide bonds, which allow redox sensor regulators to acquire specific conformations to modulate expression of target genes (Lee et al., 2018). In addition, the sulfate-binding protein CysP3 was over-expressed in the presence of mercury. It has been demonstrated that divalent mercury can react with sulfonates, and in fact in human intoxication by mercury, a recommended treatment is based on oral administration of dimercaptopropane sulfonate (Bjørklund et al., 2019). Also, it has been described a

role of the two-component regulatory RegAB system of *Acidithiobacillus ferrooxidans* in controlling ferrous iron and inorganic sulfur compounds oxidation (Moinier et al., 2017).

Mercury also provokes mitochondrial disfunctions, which may lead to alteration in calcium homeostasis and lipid peroxidation (Agarwal et al., 2010; Roos et al., 2012). Recently, it has been described that external hemin acts as an inhibitor of mitochondrial large-conductance calcium-activated potassium channel activity (Walewska et al., 2022). In the strain CECT 5344, the ATP-dependent hemin transporter HmuV was found exclusively in the CN+Hg proteome (Fig. 3.8). Mercury also reacts with pyrimidine nucleosides and nucleotides, and accordingly, over-representation of the enzymes dihydropyrimidine dehydrogenase and dihydropyrimidinase, as well as the uracil-xanthine permease and the α- and β-subunits of the ribonucleoside-diphosphate reductase, was detected in the presence of mercury. The ribonucleoside diphosphate reductase catalyses the reduction of ribonucleotides into their corresponding deoxyribonucleotides, and its activity relies on glutaredoxin and thioredoxin. As previously mentioned, glutaredoxin together with thioldisulfide isomerase/thioredoxin were found repressed by mercury, which may be related to the low amount of available glutathione. Numerous other proteins involved in DNA replication/repair and translation were down-regulated in the CN+Hg proteome, including the DNA-binding protein HU, the TusC protein, the translation initiation factor IF-1, the ribosome-binding factor A, and the ribosome-recycling factor RRF (Supplementary Materials available online in the reference Biełło et al., 2023b), which may suggest that mercury has a negative effect on general cellular processes like DNA replication and translation.

Several proteins down-represented in the CN+Hg proteome were enzymes essential for cell survival, such as non-heme iron dioxygenases, different *c*-type cytochromes and cytochrome *c*-containing proteins, the nickel/copper-containing superoxide dismutase, and the heme/Fe-S-containing bacterioferritin. These proteins contain metallic cofactors that may bind to mercury, thus leading to the impairment of the activity of these enzymes. On the other hand, the cobalt-independent methionine synthetase was found exclusively in the CN+Hg condition, whereas the precorrin-2 C20-methyltransferase, which is involved in the synthesis of vitamin B12, was over-represented in the presence of mercury (Fig. 3.8). Moreover, the formation of complexes between divalent mercury and the porphyrin ring present in the heme group and cobalamin (vitamin B12), has been well described (Hudson and Smith, 1975). Thus, the induction of both cobalt-independent methionine synthetase and precorrin-2 C20-methyltransferase might be a compensation mechanism triggered by mercury toxicity. Curiously, different pyridoxal 5'-phosphate (PLP)-dependent enzymes were also found over-represented in the CN+Hg proteome of the strain CECT 5344, such as cysteine desulfurase (IscS), alanine racemase, β-alanine-pyruvate transaminase, and D-amino acid dehydrogenase (Fig. 3.8). Cysteine desulfurase catalyzes the conversion of cysteine to alanine and sulfane sulfur through the formation of

a protein-bound cysteine persulfide intermediate on a conserved cysteine. The proposed role of this enzyme is to participate in processes involved in the biosynthesis of Fe-S clusters, thiamine, tRNA thionucleosides, biotin, lipoic acid, molybdopterin, and NAD^+ (Mihara and Esaki, 2002).

Activity of the MerR regulatory protein determines the expression of genes that are included in the *mer* clusters. MerR acts as a transcriptional repressor in the absence of mercury, hence blocking the Hg detoxification mechanism/pathway. On the other hand, when reduced mercury is present in the media, it binds to the MerR protein, which further undergoes an allosteric change that allows its release from the promoter region, leading to active transcription of the structural *mer* genes. In addition, it has been suggested, that the MerD protein has a co-regulatory function in the expression of the *mer* genes, probably by forming a complex with MerR (Mukhopadhyay et al., 1991; Barkay et al., 2003; Champier et al., 2004; Lin et al., 2012).

The genome analysis of the strain CECT 5344 has allowed the identification of six genes encoding putative MerR regulatory proteins. MerR5 and MerR6 are encoded by the two *mer* gene clusters (Fig. 3.1), whereas the genes coding for the additional four MerR proteins (MerR1-MerR4), are scattered throughout the genome of this bacterium. These MerR proteins may play an important role in the regulation of the expression of the *mer* genes, although these regulatory proteins were not detected in the proteomic analysis (Fig. 3.8). However, the MerD co-regulatory protein encoded by a gene of the *mer6T3P3T5ADE* gene cluster was found induced by mercury. Therefore, taking under consideration that proteomic analysis has several limitations, like the low detection for membrane or regulatory proteins (Bogdanow et al., 2016), a *q*RT-PCR transcriptional analysis of the six *merR* genes was performed in cells grown with 2 mM sodium cyanide in the presence or absence of 75 µM mercury chloride. This *q*RT-PCR analysis revealed that only the *merR2* gene was significatively induced by $HgCl_2$ with FC > 2 (Fig. 3.11A). Additionally, expression of the structural genes from the *merR6T3P3T5ADE* and *merP1T1R5* clusters, that code for mercury transporters, mercury reductase and the co-regulator MerD was analyzed by *q*RT-PCR, revealing that these genes were highly induced in the presence of mercury both under cyanothrophic conditions and with ammonium as N-source (Fig. 3.10). Thus, it might be suggested that MerR2 play a key role in the control of the *mer* genes, by promoting their transcription in the presence of mercury.

In addition, the bioinformatic analysis focused on distribution of MerR-type transcriptional regulators among bacteria and archaea demonstrated that MerR2 has homologs in the primitively evolved archaea and thermophilic bacteria. This might indicate a very early origin of the mercury resistance mechanism in hydrothermal habitats that could contain elevated concentrations of mercury (Boyd and Barkay, 2012; Priyadarshanee et al., 2022). The phylogenic tree also showed the existence

of three subgroups among the MerR proteins, indicating the possible close relationship between MerR5 and MerR6, MerR2 and MerR1, and also MerR3 and MerR4, which seem to belong to each one of these three subgroups of MerR proteins (Fig. 3.9). Furthermore, an additional bioinformatic analysis carried out to explore the presence of the putative MerR binding box 5'-(T/C)GTA(G/C)-N4-GTAC-3' (Brown et al., 2003) in the promoter regions of target genes of *P. pseudoalcaligenes* CECT 5344 has allowed the identification of a putative MerR regulon that could control mercury resistance/detoxification in the CECT 5344 strain, alongside with the cyanide assimilation. However, the gene coding for MerR2 does not contain the predicted MerR binding box in its promoter region. Considering all the results, and particularly the fact that *merR2* was the only regulatory gene significantly induced by mercury under cyanotrophic conditions, it may be proposed that MerR2 is a master regulator that controls expression of the different target genes that include the predicted MerR binding sites in their promoter regions (Figs. 3.12 and 3.13). Moreover, the *merR2* gene was previously described as a putative target of a regulatory small RNA (sRNA258) that could control cyanide detoxification of industrial cyanide-containing residues by *P. pseudoalcaligenes* CECT 5344 (Olaya-Abril et al., 2019).

The hypothetical regulatory model for the MerR2 regulon of *P. pseudoalcaligenes* CECT 5344 under cyanotrophic conditions, proposed by holistic approach and integration of data from proteomic, bioinformatic and transcriptional analyses, is shown in Figure 3.13. This model includes several putative MerR2-regulated genes whose function could be essential for mercury resistance in the CECT 5344 strain, all of them containing a MerR2-binding box in their promoters.

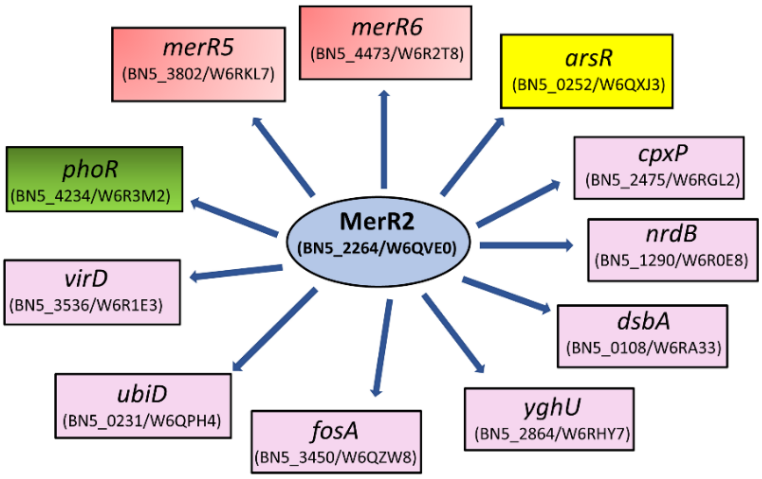

Figure 3.13. Hypothetical regulation network of the MerR2 regulon of *P. pseudoalcaligenes* CECT 5344. In this regulatory model two MerR transcriptional regulator genes, *merR5* and *merR6* (red boxes), are putatively under control of the master regulator MerR2 (blue oval), as well as the transcriptional regulator *arsR* gene (yellow box) involved in arsenic resistance, the regulatory *phoR* gene that codes for the transcriptional regulator involved in phosphate metabolism (green box), and several structural genes (violet boxes): *cpxP*, chaperone involved in resistance to metals; *nrdB*, β-subunit of the ribonucleoside-diphosphate reductase; *dsbA*, dithiol oxidoreductase (disulfide-forming); *yghU*, glutathione *S*-transferase; *fosA*, glutathione *S*-transferase; *ubiD*, 3-octaprenyl-4-hydroxybenzoate carboxy-lyase; *virD*, amino acid/peptide export protein.

The regulatory *merR5* and *merR6* genes, which are located on the *mer* gene clusters of this bacterium, were included in this regulatory network. Other putative MerR2-target genes were *cpxP*, which codes for a chaperone involved in the resistance to metals like mercury; *nrdB* gene that codes for the β-subunit of the ribonucleoside-diphosphate reductase involved in DNA replication and repair, probably related to the DNA damage that mercury causes directly or through generation of reactive oxygen species; *fosA* and *yghU* genes, which code for glutathione *S*-transferases that may contribute to increase the GSH pool biologically active in the presence of mercury; and the dithiol oxidoreductase *dsbA* gene. The Dsb system have been described to play a key role in the virulence of many pathogenic microorganisms by acting on the function of various protein secretion systems that influence the virulence (Bocian-Ostrzycka et al., 2017). Although *P. pseudoalcaligenes* CECT 5344 is not pathogenic, this could be a mechanism of defense towards mercury. Subsequently, the *virD* gene, which codes for an amino acid/peptide export protein involved in quorum sensing, was another predicted target of the MerR2 regulon. Peptides and amino acids can be very effective, and often specific, ligands for a variety of metal ions like mercury. Furthermore, the *ubiD* gene that codes for 3-octaprenyl-4-hydroxybenzoate carboxy-lyase that is involved in ubiquinone (coenzyme Q10) synthesis was also identified as a predicted MerR2-target. Recently, it has been demonstrated that coenzyme Q10 supplementation soothe the oxidative stress enforced by mercury in rats (Gamal et al., 2023).

Phosphate is an essential element for living organisms, although usually it is scarce in the environment, thus limiting bacterial growth (Biełło et al., 2023c). Additionally, mercury displays great affinity to phosphorus, making this nutrient even more restricted in mercury-containing media. Therefore, the *phoR* gene coding for a transcriptional regulator that activates *pho* gene expression to allow phosphorus metabolism was also a predicted MerR2-target. In addition, the PhoH protein, a phosphorus-related putative ATPase without clear function, was found over-represented in the presence of mercury in the proteomic analysis performed in this work (Fig. 3.8). The Pho regulon has been described in bacteria as a regulatory circuit that control phosphate homeostasis and also as a part of a regulatory network complex that is essential for stress response (Lamarche et al., 2008).

Finally, several proteins encoded by the *P. pseudoalcaligenes* CECT 5344 *ars* genes were found over-represented in the CN+Hg condition (Fig. 3.8). Although, arsenical compounds were not present in the culture media of the CECT 5344 strain used for this proteomic analysis, a significant up-regulation by mercury was observed for the ArsR2 transcriptional regulator, the thioredoxin-dependent arsenate reductase ArsC3, and the arsenic resistance protein ArsH2, which is an $NADP^+$-dependent flavoprotein that protects against oxidative stress and confers resistance to organoarsenicals (Fekih et al., 2018; Páez-Espino et al., 2020). The up-regulation of these *ars* genes was also observed by *q*RT-PCR analysis (Table 3.2). Thus, the presence of mercury chloride may trigger the induction of arsenic resistance and

detoxification mechanism, which suggests a possible crosstalk between these toxic elements, cyanide, mercury and arsenic. This result highlights the great biotechnological potential of the strain CECT 5344 for detoxification of mining wastes that are composed of complex mixtures of highly toxic compounds like cyanide, mercury and arsenic, which display different chemical properties that make their disposal very difficult. Therefore, these results make *P. pseudoalcaligenes* CECT 5344 a suitable candidate to be used in bioremediation techniques applied for the detoxification of industrial liquid wastes generated by the mining industry that usually contain elevated concentrations of cyanide, arsenic and mercury, among other metals like iron, copper and nickel.

In addition, in both proteomic and transcriptomic analyses under cyanotrophic conditions (Fig. 3.8 and Table 3.2), the precorrin-2 C20-methyltransferase CobI (BN5_4378), the alkanesulfonate monooxygenase SsuD (BN5_4162), the alkyl hydroperoxide reductase AhpC (BN5_4165), the thioredoxin reductase (BN5_3403), and the ribonucleoside-diophosphate reductase NrdB were found up-regulated in the presence of mercury (FC ≤ 2), meanwhile the glutathione peroxidase (BN5_1595), the formamidase (BN5_3204), and the nitrilase NitC (BN5_1632) were slightly down-regulated by Hg (FC ≥ 0.5). Thus, the results obtained in the proteomic and *q*RT-PCR analyses support the robustness and reliability of the study performed in this Chapter II.

Mercury resistance in *P. pseudoalcaligenes* CECT 5344 was significantly lower when ammonium chloride was used as nitrogen source than in the presence of cyanide. For this reason, the proteomic analysis was carried out only in cyanotrophic conditions. However, a transcriptional analysis by *q*RT-PCR was also performed in cells grown in the presence of 2 mM ammonium without (NH_4^+) or with 7.5 µM mercury chloride (NH_4^++Hg), a concentration of mercury 10 times lower than that used in the cyanotrophic conditions. The genes of the two *mer* clusters of the strain CECT 5344, *merP1T1R5* and *merR6T3P3T5ADE*, were significantly induced by the presence of mercury in the media, both with cyanide and with ammonium as the sole nitrogen source (Figs. 3.10 and 3.11). Interestingly, the *merR4* gene (BN5_3351) was highly induced by Hg with ammonium, whereas its expression in the CN+Hg conditions was strongly down-regulated. Conversely, the *merR2* gene (BN5_2264) was found up-regulated by Hg with cyanide, but it was down-regulated by Hg with ammonium. Therefore, it might be suggested that the presence of cyanide triggers the expression of the *merR2* gene, which acts as a main regulatory protein (Figs. 3.12 and 3.13). Furthermore, the gene encoding a GntR family transcriptional regulator (BN5_2413) was strongly up-regulated in the NH_4^++Hg conditions, meanwhile in the media with CN+Hg, its expression was significantly lower (Table 3.2). Therefore, it may be suggested that cyanide down-regulates the expression of this *gntR* gene and it could be an interesting target for further investigation of its role in mercury detoxification. On the other hand, in the transcriptomic analysis with ammonium, the genes *nitC* (BN5_1632) and *nitD* (BN5_1633) were induced by Hg, whereas under

cyanotrophic condition their expression was not significantly affected by mercury (Table 3.2). What is more, the MIC and MBC determination and the proteomic data (Fig. 3.7) demonstrate that mercury does not affect cyanide degradation and assimilation in the *P. pseudoalcaligenes* CECT 5344. Therefore, the induction of the *nitC* and *nitD* genes observed in the NH_4^++Hg condition may be a mercury detoxification response in the strain CET 5344, suggesting a possible cross-talk between cyanide and mercury resistance mechanism.

On the other hand, genes coding for proteins involved in oxidative stress response like alkanesulfonate monooxygenase SsuD (BN5_4162) and alkyl hydroperoxide reductase AhpC (BN5_4165), which were significantly up-regulated in the CN+Hg condition, were found down-regulated by the presence of mercury in media with ammonium (Table 3.2). This may suggest a synergistic effect of cyanide and mercury, which together trigger a higher oxidative stress response in bacterial cells than separately.

Considering all the results presented above, the metabolism of *P. pseudoalcaligenes* CECT 5344 under cyanotrophic conditions in the presence of mercury was summarized as shown in Figure 3.14.

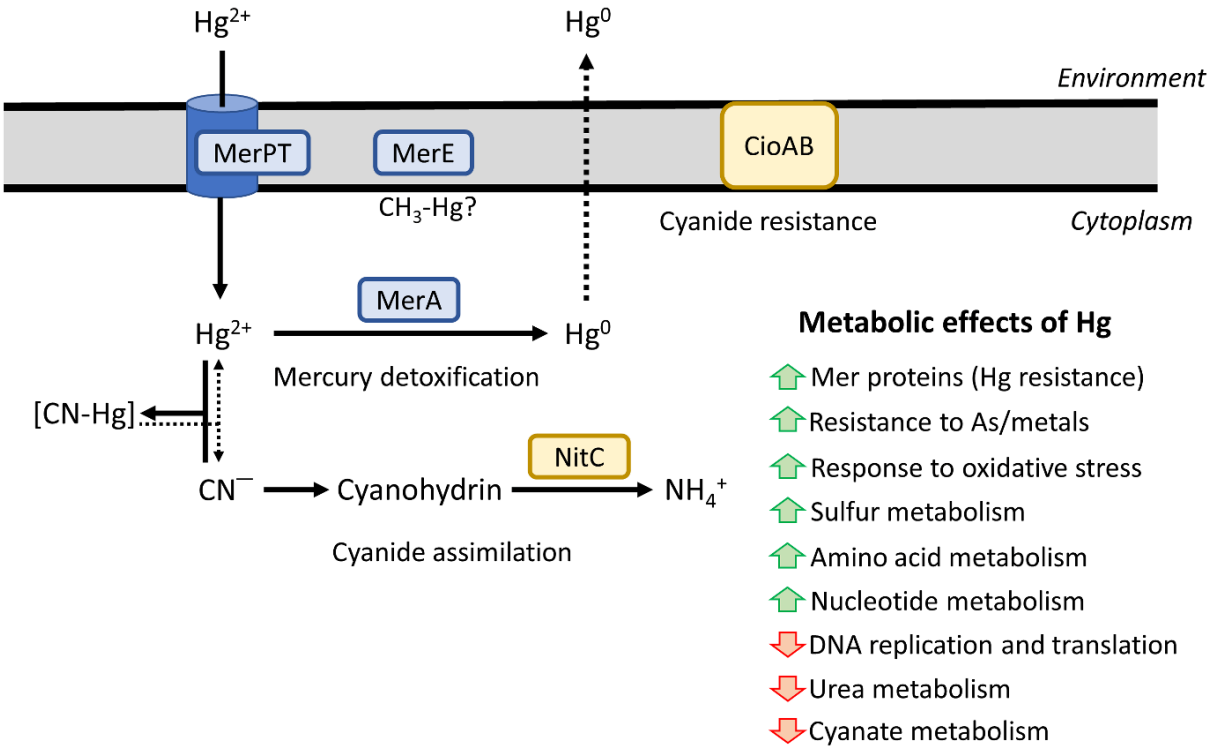

Figure 3.14. Overview of *P. pseudoalcaligenes* CECT 5344 metabolism under cyanotrophic conditions in the presence of mercury.

3.5. Conclusions

1. *Pseudomonas pseudoalcaligenes* CECT 5344 harbors two *mer* gene clusters that respond significantly to mercury chloride, regardless of the nitrogen source. In the presence of cyanide, the CECT 5344 strain shows higher mercury resistance than with ammonium, probably due to the fact that mercury forms complexes with cyanide, thus decreasing its toxicity. In any case the presence of mercury does not affect the cyanide resistance and assimilation mechanisms in this bacterium.

2. The mechanism of mercury resistance is possibly based on mercury reduction by mercuric reductase (MerA), and its further extrusion from the cells as a volatile form (Hg^0), since mercury was neither detected in the extracellular media, nor bioaccumulated extracellularly (biosorption), and only residual concentrations of mercury are accumulated inside the cells, probably chelated to biomolecules.

3. The integration of proteomic data, bioinformatics and transcriptional analysis has allowed to predict a regulatory model for the MerR2 regulon, which operates under cyanotrophic conditions, with MerR2 acting as a master regulator that controls expression of *mer* genes and other targets genes.

4. *P. pseudoalcaligenes* CECT 5344 is able to cope with the simultaneous presence of cyanide, mercury and arsenic, thus being a suitable candidate to be used for bioremediation of industrial wastewaters, which are often co-contaminated with high concentrations of these toxic chemicals.

4. Chapter III

Quantitative proteomic analysis of *Pseudomonas pseudoalcaligenes* CECT 5344 in an ammonium and iron dependent anaerobic lifestyle

Manuscript in preparation.

4.1. Introduction

Bioremediation techniques use the metabolic potential of microorganisms to remove the contaminants from the environment. Numerous treatments are focused on application of aerobic microorganisms. Nonetheless, in many polluted sites like sludges and wetlands the oxygen concentration is scarce, which constitutes a great limitation for aerobic bacteria. Although the aerobic degradation is considered to be more profitable, there are few toxic compounds, such as toluene, benzene, phenol, halogenated hydrocarbons or aromatic alcohols and aldehydes, whose degradation and/or removal is more successful under strictly anaerobic conditions (Vogel et al., 1987; Ghattas et al., 2017; Shi et al., 2017). Thus, several studies have been conducted on anaerobic degradation of petroleum hydrocarbons and in the development of anaerobic bioreactors for treatment of wastewaters (Weelink et al., 2010; Mbadinga et al., 2011; Jiménez et al., 2016; Mojiri et al., 2023). Therefore, anoxic metabolism have recently gained interest, and could be promising for developing bioremediation strategies, including those applied to residues containing cyanide and metals (Balagurusamy, 2005; Luque-Almagro et al., 2018).

In general, anaerobic metabolism encompasses two different processes to generate cellular energy: anaerobic respiration and fermentation. In the anaerobic respiration an electron transport chain is used to generate an electrochemical proton gradient, with a final electron acceptor other than oxygen, such as nitrate, nitrite, iron(III), sulphate, manganese(II), or selenate (Moodle and Ingledew, 1990; Carmona et al., 2009). On the other hand, during fermentation, organic compounds that are not fully oxidized are generated, such as lactate, butanoate or ethanol. Different anaerobic respiration pathways have been described so far, such as the well-known denitrification process that was reported in *Paracoccus denitrificans*, *Pseudomonas aeruginosa,* and *Pseudomonas denitrificans*, among other bacteria (Arat et al., 2015; Borrero-de-Acuña et al., 2016; Olaya-Abril et al., 2018); the anaerobic ammonium oxidation (Anammox) process, performed by bacteria belonging to five genera (*Brocadia*, *Kuenenia*, *Anammoxoglobus*, *Jettenia* and *Scalindua*) of the phylum Planctomycetota (Ibrahim et al., 2015; Manonmani and Joseph, 2018); and the anaerobic ammonium oxidation coupled to Fe(III)-reduction (Feammox), mainly described in *Geobacter* and *Shewanella* species, but also reported in some other bacteria (Li et al., 2015).

Pseudomonas species display a versatile metabolism that may be adapted to the presence of different pollutants. Therefore, they are commonly used in bioremediation technologies. Thus, *P. fluorescens* and *P. denitrificans* were reported as facultative anaerobes that may use an inorganic compound like nitrate as terminal electron acceptor, while *P. aeruginosa* performs anaerobic arginine

and pyruvate fermentation (Kampers et al., 2021). In addition, there were many attempts to metabolically engineered the strict aerobe *P. putida* to anaerobic lifestyle, either by performing anaerobic respiration or fermentation, but unfortunately many of these studies did not report growth under anaerobic conditions (Sohn et al., 2010; Nikel et al., 2013; Steen et al., 2013; Schmitz et al., 2015). Furthermore, *in silico* metabolic models were generated to adapt *P. putida* to anoxic conditions and as result, a genetically modified strain was able to grow under micro-oxic condition, due to increased ATP generation from acetate synthesis (Kampers et al., 2019).

The capability of the cyanotrophic bacterium *Pseudomonas pseudoalcaligenes* CECT 5344 to grow under anaerobic conditions in the presence of ammonium and iron was tested in this Chapter III. Additionally, a quantitative proteomic analysis was performed to investigate the possible metabolic processes involved in the anaerobic lifestyle of this bacterium. Considering the great biotechnological potential and the previously described ability of this strain to resist heavy metals under cyanotrophic conditions (Biełło et al., 2023a,b; Chapters I-II), the obtained results could contribute to the development of anaerobic bioremediation strategies for several pollutants in oxygen-limited sites.

4.2. Materials and methods

4.2.1. Culture media and bacterial growth conditions

P. pseudoalcaligenes CECT 5344 was cultured under aerobic or anaerobic conditions in M9 minimal media (Sambrook and Russel, 2001) at 30 °C, with pH adjusted to 9.5, although when indicated pH 7.5 was also used. 50 mM sodium acetate and 10 mM ammonium chloride were used as the sole carbon and nitrogen source, respectively. When required, potassium nitrate (KNO_3) or potassium nitrite (KNO_2) were used as nitrogen and energy sources at different concentrations. A standard metal trace solution was added to the media (1.25 mL/L) from a stock solution containing (per liter): 10.75 g $MgCl_2$, 2 g $CaCO_3$, 6.16 g $MgS0_4$ x $7H_2O$, 4.75 g $FeSO_4$ x $7H_2O$, 1.12 g $MnSO_4$ x $7H_2O$, 0.25 g $CuSO_4$ x $5H_2O$, 0.28 g $CoSO_4$ x $7H_2O$, 0.06 g H_3BO_3, 51.13 mL HCl 12 N, and distilled H_2O up to 1 L. When added this metal trace solution, the final Fe(II) concentration in the minimal media was 30 µM. When applicable, iron(II) from the standard metal traces was removed (-Fe), increased (up to 30 mM), or replaced by different concentrations of iron (III) as ferric chloride ($FeCl_3$) or ferric citrate ($C_6H_5FeO_7$). Aerobic cultures (25 mL in 100 mL Erlenmeyer flasks) were incubated in an orbital shaker MAXQ 4000 (Thermo-Scientific), while anaerobic cultures were achieved by filling completely 70 mL screw capped tubes, which were incubated in the dark during 15 days. In all cases, an aerobic overnight culture, prepared from a frozen stock in a standard M9 minimal media supplemented with 5 mM ammonium chloride, was used as

inoculum. Bacterial growth was determined, per triplicate, by measuring the absorbance at 600 nm (A_{600}) and/or by total protein quantification (Bradford, 1976).

4.2.2. Analytical determinations

The precise methodology for each analytical method was described in detail in Chapter I, Section 2.2. Extracellular ammonium concentration was determined by the previously described colorimetrical method using the Nessler reagent (Morrison, 1971). Protein concentration was quantified by the Bradford method (Bradford, 1976).

4.2.3. Detection and determination of polyhydroxyalkanoates

The detection of polyhydroxyalkanoates (PHA) was performed by staining with Nile Red dye, as previously described (Spiekerman et al., 1999; Zuriani et al., 2013). *P. pseudoalcaligenes* CECT 5344 was grown in M9 media with the standard metal trace solution (30 µM Fe), and with 50 mM sodium acetate as the carbon source and 10 mM ammonium chloride as the sole nitrogen source. Cells (per triplicate) were harvested by centrifugation at 10,000 rpm, 4 °C, 10 min, after 15 days of growth in anaerobic conditions (Ana), while the aerobic cells were collected when reached approximately A_{600} 0.4 (C_Abs) or when approximately 6 mM ammonium was consumed (C_Cons). Cells were further resuspended in 5 mL of distilled water. Subsequently, 40 µL of Nile Red dye (from a stock solution 80 µg/mL dissolved in dimethyl sulfoxide, DMSO) was added to 1 mL cell suspension and incubated at room temperature for 30 min in the dark. The stained suspension was centrifuged again at 10,000 rpm for 5 min and the resulting pellet was resuspended in 1 mL of distilled water. An aliquot of suspension was loaded into 96-well microplate, using 5 wells per replicate. The fluorescence was read at excitation wavelength 535 nm and emission wavelength 603 nm, by using a microplate reader (VarioskanLux, Thermo Fisher Scientific). In parallel, the same number of wells for each condition were used for protein quantification (Bradford, 1976) to avoid possible deviations as consequence of different growth rates derived from the growth conditions. Statistical significance was analyzed by applying a two-tailed *t*-test analysis with the Benjamini-Hochberg correction on the Nile Red staining measurements normalized by protein amount.

In addition, PHA produced by *P. pseudoalcaligenes* CECT 5344 were determined as previously described (Olaya-Abril et al., 2017), in triplicate. Briefly, cells were cultured in 350 mL of M9 minimal medium with the standard metal trace solution (30 µM Fe), and with 50 mM sodium acetate as the

carbon source and 10 mM ammonium chloride as the sole nitrogen source. As indicated above, the anaerobic cells (Ana) were harvested after 15 days of growth, while the aerobic controls were collected at A_{600} 0.4 (C_Abs) or after consumption of 6 mM ammonium (C_Cons). Then, for each replicate, 100 mL were used to determine the cell dry weight, while the remaining 250 mL were used to purify the PHA. Cultures were centrifuged (10,000 rpm, 4 °C, 10 min) and the cell pellets were resuspended in 10 mL chloroform and disrupted by cavitation with ultrasounds using a Bandelin Sonoplus H20070 equipment (5 pulses for 20 s/70 W). Samples were centrifuged for 5 min at 6,000 rpm, and chloroform soluble phase was recovered from the bottom and added, slowly and with agitation, to a clean tube containing five volumes of ice cold-methanol. Additional 10 mL cold-methanol were used to resuspend the insoluble phase, and the mixture was incubated for 30 min at 65 °C. Furthermore, an additional centrifugation step was performed for 5 min at 6,000 rpm, and the chloroform soluble fraction was added to the previously used cold methanol. The final mixture was incubated during 30 min at 4 °C on ice. The precipitated PHA were recovered by centrifugation at 7,000 rpm during 30 min, air dried, and resuspended in 500 µL of chloroform. Finally, the samples were dried overnight at 65 °C and recovered to determine the PHA dry weight, which was normalized with the dry cell weight.

4.2.4. Transmission electron microscopy

The strain CECT 5344 was grown in M9 liquid media with 50 mM acetate and 10 mM ammonium as the carbon and nitrogen sources, respectively. The cultures were collected in the three previously indicated conditions (Ana, C_Abs and C_Cons) and centrifuged at 10,000 rpm and 4 °C during 10 min. Cells were washed twice with 1 mL 20 mM Tris-HCl (pH 8) and fixed in 2% (w/v) glutaraldehyde. Afterwards, cells were suspended in 1% (w/v) OsO_4 for 1 h, gradually dehydrated in acetone 30, 50, 70, 90 and 100% (v/v), 30 min each, and finally treated with propylene oxide (two changes, 10 min each). Afterwards, cells were embedded sequentially into 2:1, 1:1, 1:2 propylene oxide-resin. Ultrathin sections (thickness 50 nm) were cut with a Leica Ultracut R ultramicrotome (Leica Inc, Buffalo, USA) using a diatome diamond knife. The sections were picked up with 200 mesh cupper grids coated with a layer of carbon and subsequently observed in a Jeol JEM-1400 (Tokyo, Japan) electron microscope (Manso et al., 2015). These analyses were carried out using the Microscopy Facilities at the Central Service for Research Support of the University of Córdoba (SCAI, UCO).

4.2.5. Quantitative proteomic analysis

P. pseudoalcaligenes CECT 5344 was cultured in M9 minimal medium with the standard metal trace solution (30 µM Fe) and with 10 mM ammonium chloride as the sole nitrogen source. The cells grown anaerobically were harvested after 15 days of incubation, while the aerobic cultures were recovered when reached approximately A_{600} 0.4 (C_Abs) and when approximately 6 mM ammonium was consumed from the media (C_Cons). Four independent cultures of each condition were harvested by centrifugation at 12,000 rpm for 10 min at 4 °C, and stored at -80 °C until used. Samples for intracellular LC-MS/MS proteomic (data-independent analysis) were prepared by following the previously described protocol (Chapter II, Section 3.2.4). In addition, the LC-MS/MS proteomic analysis of the exoproteome was also performed. Collected samples were precipitated by adding 1 volume of 100% (v/v) trichloroacetic acid (TCA) to 4 volumes of supernatant, and incubated overnight at 4 °C. The precipitates were recovered by centrifugation at 14,000 rpm for 30 min, washed twice in 1 mL 80% ice cold-acetone, and finally resuspended in 200 µL of lysis buffer (Chapter II). Afterwards, samples were re-precipitated by using the commercial 2D-Clean Up Kit (Amershamm GE Healthcare). These samples for the intracellular and exoproteome analyses were provided to the Proteomic Facility Unit of IMIBIC (Chapter II, Section 3.2.4). Relative protein quantification after LC-MS/MS analysis was performed by using MaxQuant (Cox and Mann, 2008), which uses the free available software Perseus (version 1.6.12.1) (https://maxquant.org/perseus/). The exploratory qualitative analysis was achieved by running principal component analysis (PCA) and representing relationships between expressed proteins in four experimental conditions by Venn diagram. Subsequently, the quantitative analysis was performed to define proteins differentially expressed. Proteins identified from only one peptide and/or in only one replicate were discarded. Proteins identified in all three replicates, per each condition, were used for differential pairwise comparison analysis if they were positive after considering a two-way *t*-test with the Benjamini-Hochberg correction (Olaya-Abril et al., 2018). Proteins were considered differentially expressed when the fold change (FC) was ≥ 2 ($\log_2$ FC ≥ 1) for up-regulated proteins or FC ≤ 0.5 ($\log_2$ FC ≤ -1) for down-regulated proteins, with a corrected *p* value < 0.05. Furthermore, proteins which were identified in the replicates of one condition and undetectable in the other condition were considered as exclusive. GO analysis was performed using the ClueGo software on the Cytoscape platform (version 3.10.1). Integration of final proteomic data were performed by using the tool KEGG Mapper.

4.3. Results

4.3.1. Growth of *P. pseudoalcaligenes* CECT 5344 under anaerobic conditions

To determine the *P. pseudoalcaligenes* CECT 5344 ability to grow under anoxic conditions in minimal mineral media M9 (30 µM Fe) with 50 mM acetate and 10 mM ammonium as the sole carbon and nitrogen sources, 70 mL screw capped tubes were completely filed with the media, previously inoculated at A_{600} 0.005, and incubated during 15 days in darkness. After this time, bacterial cells reached an absorbance at 600 nm of about 0.4 (A_{600} 0.4) and approximately 6 mM of ammonium was consumed (Table 4.1). Alongside, the strain CECT 5344 was grown under aerobic conditions and cells were harvested either at A_{600} 0.4 or when 6 mM ammonium was consumed, because under anoxic conditions the ammonium consumption rate was higher (i.e., cells at A_{600} 0.4 consumed 6 mM ammonium in anoxic conditions, but only around 3 mM under aerobiosis) (Table 4.1). Then, two aerobic controls were defined for subsequent experiments, considering absorbance or ammonium consumption as parameters of reference (C_Abs and C_Cons, respectively).

Table 4.1. Determination of bacterial growth under anaerobic or aerobic conditions.

Condition	A_{600}	Protein (µg/mL)	NH_4^+ (mM) in the media
T0	0.005 ± 0.00	44.9 ± 3.54	9.8 ± 0.13
Ana	0.422 ± 0.009	248.1 ± 4.07	3.78 ± 0.07
C_Abs	0.421 ± 0.008	205 ± 3.37	6.71 ± 0.27
C_Cons	0.591 ± 0.026	301.4 ± 17.85	3.93 ± 0.18

Cells were grown with 50 mM sodium acetate as the carbon source and 10 mM ammonium as the sole nitrogen source, and with the standard metal trace solution (30 µM Fe), under anoxic (Ana) or oxic (C_Abs/C_Cons) conditions. Bacterial growth was determined both by A_{600} and by protein content (µg/mL). T0 represents the initial data of the cultures at time 0, before the bacterial growth. Ammonium remained in the media was also determined.

To elucidate the mechanism by which the CECT 5344 strain could grow under anaerobic conditions, the effect of iron, nitrate and nitrite on bacterial growth was tested. First, the strain was cultured under anaerobic or aerobic conditions with the M9 minimal media in the presence of different concentrations of ferrous iron. It is wort noting that the Fe(II) concentration in the standard minimal media is 30 µM. Under anoxic conditions, bacterial growth with 0.3 µM and 3 µM Fe(II) was significantly lower than with the usual Fe concentration in the media (30 µM), and also a lower consumption of the nitrogen source was observed in both cases. Moreover, cultures with 300 µM ferrous iron, which is a

concentration 10-fold higher than that presence in the standard M9 media, showed better growth and higher ammonium consumption when compared to the standard 30 µM Fe(II)-containing cultures. However, cells were unable to growth anaerobically with very high Fe concentrations (above 3 mM) or under iron depravation (-Fe) (Table 4.2). On the other hand, under oxic conditions, *P. pseudoalcaligenes* CECT 5344 tolerated up to 10 mM Fe(II), but the ammonium consumption was residual. In addition, a low aerobic bacterial growth was still observed when iron was removed from the metal trace solution (-Fe), and about 4 mM ammonium was consumed in absence of iron (Table 4.2).

Table 4.2. Effect of iron on bacterial growth under anoxic or oxic conditions.

	Anaerobiosis (15 days)		**Aerobiosis (24 h)**	
Fe(II) Condition	**A_{600}**	**NH_4^+ (mM)**	**Protein (µg/mL)**	**NH_4^+ (mM) in the media**
T0	0.005	9.86 ± 0.14	55.5 ± 0	9.51 ± 0.49
0.3 µM	0.151 ± 0.006	7.4 ± 0.24	ND	ND
3 µM	0.168 ± 0.005	7.25 ± 0.24	ND	ND
30 µM*	0.418 ± 0.04	4.6 ± 0.87	235.1 ± 9.5	1.85 ± 0.20
300 µM	0.495 ± 0.02	2.25 ± 0.06	245.5 ± 6.8	1.99 ± 0.07
3 mM	0.126 ± 0.01	7.13 ± 0.44	213.5 ± 9.0	4.02 ± 0.45
10 mM	ND	ND	72.1 ± 3.5	9.34 ± 0.44
20 mM	ND	ND	57.3 ± 1.7	9.52 ± 0.07
30 mM	ND	ND	58.9 ± 0.9	9.50 ± 1.37
-Fe(II)	ND	ND	154.3 ± 1.8	5.95 ± 0.02

The CECT 5344 strain was grown with 50 mM sodium acetate as the carbon source and 10 mM ammonium as the sole nitrogen source in anaerobiosis (15 days) or aerobiosis (24 h) with different concentrations of Fe(II). Bacterial growth was determined by A_{600} or by the protein content (µg/mL). Ammonium remaining in the media was also determined. T0 represents initial data of the cultures at the time 0, before the bacterial growth. *Concentration of Fe(II) in the minimal media M9 with the standard metal trace solution. ND, not determined/not growth.

In addition, the effect of ferric ion and pH was also tested. For that, bacterial cells were inoculated in the M9 minimal media modified by addition of 300 µM iron (III), as ferric chloride ($FeCl_3$) or ferric citrate ($C_6H_5FeO_7$). The pH of the media was adjusted to 7.5 or 9.5 and the cells were grown under anoxic conditions during 15 days (Table 4.3). Cultures with 30 µM or 300 µM Fe(II)) were used as controls. At usual pH 9.5, both bacterial growth (A_{600}) and ammonium consumption were slightly higher in the cultures supplemented with Fe(III), specially with ferric citrate, than in the control with 30 µM Fe(II). In any case, this growth never exceeded that observed when 300 µM Fe(II) was used (Table 4.3).

In general, the growth achieved by *P. pseudoalcaligenes* CECT 5344 at pH 7.5 was lower than at pH 9.5, accordingly with the alkaliphilic nature of this bacterial strain (Luque-Almagro et al., 2005).

Table 4.3. Effect of iron(III) and pH on the anaerobic growth.

Anaerobiosis (15 days)	**A_{600}**		**NH_4^+ (mM) in the media**	
	pH 7.5	**pH 9.5**	**pH 7.5**	**pH 9.5**
T0	0.005		9.4 ± 0.4	
30 µM* Fe(II)	0.384 ± 0.03	0.405 ± 0.02	3.3 ± 0.2	4.6 ± 0.3
300 µM Fe(II)	0.418 ± 0.05	0.495 ± 0.02	3.11 ± 0.5	2.52 ± 0.06
30 µM Fe(II) + 300 µM $FeCl_3$	0.330 ± 0.04	0.423 ± 0.02	4.8 ± 0.44	3.95 ± 0.3
30 µM Fe(II) + 300 µM $C_6H_5FeO_7$	0.429 ± 0.04	0.476 ± 0.03	2.6 ± 0.5	2.83 ± 0.5

The CECT 5344 strain was grown in anaerobiosis during 15 days with 50 mM sodium acetate as the carbon source and 10 mM ammonium as the sole nitrogen source. Media contained 30 or 300 µM Fe(II), and also 300 µM Fe(III) was added as $FeCl_3$ or ferric citrate. Initial pH was 9.5 (as usual) or 7.5. Bacterial growth was determined by A_{600}. The ammonium remaining in the media was also measured. T0 represents the initial data of the cultures at the time 0, before bacterial growth *Concentration of Fe(II) with the standard metal trace added to the minimal media.

Finally, to establish the effect of nitrate and nitrite on the growth of *P. pseudoalcaligenes* CECT 5344 under anoxic condition, cells were cultured in the M9 minimal media with 30 µM Fe(II) and different concentrations of KNO_3 (10 mM, and 30 mM) or KNO_2 (1 mM, 2 mM, and 5 mM) as the sole nitrogen source, during 15 days in the dark. Only an extremely low bacterial growth was detected in the presence of nitrate or nitrite, with A_{600} around 0.13 in both cases, and protein contents lower than 30% of those obtained anaerobically with ammonium as N-source (data not shown).

4.3.2. Accumulation of polyhydroxyalkanoates

A significant accumulation of polyhydroxyalkanoates (PHA) was observed in *P. pseudoalcaligenes* CECT 5344 cells grown in M9 minimal media with 30 µM Fe(II) and 10 mM ammonium under anaerobic conditions, reaching approximately 12% dry weight, whereas in the aerobic controls C_Abs and C_Cons the PHA content reached only 4% and 6% dry weight, respectively (Fig. 4.1A). Additionally, this result was confirmed by staining with the Nile Red dye (Fig. 4.1B).

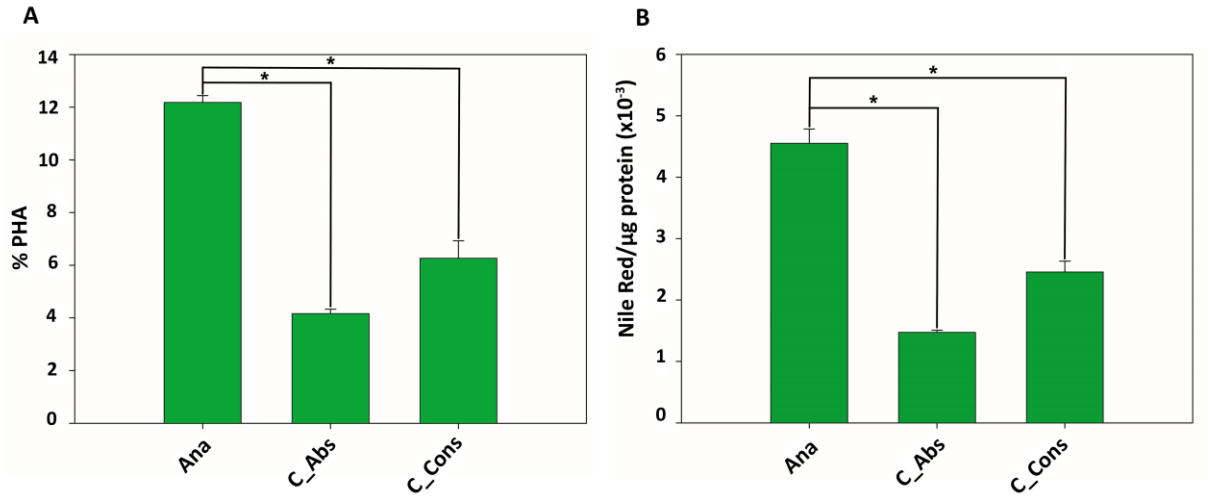

Figure 4.1. Determination of PHA accumulated by the *P. pseudoalcaligenes* CECT 5344 under anoxic or oxic conditions. The cells were grown as indicated in the Section 4.2.3. (A) The % PHA is the percentage of dry weight of PHA respect to the total dry weight of the cells. (B) Nile Red staining of PHA normalized by protein amount (µg) of cells grown under anaerobic (Ana) or aerobic (C_Abs, C_Cons) conditions. Asterisks indicate significant differences ($p < 0.05$) according to a *t*-test.

4.3.3. Transmission electron microscopy of *P. pseudoalcaligenes* CECT 5344 cells grown anaerobically

Cells of *P. pseudoalcaligenes* CECT 5344 grown under anaerobic conditions were analyzed by transmission electron microscopy (TEM) in comparison to the cells grown aerobically, as described in Section 4.2.4. As shown in the Figure 4.2, a significant increment of the periplasm space at both poles of the bacteria was observed in the cells cultured anaerobically. This widening of the periplasm was not observed in the cells grown aerobically. However, significant differences in the accumulation of PHA were not detected in the cells grown anaerobically or aerobically.

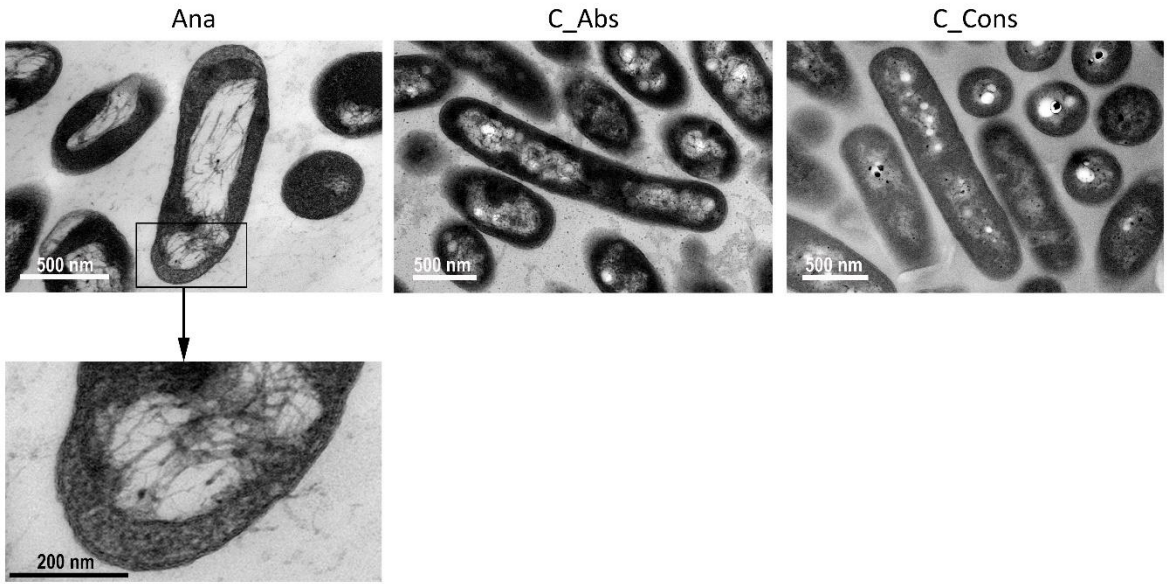

Figure 4.2. Electronic microscope images of *P. pseudoalcaligenes* CECT 5344. Cells were grown in minimal medium M9 with 10 mM ammonium and 50 mM acetate under anaerobic or aerobic condition. Images were taken after 15 days of growth for anaerobic cultures (Ana) and at A_{600} 0.4 (C_Abs) or when 6 mM ammonium was consumed (C_Cons) for aerobic conditions.

4.3.4. Proteomic analysis of *P. pseudoalcaligenes* CECT 5344 grown under anoxic conditions

To gain insights into the metabolism of *P. pseudoalcaligenes* CECT 5344 grown under anoxic condition, this strain was cultured in M9 minimal media and the intracellular proteome was analyzed in comparison to cells grown aerobically used as controls, as described in Section 4.2.5. The anaerobic cultures were harvested after 15 days, when reached an A_{600} 0.4 (Ana), whereas aerobic cultures were collected at A_{600} 0.4 (C_Abs) or when 6 mM ammonium was consumed (C_Cons). Three independent cultures were set up for intracellular LC-MS/MS data independent analysis, and a first analysis by principal component analysis (PCA) (Fig. 4.3) and qualitative Venn diagram was performed (Fig. 4.4). The PCA analysis clearly separated the three types of samples, although both aerobic controls C_Abs and C_Cons were much closely located (Fig. 4.3). As shown in the Venn diagram of the intracellular analysis, a total of 2568 unique proteins were identified from more than 1 peptide, representing the 58% of the 4435 total proteins encoded by the genome of the CECT 5344 strain, with 2495 proteins in Ana, 2537 proteins in C_Abs and 2545 proteins in C_Cons. Most of these proteins (2456 proteins) were shared among all three conditions (Fig. 4.4).

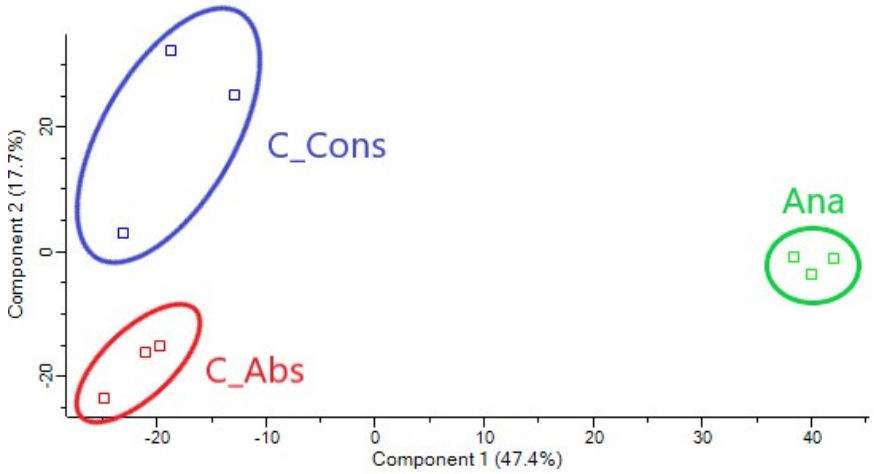

Figure 4.3. Principal component analysis (PCA) of *P. pseudoalcaligenes* CECT 5344 samples for intracellular proteomic analysis.

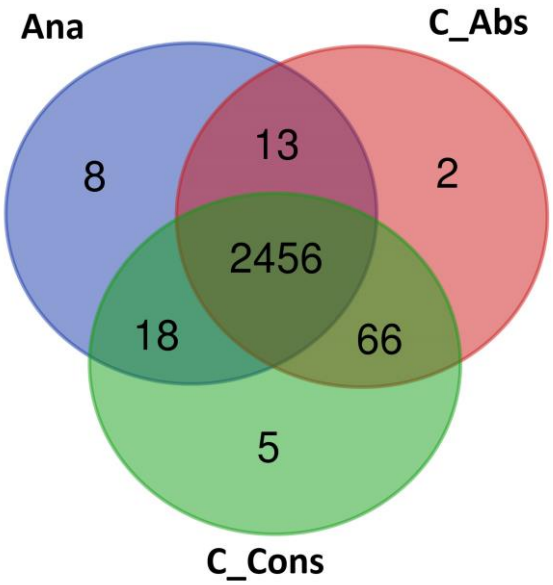

Figure 4.4. Venn diagram of proteins identified in the intracellular proteomic analysis of *P. pseudoalcaligenes* CECT 5344.

Furthermore, a differential quantitative analysis was performed to study the bacterium responses to anaerobic conditions, by comparing Ana *vs* C_Abs and Ana *vs* C_Cons, in the intracellular proteome analysis (Fig. 4.5). Proteins were considered differentially expressed when both the *q* value (adjusted *p* value) was < 0.05 and the fold change (FC) reached values ≥ 2, which is equal to $\log_2$ FC ≥ 1, (over-represented) or ≤ 0.5, which is equal to $\log_2$ FC ≤ -1 (down-represented). Likewise, the FC was calculated as the ratio of normalized peptide intensities of Ana/C_Abs or Ana/C_Cons. Proteins that were found only in one proteome (Ana, C_Abs or C_Cons), were considered 'exclusive' of that

condition. Thus, in this quantitative analysis of the intracellular proteome, when compared Ana *vs* C_Abs, 562 proteins were found differentially expressed, of which 242 proteins were over-expressed and 320 proteins were down-regulated in the Ana proteome. In addition, 21 proteins were found exclusively in the anaerobic condition (Fig. 4.5A). The comparison Ana *vs* C_Cons revealed 426 proteins differentially expressed, including 126 proteins over-represented and 300 proteins that were down-regulated in the Ana condition. Also, 17 proteins were exclusive of the anaerobic condition (Fig. 4.5B).

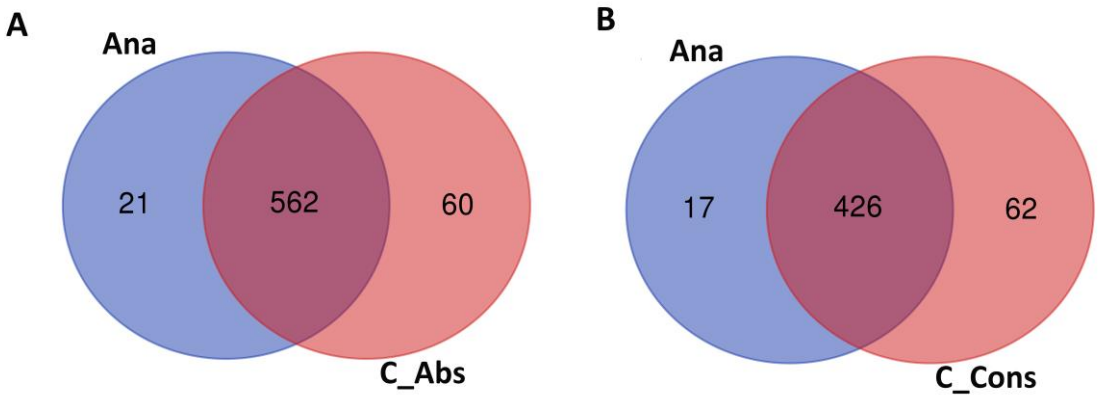

Figure 4.5. Venn diagrams of proteins identified in the comparative intracellular proteomic analyses Ana *vs* C_Abs (A) and Ana *vs* C_Cons (B) of *P. pseudoalcaligenes* CECT 5344.

The gene ontology (GO enrichment) analysis was performed to analyze the effect of anoxic condition on the global metabolism, by using the fold change values of the comparative studies from the intracellular proteomic analysis. In the Ana *vs* C_Abs comparative analysis, proteins up-regulated by the lack of oxygen gave an enrichment in some GO categories like chemotaxis and signal transduction, including methyl-accepting chemotaxis proteins (W6QTL2/BN5_0679, W6QUH0/BN5_1537, W6QV73/BN5_1791 and W6QVV2/BN5_2045); fatty acid beta-oxidation, including 3-hydroxyacyl-CoA dehydrogenase (W6QSR7/BN5_1379, W6QXU2/BN5_2237); iron ion transport, including putative hemin transport protein (W6QUB4/BN5_0956) and bacterioferritin (W6QZE8/BN5_3668); and poly-hydroxybutyrate biosynthesis process, including poly[(R)-3-hydroxyalkanoate] polymerase subunit PhaC (W6QSQ8/BN5_0414) and acetoacetyl-CoA reductase (W6R346/BN5_4103) (Fig. 4.6A). The proteins down-regulated under anaerobic conditions gave an enrichment in GO categories like protein maturation by iron-sulfur cluster transfer and iron-sulfur cluster assembly, including CyaY protein (W6QPD6/BN5_0191) and the nitrogen fixation-related protein NifU (W6R0Q7/BN5_3267); and translation, with large subunit ribosomal protein L9 (W6QQB9/BN5_0538), large subunit ribosomal protein L2 (W6QRB3/BN5_0856), and the small subunit ribosomal protein S15 (W6QRJ2/BN5_0933), among others (Fig. 4.6B).

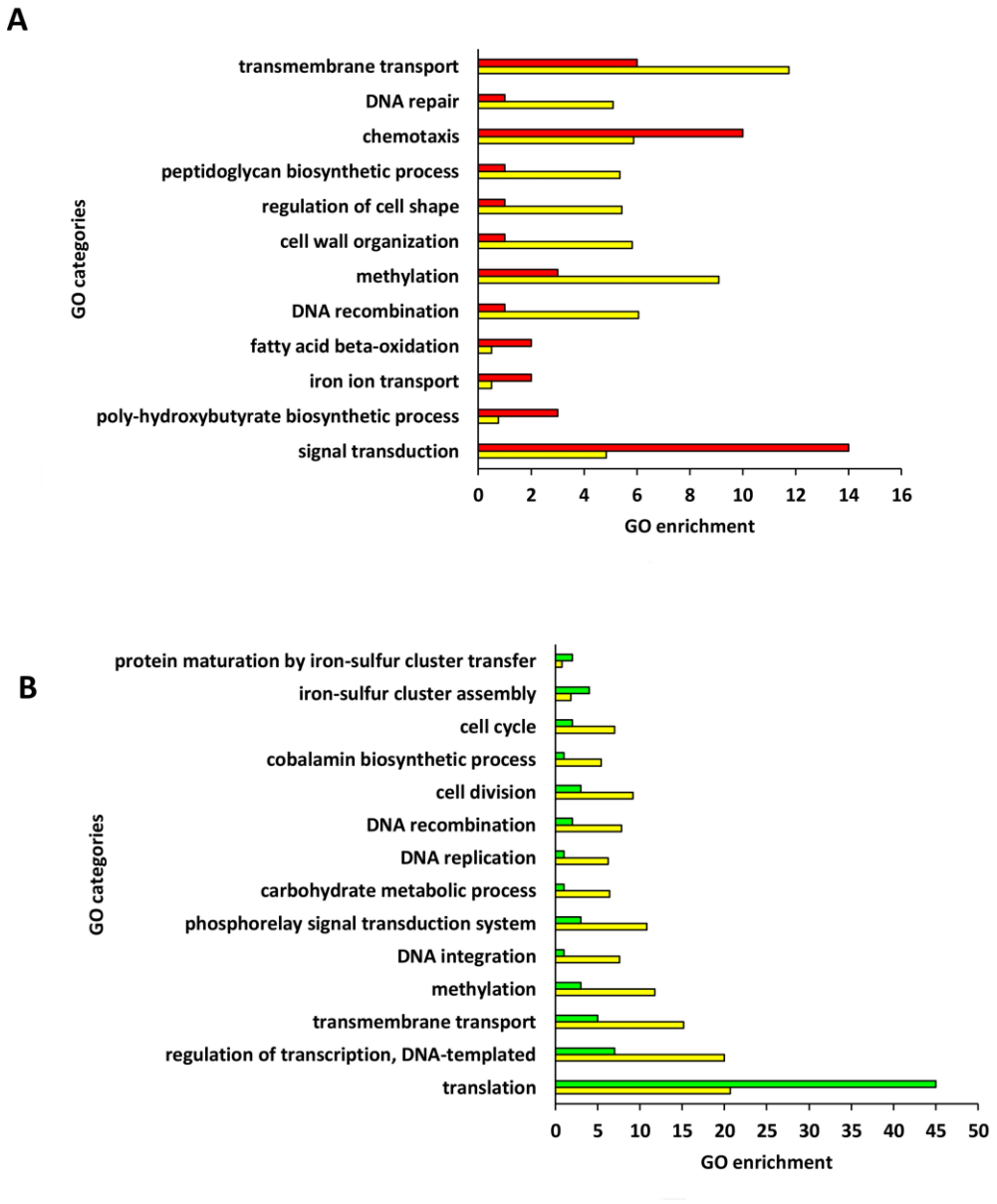

Figure 4.6. GO enrichment analysis of the anaerobic (A) and the control (C_Abs) proteomes (B). Significative changes in GO groups of proteins over-represented in each condition (red or green) for each comparison. The genome of the wild-type strain was considered as reference (yellow).

On the other hand, in the Ana *vs* C_Cons comparison, the proteins over-represented under anoxic condition were related to the protein transport categories, such as MotA/TolQ/ExbB proton channel family protein (W6R0H4/BN5_3660), biopolymer transport protein ExbB (W6RDS6/BN5_1440), and fatty acid beta-oxidation proteins like 3-hydroxyacyl-CoA dehydrogenase (W6QSR7/BN5_1379 and W6QXU2/BN5_2237) (Fig. 4.7A). Finally, the aerobic condition C_Cons yielded an enrichment in the functional groups associated with acetyl-CoA biosynthesis process, including two acetate kinase (W6QSM4/BN5_0893 and W6RL83/BN5_4099); polyamine transport, such as the putrescine transport system substrate-binding protein (W6QPL1/BN5_0266); and

translation, with the small subunit ribosomal protein S15 (W6QRJ2/BN5_0933), peptide deformylase (W6QRM0/BN5_0027), small subunit ribosomal protein S16 (W6QRW6/BN5_1073), and the small subunit ribosomal protein S18 (W6QT34/BN5_0536), among others (Fig. 4.7B).

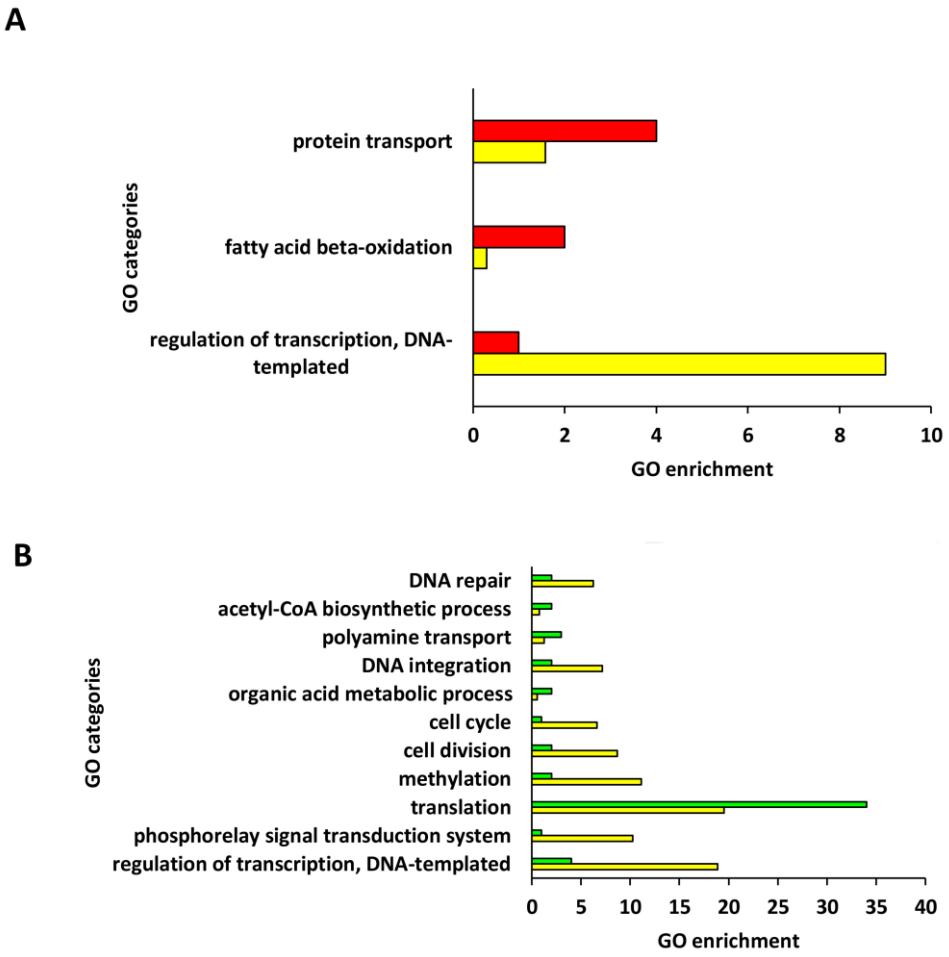

Figure 4.7. GO enrichment analysis of the anaerobic (A) and the control (C_Cons) proteomes (B). Significative changes in the GO groups proteins over-represented in each condition (red or green) for each comparison. The genome of the wild-type strain was considered as reference (yellow).

In addition to the results obtained from the functional group enrichment, the intracellular differential comparative analysis of Ana *vs* C_Abs and Ana *vs* C_Cons allowed a deeply analysis of the metabolism of *P. pseudoalcaligenes* CECT 5344 under anoxic conditions in the presence of ammonium and iron (Fig. 4.8; Supplementary Materials, Table S3). Several relevant proteins identified in this comparative quantitative analysis of the intracellular proteomes were classified functionally and grouped into iron ion transport, fatty acids synthesis/degradation, polyhydroxyalkanoates metabolism, oxidative phosphorylation, arginine metabolism, glyoxylate metabolism, and others proteins. Therefore, in the first category, proteins exclusively found in the Ana proteome, when compared to

both aerobic controls, were the ATP-binding component of hydroxamate-dependent iron transport (W6QR17/BN5_0756) and the transmembrane permease component of a heme ABC transporter (W6QRL6/BN5_0958). The outer membrane heme receptor (W6QST3/BN5_0955) was detected exclusively in the Ana proteome when compared to C_Abs control, and it was found up-regulated by anaerobiosis in the comparison Ana *vs* C_Cons. Also, proteins over-represented in Ana condition in both comparisons were the ferredoxin-NADP reductase (W6QTI1\BN5_0636), the ferric uptake regulator Fur (W6QZB3/BN5_0907), the B12 family TonB-dependent receptor (W6R745/BN5_3634) and the TonB-dependent siderophore receptor (W6QTM2/BN5_0694). Interestingly, the iron-regulated protein A (W6QS07/BN5_1133) and another TonB-dependent siderophore receptor (W6R3L4/BN5_2417) were down-regulated in the Ana proteome in the Ana *vs* C_Abs comparison, meanwhile, when compared to the C_Cons as a control, these proteins were over-represented or exclusive, respectively, under the anaerobic condition (Fig. 4.8).

Proteins related to fatty acids metabolism were found over-represented under anoxic conditions in both differential comparisons, including the fatty acid oxidation complex subunit alpha (W6QSR7/BN5_1379), the putative 3-hydroxyacyl-CoA dehydrogenase (W6QXU2/BN5_2237), the acetyl-CoA acyltransferase (W6RG21/BN5_2238), and acetyl-CoA acetyltransferase (W6RJ87/BN5_3309 and W6RL89/BN5_4104). In addition, the enzymes responsible for the synthesis of polyhydroxyalkanoates were also identified in this differential proteomic analysis. Proteins that were up-regulated in the anaerobic condition in both comparative analyses were the poly(hydroxyalkanoate) granule-associated protein (Phasin) (W6QSQ4/BN5_0409), the poly(3-hydroxyalkanoate) polymerase (W6QSQ8/BN5_0414), and the acetyl-CoA acetyltransferase (W6RJ87/BN5_3309). However, other proteins like the phasin-like protein (W6R8A0/BN5_4096), the poly(3-hydroxyalkanoate) synthetase (W6R1M3/BN5_4097) and the poly(R)-hydroxyalkanoic acid synthase, class I (W6R0M2/BN5_4105) were down-expressed in C_Abs conditions, while these proteins were up-regulated in C_Cons proteome. Similarly, a few proteins associated with oxidative phosphorylation, including the cytochrome *c* oxidase, *cbb*3-type, subunit II (W6R3N9/BN5_2442), the *cbb*3-type cytochrome *c* oxidase subunit III (W6QYC1/BN5_2444), and the cytochrome *c*-type protein (W6R4P8/BN5_2781) were induced in the Ana proteome in comparison with C_Abs, but these proteins were down-regulated in anaerobiosis when the Ana and C_Cons proteomes were compared. The β subunit of the ATP synthase (W6R1T2/BN5_4501) was over-expressed in the absence of oxygen in both comparative analyses (Fig.4.8).

Proteins associated with arginine metabolism, including the NAD-glutamate dehydrogenase (W6QZ65/BN5_2725), the arginine deiminase (ADI) (W6R686/BN5_3331), and the ornithine carbamoyltransferase (OTCase) (W6QZK4/BN5_3332), were over-expressed in the Ana proteome in

both analyses, although in the Ana *vs* C_Cons comparison these proteins showed lower induction than in the Ana *vs* C_Abs comparison. Only the glutamine synthetase (W6QVI3/BN5_2309) demonstrated similar level of induction in both comparisons. Proteins related to the glyoxylate cycle, including the malate synthase (W6QP71/BN5_0124), the isocitrate lyase (W6REY3/BN5_1853) and the succinate-CoA ligase (W6RFW4/BN5_2173), were found down-regulated in the Ana proteome compared with both aerobic controls. Finally, several other proteins including the aspartate ammonia-lyase (W6QP19/BN5_0079), the lysyl/prolyl-type hydroxylase (PKHD-type hydroxylase) (W6RBT9/BN5_0695), and the 4-hydroxyphenylpyruvate dioxygenase (W6QUG4/BN5_1532) were over-represented by anoxic conditions in both differential comparative analyses (Fig. 4.8).

Protein ID	Locus	Protein name/description	C_Abs	C_Cons
Iron ion transport				
W6RAG8	BN5_0205	HemY domain-containing protein		
W6QTI1	BN5_0636	Ferredoxin-NADP reductase		
W6QTM2	BN5_0694	TonB-dependent siderophore receptor		
W6QR17	BN5_0756	ATP-binding component of hydroxamate-dependent iron transport		
W6QZB3	BN5_0907	Ferric uptake regulation protein		
W6QST3	BN5_0955	Outer membrane heme receptor		
W6QRL6	BN5_0958	Transmembrane permease component of heme ABC transporter		
W6QS07	BN5_1133	Iron-regulated protein A		
W6R3L4	BN5_2417	TonB-dependent siderophore receptor		
W6R745	BN5_3634	B12 family TonB-dependent receptor		
W6QZE8	BN5_3668	Bacterioferritin		
W6R955	BN5_4387	Rhizobactin receptor		
Fatty acid synthesis/degradation				
W6QSR7	BN5_1379	Fatty acid oxidation complex subunit alpha		
W6QXU2	BN5_2237	Putative 3-hydroxyacyl-CoA dehydrogenase		
W6RG21	BN5_2238	Acetyl-CoA acyltransferase		
W6QYI9	BN5_2514	Acyl-CoA dehydrogenase		
W6RJ87	BN5_3309	Acetyl-CoA acetyltransferase		
W6RL89	BN5_4104	Acetyl-CoA acetyltransferase		
Polyhydroxyalkanoates metabolism				
W6QSQ4	BN5_0409	Poly(Hydroxyalkanoate) granule-associated protein		
W6QSQ8	BN5_0414	Poly(3-hydroxyalkanoate) polymerase		
W6RJ87	BN5_3309	Acetyl-CoA acetyltransferase		
W6R8A0	BN5_4096	Phasin-like protein		
W6R1M3	BN5_4097	Poly(3-hydroxyalkanoate) synthetase		
W6R1N0	BN5_4102	Transcription activator in PHB biosynthesis		
W6R346	BN5_4103	Acetoacetyl-CoA reductase		
W6RL89	BN5_4104	Acetyl-CoA acetyltransferase		
W6R0M2	BN5_4105	Poly(R)-hydroxyalkanoic acid synthase, class I		
Oxidative phosphorylation				
W6R3N9	BN5_2442	Cytochrome *c* oxidase, *cbb* 3-type, subunit II		
W6QYC1	BN5_2444	*Cbb* 3-type cytochrome *c* oxidase subunit III		
W6R1T2	BN5_4501	ATP synthase subunit *b*		

Protein ID	Locus	Protein name/description	C_Abs	C_Cons
Arginine metabolism				
W6QVI3	BN5_2309	Glutamine synthetase		
W6QZ65	BN5_2725	NAD-glutamate dehydrogenase		
W6R686	BN5_3331	Arginine deiminase (ADI)		
W6QZK4	BN5_3332	Ornithine carbamoyltransferase (OTCase)		
W6R9C4	BN5_4457	N-acetyl-gamma-glutamyl-phosphate reductase		
Glyoxylate metabolism				
W6QP71	BN5_0124	Malate synthase G		
W6REY3	BN5_1853	Isocitrate lyase		
W6RFW4	BN5_2173	Succinate-CoA ligase		
W6R168	BN5_3925	Malate synthase G		
Other proteins				
W6QP19	BN5_0079	Aspartate ammonia-lyase		
W6RBT9	BN5_0695	PKHD-type hydroxylase BN5_0695		
W6QUG4	BN5_1532	4-hydroxyphenylpyruvate dioxygenase		

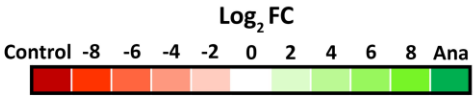

Figure 4.8. Heatmap of over-represented (green) or down-represented (red) proteins in the anaerobic condition in the differential intracellular proteomic analysis of *P. pseudoalcaligenes* CECT 5344. The differential expression of proteins is represented as Log_2 fold change (FC). The fold change has been calculated as the ratio of normalized peptide intensity form Ana/C_Abs (C_Abs) and Ana/C_Cons (C_Cons). Protein codes according to Uniprot database under the accession number UP000032841. Gene annotation corresponds to GeneBank (Accession HG916826.1).

On the other hand, an additional extracellular LC-MS/MS proteomic analysis was also performed. The samples for this analysis were harvested at the different time frame that those used for intracellular analysis. Unfortunately, high level of contamination with intracellular proteins was detected within extracellular samples, but nonetheless, it is worth to mention several proteins that were identified as induced or exclusive in the anaerobic condition, in both Ana *vs* C_Abs and Ana *vs* C_Cons comparative analysis (Fig. 4.9). Firstly, proteins like the NADPH sulfite/nitrite reductase (W6RF17/BN5_1900), the phosphoserine aminotransferase (W6QWX6/BN5_1904) and the acetylornithine aminotransferase (W6QU95/BN5_1906), which are encoded by the *cio* gene cluster involved in the cyanide-insensitive respiration, were detected over-represented in the anaerobic condition in this extracellular proteomic analysis.

Protein ID	Locus	Protein name/description	C_Abs	C_Cons
Tricarboxylic acid cycle				
W6QRS6	BN5_0087	L-asparaginase I		
W6QT92	BN5_1100	Phosphoenolpyruvate carboxylase (PEPC)		
W6RE08	BN5_1524	Fumarate hydratase class II		
W6REZ0	BN5_1863	Isocitrate dehydrogenase		
W6QUA1	BN5_1911	NADP-dependent malic enzyme		
W6QV55	BN5_2179	Succinate dehydrogenase flavoprotein subunit		
W6R327	BN5_2180	Succinate dehydrogenase hydrophobic membrane anchor subunit		
W6QXP3	BN5_2182	Citrate synthase		
W6QX86	BN5_2542	Aconitate hydratase		
W6QZ65	BN5_2725	NAD-glutamate dehydrogenase		
W6RLU2	BN5_4310	Acetyl-CoA carboxylase		
Lactate and ethanol production				
W6QSB1	BN5_0783	Alcohol dehydrogenase		
W6QSM4	BN5_0893	Acetate kinase		
W6QSM9	BN5_0898	D-lactate dehydrogenase		
W6QRR4	BN5_1018	Aldehyde dehydrogenase		
W6QVL2	BN5_2341	Aldehyde dehydrogenase		
Glutamate metabolism				
W6QXD0	BN5_0157	4-aminobutyrate aminotransferase		
W6QVI3	BN5_2309	Glutamine synthetase		
W6R8K7	BN5_4197	Putative glutamine synthetase		
W6R3X1	BN5_4339	Putative glutamine synthetase		
***cio* gene cluster**				
W6RF17	BN5_1900	NADH sulfite/nitrite reductase		
W6QWX6	BN5_1904	Phosphoserine aminotransferase		
W6QU95	BN5_1906	Acetylornithine aminotransferase		
Electron transport chain				
W6QRT0	BN5_0092	Cytochrome *c* oxidase subunit II		
W6QTJ2	BN5_0654	NADH dehydrogenase		
W6RBM7	BN5_0627	Cytochrome *d* ubiquinol oxidase, subunit I		
W6QWX9	BN5_2443	Putative membrane protein		
W6RGI6	BN5_2445	Cytochrome *c* oxidase, *cbb* 3-type, subunit I		
W6QZZ6	BN5_3480	Cytochrome *b*		
W6R9H1	BN5_4502	ATP synthase subunit *c*		
W6R2W6	BN5_4503	ATP synthase subunit *a*		
Nap system				
W6QZA5	BN5_2778	Protein NapD		
W6RHN5	BN5_2779	Nitrate reductase NapA		
W6R4P8	BN5_2781	Cytochrome *c* -type protein NapC		
W6QUD8	BN5_0991	Anaerobic nitric oxide reductase transcription regulator NorR		

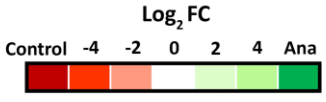

Figure 4.9. Heatmap of over-represented (green) or down-represented (red) proteins in the anaerobic condition in the differential extracellular proteomic analysis of *P. pseudoalcaligenes* CECT 5344. The differential expression of proteins is represented as Log_2 fold change (FC). The fold change has been calculated as the ratio of normalized peptide intensity form Ana/C_Abs (C_Abs) and Ana/C_Cons (C_Cons). Protein code are according to Uniprot database under the accession number UP000032841. Genes annotation are from GeneBank (Accession HG916826.1).

Interestingly, several proteins related to electron transport chain were found up-regulated in the anaerobic condition, including the cytochrome *cbb*3-type protein (W6RGI6/BN5_2445), the ATP synthase subunits *a* and *c* (W6R2W6/BN5_4503 and W6R9H1/BN5_4502), the NADH dehydrogenase (W6QTJ2/BN5_0654), and the cytochrome *b* (W6QZZ6/BN5_3480). Additionally, some proteins related to nitrate reduction were also found in this anaerobic condition, such as the periplasmic nitrate reductase NapA (W6RHN5/ BN5_2779) and the anaerobic nitric oxide reductase transcription regulator NorR (W6QUD8/ BN5_0991). In addition, the protein NapD (W6QZA5/BN5_2778) and the cytochrome *c*-type protein NapC (W6R4P8/BN5_2781) were exclusive in the Ana proteome, when C_Abs was used as a control. Regarding the central metabolic pathways, enzymes related to the tricarboxylic acid cycle were over-represented in anaerobiosis, including, among others, citrate synthase (W6QXP3/BN5_2182), fumarate hydratase (fumarase C) (W6RE08/BN5_1524), succinate dehydrogenase (W6QV55/BN5_2179 and W6R327/BN5_2180), as well as NADP-dependent malic enzyme (W6QUA1/BN5_1911). Other proteins like lactate dehydrogenase (W6QSM9/BN5_0898), aldehyde dehydrogenase (W6QVL2/BN5_2341, W6QRR4/ BN5_1018) and alcohol dehydrogenase (W6QSB1/BN5_0783) were also induced in the Ana proteome. However, the isocitrate dehydrogenase (W6REZ0/BN5_1863) was found down-regulated by anaerobiosis (Fig. 4.9).

4.4. Discussion

The intensive industrial activities have contributed significantly to the production of wastewaters. It is estimated that 2 billion tons of organic wastes are currently generated worldwide, which will increase to 3.4 billion tons by 2050 (Mushtaq et al., 2020). Therefore, the development of new technologies that will allow the bioremediation of industrial wastes, and its conversion into green energy is of great biotechnological interest. Anaerobic biodegradation, which allows for waste stabilization while providing sustainable energy source that might replace fossil fuels, has become a promising solution for wastes removal (El Asri et al., 2020; El Asri, 2023). Therefore, anaerobic processes have gained interest and importance in the development of bioremediation technologies through the recent years. The intense anthropogenic activities, especially utilization of fertilizers in agriculture, fossils burn, and disposal of food wastes, generate an excessive amount of nitrogen deposition in the environment (Fowler et al., 2013; Li et al., 2015; Chen et al., 2016). The excess of nitrogen discharged uncontrollably to the environment without treatment may lead to serious environmental problems, such as freshwater eutrophication, a decrease of dissolved oxygen levels in water, that provokes biodiversity loss, acidification, and inhibition of microbial activity, which is very sensitive to environmental conditions (Lauterböck et al., 2012; Gao et al., 2014; Chen et al., 2016). The traditional nitrification and

denitrification processes, which are applied in both aerobic and anaerobic wastewater treatments, have low efficiency for ammonium removal (Yang et al., 2018). In addition, the anaerobic ammonium oxidation (Anammox) that removes ammonium using nitrite as an electron acceptor, has been also reported insufficient (Dalsgaard et al., 2005). Thus, the discovery of a novel anaerobic ammonium oxidation process coupled to Fe(III) reduction, the so-called Feammox, has become a promising candidate for ammonium removal from wastes (Clément et al., 2005).

Iron plays a crucial role in microbial growth, being an essential micronutrient that is included in heme and non-heme cofactors present in many different proteins (Andrews et al., 2003). In addition, the Fe-reducing and Fe-oxidizing bacteria have a significant impact on the iron redox biogeochemical cycle. Fe(II) is an efficient electron donor that forms reactive oxidants in some environments, and it may also reduce some redox-sensitive contaminants (Borch et al., 2010; Tong et al., 2016; Ginn et al., 2017; Xie et al., 2020). Nonetheless, at high concentrations, Fe could be toxic for microorganisms by causing oxidative stress, precipitating on biotic surface, competing with other metals for the insertion into metalloproteins, or inhibiting the F-ATPase and other enzymes (Vuori, 1995; Dunning et al., 1998; Foster et al., 2014).

The aim of the research presented in this Chapter III was to investigate the potential of the cyanotrophic bacterium *Pseudomonas pseudoalcaligenes* CECT 5344 to grow under anaerobic conditions in the presence of iron and ammonium, by applying a data-independent proteomic analysis from cells grown with an anaerobic lifestyle. Previous works have demonstrated the great biotechnological potential of the CECT 5344 strain to degrade and assimilate cyanide under alkaline pH, and its resistance to the simultaneous presence of toxic metals like arsenic and mercury (Luque-Almagro et al., 2005; Biełło et al., 2023a,b). Nonetheless, the ability to adapt this strain to anoxic conditions has not been described yet.

P. pseudoalcaligenes CECT 5344 was able to grow anaerobically in the dark in minimal mineral medium with the normal trace amount of iron (30 µM), using 50 mM acetate as carbon source and 10 mM ammonium as the sole nitrogen source, during a period of 15 days. After this time, the bacterial cells consumed about 6 mM of the N-source (ammonium) and reached an A_{600} higher than 0.4. Under this anaerobic conditions, the increase in the protein content was even slightly higher than in aerobic cultures with similar $A_{600} \approx 0.4$ (Table 4.1). Several *Pseudomonas* species have been reported as facultative anaerobes, including *P. denitrificans* and *P. fluorescens,* which use inorganic compound like nitrate as alternative terminal electron receptor, or *P*. *aeruginosa*, which performs arginine fermentation (Eschbach et al., 2004; Wu et al., 2005; Trunk et al., 2010; Fowler et al., 2013; Glasser et al., 2014; Kampers et al., 2021).

The anaerobic growth of *P. pseudoalcaligenes* CECT 5344 was ammonium dependent, because growth with nitrate or nitrite was significantly lower than with NH_4^+. However, this strain is not able to carry out the anaerobic ammonia oxidation process (Anammox), which is almost exclusively performed by chemolithoautotrophic bacteria of the Planctomycetota group, such as *Kuenenia*, *Scalindua*, *Jettenia* and *Brocardia* (Manonmani and Joseph, 2018). Nonetheless, the anaerobic growth of the strain CECT 5344 was also dependent on the presence of iron, showing its maximal growth at an iron concentration of 300 µM (Table 4.2). *P. pseudoalcaligenes* CECT 5344 was able to resist up to 3 mM Fe(II) under anaerobic conditions, although showing a significantly impaired growth (Table 4.2). This resistance was higher than that reported for *Streptococcus mutants*, with 97% cells dead with 1 mM Fe(II), but significantly lower than in *Rhodopseudomonas palustris*, which was able to grow with 10 mM Fe(II) without showing evidence of oxidative stress damage (Dunning et al., 1998; Bryce et al., 2018). On the other hand, the growth of the strain CECT 5344 cultured with 0.3 µM or 3 µM was significantly lower than with the usual Fe concentration (30 µM) or with 300 µM Fe. Furthermore, the cells cultured under iron depravation were unable to grow anaerobically, whereas a slight growth with a significant ammonium consumption was obtained in the aerobic cultures without iron (Table. 4.2). Thus, it may be concluded, that iron is an essential element for the anaerobic growth of this bacterium, and that a process like anaerobic ammonium oxidation coupled to Fe(III) reduction (Feammox) could not be discarded, although a Fe(II)-Fe(III) cycle should be involved, as described in other bacteria, including *Pseudomonas* species (Wang et al., 2022).

A key factor for microbial growth is the pH of the media, since pH determines enzyme activity and protein conformation, and it may affect directly iron precipitation (Hoštacká et al., 2010; Aryal and Liakopoulou-Kyriakides, 2014; Huang et al., 2021). Additionally, it was suggested that a neutral pH is required for optimal Fe(III) reduction under anaerobic conditions (Rodríguez et al., 2021). Therefore, the possible anaerobic growth of *P. pseudoalcaligenes* CECT 5344 was tested at pH 7.5 or 9.5, and with Fe(III) supplementation. However, no significant differences in bacterial growth were observed (Fig. 4.3). Nonetheless, intracellular measurements of pH during bacterial growth would be required.

To get an holistic view of the *P. pseudoalcaligenes* CECT 5344 anaerobic metabolism, an intracellular proteomic data-independent LC-MS/MS analysis was performed. Foremost, the comparative GO enrichment analysis of Ana *vs* C_Abs proteomes demonstrated proteins over-represented under anoxic conditions that belonged to functional groups associated with chemotaxis, fatty acids beta-oxidation, iron ion transport, poly-hydroxybutyrate biosynthetic process, and signal transduction (Fig. 4.6). On the other hand, in the GO enrichment analysis performed for the Ana *vs* C_Cons comparison, the identified functional groups were mainly related to protein transport and fatty acid beta-oxidation (Fig. 4.7). A detailed differential analysis allowed to identify specific proteins that

might be related to adaptation of *P. pseudoalcaligenes* CECT 5344 to anaerobic lifestyle (Fig. 4.8; Supplementary Materials, Table S3). Interestingly, numerous proteins related to iron transport were over-represented in the proteome of anaerobiosis, such as the ferric uptake regulator Fur (W6QZB3/BN5_0907) and bacterioferritin (W6QZE8/BN5_3668). Also, among the proteins induced in the anaerobic proteome were the TonB-dependent siderophore receptor (W6QTM2/BN5_0694 and W6R745/BN5_3634) and the outer membrane heme receptor (W6QZB3/BN5_0955). Those proteins were induced in a Fur^- defective mutant of *P. pseudoalcaligenes* CECT 5344, and it has been reported that under iron limitation, the strain CECT 5344 expresses genes necessary for metabolism of Fe-siderophores produced by other microorganisms (Becerra et al., 2020). Thus, it might be suggested that a response similar to iron starvation is triggered due to the high iron demand during the anaerobic growth of the strain CECT 5344.

The comparative intracellular proteomic analysis (Fig. 4.8) also revealed that several proteins that might be involved in fatty acid metabolism were over-represented in Ana proteome in comparison with both aerobic controls (C_Abs and C_Cons), including 3-hydroxyacyl-CoA dehydrogenase (W6QXU2/BN5_2237), acetyl-CoA acyltransferase (W6RG21/BN5_2238), and putative 3-hydroxyacyl-CoA dehydrogenase (W6QXU2/BN5_2237). Also, proteins associated with production of polyhydroxyalkanoates (PHA), such as poly(hydroxyalkanoate) granule-associated protein (Phasin) (W6QSQ4/BN5_0409), poly(3-hydroxyalkanoate) polymerase (W6QSQ8/BN5_0414) and acetyl-CoA acetyltransferase (WRRJ87/BN5_3309 and W6RL89/BN5_4104) were induced under anaerobiosis. *P. pseudoalcaligenes* CECT 5344 was previously reported to accumulate PHA, which are biopolymers synthetized and accumulated under nutrient-limited conditions and excess of carbon source (Manso et al., 2015). Taking under consideration the fact that the strain CECT 5344 was cultured with 50 mM acetate as carbon source, it might be suggested that excess of acetate was directed to fatty acid biosynthesis, and accumulated as PHA. This is supported by the increased accumulation of PHA found in the anaerobic condition (Fig. 4.1). Interestingly, proteins like the poly(3-hydroxyalkanoate) synthetase (W6R1M3/BN5_4097), the PHB biosynthesis transcription activator (W6R1N0/BN5_4102), the acetoacetyl-CoA reductase (W6R346/BN5_4103), and the poly(R)-hydroxyalkanoic acid synthase, class I (W6R0M2/BN5_4105) were found induced by anoxic conditions when C_Abs was used as a control, whereas these proteins were down-regulated in the Ana proteome in the Ana *vs* C_Cons comparison. The observed switch in anaerobic metabolism was also confirmed by PHA detection and Nile Red staining, with the samples from C_Cons showing slightly higher PHA content than the C_Abs control (Fig. 4.1). Apart from PHAs, a significant increasement of the periplasmic space at both poles of the bacteria was observed in the cells cultured anaerobically (Fig. 4.2). This may be due to the stress conditions that are triggered by oxygen deprivation, since a similar widening of the periplasm was

observed in other *Pseudomonas* species that were cultured under different stress conditions (Ghorbal et al., 2019).

An extracellular LC-MS/MS data-independent proteomic analysis was also performed to complete the intracellular study. Unfortunately, a high level of intracellular protein contamination was detected within extracellular samples, which could be due to many factors, such as cell lysis during bacterial growth, vesicular transport, cell rupture during collection of the samples, or lack of filtration of the collected supernatant. Nonetheless, several proteins of great interest were identified in this extracellular analysis, that were not detected in the previous intracellular study. Therefore, an illustrative and preliminary view based on both intra- and extracellular data may be proposed, although an additional proteomic analysis could be required further to confirm the presented findings.

Proteins related to the tricarboxylic acid cycle were found over-represented in anaerobiosis in both Ana *vs* C_Abs and Ana *vs* C_Cons extracellular analyses (Fig. 4.9), including citrate synthase (W6QXP3/BN5_2182), aconite hydratase (W6QX86/BN5_2542), fumarate hydratase (W6RE08/BN5_1524), and succinate dehydrogenase flavoprotein (W6QV55/BN5_2179). It has been recently reported by various studies that fumarate may play a role as electron acceptor in a process called fumarate respiration (Tomasiak et al., 2007; Lin et al., 2015; Spinelli et al., 2021; Schubert and Unden, 2023). In this reaction, fumarate is reduced to succinate, by a succinate dehydrogenase isoform with fumarate reductase activity, and this is sustained by the electron input to the complex II of the electron transport chain. The presence of both fumarate reductase and succinate dehydrogenase is crucial for fumarate respiration to take place (Kröger, 1978; Maklashina et al., 1998). Subsequently, the fate of succinate produced in this process could be speculated. Firstly, it could be converted into 2-oxoglutarate by a PKHD-type hydrolase (W6RBT9/BN5_0695) that uses Fe(II) as cofactor, which is over-represented in the Ana proteome in both intracellular and extracellular analyses. This keto acid is further incorporated to the glutamate metabolism, since the NAD-glutamate dehydrogenase (W6QZ65/BN5_2725) was found up-regulated in the anoxic condition, whereas the isocitrate dehydrogenase (W6REZ0/BN5_1863), responsible for synthesis of 2-oxoglutarate from isocitrate was found down-regulated. Secondly, the excess of succinate could constrain the expression of isocitrate lyase (W6REY3/BN5_1853) of glyoxylate cycle (Pham et al., 2017; Pham et al., 2021), which was detected in all samples, but without significant changes. Finally, excess of succinate could also be excreted from the cell (Schubert and Unden, 2023).

Interestingly, the L-asparaginase (W6QRS6/BN5_0087) that catalyzes the synthesis of L-aspartate from L-asparagine, was detected exclusively in the Ana *vs* C_Abs comparison of the extracellular proteome (Fig. 4.9). The aspartate ammonia-lyase AspA (W6QP19/BN5_0079), which

reversibly convert L-asparagine into fumarate with simultaneous release of ammonia, was also found up-regulated under anoxic conditions in intracellular comparisons with both aerobic controls (C_Abs and C_Cons) (Fig. 4.8). The *aspA* gene may be important for anaerobic respiration, due to generation of fumarate, which further may be used as electron acceptor (Van Hellemond and Tielens, 1994). Additionally, the *aspA* gene might also be relevant for iron-acquisition, since it was significantly induced in several bacterial strains under iron-restricted conditions (Holmes et al., 2005; Deslandes et al., 2007; Dumpala et al., 2015; Luo et al., 2019).

The nitrate reductase NapA (W6RHN5/ BN5_2779) was over-represented in anaerobiosis in the extracellular analysis (Ana *vs* C_Abs). Also, other protein related to the periplasmic nitrate reduction like the NapD (W6QZA5/ BN5_2778) was found induced in the extracellular Ana proteome (Ana *vs* C_Abs) (Fig. 4.9), whereas the cytochrome *c*-type NapC protein (W6R4P8/BN5_2781) was over-represented under anaerobiosis when compared with C_Abs as a control, in both intracellular and extracellular comparisons. Also, the ferredoxin dependent sulphite/nitrite reductase (W6RF17/BN5_1900) was exclusive for anaerobiosis in the extracellular analysis. Nonetheless, the strain CECT 5344 is not able to perform denitrification, and the essential machinery for this process including the respiratory nitrate reductase (Nar) was not identified in the genome of *P. pseudoalcaligenes* CECT 5344. Additionally, only minor bacterial growth was detected in cells grown with KNO_2 or KNO_3 as nitrogen and energy source under anoxic conditions. Therefore, it might be suggested that the Nap system was induced under anoxic conditions due to the excess of reducing power (Moreno-Vivián et al., 1999), probably generated from an active Krebs cycle. Alongside, proteins such as lactate dehydrogenase (W6QSM9/BN5_0898), aldehyde dehydrogenase (W6QVL2/BN5_2341, W6QRR4/ BN5_1018) and alcohol dehydrogenase (W6QSB1/BN5_0783) were also found up-regulated by anoxic conditions in the extracellular differential comparisons, which may indicate that lactate and ethanol production could be related to the dissipation of the excess of reducing power to maintain redox homeostasis, allowing NAD^+ regeneration required for catabolic reactions.

On the other hand, protein related to the electron transport chain, such as cytochrome *c* oxidase *cbb*3-type subunits II and III (W6R3N9/BN5_2442 and W6QYC1/BN5_2444) were found induced by anoxic conditions in the intracellular Ana *vs* C_Abs proteomes, whereas the cytochrome *c* oxidase *cbb*3- type subunit I (W6RGI6/BN5_2445) and the putative membrane protein (W6QWX9/BN5_2443) were found induced or exclusive, respectively, in the Ana proteome in both extracellular comparisons (C_Abs and C_Cons) (Figs. 4.8 and 4.9). Likewise, proteins encoded by the *cio* gene cluster, including the sulfite/nitrite reductase (W6RF17/BN5_1900), the phosphoserine aminotransferase (W6QWX6/BN5_1904), and the acetylornithine aminotransferase (W6QU95/BN5_1906) were found over-represented or exclusive in the Ana proteome, but only in the

extracellular analysis in the comparisons with both controls (C_Abs and C_Cons). In addition, the cytochrome *bd* ubiquinol oxidase CioA1 (W6RBM7/BN5_0627) was detected exclusively under anaerobic conditions in the extracellular analysis (Fig. 4.9). The presence of these proteins solely in extracellular analysis may be due to their periplasmic or membrane location in the cell. In *P. pseudoalcaligenes* CECT 5344, the *cio* gene cluster is responsible for cyanide-insensitive respiration (Quesada et al., 2007), but this might also suggest its possible role in the anaerobic respiration. On the other hand, it has been recently described that, in addition to the anaerobic reduction of Fe(III), several bacteria are able to perform an anaerobic Fe(II) oxidation, where the *bc1* complex accepts electrons from Fe(II) to generate reduced quinones (Ilbert and Bonnefoy, 2013). Recently, Kuypers et al. (2018) suggested a new microbial nitrogen-transforming pathway that may be necessary for iron-dependent ammonium oxidation:

$$NH_4^+ + 6Fe^{3+} + 2H_2O \rightarrow NO_2^- + 6Fe^{2+} + 8H^+ \ (\Delta G^{0'} = -247 \text{ kJ mol}^{-1} \ NH_4^+)$$

Therefore, it might be speculated that, under hypoxia, Fe(II) is oxidized to Fe(III) by the *bc1* complex, which was found induced in the extracellular Ana proteome, and the resulting Fe(III) further reacts with ammonium, producing NO_2^- and recovering Fe(II) in a novel Feammox reaction, that would be able to generate ATP under anaerobiosis (Fig. 4.10).

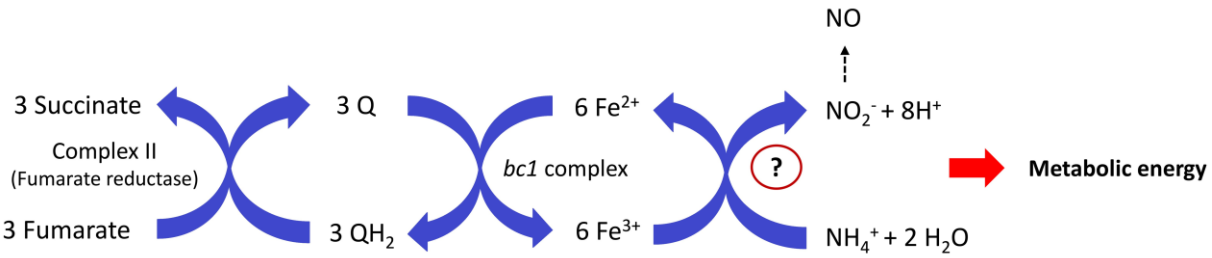

Figure 4.10. Hypothetical Feammox reaction coupled to fumarate respiration in *P. pseudoalcaligenes* CECT 5344 under anaerobic conditions. The biochemical nature of the putative protein (complex IV?) that may be involved in this reaction remains unknown so far. Q/QH_2, oxidized/reduced quinones.

Nitrite produced in the Feammox process could be reduced to nitric oxide (NO) gas by the sulfite/nitrite reductase (W6RF17/BN5_1900), or could be assimilated as a N-source by the assimilatory nitrite reductase. In this sense, traces of nitrite were detected in the media of the anaerobic cultures. Interestingly, NO is a potent and highly active signaling molecule that can inactivate the ferric uptake regulator (Fur) by binding to its iron center forming dinitrosyl complex (D'Autréaux et al., 2004). This ferrous dinitrosyl complex is unable to bind to DNA, thus leading to the induction of iron-related genes. In addition, the anaerobic nitric oxide reductase transcription regulator NorR (W6QUD8/ BN5_0991) was also identified in the extracellular Ana proteome, although this could reflect contamination of the

extracellular samples with intracellular proteins. This protein NorR is an NO stress-induced sensor that regulates the transcription of genes encoding NO-utilizing enzymes, and could play an important role in iron and cell homeostasis and protection against NO toxicity (Fleischhacker and Kiley, 2011). Eventually, NO gas could also volatilize from the cells (Sasaki et al., 2016).

Considering all the results presented in this Chapter III, the adaptation to anaerobic lifestyle of *P. pseudoalcaligenes* CECT 5344 could be summarized as shown in the Figure 4.11**.** Anaerobic Fe(II) oxidation may occur at the level of the *bc1* complex, in which Fe(II) can act as electron donor. In addition, the anaerobic bacterial metabolism is directed to synthesize fumarate, which is further used as electron acceptor in the complex II of the electron transport chain (fumarate respiration), generating succinate. Furthermore, ammonium, besides being used as a nitrogen source and assimilated via the GS/GOGAT pathway, it also participates in the Feammox redox reaction being oxidized to nitrite. Feammox coupled to Fe(III) reduction produces Fe(II), which is recycled to Fe(III) by the *bc1* complex, allowing ATP generation. This could explain the higher rate of ammonium consumption during anaerobic growth. Subsequently, nitrite formed in the Feammox process could be assimilated or used to synthesize nitric oxide, which may be involved in the regulation of the Fur protein, allowing expression of iron-related genes, and the NorR protein responsible for iron homeostasis and protection against oxidative stress. Also, tools to dissipate the excess of reducing power, such as the Nap system (periplasmic nitrate reduction) or lactate or alcohol fermentations, are induced. Finally, the excess of the carbon source leads to the accumulation of PHA.

Previously discussed results are a hypothetical, preliminary and purely illustrative view of the anaerobic metabolism of *P. pseudoalcaligenes* CECT 5344, and further investigations are required. Firstly, a new proteomic analysis is mandatory, with particular attention to minimizing contamination of extracellular samples by adjusting the cells and supernatant recovery procedure. A detailed *q*RT-PCR analysis is also necessary to validate data obtained from the proteomic analysis. Further, the determination of extracellular succinate should be performed, to reinforce the fumarate respiration hypothesis. Also, determination of analytes of fermentation products, nitric oxide and measurements of intra- and extracellular pH during the bacterial growth are required. In addition, the inhibition of the electron transport chain by using malonate to impaired complex II, myxothiazol to inhibit the *bc1* complex, and cyanide or azide to block complex IV, may be performed to confirm the involvement of these complexes in the anaerobic electron transport. Nonetheless, results derived from this study may significantly contribute to the development of anaerobic bioremediation strategies of nitrogen-rich wastes, and also for the removal of hazardous compounds, which biodegradation is more efficient or only possible in anaerobic conditions, by using the *P. pseudoalcaligenes* CECT 5344 strain.

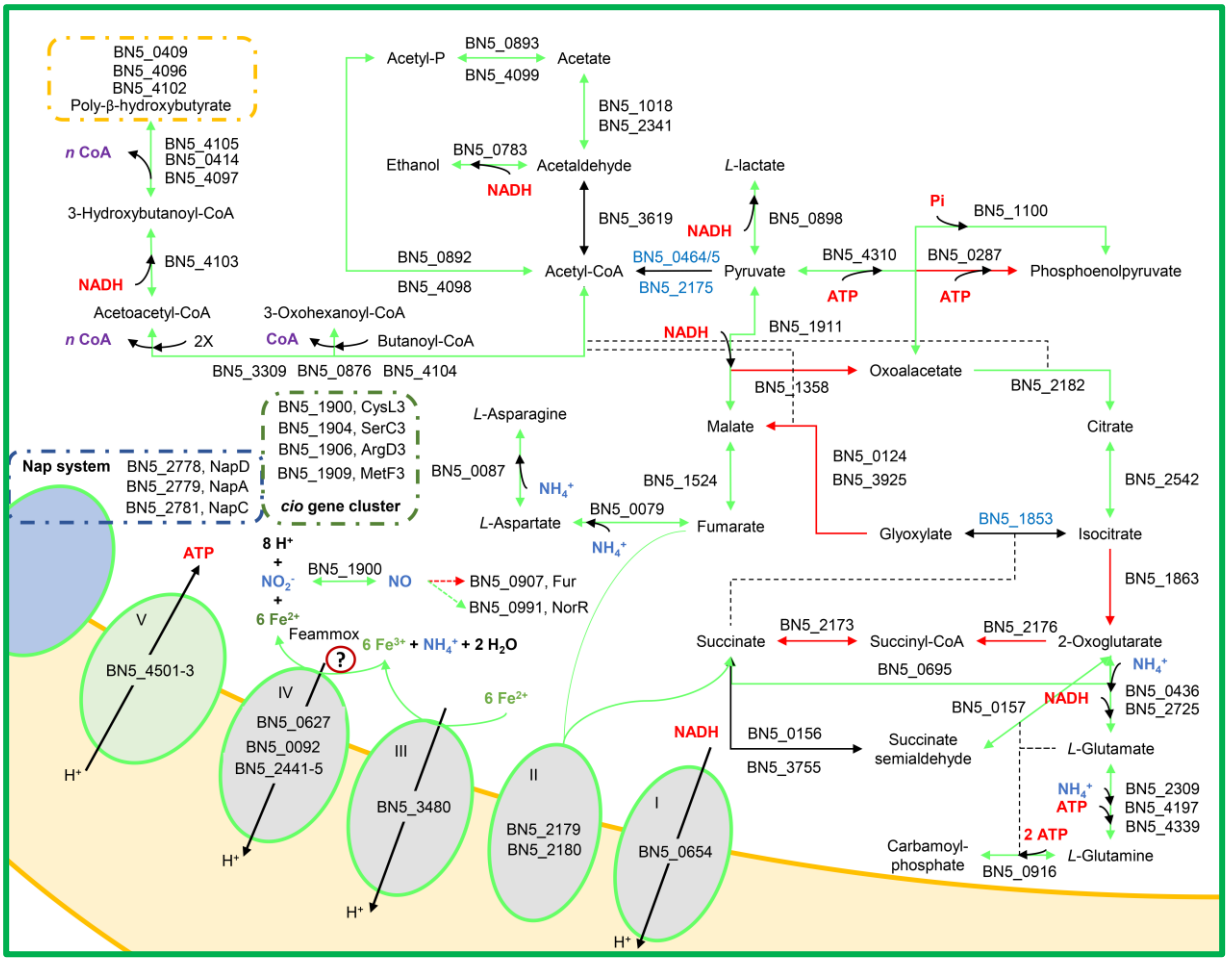

Figure 4.11. Global metabolic view of *P. pseudoalcaligenes* CECT 5344 during anaerobic grow based on integrated intracellular and extracellular proteomic analyses. Green arrows represent pathways induced in the Ana proteome, red arrows represent pathways induced in the control proteomes (C_Abs or C_Cons), and black arrows represent reactions with no significant differences. Proteins are indicated by their gene annotation: BN5_0409, poly(hydroxyalkanoate) granule-associated protein (PhaI); BN5_4096, phasin-like protein (PhaP); BN5_4102, transcription activator in PHB biosynthesis, AraC family (PhbR); BN5_4105, poly[(R)-3-hydroxyalkanoate] polymerase subunit PhaC (PhaC5); BN5_0414, poly[(R)-3-hydroxyalkanoate] polymerase subunit PhaC (PhaC1); BN5_4097, poly(3-hydroxyalkanoate) synthetase; BN5_4103, acetoacetyl-CoA reductase (PhaB); BN5_3309, acetyl-CoA C-acetyltransferase (AtoB5); BN5_0876, acetyl-CoA C-acetyltransferase; BN5_4104, acetyl-CoA C-acetyltransferase (PhaA3); BN5_1900, sulfite reductase (NADPH) hemoprotein beta-component (CysI3); BN5_1904, phosphoserine aminotransferase (SerC3); BN5_1906, succinylornithine aminotransferase (ArgD3); BN5_1909, methylenetetrahydrofolate reductase (NADH) (MetF3); BN5_2778, periplasmic nitrate reductase (NapD); BN5_2779, nitrate reductase (NapA); BN5_2781, cytochrome *c*-type protein NapC (NapC); BN5_0907, Fur family transcriptional regulator, ferric uptake regulator (Fur); BN5_0991, anaerobic nitric oxide reductase transcription regulator (NorR); BN5_4501, F-type H^+-transporting ATPase subunit *b* (AtpF); BN5_4502, F-type H^+-transporting ATPase subunit *c* (AtpE); BN5_4503, F-type H^+-transporting ATPase subunit *a* (AtpB), BN5_0627, cytochrome *bd* ubiquinol oxidase subunit I (CioA1); BN5_0092, cytochrome *c* oxidase subunit II (CoxB), BN5_2441, cytochrome *c* oxidase *cbb3*-type subunit (FixN); BN5_2442, cytochrome *c* oxidase *cbb3*-type subunit II (CcoO1); BN5_2443, cytochrome *c* oxidase *cbb3*-type subunit IV; BN5_2444, cytochrome *c* oxidase *cbb3*-type subunit III (CcoP1); BN5_2445, cytochrome *c* oxidase *cbb3*-type subunit I (CcoN3); BN5_3480, ubiquinol-cytochrome *c* reductase cytochrome *b* subunit; BN5_0654, NADH:quinone reductase (non-electrogenic); BN5_2179, succinate dehydrogenase flavoprotein subunit (SdhA); BN5_2180, succinate dehydrogenase membrane anchor subunit (SdhD); BN5_0893, acetate kinase (AckA1); BN5_4099, acetate kinase (AckA3); BN5_1018, aldehyde dehydrogenase (AldA1); BN5_2341, aldehyde dehydrogenase (AldA5); BN5_0783, alcohol/geraniol dehydrogenase ($NADP^+$); BN5_3619, acetaldehyde dehydrogenase (XylQ); BN5_0464, pyruvate dehydrogenase E2 component (AceF); BN5_0465, pyruvate dehydrogenase E2 component (AceE); BN5_2175, dihydrolipoyl

dehydrogenase (IpdA); BN5_0898, D-lactate dehydrogenase (quinone) (DId); BN5_4310, pyruvate carboxylase subunit A (PycA); BN5_0287, phosphoenolpyruvate carboxykinase (ATP) (PckA); BN5_1100, phosphoenolpyruvate carboxylase (Ppc); BN5_1911, malate dehydrogenase (oxaloacetate-decarboxylating)($NADP^+$) (MaeB3); BN5_1358, malate dehydrogenase (quinone) (MqoB); BN5_2182, citrate synthase (GltA); BN5_2542, aconitate hydratase (AcnA); BN5_1863, isocitrate dehydrogenase (Icd); BN5_0463, uncharacterized protein; BN5_2725, glutamate dehydrogenase (GdhB); BN5_2309, glutamine synthetase (GlnA5); BN5_4197, glutamine synthetase (GlnA9); BN5_4339, glutamine synthetase (GlnA11); BN5_0916, carbamoyl-phosphate synthase large subunit (CarB); BN5_0157, 5-aminovalerate/4-aminobutyrate aminotransferase (GabT); BN5_0156, succinate-semialdehyde dehydrogenase/glutarate-semialdehyde dehydrogenase (GabD1); BN5_3755, succinate-semialdehyde dehydrogenase/glutarate-semialdehyde dehydrogenase (GabD3); BN5_2176, 2-oxoglutarate dehydrogenase E2 component (dihydrolipoamide succinyltransferase) (SucB); BN5_0695, PKHD-type hydroxylase; BN5_2173, succinyl-CoA synthetase alpha subunit (SucD); BN5_1853, isocitrate lyase (AceA); BN5_0124, malate synthase (GlcB1); BN5_3925, malate synthase (GlcB3); BN5_1524, fumarate hydratase, class II (FumC); BN5_0079, aspartate ammonia-lyase (AspA); BN5_0087, L-asparaginase (AnsA). *? The biochemical nature of the putative protein (complex IV) that may be involved in this reaction remains unknown so far.

4.5. Conclusions

The main conclusions of this Chapter III are:

1. *Pseudomonas pseudoalcaligenes* CECT 5344 is able to grow under anaerobic lifestyle with 50 mM sodium acetate as carbon source and 10 mM ammonium chloride as the sole nitrogen source, in a 15 days period. This anaerobic growth is ammonium and iron-dependent. Under these anoxic conditions, the CECT 5344 strain diverts the carbon excess to the synthesis of polyhydroxyalkanoates.
2. The main basis of anaerobic metabolism may be suggested, and it is probably based on fumarate respiration, where fumarate acts as electron acceptor with Fe(II) as electron donor, and Feammox, where Fe(III) generated from Fe(II) oxidation is used for anaerobic ammonium oxidation to gain energy. Therefore during anaerobic growth, ammonium is being used as N-source and to obtain ATP through Fe(III) reduction via Feammox reaction. In addition, the Fur regulon and the possible generation of nitric oxide that leads to the expression of the *norR* gene, could contribute to control iron homeostasis.

Conclusions/Conclusiones

Conclusions

1. *Pseudomonas pseudoalcaligenes* CECT 5344 contains two main *ars* gene clusters that respond to arsenite, regardless of the nitrogen source used, although As-resistance response shows some differences between ammonium and cyanide. Therefore, *P. pseudoalcaligenes* CECT 5344 could be used for bioremediation of wastes from mining and other industries co-contaminated with cyanide and arsenic.
2. The main basis of As-resistance in this bacterium is the extrusion of As(III) through the ArsBA efflux pumps, or as organic derivatives exported through ArsP, Acr3 and ArsJ permeases. After extrusion of As(III) or organoarsenicals, As is accumulated in the bacterial biofilm, whose synthesis is enhanced in the presence of arsenite.
3. Production of arseno-phosphoglycerate by the As-inducible GAPDH enzyme, As methylation, THF metabolism, and perhaps formation of Lewis adducts in the presence of cyanide, seem to be also relevant processes involved in As detoxification. The ArsH2 protein, which is induced regardless the nitrogen source, may protect from the oxidative stress caused by both arsenic and cyanide.
4. *Pseudomonas pseudoalcaligenes* CECT 5344 harbors two *mer* gene clusters that respond significantly to mercury chloride, regardless of the nitrogen source. In the presence of cyanide, the CECT 5344 strain shows higher mercury resistance than with ammonium, probably due to the fact that mercury forms complexes with cyanide, thus decreasing its toxicity. In any case the presence of mercury does not affect the cyanide resistance and assimilation mechanisms in this bacterium.
5. The mechanism of mercury resistance is possibly based on mercury reduction by mercuric reductase (MerA), and its further extrusion from the cells as a volatile form (Hg^0), since mercury was neither detected in the extracellular media, nor bioaccumulated extracellularly (biosorption), and only residual concentrations of mercury are accumulated inside the cells, probably chelated to biomolecules.
6. The integration of proteomic data, bioinformatics and transcriptional analysis has allowed to predict a regulatory model for the MerR2 regulon, which operates under cyanotrophic conditions, with MerR2 acting as a master regulator that controls expression of *mer* genes and other targets genes.
7. *P. pseudoalcaligenes* CECT 5344 is able to cope with the simultaneous presence of cyanide, mercury and arsenic, thus being a suitable candidate to be used for bioremediation of

industrial wastewaters, which are often co-contaminated with high concentrations of these toxic chemicals.

8. *Pseudomonas pseudoalcaligenes* CECT 5344 is able to grow under anaerobic lifestyle with 50 mM sodium acetate as carbon source and 10 mM ammonium chloride as the sole nitrogen source, in a 15 days period. This anaerobic growth is ammonium and iron-dependent. Under these anoxic conditions, the CECT 5344 strain diverts the carbon excess to the synthesis of polyhydroxyalkanoates.
9. The main basis of anaerobic metabolism may be suggested, and it is probably based on fumarate respiration, where fumarate acts as electron acceptor with Fe(II) as electron donor, and Feammox, where Fe(III) generated from Fe(II) oxidation is used for anaerobic ammonium oxidation to gain energy. Therefore during anaerobic growth, ammonium is being used as N-source and to obtain ATP through Fe(III) reduction via Feammox reaction. In addition, the Fur regulon and the possible generation of nitric oxide that leads to the expression of the *norR* gene, could contribute to control iron homeostasis.

Conclusiones

1. *Pseudomonas pseudoalcaligenes* CECT 5344 contiene dos grupos principales de genes *ars* que responden al arsenito, independientemente de la fuente de nitrógeno utilizada, aunque la respuesta de resistencia al arsénico muestra algunas diferencias entre el amonio y el cianuro. Por lo tanto, *P. pseudoalcaligenes* CECT 5344 podría ser utilizada para la biorremediación de residuos de la minería y otras industrias, co-contaminados con cianuro y arsénico.
2. La base principal de la resistencia al As en esta bacteria es la extrusión de As(III) a través de las bombas tipo ArsBA, o como derivados orgánicos exportados a través de las permeasas ArsP, Acr3 y ArsJ. Tras la extrusión del As(III) o los compuestos organoarsenicales, el As se acumula en la biopelícula (biofilm) bacteriana, cuya síntesis se potencia en presencia de arsenito.
3. La producción de arseno-fosfoglicerato por la enzima GAPDH inducible por As, la metilación del As, el metabolismo del THF, y quizás la formación de aductos de Lewis en presencia de cianuro, parecen ser también procesos relevantes involucrados en la desintoxicación del As. La proteína ArsH2, que se induce independientemente de la fuente de nitrógeno, puede proteger del estrés oxidativo causado tanto por el arsénico como por el cianuro.
4. *P. pseudoalcaligenes* CECT 5344 alberga dos grupos de genes *mer* que responden significativamente al cloruro de mercurio, independientemente de la fuente de nitrógeno. En presencia de cianuro, la cepa CECT 5344 muestra mayor resistencia al mercurio que con amonio, probablemente debido a que el mercurio forma complejos con el cianuro, disminuyendo así su toxicidad. En cualquier caso, la presencia de mercurio no afecta los mecanismos de resistencia y asimilación del cianuro en esta bacteria.
5. El mecanismo de resistencia al mercurio está basado posiblemente en la reducción del mercurio por la mercurio reductasa (MerA) y su posterior salida de las células como forma volátil (Hg^0), ya que el mercurio no se detectó en medios extracelulares ni se bioacumuló extracelularmente (biosorción), y solo se detectaron concentraciones residuales de mercurio dentro de las células, probablemente quelado en biomoléculas.
6. La integración de los datos proteómicos, bioinformáticos y del análisis transcripcional ha permitido predecir un modelo regulador para el regulón MerR2, que opera en condiciones cianotróficas, con MerR2 actuando como un regulador maestro que controla la expresión de los genes *mer* y otros genes diana.
7. *P. pseudoalcaligenes* CECT 5344 es capaz de hacer frente a la presencia simultánea de cianuro, mercurio y arsénico, por lo que es un candidato adecuado para su uso en la biorremediación

de aguas residuales industriales, que a menudo están co-contaminadas con altas concentraciones de estos tóxicos.

8. *P. pseudoalcaligenes* CECT 5344 es capaz de crecer con una forma de vida anaeróbica, con acetato de sodio 50 mM como fuente de carbono y cloruro de amonio 10 mM como única fuente de nitrógeno, en un período de 15 días. Este crecimiento anaeróbico es dependiente de amonio y de hierro. En estas condiciones anóxicas, la cepa CECT 5344 desvía el exceso de carbono a la síntesis de polihidroxialcanoatos.
9. Se puede sugerir la base principal del metabolismo anaeróbico, probablemente basada en la respiración del fumarato, que actúa como aceptor de electrones, con el Fe(II) como donador de electrones, y un proceso Feammox, donde el Fe(III) generado a partir del Fe(II) se utiliza para la oxidación anaeróbica de amonio y la obtención de energía. Por lo tanto, durante el crecimiento anaeróbico, el amonio se usa como fuente de nitrógeno y para obtener ATP a través de la reducción de Fe(III) mediante la reacción de Feammox. Además, el regulón Fur y la posible generación de óxido nítrico que conduce a la expresión del gen *norR*, podrían controlar la homeostasis del hierro.

References

References

A

Abbas SZ, Rafatullah M, Hossain K, Ismail N, Tajarudin HA, Abdul Khalil HPS. A review on mechanism and future perspectives of cadmium-resistant bacteria. *Int J Environ Sci Technol* **2017**, *15*:243-262. doi:10.1007/s13762-017-1400-5.

Abdulsalam S, Bugaje I, Adefila S, Ibrahim S. Comparison of biostimulation and bioaugmentation for remediation of soil contaminated with spent motor oil. *Int J Environ Sci Technol* **2011**, *8*:187-194. doi:10.1007/BF03326208.

Abed RMM, Al-Kharusi S, Al-Hinai M. Effect of biostimulation, temperature and salinity on respiration activities and bacterial community composition in an oil polluted desert soil. *Int Biodeterior Biodegrad* **2015**, *98*:43-52. doi:10.1016/j.ibiod.2014.11.018.

Abril N, Chicano-Gálvez E, Michán C, Pueyo C, López-Barea J. iTRAQ analysis of hepatic proteins in free-living *Mus spretus* mice to assess the contamination status of areas surrounding Doñana National Park (SW Spain). *Sci Total Environ* **2015**, *523*:16-27. doi:10.1016/j.scitotenv.2015.03.116.

Abuawad A, Spratlen MJ, Parvez F, Slavkovich V, Ilievski V, Lomax-Luu AM, et al. Association between body mass index and arsenic methylation in three studies of Bangladeshi adults and adolescents. *Environ Int* **2021**, *149*:106401. doi:10.1016/j.envint.2021.106401.

Acheampong MA, Meulepas RJW, Lens PNL. Removal of heavy metals and cyanide from gold mine wastewater. *J Chem Technol Biotechnol* **2010,** *85*:590-613. doi:10.1002/jctb.2358.

Adams MD. Removal of cyanide from solution using activated carbon. *Miner Eng* **1994**, *7*:165-1177. doi:10.1016/0892-6875(94)90004-3.

Adams MD. The mechanisms of adsorption of $Hg(CN)_2$ and $HgCl_2$ on to activated carbon. *Hydrometallurgy* **1991**, *26*:201-210. doi:10.1016/0304-386X(91)90031-G.

Aderemi AV, Ayeleso AO, Oyedapo OO, Mukwevho E. Metabolomics: A scoping review of its role as a tool for disease biomarker discovery in selected non-communicable diseases. *Metabolites* **2021**, *11*:418. doi:10.3390/metabo11070418.

Adhikari P, Berish SA, Nowalk AJ, Veraldi KL, Morse SA, Mietzner TA. The *fbpABC* locus of *Neisseria gonorrhoeae* functions in the periplasm-to-cytosol transport of iron. *J Bacteriol* **1996**, *178*:2145-2149. doi:10.1128/jb.178.7.2145-2149.1996.

Aebersold RH, Leavitt J, Saavedra RA, Hood LE, Kent SB. Internal amino acid sequence analysis of proteins separated by one- or two-dimensional gel electrophoresis after *in situ* protease digestion on nitrocellulose. *Proc Natl Acad Sci* **1987**, *84*:6970-6974. doi:10.1073/pnas.84.20.6970.

Agarwal R, Raisuddin S, Tewari S, Goel SK, Raizada RB, Behari JR. Evaluation of comparative effect of pre- and posttreatment of selenium on mercury-induced oxidative stress, histological alterations, and metallothionein mRNA expression in rats. *J Biochem Mol Toxicol* **2010**, *24*:123-35. doi:10.1002/jbt.20320.

Ahn A-C, Cavalca L, Colombo M, Schuurmans JM, Sorokin DY, Muyzer G. Transcriptomic analysis of two *Thioalkalivibrio* Species under arsenite stress revealed a potential candidate gene for an alternative arsenite oxidation pathway. *Front Microbiol* **2019**, *10*:1514. doi:10.3389/fmicb.2019.01514

Akcil A. Destruction of cyanide in gold mill effluents: Biological versus chemical treatments. *Biotechnol Adv* **2003**, *21*:501- 511. doi:.1016/S0734-9750(03)00099-5.

Albergaria JT, Alvim-Ferraz MCM, Delerue-Matos C. Remediation of sandy soils contaminated with hydrocarbons and halogenated hydrocarbons by soil vapor extraction. *J Environ Manag* **2012**, *104*:195-201. doi:10.1016/j.jenvman.2012.03.033.

Ali H, Khan E. What are heavy metals? Long-standing controversy over the scientific use of the term 'heavy metals'-proposal of a comprehensive definition. *Toxicol Environ Chem* **2017**, *1*:6-19. doi:10.1080/02772248.2017.1413652.

Ali H, Khan E, Ilahi I. Environmental chemistry and ecotoxicology of hazardous heavy metals: Environmental persistence, toxicity, and bioaccumulation. *J Chem* **2019**, 6730305. doi:10.1155/2019/6730305.

Alvillo-Rivera A, Garrido-Hoyos S, Buitrón G, Thangarasu-Sarasvathi P, Rosano-Ortega G. Biological treatment for the degradation of cyanide: A review. *J Mat Res Tech* **2021**, *12*:1418-1433. doi:10.1016/j.jmrt.2021.03.030.

Amin A, Sarwar A, Saleem MA, Latif Z, Opella SJ. Expression and purification of transmembrane protein MerE from mercury-resistant *Bacillus cereus*. *J Microbiol Biotechnol* **2019**, *29*:274-282. doi:10.4014/ jmb.1704.04062.

Anand S, Samuel M, Ang CS, Keerthikumar S, Mathivanan S. Label-Based and Label-free strategies for protein quantitation. *Methods Mol Biol* **2017**, *1549*:31-43. doi:10.1007/978-1-4939-6740-7_4.

Anderson CR, Cook GM. Isolation and characterization of arsenate-reducing bacteria from arsenic-contaminated sites in New Zealand. *Curr Microbiol* **2004,** *48*:341-347. doi.org/10.1007/s00284-003-4205-3.

Anderson GL, Williams J, Hille R. The purification and characterization of arsenite oxidase from *Alcaligenes faecalis*, a molybdenum-containing hydroxylase. *J Biol Chem* **1992**, *267*:23674-23682.

Andreini C, Bertini I, Cavallaro G, Holliday GL, Thornton JM. Metal ions in biological catalysis: From enzyme databases to general principles. *J Biol Inorg Chem* **2008**, *13*:1205-1218. doi:10.1007/s00775-008-0404-5.

Andres J, Bertin PN. The microbial genomics of arsenic. *FEMS Microbio Rev* **2016**, *40*:299-322. doi:10.1093/femsre/fuv050.

Andrews JM. Determination of minimum inhibitory concentrations. *J Antimicrob Chemother* **2001**, *48*:5-16. doi:10.1093/jac/48.suppl_1.5.

Andrews SC. Iron storage in bacteria. *Adv Microb Phys* **1998**, *40*:281-351. doi:10.1016/s0065-2911(08)60134-4.

Andrews SC, Robinson AK, Rodríguez-Ouiñones F. Bacterial iron homeostasis. *FEMS Microbiol Rev* **2003**, *27*:215-237. doi:10.1016/S0168-6445(03)00055-X.

Angerer A, Gaisser S, Braun V. Nucleotide sequences of the *sfuA*, *sfuB*, and *sfuC* genes of *Serratia marcescens* suggests a periplasmic-binding protein-dependent iron transport mechanism. *J Bacteriol* **1990**, *172*:572-578. doi:10.1007/BF00205187.

Anjum A, Zuber M, Zia KM, Noreen A, Anjum MN, Tabasum S. Microbial production of polyhydroxyalkanoates (PHAs) and its copolymers: A review of recent advancements. *Int J Biol Macromol* **2016**, *89*:161-74. doi:10.1016/j.ijbiomac.2016.04.069.

Antenozio ML, Giannelli G, Marabottini R, Brunetti P, Allevato E, Marzi D, et al. Phytoextraction efficiency of *Pteris vittata* grown on a naturally as-rich soil and characterization of As-resistant rhizosphere bacteria. *Sci Rep* **2021,** *11*:6794. doi:10.1038/s41598-021-86076-7.

Antoszczyszyn T, Michalska A. The potential risk of environmental contamination by mercury contained in Polish coal mining waste. *J Sustain Min* **2016**, *15*:191-196. doi:10.1016/j.jsm.2017.04.002.

Arat S, Bullerjahn GS, Laubenbacher R. A Network biology approach to denitrification in *Pseudomonas aeruginosa*. *PLoS One* **2015**, *10*:e0118235. doi:10.1371/journal.pone.0118235.

Aryal M, Liakopoulou-Kyriakides M. Bioremoval of heavy metals by bacterial biomass. *Environ Monit Assess* **2014**, *187*:4173. doi:10.1007/s10661-014-4173-z.

Aryal M, Ziagova M, Liakopoulou-Kyriakides M. Study on arsenic biosorption using Fe(III)-treated biomass of *Staphylococcus xylosus*. *Chem Eng J* **2010**, *162*:178-185. doi.org/10.1016/j.cej.2010.05.026.

Asmus E, Garschagen H. Über die Verwendung der Barbitursäure für die Photometrische Bestimmung von Cyanid und Rhodanid. Fresenius Z. *Anal Chem* **1953**, *138*:414-422.

ATSDR, Agency for Toxic Substances and Disease Registry. Division of Toxicology and Human Health Sciences Atlanta, GA 30333. **2015**, US Department of Health and Human Services. Support document to the 2015 priority list of hazardous substances that will be candidates for toxicological profiles.

Aulitto M, Gallo G, Puopolo R, Mormone A, Limauro D, Contursi P, et al. Genomic insight of *Alicyclobacillus mali* FL18 Isolated from an arsenic-rich hot spring. *Front Microbiol* **2021**, *12*:639697. doi:10.3389/fmicb.2021.639697.

B

Bachate SP, Cavalca L, Andreoni V. Arsenic-resistant bacteria isolated from agricultural soils of Bangladesh and characterization of arsenate-reducing strains. *J Appl Microbiol* **2009**, *107*:145-156. doi:10.1111/j.1365-2672. 2009.04188.

Bache N, Geyer PE, Bekker-Jensen DB, Hoerning O, Falkenby L, Treit P, et al. A novel LC system embeds analytes in pre-formed gradients for rapid, ultra-robust proteomics. *Mol Cell Proteom* **2018**, *17*:2284-2296. doi:10.1074/mcp.TIR118.000853.

Badilla C, Osborne TH, Cole A. Watson C, Djordjevic S, Santini JM. A new family of periplasmic-binding proteins that sense arsenic oxyanions. *Sci Rep* **2018***, 8*:6282. doi:10.1038/s41598-018-24591-w.

Bae S, Kamynina E, Guetterman HM, Farinola AF, Caudill MA, Berry RJ, et al. Provision of folic acid for reducing arsenic toxicity in arsenic-exposed children and adults. *Cochrane Database Syst Rev* **2021**, *10*:CD012649. doi:10.1002/14651858.CD012649.pub2.

Balagurusamy, N. Anaerobic bioremediation-an untapped potential. *Rev Mex Ing Quím* **2005**, *4*:273-287.

Banerjee S, Majumdar J, Samal AC, Bhattachariya P, Santra SC. Biotransformation and bioaccumulation of arsenic by *Brevibacillus brevis* isolated from arsenic contaminated region of West Bengal. *IOSR J Environ Sci Toxicol Food Technol* **2013,** *3*:1-10.

Barkay T, Miller SM, Summers AO. Bacterial mercury resistance from atoms to ecosystems. *FEMS Microbiol Rev* **2003**, *27*:355-384 doi:10.1016/S0168-6445(03)00046-9.

Barkay T, Kritee K, Boyd E, Geesey G. A thermophilic bacterial origin and subsequent constraints by redox, light and salinity on the evolution of the microbial mercuric reductase. *Environ Microbiol* **2010**, *12*:2904-2917. doi:10.1111/j.1462-2920.2010.02260.x.

Barral-Fraga L, Martina-Prieto D, Barral MT, Morin S, Guasch H. Mutual interaction between arsenic and biofilm in a mining impacted river. *Sci Total Environ* **2018**, *636*:985-998. doi:10.1016/j.scitotenv.2018.04.287.

Bashir A, Malik LA, Ahad S, Manzoor T, Bhat MA, Dar GN, et al. Removal of heavy metal ions from aqueous system by ion-exchange and biosorption methods. *Environ Chem Lett* **2019**, *17*:729–754. doi:10.1007/s10311-018-00828-y.

Battle T, Srivastava U, Kopfle J, Hunter R, McClelland J. The direct reduction of iron. In: Treatise on Process Metallurgy. *Elsevier* **2014**, *3*:89-176. doi:10.1016/B978-0-08-096988-6.00016-X.

Bazzi W, Abou-Fayad AG, Nasser A, Haraoui LP, Dewachi O, Abou-Sitta G, et al. Heavy metal toxicity in armed conflicts potentiates AMR in *A. baumannii* by selecting for antibiotic and heavy metal co-resistance mechanisms. *Front Microbiol* **2020**, *11*:68. doi:10.3389/fmicb.2020.00068.

Bearden SW, Perry RD. The Yfe system of *Yersinia pestis* transports iron and manganese and is required for full virulence of plague. *Mol Microbiol* **1999**, *32*:403-414. doi:10.1046/j.1365-2958.1999.01360.x.

Beauchene NA, Myers KS, Chung D, Park DM, Weisnicht AM, Keleş S, et al. Impact of anaerobiosis on expression of the iron-responsive Fur and RyhB regulons. *mBio* **2015**, *6*:e01947-15. doi:10.1128/mBio.01947-15.

Becerra G, Igeño MI, Merchán F, Sánchez-Clemente R, Blasco R. New evolving strategies revealed by transcriptomic analysis of a fur$^-$ mutant of the cyanotrophic bacterium *Pseudomonas pseudoalcaligenes* CECT 5344. *Microbial Biotechnol* **2020**, *13*:148-161. doi:10.1111/1751-7915.13408.

Beckers F, Rinklebe J. Cycling of mercury in the environment: Sources, fate, and human health implications: A review. *Crit Rev Environ Sci Technol* **2017**, *47*:693-794. doi:10.1080/10643389.2017.1326277.

Beinert H, Holm RH, Munck E. Iron-sulfur clusters: Nature's modular, multipurpose structures. *Science* **1997**, *277*:653-659. doi:10.1126/science.277.5326.653.

Belenky P, Ye JD, Porter CB, Cohen NR, Lobritz MA, Ferrante T, et al. Bactericidal antibiotics induce toxic metabolic perturbations that lead to cellular damage. *Cell Rep* **2015**, *13*:968e980. doi:10.1016/j.celrep.2015.09.059.

Belfiore C, Ordoñez OF, Farías ME. Proteomic approach of adaptive response to arsenic stress in *Exiguobacterium* sp. S17, an extremophile strain isolated from a high-altitude Andean Lake stromatolite. *Extremophiles* **2013**, *17*:421-31. doi:10.1007/s00792-013-0523-y.

Bender DA. Perspective-the promise of metabolomics. *J Sci Food Agric* **2005**, *85***:**7-9. doi:10.1002/jsfa.2014.

Bereman MS. Tools for monitoring system suitability in LC MS/MS centric proteomic experiments. *Proteomics* **2015**, *15*:891-902. doi:10.1002/pmic.201400373.

Bermanec V, Paradžik T, Kazazić S, Venter C, Hrenović J, Vujaklija D, et al. Novel arsenic hyper-resistant bacteria from an extreme environment, Crven Dol mine, Allchar, North Macedonia. *J Hazard Mater* **2021**, *402*:123437. doi:10.1016/j.jhazmat.2020.123437hal-02920366.

Berthold DA, Andersson ME, Nordlund P. New insight into the structure and function of the alternative oxidase. *Biochim Biophys Acta* **2000**, *1460*:241-54. doi:10.1016/s0005-2728(00)00149-3. PMID: 11106766.

Bespyatykh J, Shitikov E, Guliaev A, Smolyakov A, Klimina K, Veselovsky V, et al. Proteogenomic analysis of *Mycobacterium tuberculosis* Beijing B0/W148 cluster strains. *J Proteomics* **2019**, *192*:18-26. doi:10.1016/j.jprot.2018.07.002.

Bhakta V, Balkrishna M, Thakuri C. Bacterial *mer* operon-mediated detoxification of mercurial compounds: A short review. *Arch Microbiol* **2011,** 837-44. doi:10.1007/s00203-011-0751-4.

Bhakta JN, Munekage Y, Ohnishi K, Jana BB, Balcazar JL. Isolation and characterization of cadmium-and arsenic absorbing bacteria for bioremediation. *Water Air Soil Pollut* **2014**, *225*:2151. doi:10.1007/s11270-014-2151-2

Biełło KA, Cabello P, Rodríguez-Caballero G, Sáez LP, Luque-Almagro VM, Roldán MD, et al. Proteomic analysis of arsenic resistance during cyanide assimilation by *Pseudomonas pseudoalcaligenes* CECT 5344. *Int J Mol Sci* **2023a,** *24*:7232. doi:10.3390/ijms24087232.

Biełło KA, Olaya-Abril A, Cabello P, Rodríguez-Caballero G, Sáez LP, Moreno-Vivián C, et al. Quantitative proteomic analysis of cyanide and mercury detoxification by *Pseudomonas pseudoalcaligenes* CECT 5344. *Microbiol Spectr* **2023b**, *11*:e00553-23. doi.10.1128/spectrum.00553-23.

Biełło KA, Lucena C, López-Tenllado FJ, Hidalgo-Carrillo J, Rodríguez-Caballero G, Cabello P, et al. Holistic view of biological nitrogen fixation and phosphorus mobilization in *Azotobacter chroococcum* NCIMB 8003. *Front Microbiol* **2023c**, *14*:1129721. doi:10.3389/fmicb.2023.1129721.

Birrer SC, Dafforn KA, Sun MY, Williams RBH, Potts J, Scanes P, et al. Using meta-omics of contaminated sediments to monitor changes in pathways relevant to climate regulation. *Environ Microbiol* **2019**, *21*:389-401. doi:10.1111/1462-2920.14470.

BIS, Bureau Indian Standards. Indian standard-drinking water specification. New Delhi. **1991.**

Bissen M, Frimmel FH. Arsenic-A review. Part I: Occurrence, toxicity, speciation, mobility. *Acta Hydrochim Hydrobiol* **2003**, *31*:9-18. doi.org/10.1002/aheh.200390025.

Bjørklund G, Crisponi G, Nurchi VM, Cappai R, Djordjevic AB, Aaseth J. A review on coordination properties of thiol-containing chelating agents towards mercury, cadmium, and lead. *Molecules* **2019**, *24*:3247. doi:10.3390/molecules24183247.

Blum JS, Hernández-Maldonado J, Redford K, Sing C, Bennet SC, Saltikov CW, et al. Arsenate-dependent growth is independent of an ArrA mechanism of arsenate respiration in the termite hindgut isolate *Citrobacter* sp. strain TSA-1. *Can J Microbiol* **2018**, *64*:619-627. doi:10.1139/cjm-2017-0523.

Blumer C, Haas D. Mechanism, regulation, and ecological role of bacterial cyanide biosynthesis. *Arch Microbiol* **2000**, 173:170-177. doi:10.1007/s002039900127.

Bocian-Ostrzycka KM, Grzeszczuk MJ, Banaś AM, Jagusztyn-Krynicka EK. Bacterial thiol oxidoreductases - from basic research to new antibacterial strategies. *Appl Microbiol Biotechnol* **2017**, *101*:3977-3989. doi:10.1007/s00253-017-8291-8.

Boersema PJ, Raijmakers R, Lemeer S, Mohammed S, Heck AJ. Multiplex peptide stable isotope dimethyl labeling for quantitative proteomics. *Nat Protoc* **2009**, *4*:484-94. doi:10.1038/nprot.2009.21.

Bogdanow B, Zauber H, Selbach M. Systematic errors in peptide and protein identification and quantification by modified peptides. *Mol Cell Proteom* **2016**, *15*:2791-2801. doi:10.1074/mcp.M115.055103.

Borch T, Kretzschmar R, Kappler A, Van Cappellen P, Ginder-Vogel M, Voegelin A, et al. Biogeochemical redox processes and their impact on contaminant dynamics. *Environ Sci Technol* **2010**, *44*:15-23. doi:10.1021/es9026248.

Borrero-de-Acuña JM, Rohde M, Wissing J, Jänsch L, Schobert M, Molinari G, et al. Protein network of the *Pseudomonas aeruginosa* denitrification apparatus. *J Bacteriol* **2016**, *198*:1401-13. doi:10.1128/JB.00055-16.

Boukhalfa H, Crumbliss AL. Chemical aspects of siderophore mediated iron transport. *BioMetals* **2002**, *15*:325-339. doi:10.1023/a:1020218608266.

Boyd E, Barkay T. The mercury resistance operon: From an origin in a geothermal environment to an efficient detoxification machine. *Front microbiol* **2012**, *3*:349. doi:10.3389/fmicb.2012.00349.

Bradford MM. A rapid and sensitive method for the quantitation of microgram quantities of protein utilizing the principle of protein-dye binding. *Anal Biochem* **1976**, *72*:248-254. doi:10.1006/abio.1976.9999.

Braun V. Iron uptake by Escherichia coli. *Front Biosci* **2003**, *8*:s1409-21. doi:10.2741/1232.

Bridges C, Zalups R. Mechanism involved in the transport of mercuric ions in target tissue. *Arch Toxicol* **2017**, *91*: 63-81. doi:10.1007/s00204-016-1803-y.

Broussard L, Hammett-Stabler C, Wincecker R, Ropero-Miller J. The toxicology of mercury. *Lab Med* **2002**, *33*:614-625. doi:10.1309/5HY1-V3NE-2LFL-P9MT.

Brown NL, Stoyanov JV, Kidd SP, Hobman J. The MerR family transcriptional regulators. *FEMS Microbiol Rev* **2003**, *27*:145-163. doi:10.1016/S0168-6445(03)00051-2.

Bryce C, Franz-Wachtel M, Nalpas NC, Miot J, Benzerara K, Byrne JM, et al. Proteome response of a metabolically flexible anoxygenic phototroph to Fe(II) oxidation. *Appl Environ Microbiol* **2018**, *84*:e01166-18. doi:10.1128/AEM.01166-18.

Buchanan SK, Smith BS, Venkatramani L, Xia D, Esser L, Palnitkar M, et al. Crystal structure of the outer membrane active transporter FepA from *Escherichia coli*. *Nat Struct Biol* **1999**, *6*:56-63. doi:10.1038/4931.

Bugyi F, Szabó D, Szabó G, Révész Á, Pape VFS, Soltész-Katona E, et al. Influence of post-translational modifications on protein identification in database searches. *ACS Omega* **2021**, *6*:7469-7477. doi:10.1021/acsomega.0c05997.

Burger BJ, Estrada MV, Gustin MS. What caused Earth's largest mass extinction event? New evidence from the Permian-Triassic boundary in northeastern Utah. *Glob Planet Chang* **2019**, *177*:81-100. doi:10.1016/j.gloplacha.2019.03.013.

Busairi N, Syahir A. Recent advances in mercury detection: Towards enabling a sensitive and rapid point-of-check measurement. *J Toxicol Risk Assess* **2018**, *4*:1.doi:10.23937/2572-4061.1510010.

Bustaffa E, Gorini F, Bianchi F, Minichilli F. Factors affecting arsenic methylation in contaminated Italian areas. *Int J Environ Res Public Health* **2020**, *17*:5226. doi:10.3390/ijerph17145226.

Byeon E, Kang HM, Yoon C, Lee JS. Toxicity mechanisms of arsenic compounds in aquatic organisms. *Aquat Toxicol* **2021**, *237*:105901. doi:10.1016/j.aquatox.2021.105901.

Byers BR, Arceneaux JEL. Microbial iron transport: Iron acquisition by pathogenic microorganisms. *Met Ions Biol Syst* **1998**, *35*:37-66.

C

Cabello P, Luque-Almagro VM, Olaya-Abril A, Sáez LP, Moreno-Vivián C, Roldán MD. Assimilation of cyanide and cyano-derivatives by *Pseudomonas pseudoalcaligenes* CECT5344: From omic approaches to biotechnological applications. *FEMS Microbiol Lett* **2018**, *365*:fny032. doi:10.1093/femsle/fny032.

Cai J, Salmon K, DuBow MS. A chromosomal *ars* operon homologue of *Pseudomonas aeruginosa* confers increased resistance to arsenic and antimony in *Escherichia coli*. *Microbiology* **1998**, *144*:2705-2713. doi:10.1099/00221287-144-10-2705.

Cai L, Liu G, Rensing C, Wang G. Genes involved in arsenic transformation and resistance associated with different levels of arsenic-contaminated soils. *BMC Microbiol* **2009**, *9*:4. doi:10.1186/1471-2180-9-4.

Cantu DC, Chen Y, Reilly PJ. Thioesterases: A new perspective based on their primary and tertiary structures. *Protein Sci* **2020**, *19*:1281-1295. doi:10.1002/pro.417.

Cardona GI, Escobar MC, Acosta-González A, Marín P, Marqués S. Highly mercury-resistant strains from different Colombian Amazon ecosystems affected by artisanal gold mining activities. *Appl Microbiol Biotechnol* **2022**, *106*:2775-2793. doi:10.1007/s00253-022-11860-y.

Carlin A, Shi W, Dey S, Rosen BP. The *ars* operon of *Escherichia coli* confers arsenical and antimonial resistance. *J Bacteriol* **1995**, *177*:981-986. doi:10.1128/jb.177.4.981-986.1995.

Carmona M, Zamarro MT, Blazquez B, Durante-Rodrıguez G, Juarez JF, Valderrama JA, et al. Anaerobic catabolism of aromatic compounds: a genetic and genomic view. *Microbiol Mol Biol Rev* **2009**, *73*:71-133. doi:10.1128/MMBR.00021-08.

Castillo FC, Roldán MD, Blasco RB, Huertas MJ, Caballero FJ, Moreno-Vivián C, et al. Biotecnología Ambiental. Editorial *Tébar*, **2005**.

Chakraborty R, Wu CH, Hazen TC. Systems biology approach to bioremediation. *Curr Opin Biotechnol* **2012**, *23*:483-490. doi:10.1016/j.copbio.2012.01.015.

Champier L, Duarte V, Michaud-Soret I, Coves J. Characterization of the MerD protein from *Ralstonia metallidurans* CH34: A possible role in bacterial mercury resistance by switching off the induction of the *mer* operon. *Mol Microbiol* **2004**, *52*:1475-1485. doi:10.1111/j.1365-2958.2004.04071.x.

Chareyre S, Mandin P. Bacterial iron homeostasis regulation by sRNAs. *Microbiol Spectrum* **2018**, *6*. doi:10.1128/microbiolspec.RWR-0010-2017.

Chasanah U, Nuraini Y, Handayanto E. The potential of mercury-resistant bacteria isolated from small-scale gold mine tailings for accumulation of mercury. *J Ecol Eng* **2018**, *19*:236-245. doi:10.12911/22998993/83565.

Chauhan NS, Ranjan R, Purohit HJ, Kalia VC, Sharma R. Identification of genes conferring arsenic resistance to *Escherichia coli* from an effluent treatment plant sludge metagenomic library. *FEMS Microbiol Ecol* **2009,** *67*:130-9. doi:10.1111/j.1574-6941.2008.00613.

Chen CM, Misra TK, Silver S, Rosen BP. Nucleotide sequence of the structural genes for an anion pump. The plasmid-encoded arsenical resistance operon. *J Biol Chem* **1986**, *261*:15030-15038.

Chen WJ, Tang P, Hseu YC, Chen CC, Huang KY, Chen SC. A proteome analysis of the tetracyanonickelate (II) responses in *Klebsiella oxytoca*. *Environ Microbiol* **2011**, *3*:106-111. doi:10.1111/j.1758-2229.2010.00194.x.

Chen J, Qin J, Zhu YG, de Lorenzo V, Rosen BP. Engineering the soil bacterium *Pseudomonas putida* for arsenic methylation. *Appl Environ Microbiol* **2013**, *79*:4493-4495. doi:10.1128/AEM.01133-13.

Chen H, Wang W, Xue L, Chen C, Liu G, Zhang R. Effects of ammonia on anaerobic digestion of food waste: Process Performance and Microbial Community. *Energy Fuels* **2016**, *30*. doi:10.1021/acs.energyfuels.6b00715.

Chen J, Yoshinaga M, Garbinski LD, Rosen BP. Synergistic interaction of glyceraldehydes-3-phosphate dehydrogenase and ArsJ, a novel organoarsenical efflux permease, confers arsenate resistance. *Mol Microbiol* **2016**, *100*:945-953. doi:10.1111/mmi.13371.

Chena SC, Liu JK. The respiratory responses to cyanide of a cyanide-resistant *Klebsiella oxytoca* bacterial strain. *FEMS Microbiol Lett* **1999**, *175*:37-43. doi:10.1016/S0378-1097(99)00173-1.

Chitpirom K, Akaracharanya A, Tanasupawat S, Leepipatpibooim N, Kim KW. Isolation and characterization of arsenic resistant bacteria from tannery wastes and agricultural soils in Thailand. *Ann Microbiol* **2009**, *59*:649-656. doi:10.1007/BF03179204.

Choudhury R, Srivastava S. Mutational analysis of zinc resistance in *Pseudomonas putida* strain S4. *Curr Microbiol* **2001**, *43*:316-21. doi:10.1007/s002840010309.

Chronopoulos J, Haidouti C, Chronopoulou A, Massas I. Variations in plant and soil lead and cadmium content in urban parks in Athens, Greece. *Sci Total Environ* **1997**, *196*:91-8. doi:10.1016/S0048-9697(96)05415-0.

Clément JC, Shrestha J, Ehrenfeld JG, Jaffé PR. Ammonium oxidation coupled to dissimilatory reduction of iron under anaerobic conditions in wetland soils. *Soil Biol Biochem* **2005**, *37*:2323-2328. doi:10.1016/j.soilbio.2005.03.027.

Colombo MJ, Ha J, Reinfelder JR, Barkay T, Yee N. Oxidation of Hg(0) to Hg(II) by diverse anaerobic bacteria. *Chem Geol* **2014**, *363*:334-340. doi:10.1016/j.chemgeo.2013.11.020.

Cornelis P, Wie Q, Andrews SC, Vinckx T. Iron homeostasis and management of oxidative stress response in bacteria. *Metallomics* **2011**, *3*:540-549. doi:10.1039/c1mt00022e.

Cortes M, García-Cañaveras JC, Pareja E, Lahoz A. Liver transplantation biomarkers in the metabolomics era. Biomarkers in Liver Disease. Biomarkers in Disease: Methods, Discoveries and Applications. *Springer* **2016***,* 1-29. doi:10.1007/978-94-007-7742-2_42-1.

Costa PS, Scholte LL, Reis MP, Chaves AV, Oliveira PL, Itabayana LB, et al. Bacteria and genes involved in arsenic speciation in sediment impacted by long-term gold mining. *PLoS One*. **2014**, *9*:e95655. doi:10.1371/journal.pone.0095655.

Coudert L, Bondu R, Rakotonimaro TV, Rosa E, Guittonny M, Neculita CM. Treatment of As-rich mine effluents and produced residues stability: Current knowledge and research priorities for gold mining. *J Hazard Mater* **2020**, *386*:121920. doi:10.1016/j.jhazmat.2019.121920.

Coulibaly M, Bamba D, Yao N, Zoro E, Rhazi M. Some aspects of speciation and reactivity of mercury in various martrices. *C R Chimie* **2016**, *19*:832e840. doi:10.1016/j.crci.2016.02.005.

Covington BC, McLean JA, Bachmann BO. Comparative mass spectrometry-based metabolomics strategies for the investigation of microbial secondary metabolites. *Nat Prod Rep* **2017**, *34*:6-24. doi:10.1039/c6np00048g.

Cox J, Mann M. MaxQuant enables high peptide identification rates, individualized ppb-range mass accuracies and proteome-wide protein quantification. *Nat Biotechnol* **2008**, *26*:1367-1372. doi:10.1038/nbt.1511.

Crane RA, Scott TB. Nanoscale zero-valent iron: Future prospects for an emerging water treatment technology. *J Hazard Mater* **2012**, *211-212*:112-25. doi:10.1016/j.jhazmat.2011.11.073.

D

Dalsgaard T, Thamdrup B, Canfield DE. Anaerobic ammonium oxidation (anammox) in the marine environment. *Res Microbiol* **2005**, *156*:457-464. doi:10.1016/j.resmic.2005.01.011.

Das S, Dash HR, Chakraborty J. Genetic basis and importance of metal resistant genes in bacteria for bioremediation of contaminated environments with toxic metal pollutants. *Appl Microbiol Biotechnol* **2016**, *100*:2967-2984. doi:10.1007/s00253-016-7364-4.

Dash RR, Majumder CB, Kumar A. Treatment of metal cyanide bearing wastewater by simultaneous adsorption biodegradation (SAB). *J Hazard Mater* **2008**, *152*:387-396. doi:10.1016/j.jhazmat.2007.07.009.

Dash RR, Gaur A, Balomajumder C. Cyanide in industrial wastewaters and its removal: A review on biotreatment. *J Hazard Mater* **2009**, *163*:1-11. doi:10.1016/j.jhazmat.2008.06.051.

Dash HR, Das S. Diversity, community structure, and bioremediation potential of mercury-resistant marine bacteria of estuarine and coastal environments of Odisha, India. *Environ Sci Pollut Res* **2016**, *23*:6960-6971. doi:10.1007/s11356-015-5991-4.

D'Autréaux B, Horner O, Oddou JL, Jeandey C, Gambarelli S, Berthomieu C, et al. Spectroscopic description of the two nitrosyl-iron complexes responsible for Fur inhibition by nitric oxide. *J Am Chem Soc* **2004**, *126*:6005- 6016. doi:10.1021/ja031671a.

Dawes E. Novel Biodegradable Microbial Polymers. Dordrecht, The Netherlands: Kluwer Academic Publishers. **1990**.

De J, Dash HR, Das S. Mercury pollution and bioremediation - a case study on biosorption by a mercury resistant marine bacterium. In: Microbial Biodegradation and Bioremediation. *Elsevier* **2014**, 137-167. doi:10.1016/B978-0-12-800021-2.00006-6.

De Francisco P, Martín-González A, Rodriguez-Martín D, Díaz S. Interactions with arsenic: mechanisms of toxicity and cellular resistance in eukaryotic microorganisms. *Int J Environ Res Public Health* **2021**, *18*:12226. doi:10.3390/ijerph182212226.

De Jesus AL, Rahman MM, Mazaheri M, Thompson H, Knibbs LD, Jeong C, et al. 2019. Ultrafine particles and PM2.5 in the air of cities around the world: Are they representative of each other? *Environ Int* **2019**, *129*:118-135. doi:10.1016/j.envint.2019.05.021.

De Oliveira M, Frihling BEF, Velasques J, Filho FJCM, Cavalheri PS, Migliolo L. Pharmaceuticals residues and xenobiotics contaminants: Occurrence, analytical techniques and sustainable alternatives for wastewater treatment. *Sci Total Environ* **2020**, *705*:135568. doi:10.1016/j.scitotenv.2019.135568.

Delany I, Rappuoli R, Scarlato V. Fur functions as an activator and as a repressor of putative virulence gene in *Neisseria meningitidis*. *Mol Microbiol* **2004**, *54*:1081-1090. doi:10.1111/j.1365-2958.2004.04030.x.

Delmar JA, Su CC, Yu EW. Heavy metal transport by the CusCFBA efflux system. *Protein Sci* **2015**, *24*:1720-1736. doi:10.1002/pro.2764.

Dereeper A, Guignon V, Blanc G, Audic S, Buffet S, Chevenet F, et al. Phylogeny.fr: Robust phylogenetic analysis for the non-specialist. *Nucleic Acids Res* **2008**, *1*:36. doi:10.1093/nar/gkn180.

Deslandes V, Nash JH, Harel J, Coulton JW, Jacques M. Transcriptional profiling of *Actinobacillus pleuropneumoniae* under iron-restricted conditions. *BMC Genomics* **2007**, *8*:72. doi:10.1186/1471-2164-8-72.

Di X, Beesley L, Zhang Z, Zhi S, Jia Y, Ding Y. Microbial arsenic methylation in soil and uptake and metabolism of methylated arsenic in plants: A review. *Int J Environ Res Public Health* **2019**, *16*:5012. doi:10.3390/ijerph16245012.

Diba F, Khan MZ, Uddin SZ, Istiaq A, Shuvo MS, Ul Alam AR, Hossain MA, Sultana, M. Bioaccumulation and detoxification of trivalent arsenic by *Achromobacter xylosoxidans* BHW-15 and electrochemical detection of its transformation efficiency. *Sci Rep* **2021**, *11*:21312. doi:10.1038/s41598-021-00745-1.

Ding LJ, An XL, Li S, Zhang GL, Zhu YG. Nitrogen loss through anaerobic ammonium oxidation coupled to iron reduction from paddy soils in a chronosequence. *Environ Sci Technol* **2014**, *48*:10641-10647. doi:10.1021/es503113s.

Distler U, Kuharev J, Tenzer S. Biomedical applications of ion mobility-enhanced data-independent acquisition-based label-free quantitative proteomics. *Expert Rev Proteomics* **2014**, *11*:675-84. doi:10.1586/14789450.2014.971114.

Dixon RA, Gang DR, Charlton AJ, Fiehn O, Kuiper HA, Reynolds TL, et al. Applications of metabolomics in agriculture. *J Agric Food Chem* **2006**, *54*:8984-94. doi:10.1021/jf061218t.

Dong H, Zhang A, Sun H, Wang H, Lu X, Wang M, et al. Ingenuity pathways analysis of urine metabolomics phenotypes toxicity of Chuanwu in Wistar rats by UPLC-Q-TOF-HDMS coupled with pattern recognition methods. *Mol BioSyst* **2012,** *8*:1206-1221. doi10.1039/C1MB05366C.

Dowdle PR, Laverman AM, Oremland RS. Bacterial reduction of arsenic (V) to arsenic (Ill) in anoxic sediments. *Appl Environ Microbiol* **1996**, *62*:664-1669. doi:10.1128/aem.62.5.1664-1669.1996.

Drabik A, Bodzoń-Kułakowska A, Silberring J. Gel electrophoresis. In: Proteomic Profiling and Analytical Chemistry. *Elsevier* **2016**.

Drace K, Kiefer AM, Veiga MM. Cyanidation of mercury-contaminated tailings: Potential health effects and environmental justice. *Curr Environ Health Rep* **2016**, *3*:443-449. doi:10.1007/s40572-016-0113-0.

Drechsel H, Winkelmann G. Iron Chelation and Siderophores. Harwood Academic, Amsterdam **1997**, 1-49.

Druschel GK, Emerson D, Sutka R, Suchecki P, Luther G. W. Low-oxygen and chemical kinetic constraints on the geochemical niche of neutrophilic iron(II) oxidizing microorganisms. *Geochim Cosmochim Acta* **2008**, *72*:3358-3370. doi:10.1016/J.GCA.2008.04.035

Duarte AALS, Cardoso SJA, Alcada AJ. Emerging and innovative techniques for arsenic removal applied to a small water supply system. *Sustainability* **2009**, *1*:1288-1304. doi:10.3390/su1041288

Duffus JH. Heavy metals a meaningless term? *Pure Appl Chem* **2002,** *74*:793-807.

Dumpala PR, Peterson BC, Lawrence ML, Karsi A. Identification of differentially abundant proteins of *Edwardsiella ictaluri* during iron restriction. *PLoS ONE* **2015**, *10*:e0132504. doi:10.1371/journal.pone.0132504.

Dunning JC, Ma Y, Marquis RE. Anaerobic killing of oral streptococci by reduced, transition metal cations. *Appl Environ Microbiol* **1998**, *64*:27-33. doi:10.1128/AEM.64.1.27-33.1998.

Dupree EJ, Jayathirtha M, Yorkey H, Mihasan M, Petre BA, Darie CC. A critical review of bottom-up proteomics: The good, the bad, and the future of this field. *Proteomes* **2020**, *8*:14. doi:10.3390/proteomes8030014.

Dvořák P, Nikel PI, Damborský J, de Lorenzo V. Bioremediation 3.0: Engineering pollutant-removing bacteria in the times of systemic biology. *Biotechnol Adv*. **2017**, *35*:845-866. doi:10.1016/j.biotechadv.2017.08.001.

Dwivedi N, Balomajumder C, Mondal P. Applications of microorganisms in biodegradation of cyanide from wastewater. In: Advances in Microbial Biotechnology. *CRC Press/Apple Academic Press*. **2018**, *12*:301, doi:10.1201/9781351248914-12.

E

Ehrenberg CG. Remarks on the real occurrence of fossil infusoria, and their extensive diffusion. *Taylor's Sci Mem* **1837**, *1*:400-413.

El Asri O, Afilal ME, Laiche H, Elfarh L. Evaluation of physicochemical, microbiological, and energetic characteristics of four agricultural wastes for use in the production of green energy in Moroccan farms. *Chem Biol Technol Agric* **2020**, *7*:21. doi:10.1186/s40538-020-00187-3.

El Asri O. Anaerobic biodegradation: The anaerobic digestion process. In: Handbook of Biodegradable Materials. *Springer* **2023**, doi:10.1007/978-3-031-09710-2-4.

Eschbach M, Schreiber K, Trunk K, Buer J, Jahn D, Schobert M. Long-term anaerobic survival of the opportunistic pathogen *Pseudomonas aeruginosa* via pyruvate fermentation. *J Bacteriol* **2004**, *186*:4596-604. doi:10.1128/JB.186.14.4596-4604.2004.

Esdaile LJ, Chalker JM. The mercury problem in artisanal and small-scale gold mining. *Chemistry* **2018**, *24*:6905-6916. doi:10.1002/chem.201704840.

Estepa J, Luque-Almagro VM, Manso I, Escribano MP, Martinez-Luque M, Castillo F, et al. The *nit1C* gene cluster of *Pseudomonas pseudoalcaligenes* CECT5344 involved in assimilation of nitriles is essential for growth on cyanide. *Environ Microbiol* **2012**, *4*:326-324. doi:10.1111/j.1758-2229.2012.00337.x.

F

Fairbrother L, Shapter J, Brugger J, Southam G, Pring A, Reith F. Effect of the cyanide-producing bacterium *Chromobacterium violaceum* on ultraflat Au surfaces. *Chem Geol* **2009**, 265:313-320. doi:10.1016/j.chemgeo.2009.04.010.

Fashola MO, Ngole-Jeme V M, Babalola OO. Heavy metal pollution from gold mines: Environmental effects and bacterial strategies for resistance. *Int J Environ Res Public Health* **2016**, *13*:1047. doi:10.3390/ijerph13111047.

Fekih IB, Zhang C, Li YP, Zhao Y, Alwathnani HA, Saquib Q, et al. Distribution of arsenic resistance genes in prokaryotes. *Front Microbiol* **2018**, *9*:2473. doi:10.3389/fmicb.2018.02473.

Feng C, Aldrich C, Eksteen JJ, Arrigan DWM. Removal of arsenic from gold cyanidation process waters by use of cerium-based magnetic adsorbents. *Miner Eng* **2018**, *122*:84-90, doi:10.1016/j.mineng.2018.03.026.

Ferguson AD, Hofmann E, Coulton JW, Diederichs K, Welte W. Siderophore-mediated iron transport: Crystal structure of FhuA with bound lipopolysaccharide. *Science* **1998**, *282*:2215-2220. doi:10.1126/science.282.5397.2215.

Ferguson AD, Chakraborty R, Smith BS, Esser L, Van Der Helm D, Deisenhofer J. Structural basis of gating by the outer membrane transporter FecA. *Science* **2002**, *295*:1715-1719. doi:10.1126/science.1067313.

Fernández M, Udaondo Z, Niqui JL, Duque E, Ramos JL. Synergic role of the two ars operons in arsenic tolerance in *Pseudomonas putida* KT2440. *Environ Microbiol Rep* **2014**, *6*:483-9. doi:10.1111/1758-2229.12167.

Fillat MF. The FUR (ferric uptake regulator) superfamily: diversity and versatility of key transcriptional regulators. *Arch Biochem Biophys* **2014**, *546*:41-52. doi:10.1016/j.abb.2014.01.029.

Firrincieli A, Zannoni D, Donini E, Dostálová H, Rädisch R, Iommarini L, et al. Transcriptomic analysis of the dual response of *Rhodococcus aetherivorans* BCP1 to inorganic arsenic oxyanions. *Appl Environ Microbiol* **2022**, *88*:e0220921. doi:10.1128/aem.02209-21.

Fleischhacker AS, Kiley PJ. Iron-containing transcription factors and their roles as sensors. *Curr Opin Chem Biol* **2011**, *15*:335-41. doi:10.1016/j.cbpa.2011.01.006.

Foster AW, Osman D, Robinson NJ, Metal preferences and metallation. *J Biol Chem* **2014**, *289*:28095-28103. doi:10.1074/jbc.R114.588145.

Fowler D, Coyle M, Skiba U, Sutton MA, Cape JN, Reis S, et al. The global nitrogen cycle in the twenty-first century. *Philos Trans R Soc B Biol Sci* **2013**, *368*:20130164. doi:10.1098/rstb.2013.0164.

Franchi E, Cosmina P, Pedron F, Rosellini I, Barbafieri M, Petruzzelli G, et al. Improved arsenic phytoextraction by combined use of mobilizing chemicals and autochthonous soil bacteria. *Sci Total Environ* **2019**, *655*:328-336. doi.org/10.1016/j.scitotenv.2018.11.242.

François F, Lombard C, Guigner JM, Soreau P, Jaisson FB, Martino G, et al. Isolation and characterization of environmental bacteria capable of extracellular biosorption of mercury. *Appl Environ Microbiol* **2012**, *78*:1097-1106. doi:10.1128/AEM.06522-11.

Freeman L, Angelini P, Silverman G, Merritt C. Production of hydrogen cyanide by *Pseudomonas fluorescens*. *Appl Microbiol* **1975** *29*:560- 561. doi:10.1128/am.29.4.560-561.

Fruzangohar M, Ebrahimie E, Ogunniyi AD, Mahdi LK, Paton JC, Adelson DL. Comparative GO: A web application for comparative gene ontology and gene ontology-based gene selection in bacteria. *PLoS One* **2013**, *8*:e58759. doi:10.1371/journal.pone.0058759.

G

Gadd GM. Metals, minerals and microbes: Geomicrobiology and bioremediation. *Microbiology* **2010**, *156*:609-643. doi:10.1099/mic.0.037143-0.

Gaffney J, Marley N. In-depth review of atmospheric mercury: Sources, transformations, and potential sinks. *Energy Emiss Control Technol* **2014**, *2*:1-21. doi:10.2147/EECT.S37038.

Gamal A, AboSalem M, El-Shewy E, Medhate-Hegazy A, Saber S. Coenzyme Q10 supplementation alleviates the oxidative stress on the liver imposed by mercuric chloride in albino rats. *B Vet Med J* **2023**, *43*:19-24. doi:10.21608/bvmj.2022.176212.1613.

Gao H, Zhou D, Li Y, Guo Z, Han Y, Song Y, et al. The iron-responsive Fur regulon in *Yersinia pestis*. *J Bacteriol* **2008**, *190*:3063-3075. doi:10.1128/JB.01910-07.

Gao Y, He N, Zhang X. Effects of reactive nitrogen deposition on terrestrial and aquatic ecosystems. *Ecol Eng* **2014**, *70*:312-318. doi:10.1016/j.ecoleng.2014.06.027.

Garbinski LD, Rosen BP, Chen J. Pathways of arsenic uptake and efflux. *Environ Int* **2019**, *126*:585-597. doi:10.1016/j.envint.2019.02.058.

García B, Olivera ER, Minambres B, Fernandez-Valverde M, Canedo LM, Prieto MA, et al. Novel biodegradable aromatic plastics from a bacterial source: Genetic and biochemical studies on a route of the phenylacetyl-CoA catabolon. *J Biol Chem* **1999**, *274*:29228-29241. doi:10.1074/jbc.274.41.29228.

Gavrilescu M. Environmental biotechnology: Achievements, opportunities and challenges. *Dyn Biochem Process Biotechnol Mol Biol* **2010**, *4*:1-36.

Gavrilescu M, Demnerova K, Aamand J, Agathos S, Fava F. Emerging pollutants in the environment: Present and future challenges in biomonitoring, ecological risks and bioremediation. *N Biotechnol* **2015**, *32*:147-156. doi:10.1016/j.nbt.2014.01.001.

Ge Y, Ning Z, Wang Y, Zheng Y, Zhang C, Figeys D. Quantitative proteomic analysis of *Dunaliella salina* upon acute arsenate exposure. *Chemosphere* **2016**, *145*:112-8. doi:10.1016/j.chemosphere.2015.11.049.

Genchi G, Lauria G, Catalano A, Carocci A, Sinicropi MS. Arsenic: A review on a great health issue worldwide. *Appl Sci* **2022**, *12*:6184. doi:10.3390/app12126184.

Germida J, Frick C, Farrell R. Phytoremediation of oil-contaminated soils. *Dev Soil Sci* **2002**, *28*:169-186. doi:10.1016/S0166-2481(02)80015-0.

Ghattas AK, Fischer F, Wick A, Ternes TA. Anaerobic biodegradation of (emerging) organic contaminants in the aquatic environment. *Water Res* **2017,** *116*:268-295. doi:10.1016/j.watres.2017.02.001.

Ghorbal SKB, Chourabi K, Maalej L, Ammar AB, Ouzari HI, Hassen A, et al. *Pseudomonas aeruginosa* Swarmer Cells Adaptation Toward UVC Radiations. *Front Microbiol* **2019**, *10*:556. doi:10.3389/fmicb.2019.00556.

Ghosh M, Shen J, Rosen BP. Pathways of As(III) detoxification in Saccharomyces cerevisiae. *Proc Nat Acad Sci USA* **1999**, *96*:5001-5006. doi:10.1073/pnas.96.9.5001.

Ghosh RS, Dzombak DA, Wong-Chong GM. Physical and chemical forms of cyanide. In: Cyanide in Water and Soil. Chemistry, Risk, and Management. *Taylor and Francis Group.* **2006**.

Ghosh A, Ghosh DM, Sreekrishnan TR. Recent advances in bioremediation of heavy metals and metal complex dyes: Review. *J Environ Eng* **2016**, *142*:C4015003. doi:10.1061/(ASCE)EE.1943-7870.0000965.

Ginn B, Meile C, Wilmoth J, Tang Y, Thompson A. Rapid iron reduction rates are stimulated by high-amplitude redox fluctuations in a tropical forest soil. *Environ Sci Technol* **2017**, *51*:3250-3259. doi:10.1021/acs.est.6b05709.

Giovanella P, Cabral L, Bento FM, Gianello C, Camargo FA. Mercury (II) removal by resistant bacterial isolates and mercuric (II) reductase activity in a new strain of *Pseudomonas* sp. B50A. *N Biotechnol* **2016**, *33*:216-23. doi:10.1016/j.nbt.2015.05.006.

Glasser NR, Kern SE, Newman DK. Phenazine redox cycling enhances anaerobic survival in *Pseudomonas aeruginosa* by facilitating generation of ATP and a proton-motive force. *Mol Microbiol* **2014**, *92*:399-412. doi:10.1111/mmi.12566.

González A, Angarica AE, Sancho J, Fillat MF. The FurA regulon in *Anabaena* sp. PCC 7120: In silico prediction and experimental validation of novel target genes. *Nucleic Acids Res* **2014**, *42*:4833-4846. doi:10.1093/nar/gku123.

González-Henao S, Ghneim-Herrera T. Heavy metals in soils and the remediation potential of bacteria associated with the plant microbiome. *Front Environ Sci* **2021**, doi:10.3389/fenvs.2021.604216.

González-Raymant H, Liu G, Liriano C, Li Y, Yin Y, Jiang G, et al. Elemental mercury: Its unique properties affects its behavior and fate in the environment. *Environ Pollut* **2017**, *229*:69-86, doi:10.1016/j.envpol.2017.04.101.

Goodcare R. Biomarker discovery using metabolomics and explanatory machine learning. *J Med Gen* **2005**, *42***:**S16-S16.

Green MR, Sambrook J. Molecular Cloning: a Laboratory Manual. Cold Spring Harbor, N.Y. *Cold Spring Harbor Laboratory Press*. **2012**.

Grégoire DS, Poulain AJ. Shining light on recent advances in microbial mercury cycling. *FACETS* **2018**, *3*:858-879. doi:10.1139/facets-2018-0015.

Gu Z, de Silva S, Reichman SM. Arsenic concentrations and dietary exposure in rice-based infant food in Australia. *Int J Environ Res Public Health* **2020**, *17*:415. doi:10.3390/ijerph17020415.

Guo H, Daniel JM, Seibel E, Burkhardt I, Conlon BH, Görls H, et al. Insights into the metabolomic capacity of *Podaxis* and isolation of podaxisterols A-D, ergosterol derivatives carrying nitrosyl cyanide-derived modifications. *J Nat Prod* **2022**, *85*:2159-2167. doi:10.1021/acs.jnatprod.2c00380.

Gupta N, Balomajumder C, Agarwal VK. Enzymatic mechanism and biochemistry for cyanide degradation: A review. *J Hazard Mater* **2010**, *176*:1-13. doi:10.1016/j.jhazmat.2009.11.038.

Gupta P, Diwan B. Bacterial exopolysaccharide mediated heavy metal removal: A review on biosynthesis, mechanism and remediation strategies. *Biotechnol Rep* **2017**, 13:58-71. doi:10.1016/j.btre.2016.12.006.

H

Hackethal C, Kopp JF, Sarvan I, Schwerdtle T, Lindtner O. Total arsenic and water-soluble arsenic species in foods of the first German total diet study. *Food Chem* **2021**, *346*:128913. doi:10.1016/j.foodchem.2020.128913

Hadi P, To MH, Hui CW, Lin CSK, McKay G. Aqueous mercury adsorption by activated carbons. *Water Res* **2015**, *73*:37–55. doi:10.1016/j.watres.2015.01.018.

Halter D, Cordi A, Gribaldo S, Gallien S, Goulhen-Chollet F, Heinrich-Salmeron A, et al. Taxonomic and functional prokaryote diversity in mildly arsenic-contaminated sediments. *Res Microbiol* **2011**, *162*:877-87. doi:10.1016/j.resmic.2011.06.001.

Hamlett NV, Landale EC, Davis BH, Summers AO. Roles of the Tn21 *merT*, *merP*, and *merC* gene products in mercury resistance and mercury binding. *J Bacteriol* **1992**, *174*:6377-85. doi:10.1128/jb.174.20.6377-6385.1992.

Handelsman J, Rondon MR, Brady SF, Clardy J, Goodman RM. Molecular biological access to the chemistry of unknown soil microbes: A new frontier for natural products. *Chem Biol 1998, 5***:**R245-R249. doi:10.1016/s1074-5521(98)90108-9.

Handelsman J. Metagenomics: Application of genomics to uncultured microorganisms. *Microbiol Mol Biol* **2004**, *68*:669-685. doi:10.1128/MMBR.68.4.669-685.2004.

Hansberg W. Biología de las especies de oxígeno reactivas. Instituto de Fisiología Celular, Universidad Nacional Autónoma de México. **2002.**

Hantke K. Members of the Fur protein family regulate iron and zinc transport in *E. coli* and characteristics of the Fur-regulated FhuF protein. *J Mol Microbiol Biotechnol* **2002**, *4*:217-22.

Harada M. Minamata disease: Methylmercury poisoning in Japan caused by environmental pollution. *Crit Rev Toxicol* **1995**, *25*:1-24. https://doi.org/10.3109/10408449509089885.

Hariharakrishnan J, Satpute RM, Prasad GBKS, Bhattacharya R. Oxidative stress mediated cytotoxicity of cyanide in LLC-MK2 cells and its attenuation by alpha-ketoglutarate and N-acetyl cysteine. *Toxicol Lett* **2009**, *185*:132-41. doi:10.1016/j.toxlet.2008.12.011.

Harrigan GG. Metabolic profiling—IBC's Inaugural meeting—using metabolomics to accelerate drug discovery and development, Durham, NC. *Idrugs* **2006**, *9*:28-31.

Hartmann M, Maumbach JI, Nolte J, Moyer MP, Zimmermann D. Metabolomics-a new approach for the detection of colon cancer? *Ann Oncol* **2006**, *17*:36-36.

Heidarinejad Z, Dehghani MH, Heidari M, Javedan G, Ali I, Sillanpää M. Methods for preparation and activation of activated carbon: A review. *Environ Chem Lett* **2020**, *18*:393–415. doi:10.1007/s10311-019-00955-0

Heiden SE, Sydow K, Schaefer S, Klempien I, Balau V, Bauer P, et al. Nearly identical plasmids encoding VIM-1 and mercury resistance in *Enterobacteriaceae* from North-Eastern Germany. *Microorganisms* **2021**, *9*:1345. doi:10.3390/microorganisms9071345.

Hemmat-Jou MH, Safari-Sinegani AA, Che R, Mirzaie-Asl A, Tahmourespour A, Tahmasbian I. Toxic trace element resistance genes and systems identified using the shotgun metagenomics approach in an Iranian mine soil. *Environ Sci Pollut Res Int* **2021**, *28*:4845-4856. doi:10.1007/s11356-020-10824-x.

Herigstad B, Hamilton M, Heersink J. How to optimize the drop plate method for enumerating bacteria. *J Microbiol Methods* **2001**, *44*:121-129. doi:10.1016/s0167-7012(00)00241-4.

Hery M, Rizoulis A, Sanguin H, Cooke DA, Pancost RD, Polya DA, et al. Microbial ecology of arsenic-mobilizing Cambodian sediments: Lithological controls uncovered by stable-isotope probing. *Environ Microbiol* **2015**, *17*:1857-1869. doi:10.1111/1462-2920.12412.

Higgs PI, Myers PS, Postle K. Interactions in the TonB-dependent energy transduction complex: ExbB and ExbD form homomultimers. *J Bacteriol* **1998**, *180*:6031-6038. doi:10.1128/JB.180.22.6031-6038.1998.

Holmes K, Mulholland F, Pearson BM, Pin C, McNicholl-Kennedy J, Ketley JM, et al. *Campylobacter jejuni* gene expression in response to iron limitation and the role of Fur. *Microbiology* **2005**, *151*:243-57. doi:10.1099/mic.0.27412-0.

Holzman DC. Mercury emissions not shrinking as forecast. *Environ Health Perspect* **2010**, *118*:A198. doi:10.1289/ehp.118-a198.

Homan ER. Reactions processes and materials with potential for cyanide exposure. In: Clinical and Experimental Toxicology of Cyanides. Bristol, UK. **1987**.

Hong YS, Kim YM, Lee KE. Methylmercury exposure and health effects. *J Prev Med Public Health* **2012**, *45*:353-363. doi:10.3961%2Fjpmph.2012.45.6.353.

Hoštacká A, CiŽnár I, Štefkovičová M. Temperature and pH affect the production of bacterial biofilm. *Folia Microbiol* **2010**, *55*:75-78. doi:10.1007/s12223-010-0012-y.

Hsu JL, Chen SH. Stable isotope dimethyl labelling for quantitative proteomics and beyond. *Philos Trans A Math Phys Eng Sci* **2016**, *374*:20150364. doi:10.1098/rsta.2015.0364.

Hu N, Li Z, Huang P, Tao C. Distribution and mobility of metals in agricultural soils near a copper smelter in South China. *Environ Geochem Health* **2006**, *28*:19-26. doi:10.1007/s10653-005-9007-z.

Huang EL, Lefsrud MG. Temporal analysis of xylose fermentation by *Scheffersomyces stipitis* using shotgun proteomics. *J Ind Microbiol Biotechnol* **2012**, *39*:1507-1514. doi:10.1007/s10295-012-1147-4.

Huang S, Jaffé PR. Isolation and characterization of an ammonium-oxidizing iron reducer: *Acidimicrobiaceae* sp. A6. *PLoS ONE* **2018**, *13*:e0194007. doi:10.1371/journal.pone.0194007.

Huang K, Xu Y, Packianathan C, Gao F, Chen C, Zhang J, et al. Arsenic methylation by a novel ArsM As(III) S-adenosylmethionine methyltransferase that requires only two conserved cysteine residues. *Mol Microbiol* **2018**, 107:265-276. doi:10.1111/mmi.13882.

Huang J, Jones A, Waite TD, Chen Y, Huang X, Rosso K M, et al. Fe(II) redox chemistry in the environment. *Chem Rev* **2021**, *121*:8161-8233. doi:10.1021/acs.chemrev.0c01286

Hudson MF, Smith KM. Novel mercury (II) complexes of porphyrins. *Tetrahedron* **1975**, *24*:3077-3083. doi:10.1016/0040-4020(75)80151-7.

Huertas MJ, Luque-Almagro VM, Martinez-Luque M, Blasco R, Moreno-Vivián C, Castillo F, et al. Cyanide metabolism of *Pseudomonas pseudoalcaligenes* CECT5344: Role of siderophores. *Biochem Soc Trans* **2006**, *34*:152-155. doi:10.1042/BST0340152.

Hughes WL. A physicochemical rationale for the biological activity of mercury and its compounds. *Ann N Y Acad Sci* **1957**, *65*:454-460. doi:10.1111/j.1749-6632.1956.tb36650.x.

Hughes MF. Arsenic toxicity and potential mechanisms of action. *Toxicol Lett* **2002,** *133*:1-16. doi:10.1016/s0378-4274(02)00084-x.

I

Ibáñez MI, Cabello P, Luque-Almagro VM, Saez LP, Olaya A, Sanchez de Medina V, et al. Quantitative proteomic analysis of *Pseudomonas pseudoalcaligenes* CECT5344 in response to industrial cyanide-containing wastewaters using Liquid Chromatography-Mass Spectrometry/Mass Spectrometry (LCMS/MS). *PLoS One* **2017**, *12*:e0172908. doi:10.1371/journal.pone.0172908.

Ibrahim M, Yusof N, Zulkhairi M, Yusoff M, Hassan MA. Enrichment of anaerobic ammonium oxidation (anammox) bacteria for short start-up of the anammox process: A review. *Desalin Water Treat* **2015**, *57*:1-21. doi:10.1080/19443994.2015.1063009.

Igeño MI, Becerra G, Guijo MI, Merchán F, Blasco R. Metabolic adaptation of *Pseudomonas pseudoalcaligenes* CECT5344 to cyanide: role of malate-quinone oxidoreductases, aconitase and fumarase isoenzymes. *Biochem Soc Trans* **2011**, *39*:1849-53. doi:10.1042/BST20110714

Ilari A, Stefanini S, Chiancone E, Tsernoglou D. The dodecameric ferritin from *Listeria innocua* contains a novel intersubunit iron-binding site. *Nat Struct Biol* **2000**, *7*:38-43. doi:10.1038/71236.

Ilbert M, Bonnefoy V. Insight into the evolution of the iron oxidation pathways. *Biochim Biophys Acta* **2013**, *1827*:161-75. doi:10.1016/j.bbabio.2012.10.001.

Inal JM, Ansa-Addo EA, Lange S. Interplay of host-pathogen microvesicles and their role in infectious disease. *Biochem Soc Trans* **2013**, *41*:258-62. doi:10.1042/BST20120257.

Ingvorsen K, Hojerpedersen B, Godtfredsen SE. Novel cyanide-hydrolysing enzyme from *Alcaligenes xylosoxidans* subsp. *Denitrificans*. *Appl Environ Microbiol* **1991**, *57*:1783-1789. doi:10.1128/aem.57.6.1783-1789.1991.

J

Janakiraman A, Slauch JM. The putative iron transport system SitABCD encoded on SPI1 is required for full virulence of *Salmonella typhimurium*. *Mol Microbiol* **2000**, *35*:1146-1155. doi:10.1046/j.1365-2958.2000.01783.x.

Ji G, Silver S. Regulation and expression of the arsenic resistance operon from *Staphylococcus aureus* plasmid pI258. *J Bacteriol* **1992**, *174*:3684-3694. doi:10.1128/jb.174.11.3684-3694.1992.

Jiang D, Zeng G, Huang D, Chen M, Zhang C, Huang C, et al. Remediation of contaminated soils by enhanced nanoscale zero valent iron. *Environ Res* **2018**, *163*:217-227. doi:10.1016/j.envres.2018.01.030.

Jiménez N, Richnow HH, Vogt C, Treude T, Krüger M. Methanogenic hydrocarbon degradation: Evidence from field and laboratory studies. *Microb Physiol* **2016**, *26*:227-242. doi:10.1159/000441679.

Johnson DB, Kanao T, Hedrich S. Redox transformations of iron at extremely low pH: Fundamental and applied aspects. *Front Microbiol* **2012**, *3*:96. doi:10.3389/fmicb.2012.00096.

Jones JG. Iron transformation by freshwater bacteria. *Adv Microb Ecol* **1986**, *9*:149-185.

Jünemann S. Cytochrome *bd* terminal oxidase. *Biochim Biophys Acta* **1997**, *1321*:107-27.

Jurasek L, Marchessault RH. The role of phasins in the morphogenesis of poly(3-hydroxybutyrate) granules. *Biomacromolecules* **2002**, *3*:256-261. doi:10.1021/bm010145d.

K

Kabiraj A, Biswas R, Halder U, Bandopadhyay R. Bacterial arsenic metabolism and its role in arsenic bioremediation. *Curr Microbiol* **2022**, *79*:131. doi:10.1007/s00284-022-02810-y.

Kamaladevi A, Balamurugan K. Global proteomics revealed *Klebsiella pneumoniae* induced autophagy and oxidative stress in *Caenorhabditis elegans* by inhibiting PI3K/AKT/mTOR pathway during infection. *Front Cell Infect Microbiol* **2017**, *7*:393. doi:10.3389/fcimb.2017.00393.

Kampers LFC, Koehorst JJ, van Heck RJA, Suarez-Diez M, Stams AJM, Schaap PJ. A metabolic and physiological design study of *Pseudomonas putida* KT2440 capable of anaerobic respiration. *BMC Microbiol* **2021**, *21*:9. doi:10.1186/s12866-020-02058-1.

Kampers LFC, van Heck RGA, Donati S, Saccenti E, Volkers RJM, Schaap PJ, et al. In silico-guided engineering of *Pseudomonas putida* towards growth under micro-oxic conditions. *Microb Cell Factories* **2019**, *18*:179. doi:10.1186/s12934-019-1227-5.

Kantor RS, van Zyl AW, van Hille RP, Thomas BC, Harrison ST, Banfield JF. Bioreactor microbial ecosystems for thiocyanate and cyanide degradation unraveled with genome-resolved metagenomics. *Environ Microbiol* **2015**, *17*:4929-4941. doi:10.1111/1462-2920.12936.

Kantor RS, Huddy RJ, Iyer R, Thomas BC, Brown CT, Anantharaman K, et al. Genome-resolved meta-omics ties microbial dynamics to process performance in biotechnology for thiocyanate degradation. *Environ Sci Technol* **2017**, *51*:2944-2953. doi:10.1021/acs.est.6b04477.

Kao CM, Liu JK, Lou HR, Lin CS, Chen SC. Biotransformation of cyanide to methane and ammonia by *Klebsiella oxytoca*. *Chemosphere* **2003**, *50*:1055-1061. doi:10.1016/s0045-6535(02)00624-0.

Kappler A, Bryce C, Mansor M, Lueder U, Byrne JM, Swanner ED. An evolving view on biogeochemical cycling of iron. *Nat Rev Microbiol* **2021**, *19*:360-374. doi:10.1038/s41579-020-00502-7.

Karamalidis AK, Evangelou AC, Karabika E, Koukkou AI, Drainas C, Voudrias EA. Laboratory scale bioremediation of petroleum contaminated soil by indigenous microorganisms and added *Pseudomonas aeruginosa* strain. *Spet Bioresour Technol* **2010**, *101*:6545-6552. doi:10.1016/j.biortech.2010.03.055.

Karamba KI, Mohd AS, Mohd YS, Siti AA. Effect of heavy metals on cyanide biodegradation by resting cells of *Serratia marcescens* strain AQ07. *Environ Microbiol Toxicol* **2014**, *2*:17-20.

Karamba K, Ahmad S, Zulkharnain A, Yasid N, Khalid A, Shukor M. Biodegradation of cyanide and evaluation of kinetic models by immobilized cells of *Serratia marcescens* strain AQ07. *Int J Sci Technol* **2017**, *14*:1945e58. doi:10.1007/s13762-017-1287-1.

Katoh H, Hagino N, Grossman AR, Ogawa T. Genes essential to iron transport in the cyanobacterium *Synechocystis* sp. strain PCC 6803. *J Bacteriol* **2001**, *183*:2779-2784. doi:10.1128/JB.183.9.2779-2784.2001.

Keramati P, Hoodaji M, Arezoo T. Multi-metal resistance study of bacteria highly resistant to mercury isolated from dental clinic effluent. *Afr J Microbiol Res* **2011**, *5*:831-837. doi:10.5897/AJMR10.860.

Kerrie S, Austin DW. Ancestry of pink disease (infantile acrodynia) identified as a risk factor for autism spectrum disorders. *J Toxicol Environ Health Part A* **2011**, *74*:1185-1194. doi:10.1080/15287394.2011.590097.

Khalid S, Shahid M, Niazi NK, Murtaza B, Bibi I, Dumat C. A comparison of technologies for remediation of heavy metal contaminated soils. *J Geochem Explor* **2017**, *182*:247-268. doi:10.1016/j.gexplo.2016.11.021.

Kim SH, Wei CI. Molecular characterization of biofilm formation and attachment of *Salmonella enterica serovar typhimurium* DT104 on food contact surfaces. *J Food Prot* **2009**, *72*:1841-1847. doi:10.4315/0362-028x-72.9.1841.

Kim KR, Lee BT, Kim KW. Arsenic stabilization in mine tailings using nano-sized magnetite and zero valent iron with the enhancement of mobility by surface coating. *J Geochem Explor* **2012**, *113*:124-129. doi:10.1016/j.gexplo.2011.07.002.

Kim S, Arora M, Fernandez C, Landero J, Caruso J, Chen A. Lead, mercury, and cadmium exposure and attention deficit hyperactivity disorder in children. *Environ Res* **2013**, *126*:105-110. doi:10.1016/j.envres.2013.08.008.

Kligerman AD, Tennant AH. Insights into the carcinogenic mode of action of arsenic. *Toxicol Appl Pharmacol* **2007**, *222*:281-288. doi:10.1016/j.taap.2006.10.006.

Komarek M, Vanek A, Ettler, V. Chemical stabilization of metals and arsenic in contaminated soils using oxides. *Environ Pollut* **2013**, *172*:9-22. doi:10.1016/j.envpol.2012.07.045.

Kostal J, Yang R, Wu CH, Mulchandani A, Chen W. Enhanced arsenic accumulation in engineered bacterial cells expressing ArsR. *Appl Environ Microbiol* **2004**, *70*:4582-4587. doi:10.1128/AEM.70.8.4582-4587.2004.

Koster W. ABC transporter-mediated uptake of iron, siderophores, heme and vitamin B12. *Res Microbiol* **2001**, *152*:291-301. doi:10.1016/s0923-2508(01)01200-1.

Kotwal DR, Shewale NB, Tambat US, Thakare MJ, Bholay AD. Bioremediation of mercury using mercury resistant bacteria. *Res J Life Bioinform Pham Chem Sci* **2018**, *4*:145-156. doi:10.26479/2018.0402.11.

Krijgsveld J, Ketting RF, Mahmoudi T, Johansen J, Artal-Sanz M, Verrijzer CP, et al. Metabolic labeling of *C. elegans* and *D. melanogaster* for quantitative proteomics. *Nat Biotechnol* **2003**, *21*:927-31. doi:10.1038/nbt848.

Kröger A. Fumarate as terminal acceptor of phosphorylative electron transport. *Biochim Biophys Acta* **1978**, *505*:129-145. doi:10.1016/0304-4173(78)90010-1.

Kuchma SL, O'Toole GA. Surface-induced cAMP signaling requires multiple features of the *Pseudomonas aeruginosa* type IV pili. *J Bacteriol* **2022**, *204*:e00186-22. doi:10.1128/jb.00186-22.

Kulp TR, Hoeft SE, Oremland RS. Redox transformations of arsenic oxyanions in periphyton communities. *Appl Environ Microbiol* **2004**, *70*:6428-6434. doi:10.1128/AEM.70.11.6428-6434.2004.

Kunath BJ, Minniti G, Skaugen M, Hagen LH, Vaaje-Kolstad G, Eijsink VGH, et al. Metaproteomics: Sample preparation and methodological considerations. *Adv Exp Med Bio* **2019**, *1073*:187-215. doi:10.1007/978-3-030-12298-0_8.

Kuypers MMM, Marchant HK, Kartal B. The microbial nitrogen-cycling network. *Nat Rev Microbiol* **2018**, *16*:263-276. doi:10.1038/nrmicro.2018.9.

Kuyucak N, Akcil A. Cyanide and removal options from effluents in gold mining and metallurgical processes. *Miner Eng* **2013**, *50-51*:13-29. doi:10.1016/j.mineng.2013.05.027.

Kwan YH, Zhang D, Mestre NC, Wong WC, Wang X, Lu B, et al. Comparative proteomics on deep-sea amphipods after in situ copper exposure. *Environ Sci Technol* **2019**, *53*:13981-13991. doi:10.1021/acs.est.9b04503.

L

Laemmli UK. Cleavage of structural proteins during the assembly of the head of bacteriophage T4. *Nature* **1970**, *227*:680-685. doi:10.1038/227680a0.

Lamarche MG, Wanner BL, Crépin S, Harel J. The phosphate regulon and bacterial virulence: A regulatory network connecting phosphate homeostasis and pathogenesis. *FEMS Microbiol Rev* **2008**, *32*:461-473. doi:10.1111/j.1574-6976.2008.00101.x.

Lamond AI, Uhlen M, Horning S, Makarov A, Robinson CV, Serrano L, et al. Advancing cell biology through proteomics in space and time (PROSPECTS). *Mol Cell Proteomics* **2012**, *11*:O112.017731. doi:10.1074/mcp.O112.017731.

Lampis S, Santi C, Ciurli A, Andreolli M, Vallini G. Promotion of arsenic phytoextraction efficiency in the fern *Pteris vittata* by the inoculation of As-resistant bacteria: A soil bioremediation perspective. *Front Plant Sci* **2015**, *6*:80. doi:10.3389/fpls.2015.00080.

Larive CK, Barding GA, Dinges MM. NMR spectroscopy for metabolomics and metabolic profiling. *Anal Chem* **2015**, *87*:133-146. doi:10.1021/ac504075g.

Larsen RA, Thomas MG, Wood GE, Postle K. Partial suppression of an *Escherichia coli* TonB transmembrane domain mutation (DeltaV17) by a missense mutation in ExbB. *Mol Microbiol* **1994**, *13*:627-640. doi:10.1111/j.1365-2958.1994.tb00457.x.

Lauterböck B, Ortner M, Haider R, Fuchs W. Counteracting ammonia inhibition in anaerobic digestion by removal with a hollow fiber membrane contactor. *Water Res* **2012**, *46*:4861-4869. doi:10.1016/j.watres.2012.05.022.

Lechtenberg M. Cyanogenesis in higher plants and animals. In: eLS. *John Wiley & Sons* **2011**. doi:10.1002/9780470015902.a0001921.pub2

Lee JW, Helmann JD. Functional specialization within the Fur family of metalloregulators. *Biometals* **2007**, *20*:485-499.

Lee SJ, Kim DG, Lee KY Koo JS, Lee BJ. Regulatory mechanisms of thiol-based redox sensors: lessons learned from structural studies on prokaryotic redox sensors. *Arch Pharm Res* **2018**, *41*:583593. doi:10.1007/s12272-018-1036-0.

Lelieveld J, Klingmuller K, Pozzer A, Poschl U, Fnais M, Daiber A, et al. Cardiovascular disease burden from ambient air pollution in Europe reassessed using novel hazard ratio functions. *Eur Heart J* **2019**, *40*:1590-1596. doi:10.1093/eurheartj/ehz135.

Lenney W, Gilchrist FJ. *Pseudomonas aeruginosa* and cyanide production. *Eur Respir J* **2011**, *37*:482-483; doi:10.1183/09031936.00122810.

Li J, Wang N. The *wxacO* gene of *Xanthomonas citri* ssp. *citri* encodes a protein with a role in lipopolysaccharide biosynthesis, biofilm formation, stress tolerance and virulence. *Mol Plant Pathol* **2011**, *12*:381-396. doi:10.1111/j.1364-3703.2010.00681.x

Li X, Hou L, Liu M, Zheng Y, Yin G, Lin X, et al. Evidence of nitrogen loss from anaerobic ammonium oxidation coupled with ferric iron reduction in an intertidal wetland. *Environ Sci Technol* **2015**, *49*:11560-8. doi:10.1021/acs.est.5b03419.

Li KW, Gonzalez-Lozano MA, Koopmans F, Smit AB. Recent developments in data independent acquisition (DIA) mass spectrometry: Application of quantitative analysis of the brain proteome. *Front Mol Neurosci* **2020**, *13*:564446. doi:10.3389/fnmol.2020.564446.

Li X, Liu X, Cao N, Fang S, Yu C. Adaptation mechanisms of arsenic metabolism genes and their host microorganisms in soils with different arsenic contamination levels around abandoned gold tailings. *Environ Pollut* **2021**, *291*:117994. doi:10.1016/j.envpol.2021.117994.

Liebert CA, Hall RM, Summers AO. Transposon Tn21, flagship of the floating genome. *Microbiol Mol Biol Rev* **1999**, *63*:507-22. doi:10.1128/MMBR.63.3.507-522.1999.

Lim MW, Lau EV, Poh PEA. Comprehensive guide of remediation technologies for oil contaminated soil - present works and future directions. *Mar Pollut Bull* **2016**, *109*:14-45. doi:10.1016/j.marpolbul.2016.04.023.

Lin YF, Walmsley AR, Rosen BP. An arsenic metallochaperone for an arsenic detoxification pump. *Proc Natl Acad Sci USA* **2006**, *103*:15617-15622. doi.org/10.1073/pnas.06039 74103.

Lin CC, Yee N, Barkay T. Microbial transformations in the mercury cycle. In: Environmental Chemistry and Toxicology of Mercury. *John Wiley and Sons* **2012**, 155-191. doi:10.1002/9781118146644.ch5.

Lin X, Handley KM, Gilbert JA, Kostka JE. Metabolic potential of fatty acid oxidation and anaerobic respiration by abundant members of *Thaumarchaeota* and *Thermoplasmata* in deep anoxic peat. *ISME J* **2015**, *9*:2740-4. doi:10.1038/ismej.2015.77.

Lin Y, Wang S, Wu Q, Larssen T. Material flow for the intentional use of mercury in China. *Environ Sci Technol* **2016**, *50*:2337-2344. doi:10.1021/acs.est.5b04998.

Lin X, Zhao J, Zhang W, He L, Wang L, Li H, et al. Towards screening the neurotoxicity of chemicals through feces after exposure to methylmercury or inorganic mercury in rats: A combined study using gut microbiome, metabolomics and metallomics. *J Hazard Mater* **2021a,** *409*:124923. doi:10.1016/j.jhazmat.2020.124923.

Lin X, Zhang W, He L, Xie H, Feng B, Zhu H, et al. Understanding the hepatoxicity of inorganic mercury through guts: Perturbance to gut microbiota, alteration of gut-liver axis related metabolites and damage to gut integrity. *Ecotoxicol Environ Saf* **2021b**, *225*:112791. doi:10.1016/j.ecoenv.2021.112791.

Liu S, Zhang F, Chen J, Sun G. Arsenic removal from contaminated soil via biovolatilization by genetically engineered bacteria under laboratory conditions. *J Environ Sci* **2011**, *23*:1544- 1550. doi.org/10.1016/S1001- 0742(10)60570-0.

Liu Y, Huttenhain R, Surinova S, Gillet LC, Mouritsen J, Brunner R, et al. Quantitative measurements of N-linked glycoproteins in human plasma by SWATH-MS. *Proteomics* **2013**, *13*:1247-1256. doi:10.1002/pmic.201200417.

Liu X, Hu Y, Pai P-J, Chen D, Lam H. Label-free quantitative proteomics analysis of antibiotic response in *Staphylococcus aureus* to oxacillin. *J Proteome Res* **2014**, *13*:1223-1233. doi:10.1021/pr400669d.

Liu Y, Zeng G, Zhong H, Wang Z, Liu Z, Cheng M, et al. Effect of rhamnolipid solubilization on hexadecane bioavailability: Enhancement or reduction? *J Hazard Mater* **2017**, *322*:394-401. doi:10.1016/j.jhazmat.2016.10.025.
Liu L, Li W, Song W, Guo M. Remediation techniques for heavy metal-contaminated soils: Principles and applicability. *Sci Total Environ* **2018**, *633*:206-219. doi:10.1016/j.scitotenv.2018.03.161.

Lloyd KG, Steen AD, Ladau J, Yin J, Crosby L. Phylogenetically novel uncultured microbial cells dominate Earth microbiomes. *mSystems* **2018**, *3*:e00055-18. doi:10.1128/mSystems.00055-18.

Lobritz MA, Belenky P, Porter CB, Gutierrez A, Yang JH, Schwarz EG, et al. Antibiotic efficacy is linked to bacterial cellular respiration. *Proc Natl Acad Sci USA* **2015**, *112*:8173-80. doi:10.1073/pnas.1509743112.

López-Pérez ME, Saldaña-Robles A, Zanor GA, Ibarra JE, Del Rincón-Castro MC. Microbiomes in agricultural and mining soils contaminated with arsenic in Guanajuato, Mexico. *Arch Microbiol* **2021**, *203*:499-511. doi:10.1007/s00203-020-01973-1.

Lu K, Abo RP, Schlieper KA, Graffam ME, Levine S, Wishnok JS, et al. Arsenic exposure perturbs the gut microbiome and its metabolic profile in mice: An integrated metagenomics and metabolomics analysis. *Environ Health Perspect* **2014**, *122*:284-291. doi:10.1289/ehp.1307429.

Lundholt BK, Scudder KM, Pagliaro L. A simple technique for reducing edge effect in cell-based assays. *J Biomol Screen* **2003**, *8*:566-570. doi:10.1177/1087057103256465.

Luo Q, Kong L, Dong J, Zhang T, Wang H, Zhang R, et al. Protection of chickens against fowl cholera by supernatant proteins of *Pasteurella multocida* cultured in an iron-restricted medium. *Avian Pathol* **2019**, *48*:221-229. doi:10.1080/03079457.2019.1568390.

Luque-Almagro VM, Huertas MJ, Martínez-Luque M, Moreno-Vivián C, Roldán MD, García-Gil LJ, et al. Bacterial degradation of cyanide and its metal complexes under alkaline conditions. *Appl Environ Microbiol* **2005**, *71*:940-947. doi:10.1128/AEM.71.2.940-947.2005.

Luque-Almagro VM, Huertas MJ, Roldán MD, Moreno-Vivián C, Martínez-Luque M, Blasco R, et al. The cyanotrophic bacterium *Pseudomonas pseudoalcaligenes* CECT5344 responds to cyanide by defense mechanism against iron deprivation, oxidative damage and nitrogen stress. *Environ Microbiol* **2007**, *9*:1541-1549. doi:10.1111/j.1462-2920.2007.01274.x.

Luque-Almagro VM, Huertas MJ, Sáez LP, Martínez-Luque M, Moreno-Vivián C, Castillo F, et al. Characterization of the *Pseudomonas pseudoalcaligenes* CECT5344 cyanase, an enzyme that is not essential for cyanide assimilation. *Appl Environ Microbiol* **2008**, *74*:6280-6288. doi:10.1128/AEM.00916-08.

Luque-Almagro VM, Blasco R, Martínez-Luque M, Moreno-Vivián C, Castillo F, Roldán MD. Bacterial cyanide degradation is under review: *Pseudomonas pseudoalcaligenes* CECT5344, a case of an alkaliphilic cyanotroph. *Biochem Soc Trans* **2011a**, *39*:269-274. doi:10.1042/BST0390269.

Luque-Almagro VM, Merchán F, Blasco R, Igeño MI, Martínez-Luque M, Moreno-Vivián C, et al. Cyanide degradation by *Pseudomonas pseudoalcaligenes* CECT5344 involves a malate:quinone oxidoreductase and an associated cyanide-insensitive electron transfer chain. *Microbiology* **2011b**, *157*:739-746. doi:10.1099/mic.0.045286-0.

Luque-Almagro VM, Acera F, Igeno MI, Wibberg D, Roldan MD, Saez LP et al. Draft whole genome sequence of the cyanide-degrading bacterium *Pseudomonas pseudoalcaligenes* CECT5344. *Environ Microbiol* **2013**, *15*:253-270. doi:10.1111/j.1462-2920.2012.02875.x.

Luque-Almagro VM, Escribano MP, Manso I, Sáez LP, Cabello P, Moreno-Vivián C, et al. DNA microarray analysis of the cyanotroph *Pseudomonas pseudoalcaligenes* CECT5344 in response to nitrogen starvation, cyanide and a jewelry wastewater. *J Biotechnol* **2015**, *214*:171-181. doi:10.1016/j.jbiotec.2015.09.032.

Luque-Almagro VM, Moreno-Vivián C, Roldán MD. Biodegradation of cyanide wastes from mining and jewelry industries. *Curr Opin Biotech* **2016**, *38*:9-13. doi:10.1016/j.copbio.2015.12.004.

Luque-Almagro VM, Cabello P, Saez LP, Olaya-Abril A, Moreno-Vivián C, Roldan MD. Exploring anaerobic environments for cyanide and cyano-derivatives microbial degradation. *Appl Microbiol Biotechnol* **2018**, *102*:1067-1074. doi:10.1007/s00253-017-8678-6.

M

Madison LL, Huisman GW. Metabolic engineering of poly (3hydroxyalkanoates): From DNA to plastic. *Microbiol Mol Biol Rev* **1999**, *63*:21-53. doi:10.1128/MMBR.63.1.21-53.1999.

Magdeldin S, Enany S, Yoshida Y, Xu B, Zhang Y, Zureena, et al. Basics and recent advances of two dimensional-polyacrylamide gel electrophoresis. *Clin Proteomics* **2014**, *11*:16. doi:10.1186/1559-0275-11-16.

Mahimairaja S, Bolan NS, Adriano DC. Robinson, B. Arsenic contamination and its risk management in complex environmental settings. *Adv Agron* **2005**, *86*:1-82. doi.org/10.1016/S0065-2113(05)86001-8.

Maity S, Sarkar D, Poddar K, Patil P, Sarkar A. Biofilm-mediated heavy metal removal from aqueous system by multi-metalresistant bacterial strain *Bacillus* sp. GH-s29. *Appl Biochem Biotechnol* **2022**, 8:1-19. doi:10.1007/s12010-022-04288-7.

Maklashina E, Berthold DA, Cecchini G. Anaerobic expression of *Escherichia col*i succinate dehydrogenase: Functional replacement of fumarate reductase in the respiratory chain during anaerobic growth. *J Bacteriol* **1998**, *180*:5989-5996. doi:10.1128/JB.180.22.5989-5996.1998.

Malhi H, Gores GJ. Cancer therapy-back to metabolism. *Cancer Biol Ther* **2006**, *5*:986-987. doi:10.4161/cbt.5.8.3314.

Malmir N, Allahyari-Fard N, Aminzadeh S, Moghaddassi-Jahromi ZM, Mekuto L. An overview of emerging cyanide bioremediation methods. *Processes* **2022**, *10*:1724. doi:10.3390/pr10091724.

Mandal BK, Suzuki KT. Arsenic round the world: A review. *Talanta* **2002**, *58*:201-235.

Mandeep, Shukla P. Microbial nanotechnology for bioremediation of industrial wastewater. *Front Microbiol* **2020**, *11*:590631. doi:10.3389/fmicb.2020.590631

Maniyam MG, Sjahrir F, Ibrahim AL. Bioremediation of cyanide by optimized resting cells of *Rhodococcus* strains isolated from Peninsular Malaysia. *Int J Biosci Biochem Bioinform* **2011**, *1*:98-101. doi:10.7763/IJBBB.2011.V1.18.

Manning K. Ethylene production and *β*-cyanoalanine synthase activity in carnation flowers. *Planta* **1986**, *168*:61- 66. doi:10.1007/BF00407010.

Manonmani U, Joseph K. Granulation of anammox microorganisms for autotrophic nitrogen removal from wastewater. *Environ Chem Lett* **2018**, *16*:881-901. doi:10.1007/s10311-018-0732-9.

Manso I, Ibáñez MI, de la Peña F, Sáez LP, Luque-Almagro VM, Castillo-Rodríguez F, et al. *Pseudomonas pseudoalcaligenes* CECT5344, a cyanide-degrading bacterium with by-product (polyhydroxyalkanoates) formation capacity. *Microb Cell Fact* **2015,** *14*:77. doi:10.1186/s12934-015-0267-8.

Mapelli V, Olsson L, Nielsen J. Metabolic footprinting in microbiology: Methods and applications in functional genomics and biotechnology. *Trends Biotechnol* **2008**, *26*:490e497. doi:10.1016/j.tibtech.2008.05.008.

Marquardt H, Schäfer S. G. Lehrbuch der Toxikologie. Wissenschaftsverlag, Mannheim, **1994**.

Marshall BG, Veiga MM, Kaplan RJ, Adler MR, Schudel G, Bergquist B, et al. Evidence of transboundary mercury and other pollutants in the Puyango-tubes river basin, Ecuador-Peru. *Environ Sci: Processes Impacts* **2018**, *20*:632-641 doi:10.1039/C7EM00504K.

Martínez VD, Vucic EA, Becker-Santos DD, Gil L, Lam WL. Arsenic exposure and the induction of human cancers. *J Toxicol* **2011**, 431287. doi:10.1155/2011/431287.

Massé E, Gottesman S. A small RNA regulates the expression of genes involved in iron metabolism in *Escherichia coli*. *Proc Natl Acad Sci USA* **2002**, *99*:4620-4625. doi:10.1073/pnas.032066599.

Mathema VB, Thakuri BC, Sillanpaa, M. Bacterial *mer* operon-mediated detoxification of mercurial compounds: A short review. *Arch Microbiol* **2011**, *193*:837-844. doi:10.1007/s00203-011-0751-4.

Mathivanan K, Uthaya-Chandirika J, Vinothkanna A, Yin H, Liu X, Meng D. Bacterial adaptive strategies to cope with metal toxicity in the contaminated environment- A review. *Ecotoxicol Environ Saf* **2021**, *226*:112863. doi:10.1016/j.ecoenv.2021.112863.

Matlock MM, Howerton BS, Van Aelstyn MA, Nordstrom FL, Atwood DA. Advanced mercury removal from gold leachate solutions prior to gold and silver extraction: A field study from an active gold mine in Peru. *Environ Sci Technol* **2002**, *36*:1636-1639. doi:10.1021/es0112285.

May C, Brosseron F, Chartowski P, Meyer HE, Marcus K. Differential proteome analysis using 2D-DIGE. *Methods Mol Biol* **2012**, *893*:75-82. doi:10.1007/978-1-0716-1024-4_7.

Mazumder P, Sharma SK, Taki K, Kalamdhad AS, Kumar M. Microbes involved in arsenic mobilization and respiration: A review on isolation, identification, isolates and implications. *Environ Geochem Health* **2020**, *42*:3443-3469. doi:10.1007/s10653-020-00549-8.

Mbadinga SM, Wang LY, Zhou L, Liu JF, Gu JD, Mu BZ. Microbial communities involved in anaerobic degradation of alkanes. *Int Biodeterior Biodegrad* **2011**, *65*:1-13. doi:10.1016/j.ibiod.2010.11.009.

McCarty KM, Hanh HT, Kim KW. Arsenic geochemistry and human health in South East Asia. *Rev Environ Health* **2011**, *26*:71-78. doi:10.1515/reveh.2011.010.

Meharg AA, Zhao FJ. Arsenic and rice. *Exp Agric* **2012**, *49*:151-151. doi:10.1017/S0014479712000713.

Mehta BC, Shrivastava KK. Iron in groundwater of India and its geochemistry. *Groundw Sustain Dev* **2012**, *7*:421-429. doi:10.1016/j.gsd.2017.12.011.

Meier F, Brunner AD, Koch S, Koch H, Lubeck M, Krause M, et al. Online parallel accumulation-serial fragmentation (PASEF) with a novel trapped ion mobility mass spectrometer. *Mol Cell Proteom* **2018**, *17*:2534-2545. doi:10.1074/mcp.TIR118.000900.

Meier F, Brunner AD, Frank M, Ha A, Bludau I, Voytik E, et al. DiaPASEF: Parallel accumulation-serial fragmentation combined with data-independent acquisition. *Nat Methods* **2020**, *17*:1229-1236. doi:10.1038/s41592-020-00998-0.

Melton ED, Swanner ED, Behrens S, Schmidt C, Kappler A. The interplay of microbially mediated and abiotic reactions in the biogeochemical Fe cycle. *Nat Rev Microbiol* **2014,** *12:*797-808. doi:10.1038/nrmicro3347.

Mergeay M, Monchy S, Vallaeys T, Auquier V, Benotmane A, Bertin P, et al. *Ralstonia metallidurans*, a bacterium specifically adapted to toxic metals: Towards a catalogue of metal-responsive genes. *FEMS Microbiol Rev* **2003***, 27*:358-410. doi:10.1016/S0168-6445(03)00045-7.

Meuser, H. Soil Remediation and Rehabilitation: Treatment of Contaminated and Disturbed Land. *Springer* **2013.**

Meyer JG. Qualitative and quantitative shotgun proteomics data analysis from data-dependent acquisition mass spectrometry. *Methods Mol Biol* **2021**, *2259*:297-307. doi:10.1007/978-1-0716-1178-4_19.

Meyers PR, Rawlings DE, Woods DR, Lindsey GG. Isolation and characterization of a cyanide dihydratase for *Bacillus pumilus* C1. *J Bacteriol* **1993**, *175*:6105-6112. doi:10.1128/jb.175.19.6105-6112.1993.

Michán C, Chicano-Gálvez E, Fuentes-Almagro CA, Alhama J. Redox and global interconnected proteome changes in mice exposed to complex environmental hazards surrounding Doñana National Park. *Environ Pollut* **2019***, 252*:427-439. doi:10.1016/j.envpol.2019.05.085.

Mihara H, Esaki N. Bacterial cysteine desulfurases: Their function and mechanisms. *Appl Microbiol Biotechnol* **2002**, *60*:12-23. doi:10.1007/s00253-002-1107-4.

Miller MR, Newby DE. Air pollution and cardiovascular disease: Car sick. *Cardiovasc Res* **2020**, *116*:279-294. doi:10.1093/cvr/cvz228.

Miranda-Carrazco A, Vigueras-Cortés JM, Villa-Tanaca L, Hernández-Rodríguez C. Cyanotrophic and arsenic oxidizing activities of *Pseudomonas mendocina* P6115 isolated from mine tailings containing high cyanide concentration. *Arch Microbiol* **2018**, *200*:1037-1048. doi.org/10.1007/s00203-018-1514-2.

Mohd BZ, Ibrahim Z, Jaafar J, Shahir S. Draft genome sequence of arsenic-resistant *Microbacterium* sp. strain SZ1 isolated from arsenic-bearing gold ores. *Genome Announc* **2017**, *5*:e01183-17. doi:10.1128/genomeA.01183-17.

Moinier D, Byrne D, Amouric A, Bonnefoy V. The global redox responding RegB/RegA signal transduction system regulates the genes involved in ferrous iron and inorganic sulfur compound oxidation of the acidophilic *Acidithiobacillus ferrooxidans*. *Front Microbiol* **2017**, *8*:1277. doi:10.3389/fmicb.2017.01277.

Mojiri A, Zhou JL, Karimi-Dermani B, Razmi E, Kasmuri N. Anaerobic membrane bioreactor (AnMBR) for the removal of dyes from water and wastewater: Progress, challenges, and future perspectives. *Processes* **2023**, *11*:855. doi:10.3390/pr11030855.

Moodie AD, Ingledew WJ. Microbial anaerobic respiration. In: Advances in Microbiology and Physiology. *Academic Press, London* **1990**, 225-269. doi:10.1016/s0065-2911(08)60123-x.

Moreno-Vivián C, Cabello P, Martínez-Luque M, Blasco R, Castillo F. Prokaryotic nitrate reduction: Molecular properties and functional distinction among bacterial nitrate reductases. *J Bacteriol* **1999**, *181*:6573-84. doi:10.1128/JB.181.21.6573-6584.1999.

Morillo E, Villaverde J. Advanced technologies for the remediation of pesticide-contaminated soils. *Sci Total Environ* **2017**, *586*:576-597. doi:10.1016/j.scitotenv.2017.02.020.

Morrison GR. Microchemical determination of organic nitrogen with Nessler reagent. *Anal Biochem* **1971**, *43*:527-532. doi:10.1016/0003-2697(71)90283-1.

Mudder TI, Botz MM. Cyanide and society: a critical review. *Eur Jour Mineral Process Environ Prot* **2004**, *4*:62-74.

Mueller NC, Nowack B. Nanoparticles for remediation: Solving big problems with little particles. *Elements* **2010**, *6*:395-400. doi:10.2113/gselements.6.6.395

Mukhopadhyay D, Yu HR, Nucifora G, Misra TK. Purification and functional characterization of MerD, a coregulator of the mercury resistance operon in gram-negative bacteria. *J Biol Chem* **1991**, *266*:18538-42.

Mukhopadhyay R, Bhattacharjee H, Rosen BP. Aquaglyceroporins: Generalized metalloid channels. *Biochim Biophys* **2014**, *1840*:1583-1591. doi:10.1016/j.bbagen.2013.11.021.

Muller D, Medigue C, Koechler S, Barbe V, Barakat M, et al. A tale of two oxidation states: Bacterial colonization of arsenic-rich environments. *PLoS Genet* **2007**, *3*:e53. doi:10.1371/journal.pgen.0030053.

Munyai R, Ogola HJO, Modise DM. Microbial community diversity dynamics in acid mine drainage and acid mine drainage-polluted soils: Implication on mining water irrigation agricultural sustainability. *Front Sustain Food Syst* **2021**, *5*:701870. doi:10.3389/fsufs.2021.701870.

Mushtaq J, Dar AQ, Ahsan N. Spatial-temporal variations and forecasting analysis of municipal solid waste in the mountainous city of north-western Himalayas. *SN Appl Sci* **2020**, *2*:1161. doi:10.1007/s42452-020-2975-x.

Muthubharathi BC, Gowripriya T, Balamurugan K. Metabolomics: Small molecules that matter more. *Mol Omics* **2021**, *17*:210e229. doi:10.1039/D0MO00176G.

N

Nagajyoti PC, Lee KD, Sreekanth TMV. Heavy metals, occurrence, and toxicity for plants: A review. *Environ Chem Lett* **2010**, *8*:199-216. doi:10.1007/s10311-010-0297-8.

Naghili H, Tajik H, Mardani K, Razavi-Rouhani SM, Ehsani A, Zare P. Validation of drop plate technique for bacterial enumeration by parametric and nonparametric tests. *Vet Res Forum* **2013**, *4*:179-183.

Naguib M, El-Gendy A, Khairalla A. Microbial diversity of *mer* operon genes and their potential rules in mercury bioremediation and resistance. *Open Biotechnol J* **2018**, *12*:56-77. doi:10.2174/1874070701812010056.

Nascimento AM, Chartone-Souza E. Operon *mer*: Bacterial resistance to mercury and potential for bioremediation of contaminated environments. *Genet Mol Res* **2003**, *2*:92-101.

Neneng L, Gunawan YE. Bioremediation by Isolates *Pseudomonas aeruginosa* KHY2 and *Klebsiella pneumonia* KHY3. *The J Trop Life Sci* **2018**, *8*:16-20. doi:10.11594/jtls.08.01.04.

Newby DE, Mannucci PM, Tell GS, Baccarelli AA, Brook RD, Donaldson K, et al. Expert position paper on air pollution and cardiovascular disease. *Eur Heart J* **2015**, *36*:83-93. doi:10.1093/eurheartj/ehu458.

Newcombe C, Raab A, Williams PN, Deacon C, Haris PI, Meharg AA, et al. Accumulation or production of arsenobetaine in humans? *J Environ Monit* **2010**, *12*:832-837.

Newsome L, Falagán C. The microbiology of metal mine waste: Bioremediation applications and implications for planetary health. *Geohealth* **2021**, *5*:e2020GH000380. doi:10.1029/2020GH000380.

Nicholson JK, Lindon JC, Holmes E. Metabonomics: Understanding the metabolic responses of living systems to pathophysiological stimuli via multivariate statistical analysis of biological NMR spectroscopic data. *Xenobiotica* **1999**, *29*:1181. doi:10.1080/004982599238047.

Nikel PI, de Lorenzo V. Engineering an anaerobic metabolic regime in *Pseudomonas putida* KT2440 for the anoxic biodegradation of 1,3-dichloroprop-1-ene. *Metab Eng* **2013**, *15*:98-112. doi:10.1016/j.ymben .2012.09.006.

Nordstrom DK. Public health. Worldwide occurrences of arsenic in ground water. *Science* **2002**, *296*:2143-5. doi:10.1126/science.1072375.

Novotny MV, Alley WR, Mann BF. Analytical glycobiology at high sensitivity: current approaches and directions. *Glycoconj J* **2013**, *30*:89-117. doi:10.1007/s10719-012-9444-8.

Nurfitriani S, Arisoesilaningsih E, Nuraini Y, Handayanto E. Bioaccumulation of mercury by bacteria isolated from small scale gold mining tailings in Lombok, Indonesia. *J Ecol Eng* **2020**, *21*:127-136. doi:10.12911/22998993/123247.

Nyamunda BC. Review of the impact on water quality and treatment options of cyanide used in gold ore processing. *IntechOpen* **2017**. doi:10.5772/65706.

O

O'Farrell PH. High resolution two-dimensional electrophoresis of proteins. *J Biol Chem* **1975**, *250*:4007-4021.

Obulisamy PK, Mehariya S. Polyhydroxyalkanoates from extremophiles: A review. *Bioresour Technol* **2021**, *325*:124653. doi:10.1016/j.biortech.2020.124653.

Ohmura N, Sasaki K, Matsumoto N, Saiki H. Anaerobic respiration using Fe^{3+}, S^0, and H_2 in the chemolithoautotrophic bacterium *Acidithiobacillus ferrooxidans*. *J Bacteriol* **2002**, *184*:2081-2087. doi:10.1128/JB.184.8.2081-2087.2002.

Olaya-Abril A, Luque-Almagro VM, Manso I, Gates AJ, Moreno-Vivián C, Richardson DJ, Roldán MD. Poly(3-hydroxybutyrate) hyperproduction by a global nitrogen regulator NtrB mutant strain of *Paracoccus denitrificans* PD1222. *FEMS Microbiol Lett* **2017**, *365*:fnx251. doi:10.1093/femsle/fnx251.

Olaya-Abril A, Hidalgo-Carrillo J, Luque-Almagro VM, Fuentes-Almagro C, Urbano FJ, Moreno-Vivián C, et al. Exploring the denitrification proteome of *Paracoccus denitrificans* PD1222. *Front Microbiol* **2018,** *9*:1137. doi:10.3389/fmicb.2018.01137.

Olaya-Abril A, Luque-Almagro VM, Pérez MD, López CM, Amil F, Cabello P, et al. Putative small rRNAs controlling detoxification of industrial cyanide-containing wastewaters by *Pseudomonas pseudoalcaligenes* CECT5344. *PLoS One* **2019**, *14*:e0212032. doi:10.1371/journal.pone.0212032.

Olaya-Abril A, Pérez MD, Cabello P, Martignetti D, Sáez LP, Luque-Almagro VM, et al. Role of the dihydrodipicolinate synthase DapA1 on iron homeostasis during cyanide assimilation by the alkaliphilic bacterium *Pseudomonas pseudoalcaligenes* CECT5344. *Front Microbiol* **2020**, *11*:28. doi:10.3389/fmicb.2020.00028.

Olaya-Abril A, Hidalgo-Carrillo J, Luque-Almagro VM, Fuentes-Almagro C, Urbano FJ, Moreno-Vivián C, et al. Effect of pH on the denitrification proteome of the soil bacterium *Paracoccus denitrificans* PD1222. *Sci Rep* **2021**, *11*:17276. doi:10.1038/s41598-021-96559-2.

Olaya-Abril A, Luque-Almagro VM, Hidalgo-Carrillo J, Chicano-Gálvez E, Urbano FJ, Moreno-Vivián C, et al. The NtrYX two-component system of *Paracoccus denitrificans* is required for the maintenance of cellular iron homeostasis and for a complete denitrification under iron-limited conditions. *Int J Mol Sci* **2022**, *23*:9172. doi:10.3390/ijms23169172.

Olson KR, Cihacek L. The fate of Agent Blue, the arsenic based herbicide, used in South Vietnam during the Vietnam War. *Open J Soil Sci* **2020**, *10*:518-577. doi:10.4236/ojss.2020.1011027.

Ong SE, Blagoev B, Kratchmarova I, Kristensen DB, Steen H, Pandey A, et al. Stable isotope labeling by amino acids in cell culture, SILAC, as a simple and accurate approach to expression proteomics. *Mol Cell Proteomics* **2002**, *1*:376-86. doi:10.1074/mcp.m200025-mcp200.

Ordóñez E, Letek M, Valbuena N, Gil JA, Mateos LM. Analysis of genes involved in arsenic resistance in *Corynebacterium glutamicum* ATCC13032. *Appl Environ Microbiol* **2005**, *71*:6206-6215. doi:10.1128/AEM.71.10.6206-6215.2005.

Ordoñez OF, Lanzarotti E, Kurth D, Cortez N, Farías ME, Turjanski AG. Genome comparison of two *Exiguobacterium* strains from high altitude Andean lakes with different arsenic resistance: Identification and 3D modeling of the Acr3 efflux pump. *Front Environ Sci* **2015**, *3*:50. doi:10.3389/fenvs.2015.00050.

Oremland RS, Stolz JF. The ecology of arsenic. *Science* **2003**, *300*:939-944. doi:10.1126/science.1081903.

Oremland RS, Stolz JF. Arsenic, microbes and contaminated aquifers. *Trends Microbiol* **2005**, *13*:45-9. doi:10.1016/j.tim.2004.12.002.

Oremland RS, Saltikov CW, Stolz JF, Hollibaugh JT. Autotrophic microbial arsenotrophy in arsenic-rich soda lakes. *FEMS Microbiol Lett* **2017**, *364*:fnx146. doi:10.1093/femsle/fnx146.

Osborn M, Bruce KD, Strike P, Ritchie DA. Distribution, diversity and evolution of the bacterial mercury resistance (*mer*) operon. *FEMS Microbiol Rev* **1997**, *19*:239-262. doi:10.1111/j.1574-6976.1997.tb00300.x.

Özkara A, Akyil D, Konuk M. Pesticides, environmental pollution, and health. In: Environmental Health Risk - Hazardous Factors to Living Species*. InTech* **2016**, 3-29. doi:10.5772/61472.

Özkara A, Akyil D. Environmental Pollution and Pollutants on the Ecosystem: A Review. *Turk J Sci Rev* **2018**, *11*:11-17. doi:10.3389/fpubh.2020.00014.

P

Pacyna EG, Pacyna JM, Sundseth K, Munthe J, Kindbom K, Wilson, et al. Global emission of mercury to the atmosphere from anthropogenic sources in 2005 and projections to 2020. *Atmos Environ* **2010**, *40*:2487-2499. doi:10.1016/j.atmosenv.2009.06.009.

Páez-Espino AD, Durante-Rodriguez G, de Lorenzo V. Functional coexistence of twin arsenic resistance systems in *Pseudomonas putida* KT2440. *Environ Microbiol* **2015**, *17*:229-238. doi:10.1111/1462-2920.12464.

Páez-Espino AD, Nikel PI, Chavarría M, de Lorenzo V. ArsH protects *Pseudomonas putida* from oxidative damage caused by exposure to arsenic. *Environ Microbiol* **2020**, *22*:2230-2242. doi:10.1111/1462-2920.14991.

Palama TL, Canard I, Rautureau GJ, Mirande C, Chatellier S, Herrmann BE. Identification of bacterial species by untargeted NMR spectroscopy of the exo-metabolome. *Analyst* **2016**, *141*:4558e4561. doi:10.1039/C6AN00393A.

Panagos P, Van Liedekerke M, Yigini Y, Montanarella L. Contaminated sites in Europe: Review of the current situation based on data collected through a European network. *J Environ Public Health* **2013**, 158764, doi:10.1155/2013/158764.

Pan-Hou H, Kiyono M, Omura T, Endo G. Polyphosphate produced in recombinant *Escherichia coli* confers mercury resistance. *FEMS Microbiol Lett* **2002**, *207*:159-164. doi:10.1111/j.1574-6968.2002.tb11045.x.

Pappireddi N, Martin L, Wühr M. A Review on quantitative multiplexed proteomics. *Chembiochem* **2019**, *20*:1210-1224. doi:10.1002/cbic.201800650.

Park S, Ely RL. Whole-genome transcriptional and physiological responses of *Nitrosomonas europaea* to cyanide: Identification of cyanide stress response genes. *Biotechnol Bioeng* **2009**, *102*:1645-1653.

Park JD, Zheng W. Human exposure and health effects of inorganic and elemental mercury. *J Prev Med Public Health* **2012**, *45*:344-352. doi:10.3961%2Fjpmph.2012.45.6.344.

Park JM, Sewell BT, Benedik MJ. Cyanide bioremediation: The potential of engineered nitrilases. *Appl Microbiol Biotechnol* **2017**, *101*:3029-3042. doi:10.1007/s00253-017-8204-x.

Parmar P, Soni A, Desai P. Enzymatic study of cyanide utilizing *Pseudomonas* species isolated from contaminated soil. *J Sci Innov Res* **2013**, *2*:1058-1066.

Patel BH, Percivalle C, Ritson DJ, Duffy CD, Sutherland JD. Common origins of RNA, protein and lipid precursors in a cyanosulfidic protometabolism. *Nat Chem* **2015**, *7*:301-307. doi:10.1038/nchem.2202.

Pathak A, Jaswal R, Chauhan A. Genomic characterization of a mercury resistant *Arthrobacter* sp. H-02-3 reveals the presence of heavy metal and antibiotic resistance determinants. *Front Microbiol* **2020**, *10*:3039. doi:10.3389/fmicb.2019.03039.

Patil YB, Paknikar KM. Development of a process for biodetoxification of metal cyanides from wastewaters. *Process Biochem* **2000**, *35*:1139-1151. doi:10.1016/S0032-9592(00)00150-3.

Patterson S, Aebersold R. Proteomics: The first decade and beyond. *Nat Genet* **2003**, *33*:311-323. doi:10.1038/ng1106.

Peiser GD, Wang TT, Hoffman NE, Yang SF, Liu HW, Walsh CT. Formation of cyanide from carbon 1 of 1-aminocyclopropane-1-carboxylic acid during its conversion to ethylene. *Proc Natl Acad Sci USA* **1984**, *81*:3059-3063. doi:10.1073/pnas.81.10.3059.

Pepi M, Gaggi C, Bernardini E, Focardi S, Lobianco A, Ruta M, et al. Mercury-resistant bacterial strains *Pseudomonas* and *Psychrobacter* spp. isolated from sediments of Orbetello Lagoon (Italy) and their possible use in bioremediation processes. *Int Biodeterior Biodegr* **2011**, *65*:85-91, doi:10.1016/j.ibiod.2010.09.006.

Pérez MD, Olaya-Abril A, Cabello P, Sáez LP, Roldán MD, Moreno-Vivián C, et al. Alternative pathway for 3-cyanoalanine assimilation in *Pseudomonas pseudoalcaligenes* CECT5344 under noncyanotrophic conditions. *Microbiol Spectr* **2021**, *9*:e0077721. doi:10.1128/Spectrum.00777-21.

Pesce LD. Cyanides. In: Kirk-Othmer Encyclopedia of Chemical Technology, *John Wiley and Sons* **1993**.

Petrick JS, Ayala-Fierro F, Cullen WR, Carter DE, Vasken-Aposhian H. Monomethylarsonous acid (MMA(III)) is more toxic than arsenite in Chang human hepatocytes. *Toxicol Appl Pharmacol* **2000**, *16*:*3*203-7. doi:10.1006/taap.1999.8872.

Petrikovics I, Budai M, Kovacs K, Thompson DE. Past, present and future of cyanide antagonism research: From the early remedies to the current therapies. *World J Methodol* **2015**, *5*:88-100. doi:10.5662/wjm.v5.i2.88.

Pham TV, Murkin AS, Moynihan MM, Harrris L, Tyler PC, Shetty N, et al. Mechanism-based inactivator of isocitrate lyases 1 and 2 from *Mycobacterium tuberculosis*. *Proc Natl Acad Sci* **2017**, *114:*7617-7622. doi.org/10.1073/pnas.1706134114.

Pham TV, Mellott DM, Moghadamchargari Z, Chen K, Krieger I, Laganowsky A, et al. Covalent inactivation of *Mycobacterium tuberculosis* isocitrate lyase by *cis*-2,3-epoxy-succinic acid. *ACS Chem Biol* **2021**, *16*:463-470. doi:10.1021/acschembio.0c00740.

Pirrone N, Keating T. Hemispheric transport of air pollution 2010: Mercury. *United Nations Publication* **2010**.

Pope CA, Muhlestein JB, May HT, Renlund DG, Anderson JL, Horne BD. Ischemic heart disease events triggered by short-term exposure to fine particulate air pollution. *Circulation* **2006**, *114*:2443-2448. doi:10.1161/CIRCULATIONAHA.106.636977.

Pott WA, Benjamin SA, Yang RSH. Pharmacokinetics, metabolism and carcinogenicity of arsenic. *Reviews of Envir Cont Tox* **2001**, *169*:165-214. doi:10.1007/978-1-4613-0107-3_3.

Prieto MA, de Eugenio LI, Galan B, Luengo JM, Witholt B. Synthesis and degradation of polyhydroxyalkanoates. In: *Pseudomonas*: A Model System in Biology. *Springer* **2007**. doi:10.1007/978-1-4020-6097-7_14.

Priyadarshanee M, Chatterjee S, Rath S, Dash H, Das S. Cellular and genetic mechanism of bacterial mercury resistance and their role in biogeochemistry and bioremediation. *J Hazard Mat* **2022**, *423*:126985. doi:10.1016/j.jhazmat.2021.126985.

Q

Qian C, Chen H, Johs A, Lu X, An J, Pierce EM, et al. Quantitative proteomic analysis of biological processes and responses of the bacterium *Desulfovibrio desulfuricans* ND132 upon deletion of its mercury methylation genes. *Proteomics* **2018**, *18*:e1700479. doi:10.1002/pmic.201700479.

Qian Z, Wu C, Pan W, Xiong X, Xia L, Li W. Arsenic transformation in soil-rice system affected by iron-oxidizing strain (*Ochrobactrum* sp.) and related soil metabolomics analysis. *Front Microbiol* **2022**, *13*:794950. doi:10.3389/fmicb.2022.794950.

Quatrini R, Appia-Ayme C, Denis Y, Jedlicki E, Holmes DS, Bonnefoy V. Extending the models for iron and sulfur oxidation in the extreme acidophile *Acidithiobacillus ferrooxidans*. *BMC Genom* **2009**, *10*:394. doi:10.1186/1471-2164-10-394.

Quesada A, Guijo MI, Merchán F, Blázquez B, Igeño MI, Blasco R. Essential role of cytochrome *bd* related oxidase in cyanide resistance of *Pseudomonas pseudoalcaligenes* CECT5344. *Appl Environ Microbiol* **2007**, *73*:5118-5124. doi:10.1128/AEM.00503-07.

R

Rajagopalan S, Al-Kindi SG, Brook RD. Air pollution and cardiovascular disease JACC state-of-the-art review. *J Am Coll Cardiol* **2018**, *72*:2054-2070. doi:10.1016/j.jacc.2018.07.099.

Raju NJ. Arsenic in the geo-environment: A review of sources, geochemical processes, toxicity and removal technologies. *Environ Res* **2022**, *203*, 111782. doi:10.1016/j.envres.2021.111782.

Rand MD, Caito SW. Variation in the biological half-life of methylmercury in humans: Methods, measurements and meaning. *Biochim Biophys Acta Gen Subj* **2019**, *1863*:129301. doi:10.1016/j.bbagen.2019.02.003.

Raybuck SA. Microbes and microbial enzymes for cyanide degradation. *Biodegradation* **1992**, *3*:3-18. doi:10.1007/BF00189632.

Razanamahandry LC, Karoui H, Andrianisa HA, Yacouba H. Bioremediation of soil and water polluted by cyanide: A review. *Afr J Environ Sci Technol* **2017**, *11*:272-291. doi:10.5897/AJEST2016.2264.

Reddy KR, Yaghoubi P, Yukselen-Aksoy Y. Effects of biochar amendment on geotechnical properties of landfill cover soil. *Waste Manag Res* **2015**, *33*:524-532. doi:10.1177/0734242X15580192.

Rehm BHA, Steinbüchel A. Biochemical and genetic analysis of PHA synthases and other proteins required for PHA synthesis. *Int J Biol Macromol* **1999**, *25*:3-19. doi:10.1016/s0141-8130(99)00010-0.

Reis MP, Dias MF, Costa PS, Ávila MP, Leite LR, de Araújo FMG, et al. Metagenomic signatures of a tropical mining-impacted stream reveal complex microbial and metabolic networks. *Chemosphere* **2016**, *161*:266-273. doi:10.1016/j.chemosphere.2016.06.097.

Richard JH, Bischoff C, Ahrens CG, Biester H. Mercury (II) reduction and co-precipitation of metallic mercury on hydrous ferric oxide in contaminated groundwater. *Sci Total Environ* **2016**, *539*:36-44. doi:10.1016/j.scitotenv.2015.08.

Richardson DJ. Bacterial respiration: A flexible process for a changing environment. *Microbiology* **2000**, *146*:551-571. doi:10.1099/00221287-146-3-551.

Rijavec T, Lapanje A. Cyanogenic *Pseudomonas* spp. strains are concentrated in the rhizosphere of alpine pioneer plants, *Microbiol Res* **2017**, 194:20-28. doi:10.1016/j.micres.2016.09.001.

Rimondi V, Costagliola P, Lattanzi P, Catelani T, Fornasaro S, Medas D, et al. Bioaccessible arsenic in soil of thermal areas of Viterbo, Central Italy: Implications for human health risk. *Environ Geochem Health* **2022**, *44*:465-485. doi:10.1007/s10653-021-00914-1.

Ríos-Del Toro EE, Valenzuela EI, López-Lozano NE, Cortés-Martínez MG, Sánchez-Rodríguez MA, Calvario-Martínez O, et al. Anaerobic ammonium oxidation linked to sulfate and ferric iron reduction fuels nitrogen loss in marine sediments. *Biodegradation* **2018**, *29*:429-442. doi:10.1007/s10532-018-9839-8.

Ritson DJ, Battilocchio C, Ley SV, Sutherland JD. Mimicking the surface and prebiotic chemistry of early Earth using flow chemistry. *Nat Commun* **2018**, *9*:1-10. doi:10.1038/s41467-018-04147-2.

Roberts LC, Hug SJ, Dittmar J, Voegelin A, Kretzschmar R, Wehrli B, et al. Arsenic release from paddy soils during monsoon flooding. *Nat Geosci* **2010**, *3*:53-59. doi:10.1038/ngeo723.

Robson RL, Jones R, Robson RM, Schwartz A, Richardson TH. *Azotobacter* genomes: The genome of *Azotobacter chroococcum* NCIMB 8003 (ATCC 4412). *PLoS One* **2015**, *10*:0127997. doi:10.1371/journal.pone.0127997.

Rodríguez C, Cisternas J, Serrano J, Leiva E. Nitrogen removal by an anaerobic iron-dependent ammonium oxidation (Feammox) enrichment: Potential for wastewater treatment. *Water* **2021**, *13*:3462. doi:10.3390/w13233462.

Rodríguez-Campos J, Dendooven L, Álvarez-Bernal D, Contreras-Ramos SM. Potential of earthworms to accelerate removal of organic contaminants from soil: A review. *Appl Soil Ecol* **2014**, *79*:10-25. doi:10.1016/j.apsoil.2014.02.010.

Rojas LA, Yañez C, González M, Lobos S, Smalla K, Seeger M. Characterization of the metabolically modified heavy metal-resistant *Cupriavidus metallidurans* strain MSR33 generated for mercury bioremediation. *PLoS One* **2011**, *6*:e17555. doi:10.1371/journal.pone.0017555.

Roldán MD, Olaya-Abril A, Sáez LP, Cabello P, Luque-Almagro VM, Moreno-Vivián C. Bioremediation of cyanide containing wastes: The potential of systems and synthetic biology for cleaning up the toxic leftovers from mining. *EMBO Rep* **2021**, *22*:e53720. doi:10.15252/embr.202153720.

Roos D, Seeger R, Puntel R, Vargas Barbosa N. Role of calcium and mitochondria in MeHg-mediated cytotoxicity. *J Biomed Biotechnol* **2012**, *2012*:248764. doi:10.1155/2012/248764.

Rorat A, Courtois P, Vandenbulcke F, Lemiere S. Sanitary and environmental aspects of sewage sludge management. In: Industrial and Municipal Sludge. *Elsevier* **2019**. doi:10.1016/B978-0-128159071.00008-8.

Rosen BP. Biochemistry of arsenic detoxification. *FEBS Lett* **2002**, *529*:86-92. doi:10.1016/s0014-5793(02)03186-1.

Rosen BP, Liu Z. Transport pathways for arsenic and selenium: A minireview. *Environ Int* **2009**, *35*:512-515. doi:10.1016/j.envint.2008.07.023.

Rosenberger G, Bludau I, Schmitt U, Heusel M, Hunter CL, Liu Y, et al. Statistical control of peptide and protein error rates in large-scale targeted data-independent acquisition analyses. *Nat Methods* **2017**, *14*:921-927. doi:10.1038/nmeth.4398.

Rosenstein R, Peschel A, Wieland B, Gotz F. Expression and regulation of the antimonite, arsenite, and arsenate resistance operon of *Staphylococcus xylosus* plasmid pSX267. *J Bacteriol* **1992**, *174*:3676-3683. doi:10.1128/jb.174.11.3676-3683.1992.

Rosenthaler L. Beitrage zur Blausaurefrage. Die Verbreitung der Blausaure im Pflanzenreich. *Schweizer Apothekerzeitung* **1919**, *57*:279-283, 295-297, 307-313, 324-329, 341-346.

Rudrappa T, Splaine R, Biedrzycki M, Bais H. Cyanogenic pseudomonads influence multitrophic interactions in the rhizosphere. *PLoS One* **2008**, *3*:e2073. doi:10.1371/journal.pone.0002073.

Ruelas-Inzunza J, Delgado-Álvarez C, Frías-Espericueta M, Páez-Osuna, F. Mercury in the atmospheric and coastal environments of Mexico. *Rev Environ Contam Toxicol* **2013**, *226*:65-99. doi:10.1007/978-1-4614-6898-1_3.

Ruiz ON, Álvarez D, González-Ruiz G, Torres C. Characterization of mercury bioremediation by transgenic bacteria expressing metallothionein and polyphosphate kinase. *BMC Biotechnol* **2011**, *11*:82. doi:10.1186/1472-6750-11-82

Ryall B, Lee X, Zlosnik JEA, Hoshino S, Williams HD. Bacteria of the *Burkholderia cepacia* complex are cyanogenic under biofilm and colonial growth conditions. *BMC Microbiol* **2008**, *8*:108-117. doi:10.1186/1471-2180-8-108.

S

Saal T, Christe KO, Haiges R. Lewis adduct formation of hydrogen cyanide and nitriles with arsenic and antimony pentafluoride. *Dalton Trans* **2018**, *48*:99-106. doi:10.1039/C8DT03970D

Sáez LP, Cabello P, Ibáñez MI, Luque-Almagro VM, Roldán MD, Moreno-Vivián C. Cyanate assimilation by the alkaliphilic cyanide-degrading bacterium *Pseudomonas pseudoalcaligenes* CECT5344: Mutational analysis of the *cyn* gene cluster. *Int J Mol Sci* **2019**, *20*:3008. doi:10.3390/ijms20123008.

Sager PR, Matheson DW. Mechanisms of neurotoxicity related to selective disruption of microtubules and intermediate filaments. *Toxicology* **1988**, *49*:479-492. doi:10.1016/0300-483x(88)90034-0.

Saito N, Robert M, Kitamura S, Baran R, Soga T, Mori H, et al. Metabolomics approach for enzyme discovery. *J Proteome Res* **2006**, *5*:1979-87. doi:10.1021/pr0600576

Saleem H, Ul Ain Kokab Q, Rehman Y. Arsenic respiration and detoxification by purple non-sulphur bacteria under anaerobic conditions. *C R Biol* **2019**, *342*:101-107. doi:10.1016/j.crvi.2019.02.001.

Sambrook J, Russel DW. Molecular Cloning: A Laboratory Manual. *Cold Spring Harbor Press* **2001.**

Santos MA. Managing planet earth: Perspectives on population, ecology, and the law. *Bergin and Garvey, Westport Connecticut*, Newyork. **1990**, 44.

Saranya K, Sundaramanickam A, Shekhar S, Swaminathan S, Balasubramanian T. Bioremediation of mercury by *Vibrio fluvialis* screened from industrial effluents. *BioMed Res Int* **2017**, *2017*:6. doi:10.1155/2017/6509648.

Sarkar A, Shekhar S. Iron contamination in the waters of upper Yamuna basin. *Groundw Sustain Dev* **2018**, *7*:421-429. doi:10.1016/j.gsd.2017.12.011.

Sarkar A, Kazy SK, Sar P. Characterization of arsenic resistant bacteria from arsenic rich groundwater of West Bengal, India. *Ecotoxicology* **2013**, *22*:363-376. doi:10.1007/s10646-012-1031-z.

Sasaki Y, Oguchi H, Kobayashi T, Kusama S, Sugiura R, Mariya K, et al. Nitrogen oxide cycle regulates nitric oxide levels and bacterial cell signaling. *Sci Rep* **2016***, 6*:22038. doi:10.1038/srep22038.

Schelert J, Dixit V, Hoang V, Simbahan J, Drozda M, Blum P. Occurrence and characterization of mercury resistance in the hyperthermophilic archaeon *Sulfolobus solfataricus* by use of gene disruption. *J Bacteriol* **2004**, *186*:427-37. doi:10.1128/JB.186.2.427-437.2004.

Scheller S, Yu H, Chadwick GL, McGlynn SE, Orphan VJ. Artificial electron acceptors decouple archaeal methane oxidation from sulfate reduction. *Science* **2016***, 351*:703-707. doi:10.1126/science.aad7154.

Schlichtemeier SM, Nahm CB, Xue A, Gill AJ, Smith RC, Hugh TJ. SELDI-TOF MS analysis of hepatocellular carcinoma in an Australian cohort. *J Surg Res* **2019**, *238*:127-36. doi:10.1016/j.jss.2019.01.008

Schlotterbeck G, Ross A, Dieterle F, Senn H. Metabolic profiling technologies for biomarker discovery in biomedicine and drug development. *Pharmacogenomics* **2006**, *7*:1055-75. doi:10.2217/14622416.7.7.1055.

Schmitz S, Nies S, Wierckx N, Blank LM, Rosenbaum MA. Engineering mediator-based electroactivity in the obligate aerobic bacterium *Pseudomonas putida* KT2440. *Front Microbiol* **2015**, *6*:284 doi:10.3389/fmicb.2015.00284.

Schubert C, Unden G. Fumarate, a central electron acceptor for *Enterobacteriaceae* beyond fumarate respiration and energy conservation. *Adv Microb Physiol* **2023**, *82*:267-299. doi:10.1016/bs.ampbs.2022.10.002.

Schue M, Glendinning KJ, Hobman JL, Brown NL. Evidence for direct interactions between the mercuric ion transporter (MerT) and mercuric reductase (MerA) from the Tn501 *mer* operon. *Biometals* **2007**, *21*:107-116. doi:10.1007/s10534-007-9097-4.

Schue M, Dover LG, Besra GS, Parkhill J, Brown NL. Sequence and analysis of a plasmid-encoded mercury resistance operon from *Mycobacterium marinum* identifies MerH, a new mercuric ion transporter. *J Bacteriol* **2009**, *191*:439-444. doi:10.1128/JB.01063-08.

Seccatore J, Veiga M, Origliasso C, Marin T, De Tomi G. An estimation of the artisanal small-scale production of gold in the world. *Sci Total Environ* **2014**, *496*:662-667. doi:10.1016/j.scitotenv.2014.05.003.

Seo S, Mitsuhara I, Feng J, Iwai T, Hasegawa M, Ohashi Y. Cyanide, a coproduct of plant hormone ethylene biosynthesis, contributes to the resistance of rice to blast fungus. *Plant Physiol* **2011**, *155*:502-514. doi:10.1104/pp.110.162412.

Seo SW, Kim D, Latif H, O'Brien EJ, Szubin R, Palsson BO. Deciphering Fur transcriptional regulatory network highlights its complex role beyond iron metabolism in *Escherichia coli*. *Nat Commun* **2014**, *5*:4910. doi:10.1038/ncomms5910.

Seshadri B, Bolan NS, Choppala G, Kunhikrishnan A, Sanderson P, Wang H, et al. Potential value of phosphate compounds in enhancing immobilization and reducing bioavailability of mixed heavy metal contaminants in shooting range soil. *Chemosphere* **2017**, *184*:197-206. doi:10.1016/j.chemosphere.2017.05.172.

Shang L, Jiang M, Chang HN. Poly(3-hydroxybutyrate) synthesis in fed-batch culture of *Ralstonia eutropha* with phosphate limitation under different glucose concentrations. *Biotechnol Lett* **2003**, *25*:1415-1419. doi:10.1023/a:1025047410699.

Sher S, Rehman A. Use of heavy metals resistant bacteria-a strategy for arsenic bioremediation. *Appl Microbiol Biotechnol* **2019**, *103*:6007-6021. doi:10.1007/s00253-019-09933-6.

Sher S, Rehman A, Hansen LH, Nielsen TK. Complete genome sequences of highly arsenite-resistant bacteria *Brevibacterium* sp. strain CS2 and *Micrococcus luteus* AS2. *Microbiol Resour Announc* **2019**, *8*:e00531-19. doi:10.1128/MRA.00531-19.

Sher S, Rehman A. Proteomics and transcriptomic analysis of *Micrococcus luteus* strain AS2 under arsenite stress and its potential role in arsenic removal. *Curr Res Microb Sci* **2021**, *2*:100020. doi:10.1016/j.crmicr.2021.100020.

Shi X, Ng KK, Fu C, Low SL, Ng HY. Removal of toxic component of wastewater by anaerobic processes. In: Current Developments in Biotechnology and Bioengineering. Biological Treatment of Industrial Effluents**.** *Elsevier* **2017**, *17*:443-467. doi:10.1016/B978-0-444-63665-2.00017-5.

Shi K, Li C, Rensing C, Dai X, Fan X, Wang G. Efflux transporter ArsK is responsible for bacterial resistance to arsenite, antimonite, trivalent roxarsone, and methylarsenite. *Appl Environ Microbiol* **2018**, *84*:e01842-18. doi.org/10.1128/AEM.01842-18.

Shukla SK, Rao TS. An improved crystal violet assay for biofilm quantification in 96-Well microtitre plate. *bioRxiv* **2017**, doi.org/10.1101/100214.

Singh OV. Proteomics and metabolomics: The molecular make-up of toxic aromatic pollutant bioremediation. *Proteomics* **2006**, *6***:**5481-5492. doi:10.1089/omi.2007.0005.

Singh R, Gautam N, Mishra A, Gupta R. Heavy metals and living systems: An overview. *Indian J Pharmacol* **2011**, *43*:246-53. doi:10.4103/0253-7613.81505.

Singh U, Arora NK, Sachan P. Simultaneous biodegradation of phenol and cyanide present in coke-oven effluent using immobilized *Pseudomonas putida* and *Pseudomonas stutzeri*. *Braz J Microbiol* **2018** *49*:38-44. doi:10.1016/j.bjm.2016.12.013.

Singh VK, Singh AL, Singh R, Kumar A. Iron oxidizing bacteria: Insights on diversity, mechanism of iron oxidation and role in management of metal pollution. *Environ Sustain* **2018**, *1*:221-231. doi:10.1007/s42398-018-0024-0.

Slyemi D, Bonnefoy V. How prokaryotes deal with arsenic. *Environ Microbiol Rep* **2012**, *4*:571-586. doi:10.1111/j.1758-2229.2011.00300.x.

Smedley PL, Kinniburgh DG. A review of the source, behavior and distribution of arsenic in natural waters. *Appl Geochem* **2002**, *17*:517-568. doi.org/10.1016/S0883-2927(02)00018-5.

Smith T, Pitts K, McGarvey JA, Summers AO. Bacterial oxidation of mercury metal vapor, Hg(0). *Appl Environ Microbiol* **1998**, *64*:1328-32. doi:10.1128/AEM.64.4.1328-1332.1998.

Smith AH, Lingas EO, Rahman M. Contamination of drinking-water by arsenic in Bangladesh: A public health emergency. *Bull World Health Organ* **2000**, *78*:1093-1103.

Smits THM, Pothier JF, Ruinelli M, Blom J, Frasson D, Koechli C, et al. Complete genome sequence of the cyanogenic phosphate-solubilizing *Pseudomonas* sp. strain CCOS 191, a close relative of *Pseudomonas mosselii*. *Genome Announc* **2015**, *3*:e00616-15. doi:10.1128/genomeA.00616-15.

Sohn E. Contamination: The toxic side of rice. *Nature* **2014**, *514*:S62-S63. doi:10.1038/514S62a

Sohn SB, Kim TY, Park JM, Lee SY. In silico genome-scale metabolic analysis of *Pseudomonas putida* KT2440 for polyhydroxyalkanoates synthesis, degradation of aromatics and anaerobic survival. *Biotechnol J* **2010**, *5*:739-50. doi:10.1002/biot.201000124.

Sone Y, Mochizuki Y, Koizawa K, Nakamura R, Pan-Hou H, Itoh T, et al. Mercurial-resistance determinants in *Pseudomonas* strain K-62 plasmid pMR68. *AMB Express* **2013a**, *28*:3-41. doi:10.1186/2191-0855-3-41.

Sone Y, Nakamura R, Pan-Hou H, Itoh T, Kiyono M. Role of MerC, MerE, MerF, MerT, and/or MerP in resistance to mercurials and the transport of mercurials in *Escherichia coli*. *Biol Pharm Bull* **2013b**, *36*:1835-41. doi:10.1248/bpb.b13-00554.

Song B, Chyun E, Jaffé PR, Ward BB. Molecular methods to detect and monitor dissimilatory arsenate-respiring bacteria (DARB) in sediments. *FEMS Microbiol Ecol* **2009**, *68*:108-117. doi:10.1111/j.1574-6941.2009.00657.

Song B, Zeng G, Gong J, Liang J, Xu P, Liu Z, et al. Evaluation methods for assessing effectiveness of in situ remediation of soil and sediment contaminated with organic pollutants and heavy metals. *Environ Int* **2017**, *105*:43-55. doi:10.1016/j.envint.2017.05.001.

Sonthiphand P, Ruangroengkulrith S, Mhuantong W, Charoensawan V, Chotpantarat S, Boonkaewwan S. Metagenomic insights into microbial diversity in a groundwater basin impacted by a variety of anthropogenic activities. *Environ Sci Pollut Res Int* **2019**, *26*:26765-26781. doi:10.1007/s11356-019-05905-5.

Soto J, Charles TC, Lynch MDJ, Larama G, Herrera H, Arriagada C. Genome sequence of *Brevundimonas* sp., an arsenic resistant soil bacterium. *Diversity* **2021**, *13*:344. doi:10.3390/d13080344.

Spiekermann P, Rehm BH, Kalscheuer R, Baumeister D, Steinbüchel A. A sensitive, viable-colony staining method using Nile red for direct screening of bacteria that accumulate polyhydroxyalkanoic acids and other lipid storage compounds. *Arch Microbiol* **1999**, *171*:73-80. doi:10.1007/s002030050681.

Spinelli JB, Rosen PC, Sprenger HG, Puszynska AM, Mann JL, Roessler JM, et al. Fumarate is a terminal electron acceptor in the mammalian electron transport chain. *Science* **2021**, *374*:1227-1237. doi:10.1126/science.abi7495.

Steen A, Utkur FO, Borrero-de-Acuńa JM, Bunk B, Roselius L, Bühler B, et al. Construction and characterization of nitrate and nitrite respiring *Pseudomonas putida* KT2440 strains for anoxic biotechnical applications. *J Biotechnol* **2013**, *163*:155-65. doi:10.1016/j.jbiot ec.2012.09.015.

Štefanac T, Grgas D, Dragicević LT. Xenobiotics-division and methods of detection: A review. *J Xenobiot* **2021**, *11*:130-141. doi:10.3390/jox11040009.

Steinbüchel A, Aerts K, Babel W, Follner C, Liebergesell M, Madkour MH, et al. Considerations on the structure and biochemistry of bacterial polyhydroxyalkanoic acid inclusions. *Can J Microbiol* **1995**, *41*:94-105. doi:10.1139/m95-175.

Stojiljkovic I, Baumler AJ, Hantke K. Fur regulon in gram-negative bacteria. Identification and characterization of new iron-regulated *Escherichia coli* genes by a *fur* titration assay. *J Mol Biol* **1994**, *236*:531-545. doi:10.1006/jmbi.1994.1163.

Stokes JM, Lopatkin AJ, Lobritz MA, Collins JJ. Bacterial metabolism and antibiotic efficacy. *Cell Metabol* **2019**, *30*:251e259. doi:10.1016/j.cmet.2019.06.009.

Suhadi S, Sueb S, Syamsussabri M. Mercury and cyanide pollution on the aquatic organism in Sekotong people gold mining. *J Phys Conf Ser* **2019**, *1417*:012032. doi:10.1088/1742-6596/1417/1/012032.

Sullivan C, Tyrer M, Cheeseman CR, Graham NJD. Disposal of water treatment wastes containing arsenic- A review. *Sci Total Environ* **2010**, *408*:1770-1778. doi:10.1016/j.scitotenv.2010.01.010.

Summers AO, Silver S. Mercury resistance in a plasmid-bearing strain of *Escherichia coli*. *J Bacteriol* **1972**, *112*:1228-36. doi:10.1128/jb.112.3.1228-1236.1972.

Sun R, Guangqian L, Wu H, Li X, Tian H, Yao H. Insight into mercury-laden activated carbon adsorbent product bonding nature by DFT calculations. *Chem Eng J* **2022**, *433*:134461. doi:10.1016/j.cej.2021.134461.

Suzuki K, Wakao N, Kimura T, Sakka K, Ohmiya K. Expression and regulation of the arsenic resistance operon of *Acidiphilium multivorum* AIU 301 plasmid pKW301 in *Escherichia coli*. *Appl Environ Microbiol* **1998**, *64*:411-418. doi:10.1128/AEM.64.2.411-418.1998.

T

Tajudin SAA, Azmi MAM, Nabila ATA. Stabilization/solidification remediation method for contaminated soil: A review. *IOP Conf Ser Mater Sci Eng* **2016**, *136*:012043. doi:10.1088/1757-899X/136/1/012043.

Tang P, Hseu YC, Chou HH, Huang KY, Chen SC. Proteomic analysis of the effect of cyanide on *Klebsiella oxytoca*. *Curr Microbiol* **2010**, *60*:224-228. doi:10.1007/s00284-009-9529-1.

Tchounwou PB, Yedjou CG, Patlolla AK, Sutton DJ, Heavy metal toxicity and the environment. *Exp Suppl* **2012**, *101*:133-164. doi:10.1007/978-3-7643-8340-4_6.

Thomé A, Reddy KR, Reginatto C, Cecchin I. Review of nanotechnology for soil and groundwater remediation: Brazilian perspectives. *Water Air Soil Pollut* **2015**, *226*:1-20. doi:10.1007/s11270-014-2243-z.

Thompson A, Schäfer J, Kuhn K, Kienle S, Schwarz J, Schmidt G, et al. Tandem mass tags: A novel quantification strategy for comparative analysis of complex protein mixtures by MS/MS. *Anal Chem* **2003**, *75*:1895-904. doi:10.1021/ac0262560.

Tokmina-Lukaszewska M, Shi Z, Tripet B, McDermott TR, Copié V, Bothner B, et al. Metabolic response of *Agrobacterium tumefaciens* 5A to arsenite. *Environ Microbiol* **2017**, *19*:710-721. doi:10.1111/1462-2920.13615.

Tomasiak TM, Cecchini G, Iverson TM. Succinate as donor; fumarate as acceptor. *EcoSal Plus* **2007**, *2*. doi:10.1128/ecosal.3.2.6.

Tomaszewski JE, Smithenry DW, Cho YM, Luthy RG, Lowry GV, Reible D, et al. Treatment and Containment of Contaminated Sediments. *Springer* **2006**.

Toner JD, Catling DC. Alkaline lake settings for concentrated prebiotic cyanide and the origin of life. *Geochim Cosmochim Acta* **2019**, *260*:124-132. doi:10.1016/j.gca.2019.06.031.

Tong M, Yuan SH, Ma SC, Jin MG, Liu D, Cheng D, et al. Production of abundant hydroxyl radicals from oxygenation of subsurface sediments. *Environ Sci Technol* **2016**, *50*:214-221. doi:10.1021/acs.est.5b04323.

Touati D. Iron and oxidative stress in bacteria. *Arch Biochem Biophys* **2000**, *373*:1-6. doi:10.1006/abbi.1999.1518.

Tripti K, Sayantan D, Shardendu S, Singh DN, Tripathi AK. Potential for the uptake and removal of arsenic [As(V) andAs(III)] and the reduction of As(V) to As(III) by *Bacillus licheniformis* (DAS1) under different stresses. *Korean J Microbiol Biotechnol* **2014**, *42*:238-248. doi:10.4014/kjmb.1401.01004.

Trunk K, Benkert, Quack N, Munch R, Scheer M, Garbe J, et al. Anaerobic adaptation in *Pseudomonas aeruginosa*: Definition of the Anr and Dnr regulons. *Environ Microbiol* **2010**, *12*:1719-33. doi:10.1111/j.1462-2920.2010.02252.x.

Tsai SL, Singh S, Chen W. Arsenic metabolism by microbes in nature and the impact on arsenic remediation. *Curr Opin Biotechnol* **2009**, *20*:659-667. doi:10.1016/j.copbio.2009.09.013.

Tu P, Tang Q, Mo Z, Niu H, Hu Y, Wu L, et al. Dietary administration of black raspberries and arsenic exposure: Changes in the gut microbiota and its functional metabolites. *Metabolites* **2023**, *13*:207. doi:10.3390/metabo13020207.

Tuffin IM, de Groot P, Deane SM, Rawlings DE. An unusual Tn21-like transposon containing an *ars* operon is present in highly arsenic-resistant strains of the biomining bacterium *Acidithiobacillus caldus*. *Microbiology* **2005**, *151*:3027-3039. doi:10.1099/mic.0.28131-0.

Tulasi D, Fajon V, Joze K, Shlyapnikov Y, Adotey D, Serfor-Armah Y, et al. Mercury methylation in cyanide influenced river sediments: A comparative study in Southwestern Ghana. *Environ Monit Assess* **2021**, *193*:180, doi:10.1007/s10661-021-08920-7.

U

USEPA, US Environmental Protection Agency. Drinking water criteria document for cyanide. Environment Criteria and Assessment Office, Cincinnati. **1985**. EPA/600/X-84-192-1.

V

Valko M, Morris H, Cronin MT. Metals, toxicity and oxidative stress. *Curr Med Chem* **2005**, *12*:1161-208. doi:10.2174/0929867053764635.

Van Hellemond JJ, Tielens AG. Expression and functional properties of fumarate reductase. *Biochem J* **1994**, *304*:321-31. doi:10.1042/bj3040321

Vandekerckhove J, Bauw G, Puype M, Van Damme J, Van Montagu M. Protein-blotting on polybrene-coated glass-fiber sheets. *Eur J Biochem* **1985**, *152*:9-19. doi:10.1111/j.1432-1033.1985.tb09157.x.

Vázquez V, Parga J, Valenzuela J, Figueroa G, Valenzuela A, Munive G. Recovery of silver from cyanide solutions using electrochemical process Like alternative for Merrill-Crowe process. *Mater Sci Appl* **2014**, *5*:863-870. doi:10.4236/msa.2014.512087.

Venne AS, Kollipara L, Zahedi RP. The next level of complexity: Crosstalk of posttranslational modifications. *Proteomics* **2014**, *14*:513-524. doi:10.1002/pmic.201300344.

Verlinden RA, Hill DJ, Kenward MA, Williams CD, Radecka I. Bacterial synthesis of biodegradable polyhydroxyalkanoates. *J Appl Microbiol* **2007**, *102*:1437-49. doi:10.1111/j.1365-2672.2007.03335.x.

Villas-Bôas SG, Noel S, Lane GA, Attwood G, Cookson A. Extracellular metabolomics: A metabolic footprinting approach to assess fiber degradation in complex media. *Anal Biochem* **2006**, *349*:297-305. doi:10.1016/j.ab.2005.11.019.

Vilo CA, Benedik MJ, Kunz DA, Dong Q. Draft genome sequence of the cyanide-utilizing bacterium *Pseudomonas fluorescens* strain NCIMB 11764. *J Bacteriol* **2012**, *194*:6618-6619. doi:10.1128/JB.01670-12.

Vogel TM, Criddle CS, McCarty PL. Transformations of halogenated aliphatic compounds. *Environ Sci Technol* **1987**, *21*:722e736. doi:10.1021/es00162a001.

Von Burg R. Inorganic mercury. *J Appl Toxicol* **1995**, *15*:483-493. doi:10.1002/jat.2550140315.

Vuori KM. Direct and indirect effects of iron on river ecosystems. *Ann Zool Fenn* **1995**, *32*:317-329.

W

Walewska A, Szewczyk A, Koprowski P. External hemin as an inhibitor of mitochondrial large-conductance calcium-activated potassium channel activity. *Int J Mol Sci* **2022** *23*:13391. doi:10.3390/ijms232113391.

Wang LK. Heavy Metals in the Environment. *CRC Press* **2009**. doi:10.1201/9781420073195.

Wang L, Chen S, Xiao X, Huang X, You D, Zhou X, et al. *arsRBOCT* arsenic resistance system encoded by linear plasmid pHZ227 in *Streptomyces* sp. strain FR-008. *Appl Environ Microbiol* **2006**, *72*:3738-3742. doi.org/10.1128/AEM.72.5.3738-3742.2006.

Wang Z, Liu L, Guo F, Zhang T. Deciphering cyanide-degrading potential of bacterial community associated with the coking wastewater treatment plant with a novel draft genome. *Microbiol Ecol* **2015**, *70*:701-709. doi:10.1007/s00248-015-0611-x.

Wang C, Deng H, Wang D, Wang J, Huang H, Qiu J, et al. Changes in metabolomics and lipidomics in brain tissue and their correlations with the gut microbiome after chronic food-derived arsenic exposure in mice. *Ecotoxicol Environ Saf* **2021**, *228*:112935. doi:10.1016/j.ecoenv.2021.112935.

Wang W, Ding B, Hu Y, Zhang H, He Y, She Y, et al. Evidence for the occurrence of Feammox coupled with nitrate-dependent Fe(II) oxidation in natural enrichment cultures. *Chemosphere* **2022**, *303*:134903. doi:10.1016/j.chemosphere.2022.134903

Weelink SAB, van Eekert MHA, Stams AJM. Degradation of BTEX by anaerobic bacteria: Physiology and application. *Rev Environ Sci Bio/Technol* **2010**, *9*:359-385. doi:10.1007/s11157-010-9219-2

Wen B, Zhen WF, Liao Y, Shi Z, Savage SR, Jiang W, et al. Deep learning in proteomics. *Proteomics* **2020**, *21-22*:e1900335. doi:10.1002/pmic.201900335.

WHO. WHO Guidelines for Drinking Water Quality, Recommendation; WHO: Geneva, Switzerland, **1993**, 1-11.

WHO, **2003**. Iron in Drinking-Water. WHO/SDE/WSH/03.04/08.

WHO. WHO Guidelines for Drinking-Water Quality, 4th ed. Incorporating the 1st Addendum; WHO Press: Geneva, Switzerland, **2014** Regulations, S.I. No. 122/2014.

Wibberg D, Luque-Almagro VM, Igeño MI, Bremges A, Roldán MD, Merchán F et al. Complete genome sequence of the cyanide-degrading bacterium *Pseudomonas pseudoalcaligenes* CECT5344. *J Biotechnol* **2014**, *175*:67-68. doi:10.1016/j.jbiotec.2014.02.004.

Wibberg D, Bremges A, Dammann-Kalinowski T, Maus I, Igeño MI, Vogelsang R, et al. Finished genome sequence and methylome of the cyanide-degrading *Pseudomonas pseudoalcaligenes* strain CECT5344 as resolved by single-molecule real-time sequencing. *J Biotechnol* **2016**, *232*:61-68. doi:10.1016/j.jbiotec.2016.04.008.

Wiese S, Reidegeld KA, Meyer HE, Warscheid B. Protein labeling by iTRAQ: A new tool for quantitative mass spectrometry in proteome research. *Proteomics* **2007**, *7*:340-350. doi:10.1002/pmic.200600422.

Wild SR, Rudd T, Neller A. Fate and effects of cyanide during wastewater treatment processes. *Sci Total Environ* **1994**, *156*:93-107. doi:10.1016/0048-9697(94)90346-8.

Wilkins JM, Trushina E. Application of metabolomics in Alzheimer's disease. *Front Neurol* **2018**, *8*:719. doi:10.3389/fneur.2017.00719.

Wilkins MR, Sanchez JC, Gooley AA, Appel RD, Humphery-Smith I, Hochstrasser DF, et al. Progress with proteome projects: Why all proteins expressed by a genome should be identified and how to do it. *Biotechnol Genet Eng Rev* **1995**, *13*:19-50. doi:10.1080/02648725.1996.10647923.

Wilson JR, Leang C, Morby AP, Hobman JL, Brown NL. MerF is a mercury transport protein: Different structures but a common mechanism for mercuric ion transporters? *FEBS Lett* **2000**, *472*:78-82. doi:10.1016/S0014-5793(00)01430-7.

Wireman J, Liebert CA, Smith T, Summers AO. Association of mercury resistance with antibiotic resistance in the gram-negative fecal bacteria of primates. *Appl Environ Microbiol* **1997**, *63*:4494-503. doi:10.1128/aem.63.11.4494-4503.1997.

Won TH, Bok JW, Nadig N, Venkatesh N, Nickles G, Greco C, et al. Copper starvation induces antimicrobial isocyanide integrated into two distinct biosynthetic pathways in fungi. *Nat Commun* **2022**, *13*:4828. doi:10.1038/s41467-022-32394-x.

Woundefiraw B. Review on environmental pollution and roles of institution: The missing link. *Arch of Earth and Env Sci* **2021**, *1*:1-09.

Wu M, Guina T, Brittnacher M, Nguyen H, Eng J, Miller SI. The *Pseudomonas aeruginosa* proteome during anaerobic growth. *J Bacteriol* **2005**, *187*:8185-90. doi:10.1128/JB.187.23.8185-8190.2005.

Wu X, Cobbina SJ, Mao G, Xu H, Zhang Z, Yang L. A review of toxicity and mechanisms of individual and mixtures of heavy metals in the environment. *Environ Sci Pollut Res Int* **2016a**, *23*:8244-8259. doi:10.1007/s11356-016-6333-x.

Wu CY, Mouri H, Chen SS, Zhang DZ, Koga M, Kobayashi J. Removal of trace-amount mercury from wastewater by forward osmosis. *J Water Process Eng* **2016b**, *14*:108–116. doi:10.1016/j.jwpe.2016.10.010.

Wu Y, Xiang L, Wang H, Li M, Qiu X, Liu D, et al. Transcriptome analysis of an arsenite-/antimonite-oxidizer, *Bosea* sp. AS-1 reveals the importance of the type 4 secretion system in antimony resistance. *Sci Total Environ* **2022**, *826*:154168. doi:10.1016/j.scitotenv.2022.154168.

X

Xie T, Reddym KR, Wang C, Erin Y, Kurt P. Characteristics and applications of biochar for environmental remediation: A review. *Crit Rev Environ Sci Technol* **2014**, *45*:939-969. doi:10.1080/10643389.2014.924180.

Xie WJ, Yuan SH, Tong M, Ma SC, Liao WJ, Zhang N, et al. Contaminant degradation by •OH during sediment oxygenation: Dependence on Fe(II) species. *Environ Sci Technol* **2020**, *54*:2975-2984. doi:10.1021/acs.est.9b04870.

Xue Y, Qiu T, Sun Z, Liu F, Yu B. Mercury bioremediation by engineered *Pseudomonas putida* KT2440 with adaptationally optimized biosecurity circuit. *Environ Microbiol* **2022**, *24*:3022-3036. doi:10.1111/1462-2920.16038.

Y

Yamauchi H, Fowler BA. Toxicity and metabolism of inorganic and methylated arsenicals. Arsenic in the Environment. Part II. Human Health and Ecosystem Effects. Wiley, New York, **1994,** 35-54.

Yan L, Yin H, Zhang S, Leng F, Nan W, Li H. Biosorption of inorganic and organic arsenic from aqueous solution by *Acidithiobacillus ferrooxidans* BY-3. *J Hazard Mater* **2010**, *178*:209-217. doi.org/10.1016/j.jhazm at.2010.01.065.

Yan G, Chen X, Du S, Deng Z, Wang L, Chen S. Genetic mechanisms of arsenic detoxification and metabolism in bacteria. *Curr Genet* **2019**, *65*:329-338. doi:10.1007/s00294-018-0894-9.

Yang HC, Cheng J, Finan TM, Rosen BP, Bhattacharjee H. Novel pathway for arsenic detoxification in the legume symbiont. *Sinorhizobium meliloti*. *J Bacteriol* **2005**, *187*:6991-6997. doi:10.1128/JB.187.20.6991-6997.2005.

Yang HC, Fu HL, Lin YF, Rosen BP. Pathways of arsenic uptake and efflux. *Curr Top Membr* **2012a**, *69*:325-358. doi:10.1016/B978-0-12-394390-3.00012-4.

Yang WH, Weber KA, Silver WL. Nitrogen loss from soil through anaerobic ammonium oxidation coupled to iron reduction. *Nat Geosci* **2012b**, *5*:538-541. doi:10.1038/NGEO1530.

Yang HC, Rosen BP. New mechanisms of bacterial arsenic resistance. *Biomed J* **2016**, *39*:5-13. doi:10.1016/j.bj.2015.08.003.

Yang Y, Zhang Y, Li Y, Zhao H, Peng H. Nitrogen removal during anaerobic digestion of wasted activated sludge under supplementing Fe(III) compounds. *Cheml Eng J* **2018**, *332*:711-716, doi:10.1016/j.cej.2017.09.133.

Yang Q, Zhang A, Miao J, Sun H, Han Y, Yan G, et al. Metabolomics biotechnology, applications, and future trends: A systematic review. *R Soc Chem Adv* **2019**, *9*:37245. doi:10.1039/C9RA06697G.

Ye D, Li X, Shen J, Xia X. Microbial metabolomics: From novel technologies to diversified applications. *Trends Anal Chem* **2022**, *148*:116540. doi:10.1016/j.trac.2022.116540.

Yilmaz A, Geddes T, Han B, Bahado-Singh RO, Wilson GD, Imam K, et al. Diagnostic biomarkers of Alzheimer's disease as identified in saliva using 1H NMR-based metabolomics. *J Alzheimer's Dis* **2017**, *58*:355-359. doi:10.3233/JAD-161226.

Yin K, Lv M, Wang Q, Wu Y, Liao C, Zhang W, et al. Simultaneous bioremediation and biodetection of mercury ion through surface display of carboxylesterase E2 from *Pseudomonas aeruginosa* PA1. *Water Res* **2016**, *103*:383-390. doi:10.1016/j.watres.2016.07.053.

York GM, Stubbe J, Sinskey AJ. The *Ralstonia eutropha* PhaR protein couples synthesis of the PhaP phasin to the presence of polyhydroxybutyrate in cells and promotes polyhydroxybutyrate production. *J Bacteriol* **2002**, *184*:59-66. doi:10.1128/JB.184.1.59-66.2002.

Young CA, Jordan TS. Cyanide remediation: Current and past technologies. Proceedings of the 10th Annual Conference on Hazardous Waste Research, **1995**.

Yu JG, Yue BY, Wu XW, Liu Q, Jiao FP, Jiang XY, et al. Removal of mercury by adsorption: A review. *Environ Sci Pollut Res* **2016**, *23*:5056–5076. doi:10.1007/s11356-015-5880-x.

Yuen HW, Becker W. Iron Toxicity. Treasure Island, *StatPearls Publishing* **2022**.

Z

Zagrobelny M, Søren B, Rasmussen AV, Jørgensen B, Naumann CM, Møller BL. Cyanogenic glucosides and plant-insect interactions. *Phytochemistry* **2004**, *65*:293-306. doi:10.1016/j.phytochem.2003.10.016.
Zagury GJ, Oudjehani K, Deschênes L. Characterization and availability of cyanide in solid mine tailings from gold extraction plants. *Sci Total Environ* **2004**, *320*:211-24. doi:10.1016/j.scitotenv.2003.08.012.

Zeng XX, Tagn JX, Jiang P, Liu H W, Dai ZM, Liu XD. Isolation, characterization and extraction of *mer* gene of Hg^{2+} resisting strain D2. *Trans Nonferrous Met Soc China* **2010**, *20*:507-12. doi:10.1016/S1003-6326(09)60170-9.

Zhang W, Chen L, Liu D. Characterization of a marine-isolated mercury-resistant *Pseudomonas putida* strain SP1 and its potential application in marine mercury reduction. *Appl Microbiol Biotechnol* **2012**, *93*:1305-14. doi:10.1007/s00253-011-3454-5.

Zhang A, Sun H, Wang P, Wang X. Salivary proteomics in biomedical research. *Clin Chim Acta* **2013**, *415*:261-5. doi:10.1016/j.cca.2012.11.001.

Zhang Y, Wen Z, Washburn MP, Florens L. Improving label-free quantitative proteomics strategies by distributing shared peptides and stabilizing variance. *Anal Chem* **2015a**, *87*:4749-4756. doi:10.1021/ac504740p.

Zhang J, Cao T, Tang Z, Shen Q, Rosen BP, Zhao FJ. Arsenic methylation and volatilization by arsenite *S*-adenosylmethionine methyltransferase in *Pseudomonas alcaligenes* NBRC14159. *Appl Environ Microbiol* **2015b**, *81*:2852-60. doi:10.1128/AEM.03804-14.

Zhang Z, Yin N, Cai X, Wang Z, Cui Y. Arsenic redox transformation by *Pseudomonas* sp. HN-2 isolated from arsenic-contaminated soil in Hunan, China. *J Environ Sci (China)* **2016**, *47*:165-173. doi:10.1016/j.jes.2015.11.036.

Zhang AH, Ma ZM, Sun H, Zhang Y, Liu JH, Wu FF, et al. High-throughput metabolomics evaluate the efficacy of total lignans from *Acanthophanax Senticosus* stem against ovariectomized osteoporosis. *Rat Front Pharmacol* **2019**, *10*:553. doi:10.3389/fphar.2019.00553.

Zhang J, Zeng Y, Liu B, Deng X. MerP/MerT-mediated mechanism: A different approach to mercury resistance and bioaccumulation by marine bacteria. *J Hazard Mater* **2020**, *388*:122062. doi:10.1016/j.jhazmat.2020.122062.

Zhao C, Zhang Y, Chan Z, Chen S, Yang S. Insights into arsenic multi-operons expression and resistance mechanisms in *Rhodopseudomonas palustris* CGA009. *Front Microbiol* **2015**, *6*:986. doi:10.3389/fmicb.2015.00986.

Zhao Y, Zhou C, Guo X, Hu G, Li G, Zhuang Y, et al. Exposed to mercury-induced oxidative stress, changes of intestinal microflora, and association between them in mice. *Biol Trace Elem Res* **2021**, *199*:1900-1907. doi:10.1007/s12011-020-02300-x.

Zheng R, Wu S, Ma N, Sun C. Genetic and physiological adaptations of marine bacterium *Pseudomonas stutzeri* to mercury stress. *Front Microbiol* **2018**, *9*:682. doi:10.3389/fmicb.2018.00682.

Zhou DG, Hardt WD, Galan JE. *Salmonella typhimurium* encodes a putative iron transport system within the centisome 63 pathogenicity island. *Infect Immun* **1999**, *67*:1974-1981. doi:10.1128/IAI.67.4.1974-1981.1999.

Zhou D, Qin L, Han Y, Qiu J, Chen Z, Li B, et al. Global analysis of iron assimilation and Fur regulation in *Yersinia pestis*. *FEMS Microbiol Lett* **2006**, *258*:9-17. doi:10.1111/j.1574-6968.2006.00208.x.

Zuhra K, Szabo C. The two faces of cyanide: An environmental toxin and a potential novel mammalian gasotransmitter. *FEBS J* **2022**, *289*:2481-2515. doi:10.1111/febs.16135.

Zunita M. Graphene oxide-based nanofiltration for Hg removal from wastewater: A mini-review. *Membranes* **2021**, *11*:269. doi:10.3390/membranes11040269.

Zuriani R, Vigneswari S, Azizan MNM, Majid MIA, Amirul AA. A high throughput Nile red fluorescence method for rapid quantification of intracellular bacterial polyhydroxyalkanoates. *Biotechnol Bioproc E* **2013**, *18*:472-478. doi:10.1007/s12257-012-0607-z.

Supplementary Materials

Chapter I

Table S2. Oligonucleotides used in the *q*RT-PCR analysis of *P. pseudoalcaligenes* CECT 5344.

Locus	Protein name	Forward (5'-3')	Reverse (5'-3')
BN5_0117	Phosphate transport system permease protein	CCGAACGCCATGAGCACCGTCGACA	AAGATCGCCGGGAAGATACCGCCTT
BN5_0252	ArsR family transcriptional regulator	ACGCCGCCGGGCAACTGCTCAAG	CTCGCTGACGTTGCGCTCGCCTT
BN5_0255	Hypothetical protein	CGCCGCAGGTCTGATTCTTATCGC	GGCACCACACCGATCCAACCCCA
BN5_0258	C-N hydrolase, nitrilase/cyanide hydratase, AguB	GACGGCCCCGGCTACCACGAGAA	ATCCCAGCAGATGCCGACACCGAT
BN5_0441	Nitrate/nitrite transport system ATP-binding protein	TACGTATCGACCTGCCACGGCCAC	AGCGAGCGGTTCACCAGAAAGTCCAC
BN5_1279	Uncharacterized multi-transmembrane protein, ArsP	CCAACAGCTGCGACACCACTCCGAA	CCGCCACACACCACTGTACTTCCC
BN5_1354	Sulfite reductase (NADPH) hemoprotein β-component	CGGTTACGGGCACTTCACCACACGAC	ATGCATATCGTGCTCGGCCAACCAG
BN5_1632	Nitrilase, NitC	TGAGCGTATGGTCTGGGGGCAGGG	CGCCGCATGAATCTGCTCGCCATC
BN5_1633	Radical SAM domain-containing protein, NitD	CCGTGGTGCTGCCATCCTTTGCGAAT	CAAGCGGCGAAACCAGGCGTCCTC
BN5_1902	Cytochrome *bd* ubiquinol oxidase subunit I CioA3	GGCCTTCCTGCTGGCGATCA	GCGGCGCACCGAAGATGTCA
BN5_1911	MeaB3, malate dehydrogenase	CCCGCCAACGTCTTCCGCTTCACC	AAGCGCACCGATGTTTCCCAGTCCA
BN5_1989	ArsR family transcriptional regulator, ArsR1	ACGTGGCCCGCAACACCTTGTCCT	CGGCCCTGCTGCTCAATCGAGACCA
BN5_1991	Arsenate reductase (thioredoxin), ArsC1	AGCCATCCGAAGGGCGCAGTGCAT	GGCGCACCGGGCACCACGAACTC
BN5_1992	Arsenite transporter, ArsB1	CGTGTTCCAGGCCATCGGTCGCAT	TTGGCCCAGCGCACCGAAGTCCAC
BN5_1993	Arsenate reductase (glutaredoxin), ArsC2	AAGACGCCACCCGACCGCGAGAC	CGCATCGCTCCACTTCGGGTCGTCA
BN5_2541	23S rRNA (cytidine2498-2'-O)-methyltransferase	CATCGCCTGGTTGTCCGCCTC	CGGCAAACTGGTGGACGACGC
BN5_2707	ArsR family transcriptional regulator, ArsR2	ATGCCATGTCGCCAACCGAAGTCT	CGCCTCTTCCAGTGCCGAGGTCA
BN5_2708	Arsenate reductase (thioredoxin), ArsC3	TTTTCTTTGGCCCGGCGACTCGTT	CGCTCACTCGCTTCTGGATCTGCT
BN5_2786	Arsenate reductase (glutaredoxin), ArsC5	TGCGCTATCTGGAAACGCCACCC	CTCGCCGCTACGCAGCAGGT
BN5_2838	Arsenate reductase (glutaredoxin), ArsC4	ACGAGCATGGCTGGCAGACCAT	ATCGGCTTTCTGCGCGTCGTC
BN5_3016	Glycine cleavage system H protein, GcvH3	CTGGTTACCGTCGGCATCACCCA	ACTTGGCTTCCGGCAGTTGCAC
BN5_3018	Glycine hydroxymethyltransferase, GlyA5	ACTGCTCAATGCGGGCGACACCA	AGCTTGCCCGAGGACGACACCTT
BN5_3703	DNA-directed RNA polymerase subunit beta, RpoB	AGCTGCTGCGTGCGATCTTCGGTGAGA	CCAATTGCTCGTTCAGGGCGTCGTCAG

Chapter II

Table S2. Oligonucleotides used in the *q*RT-PCR analysis of *P. pseudoalcaligenes* CECT 5344.

Primer code	Protein Name	Sequence (5'-3')
BN5_0108F	Thiol:disulfide interchange protein	CGATCGCGAAGCCTTCCTCAAGACCT
BN5_0108R		ACGATACTTGCCGCCGACGACCA
BN5_0231F	3-octaprenyl-4-hydroxybenzoate carboxy-lyase	ACGCCAGTGCCCGATACCCTC
BN5_0231R		CGCCCGGATGGATCACACCCT
BN5_0252F	ArsR family transcriptional regulator	CCTGATCGCCTGTTGCTGCTCT
BN5_0252R		ATACCGAGCAGCGCCTCCAG
BN5_0701F	MerR family transcriptional regulator	AGTCCATAGATCTGCTGCCCCATGCC
BN5_0701R		TGCCGACTTCCTCCAGCGAAAAGCC
BN5_1290F	Ribonucleoside-diphosphate reductase beta chain	ACCAACCCCGAGTGCCGCCAGT
BN5_1290R		CGCCTTCATCCATGCCCAGCGATT
BN5_1595F	Glutathione peroxidase	TCCGGTGCCAATGCCATCCCGTTG
BN5_1595R		ACTCGCCACCACCTTGCCCTG
BN5_1632F	Nitrilase NitC	TGAGCGTATGGTCTGGGGGCAGGG
BN5_1632R		CGCCGCATGAATCTGCTCGCCATC
BN5_1633F	Radical SAM domain-containing protein NitD	CCGTGGTGCTGCCATCCTTTGCGAAT
BN5_1633R		CAAGCGGCGAAACCAGGCGTCCTC
BN5_2215F	DNA polymerase III, epsilon subunit	CCCCAACAACTCGACACAACCG
BN5_2215R		GAGAAGCAAGGCGTGACAACCG
BN5_2264F	MerR family transcriptional regulator	CTCGACATCACCACCCGCGCCAT
BN5_2264R		CGCGCAGGATGAGTTTCAGCGTCACC
BN5_2322F	MerR family transcriptional regulator	ACTCTGCGCGGTCAAGCCCCAC
BN5_2322R		ACCCCGCCGCTTTACCGGAT
BN5_2412F	Glutathione *S*-transferase	AGCGAGTTTCTGCCGACCGAGCC
BN5_2412R		AGAGCTGGATGAAACGCGCCACC
BN5_2413F	GntR family transcriptional regulator	CGCCACCAAGGACCTGTATCCG
BN5_2413R		CAGCGCCTGCCACTGACCGAT
BN5_2475F	Periplasmic protein CpxP/Spy	AAGACCCTCACCGCCCTGCT
BN5_2475R		TCCTGGCGCTGCTCCTTGCT
BN5_2707F	ArsR family transcriptional regulator	ATGCCATGTCGCCAACCGAAGTCT
BN5_2707R		CGCCTCTTCCAGTGCCGAGGTCA
BN5_2708F	Arsenate reductase	TTTTCTTTGGCCCGGCGACTCGTT
BN5_2708R		CGCTCACTCGCTTCTGGATCTGCT
BN5_2819F	DNA-directed DNA polymerase	TCCCCCTTCAATGCCTCACCG
BN5_2819R		CCTGCGTCTGCGTGCCAAGCG
BN5_2864F	Putative glutathione *S*-transferase like protein	CGCCGAACAACAAGATTCCCGCCAT
BN5_2864R		CAGAATTGCCCCGGACTCGAACAGC
BN5_3204F	Formamidase	ACCGCACCGATCCGTCACTCGT
BN5_3204R		ACACACTGGCCGTCTGCATCAGGT
BN5_3351F	MerR family transcriptional regulator	CACCGGCCAATCTCGCACGCAT
BN5_3351R		TGCTTGCGGCACCTGCTCATGGTC
BN5_3397F	PhoH family protein	CGCTACCGCAGGATCATCGCCACC

BN5_3397R		GCTCTCGTCCTCCATGTGCAACGCTT
BN5_3403F	Thioredoxin reductase	CGCCAACCTGAAACCGCTGCTGA
BN5_3403R		GTCACCCGGCCAGTTGTCCACCT
BN5_3450F	Glutathione *S*-transferase domain-containing protein	CTACCCCGAGGCGCAGCTGT
BN5_3450R		CGCCAGATCCATCGGCAGGTGAC
BN5_3536F	Type IV secretion system protein VirD4	ATCGAGCGCCGCCACAAGCTAC
BN5_3536R		GCCAGCGCCGTCTCGAAGAAGTCCA
BN5_3800F	Periplasmic mercury ion-binding protein	CCGTGCTTTTCGCCTTGCCCTT
BN5_3800R		GCCGGACACCTTCTCCAGCGACT
BN5_3801F	Mercuric transport protein	TGGCATTCCGCAAGCTCTACCTGGTG
BN5_3801R		AGCACGCTGACGATCCAGAACACGAG
BN5_3802F	Mercury regulatory protein	AGTCGTGCGCCTGTGCCGAA
BN5_3802R		ATCGTTCCGCCGTCTCCCGCAT
BN5_4162F	Alkanesulfonate monooxygenase	CCAAGCTGCTCTACCCGCCGAT
BN5_4162R		CGCCCCAGGTCAGGTACAGCTC
BN5_4165F	Antioxidant, AhpC/Tsa family	ACCGGGCGCAACTTCAATGAAATCCT
BN5_4165R		CAACGACGGCACGATCACCACCT
BN5_4234F	Signal transduction histidine kinase	GGCCTGAAAACCCCGCAAGACAGC
BN5_4234R		AGTTGCCACGCTCGAAGTAGTCCT
BN5_4378F	Precorrin-2 C20-methyltransferase	CTCGCCCCGCCGCTGAGCTAC
BN5_4378R		CGCAGATCACCGCCACGTCCT
BN5_4473F	Mercuric resistance operon regulatory protein	GCACCCATTGCGAGGAAGCCAGCAG
BN5_4473R		ACCAAATCAGACAGCACGGCCTCCAT
BN5_4474F	Mercuric transport protein	CGGGTGAGGTTTGCGCGATTCCCCAA
BN5_4474R		CCGAGCGCGACCAAAACCAGCAC
BN5_4477F	Mercuric reductase (Hg(II) reductase)	CTCGCCATCCGCAACCGCAT
BN5_4477R		CGCCGCAAGCTTCAACCCCT
BN5_4478F	MerD protein	ACTACCTGCTGCGCGGATTGCT
BN5_4478R		CTCGAAGGCCGCCCGCACGAA
BN5_4479F	Putative mercuric resistance protein MerE	ACCTGTCCCTGCCATTTGCCGAT
BN5_4479R		ATCTTTGAAGGCCCGCAGCAGT

Table S3. Proteins identified in the differential intracellular proteomic analysis of *P. pseudoalcaligenes* CECT 5344 under anaerobic conditions. Relative label-free quantification (LFQ) intensity was used to calculate the fold change (FC) in the anaerobic *vs* control proteomes (Ana/C_Abs and Ana/C_Cons). Proteins not detected (-).

Protein ID	BN5	Name	Log_2 FC Ana/C_Abs	Log_2 FC ANA/C_Cons
W6QNW5	BN5_0019	Lipid A biosynthesis acyltransferase	-	2.002080523
W6QWV2	BN5_0020	Type IV pilus assembly PilZ	-6.3599996	-3.378680663
W6QRM0	BN5_0027	Peptide deformylase (PDF) (Polypeptide deformylase)	-2.630007	-2.645120292
W6R9V1	BN5_0028	LysM domain-containing protein	-4.2932395	-6.836383516
W6QQ84	BN5_0031	Quinone oxidoreductase	-2.3633501	-2.26943526
W6QRM5	BN5_0032	Oxygen-dependent coproporphyrinogen-III oxidase (CPO) (Coprogen oxidase) (Coproporphyrinogenase)	-	-2.201418346
W6R9V8	BN5_0033	Shikimate dehydrogenase (NADP(+)) (SDH)	-	-3.16630449
W6QQ87	BN5_0036	Substrate-binding region of ABC-type glycine betaine transport system	Exc.C_abs	Exc.C_Cons
W6R9W2	BN5_0038	LysR family transcriptional regulator	4.6895842	-
W6R9W6	BN5_0043	Glucose 1-dehydrogenase	4.6309879	-
W6QNY9	BN5_0044	Putative Sodium:sulfate symportert	Exc.Ana	-
W6QQ93	BN5_0046	Tryptophan synthase alpha chain	-2.0781023	-
W6QRP2	BN5_0047	Tryptophan synthase beta chain	-2.3166391	-2.606173865
W6QNZ3	BN5_0049	Uncharacterized protein	-	-6.064127135
W6QP07	BN5_0064	N5-carboxyaminoimidazole ribonucleotide synthase (N5-CAIR synthase) (5-(carboxyamino)imidazole ribonucleotide synthetase)	-2.0739772	-
W6QX02	BN5_0065	N5-carboxyaminoimidazole ribonucleotide mutase (N5-CAIR mutase) (5-(carboxyamino)imidazole ribonucleotide mutase)	-2.7008247	-2.701885742
W6QQA5	BN5_0066	Alcohol dehydrogenase, zinc-containing	3.9952894	-2.130167189
W6QX10	BN5_0070	Sulfatase family protein	Exc.C_abs	Exc.C_Cons
W6QP19	BN5_0079	Aspartate ammonia-lyase	3.4092475	3.404579606
W6QQD6	BN5_0106	Cytochrome c5-like protein	-5.2988771	-30.98332347
W6RA33	BN5_0108	Thiol:disulfide interchange protein	-2.7839501	-3.720508977
W6RA38	BN5_0113	N-acetylmuramoyl-L-alanine amidase	2.2245291	-
W6QX64	BN5_0115	Phosphate binding protein	-3.2164442	-2.48526553
W6QQE5	BN5_0116	Phosphate transport system permease protein	-	2.25792881
W6QRW0	BN5_0117	Phosphate transport system permease protein PstA	-	2.881926084
W6QP71	BN5_0124	Malate synthase G	-3.6847498	-3.142980526
W6QX98	BN5_0125	GlcG protein	-6.4449388	-4.990208171
W6QQG6	BN5_0126	Glycolate oxidase iron-sulfur subunit	-4.1647984	-4.929028536
W6RAC3	BN5_0149	Putative endoribonuclease L-PSP	-3.818043	-3.365140327
W6QPA6	BN5_0150	Cytochrome C6	Exc.C_abs	Exc.C_Cons
W6QS35	BN5_0164	D-amino acid dehydrogenase	Exc.Ana	Exc.Ana
W6QQK7	BN5_0168	Cytochrome c5-like protein	-	-3.09713299
W6QS53	BN5_0189	Uncharacterized protein	3.9067438	2.402383825
W6QPD6	BN5_0191	Protein CyaY	-3.8714303	-2.403327627
W6QPE5	BN5_0201	Two-component response regulator AlgR	2.0133063	-

W6QXF9	BN5_0202	Porphobilinogen deaminase (PBG) (Hydroxymethylbilane synthase) (HMBS) (Pre-uroporphyrinogen synthase)	-	-2.330059291
W6RAG8	BN5_0205	HemY domain-containing protein	2.2821074	2.000369713
W6QXG3	BN5_0207	Anti-RNA polymerase sigma 70 factor	-2.0644631	-2.385238177
W6QS66	BN5_0209	Alginate regulatory protein AlgP	-10.635382	-8.029257973
W6QXH2	BN5_0222	Delta-aminolevulinic acid dehydratase	2.4304666	-
W6QQP9	BN5_0223	Polyphosphate kinase (ATP-polyphosphate phosphotransferase) (Polyphosphoric acid kinase)	2.388216	-
W6QS83	BN5_0229	Thioredoxin	-2.9312175	-
W6RAJ1	BN5_0235	ABC-2 type transporter	Exc.Ana	-
W6QPI0	BN5_0236	Putative ABC transporter ATP-binding protein yhiH	Exc.Ana	-
W6QXI2	BN5_0237	Membrane-fusion protein	3.5004329	-
W6QQR6	BN5_0243	Uncharacterized protein	2.2933661	-
W6QQS0	BN5_0248	Binding protein component of ABC iron transporter	3.0899854	4.690472733
W6QPJ5	BN5_0251	Glycine cleavage system H protein	-3.1230017	-
W6QXJ3	BN5_0252	ArsR family transcriptional regulator	-	-2.936436961
W6QPJ9	BN5_0256	Cytochrome c551 peroxidase	-	-6.170411337
W6RAK9	BN5_0260	Putrescine-binding periplasmic protein	-	-4.206149124
W6RAL1	BN5_0265	Putrescine transporter periplasmic protein	-	-2.267653167
W6QPL1	BN5_0266	Putrescine transport system substrate-binding protein	-	-2.044431889
W6QPN0	BN5_0286	33 kDa chaperonin (Heat shock protein 33 homolog) (HSP33)	-2.3739672	-2.229880916
W6QXM1	BN5_0287	Phosphoenolpyruvate carboxykinase [ATP] (PCK) (PEP carboxykinase) (PEPCK)	-2.4690111	-
W6QSD9	BN5_0289	Uncharacterized protein	2.1327773	-
W6QPN4	BN5_0291	ATP-binding protein of ABC transporter	2.1015688	-
W6QSF2	BN5_0304	Uracil phosphoribosyltransferase	-	-2.357187738
W6QXN1	BN5_0307	TonB domain protein	-2.352139	-2.795888189
W6RAQ0	BN5_0310	Response regulator receiver protein	-2.739666	-
W6QQY4	BN5_0313	Protein-glutamate O-methyltransferase	2.172049	-
W6QPU0	BN5_0346	Phosphoglycerate kinase	-2.453033	-
W6QXR7	BN5_0352	Uncharacterized protein	-2.5332978	-4.173863249
W6QPV9	BN5_0361	Putative glutathione transferase	-	-2.494758214
W6QSM0	BN5_0374	Substrate-binding region of ABC-type glycine betaine transport system	-3.3479237	-4.497011791
W6RAV4	BN5_0375	Substrate-binding region of ABC-type glycine betaine transport system	-	-2.113254712
W6QSN8	BN5_0394	Lipoprotein, putative	-4.2780401	-4.886777211
W6QSP8	BN5_0404	Phosphoribosyl-AMP cyclohydrolase (PRA-CH)	-4.3167135	-4.841206612
W6QR81	BN5_0408	Putative polyhydroxyalkanoic acid system protein	-3.9354629	-
W6QSQ4	BN5_0409	Poly(Hydroxyalkanoate) granule-associated protein (Phasin)	4.7966372	20.54297661
W6RAY6	BN5_0410	Poly(Hydroxyalkanoate) granule-associated protein	-8.8364486	-10.70490435
W6QQ02	BN5_0411	TetR family transcriptional regulator phaD	3.4197243	-
W6QSQ8	BN5_0414	Poly(3-hydroxyalkanoate) polymerase	2.1263808	-
W6RAZ0	BN5_0415	Putative phosphoribosylformimino-5-aminoimidazole carboxamide ribotide isomerase	-2.3755035	-2.507877129
W6QR92	BN5_0418	Uncharacterized protein	-2.8224865	-

W6QSR5	BN5_0419	Cell division protein ftsN	Exc.C_abs	Exc.C_Cons
W6QY03	BN5_0432	Type IV pilus assembly protein PilQ	-3.4719993	-2.314926947
W6QRB7	BN5_0443	Uroporphyrinogen decarboxylase (UPD) (URO-D)	-	-2.332806536
W6QY19	BN5_0447	Putative Universal stress protein E	3.2861538	-
W6QSU3	BN5_0449	Thioredoxin	-	-2.350661278
W6QSV1	BN5_0454	Butyryl-CoA dehydrogenase	2.9031518	-
W6QQ48	BN5_0456	Ribosomal RNA large subunit methyltransferase J (23S rRNA (adenine(2030)-N6)-methyltransferase) (23S rRNA m6A2030 methyltransferase)	-	-2.417696806
W6QY35	BN5_0462	Uncharacterized protein	-2.2095001	-2.60103654
W6QQ78	BN5_0486	Putative lipoprotein	-6.3320823	-5.851527719
W6QSY8	BN5_0489	Uncharacterized protein	-2.0030591	-2.523113314
W6QY62	BN5_0492	3',5'-cyclic adenosine monophosphate phosphodiesterase CpdA (3',5'-cyclic AMP phosphodiesterase) (cAMP phosphodiesterase)	Exc.C_abs	Exc.C_Cons
W6QSZ2	BN5_0494	ADP-ribose pyrophosphatase	-3.6271842	-3.016376817
W6RB74	BN5_0495	Phosphomethylpyrimidine synthase (Hydroxymethylpyrimidine phosphate synthase) (HMP-P synthase) (HMP-phosphate synthase) (HMPP synthase) (Thiamine biosynthesis protein ThiC)	-2.1310533	-
W6RB89	BN5_0510	Chemotaxis protein	-	2.33886188
W6QT14	BN5_0514	Oligoribonuclease	-	-2.180410843
W6QRK3	BN5_0518	N-acetylmuramoyl-L-alanine amidase	-9.0944727	-10.68555546
W6QQA6	BN5_0521	RNA-binding protein Hfq	2.2711138	-
W6QRK8	BN5_0523	HflK protein	2.1320875	-
W6QT23	BN5_0524	Protein HflC	2.7736133	2.054328173
W6QQB0	BN5_0526	ATP phosphoribosyltransferase regulatory subunit	-2.1760323	-2.280947646
W6QT34	BN5_0536	30S ribosomal protein S18	-13.040555	-6.774119012
W6QQB9	BN5_0538	50S ribosomal protein L9	-2.3314594	-
W6QRM4	BN5_0540	Alanine racemase	-	-2.552309586
W6QQC6	BN5_0543	Transglutaminase domain-containing protein	2.0432608	-
W6QYC6	BN5_0544	Hypotetical protein	-9.0542805	-6.887116112
W6QT43	BN5_0546	Azurin	4.3696973	-
W6QQE4	BN5_0563	Uncharacterized protein	-2.0325629	-
W6RBE8	BN5_0567	Integral membrane protein-like protein	-	Exc.Ana
W6QYI6	BN5_0599	Bifunctional purine biosynthesis protein PurH [Includes: IMP cyclohydrolase (ATIC) (Inosinicase) (IMP synthase); Phosphoribosylaminoimidazolecarboxamide formyltransferase (AICAR transformylase)]	-2.4482202	-
W6QRT1	BN5_0600	DNA-binding protein Fis	-3.1758292	-
W6QRT7	BN5_0605	Acetyl-CoA carboxylase biotin carboxyl carrier protein subunit	-2.1085726	-
W6QQI6	BN5_0608	Methyl-accepting chemotaxis protein	2.0384888	-
W6QRU1	BN5_0610	Uncharacterized protein	-2.9543689	-4.445205143
W6RBK0	BN5_0612	Translation initiation factor 1 (EIF-1/SUI1)	-9.1787647	-5.128013287
W6QQK6	BN5_0623	Uncharacterized protein	4.3542976	-
W6QYL3	BN5_0624	Lipoprotein, putative	2.1028802	-
W6QRV6	BN5_0625	tRNA 5-carboxymethoxyuridine methyltransferase (cmo5U methyltransferase)	2.2210882	-
W6QTI1	BN5_0636	Ferredoxin-NADP reductase	-	3.321803346

W6QRZ7	BN5_0645	Uncharacterized protein	Exc.C_abs	Exc.C_Cons
W6RBQ9	BN5_0655	Uncharacterized protein	2.1242202	-
W6QYS1	BN5_0657	Uncharacterized protein	2.1801388	-
W6QTJ9	BN5_0664	Type 4 fimbrial biogenesis protein PilB	3.3646117	2.159803408
W6RBR8	BN5_0665	Fimbrillin	-	-2.170960284
W6QTL2	BN5_0679	Methyl-accepting chemotaxis sensory transducer	2.0384888	-
W6QTM2	BN5_0694	TonB-dependent siderophore receptor	34.157568	50.65619
W6RBT9	BN5_0695	PKHD-type hydroxylase BN5_0695	8.9923405	5.481763169
W6QQV7	BN5_0696	FMN-dependent alpha-hydroxy acid dehydrogenase	4.1752425	3.252817766
W6QYV1	BN5_0697	Putative outer membrane receptor	210.42175	-
W6QS37	BN5_0708	Uncharacterized protein	-9.1989339	-3.350090339
W6QTP6	BN5_0719	Extracellular solute-binding protein	-	-4.378793252
W6RBV6	BN5_0720	Uncharacterized protein	-2.8747238	-3.725214072
W6QQY1	BN5_0721	Sensor histidine kinase	4.3444092	-
W6QS61	BN5_0733	Maf-like protein BN5_0733	-3.1707849	-2.196500255
W6QS64	BN5_0738	UPF0307 protein BN5_0738	-4.8154368	-
W6QS68	BN5_0743	CBS domain-containing protein	-	-2.017217528
W6QS74	BN5_0748	Uncharacterized protein	-2.2303292	-
W6QR17	BN5_0756	ATP-binding component of hydroxymate-dependent iron transport	Exc.Ana	Exc.Ana
W6QR22	BN5_0761	Acyl-CoA dehydrogenase domain-containing protein	3.1482134	2.215859897
W6QS95	BN5_0768	CRISPR-associated Cse1 family protein	Exc.Ana	-
W6QTT9	BN5_0769	CRISPR-associated protein, Cse2 family	6.1197243	5.402323375
W6RBZ4	BN5_0770	Uncharacterized protein	2.6982051	2.309904703
W6QTV4	BN5_0784	Pseudouridine synthase	-5.1352399	-
W6RC36	BN5_0820	LysR family transcriptional regulator	-	2.392214352
W6QRA9	BN5_0851	FxsA	3.3377286	3.630999337
W6QRB3	BN5_0856	50S ribosomal protein L27	-3.0497691	-
W6RC71	BN5_0870	Peptidase M48, Ste24p	-	-2.054043403
W6QSK8	BN5_0878	Type V secretory pathway, adhesin AidA	2.4698099	-
W6QU41	BN5_0879	Uncharacterized protein	-	-3.142109228
W6QRE4	BN5_0886	Beta-lactamase domain-containing protein	-2.7587856	-2.545119389
W6QZ91	BN5_0887	OmpA/MotB domain-containing protein	-	2.02473533
W6QSM4	BN5_0893	Acetate kinase (Acetokinase)	-	-2.135291944
W6QU54	BN5_0894	Peptidyl-prolyl cis-trans isomerase	-2.8732828	-
W6QRG1	BN5_0901	GntR family transcriptional regulator	2.3811635	-
W6QZB3	BN5_0907	Ferric uptake regulation protein	-	2.071104
W6QSQ0	BN5_0918	Uncharacterized protein	2.587526	6.452075557
W6QU80	BN5_0919	Uncharacterized protein	-6.8469746	-4.687547577
W6QU89	BN5_0924	Triosephosphate isomerase (TIM) (TPI) (Triose-phosphate isomerase)	-2.2615836	-2.362694884
W6QU93	BN5_0931	Ribosome-binding factor A	-3.3956788	-
W6QRJ2	BN5_0933	30S ribosomal protein S15	-38.051111	-16.24886076
W6QRK2	BN5_0943	Pantothenate synthetase (PS) (Pantoate--beta-alanine ligase) (Pantoate-activating enzyme)	2.0789187	-
W6QZF1	BN5_0944	3-methyl-2-oxobutanoate hydroxymethyltransferase (Ketopantoate hydroxymethyltransferase) (KPHMT)	-	2.04018503
W6QRK7	BN5_0948	Two-component sensor kinase CbrA	3.662939	-
W6QUA9	BN5_0951	RNA polymerase-binding transcription factor DksA	-2.6348728	-

W6QST3	BN5_0955	Outer membrane heme receptor	Exc.Ana	-
W6QUB4	BN5_0956	Putative hemin degrading factor	Exc.Ana	-
W6RCE4	BN5_0957	Periplasmic binding protein	-	Exc.Ana
W6QRL6	BN5_0958	Transmembrane permease component of haem ABC transporter	Exc.Ana	Exc.Ana
W6QZG3	BN5_0959	Hemin import ATP-binding protein HmuV	9.9643567	13.80475456
W6QSU0	BN5_0960	Uncharacterized protein	20.352724	14.03574107
W6QZG9	BN5_0964	Pentapeptide repeat-containing protein	-	-5.26789528
W6QUD1	BN5_0981	Chromosome segregation ATPase	-	2.02459499
W6RCG3	BN5_0982	Chromosome partition protein mukE like	-2.518678	-
W6QZI7	BN5_0994	Globin	-2.545437	-
W6RCI1	BN5_0997	Uncharacterized protein	2.8431036	2.015307521
W6QUE9	BN5_1006	Putative amino-acid ABC transporter-binding protein	-2.0350534	-3.901782431
W6RCL0	BN5_1022	TRAP-type uncharacterized transport system periplasmic component-like protein	2.2705367	-
W6QT06	BN5_1025	Nuclease SbcCD subunit D	-	2.085904826
W6RCL6	BN5_1027	Uncharacterized protein	2.8597057	4.369899195
W6QRS3	BN5_1028	Putative secreted protein	-	-5.007070145
W6QZM2	BN5_1029	Uncharacterized protein	-	-2.059746323
W6QT13	BN5_1030	Uncharacterized protein	-2.0397608	-2.163249396
W6QUH1	BN5_1031	Adenine-specific DNA-methyltransferase	-2.4842322	-2.323393206
W6RCL9	BN5_1032	Uncharacterized protein	-	Exc.C_Cons
W6QRV7	BN5_1063	Uncharacterized protein	Exc.C_abs	Exc.C_Cons
W6QT48	BN5_1065	Putative Nudix hydrolase nudL	2.3240912	-
W6QUK4	BN5_1066	Carnitine operon protein caiE	-	-2.359203716
W6QRW6	BN5_1073	30S ribosomal protein S16	-8.9455282	-6.033380904
W6QUL4	BN5_1076	50S ribosomal protein L19	-4.5582077	-3.380726561
W6RCR6	BN5_1077	Putative acyl-CoA thioester hydrolase TC_0822	Exc.C_abs	Exc.C_Cons
W6QRX7	BN5_1093	HTH-type transcriptional regulator betI	-	3.264917793
W6QUN5	BN5_1101	Adenylate kinase (AK) (ATP-AMP transphosphorylase) (ATP:AMP phosphotransferase) (Adenylate monophosphate kinase)	-3.2864575	-3.700619147
W6QTA9	BN5_1115	Cys-tRNA(Pro)/Cys-tRNA(Cys) deacylase	-2.3486526	-
W6QUQ3	BN5_1121	Glutaredoxin	-3.0331146	-
W6RCW9	BN5_1122	Uncharacterized protein	2.648851	-
W6QS07	BN5_1133	Iron-regulated protein A	-	4.679183045
W6QZZ0	BN5_1134	Putative 25,5 kDa protein in gyrB 5'region	-	2.25266586
W6QTD3	BN5_1135	Uncharacterized protein	Exc.C_abs	Exc.C_Cons
W6QUS0	BN5_1136	Putative signaling protein CC_0091	2.9299953	-
W6R013	BN5_1139	Superoxide dismutase	-5.7639853	-6.275367721
W6QUU4	BN5_1146	Uncharacterized protein	4.322592	-
W6QS44	BN5_1148	Transcriptional regulator, putative	-10.289731	-5.507254705
W6QTG4	BN5_1150	Inosine-5'-monophosphate dehydrogenase	-	-4.082444671
W6RD38	BN5_1152	Methyl-accepting chemotaxis protein mcpB	2.0384888	-
W6QTG7	BN5_1155	Uncharacterized protein	-2.2256396	-
W6QS58	BN5_1168	Uncharacterized protein	-4.3426229	-3.302823785
W6RD56	BN5_1172	Oxidoreductase, short chain dehydrogenase/reductase family	-5.4420618	-4.23977195
W6R053	BN5_1174	Putative HTH-type transcriptional regulator ycgE	2.4911582	-
W6QTI2	BN5_1175	Uncharacterized protein	-	Exc.Ana

W6RD60	BN5_1177	NADPH-cytochrome P450 reductase	-3.0337454	-2.055515143
W6QUX5	BN5_1186	Sensor histidine kinase	-	Exc.Ana
W6RD68	BN5_1187	Response regulator arlR	2.5576757	-
W6QUY5	BN5_1196	Nitrilase homolog 1	2.2201646	-
W6RD81	BN5_1202	Fumarate hydratase class I	-2.5448254	-2.413845492
W6RD85	BN5_1207	Universal stress protein E	4.6765134	-
W6QS97	BN5_1208	Lipoprotein, putative	-3.1742227	-3.258865928
W6QSA3	BN5_1213	Uncharacterized protein	3.8905254	-
W6R089	BN5_1214	Uncharacterized protein	-5.338866	-3.249835439
W6QTL3	BN5_1215	Hydroxyacylglutathione hydrolase	-2.4679275	-3.227014365
W6QSB7	BN5_1233	Uncharacterized protein	-	3.121775231
W6R0A6	BN5_1239	Phosphonates-binding periplasmic protein	-2.7502574	-3.048641833
W6QTN7	BN5_1245	Soluble aldose sugar dehydrogenase ylil	-	-2.575406207
W6R0B7	BN5_1255	Uncharacterized protein	-	-4.681594566
W6QV43	BN5_1257	Probable transcriptional regulatory protein BN5_1257	-4.4894333	-2.532156664
W6QTQ2	BN5_1261	Putative membrane protein in llm 5'region	2.0921602	-
W6QV47	BN5_1262	Peptidylprolyl isomerase	-4.3658624	-
W6QTR2	BN5_1271	Uncharacterized protein	-3.0528005	-2.342312122
W6R0G5	BN5_1310	tRNA-specific cytosine deaminase	2.6704015	-
W6RDH9	BN5_1318	C4-dicarboxylate-binding periplasmic protein	-2.3636777	-4.154476414
W6R0H3	BN5_1320	CAIB/BAIF family protein	-2.4542803	-2.66998814
W6R0H7	BN5_1325	Uncharacterized protein	-5.6954112	-6.070996466
W6R0I6	BN5_1335	Uncharacterized protein	-	Exc.C_Cons
W6RDK1	BN5_1343	Putative Ubiquinone biosynthesis hydroxylase	2.2089335	-
W6QVF1	BN5_1367	Alkyl-dihydroxyacetonephosphate synthase, putative	-	2.460909608
W6RDM6	BN5_1378	Uncharacterized protein	-4.2866977	-5.808772522
W6QSR7	BN5_1379	Fatty acid oxidation complex subunit alpha [Includes: 3-hydroxyacyl-CoA dehydrogenase ; Enoyl-CoA hydratase/Delta(3)-cis-Delta(2)-trans-enoyl-CoA isomerase/3-hydroxybutyryl-CoA epimerase]	2.8538312	2.303136631
W6QSS2	BN5_1384	Uncharacterized protein	-4.8016603	-
W6QU29	BN5_1386	LexA repressor	-2.1854545	-
W6QU34	BN5_1391	Uncharacterized protein	-2.510428	-2.576001321
W6QVJ4	BN5_1409	Ferredoxin-2	-5.1757455	-2.831434848
W6QVJ8	BN5_1414	Uncharacterized protein	2.1133719	-
W6R0R6	BN5_1417	Ribosome modulation factor (RMF)	-3.3738208	-37.98215876
W6QVK4	BN5_1419	D-alanyl-D-alanine carboxypeptidase/D-alanyl-D-alanine-endopeptidase	-2.5970972	-2.974127851
W6RDQ8	BN5_1420	Uncharacterized protein yggL	-4.9876723	-
W6QU70	BN5_1433	Uncharacterized protein	Exc.C_abs	Exc.C_Cons
W6RDS6	BN5_1440	Biopolymer transport protein exbB	2.6096084	2.508050968
W6QU78	BN5_1443	UPF0434 protein BN5_1443	-2.4121729	-
W6RDT1	BN5_1445	Low molecular weight phosphotyrosine protein phosphatase	2.1758312	-
W6R0V4	BN5_1452	Uncharacterized protein	-2.4309159	-
W6QU88	BN5_1453	50S ribosomal protein L32	-7.3333209	-3.409042692
W6QSZ9	BN5_1456	3-oxoacyl-(Acyl-carrier-protein) reductase	-2.3975042	-2.618607805
W6R0W1	BN5_1457	Acyl carrier protein (ACP)	-2.2148362	-

W6QVQ1	BN5_1464	Hydrolase, TatD family	-2.1868183	-2.44884252
W6RDX8	BN5_1490	Acetylornithine aminotransferase (ACOAT)	-2.4504273	-2.60647496
W6RDY3	BN5_1495	Uncharacterized protein	-3.9824788	-4.10362813
W6RDY8	BN5_1500	Carbon storage regulator homolog	-6.5575944	-4.109985583
W6QUE2	BN5_1507	Magnesium transporter MgtE	-	2.324735638
W6RDZ3	BN5_1509	Arc	-3.8040424	-
W6R132	BN5_1526	Uncharacterized protein	-4.8548722	-
W6QUG0	BN5_1527	BolA-like protein 1	-2.5250874	-
W6QUG4	BN5_1532	4-hydroxyphenylpyruvate dioxygenase	Exc.Ana	Exc.Ana
W6QVW6	BN5_1533	Homogentisate 1,2-dioxygenase	Exc.Ana	Exc.Ana
W6RE17	BN5_1534	4-hydroxyphenylacetate degradation bifunctional isomerase/decarboxylase	Exc.Ana	-
W6QUH0	BN5_1537	Laminin subunit alphmethyl-accepting chemotaxis sensory transducer	2.0384888	-
W6QT81	BN5_1547	Alcohol dehydrogenase class-3	2.4189819	-
W6QUI6	BN5_1555	Histidine kinase	Exc.Ana	Exc.Ana
W6RE36	BN5_1557	Sensor histidine kinase	Exc.Ana	Exc.Ana
W6QT91	BN5_1558	Cysteine synthase	-2.7984087	-2.449080168
W6RE40	BN5_1562	Uncharacterized protein	-8.1979698	-3.116154289
W6QTA1	BN5_1568	N-ethylmaleimide reductase, FMN-linked	Exc.C_abs	-
W6QUL0	BN5_1576	Putative lipoprotein ygdI	-2.8399588	-2.328751449
W6R1B3	BN5_1600	Long-chain fatty acid transport protein	4.4110843	3.376511177
W6QW22	BN5_1602	Sulfurtransferase	-2.731828	-2.929118717
W6R1B9	BN5_1605	Gluconolactonase	Exc.C_abs	Exc.C_Cons
W6QW27	BN5_1607	YcgL domain-containing protein BN5_1607	-3.0256952	-
W6RE90	BN5_1608	D-isomer specific 2-hydroxyacid dehydrogenase, NAD-binding	3.8346458	-
W6QUP5	BN5_1611	RNA methyltransferase, putative	Exc.C_abs	-
W6REA8	BN5_1623	Uncharacterized protein	2.2508865	-
W6REC7	BN5_1638	Isocitrate dehydrogenase kinase/phosphatase (IDH kinase/phosphatase) (IDHK/P)	4.4414785	2.801662811
W6QUT3	BN5_1646	Small heat shock protein	3.7334256	-
W6QUV7	BN5_1651	Uncharacterized protein	2.4877934	3.046318246
W6QTN8	BN5_1669	Short chain dehydrogenase	2.0523356	-
W6REJ2	BN5_1678	DNA methylase, putative	2.1738715	-
W6QWC6	BN5_1687	Methyltransferase FkbM	-	2.514526341
W6QWD3	BN5_1697	Uncharacterized protein	-4.1733329	-6.019596007
W6QWF6	BN5_1729	Extracellular solute-binding protein	Exc.C_abs	Exc.C_Cons
W6REP1	BN5_1748	Trigger factor (TF) (PPIase)	-2.5471784	-
W6QWH2	BN5_1752	DNA-binding protein HU	-7.1484643	-4.685706747
W6QWH8	BN5_1757	Aconitate hydratase B (2-methylisocitrate dehydratase)	-2.5673856	-2.042401733
W6QTW8	BN5_1759	Universal stress protein E homolog	-	-3.376277144
W6REQ8	BN5_1768	Uncharacterized protein	8.4526282	3.889271637
W6RER7	BN5_1778	DNA methylase N-4/N-6 domain protein	-	2.713196117
W6R1U7	BN5_1780	Putative helicase	2.3284824	-
W6QV73	BN5_1791	Methyl-accepting chemotaxis protein II	2.0384888	-
W6QV79	BN5_1796	Uncharacterized protein	3.4318821	3.182292985
W6RET5	BN5_1798	Putative Acyl-CoA synthetase	4.0614644	-

W6QU10	BN5_1804	Putative hydrolases or acyltransferases	2.3554456	-
W6QV93	BN5_1811	Uncharacterized protein	3.5608788	2.231891148
W6REU6	BN5_1813	Laminin subunit alpha-5	2.0384888	-
W6QU18	BN5_1814	ATP-dependent Clp protease ATP-binding subunit clpX	2.8188369	-
W6QWM8	BN5_1817	Uncharacterized protein	2.2928363	-
W6R1X9	BN5_1820	Methyl-accepting chemotaxis protein mcpB	2.0384888	-
W6REW4	BN5_1833	Probable thiol peroxidase	-3.2633793	-2.110180877
W6QU36	BN5_1834	Multidrug resistance protein mdtA	4.0273569	3.528610037
W6R1Z0	BN5_1835	Multidrug resistance protein mdtB	2.9480241	-
W6REW8	BN5_1838	C4-dicarboxylate-binding periplasmic protein	-	-2.801695177
W6R1Z9	BN5_1845	NADH-quinone oxidoreductase subunit I (NADH dehydrogenase I subunit I) (NDH-1 subunit I)	-	-2.857129972
W6QU47	BN5_1849	NADH dehydrogenase I chain E	-3.5642536	-2.751465044
W6QWR8	BN5_1852	NADH-quinone oxidoreductase subunit A (NADH dehydrogenase I subunit A) (NDH-1 subunit A) (NUO1)	-	3.719477576
W6QVD4	BN5_1856	Acetyltransferase, GNAT family	-2.9970988	-
W6QWT3	BN5_1862	NUDIX hydrolase	-3.1220421	-
W6R217	BN5_1865	Cold shock-like protein cspG	-2.1316442	-
W6REZ4	BN5_1868	Translation initiation factor IF-1	-5.6221944	-
W6QU79	BN5_1884	Uncharacterized protein	2.0728274	-
W6RF96	BN5_1990	Lactoylglutathione lyase	Exc.C_abs	-
W6QUH3	BN5_1991	Arsenate reductase, putative	-	-2.190545225
W6QVS0	BN5_2010	Uncharacterized protein	Exc.Ana	-
W6QX70	BN5_2011	Elongation factor P (EF-P)	-3.01105	-2.251937311
W6QVT3	BN5_2025	Uncharacterized protein	-3.5397153	-2.82921144
W6QX80	BN5_2026	Sulfite reductase (Ferredoxin)	-2.9096924	-2.666042908
W6R2J3	BN5_2039	Uncharacterized protein	-	-2.750448074
W6R2J7	BN5_2044	Uncharacterized protein	Exc.Ana	-
W6QVV2	BN5_2045	Methyl-accepting chemotaxis sensory transducer	2.0384888	-
W6RFF7	BN5_2052	RND multidrug efflux transporter	-	2.855334963
W6R2L0	BN5_2054	LysR family transcriptional regulator	2.044243	-
W6QXB4	BN5_2061	UTP--glucose-1-phosphate uridylyltransferase (UDP-glucose pyrophosphorylase)	-2.1613509	-
W6R2P7	BN5_2084	Copper-exporting P-type ATPase A	-4.2361784	-
W6R2Q3	BN5_2089	Uncharacterized protein	Exc.C_abs	Exc.C_Cons
W6QVZ2	BN5_2090	Copper-resistance protein CopA	-3.3650626	-3.628651067
W6QUS5	BN5_2093	Cytochrome c family protein	-3.0214338	-3.962286865
W6R2R0	BN5_2094	Uncharacterized protein	-58.640818	-13.15281776
W6QVZ5	BN5_2095	Outer membrane porin, OprD family	-5.324207	-8.775208068
W6QXE9	BN5_2096	Uncharacterized protein	-104.53435	-77.99447368
I7K7G1	BN5_2103	Transposase for insertion sequence element IS200	2.3149804	-
W6RFP0	BN5_2133	Esterase/lipase/thioesterase family protein	-	2.939804057
W6QW30	BN5_2141	Uncharacterized protein	-2.9989691	-3.20353925
W6RFR9	BN5_2158	Uncharacterized protein	-9.7449852	-4.712175701
W6QW47	BN5_2161	ABC transporter ATP-binding protein	2.0407508	-
W6RFS6	BN5_2163	Transcription elongation factor GreB (Transcript cleavage factor GreB)	-3.740065	-

W6RFW4	BN5_2173	Succinate--CoA ligase [ADP-forming] subunit alpha	-2.6824166	-2.226688889
W6RFX5	BN5_2183	Transposase for insertion sequence element IS200	2.3149804	Exc.Ana
W6QXP9	BN5_2187	Exonuclease	2.3030302	-
W6RFY0	BN5_2188	UPF0345 protein BN5_2188	-4.481764	-4.304463199
W6QXQ5	BN5_2197	Protease HtpX (Heat shock protein HtpX)	3.2356749	3.720165145
W6R343	BN5_2200	4,5-DOPA dioxygenase extradiol	-	Exc.C_Cons
W6RFZ1	BN5_2203	Putative protease SohB	2.1864141	2.55590344
W6R347	BN5_2205	Hydroxysteroid dehydrogenase-like protein 2	-4.5625277	-
W6QV85	BN5_2209	Putative membrane protein	2.3166391	2.895341123
W6QXR8	BN5_2212	PilL protein	2.0183364	2.105700132
W6RG01	BN5_2213	Enoyl-CoA hydratase/isomerase family protein	-	-2.316264488
W6QV90	BN5_2214	Putative Orn/Lys/Arg decarboxylase	3.0273035	-
W6QWC1	BN5_2216	Ribonuclease H (RNase H)	-3.3368573	-
W6RG04	BN5_2218	Hydroxyacylglutathione hydrolase (Glyoxalase II) (Glx II)	-2.1583069	-3.16403743
W6QV95	BN5_2219	Membrane-bound lytic murein transglycosylase D	Exc.C_abs	Exc.C_Cons
W6QXS8	BN5_2222	Peptide ABC transporter, periplasmic peptide-binding protein	-	-2.474436466
W6QWE3	BN5_2236	Uncharacterized protein	-2.6119911	-15.31039926
W6QXU2	BN5_2237	Putative 3-hydroxyacyl-CoA dehydrogenase	3.9137909	2.925601625
W6RG21	BN5_2238	Acetyl-CoA acyltransferase	2.454439	2.855585669
W6QXU7	BN5_2242	Rhodanese domain-containing protein	-2.2733713	-
W6R374	BN5_2245	Uncharacterized protein	4.2282529	-
W6QWF0	BN5_2246	Uncharacterized protein	2.7752159	-
W6QXV2	BN5_2247	Sensory box histidine kinase/response regulator	3.1427917	2.440257402
W6RG31	BN5_2248	Uncharacterized protein	2.285062	-
W6R378	BN5_2250	Uncharacterized protein	3.5031838	-
W6QWF4	BN5_2251	Coenzyme PQQ synthesis protein F	-	2.041882714
W6QXY2	BN5_2277	Methyl-accepting chemotaxis sensory transducer	2.0384888	-
W6QY04	BN5_2302	2-oxoglutaroyl-CoA hydrolase	-	-2.052620142
W6R3D5	BN5_2320	Uncharacterized protein	-	-2.198876636
W6R3E0	BN5_2326	50S ribosomal protein L20	-17.618266	-5.684762197
W6QWM4	BN5_2327	50S ribosomal protein L35	Exc.C_abs	Exc.C_Cons
W6QY22	BN5_2328	Translation initiation factor IF-3	-11.176268	-5.222232417
W6QVK2	BN5_2331	FAD dependent oxidoreductase	2.2308755	4.068254688
W6QY30	BN5_2339	Pyrroloquinoline-quinone synthase (Coenzyme PQQ synthesis protein C) (Pyrroloquinoline quinone biosynthesis protein C)	2.1780444	-
W6RGA4	BN5_2340	Coenzyme PQQ synthesis protein B (Pyrroloquinoline quinone biosynthesis protein B)	2.0947334	-
W6R3F0	BN5_2342	PQQ-containing dehydrogenase	-4.4023993	-9.400407732
W6QWN6	BN5_2343	Uncharacterized protein	-4.1444098	-
W6QVL9	BN5_2346	ABC transporter, solute binding prtotein	-2.5268266	-3.609736012
W6QY39	BN5_2349	Pentapeptide repeat-containing protein	-	-2.666843811
W6RGB3	BN5_2350	LuxR transcriptional regulator	2.2218067	-
W6RGB7	BN5_2355	Beta-propeller repeat protein	-	-2.708323361
W6QY47	BN5_2359	DNA-binding response regulator	4.3785909	2.177994031
W6RGC1	BN5_2360	Uncharacterized protein	Exc.C_abs	Exc.C_Cons
W6RGC5	BN5_2365	OmpA/MotB domain-containing protein	-	-2.314926947
W6QWR9	BN5_2378	DedD protein	-5.6011899	-5.439597862

W6QVQ2	BN5_2381	N-(5'-phosphoribosyl)anthranilate isomerase (PRAI)	-3.1240986	-3.089642683
W6RGE2	BN5_2385	Aspartate-semialdehyde dehydrogenase (ASA dehydrogenase) (ASADH) (Aspartate-beta-semialdehyde dehydrogenase)	-2.3217297	-2.17261619
W6R3I5	BN5_2387	3-isopropylmalate dehydratase small subunit (Alpha-IPM isomerase) (IPMI) (Isopropylmalate isomerase)	-2.3416087	-2.602022313
W6RGE6	BN5_2390	Putative sensory box GGDEF/EAL domain protein	4.6285597	-
W6QWT9	BN5_2403	Histone family protein DNA-binding protein	-	-2.152878149
W6QY84	BN5_2404	Uncharacterized protein	Exc.C_abs	Exc.C_Cons
W6R3L4	BN5_2417	TonB-dependent siderophore receptor	-	Exc.Ana
W6QWW5	BN5_2428	Uncharacterized protein	5.7189224	-
W6R3N9	BN5_2442	Cytochrome c oxidase, cbb3-type, subunit II	6.9246125	-
W6QYC1	BN5_2444	Cbb3-type cytochrome c oxidase subunit	3.2489345	-
W6RGJ0	BN5_2450	Cytochrome c oxidase accessory protein CcoH	-2.0703385	-2.446410776
W6R3Q1	BN5_2452	Cytochrome oxidase maturation protein, cbb3-type, CcoS	4.1567232	-
W6QWY9	BN5_2453	Uncharacterized protein	-	7.977048227
W6QYC8	BN5_2454	Coproporphyrinogen-III oxidase	2.9362334	-
W6QWZ4	BN5_2458	Ion transport protein	-	2.900362716
W6QVX9	BN5_2466	Uncharacterized protein	-	Exc.C_Cons
W6QX06	BN5_2468	Segregation and condensation protein A	2.2566145	-
W6R3S3	BN5_2472	YciI like Protein	-2.454337	-
W6RGL2	BN5_2475	Uncharacterized protein	34.29477	51.17308602
W6QYH4	BN5_2499	Uncharacterized protein	Exc.C_abs	Exc.C_Cons
W6RGN7	BN5_2500	Recombination protein RecR	-2.4780409	-2.714713594
W6QYH8	BN5_2504	Uncharacterized protein	-	Exc.Ana
W6R3W1	BN5_2507	Uncharacterized protein	3.5194094	-
W6QYI9	BN5_2514	Acyl-CoA dehydrogenase	2.067136	2.407050928
W6RGQ2	BN5_2515	Uncharacterized protein	-3.2061309	-
W6QW24	BN5_2516	Uncharacterized protein	Exc.C_abs	Exc.C_Cons
W6R3X8	BN5_2522	Cytochrome D ubiquinol oxidase subunit I	Exc.C_abs	Exc.C_Cons
W6QW33	BN5_2530	Uncharacterized protein	-3.1643884	-2.975832519
W6R3Z0	BN5_2536	Glutathione peroxidase	-2.0166117	-2.22622591
W6RGS0	BN5_2539	Uncharacterized protein	Exc.C_abs	-
W6QX86	BN5_2542	Aconitate hydratase (Aconitase)	-2.2324069	-2.911642712
W6QYL0	BN5_2543	Aerotaxis receptor	2.0384888	-
W6RGT2	BN5_2554	Uncharacterized protein	Exc.C_abs	Exc.C_Cons
W6QYM5	BN5_2558	Putative isochorismatase family protein yrdC	-	-2.139934541
W6RGT5	BN5_2559	Uncharacterized protein	3.455633	3.991368092
W6QW61	BN5_2565	Chromosome partition protein Smc	-	2.260068762
W6R427	BN5_2566	Uncharacterized HTH-type transcriptional regulator yncC	3.756485	3.564286566
W6QW66	BN5_2575	2-oxo-4-hydroxy-4-carboxy-5-ureidoimidazoline decarboxylase	-3.4675419	-2.671555521
W6RGY1	BN5_2609	Lipoprotein, putative	Exc.C_abs	Exc.C_Cons
W6QXG0	BN5_2612	Probable thiol:disulfide interchange protein dsbE-2	2.3775901	-
W6RH00	BN5_2629	Protein phosphatase CheZ (Chemotaxis protein CheZ)	2.4074959	2.945338264
W6R4A2	BN5_2631	RNA polymerase sigma factor FliA (RNA polymerase sigma factor for flagellar operon) (Sigma F) (Sigma-28)	-	-3.47791659

W6QWC4	BN5_2635	Flagellar biosynthetic protein flhB	2.8075207	2.371856399
W6RH14	BN5_2644	Hpt domain protein	-	2.664195589
W6RH27	BN5_2654	Uncharacterized protein	4.66098	5.176223817
W6QZ06	BN5_2678	Chemotaxis protein methyltransferase	-	-2.005784576
W6QXQ8	BN5_2682	Putative flagella synthesis protein FlgN	-4.2511898	-3.205242104
W6QZ36	BN5_2694	5-methyltetrahydropteroyltriglutamate--homocysteine methyltransferase (Cobalamin-independent methionine synthase) (Methionine synthase, vitamin-B12 independent isozyme)	4.6146887	6.40397052
W6QZ56	BN5_2714	Tyrosine recombinase xerC	-	-2.275352395
W6QXU6	BN5_2724	Putative beta-barrel assembly-enhancing protease	-	-2.634872831
W6QWR3	BN5_2727	Uncharacterized protein Mb1516	5.9801016	-
W6R4L4	BN5_2728	Uncharacterized protein	2.9682309	-
W6R4L6	BN5_2733	Putative membrane protein MJ1562	2.6983298	-
W6QXV5	BN5_2734	Ycf48-like protein	3.1331923	-
W6QZ71	BN5_2735	Uncharacterized protein PA3922	-	-2.094104349
W6QZA0	BN5_2773	Sensor protein PhoQ	2.8560739	2.233283908
W6RHN0	BN5_2774	Alkaline phosphatase synthesis transcriptional regulatory protein sphR	2.0402793	-
W6QWU9	BN5_2775	Uncharacterized protein	4.4321294	-
W6QZA5	BN5_2778	Protein napD	3.8259906	-
W6RHN5	BN5_2779	Nitrate reductase	-	-4.204885939
W6R4P8	BN5_2781	Cytochrome c-type protein	2.5648421	-
W6QXZ5	BN5_2782	Thiol-disulfide oxidoreductase resA	2.0288563	-
W6R4Q4	BN5_2786	Arsenate reductase	-2.6622265	-2.248401995
W6QY01	BN5_2787	NAD(P)H dehydrogenase (quinone) (NAD(P)H:quinone oxidoreductase) (NQO)	-2.1318905	-2.521997187
W6QZB9	BN5_2793	Phosphoribosylglycinamide formyltransferase (5'-phosphoribosylglycinamide transformylase) (GAR transformylase) (GART)	-2.4205809	-
W6RHP8	BN5_2794	Uncharacterized protein	-2.3516934	-2.696148574
W6RHR3	BN5_2804	Protein-L-isoaspartate O-methyltransferase (L-isoaspartyl protein carboxyl methyltransferase) (Protein L-isoaspartyl methyltransferase) (Protein-beta-aspartate methyltransferase) (PIMT)	2.5444138	-
W6QWX7	BN5_2805	5'-nucleotidase SurE (Nucleoside 5'-monophosphate phosphohydrolase)	-	-2.055135238
W6QY17	BN5_2807	2-C-methyl-D-erythritol 2,4-cyclodiphosphate synthase (MECDP-synthase) (MECPP-synthase) (MECPS)	-2.0474573	-2.268806126
W6RHT1	BN5_2814	Enolase (2-phospho-D-glycerate hydro-lyase) (2-phosphoglycerate dehydratase)	-2.4156867	-
W6R4U4	BN5_2831	Ribosome-recycling factor (RRF) (Ribosome-releasing factor)	-2.6965847	-
W6QZG2	BN5_2833	Elongation factor Ts (EF-Ts)	-2.1635993	-
W6QZG8	BN5_2838	Arsenate reductase glutaredoxin family protein	-3.10846	-2.386340646
W6QY53	BN5_2847	Uncharacterized protein	-3.2206086	-
W6QZH6	BN5_2848	Cold shock protein (Beta-ribbon, CspA family)	-4.5594717	-2.646159456
W6RHW6	BN5_2849	Uncharacterized protein	3.6379692	2.565606653

W6QX24	BN5_2850	ABC-type uncharacterized transport system involved in gliding motility auxiliary component-like protein	2.989215	2.898821836
W6R4W2	BN5_2851	ABC transporter, permease protein	3.391719	3.19983312
W6QY58	BN5_2852	Putative ABC-2 type transport system ATP-binding protein	2.8271204	2.391860638
W6QZH9	BN5_2853	Uncharacterized protein	-4.983675	-2.576971652
W6QZI6	BN5_2858	3-oxoacyl-(Acyl-carrier-protein) synthase III, putative	-2.1494487	-2.025296783
W6QY71	BN5_2867	Periplasmic protein-like protein	-2.5759775	-3.682417831
W6QZJ4	BN5_2868	Uncharacterized protein	4.0003697	5.44148341
W6RI05	BN5_2874	Uncharacterized protein	Exc.C_abs	Exc.C_Cons
W6QY80	BN5_2877	Acyl-CoA synthetase	2.702073	-
W6RI15	BN5_2879	MaoC-like domain protein	-4.1918875	-2.817274229
W6QZN5	BN5_2913	Putative signal transduction protein	-	-2.767084434
W6QYC2	BN5_2917	Outer membrane porin	2.5896133	-
W6QZP0	BN5_2918	Putative tricarboxylic transport membrane protein	-	-5.975806085
W6QX99	BN5_2930	Multicomponent K+:H+ antiporter subunit C	3.1883058	4.224185919
W6QZQ6	BN5_2933	Glycerate kinase	2.9654033	-
W6R536	BN5_2936	ProP effector	-14.65885	-6.360616772
W6QZR2	BN5_2938	N-ethylmaleimide reductase	-	-2.754292286
W6RI69	BN5_2939	Pyridoxine/pyridoxamine 5'-phosphate oxidase (PNP/PMP oxidase) (PNPOx) (Pyridoxal 5'-phosphate synthase)	-	-3.13514753
W6QXA7	BN5_2940	OmpA/MotB domain-containing protein	-7.9525819	-
W6R541	BN5_2941	Beta-lactamase	-	-2.112293048
W6QXB2	BN5_2945	Cation antiporter	3.4090427	-
W6QXB9	BN5_2950	Uncharacterized protein	Exc.C_abs	Exc.C_Cons
W6QZT5	BN5_2958	Uncharacterized protein	-2.7376411	-
W6RI90	BN5_2959	Water stress/hypersensitive response protein	2.6738095	2.235958379
W6RI94	BN5_2964	Isochorismatase hydrolase	-2.5887698	-2.31326947
W6QZU8	BN5_2968	Cold shock protein (Beta-ribbon, CspA family)	-9.007333	-4.082161708
W6QYH7	BN5_2972	Electron transport complex subunit B	Exc.C_abs	-
W6QZV3	BN5_2973	Electron transport complex subunit C	-2.377233	-
W6R581	BN5_2981	Dihydroorotase (DHOase)	-	-2.201977916
W6R587	BN5_2986	Uncharacterized protein	-2.5508298	-
W6QZX4	BN5_2993	Uracil-DNA glycosylase (UDG)	2.0526296	-
W6QZX9	BN5_2998	Acyl-CoA dehydrogenase	2.1284846	-
W6QXG9	BN5_3000	Enoyl-CoA hydratase/isomerase family protein	2.0058309	-
W6RIH2	BN5_3010	Methyl-accepting chemotaxis sensory transducer	2.0384888	-
W6QZZ4	BN5_3014	Putative PAS/PAC sensor protein	4.3100811	-
W6RIH7	BN5_3015	Superoxide dismutase [Cu-Zn]	-2.1141338	-
W6QXI4	BN5_3016	Glycine cleavage system H protein	-2.8931344	-
W6RII4	BN5_3025	Sel1 domain-containing protein	Exc.C_abs	Exc.C_Cons
W6R5D0	BN5_3027	ABC-type Fe3+ transport system periplasmic component-like protein	-2.3288537	-12.23537714
W6QXJ7	BN5_3031	ABC transporter, ATP-binding protein	-2.0523356	-
W6R5D5	BN5_3032	Phosphoserine phosphatase	2.5669704	-
W6R009	BN5_3034	Uncharacterized protein	2.5352886	-
W6QYP0	BN5_3038	Carboxyl-terminal protease	-3.8251951	-4.937565888
W6R020	BN5_3044	Peptidyl-prolyl cis-trans isomerase	-2.0587947	-

W6QYQ0	BN5_3050	Methylglyoxal synthase (MGS)	-2.3686198	-3.153338398
W6QXM0	BN5_3058	FMN-dependent NADH-azoreductase (Azo-dye reductase) (FMN-dependent NADH-azo compound oxidoreductase)	-	2.336145288
W6RIL1	BN5_3062	Peptidyl-prolyl cis-trans isomerase (PPIase)	-2.2572507	-3.015018108
W6R5H8	BN5_3069	Uncharacterized protein	-2.2971844	-
W6R045	BN5_3071	Phosphoketolase	2.3107588	-
W6RIL9	BN5_3072	Metallo-beta-lactamase family protein	2.7403623	-
W6RIM5	BN5_3083	MotA/TolQ/ExbB proton channel	2.3478388	2.81890202
W6R5J7	BN5_3085	Holliday junction ATP-dependent DNA helicase RuvB	2.2008589	-
W6R062	BN5_3087	Crossover junction endodeoxyribonuclease RuvC (Holliday junction nuclease RuvC) (Holliday junction resolvase RuvC)	Exc.C_abs	Exc.C_Cons
W6RIN3	BN5_3093	Cold-shock DNA-binding protein family protein	-	2.618849827
W6QYV0	BN5_3096	Porin D	3.4482555	-
W6QXQ4	BN5_3099	Uncharacterized protein	-4.7459602	-4.257185634
W6R5M0	BN5_3105	Uncharacterized protein	-5.1074388	-3.976594163
W6QXS7	BN5_3119	Putative quercetin 2,3-dioxygenase PA3240	-2.900671	-3.916830417
W6R0B8	BN5_3142	Peptidyl-prolyl cis-trans isomerase	-2.9589117	-
W6QXV7	BN5_3144	Response regulator receiver:metal-dependent phosphohydrolase, HD subdomain	-4.6099997	-
W6R5R4	BN5_3145	Chemotaxis sensory transducer	2.0384888	-
W6RIU4	BN5_3148	Uncharacterized protein	Exc.C_abs	Exc.C_Cons
W6QXW2	BN5_3149	UPF0114 protein BN5_3149	4.0484416	7.666917558
W6QXW9	BN5_3154	Uncharacterized protein	-	-3.864727427
W6QZ04	BN5_3156	Uncharacterized protein	-	-8.843392977
W6RIV3	BN5_3158	Putative phage integrase	Exc.C_abs	Exc.C_Cons
W6QY54	BN5_3194	Spermidine/putrescine import ATP-binding protein potA	2.147339	-
W6QZ88	BN5_3196	Cytokinin riboside 5'-monophosphate phosphoribohydrolase	-	-2.080576497
W6R0K6	BN5_3197	Uncharacterized protein	-	Exc.C_Cons
W6R5Z8	BN5_3200	Uncharacterized protein	-2.5447254	-4.258002116
W6QZD7	BN5_3251	Nitrilase/cyanide hydratase and apolipoprotein N-acyltransferase	-2.2860971	-2.623913208
W6RJ51	BN5_3253	GTPase Der (GTP-binding protein EngA)	-	2.490093647
W6QYB5	BN5_3259	Type IV pilus biogenesis/stability protei	-3.5330153	-4.663996373
W6QZE7	BN5_3261	Nucleoside diphosphate kinase (NDK) (NDP kinase) (Nucleoside-2-P kinase)	-2.139193	-2.142061646
W6R0Q3	BN5_3262	Uncharacterized protein	-3.5917825	-
W6RJ57	BN5_3263	2Fe-2S ferredoxin	-3.3719115	-
W6QZF2	BN5_3266	Iron-binding protein IscA	-6.2964268	-
W6R0Q7	BN5_3267	Iron-sulfur cluster assembly scaffold protein IscU	-4.8510599	-
W6RJ65	BN5_3273	Uncharacterized protein	-42.2304	-18.25234597
W6R648	BN5_3281	Uncharacterized protein	-9.6683297	-4.551893068
W6RJ69	BN5_3284	Permease YjgP/YjgQ family protein	2.117458	-
W6QZH0	BN5_3287	Uncharacterized protein	Exc.C_abs	Exc.C_Cons
W6R0S4	BN5_3288	Valine--tRNA ligase (Valyl-tRNA synthetase) (ValRS)	-2.1399345	-
W6R654	BN5_3291	Sodium/sulfate symporter	-	4.092634982
W6QZI3	BN5_3307	3-oxoacid CoA-transferase	13.424254	2.375777946
W6R0U1	BN5_3308	Butyryl-CoA:acetate CoA transferase	6.808939	2.78871403

W6RJ87	BN5_3309	Acetyl-CoA acetyltransferase	5.0265435	-
W6RJ95	BN5_3319	UspA domain-containing protein	3.42072	-
W6QYG8	BN5_3320	ATPase, P-type (Transporting), HAD superfamily, subfamily IC	2.8440497	-
W6R0V5	BN5_3323	NADH:flavin oxidoreductase/NADH oxidase	-	-2.346049305
W6RJA0	BN5_3324	Uncharacterized protein	2.026467	2.215092072
W6R686	BN5_3331	Arginine deiminase (ADI) (Arginine dihydrolase) (AD)	6.6064107	-
W6QZK4	BN5_3332	Ornithine carbamoyltransferase (OTCase)	5.6590766	-
W6R0W2	BN5_3333	Carbamate kinase	2.8561663	-
W6RJA6	BN5_3334	Uncharacterized protein	3.8098213	-
W6RJB1	BN5_3339	Uncharacterized protein	3.5301268	2.813436367
W6QZL1	BN5_3342	Putative glutamine amidotransferase	2.3438442	-
W6R0X0	BN5_3343	Uncharacterized protein	-4.1463541	-4.035022356
W6R697	BN5_3346	Ferrochelatase (Heme synthase) (Protoheme ferro-lyase)	-	-2.59781735
W6QYJ2	BN5_3350	Uncharacterized protein	Exc.C_abs	-
W6R6A1	BN5_3351	MerR family transcriptional regulator	Exc.C_abs	Exc.C_Cons
W6RJC3	BN5_3354	Short-chain dehydrogenase/reductase SDR	Exc.C_abs	Exc.C_Cons
W6QYJ6	BN5_3355	Amine oxidase	Exc.C_abs	Exc.C_Cons
W6QZM5	BN5_3357	Cyclopropane-fatty-acyl-phospholipid synthase	Exc.C_abs	Exc.C_Cons
W6QYL1	BN5_3372	50S ribosomal protein L25 (General stress protein CTC)	-2.2920418	-
W6R109	BN5_3396	Cyclic pyranopterin monophosphate synthase accessory protein (Molybdenum cofactor biosynthesis protein C)	-2.9711058	-3.590372008
W6QYN6	BN5_3408	NADH:flavin oxidoreductase/NADH oxidase	-	-4.215235787
W6QZT6	BN5_3420	Type IV pilus assembly protein PilW	Exc.C_abs	Exc.C_Cons
W6R129	BN5_3421	Type IV pilus assembly protein PilX	Exc.C_abs	Exc.C_Cons
W6RJH5	BN5_3422	Putative Tfp pilus assembly protein	-2.027919	-2.417082417
W6QYP8	BN5_3423	Fimbrial protein pilin	-5.4648618	-6.680633895
W6R134	BN5_3426	Uncharacterized protein	-6.0913767	-
W6QYQ2	BN5_3428	Lipoprotein signal peptidase (Prolipoprotein signal peptidase) (Signal peptidase II) (SPase II)	-	6.796820394
W6RJI2	BN5_3432	30S ribosomal protein S20	-19.396171	-10.21652975
W6QYQ6	BN5_3433	Uncharacterized protein	-2.438961	-
W6RJJ1	BN5_3442	Mechanosensitive ion channel	-	2.238191274
W6R6K4	BN5_3459	Cell division protein FtsQ	Exc.C_abs	Exc.C_Cons
W6RJL8	BN5_3467	UDP-N-acetylmuramoyl-L-alanyl-D-glutamate--2,6-diaminopimelate ligase (Meso-A2pm-adding enzyme) (Meso-diaminopimelate-adding enzyme) (UDP-MurNAc-L-Ala-D-Glu:meso-diaminopimelate ligase) (UDP-MurNAc-tripeptide synthetase) (UDP-N-acetylmuramyl-tripeptide synthetase)	-2.2092142	-2.816688454
W6QYU2	BN5_3468	Peptidoglycan synthetase FtsI	Exc.C_abs	Exc.C_Cons
W6R6L3	BN5_3469	Cell division protein FtsL	-3.8313823	-
W6R184	BN5_3476	Transport-associated	2.8715573	-
W6RJN2	BN5_3482	30S ribosomal protein S9	-7.312172	-3.636120473
W6QYV7	BN5_3483	50S ribosomal protein L13	-3.798597	-3.128562662
W6R000	BN5_3485	Acyl-CoA dehydrogenase domain-containing protein	2.7629255	2.719120336
W6R6N0	BN5_3489	Alpha/beta fold family hydrolase-like protein	-	2.062408336
W6R6N7	BN5_3494	2-alkenal reductase	-4.1733666	-4.281585099

W6R1A2	BN5_3496	Histidinol dehydrogenase (HDH)	-2.3200673	-2.1271179
W6R6P1	BN5_3499	BolA family protein	-4.8791618	-
W6R1A7	BN5_3501	Toluene tolerance family protein	-2.2724785	-
W6R017	BN5_3505	Arabinose 5-phosphate isomerase (API)	-2.646404	-
W6R1B1	BN5_3506	3-deoxy-D-manno-octulosonate 8-phosphate phosphatase	-3.7853237	-3.686836231
W6R1B7	BN5_3511	SSU ribosomal protein S30P / sigma 54 modulation protein	-2.4996048	-
W6QYZ1	BN5_3523	Lytic murein transglycosylase	-3.8429122	-4.982258927
W6R6U6	BN5_3549	Putative lipoprotein	Exc.C_abs	Exc.C_Cons
W6R064	BN5_3550	Transcriptional regulator, XRE family	-	-4.365302608
W6RJY0	BN5_3562	Uncharacterized protein	-	2.333124563
W6QZ32	BN5_3568	Uncharacterized protein	Exc.C_abs	Exc.C_Cons
W6R6X2	BN5_3569	Rare lipoprotein A	-7.9423173	-8.397888693
W6R085	BN5_3570	Lytic murein transglycosylase B	-6.9837407	-10.24276514
W6R1H2	BN5_3571	Rod shape-determining protein rodA	Exc.Ana	Exc.Ana
W6RJY9	BN5_3572	Peptidoglycan glycosyltransferase	Exc.C_abs	Exc.C_Cons
W6R6X7	BN5_3574	Ribosomal silencing factor RsfS	-2.8442863	-
W6RK00	BN5_3582	Dehydratase	2.0611269	-
W6R0A3	BN5_3590	Fatty-acyl-CoA synthase	5.441232	3.899709524
W6R1I7	BN5_3591	Uncharacterized protein	11.87859	8.41551561
W6RK11	BN5_3592	Acyl-CoA dehydrogenase family protein	5.4181487	4.146325374
W6R1J6	BN5_3601	Inorganic pyrophosphatase (Pyrophosphate phospho-hydrolase) (PPase)	-2.8211173	-2.559389996
W6R1K4	BN5_3611	Phosphate-selective porin O and P superfamily	2.4617882	-
W6RK34	BN5_3617	4-oxalocrotonate decarboxylase	4.5960675	2.506023598
W6QZ86	BN5_3618	4-hydroxy-2-oxovalerate aldolase (HOA) (4-hydroxy-2-keto-pentanoic acid aldolase) (4-hydroxy-2-oxopentanoate aldolase)	3.5416214	-
W6R0D0	BN5_3620	2-oxypent-4-enoate hydratase	6.2395414	-
W6QZ93	BN5_3623	Transcriptional regulator, MarR family	2.5004712	2.371335842
W6RK53	BN5_3632	Alpha/beta hydrolase fold	Exc.Ana	-
W6R745	BN5_3634	B12 family TonB-dependent receptor	2.6569419	2.564006643
W6R1N2	BN5_3636	Uncharacterized protein	4.9186305	5.382264658
W6RK60	BN5_3637	GTP cyclohydrolase-2 (GTP cyclohydrolase II)	-2.1752783	-
W6QZA9	BN5_3638	Aspartyl protease-like protein	Exc.C_abs	Exc.C_Cons
W6RK65	BN5_3642	N utilization substance protein B homolog (Protein NusB)	-4.4299794	-2.266134253
W6RK74	BN5_3647	Transcriptional repressor NrdR	2.5011646	2.945202164
W6QZC1	BN5_3648	Uncharacterized protein	Exc.C_abs	Exc.C_Cons
W6R1P6	BN5_3651	Uncharacterized protein	2.040515	-
W6RK79	BN5_3652	Uncharacterized protein	-2.9986227	-
W6RK87	BN5_3657	Protein TonB	-	3.780433473
W6R770	BN5_3659	MotA/TolQ/ExbB proton channel	-	Exc.Ana
W6R0H4	BN5_3660	MotA/TolQ/ExbB proton channel	8.6398125	13.70502765
W6R1Q7	BN5_3661	Uncharacterized protein	3.9007909	11.15253677
W6RK91	BN5_3662	OmpW family outer membrane protein	5.3404698	-2.03632335
W6QZE8	BN5_3668	Bacterioferritin	3.3840088	2.689491321
W6R0I3	BN5_3670	50S ribosomal protein L17	-34.341155	-8.14661088
W6RKA2	BN5_3672	30S ribosomal protein S4	-3.3974838	-

W6QZF3	BN5_3673	30S ribosomal protein S11	-7.4492749	-2.468326658
W6R788	BN5_3674	30S ribosomal protein S13	-6.6827103	-2.983763799
W6RKA7	BN5_3677	50S ribosomal protein L15	-32.616574	-8.182074462
W6QZF8	BN5_3678	50S ribosomal protein L30	-4.1491045	-3.723174754
W6R793	BN5_3679	30S ribosomal protein S5	-5.328145	-
W6R0J3	BN5_3680	50S ribosomal protein L18	-9.2933581	-3.993904953
W6R1S9	BN5_3681	50S ribosomal protein L6	-2.0584618	-
W6RKB4	BN5_3682	30S ribosomal protein S8	-5.2522418	-4.029870095
W6QZG6	BN5_3683	30S ribosomal protein S14	-41.693002	-15.54846226
W6R0J9	BN5_3685	50S ribosomal protein L24	-35.860739	-11.12756996
W6RKD3	BN5_3687	30S ribosomal protein S17	-2.551714	-
W6QZJ6	BN5_3688	50S ribosomal protein L29	-4.4777273	-5.35158657
W6R7B8	BN5_3689	50S ribosomal protein L16	-16.938098	-4.644746952
W6R1W4	BN5_3691	50S ribosomal protein L22	-15.67507	-6.233028604
W6RKF0	BN5_3692	30S ribosomal protein S19	-108.98356	-32.00887351
W6QZL4	BN5_3693	50S ribosomal protein L2	-19.03347	-6.361792573
W6R7C1	BN5_3694	50S ribosomal protein L23	-9.6806237	-3.423882834
W6R1Y1	BN5_3696	50S ribosomal protein L3	-2.2154504	-
W6RKF5	BN5_3697	30S ribosomal protein S10	-3.9738388	-3.640744082
W6R7C5	BN5_3699	Elongation factor G (EF-G)	-2.1271179	-
W6R0P2	BN5_3700	30S ribosomal protein S7	-8.3969574	-6.335828714
W6R1Y8	BN5_3701	30S ribosomal protein S12	-24.899301	-6.353713333
W6R7C9	BN5_3704	50S ribosomal protein L7/L12	-2.3275304	-
W6R1Z2	BN5_3706	50S ribosomal protein L1	-2.9892841	-2.052003701
W6RKG0	BN5_3707	50S ribosomal protein L11	-2.1436955	-
W6R7D0	BN5_3709	Protein translocase subunit SecE	2.1763843	2.589415835
W6R7D8	BN5_3728	Anhydro-N-acetylmuramic acid kinase (AnhMurNAc kinase)	2.7771081	2.176203292
W6R0R1	BN5_3729	Iron-sulfur cluster insertion protein ErpA	-4.4098615	-
W6RKH2	BN5_3731	Uncharacterized protein	-3.7763828	-5.778806916
W6R209	BN5_3735	Alanine racemase 1	2.8688715	-
W6R7E7	BN5_3743	Indole-3-glycerol phosphate synthase (IGPS)	-2.4834287	-2.069668918
W6R216	BN5_3745	Anthranilate synthase, component II	-	-2.75993317
W6RKJ4	BN5_3761	Extracellular solute-binding protein	-7.1691397	-5.577556927
W6RKJ6	BN5_3766	DnaJ like chaperone protein	-	Exc.C_Cons
W6R7H3	BN5_3773	Protein ApaG	-2.1433488	-
W6R245	BN5_3775	Thiosulfate sulfurtransferase GlpE	-2.8451407	-
W6RKK5	BN5_3776	Putative serine protein kinase, PrkA	3.0962029	-
W6R0V6	BN5_3784	30S ribosomal protein S21	-83.896187	-37.55847724
W6RKL9	BN5_3807	Uncharacterized protein	Exc.C_abs	Exc.C_Cons
W6R7L0	BN5_3819	Uncharacterized protein	Exc.C_abs	Exc.C_Cons
W6R293	BN5_3821	Transcriptional regulator, putative	-5.1770611	-2.977772079
W6QZX0	BN5_3828	Uncharacterized protein	Exc.C_abs	Exc.C_Cons
W6QZY6	BN5_3848	Uncharacterized protein	Exc.C_abs	Exc.C_Cons
W6R105	BN5_3850	Protease	Exc.C_abs	Exc.C_Cons
W6R7P2	BN5_3864	Putative secreted protein	-	Exc.C_Cons
W6R016	BN5_3888	Diguanylate cyclase	Exc.Ana	-
W6R2F9	BN5_3891	TRAP dicarboxylate transporter, DctP subunit	-3.2252999	-4.18028122
W6R2G4	BN5_3896	NADPH:quinone oxidoreductase 1	-	-2.580946077

W6RKR8	BN5_3897	TetR family transcriptional regulator	Exc.C_abs	Exc.C_Cons
W6R7R9	BN5_3899	Endonuclease I	-	-4.239311565
W6R2H4	BN5_3906	Acyl-CoA dehydrogenase domain-containing protein	5.6362411	4.271570717
W6R155	BN5_3910	Acyl-CoA dehydrogenase domain-containing protein	5.6362411	4.271570717
W6RKS6	BN5_3912	Uncharacterized protein	-	-4.450908985
W6RKS8	BN5_3917	Biotin synthase	-2.4971803	-
W6R7T9	BN5_3924	Putative acetyltransferase	-4.2302903	-4.310305123
W6R168	BN5_3925	Malate synthase G	-3.6847498	-3.142980526
W6R7X3	BN5_3959	Uncharacterized protein	-2.6890564	-4.455950893
W6R7Y2	BN5_3969	Pyrroline-5-carboxylate reductase (P5C reductase) (P5CR) (PCA reductase)	-2.2769985	-2.130167189
W6R1B4	BN5_3970	Uncharacterized protein	3.8124013	5.536867508
W6R2Q7	BN5_3971	UPF0235 protein BN5_3971	Exc.C_abs	Exc.C_Cons
W6R1B8	BN5_3975	Uncharacterized protein	-3.8641024	-4.599998317
W6R2R2	BN5_3976	Non-canonical purine NTP pyrophosphatase (Non-standard purine NTP pyrophosphatase) (Nucleoside-triphosphate diphosphatase) (Nucleoside-triphosphate pyrophosphatase) (NTPase) (Nucleotide diphosphatase)	-2.8503386	-
W6R7Z4	BN5_3979	Uncharacterized protein	-	-3.20198526
W6R2R8	BN5_3981	Thiazole synthase	-	-2.219703019
W6RKX0	BN5_3982	Uncharacterized protein	-2.0463695	-
W6R0A5	BN5_3988	Methionine import ATP-binding protein metN	4.5841524	3.249865474
W6RKY3	BN5_3997	Aldehyde dehydrogenase	4.7235341	3.445627318
W6R814	BN5_3999	Oxidoreductase, GMC family	2.8723801	2.46080442
W6RKY6	BN5_4002	Gamma-glutamyltranspeptidase	-	-2.14979635
W6R819	BN5_4004	Uncharacterized protein	Exc.C_abs	Exc.C_Cons
W6R0C3	BN5_4008	UPF0064 protein yccW	-2.2613746	-2.018569602
W6R1F1	BN5_4010	Spermidine/putrescine-binding periplasmic protein 1	-	-5.813068866
W6R1G0	BN5_4020	Lactoylglutathione lyase	-	-3.180234906
W6R844	BN5_4034	Uncharacterized protein	-	3.921475717
W6R2Y6	BN5_4036	Ribose-5-phosphate isomerase A (Phosphoriboisomerase A) (PRI)	-3.557425	-3.151051499
W6R1H7	BN5_4040	Uncharacterized protein yjiK	-	-2.025147047
W6R1I9	BN5_4055	Protein-export protein SecB	-2.9792861	-2.284586921
W6R302	BN5_4056	Glutaredoxin-C6	-3.8470876	-
W6R1J4	BN5_4060	Glycyl-glycine endopeptidase ALE-1	-3.5907827	-6.110109917
W6R307	BN5_4061	Carboxyl-terminal protease	-2.0189427	-2.130364067
W6RL49	BN5_4062	Uncharacterized protein	-	-2.104970478
W6R0I0	BN5_4063	Uncharacterized protein	-2.5854224	-3.418981619
W6R312	BN5_4066	1-(5-phosphoribosyl)-5-[(5-phosphoribosylamino)methylideneamino] imidazole-4-carboxamide isomerase (Phosphoribosylformimino-5-aminoimidazole carboxamide ribotide isomerase)	-2.4407649	-
W6R0J1	BN5_4073	Probable Fe(2+)-trafficking protein	-3.6345246	-
W6R0J6	BN5_4079	Membrane-bound lytic murein transglycosylase F	-	-2.100840548
W6RL79	BN5_4094	Uncharacterized protein	Exc.C_abs	Exc.C_Cons
W6R8A0	BN5_4096	Phasin-like protein	14.360161	-
W6R1M3	BN5_4097	Poly(3-hydroxyalkanoate) synthetase	3.4845765	-2.280526076
W6R342	BN5_4098	Phosphate acetyl/butaryl transferase	3.8160586	-

W6RL83	BN5_4099	Acetate kinase (Acetokinase)	3.1715102	-3.176680509
W6R1N0	BN5_4102	Transcription activator in PHB biosynthesis, AraC family	3.2977225	-
W6R346	BN5_4103	Acetoacetyl-CoA reductase	6.1951247	-
W6RL89	BN5_4104	Acetyl-CoA acetyltransferase	5.0265435	-
W6R0M2	BN5_4105	Poly(R)-hydroxyalkanoic acid synthase, class I	4.6705636	-
W6R8B1	BN5_4106	Secretion protein HlyD family protein	3.5004329	-
W6R1N4	BN5_4107	Putative ABC transporter ATP-binding protein yhiH	2.9925389	-
W6R351	BN5_4108	Putative ABC transporter ATP-binding protein yhiH	4.1853163	-
W6R0M7	BN5_4110	Uncharacterized lipoprotein ygdI	-	-4.343726698
W6R358	BN5_4113	Uncharacterized protein	Exc.C_abs	Exc.C_Cons
W6R384	BN5_4139	Sensor histidine kinase	-	2.789577565
W6RLC1	BN5_4140	Acetoacetate metabolism regulatory protein atoC	2.058985	-
W6R0R2	BN5_4141	C4-dicarboxylate-binding periplasmic protein	-2.3636777	-4.154476414
W6R8F5	BN5_4147	General secretion pathway protein E	3.3646117	2.159803408
W6R1T3	BN5_4158	Sulfate-binding protein	-4.7084972	-5.219216808
W6RLE3	BN5_4165	Antioxidant, AhpC/Tsa family	-3.7419752	-2.304786848
W6R1U4	BN5_4168	Two-component system sensor protein	-	2.637680824
W6R1W0	BN5_4183	Sulfate-binding protein	Exc.C_abs	Exc.C_Cons
W6R8K1	BN5_4192	Uncharacterized protein	-	-4.176516102
W6R1X7	BN5_4198	Laminin subunit gamma-1	2.0384888	-
W6R8N2	BN5_4202	50S ribosomal protein L33	-16.765226	-7.992979191
W6R202	BN5_4203	50S ribosomal protein L28	-7.8178216	-3.197918858
W6R3H6	BN5_4204	Heme-binding protein A	-	-2.459218631
W6RLL0	BN5_4205	DNA repair protein radC homolog	5.2237409	3.975556068
W6R218	BN5_4208	Deoxyuridine 5'-triphosphate nucleotidohydrolase (dUTPase) (dUTP pyrophosphatase)	-2.3734188	-2.758084517
W6R131	BN5_4211	Keratin, type II cytoskeletal 75	-2.0040706	-
W6R3K3	BN5_4214	Uncharacterized protein	4.0230788	6.104190557
W6RLL5	BN5_4215	Ribonuclease PH (RNase PH) (tRNA nucleotidyltransferase)	-2.3803384	-
W6R8R7	BN5_4217	Guanylate kinase (GMP kinase)	-2.072157	-2.742769403
W6R230	BN5_4218	DNA-directed RNA polymerase subunit omega (RNAP omega subunit) (RNA polymerase omega subunit) (Transcriptase subunit omega)	-5.1357204	-3.376667209
W6R3K8	BN5_4219	Guanosine-3',5'-bis(Diphosphate) 3'-pyrophosphohydrolase	2.0219771	-
W6RLM0	BN5_4220	UPF0076 protein PH0854	-2.1155508	-
W6R3L7	BN5_4229	Uncharacterized protein	-3.2901803	-
W6RLM7	BN5_4230	Integration host factor subunit alpha	-2.3845218	-3.785279944
W6R267	BN5_4258	Uncharacterized protein	-	2.325863881
W6R172	BN5_4261	Sulfatase-modifying factor 1	-2.0462277	-2.130659419
W6R3P5	BN5_4264	PpkA-related protein	-2.303935	-2.462516401
W6R8V3	BN5_4272	Uncharacterized protein	2.6568375	-
W6RLQ8	BN5_4275	31 kDa immunogenic protein	-	-2.362039897
W6R8V9	BN5_4277	Uncharacterized protein	-	-3.31099921
W6R287	BN5_4278	Uncharacterized protein	Exc.Ana	-
W6R3Q9	BN5_4279	Aerotaxis receptor	2.0384888	-
W6R3R9	BN5_4289	Uncharacterized protein	-5.5303981	-2.593589221
W6R3S5	BN5_4294	Uncharacterized protein	2.2118701	-

W6R2B9	BN5_4313	Putative exported oxidoreductase subunit	-	-2.336798494
W6R3U8	BN5_4314	Putative oxidoreductase subunit	-	-2.902440851
W6R1C9	BN5_4326	D-methionine-binding lipoprotein metQ	-3.1468317	-2.450767005
W6R3W3	BN5_4329	Uncharacterized protein	-	2.06133645
W6RLW0	BN5_4335	UPF0039 protein	-2.1582321	-2.330947752
W6R1F7	BN5_4356	Antitoxin	-2.420827	-
W6R1G2	BN5_4361	Uncharacterized protein	Exc.Ana	-
W6R936	BN5_4362	Uncharacterized protein in lpd-3 5'region	Exc.C_abs	Exc.C_Cons
W6R2G7	BN5_4368	Cyclopropane-fatty-acyl-phospholipid synthase	2.7567721	-
W6R2I3	BN5_4383	Uncharacterized protein PYRAB12460	-2.6011387	-
W6R420	BN5_4384	Putative oxidoreductase	2.7529912	-
W6R955	BN5_4387	Rhizobactin receptor	4.1293175	Exc.Ana
W6R1I6	BN5_4391	Alkyl hydroperoxide reductase AhpD	-	-2.080408254
W6RM13	BN5_4400	Precorrin-4 C11-methyltransferase	-2.3785131	-
W6R2K3	BN5_4403	Methionine aminopeptidase (MAP) (MetAP) (Peptidase M)	3.467558	2.539656419
W6RM20	BN5_4410	Probable transcriptional regulator ycf27	-4.7867064	-3.632509741
W6R2L7	BN5_4413	Porin D	-5.324207	-8.775208068
W6R2N9	BN5_4433	Peptide methionine sulfoxide reductase MsrB (Peptide-methionine (R)-S-oxide reductase)	-4.8100993	-3.305724893
W6R473	BN5_4434	Peptide methionine sulfoxide reductase MsrA (Protein-methionine-S-oxide reductase) (Peptide-methionine (S)-S-oxide reductase) (Peptide Met(O) reductase)	-6.4358617	-3.872145953
W6R9A9	BN5_4442	Uncharacterized protein	2.1266756	-
W6R2R6	BN5_4453	Uncharacterized protein	-	-2.289448321
W6R2S9	BN5_4463	Spermidine/putrescine-binding periplasmic protein	Exc.C_abs	Exc.C_Cons
W6R1Q1	BN5_4471	Uncharacterized protein	-2.3551735	-
W6R9E0	BN5_4472	Uncharacterized protein	-2.082813	-
W6RM71	BN5_4475	Periplasmic mercury ion-binding protein	-3.3672403	-7.872926448
W6R9F0	BN5_4482	Transposition protein TniB	2.2151433	-
W6R1T2	BN5_4501	ATP synthase subunit b (ATP synthase F(0) sector subunit b) (ATPase subunit I) (F-type ATPase subunit b) (F-ATPase subunit b)	2.4341757	3.192898445
W6R2X6	BN5_4513	50S ribosomal protein L34	-191.75827	-39.26698707
G9HWE9	PPSAL_0901	Ferric uptake regulation protein (Ferric uptake regulator) (Fur family transcriptional regulator)	-	2.071104

Annexes

Annex I

Biełło, K.A.; Cabello, P.; Rodríguez-Caballero, G.; Sáez, L.P.; Luque-Almagro, V.M.; Roldán, M.D.; Olaya-Abril, A.; Moreno-Vivián, C. Proteomic Analysis of Arsenic Resistance during Cyanide Assimilation by *Pseudomonas pseudoalcaligenes* CECT 5344. *International Journal of Molecular Sciences* (2023), *24*:7232. doi:10.3390/ijms24087232.

Annex II

Biełło, K.A.; Olaya-Abril, A.; Cabello, P., Rodríguez-Caballero, G.; Sáez, L.P.; Moreno-Vivián, C.; Luque-Almagro, V.M.; Roldán, M.D. Quantitative proteomic analysis of cyanide and mercury detoxification by *Pseudomonas pseudoalcaligenes* CECT 5344. *Microbiology Spectrum* (2023), *11*:e0055323. doi:10.1128/spectrum.00553-23.

International Journal of
Molecular Sciences

MDPI

Article

Proteomic Analysis of Arsenic Resistance during Cyanide Assimilation by *Pseudomonas pseudoalcaligenes* CECT 5344

Karolina A. Biełło [1,†], Purificación Cabello [2,†], Gema Rodríguez-Caballero [1], Lara P. Sáez [1], Víctor M. Luque-Almagro [1], María Dolores Roldán [1], Alfonso Olaya-Abril [1,*] and Conrado Moreno-Vivián [1]

[1] Departamento de Bioquímica y Biología Molecular, Edificio Severo Ochoa, Campus de Rabanales, Universidad de Córdoba, 14071 Córdoba, Spain; karolinabiello@gmail.com (K.A.B.); b42lualv@uco.es (V.M.L.-A.); bb2rorum@uco.es (M.D.R.); bb1movic@uco.es (C.M.-V.)
[2] Departamento de Botánica, Ecología y Fisiología Vegetal, Edificio Celestino Mutis, Campus de Rabanales, Universidad de Córdoba, 14071 Córdoba, Spain; bv1cahap@uco.es
* Correspondence: b22olaba@uco.es
† These authors contributed equally to this work.

Abstract: Wastewater from mining and other industries usually contains arsenic and cyanide, two highly toxic pollutants, thereby creating the need to develop bioremediation strategies. Here, molecular mechanisms triggered by the simultaneous presence of cyanide and arsenite were analyzed by quantitative proteomics, complemented with qRT-PCR analysis and determination of analytes in the cyanide-assimilating bacterium *Pseudomonas pseudoalcaligenes* CECT 5344. Several proteins encoded by two *ars* gene clusters and other Ars-related proteins were up-regulated by arsenite, even during cyanide assimilation. Although some proteins encoded by the *cio* gene cluster responsible for cyanide-insensitive respiration decreased in the presence of arsenite, the nitrilase NitC required for cyanide assimilation was unaffected, thus allowing bacterial growth with cyanide and arsenic. Two complementary As-resistance mechanisms were developed in this bacterium, the extrusion of As(III) and its extracellular sequestration in biofilm, whose synthesis increased in the presence of arsenite, and the formation of organoarsenicals such as arseno-phosphoglycerate and methyl-As. Tetrahydrofolate metabolism was also stimulated by arsenite. In addition, the ArsH2 protein increased in the presence of arsenite or cyanide, suggesting its role in the protection from oxidative stress caused by both toxics. These results could be useful for the development of bioremediation strategies for industrial wastes co-contaminated with cyanide and arsenic.

Keywords: arsenic resistance; biofilm; cyanide assimilation; quantitative proteomics; *Pseudomonas pseudoalcaligenes*

Citation: Biełło, K.A.; Cabello, P.; Rodríguez-Caballero, G.; Sáez, L.P.; Luque-Almagro, V.M.; Roldán, M.D.; Olaya-Abril, A.; Moreno-Vivián, C. Proteomic Analysis of Arsenic Resistance during Cyanide Assimilation by *Pseudomonas pseudoalcaligenes* CECT 5344. *Int. J. Mol. Sci.* **2023**, *24*, 7232. https://doi.org/10.3390/ijms24087232

Academic Editor: Rosa María Martínez-Espinosa

Received: 9 March 2023
Revised: 12 April 2023
Accepted: 13 April 2023
Published: 13 April 2023

1. Introduction

The biogeochemical cycle of arsenic (As), a metalloid widely distributed in the lithosphere, encompasses both natural and anthropic processes [1–4]. Due to human activities, arsenic can reach molar range concentrations in gold mining effluents [5], where other toxic pollutants such as cyanide and heavy metals are also present. Arsenic is considered a serious environmental pollutant that is highly toxic to humans [6–8]. In fact, arsenic-contaminated groundwater caused the largest poisoning in human history in Bangladesh [9].

Microbes may transform arsenic into different inorganic and organic forms [10]. Trivalent arsenite and pentavalent arsenate are the most abundant inorganic forms, with As(III) being 100 times more toxic than As(V) [4]. Arsenate toxicity is mainly derived from its ability to compete with phosphate oxyanions for both transport and energetic functions [11], whereas arsenite binds to sulfhydryl groups of proteins and biomolecules such as glutathione and lipoic acid [1]. Both forms enter adventitiously into the cells through different

uptake systems [12]. Thus, arsenate is a phosphate analog that uses the phosphate permeases, whereas the internalization of arsenite may occur through aquaglyceroporins, such as GlpF in *E. coli* and AqpS in *Sinorhizobium meliloti* [13]. Organic arsenical compounds, such as monomethy larsenate (MMAV), dimethy larsenate (DMAV), and trimethylarsine (TMA), also occur in nature. These methyl arsenicals are usually less toxic than their inorganic counterparts, except for the highly toxic trivalent derivatives monomethy larsenite (MMAIII) and dimethylarsenite (DMAIII) [14].

Ancient and ongoing exposure to arsenic has allowed the evolution or acquisition of various arsenic resistance systems in microorganisms, but with different degrees of efficiency [15,16]. A common strategy for tolerating inorganic arsenic is its extrusion from the cytosol [12,17], although other mechanisms have been also described, such as intracellular chelation by metal-binding peptides [18], bioaccumulation [19], immobilization, and transformation to potentially less toxic organic forms [20]. Prokaryotes show the greatest metabolic diversity with respect to arsenic metabolism, which is the detoxification pathway encoded by the *ars* genes most widely distributed among bacteria and archaea [16,21–24]. The As-resistance systems (Ars) require at least three components: an arsenite-responsive regulatory protein (ArsR), an efflux pump (ArsB), and an arsenate reductase (ArsC), although other *ars* genes are also included in some microbial *ars* gene clusters [25]. ArsR is a repressor that, after binding arsenite, dissociates from the promoter region to allow transcription of structural *ars* genes [26]. ArsB is a transmembrane protein that mediates arsenite export to the extracellular media [27]. The ATPase ArsA may form a complex with ArsB to yield a high-efficiency ATP-driven efflux pump. Additionally, the permease Acr3 may be present or replace the ArsB efflux pump [28]. The arsenate reductase ArsC transforms As(V) into As(III), which is extruded by the efflux pump. Depending on the electron donor used, two unrelated types of arsenate reductases are found, glutaredoxin- and thioredoxin-dependent ArsC [16,23].

Microbial formation of organoarsenicals, mainly by methylation, has also an important role in the arsenic biogeochemical cycle [16,21,23]. Arsenic methylation is usually considered a detoxification mechanism, but when toxic methyl-As(III) derivatives such as MMAIII or DMAIII are formed, demethylation may be part of the detoxification process [29]. Bacterial organoarsenical detoxification proteins include the *S*-adenosylmethionine (SAM)-dependent methyltransferase ArsM, which may have both methylating and demethylating activity, the NADPH-dependent FMN reductase ArsH, a protein that reduces ferric and chromate ions and shows methyl arsenite oxidase activity to confer resistance to methyl-As(III) derivatives, but also protects from oxidative damage caused by exposure to As [25], the permease ArsP that confers tolerance to MMAIII and DMAIII, and the non-heme iron-dependent dioxygenase ArsI, which shows C-As lyase activity [30]. Arsenic resistance in *Pseudomonas aeruginosa* DK2 involves the *gapdh* and *arsJ* gene products. The glyceraldehyde-3-phosphate dehydrogenase GAPDH uses arsenate, an inorganic phosphate analog, to form 1-arseno-3-phosphoglycerate, and this unstable organoarsenical compound is extruded by ArsJ, a major facilitator superfamily (MFS) permease, before its dissociation into As(V) and 3-phosphoglycerate [31].

Arsenic and cyanide are usually co-contaminants of industrial wastewater from mining and other industries. Environments co-contaminated with different metals or chemicals are less understood, and more difficult to remediate than single-polluted systems [32]. Although As-resistance has been well characterized in different bacteria, the capability to tolerate and detoxify arsenic in the presence of cyanide has not been studied yet. In this work, the first holistic approach combining quantitative proteomics and qRT-PCR transcriptional analysis of relevant genes was carried out to characterize arsenic and cyanide detoxification in *Pseudomonas pseudoalcaligenes* CECT 5344, a bacterium isolated from the sludges of the Guadalquivir River (Córdoba, Spain) that can grow with cyanide, cyanate, 3-cyano alanine and other nitriles, and industrial residues containing cyanide and metals [33–36]. In this strain, the cyanide-insensitive respiration and the cyanide assimilation pathway are linked. Thus, the alternative oxidase CioAB encoded by the *cio* gene

cluster is coupled to malate:quinone oxidoreductase that oxidizes malate to oxalacetate, which reacts with cyanide forming a 2-hydroxy nitrile. This nitrile is further hydrolyzed by the nitrilase NitC encoded by the *nit1C* gene cluster, generating ammonium used as a nitrogen source for growth [34]. The genome of this strain was completely sequenced [37,38], and omic studies on the cyanide assimilation were previously performed [39–44], making this bacterium a suitable model to develop system and synthetic biology strategies for bioremediation of residues co-contaminated with cyanide and arsenic [45]. Knowledge of the mechanisms involved in the resistance and detoxification of arsenic and cyanide is essential for the bioremediation of mining wastes and systems polluted with both contaminants.

2. Results and Discussion

2.1. Bioinformatic Analysis of Arsenic Detoxifying Potential in P. pseudoalcaligenes CECT 5344

The presence in the P. pseudoalcaligenes CECT 5344 genome of putative genes involved in arsenic tolerance was analyzed by protein-BLAST using available information from sequences deposited in UniProt. Genes coding for three arsenate reductases (ArsC), two arsenite efflux pumps (ArsB), two regulatory proteins (ArsR), and other putative proteins involved in arsenic detoxification were identified in two different *ars* gene clusters (Figure 1A), but other *ars* genes were also distributed throughout the genome. The *ars* gene cluster 1 of P. pseudoalcaligenes CECT 5344 showed the gene arrangement arsRICBCH (BN5_1989–BN5_1994), with two genes coding for different arsenate reductases, the thioredoxin-dependent ArsC1 (BN5_1991), and the glutaredoxin-dependent ArsC2 (BN5_1993). The *ars* gene region 2, comprising from BN5_2705 to BN5_2712, displayed the arsABRCH gene organization, in which the arsC gene (BN5_2708) codes for a thioredoxin-dependent arsenate reductase (ArsC3). Additionally, the *gapdh* (BN5_2711) and *arsJ* (BN5_2712) genes were included in this *ars* gene arrangement, which code for a glyceraldehyde-3-phosphate dehydrogenase and an organoarsenical MSF-type transporter, respectively (Figure 1A). In addition to these *ars* gene regions, the genome of P. pseudoalcaligenes CECT 5344 includes two other arsC genes (BN5_2838 and BN5_2786) for putative glutaredoxin-dependent arsenate reductases (ArsC4 and ArsC5, respectively), and genes coding for an ArsR-family transcriptional regulator (BN5_0252), an Acr3-type permease/multidrug resistance protein MdtC (BN5_2698), and a multi-transmembrane protein (BN5_1279) that contains an ArsP domain according to the Pfam protein family database. In addition, several predicted proteins of the strain CECT 5344 showed similarity (40–50%) with bacterial ArsM methyltransferases, mainly aligned in the central methylase domain. These ArsM-like proteins are annotated in the P. pseudoalcaligenes CECT 5344 genome as 3-demethylubiquinone-9 3-methyltransferase (BN5_1671), bifunctional demethylmenaquinone methyltransferase/2-methoxy-6-polyprenyl-1,4-benzoquinol methylase UbiE (BN5_0407), quinone oxidoreductase (BN5_0233), ubiquinone/menaquinone biosynthesis methylase (BN5_3586), biotin synthesis protein BioC (BN5_3914), and uncharacterized protein (BN5_4176). However, homologs to the aio, arx, or arr genes, which are involved in As(III) oxidation or dissimilatory As(V) reduction, were not found in the genome of P. pseudoalcaligenes CECT 5344.

2.2. Arsenic Resistance of P. pseudoalcaligenes CECT 5344

The minimal inhibitory concentration (MIC) and the minimal bactericidal concentration (MBC) were calculated by growing the strain CECT 5344 with 2 mM ammonium chloride or 2 mM sodium cyanide as the sole nitrogen source in the presence of different As(III) or As(V) concentrations. For As(III), the MIC and MBC values were 35 and 40 mM, respectively, regardless of the N-source used (ammonium or cyanide). These values are similar to those found in Bacillus licheniformis DAS1 [46] or in several bacterial isolates from tannery wastes [47]. Interestingly, the MIC and MBC values for cyanide, which were 25 and 50 mM in absence of arsenite, dropped to 20 and 25 mM, respectively, in the presence of 0.25 mM arsenite, thus indicating that As(III) decreases cyanide tolerance of P. pseudoalcaligenes CECT 5344. This fact should be considered for the bioremediation of

wastes co-contaminated with both toxics. Regarding As(V), this bacterium showed MIC values of 1.25 M (with cyanide as N-source) or 1.75 M (with ammonium), and MBC values of 2 M (with cyanide) or 2.5 M (with ammonium), in accordance with the lower toxicity of arsenate compared to arsenite described by other authors [48–50].

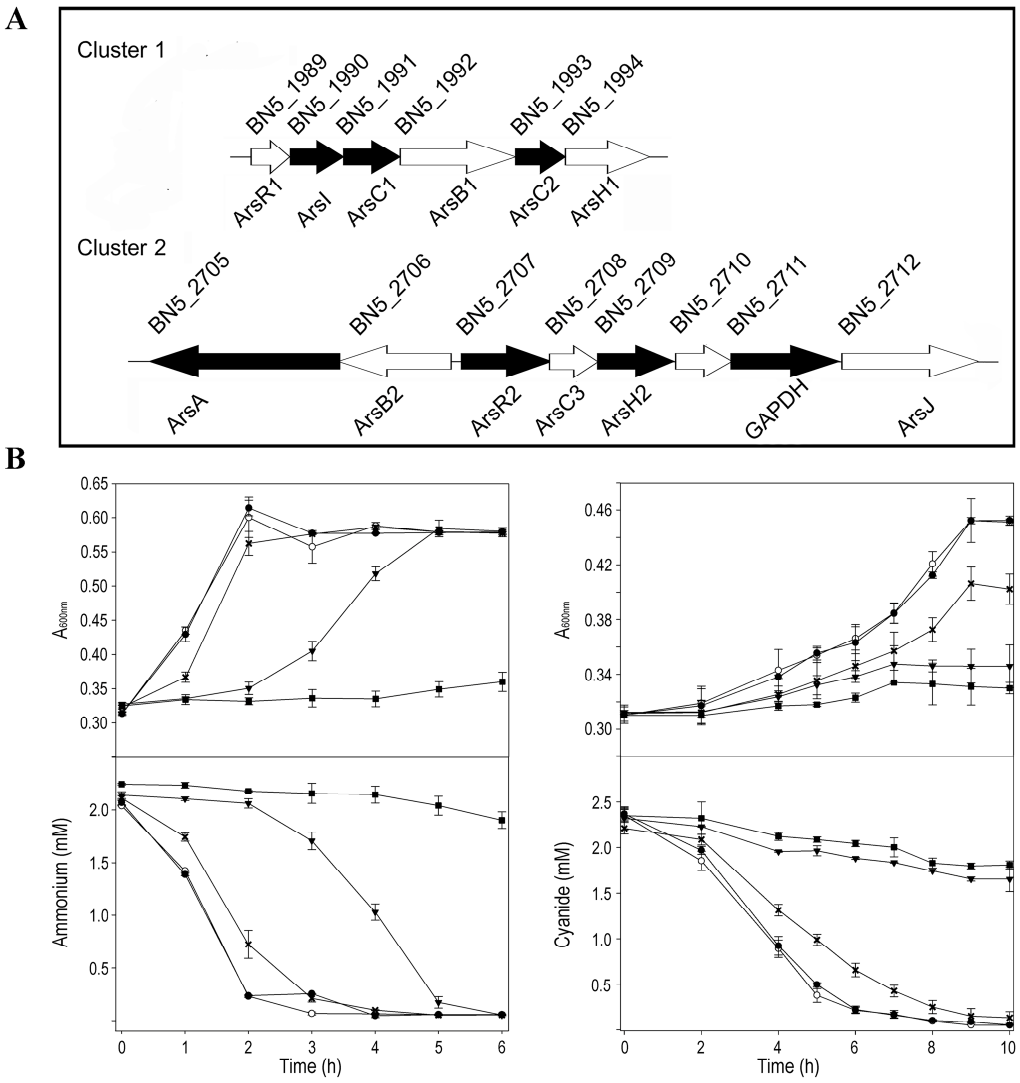

Figure 1. *P. pseudoalcaligenes* CECT 5344 *ars* gene clusters and physiological characterization of arsenic tolerance. (**A**) Genes coding for putative proteins related to arsenic detoxification. The reference numbers correspond with UniProt annotation (UP000032841). Black genes code for proteins identified by LC-MS/MS proteomic analysis in cells grown in the presence of arsenite. Gene descriptions are provided in Supplementary Data Set S1 (SDS1). (**B**) Arsenite tolerance of the strain CECT 5344. Cells were grown in M9 minimal medium with 50 mM sodium acetate as carbon source and 2 mM ammonium chloride (panels left) or 2 mM sodium cyanide (panels right) as nitrogen source, without (open circles) or with arsenite 0.1 mM (filled circles), 0.25 mM (asterisks), 0.5 mM (filled triangles), and 1 mM (filled squares). Bacterial growth, upper panels; N-source consumption, lower panels.

Before performing the quantitative proteomics and qRT-PCR analyses, a physiological characterization was carried out to determine an arsenite concentration that could affect cell growth and, therefore, metabolism without completely inhibiting bacterial growth. P. pseudoalcaligenes CECT 5344 was grown with different concentrations of arsenite (up to 1 mM), using either ammonium or cyanide as the sole nitrogen source (Figure 1B). It was observed that, with both nitrogen sources, a concentration of 0.25 mM of arsenite, almost 10 times higher than the average concentration of arsenic in the lithosphere [51],

conditioned cell growth sufficiently without being highly detrimental to bacterial growth (Figure 1B). Likewise, P. pseudoalcaligenes CECT 5344 was highly resistant to As(V), but it was observed that 200 mM arsenate negatively affected bacterial growth (Figure S1). Therefore, 0.25 mM arsenite and 200 mM arsenate were used for the subsequent analyses.

2.3. Global Changes in the Proteome of P. pseudoalcaligenes CECT 5344 in Response to Arsenite

To study the general response against As(III) in this bacterium, quantitative proteomic analysis by LC-MS/MS was carried out using cells grown under four conditions: 2 mM ammonium chloride as the sole nitrogen source, without or with 0.25 mM arsenite addition (conditions N or NAs, respectively), and 2 mM sodium cyanide as sole nitrogen source, without or with 0.25 mM arsenite (conditions CN or CNAs, respectively). The samples were collected before exhausting the nitrogen source to prevent a nitrogen starvation response. The three biological replicas carried out for each condition were grouped according to both the nitrogen source and the presence or absence of arsenite (Figure S2A). A total of 1659 unique proteins were identified from more than one peptide: 1177 in N, 1312 in NAs, 1591 in CN, and 1581 in CNAs (Supplementary Data Set SDS1, Figure S2B), although most of them (1105 proteins; 66.6% of identified proteins) were shared among all conditions (Figure S2C).

In the differential expression analyses, the comparisons of CNAs vs. CN and NAs vs. N revealed the protein expression changes that are due to the presence of arsenite with both nitrogen sources (Supplementary Data Set S2 SDS2). The comparison CNAs vs. CN revealed that 24 proteins were up-regulated in the CNAs cultures, of which 17 were 'exclusive' (that is, found in at least two replicas of the condition CNAs and not detected in CN), and 7 were over-represented (fold change FC $\geq$ 2) in the presence of As(III). Conversely, 41 proteins were up-regulated in the CN condition, with 18 proteins exclusive and 23 proteins over-represented in the absence of arsenite. The comparison of NAs vs. N showed that 87 proteins were up-regulated by arsenite in the NAs cultures, of which 86 were exclusive (not found in N), and only one protein was over-represented in NAs with respect to N, whereas 18 proteins were exclusive of the N cultures (not detected in NAs).

The differential proteomic analyses CN vs. N and CNAs vs. NAs reflected how the bacterium responds to cyanide in the absence or presence of arsenite, respectively. The analysis CN vs. N showed 353 proteins exclusive plus 188 proteins over-represented in CN, and 18 proteins exclusive plus 164 proteins over-represented in N. Comparing CNAs vs. NAs, 241 proteins were found exclusively in CNAs, and 168 proteins were over-represented, whereas 23 proteins were exclusive and 137 proteins were over-represented in NAs (SDS2).

Results obtained in the differential proteomic analysis CN vs. N presented a high degree of overlap with omic results previously described in this cyanide-degrading strain [39,41,43,44], thus supporting the robustness and reliability of the analysis. The four nitrilases (NitC, Nit4, Nit1, and Nit2) that are present in P. pseudoalcaligenes CECT 5344 [37] were identified in the proteomic analysis (Table 1). As previously described, cyanide up-regulated the nitrilases NitC and Nit4, which are required for cyanide and 3-cyanoalanine assimilation, respectively [34,44]. NitC is encoded by the nitC (BN5_1632) gene of the nit1C cluster, whereas nit4 (BN5_1912) belongs to the cio gene cluster involved in the cyanide-insensitive respiration [37]. NitC was not significantly affected by arsenite (FC 0.91 in CNAs/CN), but the other two proteins encoded by the nit1C gene cluster, NitD, and NitG, were decreased in the CNAs condition. Similarly, Nit4 and most proteins encoded by the cio gene cluster were up-regulated by cyanide but decreased significantly in the presence of arsenite, showing FC values lower than 0.5 in CNAs/CN (Table 1). This may explain the drop in the MIC and MBC values for cyanide observed when the strain CECT 5344 was grown in the presence of arsenite 0.25 mM. Induction by arsenite, regardless of the nitrogen source used, was observed for the phosphate permease PstA, the protein PilJ involved in type IV pili formation, mobility and biofilm synthesis [52], the multidrug resistance/Acr3-type permease MdtC, the glycerol-3-phosphate dehydrogenase GlpD1,

the protein translocase component SecY, and a LuxR family regulator, whereas the DNA repair protein RecN, the diguanylate cyclase YddV, and the membrane transport ATPase component ZntA, among other proteins, were exclusive of CNAs (Table 1). Interestingly, when comparing proteins up-regulated by cyanide in the absence of arsenite (CN vs. N) with those induced by arsenite in the absence of cyanide (NAs vs. N), it was found that 77 exclusive proteins were shared between the CN and NAs proteomes (SDS2). Some of these proteins are related to oxidative stress, such as the glutathione S-transferase and the hydrogen peroxide-inducible activator encoded by the BN5_4225 gene; mobility, cell communication, and biofilm formation, such as FlgN and PilJ proteins; cyanide metabolism such as the aliphatic nitrilase Nit1; and arsenic metabolism such as the ArsA and ArsH2 proteins, among others (SDS2). Therefore, cyanide and arsenic detoxification processes show a certain degree of interrelation, being affected by each other, probably because both toxics trigger general stress response mechanisms.

Comparative gene ontology (GO enrichment) was carried out to analyze the arsenite effect on global metabolism. In general, the response to arsenite was influenced by the nitrogen source (Figure S3). Thus, in ammonium-grown cells, proteins up-regulated by As gave an enrichment in the GO categories SOS response proteins, nucleoside metabolic process related proteins, and aromatic amino acid family biosynthetic process/chorismate biosynthetic process proteins. On the other hand, the response to arsenite in the presence of cyanide triggered non-specific responses related to nitrate assimilation and redox processes through the down-regulation of the assimilatory nitrate and nitrite reductases, and the cytochrome c oxidase cbb3-type CcoG, among other proteins. Arsenite may provoke changes in the metabolism of nitrogen compounds, as suggested by the induction of the glutamate synthase, the N-carbamoyl-L-amino acid amidohydrolase, and the molybdopterin molybdochelatase MoeA and siroheme synthase CysG proteins involved in the biosynthesis of the molybdopterin and siroheme cofactors of the nitrate and nitrite reductases, respectively (Table 1). Regarding other metabolic processes, the induction of enzymes involved in tetrahydrofolate (THF) metabolism was also observed in the arsenic cultures NAs and CNAs (Figure 2).

Concerning As metabolism, the differential proteomic analyses NAs vs. N and CNAs vs. CN revealed the metabolic strategy followed by P. pseudoalcaligenes to resist and detoxify arsenic. According to proteomic data, the *ars* gene clusters 1 and 2 responded significantly to the presence of arsenite. Thus, several proteins encoded by these gene clusters, such as the arsenate reductases ArsC1 and ArsC2, the pump-driving ATPase ArsA, the regulatory protein ArsR2, and the glyceraldehyde-3-phosphate dehydrogenase GAPDH, among other proteins, were up-regulated by arsenite (Table 1). In contrast, the putative arsenate reductases encoded by the non-clustered arsC genes BN5_2786 (ArsC5) and BN5_2838 (ArsC4) were not detected in the proteomic analysis.

Arsenite also induced the phosphate permease PstA, an arsenate transporter (Table 1). Once inside the cells, As(V) could be reduced to As(III) by the arsenate reductases ArsC1-C3, with arsenite directly expelled to the extracellular media by the ATP-driven efflux pump ArsBA or by other permeases such as ArsP or the multidrug resistance Acr3-type permease, which are also induced by As (Table 1). Although ArsB proteins were not identified by proteomics, probably because of technical limitations due to its transmembrane location [53], the ArsA component of the ArsBA efflux pump, and other proteins encoded by the *ars* clusters 1 and 2, were up-regulated by arsenite according to proteomic data (Table 1, Figure 1A).

Intracellular As bioaccumulation is not common in prokaryotes [54]. Accordingly, the induction of proteins related to this mechanism was not observed in the CECT 5344 strain. However, the synthesis of organoarsenic compounds, which later would be expelled from the cells, also contributes to arsenic detoxification in bacteria [21,23,55]. The proteomic analysis revealed that some ArsM-like proteins were constitutively expressed or induced by cyanide, suggesting that As(III) methylation may occur in P. pseudoalcaligenes CECT 5344, although these putative methyltransferases were not directly regulated by arsenite. Proteins

related to THF metabolism (Figure 2) and also proteins involved in the synthesis of chorismate, a precursor of p-aminobenzoate, were induced in the presence of As(III), suggesting a relationship between THF metabolism and arsenic resistance. It has been shown that the administration of folic acid reduces arsenic toxicity in humans [56], and this effect could be due to the requirement of THF for arsenic methylation, either directly or allowing the synthesis and recycling of SAM, which is required for ArsM-type methyltransferases [57,58]. In addition, the enzyme GAPDH catalyzes the formation of arseno-phosphoglycerate, which is exported by the permease ArsJ [30,31]. In P. pseudoalcaligenes CECT 5344, both *gapdh* (BN5_2711) and *arsJ* (BN5_2712) genes are present in the arsenite-induced *ars* cluster 2 (Figure 1A). In addition, the glycerol-3-phosphate dehydrogenase GlpD1 was induced in both NAs and CNAs conditions (Table 1). On the other hand, nitriles and CN derivatives may react with arsenic forming Lewis adducts [59]. Dissociation of these possible adducts could be mediated by the putative C-As lyase ArsI encoded by the BN5_1990 gene of the *ars* cluster 1, which was found to be induced by arsenite (Table 1). Interestingly, the ArsH2 protein encoded by the BN5_2709 gene of the *ars* cluster 2 was up-regulated by arsenite and cyanide in the absence of arsenite, being exclusive to the CN condition in the CN vs. N comparison (Table 1). It has been recently described that ArsH2 contributes to relieving As toxicity in Pseudomonas putida, protecting from oxidative damage caused by exposure to arsenic and diamide [25]. Therefore, ArsH2 could be also involved in the defense against the oxidative stress caused by both arsenic and cyanide in P. pseudoalcaligenes CECT 5344.

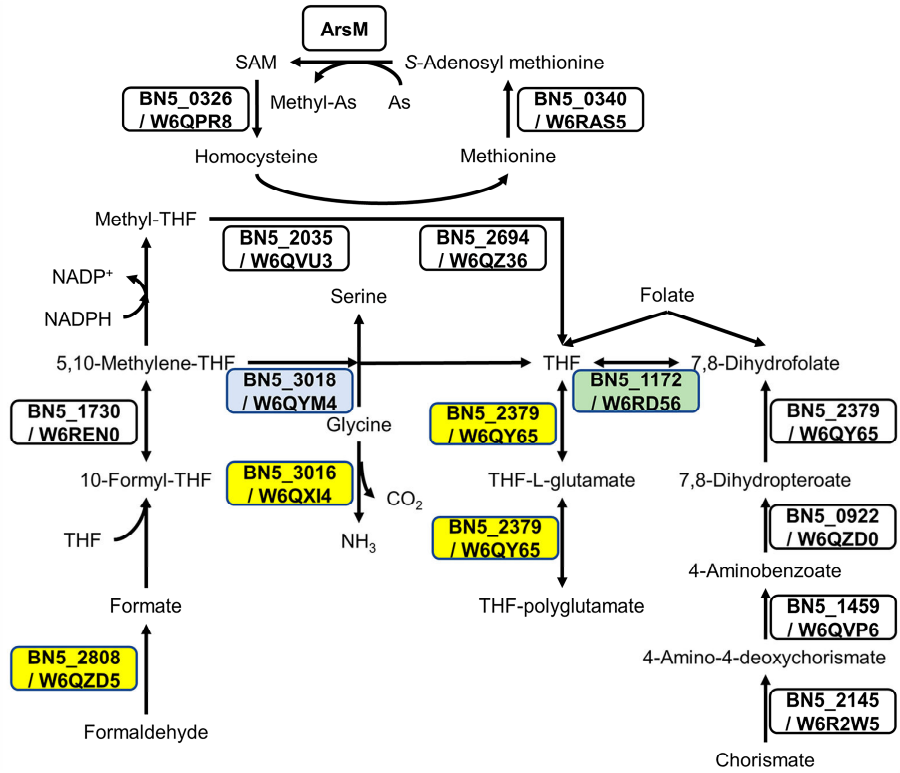

Figure 2. The effect of arsenite on proteins involved in tetrahydrofolate (THF) metabolism. Folate biosynthesis (ppse00790), biosynthesis of cofactors (ppse01240), and carbon metabolism (ppse01200) from KEGG were analyzed to build the metabolic pathways. Proteins W6QZD5 (*S*-formylglutathione hydrolase encoded by BN5_2808), W6QXI4 (glycine cleavage system H protein encoded by BN5_3016), and W6QY65 (dihydrofolate/folylpolyglutamate synthase encoded by BN5_2379), marked in yellow boxes, were induced by As(III) when ammonium was used as N-source. The protein W6QYM4 (serine methylase encoded by BN5_3018), shown in a blue box, was induced by As(III) with cyanide as N-source. The protein W6RD56 (dihydrofolate reductase encoded by BN5_1172), boxed in green, was identified only in cyanide, with or without arsenite.

Table 1. Proteomic analysis of proteins with a possible role in arsenic and/or cyanide detoxification. Relative label-free quantification (LFQ) intensity was used to calculate the FC in the four comparisons NAs/N, CNAs/CN, CN/N, and CNAs/NAs. NAs, ammonium as N-source, with 0.25 mM arsenite; N, ammonium as N-source, without arsenite; CNAs, cyanide as N-source, with 0.25 mM arsenite; and CN, cyanide as N-source, without arsenite. Proteins exclusively found in a condition are indicated with the name of that condition. Proteins not detected (-).

Protein ID	Locus	Protein Names	Short Name	FC NAs/N	FC CNAs/CN	FC CN/N	FC CNAs/NAs
			***ars* gene cluster 1**				
W6QX55	BN5_1989	Putative transcriptional regulator ArsR	ArsR1	-	-	-	-
W6RF96	BN5_1990	Lactoylglutathione lyase, C-As lyase	ArsI	NAs	CNAs	-	0.15
W6QUH3	BN5_1991	Arsenate reductase (thioredoxin-dependent)	ArsC1	15.27	3.21	3.01	0.63
W6R2E3	BN5_1992	Arsenical-resistance protein (arsenite ArsB efflux pump)	ArsB1	-	-	-	-
W6QVQ7	BN5_1993	Arsenate reductase (glutaredoxin-dependent)	ArsC2	3.21	CNAs	-	0.3
W6QX59	BN5_1994	Arsenical resistance protein	ArsH1	-	-	-	-
			***ars* gene cluster 2**				
W6RHD6	BN5_2705	Arsenical pump-driving ATPase, ArsA	ArsA	NAs	2.38	CN	0.72
W6QWP7	BN5_2706	Arsenite transporter ArsB efflux pump	ArsB2	-	-	-	-
W6R4K3	BN5_2707	Regulatory protein ArsR	ArsR2	NAs	8.98	CN	0.67
W6QXT2	BN5_2708	Arsenate reductase (thioredoxin-dependent)	ArsC3	-	-	-	-
W6QZ50	BN5_2709	Arsenical resistance protein, ArsH	ArsH2	NAs	3.88	CN	0.99
W6RHD9	BN5_2710	Protein tyrosine phosphatase domain-containing protein 1		-	-	-	-
W6QWQ1	BN5_2711	Glyceraldehyde-3-phosphate dehydrogenase	GADPH	8.49	2.00	2.16	0.51
W6R4K6	BN5_2712	MFS transporter 1-arseno-3-phosphoglycerate exporter	ArsJ	-	-	-	-
			***nit1C* gene cluster**				
H9N5E0	BN5_1630	Sigma-54-dependent transcriptional regulator	NitA	-	0.8	CN	CNAs
H9N5E2	BN5_1631	Uncharacterized protein	NitB	1.66	1.03	56.13	34.72
H9N5E1	BN5_1632	Nitrilase NitC	NitC	2.29	0.91	769.53	305.89
H9N5E3	BN5_1633	Radical SAM domain-containing protein	NitD	0.32	0.13	164.02	67.29
H9N5E4	BN5_1634	GCN5-related N-acetyltransferase	NitE	NAs	1.83	CN	30.76
H9N5E5	BN5_1635	AIR synthase-like protein	NitF	-	0.95	CN	CNAs
H9N5D9	BN5_1636	Uncharacterized protein	NitG	-	0.35	CN	CNAs
H9N5D8	BN5_1637	FAD dependent oxidoreductase	NitH	1.32	0.94	74.27	52.98
			***cio* gene cluster**				
W6QWX1	BN5_1899	GntR family transcriptional regulator	MocR	-	CN	CN	-
W6RF17	BN5_1900	Sulfite reductase (NADPH) hemoprotein beta-component	CysL3	0.75	0.09	17.44	2.05
W6QU90	BN5_1901	Uncharacterized protein	CioC3	NAs	0.22	CN	30.15
W6R254	BN5_1902	Terminal oxidase subunit I	CioA3	-	CN	CN	-
W6QVH5	BN5_1903	Cytochrome *d* ubiquinol oxidase, subunit II	CioB3	-	-	-	-
W6QWX6	BN5_1904	Phosphoserine aminotransferase	SerC3	0.45	0.21	53.62	25.19
W6RF21	BN5_1905	Histidinol-phosphate aminotransferase	HisC3	0.59	0.22	33.33	12.33
W6QU95	BN5_1906	Acetylornithine aminotransferase	ArgD3	0.91	0.11	399.11	47.46
W6R260	BN5_1907	4-hydroxy-tetrahydrodipicolinate synthase	DapA1	2.11	0.3	182.98	26.06
W6QVI0	BN5_1908	High-affinity glucose transporter	-	-	-	-	-
W6QWY1	BN5_1909	Methylenetetrahydrofolate reductase	MetF3	-	0.13	CN	CNAs
W6RF25	BN5_1910	Cysteine synthase	CysM3	-	-	-	-
W6QUA1	BN5_1911	NADP-dependent malic enzyme	MaeB3	1.76	0.08	104.5	4.8
W6R265	BN5_1912	Nitrilase Nit4	Nit4	1.35	0.29	6.15	1.34

Table 1. *Cont.*

Protein ID	Locus	Protein Names	Short Name	FC NAs/N	FC CNAs/CN	FC CN/N	FC CNAs/NAs
Other nitrilases and C-N hydrolases							
W6RF39	BN5_1925	Aliphatic nitrilase	Nit1	NAs	1.65	CN	1.43
W6R989	BN5_4427	Bifunctional nitrilase/nitrile hydratase NIT4B	Nit2/Nit4B	-	1.15	CN	CNAs
W6QQS6	BN5_0258	C-N hydrolase, nitrilase/cyanide hydratase	C-N11/AguB	-	-	-	-
W6QQZ6	BN5_0736	C-N hydrolase, nitrilase/cyanide hydratase	C-N10/Nit1B	NAs	0.86	CN	1.4
W6QUY5	BN5_1196	Nitrilase homolog 1	C-N12/Nit1A	-	-	-	-
W6QZ84	BN5_2750	Hydrolase, carbon-nitrogen family	C-N12	-	-	-	-
W6QY63	BN5_3204	Formamidase	C-N2/AmiF	1.95	1.28	5.32	3.49
W6QZD7	BN5_3251	C-N hydrolase, nitrilase/cyanide hydratase	CN-13/Nit3B	1.43	1.02	2.07	1.49
***cyn* gene cluster**							
W6QRB2	BN5_0438	Fis family transcriptional regulator	CynF	NAs	CN	CN	NAs
W6QST4	BN5_0439	ABC-type transporter periplasmic component protein	CynA	0.6	0.54	16.22	14.5
W6RB18	BN5_0440	ABC transporter inner membrane subunit protein	CynB	-	-	-	-
W6QQ36	BN5_0441	ABC transporter/ATPase component protein	CynD	1.06	1.53	61.12	88.16
W6QY14	BN5_0442	Cyanase	CynS	0.45	0.87	164.76	318.2
Other proteins							
W6QRW0	BN5_0117	Phosphate transport system permease protein	PstA	NAs	1.41	CN	2.04
W6QXN5	BN5_0312	Methyl-accepting chemotaxis sensory transducer	PilJ	NAs	2.08	CN	9.80
W6QSH6	BN5_0328	Glutamate synthase	PydA	NAs	1.26	CN	0.82
W6QXQ0	BN5_0332	*N*-carbamoyl-L-amino acid amidohydrolase	-	NAs	1.37	CN	2.10
W6QTB1	BN5_1579	Molybdopterin molybdochelatase	MoeA	NAs	0.84	CN	2.73
W6QWV1	BN5_1877	Siroheme synthase	CysG	NAs	1.31	CN	3.94
W6QRZ0	BN5_1113	Glycerol-3-phosphate dehydrogenase	GlpD1	NAs	CNAs	-	1.89
W6QSH3	BN5_1279	UPF0718 protein MJ0584	ArsP	NAs	CNAs	-	1.51
W6QXS5	BN5_2698	Multidrug resistance protein MdtC, Acr3-type permease	Acr3/MdtC	NAs	CNAs	-	0.22
W6R038	BN5_3066	Two component LuxR family transcriptional regulator	LuxR	NAs	CNAs	-	2.78
W6R1S4	BN5_3676	Protein translocase subunit SecY	SecY	NAs	CNAs	-	4.28
W6R067	BN5_3092	Diguanylate cyclase YddV	YddV	-	CNAs	-	CNAs
W6RL26	BN5_4037	Putative membrane transport ATPase	ZntA	-	CNAs	-	CNAs
W6R8E4	BN5_4137	dTDP-4-dehydrorhamnose 3,5-epimerase	RfbC	-	CNAs	-	CNAs
W6R0W4	BN5_4181	Uncharacterized protein	-	-	CNAs	-	CNAs
W6RM49	BN5_4450	AraC family transcriptional regulator	AraC	-	CNAs	-	CNAs
W6QSN9	BN5_0908	DNA repair protein RecN	RecN	-	CNAs	-	CNAs
W6RCR6	BN5_1077	Putative acyl-CoA thioester hydrolase	-	-	CNAs	-	CNAs

2.4. Accumulation of Arsenic in Biofilm

It has been recently reported that As may be retained by the bacterial biofilm [17,55,60]. In addition, some proteins such as PilJ (BN5_0312), RfbA (BN5_4136), and RfbC (BN5_4137), which are involved in biofilm formation [52,61,62] were found to be up-regulated by arsenite in the proteomic analysis (Table 1, SDS2). Therefore, the capacity to synthesize biofilm and the possible accumulation of arsenic inside the cells or in the biofilm was determined. Biofilm formation was significantly increased in cells grown with arsenite, being the CNAs condition where the highest amount of biofilm was produced (Figure 3A). On the other hand, it was also observed that arsenic was retained mainly in biofilm, and intracellular accumulation of arsenic was residual. The accumulation of arsenic in biofilm was also significantly higher in the CNAs condition than in NAs (Figure 3B). These results indicate that As is extruded from the cytoplasm to the extracellular media, being retained and accumulated in the cell biofilm.

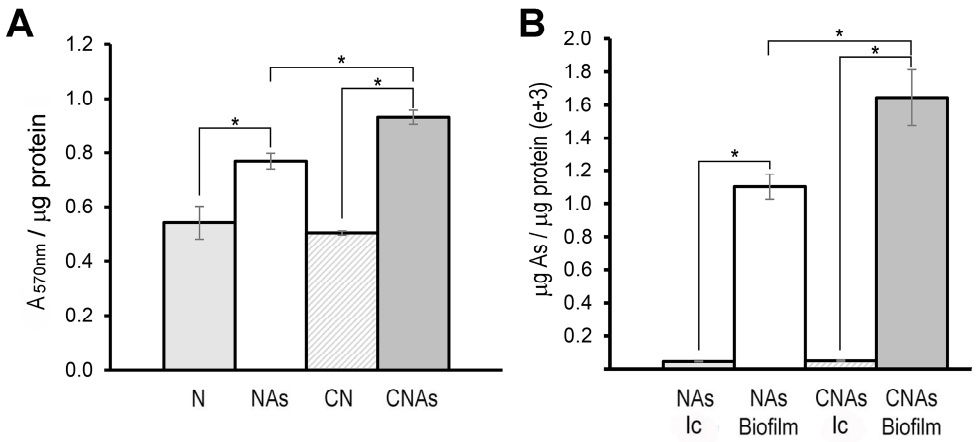

Figure 3. Biofilm production in *P. pseudoalcaligenes* CECT 5344 and arsenic accumulation in the biofilm. (**A**) Biofilm formation (measured with crystal violet as A_{570nm}) normalized by protein amount (µg) in cells grown with 2 mM ammonium as a nitrogen source in the absence (N) or the presence of 0.25 mM arsenite (Nas), or with 2 mM cyanide as nitrogen source, without (CN) or with 0.25 mM arsenite (CNAs). (**B**) Intracellular (Ic) and biofilm As accumulation in cells grown with 0.25 mM arsenite using ammonium (Nas) or cyanide (CNAs) as the sole nitrogen source. Asterisks indicate that the differences are significant ($p < 0.05$) according to a *t*-test.

2.5. Transcriptional qRT-PCR Analysis

A qRT-PCR transcriptional analysis of some genes coding for relevant proteins identified by proteomics was also performed. First, the arsenate reductase genes of the strain CECT 5344 were analyzed in cells grown in the presence of 0.25 mM arsenite or 200 mM arsenate, with ammonium or cyanide (2 mM) as the sole nitrogen source. The expression of the arsenate reductases *arsC1* and *arsC2* genes (BN5_1991 and BN5_1993, respectively), located in the *ars* cluster 1, as well as *arsC3* (BN5_2708), located in the *ars* cluster 2, were induced by As(III) and As(V) regardless of the nitrogen source, cyanide, or ammonium (Figure 4). However, the expression of the putative genes *arsC5* (BN5_2786) and *arsC4* (BN5_2838) was residual and resulted in being unaffected by arsenite or arsenate (not shown). Therefore, proteomic and qRT-PCR data are coincident and suggest that the arsC1-C3 genes are involved in As-resistance, but the *arsC4* and *arsC5* genes could be the result of gene duplications or horizontal gene transfer events, being either non-functional or controlled by different environmental conditions, such as what occurs in *Pseudomonas putida* [63] and *Rhodopseudomonas palustris* [64].

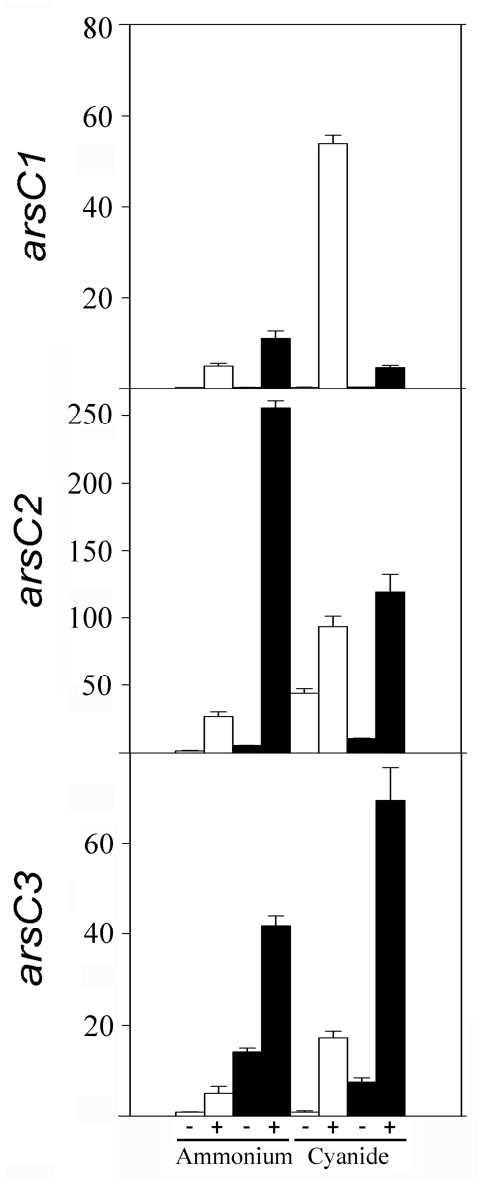

Figure 4. Relative expression of arsenate reductase genes (*arsC1*, *arsC2*, and *arsC3*) of P. pseudoalcaligenes CECT 5344 in response to arsenic. Gene expression was analyzed by qRT-PCR in cells grown with 2 mM ammonium chloride or 2 mM sodium cyanide as the sole nitrogen source, without (−) or with (+) arsenite 0.25 mM (white bars) or arsenate 200 mM (black bars).

In general, the proteomic results were confirmed when the expression of selected genes was analyzed by qRT-PCR (Figure S4). Thus, qRT-PCR analysis showed that the expression of the arsP gene (BN5_1279) encoding a putative permease and the gcvH3 (BN5_3016) and glyA5 (BN5_3018) genes, which are related to THF biosynthesis (Figure 2), were induced by arsenite. Increases of both protein and mRNA in the presence of arsenite were also observed for the phosphate permease PstA. Arsenite induction of the arsB1 (BN5_1992) and arsR1 (BN5_1989) genes (*ars* cluster 1) was observed only at the transcriptional level (Figure S4). This may be due to the difficulty to detect proteomics membrane proteins or regulators that may be present in the cells at very low concentrations [53]. On the other hand, the negative effect of arsenite on the cio gene cluster (cioA3 and maeB3 genes) was confirmed by qRT-PCR. For the maeB3 gene, this inhibition was observed both by transcriptional and proteomic analyses, but for the cioA3 gene, it was observed only at the protein level. Proteomic and qRT-PCR data revealed that the nitrilase NitC, which is essential for cyanide assimilation [34], was not affected by arsenite (Figure S4), thus

allowing bacterial growth in the presence of both toxins, cyanide, and arsenite. However, the proteins NitD and NitG, which are also encoded by the nit1C gene cluster were found to decrease in the presence of arsenite (Table 1). Significant differences were not observed at the transcript level for nitD and nitG in the CN and CNAs conditions (Figure S4), suggesting that As(III) affects NitD and NitG only post-translationally.

2.6. Overview of the As Resistance Mechanisms in P. pseudoalcaligenes CECT 5344

Considering all the results of this work, the arsenic metabolism in P. pseudoalcaligenes CECT 5344 could be summarized as shown in Figure 5. Arsenite induces the expression of the *ars* gene clusters 1 and 2, probably through the inactivation of ArsR. Arsenate enters the cells through the PstA phosphate permease, and then is reduced to As(III) by the arsenate reductases ArsC1-C3. The main mechanism of arsenite tolerance is its extrusion through the ArsBA-type efflux pump. The formation of organoarsenical compounds also contributes to As detoxification. Methylated derivatives could be formed by methyltransferases that show similarity to bacterial ArsM proteins, and proteomic data suggest that THF metabolism may play a role in the methylation processes. Moreover, an arsenic-phosphoglycerate derivative may be formed by the arsenite-inducible glyceraldehyde-3-phosphate dehydrogenase GAPDH. Organoarsenicals could be extruded by ArsJ, Acr3, and ArsP permeases. Once outside, arsenic is retained and accumulated on the biofilm. Moreover, when cyanide is used as the nitrogen source, arsenite and cyanide could form Lewis adducts, which could be processed by ArsI. Additionally, the protein ArsH2, which is induced by arsenite or cyanide, could increase the tolerance to these compounds by protecting them from oxidative stress caused by these toxins. Results derived from this work may contribute to the development of strategies for the bioremediation of wastes containing cyanide and arsenic as co-pollutants by using the P. pseudoalcaligenes CECT 5344 strain and taking into account that cyanide and arsenic detoxification processes affect each other.

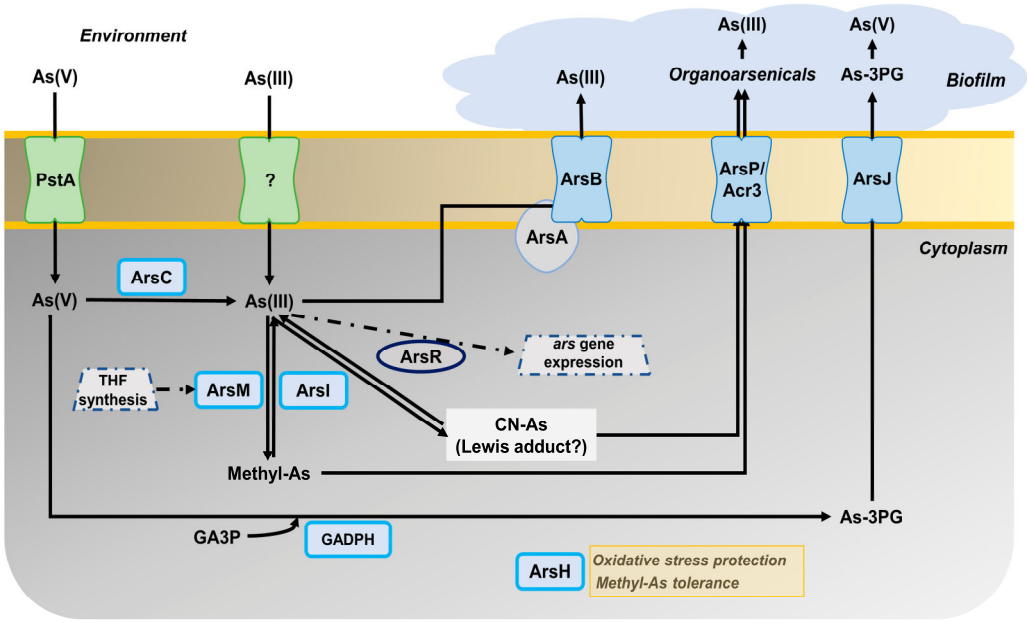

Figure 5. Overview of the arsenic metabolism in P. pseudoalcaligenes CECT 5344. The different proteins (encoded by the genes indicated in brackets) that are involved in the As tolerance of the strain CECT 5344 are: ArsC (BN5_1991; BN5_1993; BN5_2708); ArsR (BN5_1989; BN5_2707); ArsB (BN5_1992; BN5_2706); ArsA (BN5_2705); ArsI (BN5_1990); ArsH (BN5_1994; BN5_2709); glyceraldehyde-3-phosphate dehydrogenase GAPDH (BN5_2711); ArsJ (BN5_2712); ArsP (BN5_1279); Acr3 (BN5_2698); ArsM (BN5_1671; BN5_0407; BN5_4176); PstA (BN5_0117).

3. Materials and Methods

3.1. Culture Media and Growth Conditions

P. pseudoalcaligenes CECT 5344 was cultured in M9 minimal medium, pH 9.5 (NaOH adjusted), at 30 °C under aerobic conditions in an orbital shaker at 220 rpm [33]. Sodium acetate (50 mM) and ammonium chloride or sodium cyanide (2 mM) were used as carbon and nitrogen sources, respectively. When applicable, sodium arsenite or sodium arsenate dibasic (Sigma-Aldrich, St. Louis, MO, USA) was added at different concentrations from stock solutions. When agar plates were required, 15 g/L bacteriological agar was added to the liquid LB medium.

3.2. Determination of Bacterial Growth and Arsenic Tolerance

Cell growth was monitored in triplicate liquid cultures by measuring the absorbance at 600 nm (A_{600nm}) in a spectrophotometer. On agar plates, growth was determined by counting colony-forming units (CFU) with the drop plate technique [65].

Tolerance of *P. pseudoalcaligenes* CECT 5344 to arsenite and arsenate was determined by calculating the minimal inhibitory concentration (MIC) and the minimal bactericidal concentration (MBC) [66], using cultures in M9 liquid medium inoculated in U-shaped 96-well microtiter plates (in quintuplicate). After incubation at 30 °C with shaking at 220 rpm for 48 h, MIC was estimated as the lowest As concentration that inhibits visible growth as a dot at the bottom of the well, and MBC was calculated as the lowest As concentration that kills the bacteria, checked by CFU counting. To determine MIC and MBC for As(III), ammonium or cyanide (2 mM) was used as a nitrogen source with increasing concentrations of arsenite up to 75 mM. For As(V), the concentration range was increased up to 2.5 M. The influence of As(III) in the cyanide tolerance was determined by calculating the MIC and MBC values for cyanide (with increasing concentrations of cyanide up to 50 mM) in the absence or the presence of 0.25 mM arsenite.

3.3. Analytical Determinations and Biofilm Quantification

Extracellular ammonium was determined using the Nessler reagent according to the previously described colorimetrical method [67]. Cyanide was measured using chloramine T, barbituric acid, and pyridine reagents, as previously described [68]. Protein was quantified by the dye-binding method [69].

Biofilm production in *P. pseudoalcaligenes* CECT 5344 was quantified with crystal violet (absorbance at 570 nm) into 96-well microtiter plates in triplicate, taking into consideration the 'edge effect' [70]. Biofilm formation was normalized by protein quantification to avoid possible differences in growth derived from the nitrogen source used. For this purpose, the same number and position of wells were used for a parallel protein determination [69]. Statistical significance was analyzed by applying a two-tailed *t*-test analysis (Benjamini-Hochberg corrected) on the normalized protein crystal violet measurements.

Determination of intracellular arsenic was carried out by harvesting 100 mL of cells cultured in M9 minimal medium with 0.25 mM arsenite, using either 2 mM ammonium chloride (condition named NAs) or 2 mM sodium cyanide (condition named CNAs) as the sole nitrogen source. After centrifugation (10,000 rpm, 4 °C, 10 min), cells were resuspended and washed three times with 1 mL 0.85% NaCl and dried at 80 °C for 96 h to determine cell dry weight. Then, pellets were resuspended in 1 mL HNO_3 (69%, trace-metal grade, Fisher). On the other hand, the determination of arsenic present in the biofilm was carried out in cultures on microtiter plates, using six wells per replica, which were washed with 0.85% NaCl after growing for 48 h in the conditions NAs and CNAs. Then, 100 µL of HNO_3 was used to collect biofilm. In parallel, the same number of wells for each condition were used for protein quantification [69]. Samples from both approaches (intracellular and biofilm) were heated up to 95 °C and digested at 25 °C for 1 h with shaking, and after dilution of the samples in 2% HNO_3, arsenic content was analyzed on an ICP/MS equipment (PerkinElmer, model Nexion 350X) at the Central Service for Research Support of the University of Córdoba (SCAI-UCO). Three biological samples were analyzed for each

condition (NAs and CNAs). Statistical significance was analyzed by applying a two-tailed *t*-test analysis (Benjamini-Hochberg corrected).

3.4. Quantitative Proteomic Analysis

Proteomic analysis was carried out in cells grown in M9 minimal medium under four conditions: 2 mM ammonium as sole nitrogen source, without arsenite (condition N) or with 0.25 mM arsenite (condition NAs); and 2 mM cyanide as sole nitrogen source, without (condition CN) or with 0.25 mM arsenite (condition CNAs). Before total consumption of the nitrogen source, three independent cultures were harvested by centrifugation, and pellets were resuspended in 300 µL of a lysis buffer that contained 50 mM Tris-HCl (pH 7.5), 4% CHAPS, and urea 8 M. Then, samples were disrupted by sonication in a Bandelin Sonoplus H2070 equipment (8 pulses for 20 s, at 25 W). Cell debris was removed by centrifugation (12,000 rpm, 10 min, 4 °C), and supernatants were precipitated using the 2D-Clean Up Kit (Amersham GE Healthcare). Pellets resuspended in 100 µL lysis buffer were used for protein determination [69] and LC-MS/MS analysis, as previously described [71,72]. The search against P. pseudoalcaligenes CECT 5344 proteome (UniProt UP000032841) and quantification parameters used for the proteomic analysis are shown in Table S1. Data were analyzed using the Perseus software (1.6.12.1) (https://maxquant.org/perseus/ (accessed on 8 March 2023), and their statistical significance was determined by *t*-test analysis (Benjamini-Hochberg corrected). Proteins were considered differentially expressed when the fold change (FC), defined as the ratio of the normalized peptide intensity values in the non-reference condition vs. the reference condition, was $\geq$2 (for over-represented proteins) or $\leq$0.5 (for down-represented proteins), with an adjusted *p*-value < 0.05. The gene ontology GO enrichment analysis was carried out by using the Comparative GO application [73]. Data were deposited to the ProteomeXchange Consortium (http://proteomecentral.proteomexchange.org (accessed on 8 March 2023)) with the dataset identifier PXD033539.

3.5. Quantitative Real-Time PCR Analysis

The transcriptional expression of several selected genes was analyzed by qRT-PCR using three biological samples, each with two technical replicas, as previously described [72]. Gene-specific primers were designed using the Oligo 7.0 software (Table S2). Data were normalized to the rpoB and 23S rRNA housekeeping genes. Finally, data were analyzed by a *t*-test (Benjamini-Hochberg corrected), and relative quantification was calculated by the ΔΔCt method [74].

4. Conclusions

The following conclusions may be addressed: (1) P. pseudoalcaligenes CECT 5344 contains two main *ars* gene clusters that respond to arsenite, regardless of the nitrogen source used, although As-resistance response shows some differences between ammonium and cyanide; (2) the main basis of As-resistance in this bacterium is the extrusion of As(III) through ArsBA efflux pumps, or as organic derivatives exported through ArsP, Acr3, and ArsJ permeases; (3) production of arseno-phosphoglycerate by the As-inducible GAPDH enzyme, As methylation, THF metabolism, and perhaps formation of Lewis adducts in the presence of cyanide, could be also relevant processes involved in As detoxification; (4) after extrusion of As(III) or organoarsenicals, As is accumulated in the bacterial biofilm, whose synthesis is enhanced in the presence of arsenite; (5) the ArsH2 protein may protect from the oxidative stress caused by both arsenic and cyanide; and (6) P. pseudoalcaligenes CECT 5344 could be used for bioremediation of wastes from mining and other industries co-contaminated with cyanide and arsenic.

Supplementary Materials: The following supporting information can be downloaded at: https://www.mdpi.com/article/10.3390/ijms24087232/s1.

Author Contributions: Conceptualization, V.M.L.-A., M.D.R., A.O.-A. and C.M.-V.; methodology, K.A.B., P.C., G.R.-C. and L.P.S.; software, V.M.L.-A., M.D.R. and A.O.-A.; validation, K.A.B., P.C., A.O.-A. and C.M.-V.; formal analysis, K.A.B., P.C., A.O.-A. and C.M.-V.; investigation, K.A.B., P.C. and G.R.-C.; data curation, K.A.B., P.C., G.R.-C. and L.P.S.; writing-original draft preparation, A.O.-A. and C.M.-V.; writing-review and editing; A.O.-A. and C.M.-V.; supervision; L.P.S., V.M.L.-A., M.D.R., A.O.-A. and C.M.-V.; project administration, C.M.-V.; funding acquisition, V.M.L.-A., M.D.R. and C.M.-V. All authors have read and agreed to the published version of the manuscript.

Funding: This research was funded by Junta de Andalucía (grant number P18-RT-3048), Ministerio de Ciencia, Innovación y Universidades (grant number RTI2018-099573-B-100), and Fundación Torres Gutiérrez, Spain.

Institutional Review Board Statement: Not applicable.

Informed Consent Statement: Not applicable.

Data Availability Statement: Supplementary data associated with this work are available online, and it can be only found in the online version of this paper.

Acknowledgments: The authors thank MAGTEL, FCC-AMBITO (GEMASUR), SAVECO and AVENIR for fruitful collaborations. The Servicio Central de Apoyo a la Investigación (SCAI), Universidad de Córdoba, is also acknowledged for technical support in LC-MS/MS.

Conflicts of Interest: The authors declare no conflict of interest.

References

1. Oremland, R.S.; Stolz, J.F. The ecology of arsenic. *Science* **2003**, *300*, 939–944. [CrossRef] [PubMed]
2. Hery, M.; Rizoulis, A.; Sanguin, H.; Cooke, D.A.; Pancost, R.D.; Polya, D.A.; Lloyd, J.R. Microbial ecology of arsenic-mobilizing Cambodian sediments: Lithological controls uncovered by stable-isotope probing. *Environ. Microbiol.* **2015**, *17*, 1857–1869. [CrossRef] [PubMed]
3. Sher, S.; Rehman, A. Use of heavy metals resistant bacteria-a strategy for arsenic bioremediation. *Appl. Microbiol. Biotechnol.* **2019**, *103*, 6007–6021. [CrossRef] [PubMed]
4. Raju, N.J. Arsenic in the geo-environment: A review of sources, geochemical processes, toxicity and removal technologies. *Environ. Res.* **2022**, *203*, 111782. [CrossRef]
5. Coudert, L.; Bondu, R.; Rakotonimaro, T.V.; Rosa, E.; Guittonny, M.; Neculita, C.M. Treatment of As-rich mine effluents and produced residues stability: Current knowledge and research priorities for gold mining. *J. Hazard Mater.* **2020**, *386*, 121920. [CrossRef] [PubMed]
6. Tapia-Gatica, J.; Selles, I.; Bravo, M.A.; Tessini, C.; Barros-Parada, W.; Novoselov, A.; Neaman, A. Global issues in setting legal limits on soil metal contamination: A case study of Chile. *Chemosphere* **2022**, *290*, 133404. [CrossRef] [PubMed]
7. Martínez, V.D.; Vucic, E.A.; Becker-Santos, D.D.; Gil, L.; Lam, W.L. Arsenic exposure and the induction of human cancers. *J. Toxicol.* **2011**, *2011*, 431287. [CrossRef]
8. Sun, H.J.; Rathinasabapathi, B.; Wu, B.; Luo, J.; Pu, L.P.; Ma, L.Q. Arsenic and selenium toxicity and their interactive effects is humans. *Environ. Int.* **2014**, *69*, 148–158. [CrossRef]
9. Smith, A.H.; Lingas, E.O.; Rahman, M. Contamination of drinking-water by arsenic in Bangladesh: A public health emergency. *Bull. World Health Organ.* **2000**, *78*, 1093–1103.
10. Muller, D.; Médigue, C.; Koechler, S.; Barbe, V.; Barakat, M.; Talla, E.; Bonnefoy, V.; Krin, E.; Arsène-Ploetze, F.; Carapito, C.; et al. A tale of two oxidation states: Bacterial colonization of arsenic-rich environments. *PLoS Genet.* **2007**, *3*, e53. [CrossRef]
11. Yang, H.C.; Cheng, J.; Finan, T.M.; Rosen, B.P.; Bhattacharjee, H. Novel pathway for arsenic detoxification in the legume symbiont *Sinorhizobium meliloti*. *J. Bacteriol.* **2005**, *187*, 6991–6997. [CrossRef] [PubMed]
12. Garbinski, L.D.; Rosen, B.P.; Chen, J. Pathways of arsenic uptake and efflux. *Environ. Int.* **2019**, *126*, 585–597. [CrossRef] [PubMed]
13. Mukhopadhyay, R.; Bhattacharjee, H.; Rosen, B.P. Aquaglyceroporins: Generalized metalloid channels. *Biochim. Biophys. Acta* **2014**, *1840*, 1583–1591. [CrossRef] [PubMed]
14. Oremland, R.S.; Saltikov, C.W.; Stolz, J.F.; Hollibaugh, J.T. Autotrophic microbial arsenotrophy in arsenic-rich soda lakes. *FEMS Microbiol. Lett.* **2017**, *364*, fnx146. [CrossRef]
15. Rosen, B.P.; Liu, Z. Transport pathways for arsenic and selenium: A minireview. *Environ. Int.* **2009**, *35*, 512–515. [CrossRef]
16. Slyemi, D.; Bonnefoy, V. How prokaryotes deal with arsenic. *Environ. Microbiol. Rep.* **2012**, *4*, 571–586. [CrossRef]
17. Barral-Fraga, L.; Martina-Prieto, D.; Barral, M.T.; Morin, S.; Guasch, H. Mutual interaction between arsenic and biofilm in a mining impacted river. *Sci. Total Environ.* **2018**, *636*, 985–998. [CrossRef]

18. Morelli, E.; Mascherpa, M.C.; Scarano, G. Biosynthesis of phytochelatins and arsenic accumulation in the marine microalga *Phaeodactylum tricornutum* in response to arsenate exposure. *Biometals* **2005**, *18*, 587–593. [CrossRef]
19. Diba, F.; Khan, M.Z.; Uddin, S.Z.; Istiaq, A.; Shuvo, M.S.; Ul Alam, A.R.; Hossain, M.A.; Sultana, M. Bioaccumulation and detoxification of trivalent arsenic by *Achromobacter xylosoxidans* BHW-15 and electrochemical detection of its transformation efficiency. *Sci. Rep.* **2021**, *11*, 21312. [CrossRef]
20. Yang, H.C.; Rosen, B.P. New mechanisms of bacterial arsenic resistance. *Biomed. J.* **2016**, *39*, 5–13. [CrossRef]
21. Andres, J.; Bertin, P.N. The microbial genomics of arsenic. *FEMS Microbiol. Rev.* **2016**, *40*, 299–322. [CrossRef] [PubMed]
22. Ben Fekih, I.; Zhang, C.; Li, Y.P.; Zhao, Y.; Alwathnani, H.A.; Saquib, Q.; Rensing, C.; Cervantes, C. Distribution of arsenic resistance genes in prokaryotes. *Front. Microbiol.* **2018**, *9*, 2473. [CrossRef] [PubMed]
23. Yan, G.; Chen, X.; Du, S.; Deng, Z.; Wang, L.; Chen, S. Genetic mechanisms of arsenic detoxification and metabolism in bacteria. *Curr. Genet.* **2019**, *65*, 329–338. [CrossRef] [PubMed]
24. Mazumder, P.; Sharma, S.K.; Taki, K.; Kalamdhad, A.S.; Kumar, M. Microbes involved in arsenic mobilization and respiration: A review on isolation, identification, isolates and implications. *Environ. Geochem. Health* **2020**, *42*, 3443–3469. [CrossRef]
25. Páez-Espino, A.D.; Nikel, P.I.; Chavarría, M.; de Lorenzo, V. ArsH protects *Pseudomonas putida* from oxidative damage caused by exposure to arsenic. *Environ. Microbiol.* **2020**, *22*, 2230–2242. [CrossRef]
26. Rawle, R.; Saley, T.C.; Kang, Y.S.; Wang, Q.; Walk, S.; Bothner, B.; McDermott, T.R. Introducing the ArsR-regulated arsenic stimulon. *Front. Microbiol.* **2021**, *12*, 630562. [CrossRef]
27. Yang, H.C.; Fu, H.L.; Lin, Y.F.; Rosen, B.P. Pathways of arsenic uptake and efflux. *Curr. Top. Membr.* **2012**, *69*, 325–358. [CrossRef]
28. Ghosh, M.; Shen, J.; Rosen, B.P. Pathways of As(III) detoxification in *Saccharomyces cerevisiae*. *Proc. Nat. Acad. Sci. USA* **1999**, *96*, 5001–5006. [CrossRef]
29. Di, X.; Beesley, L.; Zhang, Z.; Zhi, S.; Jia, Y.; Ding, Y. Microbial arsenic methylation in soil and uptake and metabolism of methylated arsenic in plants: A review. *Int. J. Environ. Res. Public Health* **2019**, *16*, 5012. [CrossRef]
30. Huang, K.; Xu, Y.; Packianathan, C.; Gao, F.; Chen, C.; Zhang, J.; Shen, Q.; Rosen, B.P.; Zhao, F.J. Arsenic methylation by a novel ArsM As(III) S-adenosylmethionine methyltransferase that requires only two conserved cysteine residues. *Mol. Microbiol.* **2018**, *107*, 265–276. [CrossRef]
31. Chen, J.; Yoshinaga, M.; Garbinski, L.D.; Rosen, B.P. Synergistic interaction of glyceraldehydes-3-phosphate dehydrogenase and ArsJ, a novel organoarsenical efflux permease, confers arsenate resistance. *Mol. Microbiol.* **2016**, *100*, 945–953. [CrossRef] [PubMed]
32. Liu, H.; Hong, Z.; Lin, J.; Huang, D.; Ma, L.Q.; Xu, J.; Dai, Z. Bacterial coculture enhanced Cd sorption and as bioreduction in co-contaminated systems. *J. Hazard. Mater.* **2023**, *444*, 130376. [CrossRef] [PubMed]
33. Luque-Almagro, V.M.; Huertas, M.J.; Martínez-Luque, M.; Moreno-Vivián, C.; Roldán, M.D.; García-Gil, L.J.; Castillo, F.; Blasco, R. Bacterial degradation of cyanide and its metal complexes under alkaline conditions. *Appl. Environ. Microbiol.* **2005**, *71*, 940–947. [CrossRef] [PubMed]
34. Estepa, J.; Luque-Almagro, V.M.; Manso, I.; Escribano, M.P.; Martínez-Luque, M.; Castillo, F.; Moreno-Vivián, C.; Roldán, M.D. The *nit1C* gene cluster of *Pseudomonas pseudoalcaligenes* CECT5344 involved in assimilation of nitriles is essential for growth on cyanide. *Environ. Microbiol. Rep.* **2012**, *4*, 326–334. [CrossRef] [PubMed]
35. Cabello, P.; Luque-Almagro, V.M.; Olaya-Abril, A.; Sáez, L.P.; Moreno-Vivián, C.; Roldán, M.D. Assimilation of cyanide and cyano-derivatives by *Pseudomonas pseudoalcaligenes* CECT5344: From omic approaches to biotechnological applications. *FEMS Microbiol. Lett.* **2018**, *365*, fny032. [CrossRef]
36. Sáez, L.P.; Cabello, P.; Ibáñez, M.I.; Luque-Almagro, V.M.; Roldán, M.D.; Moreno-Vivián, C. Cyanate assimilation by the alkaliphilic cyanide-degrading bacterium *Pseudomonas pseudoalcaligenes* CECT5344: Mutational analysis of the *cyn* gene cluster. *Int. J. Mol. Sci.* **2019**, *20*, 3008. [CrossRef] [PubMed]
37. Luque-Almagro, V.M.; Acera, F.; Igeño, M.I.; Wibberg, D.; Roldán, M.D.; Sáez, L.P.; Hennig, M.; Quesada, A.; Huertas, M.J.; Blom, J.; et al. Draft whole genome sequence of the cyanide-degrading bacterium *Pseudomonas pseudoalcaligenes* CECT5344. *Environ. Microbiol.* **2013**, *15*, 253–270. [CrossRef]
38. Wibberg, D.; Bremges, A.; Dammann-Kalinowski, T.; Maus, I.; Igeño, M.I.; Vogelsang, R.; König, C.; Luque-Almagro, V.M.; Roldán, M.D.; Sczyrba, A.; et al. Finished genome sequence and methylome of the cyanide-degrading *Pseudomonas pseudoalcaligenes* strain CECT5344 as resolved by single-molecule real-time sequencing. *J. Biotechnol.* **2016**, *232*, 61–68. [CrossRef]
39. Luque-Almagro, V.M.; Escribano, M.P.; Manso, I.; Sáez, L.P.; Cabello, P.; Moreno-Vivián, C.; Roldán, M.D. DNA microarray analysis of the cyanotroph *Pseudomonas pseudoalcaligenes* CECT5344 in response to nitrogen starvation, cyanide and a jewelry wastewater. *J. Biotechnol.* **2015**, *214*, 171–181. [CrossRef]
40. Luque-Almagro, V.M.; Moreno-Vivián, C.; Roldán, M.D. Biodegradation of cyanide wastes from mining and jewellery industries. *Curr. Opin. Biotechnol.* **2016**, *38*, 9–13. [CrossRef]
41. Ibáñez, M.I.; Cabello, P.; Luque-Almagro, V.M.; Saez, L.P.; Olaya, A.; Sánchez de Medina, V.; Luque de Castro, M.D.; Moreno-Vivian, C.; Roldán, M.D. Quantitative proteomic analysis of *Pseudomonas pseudoalcaligenes* CECT5344 in response to industrial cyanide-containing wastewaters using Liquid Chromatography-Mass Spectrometry/Mass Spectrometry (LC-MS/MS). *PLoS ONE* **2017**, *12*, e0172908. [CrossRef] [PubMed]

42. Olaya-Abril, A.; Luque-Almagro, V.M.; Pérez, M.D.; López, C.M.; Amil, F.; Cabello, P.; Sáez, L.P.; Moreno-Vivian, C.; Roldán, M.D. Putative small rRNAs controlling detoxification of industrial cyanide-containing wastewaters by *Pseudomonas pseudoalcaligenes* CECT5344. *PLoS ONE* **2019**, *14*, e0212032. [CrossRef] [PubMed]
43. Olaya-Abril, A.; Pérez, M.D.; Cabello, P.; Martignetti, D.; Sáez, L.P.; Luque-Almagro, V.M.; Moreno-Vivián, C.; Roldán, M.D. Role of the dihydrodipicolinate synthase DapA1 on iron homeostasis during cyanide assimilation by the alkaliphilic bacterium *Pseudomonas pseudoalcaligenes* CECT5344. *Front. Microbiol.* **2020**, *11*, 28. [CrossRef] [PubMed]
44. Pérez, M.D.; Olaya-Abril, A.; Cabello, P.; Sáez, L.P.; Roldán, M.D.; Moreno-Vivián, C.; Luque-Almagro, V.M. Alternative pathway for 3-cyanoalanine assimilation in *Pseudomonas pseudoalcaligenes* CECT5344 under noncyanotrophic conditions. *Microbiol. Spectr.* **2021**, *9*, e0077721. [CrossRef] [PubMed]
45. Roldán, M.D.; Olaya-Abril, A.; Sáez, L.P.; Cabello, P.; Luque-Almagro, V.M.; Moreno-Vivián, C. Bioremediation of cyanide-containing wastes: The potential of systems and synthetic biology for cleaning up the toxic leftovers from mining. *EMBO Rep.* **2021**, *22*, e53720. [CrossRef] [PubMed]
46. Tripti, K.; Sayantan, D.; Shardendu, S.; Singh, D.N.; Tripathi, A.K. Potential for the uptake and removal of arsenic [As(V) and As(III)] and the reduction of As(V) to As(III) by *Bacillus licheniformis* (DAS1) under different stresses. *Korean J. Microbiol. Biotechnol.* **2014**, *42*, 238–248. [CrossRef]
47. Chitpriom, K.; Akaracharanya, A.; Tanasupawat, S.; Leepipatpiboom, N.; Kim, K. Isolation and characterization of arsenic resistant bacteria from tannery wastes and agricultural soils in Thailand. *Ann. Microbiol.* **2009**, *59*, 649–656. [CrossRef]
48. Cai, L.; Liu, G.; Rensing, C.; Wang, G. Genes involved in arsenic transformation and resistance associated with different levels of arsenic-contaminated soils. *BMC Microbiol.* **2009**, *9*, 4. [CrossRef]
49. Byeon, E.; Kang, H.M.; Yoon, C.; Lee, J.S. Toxicity mechanisms of arsenic compounds in aquatic organisms. *Aquat. Toxicol.* **2021**, *237*, 105901. [CrossRef]
50. Kabiraj, A.; Biswas, R.; Halder, U.; Bandopadhyay, R. Bacterial arsenic metabolism and its role in arsenic bioremediation. *Curr. Microbiol.* **2022**, *79*, 131. [CrossRef]
51. Newsome, L.; Falagán, C. The microbiology of metal mine waste: Bioremediation applications and implications for planetary health. *GeoHealth* **2021**, *5*, e2020GH000380. [CrossRef] [PubMed]
52. Kuchma, S.L.; O'Toole, G.A. Surface-induced cAMP signaling requires multiple features of the *Pseudomonas aeruginosa* type IV pili. *J. Bacteriol.* **2022**, *204*, e00186-22. [CrossRef] [PubMed]
53. Bogdanow, B.; Zauber, H.; Selbach, M. Systematic errors in peptide and protein identification and quantification by modified peptides. *Mol. Cell. Proteom.* **2016**, *15*, 2791–2801. [CrossRef] [PubMed]
54. Bazzi, W.; Abou Fayad, A.G.; Nasser, A.; Haraoui, L.P.; Dewachi, O.; Abou-Sitta, G.; Nguyen, V.K.; Abara, A.; Karah, N.; Landecker, H.; et al. Heavy metal toxicity in armed conflicts potentiates AMR in *A. baumannii* by selecting for antibiotic and heavy metal co-resistance mechanisms. *Front. Microbiol.* **2020**, *11*, 68. [CrossRef] [PubMed]
55. Mathivanan, K.; Uthaya-Chandirika, J.; Vinothkanna, A.; Yin, H.; Liu, X.; Meng, D. Bacterial adaptive strategies to cope with metal toxicity in the contaminated environment—A review. *Ecotoxicol. Environ. Saf.* **2021**, *226*, 112863. [CrossRef] [PubMed]
56. Bae, S.; Kamynina, E.; Guetterman, H.M.; Farinola, A.F.; Caudill, M.A.; Berry, R.J.; Cassano, P.A.; Stover, P.J. Provision of folic acid for reducing arsenic toxicity in arsenic-exposed children and adults. *Cochrane Database Syst. Rev.* **2021**, *10*, CD012649. [CrossRef]
57. Bustaffa, E.; Gorini, F.; Bianchi, F.; Minichilli, F. Factors affecting arsenic methylation in contaminated Italian areas. *Int. J. Environ. Res. Public Health* **2020**, *17*, 5226. [CrossRef]
58. Abuawad, A.; Spratlen, M.J.; Parvez, F.; Slavkovich, V.; Ilievski, V.; Lomax-Luu, A.M.; Saxena, R.; Shahriar, H.; Uddin, M.N.; Islam, T.; et al. Association between body mass index and arsenic methylation in three studies of Bangladeshi adults and adolescents. *Environ. Int.* **2021**, *149*, 106401. [CrossRef]
59. Saal, T.; Christe, K.O.; Haiges, R. Lewis adduct formation of hydrogen cyanide and nitriles with arsenic and antimony pentafluoride. *Dalton Trans.* **2018**, *48*, 99–106. [CrossRef]
60. Maity, S.; Sarkar, D.; Poddar, K.; Patil, P.; Sarkar, A. Biofilm-mediated heavy metal removal from aqueous system by multi-metal-resistant bacterial strain *Bacillus* sp. GH-s29. *Appl. Biochem. Biotechnol.* **2022**, 1–19. [CrossRef]
61. Kim, S.H.; Wei, C.I. Molecular characterization of biofilm formation and attachment of *Salmonella enterica* serovar typhimurium DT104 on food contact surfaces. *J. Food Prot.* **2009**, *72*, 1841–1847. [CrossRef] [PubMed]
62. Li, J.; Wang, N. The *wxacO* gene of *Xanthomonas citri* ssp. *citri* encodes a protein with a role in lipopolysaccharide biosynthesis, biofilm formation, stress tolerance and virulence. *Mol. Plant Pathol.* **2011**, *12*, 381–396. [CrossRef]
63. Páez-Espino, A.D.; Durante-Rodríguez, G.; de Lorenzo, V. Functional coexistence of twin arsenic resistance systems in *Pseudomonas putida* KT2440. *Environ. Microbiol.* **2015**, *17*, 229–238. [CrossRef] [PubMed]
64. Zhao, C.; Zhang, Y.; Chan, Z.; Chen, S.; Yang, S. Insights into arsenic multi-operons expression and resistance mechanisms in *Rhodopseudomonas palustris* CGA009. *Front. Microbiol.* **2015**, *6*, 986. [CrossRef] [PubMed]
65. Naghili, H.; Tajik, H.; Mardani, K.; Razavi Rouhani, S.M.; Ehsani, A.; Zare, P. Validation of drop plate technique for bacterial enumeration by parametric and nonparametric tests. *Vet. Res. Forum* **2013**, *4*, 179–183.
66. Andrews, J.M. Determination of minimum inhibitory concentrations. *J. Antimicrob. Chemother.* **2001**, *48*, 5–16. [CrossRef]
67. Morrison, G.R. Microchemical determination of organic nitrogen with nessler reagent. *Anal. Biochem.* **1971**, *43*, 527–532. [CrossRef]
68. Asmus, E.; Garschagen, H. Über die Verwendung der Barbitursäure für die Photometrische Bestimmung von Cyanid und Rhodanid. *Fresenius' Z. Anal. Chem.* **1953**, *138*, 414–422. [CrossRef]

69. Bradford, M.M. A rapid and sensitive method for the quantitation of microgram quantities of protein utilizing the principle of protein-dye binding. *Anal. Biochem.* **1976**, *72*, 248–254. [CrossRef]
70. Lundholt, B.K.; Scudder, K.M.; Pagliaro, L. A simple technique for reducing edge effect in cell-based assays. *J. Biomol. Screen* **2003**, *8*, 566–570. [CrossRef]
71. Olaya-Abril, A.; Hidalgo-Carrillo, J.; Luque-Almagro, V.M.; Fuentes-Almagro, C.; Urbano, F.J.; Moreno-Vivián, C.; Richardson, D.J.; Roldán, M.D. Exploring the denitrification proteome of *Paracoccus denitrificans* PD1222. *Front. Microbiol.* **2018**, *9*, 1137. [CrossRef] [PubMed]
72. Olaya-Abril, A.; Hidalgo-Carrillo, J.; Luque-Almagro, V.M.; Fuentes-Almagro, C.; Urbano, F.J.; Moreno-Vivián, C.; Richardson, D.J.; Roldán, M.D. Effect of pH on the denitrification proteome of the soil bacterium *Paracoccus denitrificans* PD1222. *Sci. Rep.* **2021**, *11*, 17276. [CrossRef] [PubMed]
73. Fruzangohar, M.; Ebrahimie, E.; Ogunniyi, A.D.; Mahdi, L.K.; Paton, J.C.; Adelson, D.L. Comparative GO: A web application for comparative gene ontology and gene ontology-based gene selection in bacteria. *PLoS ONE* **2013**, *8*, e58759. [CrossRef] [PubMed]
74. Olaya-Abril, A.; Luque-Almagro, V.M.; Hidalgo-Carrillo, J.; Chicano-Gálvez, E.; Urbano, F.J.; Moreno-Vivián, C.; Richardson, D.J.; Roldán, M.D. The NtrYX two-component system of *Paracoccus denitrificans* is required for the maintenance of cellular iron homeostasis and for a complete denitrification under iron-limited conditions. *Int. J. Mol. Sci.* **2022**, *23*, 9172. [CrossRef] [PubMed]

AMERICAN SOCIETY FOR MICROBIOLOGY | Microbiology Spectrum

RESEARCH ARTICLE

Quantitative Proteomic Analysis of Cyanide and Mercury Detoxification by *Pseudomonas pseudoalcaligenes* CECT 5344

Karolina A. Biełło,[a] Alfonso Olaya-Abril,[a] Purificación Cabello,[b] Gema Rodríguez-Caballero,[a] Lara P. Sáez,[a] Conrado Moreno-Vivián,[a] Víctor Manuel Luque-Almagro,[a] María Dolores Roldán[a]

[a]Departamento de Bioquímica y Biología Molecular, Edificio Severo Ochoa, Campus de Rabanales, Universidad de Córdoba, Córdoba, Spain
[b]Departamento de Botánica, Ecología y Fisiología Vegetal, Edificio Celestino Mutis, Campus de Rabanales, Universidad de Córdoba, Córdoba, Spain

Karolina A. Biełło and Alfonso Olaya-Abril contributed equally to this work. The order of two first coauthors was determined alphabetically.

ABSTRACT The cyanide-degrading bacterium *Pseudomonas pseudoalcaligenes* CECT 5344 uses cyanide and different metal-cyanide complexes as the sole nitrogen source. Under cyanotrophic conditions, this strain was able to grow with up to 100 μM mercury, which was accumulated intracellularly. A quantitative proteomic analysis by liquid chromatography-tandem mass spectrometry (LC-MS/MS) has been applied to unravel the molecular basis of the detoxification of both cyanide and mercury by the strain CECT 5344, highlighting the relevance of the cyanide-insensitive alternative oxidase CioAB and the nitrilase NitC in the tolerance and assimilation of cyanide, independently of the presence or absence of mercury. Proteins overrepresented in the presence of cyanide and mercury included mercury transporters, mercuric reductase MerA, transcriptional regulator MerD, arsenate reductase and arsenical resistance proteins, thioredoxin reductase, glutathione *S*-transferase, proteins related to aliphatic sulfonates metabolism and sulfate transport, hemin import transporter, and phosphate starvation induced protein PhoH, among others. A transcriptional study revealed that from the six putative *merR* genes present in the genome of the strain CECT 5344 that could be involved in the regulation of mercury resistance/detoxification, only the *merR2* gene was significantly induced by mercury under cyanotrophic conditions. A bioinformatic analysis allowed the identification of putative MerR2 binding sites in the promoter regions of the regulatory genes *merR5*, *merR6*, *arsR*, and *phoR*, and also upstream from the structural genes encoding glutathione *S*-transferase (*fosA* and *yghU*), dithiol oxidoreductase (*dsbA*), metal resistance chaperone (*cpxP*), and amino acid/peptide extruder involved in quorum sensing (*virD*), among others.

IMPORTANCE Cyanide, mercury, and arsenic are considered very toxic chemicals that are present in nature as cocontaminants in the liquid residues generated by different industrial activities like mining. Considering the huge amounts of toxic cyanide- and mercury-containing wastes generated at a large scale and the high biotechnological potential of *P. pseudoalcaligenes* CECT 5344 in the detoxification of cyanide present in these industrial wastes, in this work, proteomic, transcriptional, and bioinformatic approaches were used to characterize the molecular response of this bacterium to cyanide and mercury, highlighting the mechanisms involved in the simultaneous detoxification of both compounds. The results generated could be applied for developing bioremediation strategies to detoxify wastes cocontaminated with cyanide, mercury, and arsenic, such as those generated at a large scale in the mining industry.

KEYWORDS arsenic, biodegradation, cyanide, heavy metals, mercury, *Pseudomonas*

Mercury is an environmental hazard that is accumulated in nature at low concentrations as both inorganic and organic forms, such as elemental/metallic (Hg^0) or bivalent (Hg^{II}) mercury, and organomercurials (R-Hg). In addition to natural processes,

Editor Giordano Rampioni, Universita degli Studi Roma Tre Dipartimento di Scienze

Address correspondence to Víctor Manuel Luque-Almagro, b42lualv@uco.es.

The authors declare no conflict of interest.

Received 24 March 2023
Accepted 21 June 2023
Published 11 July 2023

anthropogenic activities produce up to 7,000 metric tons of mercury per year, which may be toxic disposals in the absence of appropriate waste management strategies (1, 2). Among these human activities include fossil fuel combustion, especially coal; metal ore mining; mercury-containing pesticides used in agriculture; and mercury-based catalysts applied to industrial purposes (1–4). The largest amounts of mercury released to the environment correspond to mining activities, mainly related to gold extraction. In the recovery of precious metals from ores, elevated concentrations of cyanide are also used in the so-called cyanidation process (cyanide leaching), and other pollutants like arsenic, lead, copper, or zinc are usually present as cocontaminants of the cyanide-containing wastes generated from mining industries (5–8). About one million tons/year of these wastewaters from mines are produced, which are stored in artificial ponds that are prone to leaching or dam breaks, posing a major threat to the environment and human health (8).

Elemental mercury is dangerous because of its volatility, and pollution caused by this form of mercury is not restricted to the specific areas where it is released since it may be easily scattered by the wind. Elemental mercury is chemically oxidized to the bivalent form and deposited in aquatic or terrestrial ecosystems (2, 9, 10). Additionally, mercury can undergo further reactions like reduction or methylation. Methylmercury bioaccumulates and biomagnifies in the food chain (11, 12), and humans may be exposed to methylmercury from contaminated fish when ingested. Likewise, mercury salts like mercury chloride also display great acute toxicity (13). Organomercurials are considered very potent toxins that threaten human health and ecosystems. Methylmercury has a half-life of about 44 days in the human body and constitutes a neurotoxin that accumulates in brain, kidney, and liver. Additionally, methylmercury may pass through the placenta, affecting the fetus (1, 2, 14). Mercury is associated with a broad range of severe diseases, such as Minamata disease, acrodynia, attention deficit disorder, and hyperactivity (15, 16).

Considering that mercury may be present naturally in the environment, many different microorganisms have evolved mechanisms to tolerate and detoxify this toxic metal. Microorganisms play a major role in mercury cycling in nature through reduction, oxidation, and/or bioaccumulation (chelation or biosorption) processes (1, 2, 17). Some bacteria like *Escherichia coli*, *Bacillus*, or *Streptomyces* display an oxidative mechanism that produces the bivalent form of mercury from elemental mercury through a hydroperoxidase-catalase activity (2, 18). Some dissimilatory sulfate-reducing bacteria and dissimilatory iron-reducing bacteria are able to carry out mercury methylation under anaerobic conditions (19, 20), although it is still controversial if methylation may confer resistance to mercury. On the other hand, extracellular biosorption of mercury has been described in several bacterial strains, occurring mainly through the secretion of negatively charged extracellular polymers (17). However, the most widespread mechanism of resistance triggered by bacteria in response to mercury toxicity is based on the occurrence of the *mer* genes (21). The *mer* operons described up to date are considered narrow spectrum when they confer resistance only to inorganic mercury salts or broad spectrum when they facilitate resistance to both organomercurials and inorganic mercury (21–23).

The alkaliphilic bacterium *Pseudomonas pseudoalcaligenes* CECT 5344 was isolated from sludges of the Guadalquivir River (Córdoba, Spain) near an industrial area with elevated jewelry activity, in which cyanide is used for gold electroplating. The strain CECT 5344 uses free cyanide, metal-cyanide complexes, and cyano derivatives, including cyanate and 3-cyanoalanine, as the sole nitrogen source under alkaline conditions that prevent cyanhydric acid volatilization (24). *P. pseudoalcaligenes* CECT 5344 harbors in its genome, in addition to the gene clusters involved in cyanide resistance and assimilation, several *mer* and *ars* operons that could confer to this bacterium a wide capability to tolerate and detoxify mercury and arsenic (25).

Considering the large amounts of cyanide- and mercury-containing wastes generated in the mining industry and the high biotechnological potential of *P. pseudoalcaligenes* CECT 5344 in the bioremediation of these industrial wastes (8), in this work, the

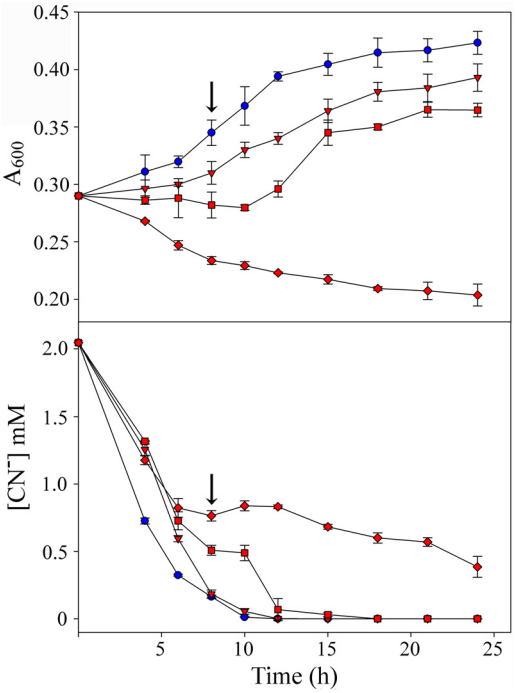

FIG 1 Physiological characterization of *P. pseudoalcaligenes* CECT 5344 cells grown with cyanide as the sole nitrogen source, in the presence or absence of mercury. Growth (top) and cyanide consumption (bottom) of *P. pseudoalcaligenes* CECT 5344 cells in media without mercury (blue circles) or with mercury (red symbols) at 75 μM (triangles), 100 μM (squares), and 150 μM (diamonds). Cells were grown in M9 minimal media with 50 mM sodium acetate and 2 mM sodium cyanide as the carbon and nitrogen source, respectively. CECT 5344 cells for proteomic and qRT-PCR analyses were harvested at 7.5 h of growth (time indicated by the arrow).

molecular response to cyanide and mercury of this cyanide-degrading bacterium was characterized through liquid chromatography-tandem mass spectrometry (LC-MS/MS), reverse transcription-quantitative PCR (qRT-PCR), and bioinformatic approaches. The results generated could be useful to develop further bioremediation techniques for the detoxification of wastes cocontaminated with cyanide, mercury, and arsenic.

RESULTS

Detoxification of cyanide and mercury by *P. pseudoalcaligenes*. To evaluate the ability of the cyanide-degrading bacterium *P. pseudoalcaligenes* CECT 5344 to detoxify cyanide in the presence of mercuric chloride, the MIC and the minimum bactericidal concentration (MBC) were determined in this bacterium. The MIC and MBC of mercury for CECT 5344 cells grown aerobically in M9 minimal media, with 50 mM acetate and 2 mM sodium cyanide as the sole carbon and nitrogen sources, were 200 μM and 300 μM, respectively. In contrast, in the absence of cyanide and with 2 mM ammonium chloride as the nitrogen source, the MIC and MBC of mercury were considerably lower, namely, 10 μM and 17.5 μM, respectively. The growth curves of the CECT 5344 strain were carried out in minimal medium M9 with 2 mM cyanide as the sole nitrogen source in the absence or the presence of different concentrations of mercury, ranging from 75 μM to 150 μM (Fig. 1). The strain CECT 5344 was able to grow with 100 μM mercury, consuming cyanide from the extracellular medium, although this growth was slower than growth with 75 μM mercury. Accordingly, cyanide was totally removed from the medium at 12 h in the presence of 75 μM mercury, but about 18 h were required for the complete consumption of cyanide in the presence of 100 μM mercury (Fig. 1). At higher mercury concentrations, such as 150 μM or above, bacterial growth and cyanide uptake were severely impaired (Fig. 1). Therefore, 75 μM mercury chloride was used to perform further analyses.

Additionally, mercury concentration remaining in the extracellular media or bioaccumulated extracellularly (biosorption) and intracellularly (chelated to biomolecules) was determined by inductively coupled plasma-mass spectrometry (ICP-MS) from CECT 5344 cultures at 7.5 h of growth in media with 2 mM NaCN and 75 μM $HgCl_2$, as described in the Materials and Methods. Mercury was neither detected in the extracellular media nor bioaccumulated extracellularly, while the intracellular concentration of mercury was 0.010 $\pm$ 0.003 μg/mg protein. In a control experiment carried out without cells, the mercury concentration remained constant throughout the experiment (data not shown).

The analysis of the *P. pseudoalcaligenes* CECT 5344 genome sequence revealed the presence of two *mer* gene clusters in the loci BN5_3800-BN5_3802 (*merP1T1R5*) and BN5_4473-BN5_4479 (*merR6T3P3T5ADE*). These mercury resistance genes code for putative transcriptional regulators MerR and MerD; mercuric transport proteins MerT, MerP, and MerE; and mercuric reductase MerA. In addition, other four *merR* genes (*merR1* to *merR4*), encoding putative MerR transcriptional regulators, were also found scattered throughout the CECT 5344 genome.

Proteomic analysis of *P. pseudoalcaligenes* grown under cyanotrophic conditions with mercury. To investigate the global changes in the proteome of *P. pseudoalcaligenes* CECT 5344 provoked by the combination of the two toxic chemicals cyanide and mercury, a proteomic analysis by liquid chromatography-tandem mass spectrometry (LC-MS/MS) was performed in CECT 5344 cells grown under aerobic conditions with 2 mM sodium cyanide as the sole nitrogen source, in the absence (CN) or presence of 75 μM $HgCl_2$ (CN + Hg). Cells were harvested at 7.5 h of growth, when they were actively growing, and low concentrations of cyanide remained in the media (Fig. 1). Four independent biological replicates were used in this study, and the principal-component analysis (PCA), clustering of the replicates, and volcano plot were obtained (see Fig. S1 to S3 in the supplemental material). The preliminary qualitative analysis revealed that the overall number of identified proteins (2,689) represented about 60% of the total predicted protein-coding genes (4,435 genes) of the CECT 5344 strain (26).

A further quantitative differential analysis was performed by a comparison of the CN + Hg and CN proteomes (see Table S1 in the supplemental material). In this comparative analysis, the parameter fold change (FC) was used to measure differences in protein expression, which was calculated as the ratio of normalized peptide intensities, CN + Hg/CN. Therefore, proteins shared by both CN + Hg and CN proteomes, but that were nevertheless differentially represented, were considered "overrepresented" in the CN + Hg proteome when the $\log_2$ FC was $\geq$1 or "downrepresented" in the CN + Hg proteome when the $\log_2$ FC was ≤ -1. Proteins that were found only in one proteome (either CN + Hg or CN) were considered "exclusive" of that condition. In this quantitative analysis, 21 proteins were exclusive of the CN + Hg proteome and 209 proteins were found differentially expressed (see Fig. S4 in the supplemental material; Table S1). Among these proteins differentially expressed, 45 proteins were overrepresented in the CN + Hg proteome, while 164 proteins were downrepresented in the CN + Hg proteome (Table S1). The gene ontology (GO) analysis (27) using the comparative study between the proteomes CN and CN + Hg revealed insight into functional protein categories that were affected by the presence of mercury under cyanotrophic conditions. Proteins overrepresented in the absence of mercury (or downrepresented with mercury) belonged mainly to the GO category "urea metabolism," while proteins overrepresented in the presence of mercury (or downrepresented without mercury) belonged to the GO groups "response to metal ion," "response to toxic substance," "response to mercury ion," "detoxification of inorganic compound," and "oxidoreductase activity, acting on the CH-NH_2 group of donors," among others (see Fig. S5 in the supplemental material).

The proteins encoded by the *nit1C* and *cio* gene clusters, which are essential for cyanide assimilation and cyanide-insensitive respiration, respectively (25, 28), were found in both proteomes (CN and CN + Hg) and were not affected significantly by the presence of mercury (Fig. 2).

Protein ID[(1)]	Gene ID[(2)]	Protein description/name	CN	CN+Hg
		nit gene cluster		
H9N5E0	BN5_1630	Sigma-54-dependent transcriptional regulator (NitA)		
H9N5E2	BN5_1631	Uncharacterized protein (NitB)		
H9N5E1	BN5_1632	Nitrilase (NitC)		
H9N5E3	BN5_1633	Radical SAM domain-containing protein (NitD)		
H9N5E4	BN5_1634	GCN5-related *N*-acetyltransferase (NitE)		
H9N5E5	BN5_1635	AIR synthase-like protein (NitF)		
H9N5D9	BN5_1636	Uncharacterized protein (NitG)		
H9N5D8	BN5_1637	FAD-dependent oxidoreductase (NitH)		
		cio gene cluster		
W6QWX1	BN5_1899	GntR family transcriptional regulator (MocR)		
W6RF17	BN5_1900	Sulfite reductase (NADPH) hemoprotein beta-component (CysL3)		
W6QU90	BN5_1901	Uncharacterized protein (CioC3)		
W6R254	BN5_1902	Terminal oxidase subunit I (CioA3)		
W6QVH5	BN5_1903	Cytochrome *d* ubiquinol oxidase, subunit II (CioB3)		
W6QWX6	BN5_1904	Phosphoserine aminotransferase (SerC3)		
W6RF21	BN5_1905	Histidinol-phosphate aminotransferase (HisC3)		
W6QU95	BN5_1906	Acetylornithine aminotransferase (ArgD3)		
W6R260	BN5_1907	4-hydroxy-tetrahydrodipicolinate synthase (DapA1)		
W6QVI0	BN5_1908	High-affinity glucose transporter		
W6QWY1	BN5_1909	Methylenetetrahydrofolate reductase (MetF3)		
W6RF25	BN5_1910	Cysteine synthase (CysM3)		
W6QUA1	BN5_1911	NADP-dependent malic enzyme (MaeB3)		
W6R265	BN5_1912	Nitrilase (Nit4)		
		C-N hydrolase and other nitrilase genes		
W6QQS6	BN5_0258	C-N hydrolase, nitrilase/cyanide hydratase (AguB)		
W6QQZ6	BN5_0736	C-N hydrolase, nitrilase/cyanide hydratase (Nit1B)		
W6QUY5	BN5_1196	Nitrilase homolog 1 (Nit1A)		
W6RF39	BN5_1925	Aliphatic nitrilase (Nit1)		
W6QZ84	BN5_2750	Hydrolase, carbon-nitrogen family		
W6QY63	BN5_3204	Formamidase (AmiF)		
W6R989	BN5_4427	Bifunctional nitrilase/nitrile hydratase NIT4B (Nit2)		
W6QZD7	BN5_3251	C-N hydrolase, nitrilase/cyanide hydratase (Nit3B)		

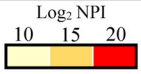

FIG 2 Effect of mercury on proteins involved in cyanide detoxification/assimilation in the *P. pseudoalcaligenes* CECT 5344 strain. Data are shown as a heatmap of the $\log_2$ of normalized peptide intensity ($\log_2$ NPI). CN, cyanide-containing media without added mercury; CN + Hg, cyanide-containing media with 75 μM $HgCl_2$. (1) Protein code according to the Uniprot database under the accession number UP000032841. (2) Gene annotation from GenBank (accession HG916826.1).

Some proteins identified in the quantitative analysis were classified functionally. Proteins were grouped into carbohydrate and energy metabolism, nucleotide metabolism, amino acid metabolism, metabolism of cofactors and vitamins, transporters, regulators, mercury and arsenic resistance, and other proteins (Fig. 3). In the first category, proteins involved in sulfur metabolism were highly overrepresented in the CN + Hg proteome, such as the SsuB and SsuC proteins for the transport of aliphatic sulfonates, the alkanesulfonate monooxygenase SsuD, and the sulfate-binding protein CysP3, whereas formamidase and proteins involved in cyanate metabolism were downrepresented in the presence of Hg (Fig. 3; Table S1). Among proteins highly overrepresented in the CN + Hg proteome were Mer proteins for mercury resistance (MerP1, MerP3, MerA, and MerD), arsenical resistance proteins (ArsR2, ArsC3, and ArsH2), proteins involved in the metabolism of amino acids (cobalamin-independent methionine synthase MetE and glutathione *S*-transferase) and nucleotides (dihydropyrimidine dehydrogenase, dihydropyrimidase, and ribonucleotide-diphosphate reductase), the synthesis of cofactors (precorrin-2 C20-methyltransferase CobI), and some transporters (hemin import ATP-binding HmuV) and regulators

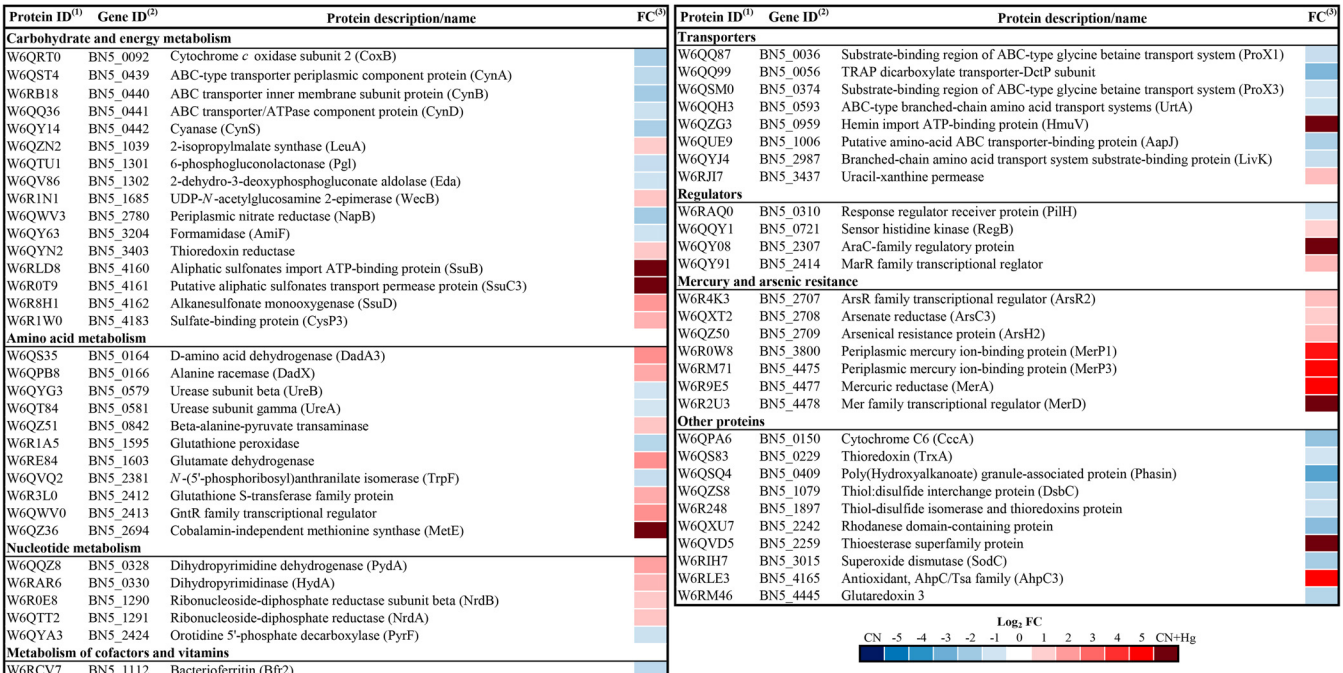

FIG 3 Heatmap of *P. pseudoalcaligenes* CECT 5344 proteins affected by mercury under cyanotrophic conditions. The differential expression of proteins is represented as the $\log_2$ fold change (FC). The fold change has been calculated as the ratio normalized peptide intensity in CN + Hg/normalized peptide intensity in CN. (1) Protein code according to Uniprot database under the accession number UP000032841. (2) Gene annotation from GenBank (accession HG916826.1).

(RegB, AraC, and GntR family regulators). In contrast, some proteins downrepresented in the CN + Hg proteome were related to polyhydroxyalkanoate production, dicarboxylate transport, and urea metabolism (Fig. 3; Table S1).

Additionally, a quantitative transcriptional analysis by qRT-PCR was applied to study the transcriptional expression of several genes that code for proteins that were found over- or downrepresented in the CN + Hg proteome (Table 1). Genes induced in the presence of mercury were those coding for phosphate starvation-induced protein PhoH, precorrin-2 C20-methyltransferase CobI, alkanesulfonate monooxygenase SsuD, alkyl hydroperoxide reductase AhpC, thioredoxin reductase, transcriptional regulator ArsR2, arsenate reductase ArsC3, glutathione *S*-transferase, and ribonucleoside-diphosphate reductase NrdB. Conversely, genes with a decreased expression in the presence of mercury included those coding for glutathione peroxidase and formamidase (Table 1). The expression of the *nitC* gene coding for the nitrilase NitC that is essential for cyanide assimilation was slightly decreased in the presence of mercury, although mercury had no effect on the expression of the *nitD* gene that is clustered together the *nitC* gene (Table 1).

Transcriptional and bioinformatic analyses of MerR regulators. The genome of *P. pseudoalcaligenes* CECT 5344 contains six genes that code for the following putative MerR-type transcriptional regulators: MerR1 (W6QQW2 protein/BN5_0701 gene), MerR2 (W6QVE0/BN5_2264), MerR3 (W6QWL9/BN5_2322), MerR4 (W6R6A1/BN5_3351), MerR5 (W6RKL7/BN5_3802), and MerR6 (W6R2T8/BN5_4473). BLASTP sequence comparisons of these six regulators revealed that MerR5 and MerR6 were homologs, displaying 50% identity. MerR2 showed 33% and 34% identity with MerR1 and MerR6, respectively, and MerR5 presented with 36.5% identity compared with MerR1 (see Table S2 in the supplemental material).

A quantitative gene expression analysis of the *P. pseudoalcaligenes merR* genes was performed using mRNA from cells grown under cyanotrophic conditions in CN or CN + Hg media (Fig. 4A). Only *merR2* (BN5_2264) showed a significative induction by mercury,

TABLE 1 Transcriptional expression analysis by qRT-PCR of some *P. pseudoalcaligenes* CECT 5344 genes encoding proteins affected by mercury in the proteomic analysis

Gene[a]/protein ID[b]	Gene/protein name	Gene expression[c] in:		Fold change[d]
		CN + Hg media	CN media	
BN5_3397/W6RJF8	PhoH family protein	0.156	0.086	1.82
BN5_4378/W6R2H6	Precorrin-2 C20-methyltransferase (CobI)	0.026	0.011	2.38
BN5_4162/W6R8H1	Alkanesulfonate monooxygenase (SsuD)	0.041	0.009	4.18
BN5_4165/W6RLE3	Antioxidant, AhpC/Tsa family (AhpC)	0.293	0.066	4.43
BN5_3403/W6QYN2	Thioredoxin reductase	0.418	0.083	5.00
BN5_2707/W6R4K3	ArsR family transcriptional regulator (ArsR2)	4.655	1.380	3.37
BN5_2708/W6QXT2	Arsenate reductase (ArsC3)	0.785	0.077	10.25
BN5_2412/W6R3L0	Glutathione *S*-transferase family protein	0.701	0.189	3.69
BN5_1290/W6R0E8	Ribonucleoside-diphosphate reductase (NrdB)	5.802	2.154	2.69
BN5_1595/W6R1A5	Glutathione peroxidase	0.528	0.650	0.81
BN5_3204/W6QY63	Formamidase (AmiF)	0.270	0.512	0.53
BN5_1632/H9N5E1	Nitrilase (NitC)	7.40	9.40	0.79
BN5_1633/H9N5E3	Radical SAM domain-containing protein (NitD)	5.524	5.536	1.00

[a]Protein code according to the Uniprot database under the accession number UP000032841.
[b]Gene annotation from GenBank (accession HG916826.1).
[c]Relative gene expression from cells grown in cyanide and mercury.
[d]Fold change represented as the ratio gene expression CN + Hg/CN.

displaying a fold change of 2.2, whereas *merR4* (BN5_3351) was downregulated in the presence of mercury (Fig. 4A). Additionally, a transcriptional expression analysis of other genes that belong to the *merR6T3P3T5ADE* (BN5_4473 to BN5_4479) and *merP1T1R5* (BN5_3800 to BN5_3802) gene clusters of *P. pseudoalcaligenes* CECT 5344 was carried out by qRT-PCR. Genes included in these two *mer* operons of the CECT 5344 strain were highly induced in the presence of mercury. However, the transcriptional expression of the *merP1* and *merT1* genes located in the *merP1T1R5* gene cluster was higher than that displayed by genes of the *merR6T3P3T5ADE* gene cluster. In addition, the transcriptional expression of the mercuric (II) reductase *merA* gene (BN5_4477) was higher than the expression of the *merT3*, *merD*, and *merE* genes that are located in the same gene cluster (Fig. 4B).

A bioinformatic analysis was performed to identify MerR orthologs in the KEGG database, revealing that MerR-type transcriptional regulators are distributed widely among proteobacteria and eubacteria, without significative differences in their distribution within the different phyla. Among the six MerR-type regulators of *P. pseudoalcaligenes* CECT 5344, MerR1 was the closest relative to MerR2 in the phylogenetic tree (Fig. 5). Curiously, the transcriptional regulator MerR2 was also very close, in evolutive distance, to those found in archaea and thermophilic bacteria (Fig. 5). An additional bioinformatic analysis was carried out to identify putative MerR2 binding boxes in the promoter gene regions of *P. pseudoalcaligenes* CECT 5344, according to the MerR binding sequence described previously in *Escherichia coli* (29). Thus, a predicted MerR2 binding sequence of 5′-(T/C)GTA(G/C)-N_4-GTAC-3′ was identified in *P. pseudoalcaligenes* CECT 5344. This predicted MerR binding sequence was found in the promoters of several regulatory genes, including those involved in mercuric resistance (*merR5*, BN5_3802; and *merR6*, BN5_4473), in arsenic resistance (*arsR*, BN5_0252), and in phosphate metabolism (*phoR*, BN5_4234). It was also found in the promoters of structural genes for metal resistance (*cpxP*, BN5_2475), ribonucleoside-diphosphate reductase/β-subunit (*nrdB*, BN5_1290), dithiol oxidoreductase/disulfide-forming (*dsbA*, BN5_0108), two glutathione *S*-transferases (*yghU*, BN5_2864; and *fosA*, BN5_3450), 3-octaprenyl-4-hydroxybenzoate carboxy-lyase (*ubiD*, BN5_0231), and amino acid/peptide exporter (*virD*, BN5_3536) (Fig. 6A). Additionally, a transcriptomic study using qRT-PCR of the predicted MerR target genes was performed. In this analysis, six of the predicted target genes were significantly induced (FC >2) in the presence of mercury, including *arsR*, *cpxP*, *nrdB*, *dsbA*, *yghU*, and *fosA* genes. However, the expression of the genes *merR5*, *merR6*, and *phoR*, which code for regulatory proteins, was not significantly affected by mercury (Fig. 6B).

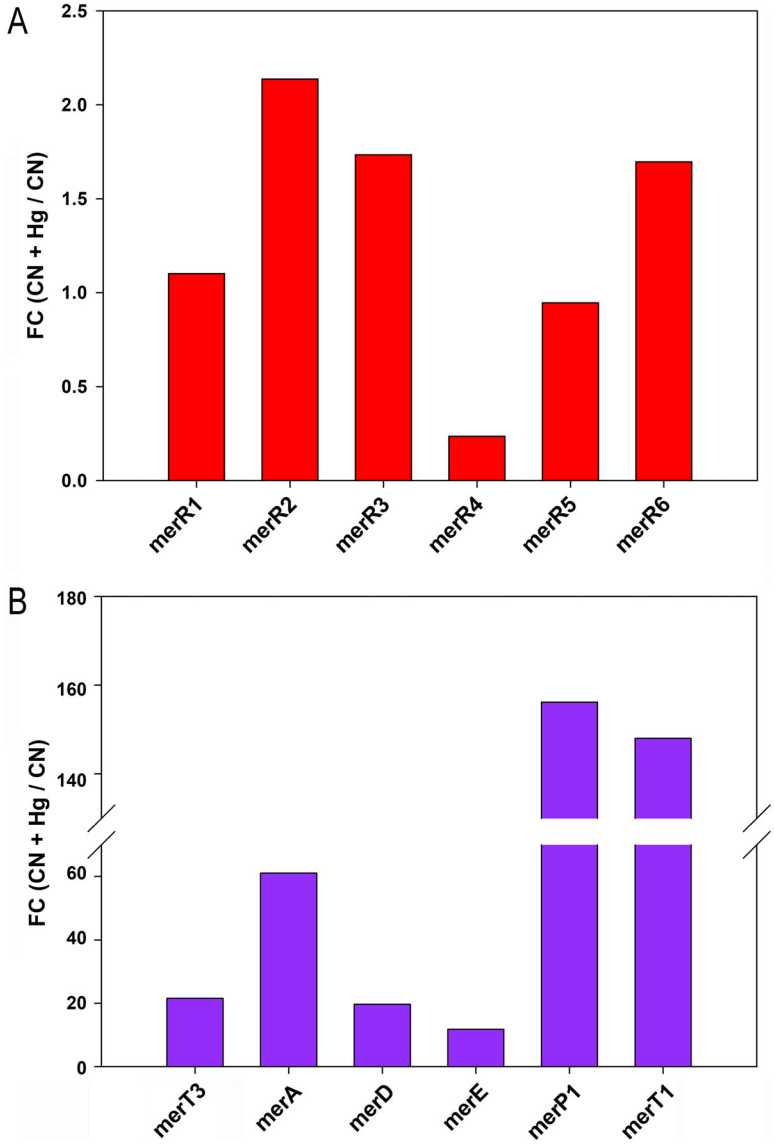

FIG 4 Transcriptional gene expression analysis by qRT-PCR of *P. pseudoalcaligenes* CECT 5344 *mer* genes. (A) Differential relative gene expression of *merR* genes. (B) Differential relative gene expression of other mercury-related genes. Gene expression was analyzed by qRT-PCR from cells grown with 2 mM sodium cyanide as the sole nitrogen source, without or with 75 μM $HgCl_2$. The differential gene expression is represented as the fold change (FC) of the ratio relative gene expression (CN + Hg/CN). Gene/protein identifiers (IDs) are as follows: *merR1* (BN5_0701/W6QQW2), *merR2* (BN5_2264/W6QVE0), *merR3* (BN5_2322/W6QWL9), *merR4* (BN5_3351/W6R6A1), *merR5* (BN5_3802/W6RKL7) *merR6* (BN5_4473/W6R2T83), *merT3* (BN5_4474/W6R4B5), *merA* (BN5_4477/W6R9E5), *merD* (BN5_4478/W6R2U3), *merE* (BN5_4479/W6R4C0), *merP1* (BN5_3800/W6R0W8), and *merT1* (BN5_3801/W6R273).

DISCUSSION

Mercury and cyanide resistance/detoxification by *P. pseudoalcaligenes* CECT 5344. Mercury is considered one of most toxic elements that is present in the environment, threatening ecosystems and human health (2, 30). Mercury may form strong complexes with inorganic anions, such as sulfide, hydroxide, or chloride, and also with other metals like gold and silver (31, 32). In the environment, microorganisms can also produce organomercurial derivatives, mainly methylmercury (2, 33). Additionally, mercury can bind to cyanide, which is used at a large scale in mining activities through the cyanidation process (5). It has been proposed that cyanide might facilitate the methylation of mercury, thus increasing its solubility in anaerobic aqueous environments and

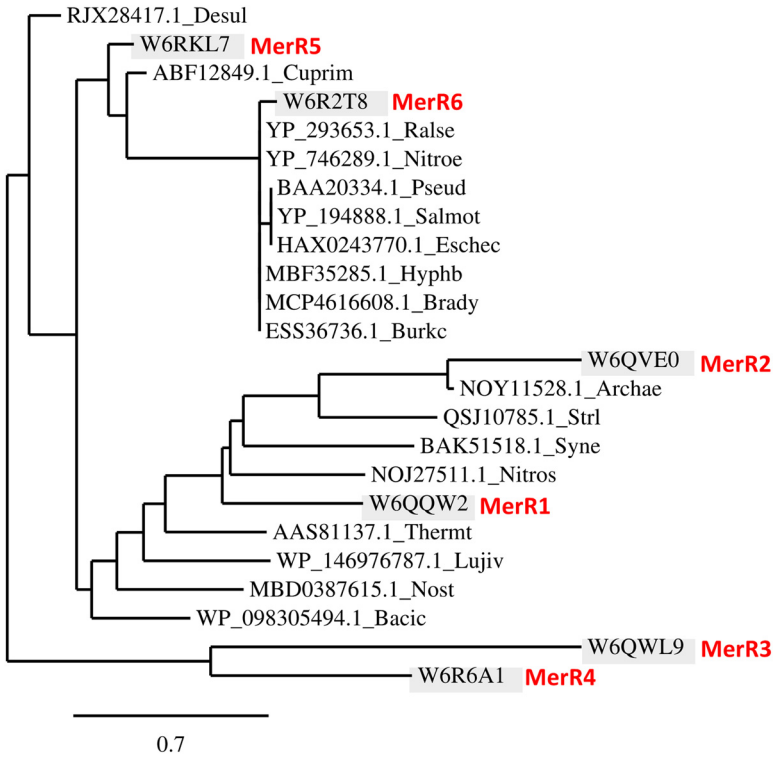

FIG 5 Phylogenetic distribution of MerR proteins in bacteria and archaea. The tree was constructed using the Phylogeny.fr platform (65). Sequences were aligned with MUSCLE v3.8.31 with default settings. Ambiguous regions were removed with Gblocks v0.91b. The phylogenetic tree was reconstructed using the maximum likelihood method implemented in the PhyML program 3.1/3.0 aLRT. The graphical representation and edition of the phylogenetic tree were performed with TreeDyn v198.3. The *P. pseudoalcaligenes* CECT 5344 MerR sequences are highlighted in red. Protein names (protein/gene IDs) are as follows: MerR1 (W6QQW2/BN5_0701), MerR2 (W6QVE0/BN5_2264), MerR3 (W6QWL9/BN5_2322), MerR4 (W6R6A1/BN5_3351), MerR5 (W6RKL7/BN5_3802), and MerR6 (W6R2T83/BN5_4473). Protein sequences correspond to the following phyla and organisms: *Alphaproteobacteria* (Hyphb, *Hyphomonadaceae bacterium*; Brady, *Bradyrhizobium* sp.), *Betaproteobacteria* (Burkc, *Burkholderia cenocepacia* KC-01; Nitroe, *Nitrosomonas eutropha* C91; Ralse, *Ralstonia eutropha* JMP134; Cuprim, *Cupriavidus metallidurans* CH34), *Deltaproteobacteria* (Desul, *Desulfarculus* sp.; Lujiv, *Lujinxingia vulgaris*), *Gammaproteobacteria* (Pseud, *Pseudomonas* sp. K-62), *Enterobacteria* (Salmot, *Salmonella enterica* subsp. *enterica* serovar Typhimurium; Eschec, *Escherichia coli* JJ1897), *Firmicutes* (Bacic, *Bacillus cereus*), *Actinobacteria* (Strl, *Streptomyces lividans*), *Cyanobacteria* (Syne, *Synechocystis* sp. PCC 6803; Nost, *Nostoc* sp. C3-bin3), *Deinococcus-Thermus* (Thermt, *Thermus thermophilus* HB27), and *Archaea* (Nitros, *Nitrososphaera* sp.; Archae, *Archaeoglobi archaeon*).

the human body (34). Methylmercury is a highly toxic form of mercury that is also produced by anaerobic bacteria that harbor the *hgcAB* genes (35).

The method used most extensively in the laboratory for mercury removal from polluted wastewaters is based on ion-exchange resin adsorption, which is not suitable for environmental conditions. Bacterial-mediated detoxification of mercury is an advantageous technology because it is inexpensive, feasible, and allows the sequestration of mercury in diverse environments (2). Mercury-resistant bacteria usually contain *mer* genes that confer these microorganisms a great potential to be applied in mercury bioremediation techniques. These bacterial *mer* genes are relevant for the conversion of both reactive inorganic and organic forms of mercury to the volatile Hg^0. Once in the atmosphere, Hg^0 can be oxidized photochemically to Hg^{II}, which is deposited back into terrestrial and aquatic ecosystems. Therefore, the occurrence of the Mer system in microorganisms can regulate the fate of mercury in the biogeochemical cycle of a specific environment (1, 36).

The cyanotrophic bacterium *P. pseudoalcaligenes* CECT 5344 uses free cyanides, metal cyanide complexes and cyano derivatives as the sole nitrogen source (24). In this bacterial strain, the cyanide degradation pathway occurs through the production of

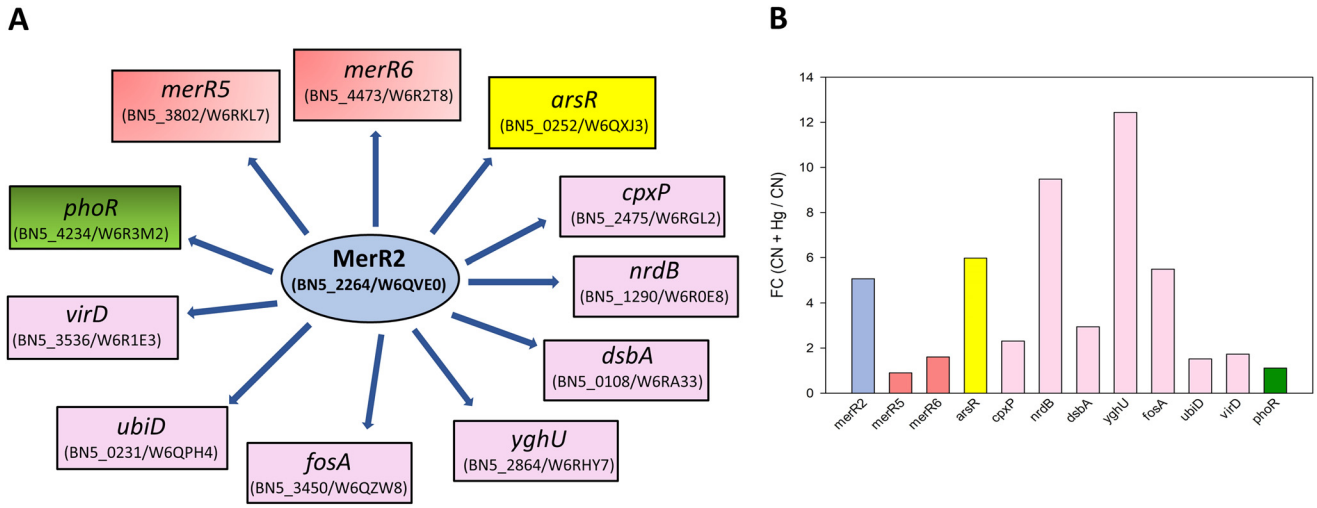

FIG 6 Hypothetical regulation network of the MerR2 regulon of *P. pseudoalcaligenes* CECT 5344 (A) and transcriptional qRT-PCR analysis of the MerR2-regulated genes (B). In this regulatory model, two MerR transcriptional regulator genes, namely, *merR5* and *merR6* (red boxes), are putatively under the control of the master regulator MerR2 (blue oval), as well as the transcriptional regulator *arsR* gene (yellow box) involved in arsenic resistance, the regulatory *phoR* gene that codes for the transcriptional regulator involved in phosphate metabolism (green box), and several structural genes (violet boxes), as follows: *cpxP*, chaperone involved in resistance to metals; *nrdB*, β-subunit of the ribonucleoside-diphosphate reductase; *dsbA*, dithiol oxidoreductase (disulfide-forming); *yghU*, glutathione *S*-transferase; *fosA*, glutathione *S*-transferase; *ubiD*, 3-octaprenyl-4-hydroxybenzoate carboxy-lyase; and *virD*, amino acid/peptide export protein. The transcriptional analysis by qRT-PCR shown in B was performed with mRNA from CECT 5344 cells harvested after 10 h of growth, when these genes showed the highest expression.

oxaloacetate, which reacts chemically with cyanide to generate a cyanohydrin that is converted into the corresponding carboxylic acid and ammonium by the nitrilase NitC. The ammonium released in the nitrilase reaction is incorporated into carbon skeletons through the glutamine synthetase/glutamate synthase cycle (8, 28). Sequencing of the whole genome of the strain CECT 5344 (25, 26) has allowed the development of different omic techniques applied to the degradation of cyanide present in different industrial wastes, including those generated from mining. Mercury and arsenic are usually present in these liquid residues that contain large amounts of cyanide, thus increasing their toxicity (7, 8). In this work, the simultaneous cyanide and mercury detoxifications by the cyanotrophic bacterium *P. pseudoalcaligenes* CECT 5344 have been characterized in minimal media with acetate and cyanide as the sole carbon and nitrogen source, respectively, in the presence or absence of mercuric chloride (Fig. 1). It is important to highlight that *P. pseudoalcaligenes* CECT 5344 showed higher MIC and MBC values for mercury in the presence of cyanide (200 μM and 300 μM, respectively) than with ammonium (10 μM and 17.5 μM, respectively), probably due to a lower toxicity of this metal when it forms complexes with cyanide. This result shows the advantage of using the strain CECT 5344 in the detoxification of industrial wastewaters containing both cyanide and mercury. Under cyanotrophic conditions, this bacterium tolerated elevated concentrations of mercury, displaying growth in the presence of 100 μM mercuric chloride. However, better growth and cyanide consumption rates were achieved in the presence of 75 μM mercuric chloride (Fig. 1). Additionally, the extracellular and intracellular determinations of mercury concentration by ICP-MS in the CECT 5344 cells grown with cyanide and mercury have revealed that this bacterial strain accumulated intracellularly a low amount of mercury, which is probably chelated to biomolecules. Likewise, most of the mercury added to the media was removed rapidly since mercury was not detected in the extracellular media after 7.5 h of growth, indicating that this bacterial strain detoxifies mercury efficiently in the presence of cyanide by transporting this metal inside the cell for its bioaccumulation/metabolization.

Proteomic study of the resistance to mercury in *P. pseudoalcaligenes* CECT 5344 under cyanotrophic conditions. To characterize at the molecular level the simultaneous detoxification by the strain CECT 5344 of these two potent toxics, namely, cyanide and mercury, and to determine the possible mechanisms involved in the

mercury tolerance of this strain, a quantitative proteomic analysis was carried out. The proteomes from *P. pseudoalcaligenes* cells grown in the presence of 2 mM sodium cyanide as the sole nitrogen source, with 75 μM mercury chloride (CN + Hg) or without mercury (CN), were established (Fig. S1 to S4). A total of 2,689 proteins were identified in both proteomes, of which 209 proteins were differentially expressed and 21 were proteins found exclusively under the CN + Hg condition (Fig. S4; Table S1). Among the proteins identified in both proteomes, namely, CN and CN + Hg, were those encoded by the *nit1C* gene cluster, which codes for the nitrilase NitC and other proteins essential for cyanide assimilation in the strain CECT 5344 (28). Additionally, proteins encoded by the *cio* gene cluster were also identified in both proteomes (Fig. 2). These proteins include the cytochrome *bd*-type alternative oxidase CioAB that replaces the cytochrome *c* oxidase for a cyanide-independent respiration and the 4-hydroxy-tetrahydropicolinate synthase DapA1 and the nitrilase Nit4, which play a key role in intracellular iron homeostasis and 3-cyanoalanine assimilation, respectively (37, 38). Other members of the C-N hydrolase superfamily, including the nitrilases Nit1 and Nit2, were also detected in the proteomes from cells grown both in CN and CN + Hg media (Fig. 2). A mutational analysis of these nitrilase genes has revealed that they are not essential for cyanide degradation in the strain CECT 5344, but all together, they could contribute to the alleviation of cyanide toxicity, thus contributing to bacterial cyanide resistance (38). The fact that mercury did not significantly affect proteins involved in cyanide resistance and assimilation constitutes an advantage to apply *P. pseudoalcaligenes* CECT 5344 for cyanide and mercury bioremediation processes.

When the CN and CN + Hg proteomes were compared, the analysis of functional protein categories revealed that proteins overrepresented in the presence of mercury belonged to GO groups mainly related to the response to mercury ion, response to toxic substances, and detoxification of inorganic compounds (Fig. S5). Among proteins exclusive or overrepresented in the CN + Hg proteome were several proteins encoded by the two *mer* gene clusters of *P. pseudoalcaligenes* CECT 5344, including the MerR-family transcriptional regulator MerD, the mercuric reductase MerA, and the periplasmic mercury ion-binding proteins MerP1 and MerP3 (Fig. 3; Table S1). MerP and MerT proteins have been described to be essential to import mercury inside the cell. Mercury binds to two cysteine residues of the periplasmic protein MerP, being next transferred to the cytoplasmic protein MerT, which is also responsible for the uptake of organomercurials (39). MerT contains four cysteine residues by which reduced mercury is bound and transferred to the active side of the NADPH-dependent mercuric reductase MerA (23). The *merR6T3P3T5ADE* gene cluster (BN5_4473 to BN5_4479) of *P. pseudoalcaligenes* codes for additional proteins that were not identified in this proteomic study, including the mercuric resistance regulatory protein MerR6, the mercuric transport proteins MerT3 and MerT5, and the mercuric resistance protein MerE that functions as an inorganic/organic mercury transporter (40, 41). The second *merP1T1R5* gene cluster of the strain CECT 5344 (BN5_3800 to BN5_3802) also encodes two proteins that were not identified in this proteomic analysis, namely, the mercuric transport protein MerT1 and the mercuric resistance regulatory protein MerR5. It is worth noting that the detection of hydrophobic integral membrane proteins and regulators present in the cells at low concentrations are well-known limitations of proteomic techniques (42).

Mercury causes alterations in cell membrane permeability and DNA structure and provokes changes in the structure/function of proteins because it shows a high affinity to sulfhydryl groups (43). Glutathione (GSH) has a relevant role as an antioxidant, preventing the damage of essential cellular molecules in the presence of some metals or ion peroxides. Thus, mercury preferably binds to glutathione, cysteine, or homocysteine as a mercury resistance mechanism. GSH can also conjugate organomercurial compounds like methylmercury. In the proteomic study performed in this work, a glutathione *S*-transferase was found induced in the presence or mercury (Fig. 3; Table S1). This enzyme has a primary role in the conjugation of toxic substances to GSH and probably plays a crucial role in the cellular detoxification of mercury (43). Two GSH-dependent enzymes that were found downregulated in media with mercury, glutaredoxin, and

glutathione peroxidase (Fig. 3; Table S1) are involved in redox reactions and protection from oxidative damage. This process is probably related to a decreased pool of biologically active GSH in the presence of mercury. In this sense, a thioesterase family protein was exclusive of the CN + Hg proteome (Fig. 3; Table S1). Thioesterases catalyze the cleavage of thioester groups present in a wide variety of molecules like coenzyme A, acyl carrier protein, and GSH, among others (44).

On the other hand, mercury induces oxidative stress by increasing reactive oxygen species, acting as a catalyst in Fenton-type reactions (45). Mercury also causes mitochondrial dysfunction, which can provoke alterations in calcium homeostasis and lipid peroxidation. In the proteomic analysis, the ATP-dependent hemin transporter HmuV was found exclusively in the CN + Hg proteome (Fig. 3; Table S1). Recently, it has been described that external hemin acts as an inhibitor of mitochondrial large-conductance calcium-activated potassium channel activity (46). Additionally, the antioxidant protein alkyl hydroperoxide reductase AhpC, which is a thiol-dependent enzyme, and the thiol-based redox sensor RegB were overrepresented in the CN + Hg proteome (Fig. 3; Table S1). Most redox signals are recognized by cysteine residues, which can be oxidized into different redox states like sulfenic, sulfinic, and sulfonic groups that can sense a range of oxidative signals. Thus, sulfenic acids can form complexes to GSH, and also two adjacent cysteine sulfenic acids can form intra- or intermolecular disulfide bonds, which allow redox sensor regulators to acquire specific conformations to modulate the expression of target genes (47). In this sense, components of an ABC-type sulfonate transporter, and also an alkanesulfonate monooxygenase that catalyzes the conversion of sulfonates into sulfite and the corresponding aldehyde, were found overrepresented in the CN + Hg proteome. Additionally, the sulfate-binding protein CysP3 was overrepresented in the presence of mercury (Fig. 3; Table S1). It has been described that Hg^{II} can react with sulfonates, and in fact, in human intoxication by mercury, a treatment based on oral administration of dimercaptopropane sulfonate, is recommended (43). It has also been described the role of the two-component regulatory RegAB system of *Acidithiobacillus ferrooxidans* in controlling ferrous iron and inorganic sulfur compounds oxidation (48).

Mercury may also react with pyrimidine nucleosides and nucleotides. In this sense, the enzymes dihydropyrimidine dehydrogenase and dihydropyrimidinase were overrepresented in the presence of mercury, as well as the uracil-xanthine permease and the α- and β-subunits of the ribonucleoside-diphosphate reductase (Fig. 3; Table S1). The ribonucleoside-diphosphate reductase catalyzes the reduction of ribonucleotides into their corresponding deoxyribonucleotides, and its activity relies on glutaredoxins and thiorredoxins. As mentioned above, glutaredoxin and thioredoxin were downregulated in the presence of mercury, as well as a thiol-disulfide isomerase/thioredoxin (Fig. 3; Table S1). Other proteins involved in DNA replication/repair and translation that were downregulated in the CN + Hg proteome included the DNA-binding protein HU, the TusC protein, the translation initiation factor IF-1, the ribosome-binding factor A, and the ribosome-recycling factor RRF (Table S1), suggesting that general cellular processes like DNA replication and translation are negatively affected by mercury.

Mercury also binds to several metallic cofactors present in enzymes that are essential for cell survival, leading to their downrepresentation in the CN + Hg proteome, such as several nonheme iron dioxygenases, different *c*-type cytochromes and several cytochrome *c*-containing proteins, the nickel/copper-containing superoxide dismutase, and the heme/Fe-S containing bacterioferritin (Fig. 3; Table S1). The formation of complexes between mercury (II) and the porphyrin ring, which is present in the heme group and cobalamin (vitamin B_{12}), has been well described (49). In fact, a protein found exclusively in the presence of mercury was the cobalamin-independent methionine synthase, while the precorrin-2 C20-methyltransferase, which is involved in the synthesis of vitamin B_{12}, was overrepresented in the presence of mercury, perhaps as a compensation mechanism. Curiously, different pyridoxal 5′-phosphate (PLP)-dependent enzymes were also found overrepresented in the CN + Hg proteome of the strain

CECT 5344, such as cysteine desulfurase IscS, alanine racemase, β-alanine-pyruvate transaminase, and D-amino acid dehydrogenase (Fig. 3; Table S1). Cysteine desulfurase catalyzes the conversion of L-cysteine to L-alanine and sulfane sulfur through the formation of a protein-bound cysteine persulfide intermediate on a conserved cysteine. The proposed role of this enzyme is to participate in processes for the biosynthesis of Fe-S clusters, thiamine, tRNA thionucleosides, biotin, lipoic acid, molybdopterin, and NAD^+ (50).

Transcriptional and bioinformatic analysis of mercury detoxification in *P. pseudoalcaligenes* CECT 5344: an integrative view. The expression of the *mer* genes depends on the activity of the regulator MerR, which acts as a transcriptional repressor in the absence of mercury. In the presence of reduced mercury, this metal binds to MerR, which undergoes an allosteric change that provokes its release from the promoter region, allowing active transcription of the structural *mer* genes. It has been proposed that the protein MerD may assist in the dissociation of MerR from DNA, probably by forming a complex with MerR, and therefore playing a coregulatory function in the expression of the *mer* genes (41). Although MerD was annotated in the genome of the strain CECT 5344 as a MerR-type transcriptional regulator, it is not homologous to the MerR regulators that are present in this bacterium. In addition to the mercuric regulatory proteins MerR6 and MerR5 encoded by the *mer* gene clusters from the CECT 5344 strain, four additional genes coding for putative MerR proteins (MerR1 to MerR4) were also identified in different *loci* of the genome. The transcriptional analysis of these six *merR* genes (*merR1* to *merR6*) encoding putative MerR transcriptional regulators in *P. pseudoalcaligenes* revealed that only the *merR2* gene was significatively induced by mercury when cyanide was the sole nitrogen source (Fig. 4A), suggesting that MerR2 may have a key role in the control of the *mer* genes. However, the expression of other *merR* genes slightly increased in the presence of mercury, and therefore, their role in the regulation of mercury resistance/detoxification in the strain CECT 5344 cannot be ruled out. The bioinformatic analysis of the distribution of MerR-type transcriptional regulators among bacteria and archaea showed that MerR2 has homologs in the primitively evolved archaea and thermophilic bacteria (Fig. 5), which indicates a very early origin of the mercury resistance mechanism in hydrothermal habitats that could contain elevated concentrations of mercury (2). Structural genes belonging to the *merR6T3P3T5ADE* and *merP1T1R5* gene clusters were highly induced in the presence of cyanide and mercury (Fig. 4B), thus indicating that probably MerR2 promotes in the presence of mercury the transcription of these *mer* genes that code for mercury transporters, mercury reductase, and the coregulator MerD. Thus, the strain CECT 5344 is a suitable candidate to be used in bioremediation techniques applied for the detoxification of industrial liquid wastes generated by the mining industry that usually contain elevated concentrations of cyanide and mercury, among other metals and metalloids like iron, copper, nickel, and arsenic (51). The results included in this work contribute to highlighting the great biodegradative potential of the CECT strain to detoxify highly toxic complex mixtures of contaminants (Fig. 7).

An additional bioinformatic analysis for searching MerR binding sites in the promoter regions of target genes of *P. pseudoalcaligenes* CECT 5344 allowed the identification of a putative MerR regulon that could control the mercury resistance/detoxification mechanisms in this bacterial strain, paralleling with cyanide detoxification/assimilation. The gene coding for MerR2 does not contain the predicted MerR binding box [5′-(T/C)GTA (G/C)-N_4-GTAC-3′] in its promoter region. This result, together with the fact that *merR2* was the only *merR* gene of this bacterium that was significantly induced by mercury (Fig. 4A), lead us to propose that MerR2 could be a master regulator that controls the expression of different target genes that include the predicted MerR2 binding box in their promoter regions. Thus, different MerR2-regulated genes were induced in the presence of mercury, as described in the proteomic and/or transcriptional analyses carried out in this work (Fig. 3 and 6A; Table S1). Additionally, the *merR2* gene was identified previously as a putative target of a regulatory small RNA (sRNA258) that may control the detoxification of an industrial cyanide-containing residue by *P. pseudoalcaligenes* CECT 5344 (52). Integration of the proteomic data, transcriptional analysis, and bioinformatics

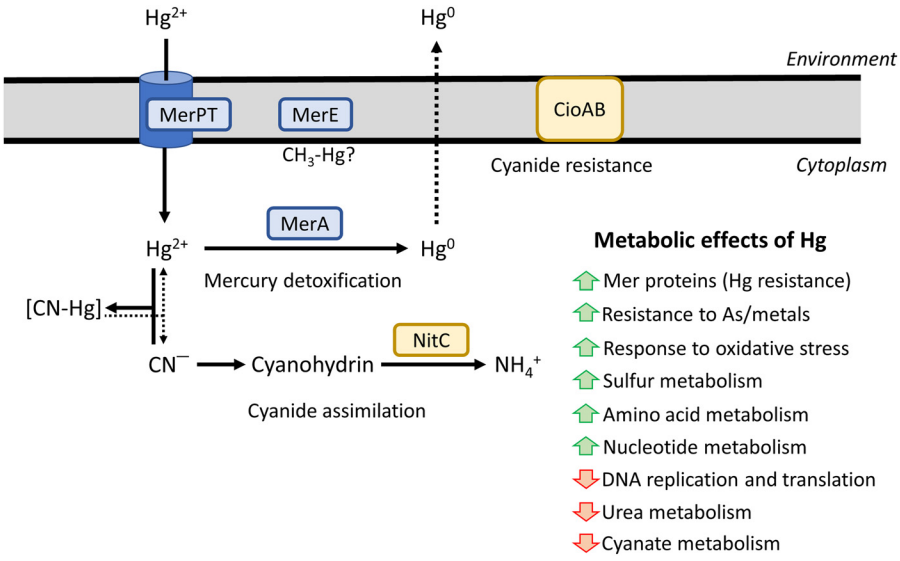

FIG 7 Overview of *P. pseudoalcaligenes* CECT 5344 metabolism under cyanotrophic conditions in the presence of mercury.

has allowed us to predict a regulatory model for the MerR2 regulon of *P. pseudoalcaligenes* CECT 5344 that operates under cyanotrophic conditions (Fig. 6A). Among putative MerR2-regulated genes were *merR5* and *merR6*, which are located in the two *mer* gene clusters of this strain. Other putative MerR2-target genes were *cpxP*, which codes for a chaperone involved in the resistance to metals like mercury; the *nrdB* gene that codes for the β-subunit of the ribonucleoside-diphosphate reductase involved in DNA replication and repair, probably related to the damage that mercury causes directly to DNA; the *fosA* and *yghU* genes, which code for glutathione *S*-transferases that may contribute to increasing the GSH pool biologically active in the presence of mercury; and the dithiol oxidoreductase *dsbA gene*. Proteins of the Dsb system have been described to play a key role in the virulence of many pathogenic microorganisms by acting on the function of various protein secretion systems that influence the virulence (53). The bacterial strain CECT 5344 is not pathogenic but could be a mechanism of defense toward mercury toxicity. In this sense, another predicted target of MerR2 was the *virD* gene that codes for an amino acid/peptide export protein involved in quorum sensing. However, peptides and amino acids can be very effective, and often specific, ligands for a variety of metal ions like mercury. Additionally, the 3-octaprenyl-4-hydroxybenzoate carboxy-lyase *ubiD* gene involved in ubiquinone (coenzyme Q10) synthesis was also identified as a predicted MerR2 target. Recently, it has been shown that coenzyme Q10 supplementation alleviates the oxidative stress imposed by mercury in rats (54). On the other hand, the predicted MerR2-target *phoR* gene codes for a transcriptional regulator involved in phosphorus metabolism. Additionally, the phosphorus-related PhoH protein was found overrepresented in the presence of mercury in the proteomic study carried out in this work (Fig. 3; Table S1). PhoR is a transcriptional regulator that activates *pho* gene expression, while PhoH is a putative ATPase, without clear function. The Pho regulon in bacteria has been described to function not only as a simple regulatory circuit for controlling phosphate homeostasis but also as part of a complex regulatory network relevant for stress response (55). Phosphate is an essential nutrient for living organisms, including bacteria, and usually is scarce in the environment, thus limiting bacterial growth. Furthermore, mercury displays high affinity to phosphorus, making this nutrient even more limited in mercury-containing media. Finally, another predicted MerR2-target gene was *arsR* (BN5_0252), which codes for a transcriptional repressor that may control the expression of *ars* genes. Although arsenical compounds were not present in the culture media of the strain CECT 5344 in this study, several proteins encoded by the *P. pseudoalcaligenes*

CECT 5344 *ars* genes involved in arsenic resistance were overrepresented in the CN + Hg proteome of this bacterium (Fig. 3; Table S1), including the thioredoxin-dependent arsenate reductase ArsC3, the ArsR2 transcriptional regulator, and the arsenic resistance protein ArsH2, which is an $NADP^+$-dependent flavoprotein that protects against oxidative stress and confers resistance to organoarsenicals (56, 57). The presence of mercury in the growth media of *P. pseudoalcaligenes* leads to the induction of these proteins involved in arsenic resistance and detoxification, suggesting a possible cross talk between these two toxic elements, namely, mercury and arsenic. This result highlights the great biotechnological potential of the strain CECT 5344 for use in the detoxification of mining wastes that are composed of complex mixtures of highly toxic compounds like cyanide, mercury, and arsenic, which display different chemical properties that make their disposal very difficult.

MATERIALS AND METHODS

Culture media and bacterial growth conditions. *Pseudomonas pseudoalcaligenes* CECT 5344 was cultured in M9 minimal media, at pH 9.5 and 30°C, under aerobic conditions with agitation of 220 rpm in an orbital shaker (24, 28). Sodium acetate (50 mM) was used as the carbon source, and sodium cyanide (2 mM) or ammonium chloride (2 mM) was used as the nitrogen source where indicated. When applicable, mercury chloride (Sigma-Aldrich) was added to the M9 media (from a 5 mM stock solution) to achieve the indicated concentration for each experiment. Agar plates were prepared by addition of 1.5% bacteriological agar to LB liquid medium.

Determination of bacterial growth and mercury tolerance. Bacterial growth was determined in liquid cultures by measuring the absorbance at 600 nm (A_{600}) in a spectrophotometer (Spectronic; Thermo Fisher Scientific, USA). The tolerance of *P. pseudoalcaligenes* CECT 5344 to mercury was determined by calculation of the MIC and the minimum bactericidal concentration (MBC) (58). For this purpose, the strain CECT 5344 was grown (in quintuplicate) in U-shaped 96-well microtiter plates, containing M9 liquid medium, at 30°C with shaking at 220 rpm. After 48 h of incubation, the MIC of mercury that impairs visible growth of bacteria (MIC) and the minimum bactericide concentration of mercury that kills bacteria (MBC) were determined by measuring bacterial growth in agar plates by counting CFU with the drop plate technique (59).

Analytical determinations. Cyanide was determined colorimetrically in the presence of chloramine T, barbituric acid, and pyridine reagents as described previously (60). Protein was quantified by the method of Bradford (61).

The determination of mercury in the culture media or that accumulated extracellularly (biosorption) or intracellularly (chelated to biomolecules) was determined from 100-mL liquid cultures in M9 minimal media with 75 μM $HgCl_2$ and 2 mM sodium cyanide, as the sole nitrogen source (CN + Hg media). Four biological samples were analyzed. Cells were centrifuged (10,000 rpm, 10 min, and 4°C) at 7.5 h of growth, and after centrifugation, supernatants were used to determine the mercury concentration. Pellets with cells were washed with 1 mL of a solution containing 0.85% NaCl. Cells were heated at 80°C for 96 h, and cell dry weight was determined. Pellets were digested in 69% HNO_3 (trace-metal grade; Fisher). Mercury concentration was determined by inductively coupled plasma-mass-spectrometry (ICP-MS; PerkinElmer; model Nexion 350X) at the Central Service for Research Support of the University of Córdoba (SCAI-UCO).

Quantitative proteomic analysis by LC-MS/MS. Proteomic analysis was carried out from *P. pseudoalcaligenes* CECT 5344 cells grown in M9 minimal medium containing 50 mM sodium acetate and 2 mM sodium cyanide as the carbon and nitrogen sources, respectively, and in the presence of 75 μM $HgCl_2$ (CN + Hg) or without mercury (CN). Four independent biological replicates were used for each medium. Cells were harvested by centrifugation at 12,000 rpm for 10 min at 4°C after 7.5 h of growth, when they were actively growing and most of the cyanide was depleted from the media. Pellets with cells were resuspended in 300 μL of a lysis buffer, containing 8 M urea, 50 mM Tris-HCl (pH 7.5), 4% 3-[(3-cholamidopropyl)-dimethylammonio]-1-propanesulfonate (CHAPS), and 1% SDS. Samples were disrupted by sonication in Bandelin Sonoplus H2070 equipment (8 pulses for 20 s, at 25 W). After centrifugation at 12,000 rpm for 10 min at 4°C, supernatants were cleaned by using the 2D-clean up kit (Amersham GE Healthcare). The LC-MS protocol, acquisition modes, data-independent acquisition-parallel accumulation serial fragmentation (DIA-PASEF) parameters, building up *in silico* library by using DIA-NN software, and searching criteria and quantification mode were carried out as described previously (62). The *P. pseudoalcaligenes* CECT 5344 proteome is available in Uniprot (UP000032841). Data were analyzed by using Perseus software (1.6.12.1). The principal-component analysis (PCA) was carried out, and a heat map and a volcano plot were generated by using default parameters (Fig. S1 to S3). Then a *t* test was applied, and differentially expressed proteins were defined as those with an adjusted *P* value of $\leq$0.05 and a $\log_2$ FC of $\geq$1 (overexpressed in CN + Hg media) or ≤ -1 (overexpressed in CN media). Proteins indicated as exclusive were identified only under one condition (either CN + Hg or CN) in at least three of the four replicates from the same culture media. After data were filtered, a GO enrichment analysis was carried out by using the ComparativeGO application (27). Data were deposited to the ProteomeXchange Consortium (http://proteomecentral.proteomexchange.org) via the PRIDE partner repository with the data set identifier PXD038659.

Quantitative real-time PCR analysis. The transcriptional expression of selected genes was analyzed by qRT-PCR using three biological samples, each with two technical replicates. RNA isolation was performed following the Qiagen RNA extraction kit (RNeasy midi kit), and the synthesis of total cDNA was achieved with the SuperScript II reverse transcriptase (Invitrogen). The detailed procedure was described previously (63). Oligonucleotides sequences used as primers (see Table S3 in the supplemental material) in the qRT-PCRs were designed using the Oligo 7.0 software. The obtained data were normalized to the *dnaQ1* (BN5_2215) and the *dnaE* (BN5_2819) housekeeping genes. Gene expression was calculated by the threshold cycle $\Delta\Delta C_T$ method (62).

Bioinformatic analysis of the MerR binding sequence in the genome of *P. pseudoalcaligenes*. The pattern locator (PatLoc) software (https://academic.oup.com/bioinformatics/article/22/24/3099/210155) described previously (64) was used for the identification of MerR sequence patterns in the genome of *P. pseudoalcaligenes* CECT 5344 with the restriction of searching in intergenic regions. For that purpose, the sequence 5′-(T/C)GTA(G/C)-N_4-GTAC-3′ was used as the predicted MerR binding box in *P. pseudoalcaligenes* CECT 5344, as deduced from the one described previously in *E. coli* (29).

Statistical analysis. Statistical significance was determined by a two-tailed *t* test analysis by using the Benjamini-Hochberg correction method. Data were analyzed by using Perseus software (v1.6.12.1) (https://maxquant.org/perseus/). Log_2 LFQ intensity data were used for proteomics and normalized data for qRT-PCR. A pair of samples were considered significantly different when the adjusted *P* value was lower than 0.05. Perseus (v1.6.12.1) software was used for the proteomic data analysis. To identify the *merR* gene orthologs, the KEGG database was used (https://www.kegg.jp/kegg/kegg2.html). Other data were compared using the IBM SPSS Statistics v22 software.

SUPPLEMENTAL MATERIAL

Supplemental material is available online only.

SUPPLEMENTAL FILE 1, DOCX file, 1.1 MB.

ACKNOWLEDGMENTS

We thank the companies MAGTEL, FCC-AMBITO (GEMASUR), SAVECO, and AVENIR for fruitful collaborations.

This work was funded by Junta de Andalucía (grant P18-RT-3048) and Fundación Torres Gutiérrez, Spain.

K.A.B., and A.O.-A. performed the experiments and data collection. P.C., G.R.-C., and L.P.S. performed the data collection and curation. V.M.L.-A., A.O.-A., C.M.-V., and M.D.R. were involved in conceptualization and supervision. C.M.-V. and M.D.R. were involved in funding acquisition/project administration. V.M.L.-A. and M.D.R. performed writing – review and editing. All authors read and approved the final manuscript.

We report no potential conflict of interest.

REFERENCES

1. Selin NE. 2009. Global biogeochemical cycling of mercury: a review. Annu Rev Environ Resour 34:43–63. https://doi.org/10.1146/annurev.environ.051308.084314.
2. Priyadarshanee M, Chatterjee S, Rath S, Dash H, Das S. 2022. Cellular and genetic mechanism of bacterial mercury resistance and their role in biogeochemistry and bioremediation. J Hazard Mater 423:126985. https://doi.org/10.1016/j.jhazmat.2021.126985.
3. Ruelas-Inzunza J, Delgado-Alvarez C, Frías-Espericueta M, Páez-Osuna F. 2013. Mercury in the atmospheric and coastal environments of Mexico, review of environmental contamination and toxicology. Rev Environ Contam Toxicol 226:65–99. https://doi.org/10.1007/978-1-4614-6898-1_3.
4. Lin Y, Wang S, Wu Q, Larssen T. 2016. Material flow for the intentional use of mercury in China. Environ Sci Technol 50:2337–2344. https://doi.org/10.1021/acs.est.5b04998.
5. Drace K, Kiefer AM, Veiga MM. 2016. Cyanidation of mercury-contaminated tailings: potential health effects and environmental justice. Curr Environ Health Rep 3:443–449. https://doi.org/10.1007/s40572-016-0113-0.
6. Chen M, Lu W, Hou Z, Zhang Y, Jiang X, Wu J. 2017. Heavy metal pollution in soil associated with a large-scale cyanidation gold mining region in southeast of Jilin, China. Environ Sci Pollut Res Int 24:3084–3096. https://doi.org/10.1007/s11356-016-7968-3.
7. Aghaei E, Diaz-Alorro R, Tadesse B, Browner R. 2019. A review on current practices and emerging technologies for sustainable management, sequestration and stabilization of mercury from gold processing streams. J Environ Manage 249:109367. https://doi.org/10.1016/j.jenvman.2019.109367.
8. Roldán MD, Olaya-Abril A, Sáez LP, Cabello P, Luque-Almagro VM, Moreno-Vivián C. 2021. Bioremediation of cyanide-containing wastes: the potential of systems and synthetic biology for cleaning up the toxic leftovers from mining. EMBO Rep 22:e53720. https://doi.org/10.15252/embr.202153720.
9. Holzman DC. 2010. Mercury emissions not shrinking as forecast. Environ Health Perspect 118:A198. https://doi.org/10.1289/ehp.118-a198.
10. Bridges C, Zalups R. 2017. Mechanism involved in the transport of mercuric ions in target tissue. Arch Toxicol 91:63–81. https://doi.org/10.1007/s00204-016-1803-y.
11. Gentès S, Löhrer B, Legeay A, Mazel AF, Anschutz P, Charbonnier C, Tessier E, Maury-Brachet R. 2021. Drivers of variability in mercury and methylmercury bioaccumulation and biomagnification in temperate freshwater lakes. Chemosphere 267:128890. https://doi.org/10.1016/j.chemosphere.2020.128890.
12. Bjørklund G, Antonyak H, Polishchuk A, Semenova Y, Lesiv M, Lysiuk R, Peana M. 2022. Effect of methylmercury on fetal neurobehavioral development: an overview of the possible mechanisms of toxicity and the neuroprotective effect of phytochemicals. Arch Toxicol 96:3175–3199. https://doi.org/10.1007/s00204-022-03366-3.
13. Rand MD, Caito SW. 2019. Variation in the biological half-life of methylmercury in humans: methods, measurements and meaning. Biochim Biophys Acta 1863:129301. https://doi.org/10.1016/j.bbagen.2019.02.003.
14. Hong YS, Kim YM, Lee KE. 2012. Methylmercury exposure and health effects. J Prev Med Public Health 45:353–363. https://doi.org/10.3961/jpmph.2012.45.6.353.

15. Harada M. 1995. Minamata disease: methylmercury poisoning in Japan caused by environmental pollution. Crit Rev Toxicol 25:1–24. https://doi.org/10.3109/10408449509089885.
16. Kim S, Arora M, Fernandez C, Landero J, Caruso J, Chen A. 2013. Lead, mercury, and cadmium exposure and attention deficit hyperactivity disorder in children. Environ Res 126:105–110. https://doi.org/10.1016/j.envres.2013.08.008.
17. François F, Lombard C, Guigner JM, Soreau P, Jaisson FB, Martino G, Vandervennet M, Garcia D, Molinier AL, Pignol D, Peduzzi J, Zirah S, Rebuffat S. 2012. Isolation and characterization of environmental bacteria capable of extracellular biosorption of mercury. Appl Environ Microbiol 78:1097–1106. https://doi.org/10.1128/AEM.06522-11.
18. Smith T, Pitts K, McGarvey JA, Summers AO. 1998. Bacterial oxidation of mercury metal vapor, Hg(0). Appl Environ Microbiol 64:1328–1332. https://doi.org/10.1128/AEM.64.4.1328-1332.1998.
19. Gilmour CC, Elias DA, Kucken AM, Brown SD, Palumbo AV, Schadt CW, Wall JD. 2011. Sulfate-reducing bacterium Desulfovibrio desulfuricans ND132 as a model for understanding bacterial mercury methylation. Appl Environ Microbiol 77:3938–3951. https://doi.org/10.1128/AEM.02993-10.
20. Si Y, Zou Y, Liu X, Si X, Mao J. 2015. Mercury methylation coupled to iron reduction by dissimilatory iron-reducing bacteria. Chemosphere 122:206–212. https://doi.org/10.1016/j.chemosphere.2014.11.054.
21. Mathema VB, Thakuri BC, Sillanpää M. 2011. Bacterial mer operon-mediated detoxification of mercurial compounds: a short review. Arch Microbiol 193:837–844. https://doi.org/10.1007/s00203-011-0751-4.
22. Mergeay M, Monchy S, Vallaeys T, Auquier V, Benotmane A, Bertin P, Taghavi S, Dunn J, van der Lelie D, Wattiez R. 2003. Ralstonia metallidurans, a bacterium specifically adapted to toxic metals: towards a catalogue of metal-responsive genes. FEMS Microbiol Rev 27:385–410. https://doi.org/10.1016/S0168-6445(03)00045-7.
23. Sone Y, Nakamura R, Pan-Hou H, Itoh T, Kiyono M. 2013. Role of MerC, MerE, MerF, MerT, and/or MerP in resistance to mercurials and the transport of mercurials in Escherichia coli. Biol Pharm Bull 36:1835–1841. https://doi.org/10.1248/bpb.b13-00554.
24. Luque-Almagro VM, Blasco R, Huertas MJ, Martínez-Luque M, Moreno-Vivián C, Castillo F, Roldán MD. 2005. Alkaline cyanide biodegradation by Pseudomonas pseudoalcaligenes CECT5344. Biochem Soc Trans 33:168–169. https://doi.org/10.1042/BST0330168.
25. Luque-Almagro VM, Acera F, Igeño MI, Wibberg D, Roldán MD, Sáez LP, Hennig M, Quesada A, Huertas MJ, Blom J, Merchán F, Escribano MP, Jaenicke S, Estepa J, Guijo MI, Martínez-Luque M, Macías D, Szczepanowski R, Becerra G, Ramirez S, Carmona MI, Gutiérrez O, Manso I, Pühler A, Castillo F, Moreno-Vivián C, Schlüter A, Blasco R. 2013. Draft whole genome sequence of the cyanide-degrading bacterium Pseudomonas pseudoalcaligenes CECT5344. Environ Microbiol 15:253–270. https://doi.org/10.1111/j.1462-2920.2012.02875.x.
26. Wibberg D, Bremges A, Damman-Kalinowski T, Maus I, Igeño MI, Vogelsang R, König C, Luque-Almagro VM, Roldán MD, Sczyrba A, Moreno-Vivián C, Blasco R, Pühler A, Schlüter A. 2016. Finished genome sequence and methylome of the cyanide-degrading Pseudomonas pseudoalcaligenes strain CECT5344 as resolved by single-molecule real-time sequencing. J Biotechnol 232:61–68. https://doi.org/10.1016/j.jbiotec.2016.04.008.
27. Fruzangohar M, Ebrahimie E, Ogunniyi AD, Mahdi LK, Paton JC, Adelson DL. 2013. Comparative GO: a Web application for comparative gene ontology and gene ontology-based gene selection in bacteria. PLoS One 8:e58759. https://doi.org/10.1371/journal.pone.0058759.
28. Estepa J, Luque-Almagro VM, Manso I, Escribano MP, Martínez-Luque M, Castillo F, Moreno-Vivián C, Roldán MD. 2012. The nit1C gene cluster of Pseudomonas pseudoalcaligenes CECT5344 involved in assimilation of nitriles is essential for growth on cyanide. Environ Microbiol Rep 4:326–334. https://doi.org/10.1111/j.1758-2229.2012.00337.x.
29. Brown NL, Stoyanov JV, Kidd SP, Hobman JL. 2003. The MerR family transcriptional regulators. FEMS Microbiol Rev 27:145–163. https://doi.org/10.1016/S0168-6445(03)00051-2.
30. Wedepohl KH. 1995. The composition of the continental crust. Geochim Cosmochim Acta 59:1217–1232. https://doi.org/10.1016/0016-7037(95)00038-2.
31. Vázquez V, Parga J, Valenzuela J, Figueroa G, Valenzuela A, Munive G. 2014. Recovery of silver from cyanide solutions using electrochemical process like alternative for Merrill-Crowe process. Mater Sci Appl 5:863–870. https://doi.org/10.4236/msa.2014.512087.
32. Coulibaly M, Bamba D, Yao N, Zoro E, Rhazi M. 2016. Some aspects of speciation and reactivity of mercury in various matrices. Comptes Rendus Chimie 19:832–840. https://doi.org/10.1016/j.crci.2016.02.005.
33. Sun R, Guangqian L, Wu H, Li X, Tian H, Yao H. 2022. Insight into mercury-laden activated carbon adsorbent product bonding nature by DFT calculations. Chem Engineer J 433:134461. https://doi.org/10.1016/j.cej.2021.134461.
34. Tulasi D, Fajon V, Joze K, Shlyapnikov Y, Adotey D, Serfor-Armah Y, Horvat M. 2021. Mercury methylation in cyanide influenced river sediments: a comparative study in Southwestern Ghana. Environ Monit Assess 193:180. https://doi.org/10.1007/s10661-021-08920-7.
35. Lin H, Ascher DB, Myung Y, Lamborg CH, Hallam SJ, Gionfriddo CM, Holt KE, Moreau JW. 2021. Mercury methylation by metabolically versatile and cosmopolitan marine bacteria. ISME J 15:1810–1825. https://doi.org/10.1038/s41396-020-00889-4.
36. Si L, Branfireun BA, Fierro J. 2022. Chemical oxidation and reduction pathways of mercury relevant to natural waters: a review. Water 14:1891. https://doi.org/10.3390/w14121891.
37. Olaya-Abril A, Pérez MD, Cabello P, Martignetti D, Sáez LP, Luque-Almagro VM, Moreno-Vivián C, Roldán MD. 2020. Role of the dihydrodipicolinate synthase DapA1 on iron homeostasis during cyanide assimilation by the alkaliphilic bacterium Pseudomonas pseudoalcaligenes CECT 5344. Front Microbiol 11:28. https://doi.org/10.3389/fmicb.2020.00028.
38. Pérez MD, Olaya-Abril A, Cabello P, Sáez LP, Roldán MD, Moreno-Vivián C, Luque-Almagro VM. 2021. Alternative pathway for 3-cyanoalanine assimilation in Pseudomonas pseudoalcaligenes CECT5344 under non cyanotrophic conditions. Microbiol Spectr 9:e0077721. https://doi.org/10.1128/Spectrum.00777-21.
39. Zheng R, Wu S, Ma N, Sun C. 2018. Genetic and physiological adaptations of marine bacterium Pseudomonas stutzeri 273 to mercury stress. Front Microbiol 9:682. https://doi.org/10.3389/fmicb.2018.00682.
40. Amin A, Sarwar A, Saleem MA, Latif Z, Opella SJ. 2019. Expression and purification of transmembrane protein MerE from mercury-resistant Bacillus cereus. J Microbiol Biotechnol 29:274–282. https://doi.org/10.4014/jmb.1704.04062.
41. Naguib M, El-Gendy A, Khairalla A. 2018. Microbial diversity of mer operon genes and their potential rules in mercury bioremediation and resistance. Open Biotechnol J 12:56–77. https://doi.org/10.2174/1874070701812010056.
42. Bogdanow B, Zauber H, Selbach M. 2016. Systematic errors in peptide and protein identification and quantification by modified peptides. Mol Cell Proteomics 15:2791–2801. https://doi.org/10.1074/mcp.M115.055103.
43. Bjørklund G, Crisponi G, Nurchi VM, Cappai R, Djordjevic AB, Aaseth J. 2019. A review on coordination properties of thiol-containing chelating agents towards mercury, cadmium, and lead. Molecules 24:3247. https://doi.org/10.3390/molecules24183247.
44. Cantu DC, Chen Y, Reilly PJ. 2010. Thioesterases: a new perspective based on their primary and tertiary structures. Protein Sci 19:1281–1295. https://doi.org/10.1002/pro.417.
45. Zhao Y, Zhou C, Guo X, Hu G, Li G, Zhuang Y, Cao H, Li L, Xing C, Zhang C, Yang F, Liu P. 2021. Exposed to mercury-induced oxidative stress, changes of intestinal microflora, and association between them in mice. Biol Trace Elem Res 199:1900–1907. https://doi.org/10.1007/s12011-020-02300-x.
46. Walewska A, Szewczyk A, Koprowski P. 2022. External hemin as an inhibitor of mitochondrial large-conductance calcium-activated potassium channel activity. Int J Mol Sci 23:13391. https://doi.org/10.3390/ijms232113391.
47. Lee SJ, Kim DG, Lee KY, Koo JS, Lee BJ. 2018. Regulatory mechanisms of thiol-based redox sensors: lessons learned from structural studies on prokaryotic redox sensors. Arch Pharm Res 41:583–593. https://doi.org/10.1007/s12272-018-1036-0.
48. Moinier D, Byrne D, Amouric A, Bonnefoy V. 2017. The global redox responding RegB/RegA signal transduction system regulates the genes involved in ferrous iron and inorganic sulfur compound oxidation of the acidophilic Acidithiobacillus ferrooxidans. Front Microbiol 8:1277. https://doi.org/10.3389/fmicb.2017.01277.
49. Hudson MF, Smith KM. 1975. Novel mercury (II) complexes of porphyrins. Tetrahedron 31:3077–3083. https://doi.org/10.1016/0040-4020(75)80151-7.
50. Mihara H, Esaki N. 2002. Bacterial cysteine desulfurases: their function and mechanisms. Appl Microbiol Biotechnol 60:12–23. https://doi.org/10.1007/s00253-002-1107-4.
51. Meloni F, Montegrossi G, Lazzaroni M, Rappuoli D, Nisi B, Vaselli O. 2021. Total and leached arsenic, mercury and antimony in the mining waste dumping area of abadie San Salvatore (Mt. Amiata, central Italy). Appl Sci 11:7893. https://doi.org/10.3390/app11177893.
52. Olaya-Abril A, Luque-Almagro VM, Pérez MD, López CM, Amil F, Cabello P, Sáez LP, Moreno-Vivián C, Roldán MD. 2019. Putative small RNAs controlling detoxification of industrial cyanide-containing wastewaters by

Pseudomonas pseudoalcaligenes CECT 5344. PLoS One 14:e0212032. https://doi.org/10.1371/journal.pone.0212032.
53. Bocian-Ostrzycka KM, Grzeszczuk MJ, Banaś AM, Jagusztyn-Krynicka EK. 2017. Bacterial thiol oxidoreductases—from basic research to new antibacterial strategies. Appl Microbiol Biotechnol 101:3977–3989. https://doi.org/10.1007/s00253-017-8291-8.
54. Gamal A, AboSalem M, El-Shewy E, Medhate-Hegazy A, Saber S. 2023. Coenzyme Q10 supplementation alleviates the oxidative stress on the liver imposed by mercuric chloride in albino rats. Benha Vet Med J 43:19–24. https://doi.org/10.21608/bvmj.2022.176212.1613.
55. Lamarche MG, Wanner BL, Crépin S, Harel J. 2008. The phosphate regulon and bacterial virulence: a regulatory network connecting phosphate homeostasis and pathogenesis. FEMS Microbiol Rev 32:461–473. https://doi.org/10.1111/j.1574-6976.2008.00101.x.
56. Ben Fekih I, Zhang C, Li YP, Zhao Y, Alwathnani HA, Saquib Q, Rensing C, Cervantes C. 2018. Distribution of arsenic resistance genes in prokaryotes. Front Microbiol 9:2473. https://doi.org/10.3389/fmicb.2018.02473.
57. Páez-Espino AD, Nikel PI, Chavarría M, de Lorenzo V. 2020. ArsH protects Pseudomonas putida from oxidative damage caused by exposure to arsenic. Environ Microbiol 22:2230–2242. https://doi.org/10.1111/1462-2920.14991.
58. Andrews JM. 2001. Determination of minimum inhibitory concentrations. J Antimicrob Chemother 48:5–16. https://doi.org/10.1093/jac/48.suppl_1.5.
59. Naghili H, Tajik H, Mardani K, Razavi-Rouhani SM, Ehsani A, Zare P. 2013. Validation of drop plate technique for bacterial enumeration by parametric and nonparametric tests. Vet Res Forum 4:179–183.
60. Asmus E, Garschagen H. 1953. The use of barbituric acid for the photometric determination of cyanide and thiocyanate. Z Anal Chem 138:414–422. https://doi.org/10.1007/BF00461093.
61. Bradford MM. 1976. A rapid and sensitive method for the quantitation of microgram quantities of protein utilizing the principle of protein-dye binding. Anal Biochem 72:248–254. https://doi.org/10.1006/abio.1976.9999.
62. Olaya-Abril A, Luque-Almagro VM, Hidalgo-Carrillo J, Chicano-Gálvez E, Urbano FJ, Moreno-Vivián C, Richardson DJ, Roldán MD. 2022. The NtrYX two-component system of Paracoccus denitrificans is required for the maintenance of cellular iron homeostasis and for a complete denitrification under iron-limited conditions. Int J Mol Sci 23:9172. https://doi.org/10.3390/ijms23169172.
63. Olaya-Abril A, Hidalgo-Carrillo J, Luque-Almagro VM, Fuentes-Almagro C, Urbano FJ, Moreno-Vivián C, Richardson DJ, Roldán MD. 2021. Effect of pH on the denitrification proteome of the soil bacterium Paracoccus denitrificans PD1222. Sci Rep 11:17276. https://doi.org/10.1038/s41598-021-96559-2.
64. Mrázek J, Xie S. 2006. Pattern locator: a new tool for finding local sequence patterns in genomic DNA sequences. Bioinformatics 22:3099–3100. https://doi.org/10.1093/bioinformatics/btl551.
65. Dereeper A, Guignon V, Blanc G, Audic S, Buffet S, Chevenet F, Dufayard JF, Guindon S, Lefort V, Lescot M, Claverie JM, Gascuel O. 2008. Phylogeny.fr: robust phylogenetic analysis for the non-specialist. Nucleic Acids Res 36:W465–W469. https://doi.org/10.1093/nar/gkn180.